



Fundamentals of Vehicle Dynamics

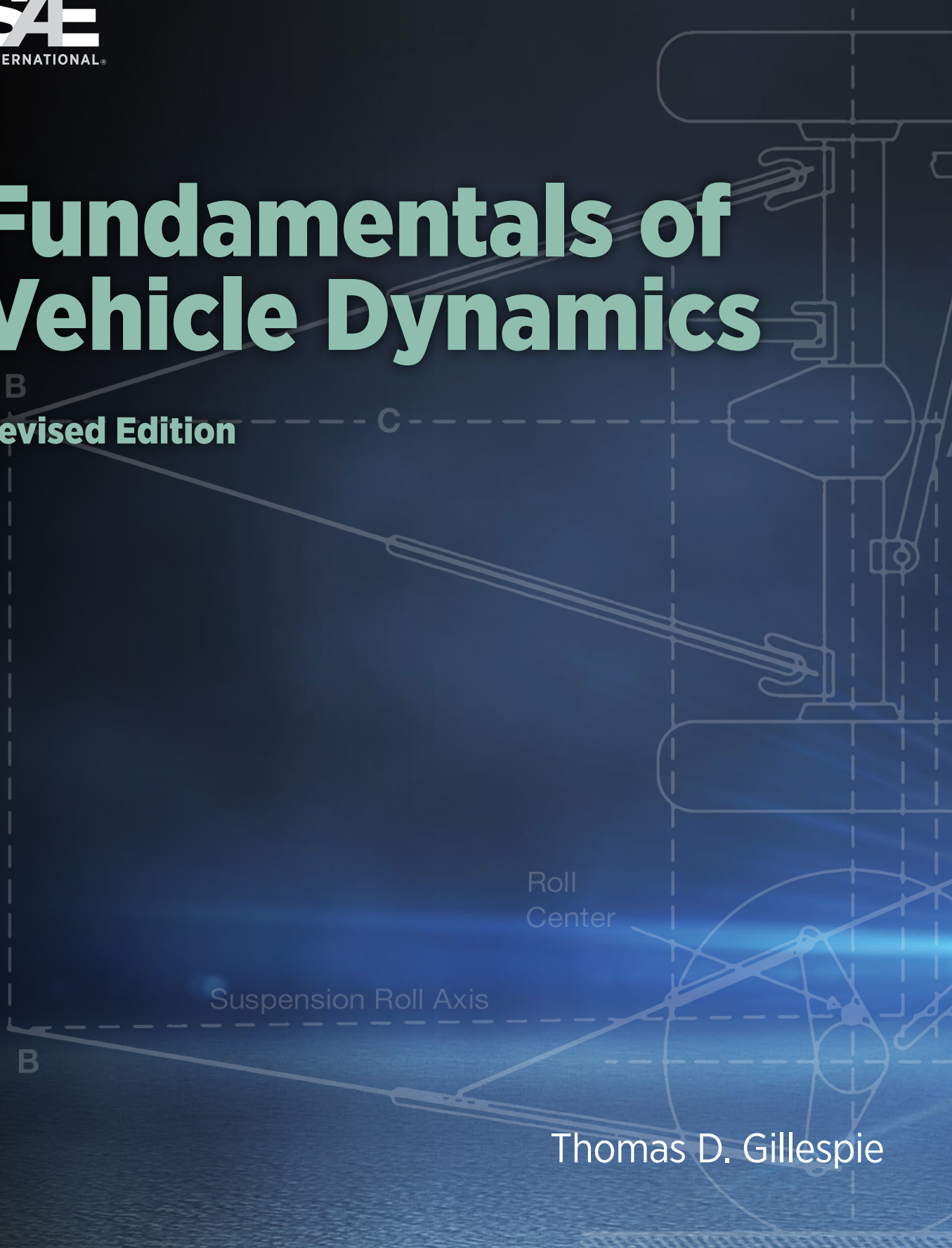
Revised Edition

Thomas D. Gillespie

B

Suspension Roll Axis

Roll
Center



Fundamentals of Vehicle Dynamics

Revised Edition

Fundamentals of Vehicle Dynamics

Revised Edition

THOMAS D. GILLESPIE

Revised Edition Editors:

**SAIED TAHERI
CORINA SANDU
BENJAMIN L. DUPREY**



Warrendale, Pennsylvania, USA



400 Commonwealth Drive
Warrendale, PA 15096-0001 USA
E-mail: CustomerService@sae.org
Phone: 877-606-7323 (inside USA and Canada)
724-776-4970 (outside USA)

Copyright © 2021 SAE International. All rights reserved.

No part of this publication may be reproduced, stored in a retrieval system, or transmitted, in any form or by any means, electronic, mechanical, photocopying, recording, or otherwise, without the prior written permission of SAE International. For permission and licensing requests, contact SAE Permissions, 400 Commonwealth Drive, Warrendale, PA 15096-0001 USA; e-mail: copyright@sae.org; phone: 724-772-4028.

Library of Congress Catalog Number 2020947766

<http://dx.doi.org/10.4271/9781468601770>

Information contained in this work has been obtained by SAE International from sources believed to be reliable. However, neither SAE International nor its authors guarantee the accuracy or completeness of any information published herein and neither SAE International nor its authors shall be responsible for any errors, omissions, or damages arising out of use of this information. This work is published with the understanding that SAE International and its authors are supplying information but are not attempting to render engineering or other professional services. If such services are required, the assistance of an appropriate professional should be sought.

ISBN-Print 978-1-4686-0176-3

ISBN-PDF 978-1-4686-0177-0

ISBN-epub 978-1-4686-0356-9

To purchase bulk quantities, please contact: SAE Customer Service

E-mail: CustomerService@sae.org
Phone: 877-606-7323 (inside USA and Canada)
724-776-4970 (outside USA)
Fax: 724-776-0790

Visit the SAE International Bookstore at books.sae.org

Chief Product Officer

Frank Menchaca

Publisher

Sherry Dickinson Nigam

Director of Content Management

Kelli Zilkoski

Production and Manufacturing

Associate

Erin Mendicino

contents

Foreword	xiii
Preface	xv
Acknowledgments	xvii
From the Publisher	xix
About the Author	xxi
About the Editors	xxiii
List of Symbols	xxv

CHAPTER 1

Introduction	<u>1</u>
Dawn of the Motor Vehicle Age	<u>1</u>
Introduction to Vehicle Dynamics	<u>5</u>
Fundamental Approach to Modeling	<u>6</u>
Lumped Mass	<u>6</u>
Vehicle-Fixed Coordinate System	<u>7</u>
ISO/SAE Z-up Vehicle-Fixed Coordinate System	<u>8</u>
Motion Variables	<u>8</u>
Earth-Fixed Coordinate System	<u>8</u>
Euler Angles	<u>9</u>
Forces	<u>9</u>
Newton's Second Law	<u>9</u>
Dynamic Axle Loads	<u>10</u>
Static Loads on Level Ground	<u>11</u>
Low-Speed Acceleration	<u>11</u>
Loads on Grades	<u>12</u>
Climbing a Grade	<u>12</u>
Road Grade	<u>12</u>
Composite Mass	<u>13</u>
Moments of Inertia	<u>13</u>
Example Problems	<u>14</u>
References	<u>18</u>

CHAPTER 2

Acceleration Performance	<u>21</u>
Power-Limited Acceleration	<u>21</u>
Engines	<u>21</u>
Powertrain	<u>23</u>
Automatic Transmissions	<u>27</u>
Example Problems	<u>30</u>
Traction-Limited Acceleration	<u>32</u>
Transverse Weight Shift due to Drive Torque	<u>32</u>
Traction Limits	<u>35</u>
Parts of a Differential	<u>36</u>
Differential Rules	<u>37</u>
Example Problems	<u>37</u>
References	<u>39</u>

CHAPTER 3

Braking Performance	<u>41</u>
Basic Equations	<u>41</u>
Constant Deceleration	<u>42</u>
Deceleration with Wind Resistance	<u>43</u>
Energy/Power	<u>43</u>
Braking Forces	<u>43</u>
Rolling Resistance	<u>44</u>
Aerodynamic Drag	<u>44</u>
Driveline Drag	<u>44</u>
Grade	<u>44</u>
Brakes	<u>45</u>
Brake Factor	<u>45</u>
Tire-Road Friction	<u>47</u>
Velocity	<u>49</u>
Inflation Pressure	<u>49</u>
Vertical Load	<u>49</u>
Example Problems	<u>49</u>
Federal Requirements for Braking Performance	<u>51</u>
Brake Proportioning	<u>52</u>
Anti-lock Brake Systems	<u>57</u>
Braking Efficiency	<u>58</u>
Rear Wheel Lockup	<u>59</u>
Pedal Force Gain	<u>61</u>
Example Problem	<u>63</u>
References	<u>64</u>

CHAPTER 4

Road Loads	67
Aerodynamics	67
Mechanics of Air Flow around a Vehicle	68
Pressure Distribution on a Vehicle	70
Aerodynamic Forces	73
Drag Components	74
Aerodynamic Aids	78
Bumper Spoilers	78
Air Dams	78
Deck Lid Spoilers	78
Window and Pillar Treatments	78
Optimization	79
Drag	79
Air Density	79
Drag Coefficient	81
Side Force	83
Lift Force	84
Pitching Moment	85
Yawing Moment	85
Rolling Moment	86
Crosswind Sensitivity	87
Rolling Resistance	90
Factors Affecting Rolling Resistance	91
Tire Temperature	91
Tire Inflation Pressure/Load	91
Velocity	92
Tire Material and Design	92
Tire Slip	94
Typical Coefficients	94
Total Road Loads	96
Fuel Economy Effects	97
Example Problems	97
References	99

CHAPTER 5

Ride	103
Excitation Sources	104
Road Roughness	104
Tire/Wheel Assembly	109
Driveline Excitation	113
Engine and Transmission	116

Vehicle Response Properties	<u>119</u>
Suspension Isolation	<u>119</u>
Example Problem	<u>124</u>
Suspension Stiffness	<u>124</u>
Air Spring Suspensions	<u>126</u>
Suspension Damping	<u>127</u>
Tuning – Damping	<u>128</u>
Tuning – Unsprung Mass	<u>128</u>
Active Control	<u>130</u>
Wheel Hop Resonances	<u>134</u>
Suspension Nonlinearities	<u>135</u>
Rigid Body Bounce/Pitch Motions	<u>137</u>
Bounce/Pitch Frequencies	<u>140</u>
Special Cases	<u>144</u>
Example Problem	<u>145</u>
Perception of Ride	<u>147</u>
Tolerance to Seat Vibrations	<u>147</u>
Other Vibration Forms	<u>152</u>
Conclusion	<u>153</u>
References	<u>153</u>

CHAPTER 6

Steady-State Cornering	<u>157</u>
Introduction	<u>157</u>
Low-Speed Turning	<u>158</u>
High-Speed Cornering	<u>159</u>
Tire Cornering Forces	<u>159</u>
Cornering Equations	<u>160</u>
Understeer Gradient	<u>163</u>
Characteristic Speed	<u>164</u>
Critical Speed	<u>164</u>
Lateral Acceleration Gain	<u>165</u>
Yaw Velocity Gain	<u>165</u>
Sideslip Angle	<u>165</u>
Static Margin	<u>167</u>
Suspension Effects on Cornering	<u>168</u>
Roll Moment Distribution	<u>168</u>
Camber Change	<u>174</u>
Roll Steer	<u>176</u>
Lateral Force Compliance Steer	<u>177</u>
Aligning Torque	<u>178</u>
Effect of Tractive Forces on Cornering	<u>178</u>

Summary of Understeer Effects	<u>181</u>
Experimental Measurement of Understeer Gradient	<u>181</u>
Constant Radius Method	<u>182</u>
Constant Speed Method	<u>183</u>
Example Problems	<u>184</u>
References	<u>187</u>

CHAPTER 7

Suspensions	<u>191</u>
Solid Axles	<u>192</u>
Hotchkiss	<u>192</u>
Four Link	<u>193</u>
De Dion	<u>193</u>
Independent Suspensions	<u>194</u>
Trailing Arm Suspension	<u>194</u>
SLA Front Suspension	<u>195</u>
MacPherson Strut	<u>195</u>
Multi-link Rear Suspension	<u>196</u>
Trailing-Arm Rear Suspension	<u>196</u>
Semi-trailing Arm	<u>197</u>
Swing Axle	<u>198</u>
Anti-Squat and Anti-Pitch Suspension Geometry	<u>199</u>
Equivalent Trailing Arm Analysis	<u>199</u>
Rear Solid Drive Axle	<u>201</u>
Independent Rear Drive	<u>202</u>
Front Solid Drive Axle	<u>203</u>
Independent Front-Drive Axle	<u>203</u>
Four-Wheel Drive	<u>204</u>
Anti-Dive Suspension Geometry	<u>204</u>
Examples	<u>205</u>
Roll Center Analysis	<u>206</u>
Solid Axle Roll Centers	<u>207</u>
Four-Link Rear Suspension	<u>208</u>
Three-Link Rear Suspension	<u>209</u>
Four-Link with Parallel Arms	<u>209</u>
Hotchkiss Suspension	<u>210</u>
Independent Suspension Roll Centers	<u>211</u>
Positive Swing Arm Geometry	<u>212</u>
Negative Swing Arm Geometry	<u>212</u>
Parallel Horizontal Links	<u>213</u>
Inclined Parallel Links	<u>213</u>
MacPherson Strut	<u>214</u>
Swing Axle	<u>215</u>

Active Suspensions	<u>215</u>
Suspension Categories	<u>215</u>
Functions	<u>216</u>
Performance	<u>217</u>
References	<u>218</u>

CHAPTER 8

The Steering System	<u>221</u>
Introduction	<u>221</u>
The Steering Linkages	<u>222</u>
Steering Geometry Error	<u>224</u>
Toe Change	<u>225</u>
Roll Steer	<u>226</u>
Front-Wheel Geometry	<u>227</u>
Steering System Forces and Moments	<u>229</u>
Vertical Force	<u>230</u>
Lateral Force	<u>233</u>
Tractive Force	<u>233</u>
Aligning Torque	<u>234</u>
Rolling Resistance and Overturning Moments	<u>234</u>
Steering System Models	<u>234</u>
Examples of Steering System Effects	<u>236</u>
Steering Ratio	<u>237</u>
Understeer	<u>237</u>
Braking Stability	<u>238</u>
Influence of Front-Wheel Drive	<u>240</u>
Driveline Torque about the Steer Axis	<u>240</u>
Influence of Tractive Force on Tire Cornering Stiffness	<u>241</u>
Influence of Tractive Force on Aligning Moment	<u>242</u>
Fore/Aft Load Transfer	<u>242</u>
Summary of FWD Understeer Influences	<u>242</u>
Four-Wheel Steer	<u>243</u>
Low-Speed Turning	<u>243</u>
High-Speed Cornering	<u>244</u>
References	<u>245</u>

CHAPTER 9

Rollover	<u>249</u>
Quasi-Static Rollover of a Rigid Vehicle	<u>250</u>
Quasi-Static Rollover of a Suspended Vehicle	<u>253</u>

Transient Rollover	<u>255</u>
Simple Roll Models	<u>256</u>
Yaw-Roll Models	<u>259</u>
Tripping	<u>260</u>
Accident Experience	<u>262</u>
Dynamic Stability Testing	<u>265</u>
Electronic Stability Control (ESC)	<u>266</u>
Sine with Dwell: ESC Performance Requirements	<u>267</u>
Hardware-in-the-Loop Testing of ESC Systems	<u>268</u>
Fishhook Maneuver	<u>269</u>
Slowly Increasing Steer	<u>269</u>
Fishhook Maneuver	<u>269</u>
References	<u>271</u>

CHAPTER 10

Tires	<u>275</u>
Tire Construction	<u>276</u>
Size and Load Rating	<u>277</u>
Tire Load Index	<u>278</u>
Terminology and Axis System	<u>279</u>
Mechanics of Force Generation	<u>280</u>
Tractive Properties	<u>281</u>
Vertical Load	<u>283</u>
Inflation Pressure	<u>283</u>
Surface Friction	<u>284</u>
Speed	<u>285</u>
Relevance to Vehicle Performance	<u>285</u>
Cornering Properties	<u>286</u>
Slip Angle	<u>286</u>
Tire Type	<u>289</u>
Load	<u>290</u>
Inflation Pressure	<u>290</u>
Size and Width	<u>290</u>
Tread Design	<u>291</u>
Relevance to Vehicle Performance	<u>291</u>
Camber Thrust	<u>291</u>
Tire Type	<u>292</u>
Load	<u>293</u>

Inflation Pressure	<u>293</u>
Tread Design	<u>294</u>
Other Factors	<u>294</u>
Relevance to Vehicle Performance	<u>294</u>
Aligning Moment	<u>294</u>
Slip Angle	<u>294</u>
Path Curvature	<u>296</u>
Relevance to Vehicle Performance	<u>296</u>
Combined Braking and Cornering	<u>297</u>
Friction Circle	<u>297</u>
Variables	<u>299</u>
Relevance to Vehicle Performance	<u>299</u>
Conicity and Ply Steer	<u>300</u>
Relevance to Vehicle Performance	<u>301</u>
Durability Forces	<u>302</u>
Tire Vibrations	<u>303</u>
References	<u>306</u>
Appendix A: (R) Vehicle Dynamics Terminology	<u>307</u>
Appendix B: SAE J6a Ride and Vibration Data Manual	<u>395</u>
Appendix C: Ride Index Structure and Development Methodology	<u>437</u>
Index	<u>473</u>

foreword

For more than a generation, the first edition of *Fundamentals of Vehicle Dynamics* has served as a textbook for aspiring automotive engineers and provided a desk reference for practicing engineers interested in vehicle dynamics. It was written to introduce the basic mechanics governing vehicle dynamic performance, present the analytical methods available for predicting performance, and familiarize readers with standard terminology. Published in 1992, *Fundamentals of Vehicle Dynamics* emphasizes a system-level examination of critical aspects of performance, including acceleration, braking, cornering, road loads, ride, and rollover. To support this understanding, the book examines critical components, such as tires, suspensions, and steering systems and their effect on system behavior.

The wide circulation of the first edition – more than 35,000 copies – demonstrates its success as a resource for understanding basic vehicle dynamics and the fundamental engineering principals needed to analyze vehicle performance. This Revised Edition is offered with an updated presentation of the basics to serve a new generation of automotive engineers. Recent developments have created novel vehicle configurations for this generation of automotive engineers to consider. Automated shuttles, automated vehicles without a forward-facing driver's seat, and automated delivery vehicles are being developed with unusual physical layouts, unconventional weight distribution, and access to restricted routes. Their successful deployment depends on vehicle dynamic performance that ensures vehicle safety and protects their occupants (or cargo) against excessive vibration. Furthermore, as the market for active safety systems and automated vehicles increases, so will the need to understand the core dynamics of the vehicle. This is needed meet the performance goals of the closed-loop system, and will often be required to ensure safe performance during a control system failure.

The author, Dr. Thomas D. Gillespie, has over 50 years of combined professional experience in the military, industry, government, and academia relevant to the dynamics of both passenger cars and commercial trucks. His experience includes responsibilities as a Project Officer with the U.S. Army Corps of Engineers directing engineering and service tests on new military construction equipment; work at Ford as a group leader in development testing of new heavy truck products and development of analytical methods and computer programs for predicting truck braking, handling, and ride performance; service on the White House staff as a Senior Policy Analyst for Dr. William R. Graham, Science Adviser to President Reagan; and 30 years of research at the University of Michigan Transportation Research Institute.

Dr. Gillespie has authored over 100 technical publications that describe a wide range of contributions he has made to the field of vehicle dynamics. In support of his research, Dr. Gillespie has demonstrated methods of examining vehicle dynamic performance using laboratory measurement, theory, numerical simulation, and test track evaluation. His work contributed to some of the early computer simulation programs used to evaluate and improve the safety of commercial vehicles, including articulated heavy trucks. His publications address several vehicle performance modes, including braking, handling, ride, and rollover. Dr. Gillespie has also contributed to our understanding of the way roads affect vehicles by examining skid resistance and vehicle response to road roughness, and our understanding of the way vehicles affect roads by examining dynamic

pavement loading by heavy trucks. Dr. Gillespie performed research for the National Academy of Sciences and the World Bank that led to the development of the International Roughness Index (IRI). The IRI is an international standard measure of the ride quality and functional status of road surfaces and the primary indicator of pavement performance on the U.S. National Highway System.

Dr. Gillespie presents the content in *Fundamentals of Vehicle Dynamics* with a balance between practical explanations and technical depth that is accessible to readers with a wide range of education and experience. This is a hallmark of Dr. Gillespie's approach to sharing his knowledge of vehicle dynamics. He has taught vehicle dynamics to thousands of students on five continents, and presented his research on six continents. In those endeavors, Dr. Gillespie consistently structured his materials with the needs of practitioners in mind, and often explicitly began with the question: "What do they need to know to succeed?" In large lecture halls and in one-on-one conversations, Dr. Gillespie consistently shared his vehicle dynamics expertise using a mix of fundamental knowledge, historical insight, and practicality. For my part, I have been privileged to learn from Dr. Gillespie in both settings, and my knowledge of vehicle dynamics and enthusiasm for the subject consistently grew each time I interacted with him. This was due in part to Dr. Gillespie's natural inclinations as an educator, and in part to his humility, kindness, generosity, and intellectual curiosity.

Steven M. Karamihas, Ph.D.

Senior Research Specialist

University of Michigan Transportation Research Institute (UMTRI)

preface

Throughout all of history it is doubtful that any invention has so effectively captured the interest and devotion of man as the automobile. The mobility enjoyed by humanity in the twentieth century has become an integral component of the modern lifestyle. In this first century of its history, more than a billion automobiles have been manufactured to satisfy the appetite for personal mobility. The marvels of mass production at times have reduced the cost of an automobile to only a few months of personal income. Most profoundly, however, for many people automobiles are a first love at some point in their lives, taking first priority with their interest and finances. In the words from a poem penned in earlier days:

I drive my “Lizzie” every day,

Up hill, down dale, and every way.

A faithful auto it has been

Even if it is of tin.

I'll have to say—It's rattling good.

—The engine, it's beneath the hood,

—The wheels turn backward in reverse,

—The paint it's looking worse and worse.

When I have money in my jeans,

I'll not ride in a can of beans,

I'll buy what's called an “automobile.”

Won't I look fine behind the wheel.

—T. N. Gillespie

Much of the infatuation with the automobile has centered around performance—acceleration, braking, cornering and ride. The art is practiced by the backyard mechanic, the racing enthusiast, and the automotive engineer. A library of books, magazine articles, and technical papers has been written to explain the engineering principles, the rules of thumb, and sometimes the “wrong way” to enhance the performance of an automobile. Most of the books written by practitioners from the racing circuits expound the wisdom of experience but without rigorous engineering explanation. A few textbooks have been written by those knowledgeable in automotive engineering, but the books are often rather analytical and theoretical in nature. This book attempts to find the middle ground—to provide a foundation of engineering principles and analytical methods to explain the performance of an automotive vehicle, when those explanations are not too laborious, and to smooth the way between the doses of equations with practical explanations of the mechanics involved. The inclusion of engineering principles and equations biases the book to interest only the engineer, but it is hoped that the explanations are complete enough that those without a formal engineering degree can still comprehend and use most of the principles discussed.

Those responsible for the design and development in the manufacturing companies today are challenged by questions about the qualities desired in the product by the customer, and how these qualities are related to design and manufacturing processes.

In recent years the complexity of the automotive design process has been increased by regulatory actions arising from the social and environmental consequences of the millions of motor vehicles operating on our highways. Added to this is the competitive pressure of the modern automotive manufacturing industry. In order to remain competitive in the future the manufacturers must seek ways to improve the efficiency of the design and development processes and shorten the time span from concept to production. Achievement of these goals requires a better understanding of the automobile as a system, so that qualities and performance of proposed designs can be predicted at an early stage in the design evolution, allowing refinements to be introduced while there is minimal impact to program costs.

Acceleration, braking, turning and ride are among the most fundamental properties of a motor vehicle and, therefore, should be well understood by every automotive engineer. Performance in one mode is closely linked to the others as a consequence of the dependence on a common set of vehicle mechanical properties. To understand the vehicle as a system it is necessary to acquire a knowledge of all the modes. Motion is the common denominator of all these modes; thus, the study of this field is denoted as vehicle dynamics.

The objectives in writing this book were:

1. *To introduce the basic mechanics governing vehicle dynamic performance* in the longitudinal (acceleration and braking modes), ride (vertical and pitch motions), and handling (lateral, yaw, and roll modes). Engineering analysis techniques will be applied to basic systems and subsystems to derive the controlling equations. The equations reveal which vehicle properties are influential to a given mode of performance and provide a tool for its prediction. By understanding the derivation of the equations, the practitioner is made aware of the range of validity and limitations of the results.
2. *Familiarization with analytical methods available.* Over past decades analytical methods have been developed for predicting many aspects of automotive performance. Although the engineer has no need to master and utilize these techniques in daily activity, a knowledge of their existence greatly increases his/her value to the company. Awareness of these methods is the first step in knowing what is possible and where to find the necessary tools when the need arises.
3. *Familiarization with terminology.* Clarity in communication is vital to problem solving. Over the years, appropriate terminology for automotive engineering has been defined to facilitate communication. The study of vehicle dynamics provides the opportunity to become familiar with the terminology.

Thomas D. Gillespie

acknowledgments

This book is dedicated to my wife, Susan, and our four wonderful children, Dave, Darren, Devin and Jessica. Throughout the long hours necessary to prepare these materials they have shown me patience and encouragement—two ingredients essential to any such endeavor.

The author is also indebted to many colleagues in the vehicle dynamics community who have provided comments and encouragement in preparation of this manuscript. Among those who have contributed their time and energy are Paul Fancher, Sam Clark, Charles MacAdam, Ray Murphy, James Bernard, Bill Fogarty, Manfred Rumple, Bill Stewart, Chuck Houser, Don Tandy, and the many dedicated staff members of the Society of Automotive Engineers.

from the publisher

Dr. Thomas D. Gillespie authored the first edition of this book nearly 30 years ago. Published on February 1, 1992, *Fundamentals of Vehicle Dynamics* withstands the test of time and remains a key reference for engineers and students alike. From the moment I met Dr. Gillespie in 2017, his vision for a revised edition was clear. He wanted to remain true to the original mission of the book – to introduce the fundamental properties of motor vehicles: acceleration, braking, turning, and ride. Even in the era of hybrid and electric vehicles, basic mechanics governing vehicle dynamics performance remains consistent as the laws of physics are universal.

To prepare the revised edition, assembling a team of experts well-versed in this book became a top priority. Dr. Saeid Taheri and Dr. Corina Sandu of Virginia Polytechnic Institute and State University (Virginia Tech) enthusiastically signed on first. Highly respected and globally recognized for their achievements, they carefully edited the manuscript ensuring the content was complete and accurate. Next Mr. Benjamin Duprey, Senior Modeling and Simulation Engineer of Mechanical Simulation Corporation, joined our team and was responsible for incorporating updates from Dr. Gillespie's professional development course into the book. Mr. Duprey meticulously reviewed each chapter folding in new content, updating terminology, and reviewing each equation. Finally, SAE provided new illustrations and photographs then applied a modern text design to increase the readability and functionality of the material. For the convenience of the readers, the revised edition includes J670 JAN2008 and J2834™ as well as J6a which is no longer available from SAE International.

The Fundamentals of Vehicle Dynamics, Revised Edition was a labor of love for all of us with the utmost care going to honor Dr. Gillespie's vision. We hope this book inspires a new generation of engineers.

Sherry Nigam
Publisher, SAE Books

about the author

Dr. Thomas D. Gillespie's professional career has been primarily concerned with advanced engineering and research in the automotive and highway areas. From the beginning, his career spanned the breadth of these areas, ranging from applied research at the Pennsylvania State University in automatic controls and pavement friction test methods, to responsibilities as a Project Officer with the U.S. Army Corps of Engineers directing engineering and service tests on new military construction equipment. While working at Ford Motor Company, he served as a group leader in development testing of new heavy truck products, as well as development of analytical methods and computer programs for predicting truck braking, handling, and ride performance. His expertise in the area of road roughness and vehicle dynamic interactions led to consultation with the World Bank directing an international experiment in roughness measurement. From there Dr. Gillespie, Dr. Michael Sayers and others developed a worldwide standard - the International Roughness Index.



In 1987-88, he served on the White House staff as a Senior Policy Analyst in the Office of Science and Technology Policy. He later served as a consultant to the White House, chairing the Interagency Task Force to develop a National Action Plan on Advanced Superconductivity Research and Development.

In 1996, Dr. Gillespie and Dr. Sayers founded the Mechanical Simulation Corporation to provide car, truck and motorcycle simulation packages, training and ongoing support worldwide to more than 110 OEMs and Tier 1 suppliers, and over 200 universities and government research groups. Today, Mechanical Simulation Corporation is the world leader in the development and distribution of advanced software used to simulate vehicle behavior involving interactions between the 3D dynamic vehicle response, advanced, controllers, driver controls, and 3D roads.

Dr. Gillespie is a Research Professor Emeritus at the University of Michigan. He is retired from a 30-year career as a researcher at the University's Transportation Research Institute where his research focused on vehicle dynamics, road roughness, tire uniformity, tire-roadway interaction and simulation of these phenomena.

about the editors

Saied Taheri

Dr. Saied Taheri is a Professor of Mechanical Engineering at Virginia Polytechnic Institute and State University, known as Virginia Tech (VT). He has been the founding director of the NSF I/UCRC Center for Tire Research (CenTiRe) since 2012 and the director of the Intelligent Transportation Laboratory since 2008. He was also the co-founder of the National Tire Research Center in 2009. He has 31 years of academic and industrial experience in automotive engineering (tire and vehicle dynamic modeling and design), dynamics and control, intelligent systems, Wavelets, and machine learning with applications in intelligent tires and vehicles, vehicle dynamics and control, automotive and transportation safety, and railroads.



Prior to joining VT in 2007, he was a senior engineer at Goodyear Tire& Rubber Company and an adjunct professor at the University of Akron (1998-2007) and earlier worked as an assistant professor at Tehran Polytechnic Institute (1991-1998). He has directed 10 post-docs/visiting scholars, 19 doctoral dissertations and 21 master theses. His sponsored research has reached \$16M. He received his B.S., M.S., and Ph.D. degrees in Mechanical Engineering from Clemson University in 1984, 1986, and 1990, respectively.

Corina Sandu

Dr. Corina Sandu is Robert E. Hord Jr. Professor in the Mechanical Engineering Department at Virginia Tech, Associate Department Head for Graduate Studies, and Director of the Terramechanics, Multibody, and Vehicle Systems Laboratory. She graduated with an Engineer Diploma from the University "Politehnica" of Bucharest, Romania (1991), and M.S. (1995) and Ph.D. (2000) degrees in Mechanical Engineering from the University of Iowa. Dr. Sandu's research expertise lies in vehicle dynamics (suspension, handling, ride, performance), terramechanics (vehicle-terrain interaction, tire/track modeling, vehicle mobility, soil/terrain modeling) and multibody dynamics (modeling, simulation, uncertainty quantification, parameter estimation, sensitivity analysis, design optimization).



Dr. Sandu is ASME Fellow, SAE Fellow, and Marie Skłodowska-Curie Fellow. She published over 200 peer-reviewed papers, and 9 book chapters. Dr. Sandu is the Editor-in-Chief of SAE International Journal of Commercial Vehicles. She is past recipient of SAE Ralph R. Teetor Educational Award (2007), SAE EMB Outstanding Oral Presentation Award (2007), SAE Forest R. McFarland Award (2013 and 2019), and Rodica Baranescu Award for Technical and Leadership Excellence in Commercial Vehicles Engineering (2013). She served as Chair of the SAE Chassis Design and Vehicle Dynamics committee, as Chair of the ASME Design Engineering Division, and as Chair of the ASME Vehicle Design Committee.

Dr. Sandu is currently the Chair of the SAE Fellow Committee and the President of the International Society for Terrain-Vehicle Systems.

**Benjamin L. Duprey**

Benjamin L. Duprey is a Senior Modeling and Simulation Engineer with Mechanical Simulation Corporation. He received his BS degree from the Rochester Institute of Technology in Rochester, NY, and his MS degree from Virginia Tech, both in mechanical engineering. Prior to joining Mechanical Simulation he worked in the Vehicle Test Department at Continental Corporation, performing in-vehicle calibration of Electronic Stability Control Systems.

While at Virginia Tech under the guidance of Dr. Saied Taheri, Dr. Mehdi Amadian, and Dr. R. Gordon Kirk, Mr. Duprey's Masters thesis focused on developing a fuzzy logic-based stability index using predictive vehicle modeling and GPS data. This included development of a vehicle math model and the construction of a driving simulator. His current work at Mechanical Simulation focuses on multibody dynamics, the simulation of ADAS and Automated Driving technologies, Engineering Support, and data-driven test methods.

He has co-authored four SAE papers, all presented at the SAE ComVec conference. His responsibilities to ComVec include serving on the Executive Council and as past-chair of the Chassis and Suspension Committee. Mr. Duprey is an Associate Editor for the ASME journal Autonomous Vehicles and Systems, the SAE International Journal of Commercial Vehicles, and serves as a reviewer for the iMechE Journal of Automobile Engineering.

Mr. Duprey serves on the SAE Vehicle Dynamics Standards Committee and is a member of ASME, the Association for the Advancement of Artificial Intelligence, and the Game Theory Society.

list of symbols

- a** - Tire cornering stiffness parameter
b - Tire cornering stiffness parameter
A - Frontal area of a vehicle
A_f - Lateral force compliance steer coefficient on the front axle
A_r - Lateral force compliance steer coefficient on the rear axle
a_x - Acceleration in the x-direction
a_y - Acceleration in the lateral direction
b - Longitudinal distance from front axle to center of gravity
C - Longitudinal distance from center of gravity to rear axle
C_a - Cornering stiffness of the tires on an axle
C_{a'} - Cornering stiffness of one tire
CC_a - Tire cornering coefficient
C_y - Tire camber stiffness
C_D - Aerodynamic drag coefficient
C_h - Road surface rolling resistance coefficient
C_L - Aerodynamic lift coefficient
C_{pM} - Aerodynamic pitching moment coefficient
C_{RM} - Aerodynamic rolling moment coefficient
C_{yM} - Aerodynamic yawing moment coefficient
C_s - Suspension damping coefficient
C_s - Aerodynamic side force coefficient
CP - Center of pressure location of aerodynamic side force
 d - Lateral distance between steering axis and center of tire contact at the ground
 d_h - Distance from axle to the hitch point
 d_{ns} - Distance from center of mass to the neutral steer point
 D - Tire diameter
DI - Dynamic index
D_X - Linear deceleration
D_A - Aerodynamic drag force
 e - Height of the pivot for an “equivalent torque arm”
 Drum brake geometry factor
E[y²] - Mean square vibration response
 f - Longitudinal length for an “equivalent torque arm”
 f_a - Wheel hop resonant frequency (vertical)
 f_n - Undamped natural frequency of a suspension system (Hz)
 f_r - Rolling resistance coefficient
F_b - Braking force
 Vertical disturbance force on the sprung mass
F_i - Imbalance force in a tire
F_x - Force in the x-direction (tractive force)
F_{xm} - Maximum brake force on an axle
F_{xt} - Total force in the x-direction

F_y	- Force in the y-direction (lateral force) Lateral force on an axle
$F_{y'}$	- Lateral force on one tire
F_z	- Force in the z-direction (vertical force)
F_{zi}	- Vertical force on inside tire in a turn
F_{zo}	- Vertical force on outside tire in a turn
F_w	- Tire/wheel nonuniformity force on the unsprung mass
g	- Acceleration of gravity (32.2 ft/sec ² , 9.81 m/sec ²)
G	- Brake gain
G_o	- Road roughness magnitude parameter
G_z	- Power spectral density amplitude of road roughness
G_{zs}	- Power spectral density amplitude of sprung mass acceleration
h	- Center of gravity height
h_a	- Height of the aerodynamic drag force
h_h	- Hitch height
h_l	- Height of the sprung mass center of gravity above the roll axis
h_r	- Height of suspension roll center
h_t	- Tire section height
H_p	- Engine or brake horsepower
HP_A	- Aerodynamic horsepower
HP_R	- Rolling resistance horsepower
HP_{RL}	- Road load horsepower
H_v	- Response gain function
I_d	- Moment of inertia of the driveshaft
I_e	- Moment of inertia of the engine
I_t	- Moment of inertia of the transmission
I_w	- Moment of inertia of the wheels
I_{xx}	- Moment of inertia about the x-axis
I_{yy}	- Moment of inertia about the y-axis
I_{zz}	- Moment of inertia about the z-axis
k	- Radius of gyration
K	- Understeer gradient
K_{at}	- Understeer gradient due to aligning torque
K_{llt}	- Understeer gradient due to lateral load transfer on the axles
K_{lfcs}	- Understeer gradient due to lateral force compliance steer
K_s	- Vertical stiffness of a suspension
K_{ss}	- Steering system stiffness
K_{strg}	- Understeer gradient due to the steering system
K_t	- Vertical stiffness of a tire
K_ϕ	- Suspension roll stiffness
L	- Wheelbase
L_A	- Aerodynamic lift force
m	- Drum brake geometry parameter
M	- Mass of the vehicle
M_{AT}	- Moment around the steer axis due to tire aligning torques
M_L	- Moment around the steer axis due to tire lateral forces
M_r	- Equivalent mass of the rotating components
M_{SA}	- Moment around the steer axis due to front-wheel-drive forces and torques
M_T	- Moment around the steer axis due to tire tractive forces
M_V	- Moment around the steer axis due to tire vertical forces
M_ϕ	- Rolling moment

- n** - Drum brake geometry parameter
N - Normal force
N_t - Numerical ratio of the transmission
N_f - Numerical ratio of the final drive
N_{tf} - Numerical ratio of the combined transmission and final drive
NSP - Neutral steer point
p - Pneumatic trail
P_a - Brake application pressure/effort
P_{atm} - Atmospheric pressure
P_f - Front brake application pressure
P_r - Rear brake application pressure
P_s - Static pressure
P_t - Total pressure
PM - Aerodynamic pitching moment
 p - Roll velocity about the x-axis of the vehicle
 q - Pitch velocity about the y-axis of the vehicle
 q - Dynamic pressure
 r - Yaw velocity about the z-axis of the vehicle
 r - Rolling radius of the tires
r_k - Ratio of tire to suspension stiffness
R - Radius of turn
R_h - Hitch force
R_g - Grade force
R_x - Rolling resistance force
R_{RL} - Road load
RM - Aerodynamic rolling moment
RR - Ride rate of a tire/suspension system
R_φ - Roll rate of the sprung mass
 s - Lateral separation between suspension springs
S_A - Aerodynamic side force
S_o - Spectral density of white-noise
SD - Stopping distance
 t - Tread
 t_s - Length of time of a brake application
T_a - Torque in the axle
T_b - Brake torque
T_c - Torque at the clutch
T_d - Torque in the driveshaft
T_e - Torque of the engine
T_{sf} - Roll torque in a front suspension
T_{sr} - Roll torque in a rear suspension
T_{amb} - Ambient temperature
 T_x - Torque about the x-axis
 V - Forward velocity
V_w - Ambient wind velocity
V_f - Final velocity resulting from a brake application
V_o - Initial velocity in a brake application
 w - Tire section width
 w - Weight of the vehicle
W_a - Axle weight
W_d - Dynamic load transfer

W_f	- Dynamic weight on the front axle
W_r	- Dynamic weight on the rear axle
W_{rr}	- Dynamic weight on the right rear wheel
W_{fs}	- Static weight on the front axle
W_{rs}	- Static weight on the rear axle
W_y	- Lateral weight transfer on an axle
x	- Forward direction on the longitudinal axis of the vehicle
y	- Lateral direction out the right side of the vehicle
YM	- Aerodynamic yawing moment
z	- Vertical direction with respect to the plane of the vehicle
X	- Forward direction of travel
Y	- Lateral direction of travel
Z	- Vertical direction of travel
	Vertical displacement of the sprung mass
Z_r	- Road profile elevation
Z_u	- Vertical displacement of the unsprung mass
α	- Tire slip angle
	Coefficient in the pitch plane equations
α_{cw}	- Aerodynamic wind angle
α_d	- Rotational acceleration of the driveshaft
α_e	- Rotational acceleration of the engine
α_w	- Rotational acceleration of the wheels
α_x	- Rotational acceleration about the x-axis
β	- Sideslip angle
	Rotation angle of a U-joint
	Coefficient in the pitch plane equations
γ	- Camber angle
	Coefficient in the pitch plane equations
γ_g	- Wheel camber with respect to the ground
γ_b	- Wheel camber with respect to the vehicle body
δ	- Steer angle
δ_c	- Compliance steer
δ_i	- Steer angle of the inside wheel in a turn
δ_o	- Steer angle of the outside wheel in a turn
Δ	- Off-tracking distance in a turn
ϵ	- Roll steer coefficient
	Inclination of the roll axis
ζ	- Moment arm related to tire force yaw damping
	Half-shaft angle on a front-wheel drive
ζ_s	- Damping ratio of the suspension
η_b	- Braking efficiency
η_t	- Efficiency of the transmission
η_f	- Efficiency of the final drive
η_{tf}	- Combined efficiency of the transmission and final drive
θ	- Pitch angle
	Angle of a U-joint
θ_p	- Body pitch due to acceleration squat or brake dive
Θ	- Grade angle
λ	- Lateral inclination angle of the steer axis (kingpin inclination angle)

- μ - Coefficient of friction
 μ_p - Peak coefficient of friction
 μ_s - Sliding coefficient of friction
 ν - Wavenumber of road roughness spectrum
 ξ - Fraction of the drive force developed on the front axle of a 4WD
 Fraction of the brake force developed on the front axle
 Rear steer proportioning factor on a 4WS vehicle
 ρ - Density of air
 ν - Caster angle of the steer axis
 ϕ - Roll angle
 φ - Road cross-slope angle
 χ - Ratio of unsprung to sprung mass
 ψ - Heading angle
 Yaw angle
 ω - Rotational speed
 ω_d - Damped natural frequency of a suspension system (radians/sec)
 Rotational speed of the driveshaft
 ω_e - Rotational speed of the engine
 ω_i - Rotational speed at the input of a U-joint
 ω_n - Undamped natural frequency of a suspension system (radians/sec)
 ω_o - Rotational speed at the output of a U-joint
 ω_u - Natural frequency of the unsprung mass
 ω_w - Rotational speed of the wheels



Introduction

© Shutterstock



Hot Wheels 50th Anniversary Camaro.

Dawn of the Motor Vehicle Age

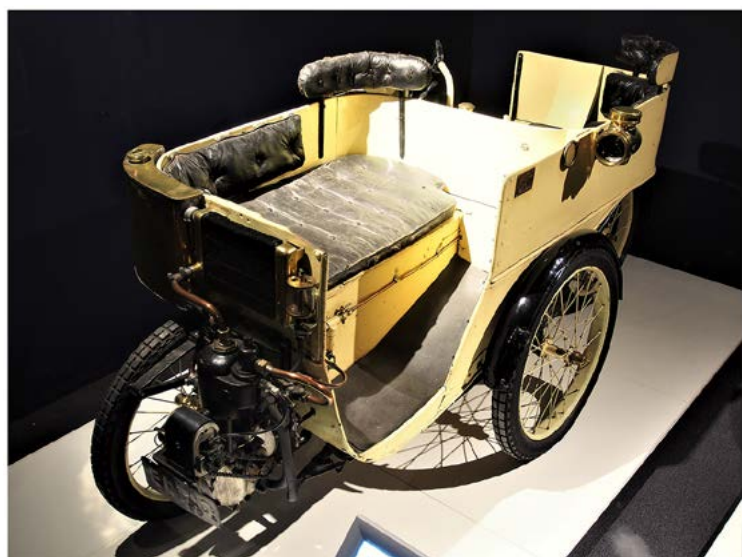
The dawn of the motor vehicle age occurred around 1769 when the French military engineer, Nicholas Joseph Cugnot (1725-1804), built a three-wheeled, steam-driven vehicle for the purpose of pulling artillery pieces ([Figure 1.1](#)) [1]. Within a few years an improved model was built, only to cause the first automotive accident when it ran into a wall! This was followed by a steam-powered vehicle built in 1784 by the Scottish engineer, James Watt (1736-1819), which proved unworkable. By 1802, Richard Trevithick (1771-1833), an Englishman, developed a steam coach that traveled from Cornwall to London. The coach met its demise by burning one night after Trevithick forgot to extinguish the boiler fire. Nevertheless, the steam coach business thrived in England until about 1865 when competition from the railroads and strict anti-speed laws brought it to an end [2].

FIGURE 1.1 First motor vehicle, circa 1769, built by Cugnot. Photo courtesy of Joe deSousa.



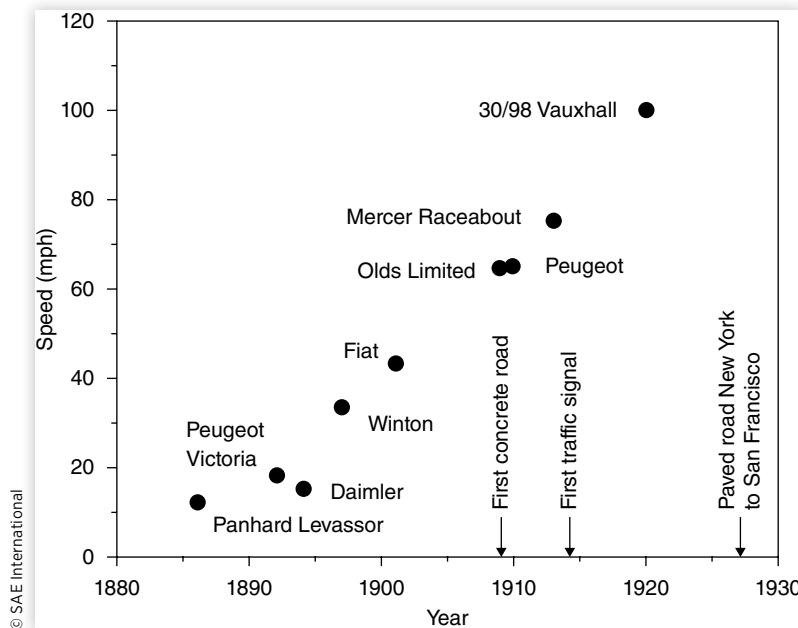
Courtesy of Joe deSousa

The first practical automobiles powered by gasoline engines arrived in 1886 with the credit generally going to Karl Benz (1844-1929) and Gottlieb Daimler (1834-1900) working independently. Over the next decade, automotive vehicles were developed by many other pioneers with familiar names such as Rene Panhard, Emile Levassor, Armand Peugeot, Frank and Charles Duryea, Henry Ford, and Ransom Olds. By 1908 the automotive industry was well established in the United States with Henry Ford manufacturing the Model T and the General Motors Corporation being founded. In Europe, the familiar companies like Daimler, Opel, Renault, Benz, and Peugeot were becoming recognized as automotive manufacturers. By 1909, over 600 makes of American cars had been identified [3].



1901 Sunbeam Mabley. (Photo courtesy of Alf van Beem.)

Courtesy of Alf van Beem

FIGURE 1.2 Travel speeds of production automobiles.

In the early decades of the 1900s, most of the engineering energy of the automotive industry went into invention and design that would yield faster, more comfortable, and more reliable vehicles. The speed capability of motor vehicles climbed quickly in the embryonic industry, as illustrated by the top speeds of some typical production cars, as shown in [Figure 1.2](#).

In general, motor vehicles achieved high speed capability well before good paved roads existed on which to use it. With higher speeds, the dynamics of the vehicles, particularly turning and braking, assumed greater importance as an engineering concern. The status of automotive engineering during this period was characterized in the reminiscences of Maurice Olley [4] as follows:

"There had been sporadic attempts to make the vehicle ride decently, but little had been done. The rear passengers still functioned as ballast, stuck out behind the rear wheels. Steering was frequently unstable and the front axle with front brakes made shimmy almost inevitable. The engineers had made all the parts function excellently, but when put together the whole was seldom satisfactory."

One of the first engineers to write on automotive dynamics was Frederick William Lanchester (1868–1946). (In a 1908 paper [5] he observed that a car with tiller steering “oversteers” if the centrifugal force on the driver’s hands pushes toward greater steer angle [6].) Steering shimmy problems were prevalent at that time as well [7, 8]. But, as described by Segel [6], the understanding of both — the turning behavior and the shimmy problems — was hampered by a lack of knowledge of tire mechanics in these early years.

In 1931, a test device — a tire dynamometer — was built which could measure the mechanical properties of the pneumatic tire, allowing engineers to begin to gain insight into how tires developed force and moment properties [9]. With this new-found knowledge, engineers like Lanchester [10], Olley [11], Rieckert and Schunk [12], Rocard [13], Segel [14], and others developed mechanistic explanations of the turning behavior of automobiles and laid the groundwork for much of our understanding today.

FIGURE 1.3 Over 110 years of progress from the Model T to the Ford Fusion. (Photos courtesy of the Collections of The Henry Ford and Shutterstock 2021.)



Reprinted with permission from © The Collections of The Henry Ford

© Shutterstock

The industry is well into its second century, with advances in control systems and autonomy becoming dominant factors in the engineering priorities of motor vehicles. Engineers have achieved dramatic advancements in the technologies employed in automobiles from the Model T to the Fusion Hybrid. ([Figure 1.3](#)). More than ever, dynamics plays an important role in vehicle design and development. A number of textbooks have been written to help the engineer in this discipline [15–24], but there remains a need for books that lay out the fundamental aspects of vehicle dynamics. This book attempts to fill that need.

Introduction to Vehicle Dynamics

It has often been said that the primary forces by which a high-speed motor vehicle is controlled are developed in four patches—each the size of a man’s hand—where the tires contact the road. This is indeed the case. A knowledge of the forces and moments generated by pneumatic (rubber) tires at the ground is essential to understanding highway vehicle dynamics. Vehicle dynamics in its broadest sense encompasses all forms of conveyance—ships, airplanes, railroad trains, track-laying vehicles, as well as rubber-tired vehicles. The principles involved in the dynamics of these many types of vehicles are diverse and extensive. Therefore, this book focuses only on rubber-tired vehicles. Most of the discussion and examples will concentrate on the automobile, although the principles are directly applicable to trucks and buses, large and small. Where warranted, trucks will be discussed separately when the functional design or performance qualities distinguish them from the automobile.

Inasmuch as the performance of a vehicle—the motions accomplished in accelerating, braking, cornering, and ride—is a response to forces imposed, much of the study of vehicle dynamics must involve the study of how and why the forces are produced. The dominant forces acting on a vehicle to control performance are developed by the tire against the road. Thus, it becomes necessary to develop an intimate understanding of the behavior of tires, characterized by the forces and moments generated over the broad range of conditions over which they operate. Studying tire performance without a thorough understanding of its significance to the vehicle is unsatisfying, as is the inverse. Therefore, the relevant properties of tires are introduced at appropriate points in the early chapters of the text, while the reader is referred to Chapter 10 for a more comprehensive discussion of tire properties.

At the outset it is worth noting that the term “handling” is often used interchangeably with cornering, turning, or directional response, but there are nuances of difference between these terms. Cornering, turning, and directional response refer to objective properties of the vehicle when changing direction and sustaining lateral acceleration in the process. For example, cornering ability may be quantified by the level of lateral acceleration that can be sustained in a stable condition. Similarly, directional response may be quantified by the time required for lateral acceleration to develop following a steering input. Handling, on the other hand, adds to this the vehicle qualities that feed back to the driver and affect the ease of the driving task or the driver’s ability to maintain control. Handling implies, then, not only the vehicle’s explicit capabilities, but its contributions to the system performance of the driver/vehicle combination, as well. Throughout the book the various terms will be used in a manner most appropriate to the discussion at hand.

Understanding vehicle dynamics can be accomplished at two levels—the empirical level and the analytical level. The empirical understanding derives from trial and error by which one learns which factors influence vehicle performance, in which way, and under what conditions. The empirical method, however, can often lead to failure. Without a mechanistic understanding of how changes in vehicle design or properties affect performance, extrapolating past experience to new conditions may involve unknown factors that may produce a new result, defying the prevailing rules of thumb. For this reason, engineers favor the analytical approach. The analytical approach attempts to describe the mechanics of interest based on the known laws of physics, facilitating the establishment of an analytical model. In the simpler cases, these models can be represented by algebraic or differential equations that relate forces or motions of interest to control inputs and vehicle or tire properties. These equations then allow one to evaluate the role of each vehicle property in the phenomenon of interest. The existence of the model thereby provides means to identify the important factors, the way in which they operate, and under what conditions. The model provides a predictive capability as well, so that changes necessary to reach a given performance goal can be identified.

It might be noted that analytical methods are not foolproof either, because by their very nature serves as approximations of physical systems. As many have experienced, the assumptions that must be made to obtain manageable models may often prove fatal to an application of the analysis. Therefore, it is very important for the engineer to understand the assumptions that have been made in modeling any aspect of dynamics to avoid these errors.

In the past, many of the shortcomings of analytical methods were a consequence of the mathematical limitations in solving problems. Before the advent of computers, analysis was only considered successful if the “problem” could be reduced to a closed form solution. That is, only if the mathematical expression could be manipulated to a form which allowed the analyst to extract relationships between the variables of interest. To a large extent, this limited the functionality of the analytical approach to solutions of problems in vehicle dynamics. The existence of large numbers of components, systems, subsystems, and nonlinearities in vehicles made comprehensive modeling virtually impossible, and the only utility obtained came from rather simplistic models of certain mechanical systems. Though useful, the simplicity of the models often constituted deficiencies that handicapped the engineering approach used in vehicle development.

With the computational power of modern computers, a major shortcoming of the analytical method has been overcome. It is now possible to assemble models (equations) for the behavior of individual components of a vehicle that can be integrated into comprehensive models of the overall vehicle, allowing simulation and evaluation of its behavior before being rendered in hardware. Such models can calculate performance that could not be solved for in the past. In cases where the engineer is uncertain of the importance of specific properties, those properties can be included in the model and their importance assessed by evaluating their influence on simulated behavior. This provides the engineer with a powerful tool as a way to test our understanding of a complex system and investigate means of improving performance. In the end, we are forced to confront all the variables that may influence the performance of interest, and recognize everything that is important.

Fundamental Approach to Modeling

The subject of “vehicle dynamics” is concerned with the movements of vehicles—automobiles, trucks, buses, and special-purpose vehicles—on a road surface. The movements of interest are acceleration and braking, ride, and turning. Dynamic behavior is determined by the forces imposed on the vehicle from the tires, gravity, and aerodynamics. The vehicle and its components are studied to determine what forces will be produced by each of these sources at a particular maneuver and trim condition, and how the vehicle will respond to these forces. For that purpose it is essential to establish a rigorous approach to modeling the systems and the conventions that will be used to describe motions.

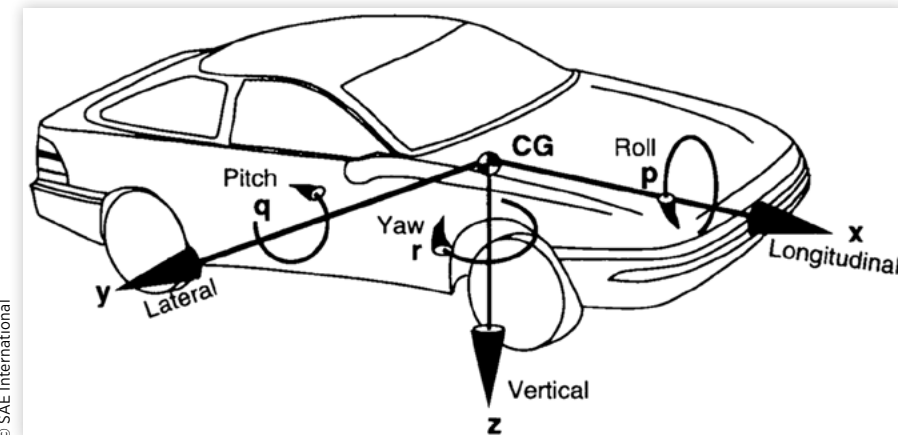
Lumped Mass

A motor vehicle is made up of many components distributed within its exterior envelope. Yet, for many of the more elementary analyses applied to it, all components move together. For example, under braking, the entire vehicle slows down as a unit; thus it can be represented as one lumped mass located at its center of gravity (C.G.) with appropriate mass and inertia properties. For acceleration, braking, and most turning analyses, one mass is sufficient. For ride analysis, it is often necessary to treat the wheels as separate lumped masses. In that case the lumped mass representing the body is the “sprung mass,” and the wheels are denoted as “unsprung masses.”

For a single mass representation, the vehicle is treated as a mass concentrated at its center of gravity (C.G.) as shown in [Figure 1.4a](#) and [Figure 1.4b](#). The point mass at the

C.G., with appropriate rotational moments of inertia, is dynamically equivalent to the vehicle itself for all motions in which it is reasonable to assume the vehicle to be rigid.

FIGURE 1.4a SAE vehicle axis system.



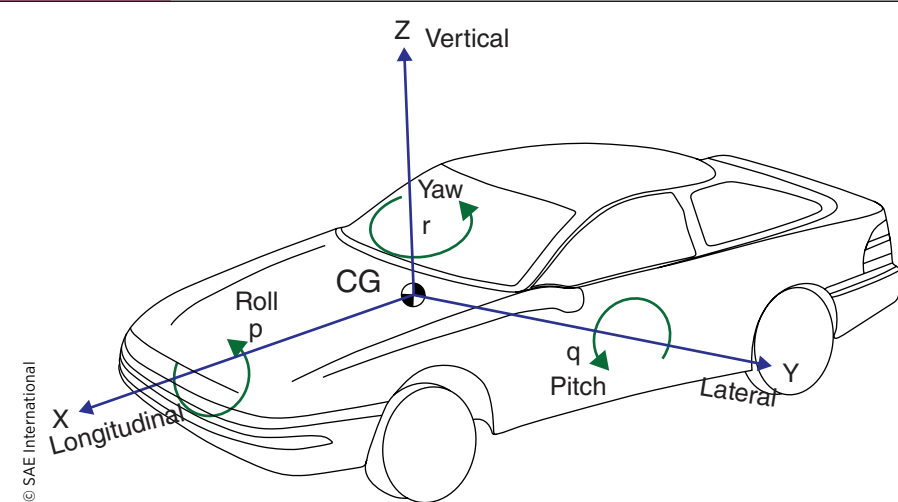
© SAE International

Vehicle-Fixed Coordinate System

The vehicle motions are defined with reference to a right-hand orthogonal coordinate system (the vehicle-fixed coordinate system) which originates at the C.G. and travels with the vehicle. By SAE convention [25] the coordinates are:

- x - Forward and on the longitudinal plane of symmetry
- y - Lateral out the right side of the vehicle
- z - Downward with respect to the vehicle
- p - Roll velocity about the x-axis
- q - Pitch velocity about the y-axis
- r - Yaw velocity about the z-axis

FIGURE 1.4b ISO vehicle coordinate system.



© SAE International

ISO/SAE Z-up Vehicle-Fixed Coordinate System

Another commonly used vehicle-fixed coordinate system has the Z-axis positive when pointing up and the X-axis positive pointing forward. This results in the Y-axis positive pointing to the vehicle's left:

- x - Forward and on the longitudinal plane of symmetry
- y - Lateral, out the left side of the vehicle
- z - Upward with respect to the vehicle
- p** - Roll velocity about the x-axis. Positive roll is to the right
- q** - Pitch velocity about the y-axis. Positive pitch is nose-down
- r** - Yaw velocity about the z-axis. Positive yaw is to the left

Motion Variables

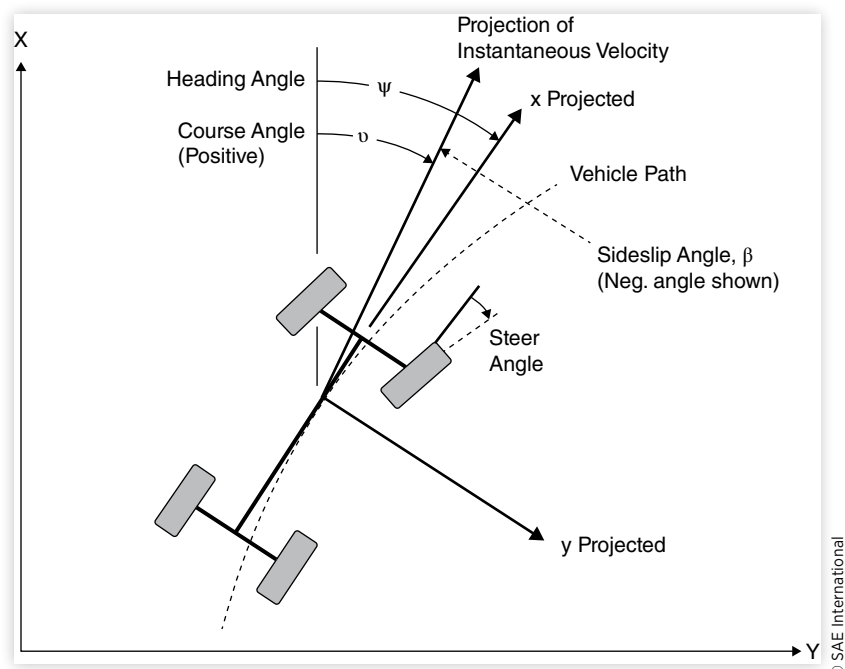
Vehicle motion is usually described by the velocities (forward, lateral, vertical, roll, pitch, and yaw) with respect to the vehicle-fixed coordinate system, where the velocities are referenced to the earth-fixed coordinate system.

Earth-Fixed Coordinate System

Vehicle attitude and trajectory through the course of a maneuver are defined with respect to a right-hand orthogonal axis system fixed on the earth. It is normally selected to coincide with the vehicle-fixed coordinate system at the point where the maneuver is started. As shown in [Figure 1.5](#), the coordinates corresponding to the SAE Z-down coordinate system (Figure 1.4a) are:

- X - Forward travel
- Y - Travel to the right

FIGURE 1.5 Vehicle in an earth fixed coordinate system.



Z - Vertical travel (positive downward)

ψ - Heading angle (angle between x and X in the ground plane)

ν - Course angle (angle between the vehicle's velocity vector and X-axis)

β - Sideslip angle (angle between x-axis and the vehicle velocity vector)

Euler Angles

The relationship between the vehicle-fixed coordinate system and the earth-fixed coordinate system is defined by Euler angles. Euler angles are determined by a sequence of three angular rotations. Beginning at the earth-fixed system, the axis system is first rotated in yaw (around the z-axis), then in pitch (around the y-axis), and then in roll (around the x-axis) to line up with the vehicle-fixed coordinate system. The three angles obtained are the Euler angles. It is necessary to adhere strictly to the defined sequence of rotations, because the resultant vehicle attitude will vary with the order of rotations.

Forces

Forces and moments are normally defined as they act on the vehicle. Thus, a positive force in the longitudinal (x-axis) direction on the vehicle is forward. The force corresponding to the load on a tire acts in the upward direction and is therefore negative in magnitude (in the negative z-direction). Because of the inconvenience of this convention, the SAE J670, "Vehicle Dynamics Terminology," gives the name Normal Force as that acting downward, and Vertical Force as the negative of the Normal Force. (See Appendix A.) Thus, the Vertical Force is the equivalent of tire load with a positive convention in the upward direction. In other countries, different conventions may be used.

Given these definitions of coordinate systems and forces, it is now possible to begin formulating equations by which to analyze and describe the behavior of a vehicle.

Newton's Second Law

The fundamental law from which most vehicle dynamics analyses begin is the second law formulated by Sir Isaac Newton (1642-1727). The law applies to both translational and rotational systems [26].

Translational systems: The sum of the external forces acting on a body in a given direction is equal to the product of its mass and the acceleration in that direction (assuming the mass is fixed).

$$\Sigma F_x = M \cdot a_x \quad (1.1)$$

where:

F_x = Forces in the x-direction

M = Mass of the body

a_x = Acceleration in the x-direction

Rotational systems: The sum of the torques acting on a body about a given axis is equal to the product of its rotational moment of inertia and the rotational acceleration about that axis.

$$\Sigma T_x = I_{xx} \cdot \alpha_x \quad (1.2)$$

where:

T_x = Torques about the x-axis

I_{xx} = Moment of inertia about the x-axis

α_x = Angular acceleration about the x-axis

Newton's Second Law is applied by visualizing a boundary around the body of interest. The appropriate forces and/or moments are substituted at each point of contact with the outside world, along with any gravitational forces. This forms a free-body diagram and Newton's Second Law may then be written for each of the three independent directions (normally the vehicle fixed axes).

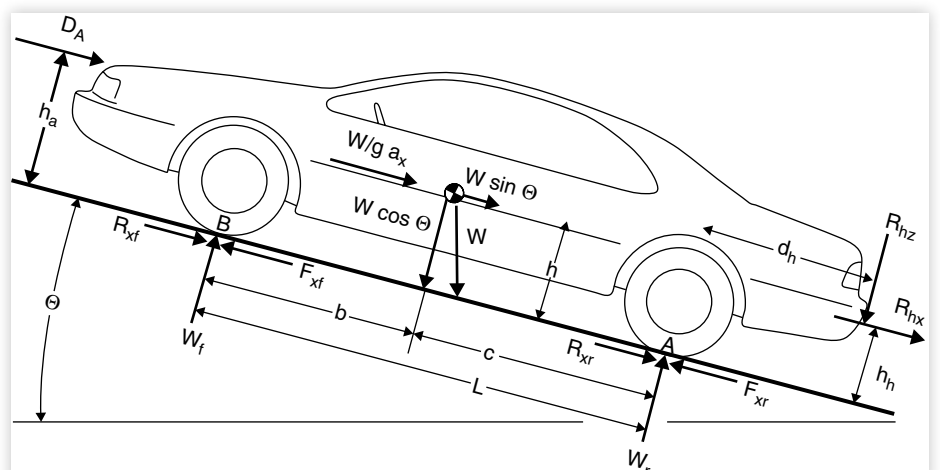
Dynamic Axle Loads

Determining the axle loadings on a vehicle under arbitrary conditions is a first simple application of Newton's Second Law. It is an important first step in the analysis of acceleration and braking performance because the axle loads determine the tractive effort obtainable at each axle, affecting the acceleration, gradeability, maximum speed, and drawbar effort.

Consider the vehicle shown in [Figure 1.6](#), in which most of the significant forces on the vehicle are shown.

- W is the weight of the vehicle acting at its C.G. with a magnitude equal to its mass times the acceleration of gravity. On a grade it may have two components, a cosine component which is perpendicular to the road surface, and a sine component, parallel to the road.
- If the vehicle is accelerating along the road, it is convenient to represent the effect by an equivalent inertial force known as a "d'Alembert force" (Jean le Rond d'Alembert, 1717-1783) denoted by $W/g \cdot a_x$ acting at the C.G. opposite to the direction of the acceleration [26].
- The tires will experience a force normal to the road, denoted by W_f and W_r , representing the dynamic weights carried on the front and rear wheels, respectively.
- Tractive forces, F_{xf} and F_{xr} , or rolling resistance forces, R_{xf} and R_{xr} , may act in the ground plane in the tire contact patch.
- D_A is the aerodynamic force acting on the body of the vehicle. It may be represented as acting at a point above the ground indicated by the height, h_a , or by a longitudinal force of the same magnitude in the ground plane with an associated moment (the aerodynamic pitching moment) equivalent to D_A times h_a .
- R_{hz} and R_{hx} are vertical and longitudinal forces acting at the hitch point when the vehicle is towing a trailer.

FIGURE 1.6 Forces acting on a vehicle under arbitrary conditions.



The loads carried on each axle will consist of a static component, plus load transferred from front to rear (or vice versa) due to the other forces acting on the vehicle. The load on the front axle can be found by summing torques about the point “A” under the rear tires. Presuming that the vehicle is not accelerating in pitch, the sum of the torques at point A must be zero.

By the SAE convention, a clockwise torque about A is positive. Then:

$$W_f L + D_A h_a + \frac{W}{g} a_x h + R_{hx} h_h + R_{hz} d_h + Wh \sin \Theta - Wc \cos \Theta = 0 \quad (1.3)$$

Note that an uphill attitude corresponds to a positive angle, Θ , such that the sine term is positive. A downhill attitude produces a negative value for this term.

From [Equation \(1.3\)](#) we can solve for W_f and from a similar equation about point B we can solve for W_r . The axle load expressions then become:

$$W_f = \left(Wc \cos \Theta - R_{hx} h_h - R_{hz} d_h - \frac{W}{g} a_x h - D_A h_a - Wh \sin \Theta \right) / L \quad (1.4)$$

$$W_r = \left(Wb \cos \Theta + R_{hx} h_h + R_{hz} (d_h + L) + \frac{W}{g} a_x h + D_a h_a + Wh \sin \Theta \right) / L \quad (1.5)$$

Static Loads on Level Ground

When the vehicle sits statically on level ground, the load equations simplify considerably. The sine is zero and the cosine is one, and the variables R_{hx} , R_{hz} , a_x , and D_A are zero. Thus:

$$W_{fs} = W \frac{c}{L} \quad (1.6)$$

$$W_{rs} = W \frac{b}{L} \quad (1.7)$$

Low-Speed Acceleration

When the vehicle is accelerating on level ground at a low speed, such that D_A is zero (and presuming no trailer hitch forces), the loads on the axles are:

$$W_f = W \left(\frac{c}{L} - \frac{a_x}{g} \frac{h}{L} \right) = W_{fs} - W \frac{a_x}{g} \frac{h}{L} \quad (1.8)$$

$$W_r = W \left(\frac{b}{L} + \frac{a_x}{g} \frac{h}{L} \right) = W_{rs} + W \frac{a_x}{g} \frac{h}{L} \quad (1.9)$$

Thus, when the vehicle accelerates, load is transferred from the front axle to the rear axle in proportion to the acceleration (normalized by the gravitational acceleration) and the ratio of the C.G. height to the wheelbase.

Loads on Grades

The influence of grade on axle loads is also worth considering. Grade is defined as the “rise” over the “run.” That ratio is the tangent of the grade angle, Θ . The common grades on interstate highways are limited to 4 percent wherever possible. On primary and secondary roads they occasionally reach 10 to 12 percent. The cosines of angles this small are very close to one, and the sine is very close to the angle itself. That is:

$$\cos \Theta = 0.99^+ \cong 1$$

$$\sin \Theta \cong \Theta$$

Thus the axle loads as influenced by grades will be:

$$W_f = W \left(\frac{c}{L} - \frac{h}{L} \Theta \right) = W_{fs} - W \frac{h}{L} \Theta \quad (1.10)$$

$$W_r = W \left(\frac{b}{L} + \frac{h}{L} \Theta \right) = W_{rs} + W \frac{h}{L} \Theta \quad (1.11)$$

where a positive grade causes load to be transferred from the front to the rear axle.

Climbing a Grade

No aerodynamic or acceleration effects:

$$W_f = W \left(\frac{c \cdot \cos \theta}{L} - \frac{h \cdot \sin \theta}{L} \right) \quad W_r = W \left(\frac{b \cdot \cos \theta}{L} + \frac{h \cdot \sin \theta}{L} \right)$$

For small angles: $\cos \theta = 1$, $\sin \theta = \theta$

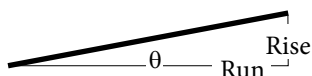
$$W_f = W_{fs} - W \frac{h}{L} \theta \quad W_r = W_{rs} + W \frac{h}{L} \theta$$

θ = Grade angle (in radians).

Road Grade

Road Grade is usually expressed in %

$$\text{Grade (\%)} = 100 \frac{\text{Rise}}{\text{Run}}$$



$$\theta = \tan^{-1} (\text{Rise}/\text{Run})$$

Example: 5% grade Rise/Run = 0.05.

$$\theta = \tan^{-1} (0.05) = 2.86 \text{ deg} = 0.0499 \text{ rad} \cong 0.05 \text{ rad}$$

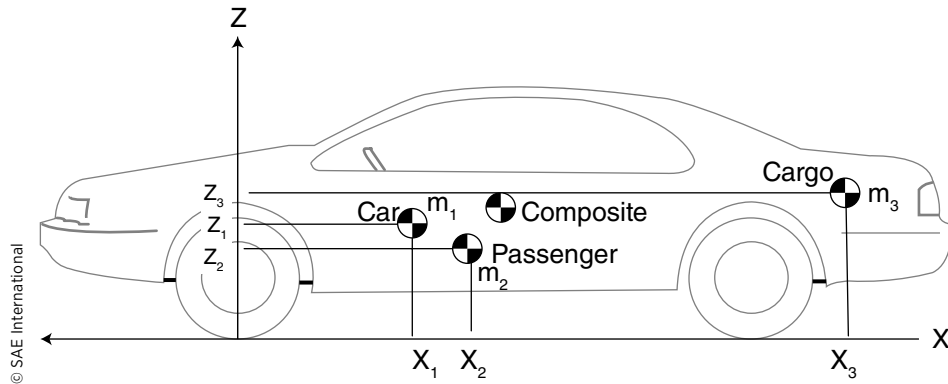
$$\cos(2.862^\circ) = 0.999 \cong 1 \quad \sin(2.862^\circ) = 0.0499 \cong 0.05$$

Good to about 20% (<2% error).

Composite Mass

As can be seen in the figure below, there exists many mass bodies whose contributions add up to the total mass and C.G. location of the vehicle as a system. These bodies typically represent passengers and cargo, but could just as easily be fuel loads and ancillary components such as those that are typically attached to the frame of a commercial vehicle.

Consider the figure, below.



Longitudinal

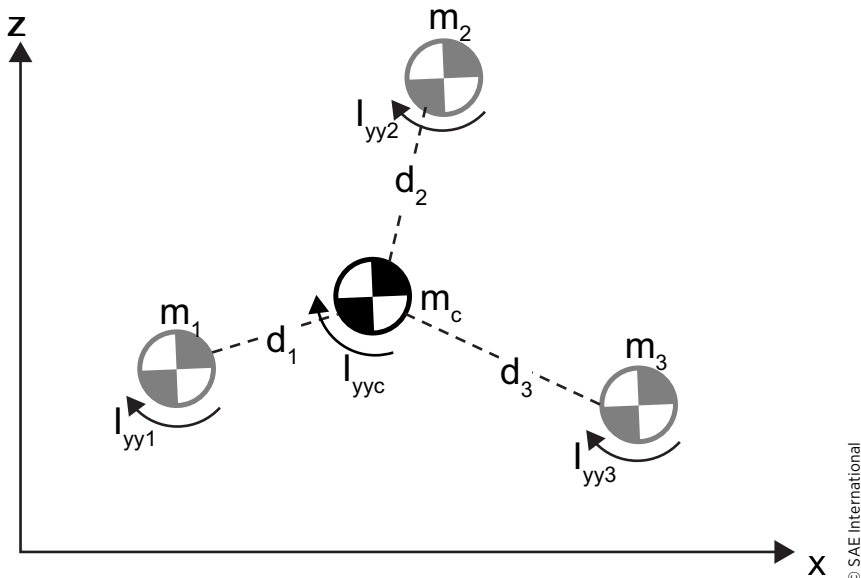
$$X_{\text{composite}} = \frac{\sum_{i=1}^n m_i x_i}{\sum_{i=1}^n m_i}$$

Vertical

$$Z_{\text{composite}} = \frac{\sum_{i=1}^n m_i z_i}{\sum_{i=1}^n m_i}$$

Moments of Inertia

Calculating moments of inertia for a composite mass can be accomplished using the method shown in figure to the next page and the corresponding equation. Here, we consider the various masses present in the vehicle. By taking the square of the distance from the individual masses to the composite mass, multiplying it by the mass (e.g., in kg), and adding this product to the inertia of the individual masses we can consider the contribution of any individual mass to the composite mass that represents the vehicle as a system.



© SAE International

$$I_{yyc} = \sum_{i=1}^n (I_{yyi} + m_i d_i^2)$$

where:

I_{yyc} = Moment of inertia about the "y" axis of the composite mass

I_{yyi} = Moments of inertia about the "y" axis of the individual masses

d_i = Distance from the C.G. of mass "i" to the composite C.G.

Example Problems

1. The curb weights of a 4-door sedan without passengers or cargo are 2,313 lb on the front axle and 1,322 lb on the rear axle. The wheelbase, L, is 109 in. Determine the fore/aft position of the center of gravity for the vehicle.

Solution:

The fore/aft position of the C.G. is defined by either parameter c or b in [Equation \(1.6\)](#) or [\(1.7\)](#), which apply to a vehicle sitting at rest on level ground. Using [Equation \(1.7\)](#) we can solve for b:

$$b = L \frac{W_{rs}}{W} = 109'' \frac{1,322 \text{ lb}}{(2,313 + 1,322) \text{ lb}} = 39.64''$$

i.e., the C.G. of the vehicle is 39.64 inches aft of the front axle.

2. A 4-door sedan with 3.0 L engine accelerates from a standing start up a 6 percent grade with an acceleration of 6 ft/sec². Find the load distribution on the axles under these conditions.

Solution:

Assume that aerodynamic forces are negligible since the vehicle starts from zero speed. Also assume that there are no trailer hitch forces. [Equations \(1.4\)](#) and [\(1.5\)](#) are

the fundamental equations from which to start, but to use them the values for the parameters b and c must be determined. For the 4-door sedan, the curb weights are 1,949 lb on the front axle and 1,097 lb on the rear axle; the wheelbase is 106 in; and the passenger's weight is distributed 49 percent on the front axle and 51 percent on the rear axle. Assuming a 200 lb driver, this gives weights as follows:

$$W_{fs} = 2,047 \text{ lb} \quad W_{rs} = 1,199 \text{ lb} \quad W = 3,246 \text{ lb}$$

Equations (1.6) and (1.7) are used to find that $b = 39.15$ inches and $c = 66.85$ inches. From a pocket calculator we determine that a 6 percent grade corresponds to a 3.433 degree angle (arctangent of 0.06). Assume the C.G. height, h , is 20 inches. Now all of the information is available to solve Equation (1.4).

$$W_f = \frac{W(c \cos \Theta - h a_x / g - h \sin \Theta)}{L}$$

$$W_f = \frac{3246 \text{ lb} (66.85'' \times 0.998 - 20'' \times 6/32.2 - 20'' \times 0.0599)}{106''} = 1,892.2 \text{ lb}$$

Using the same approach the rear axle load is found to be 1,347.3 lb. Curiously, these only add up to about 3,239.5 lb, not the 3,246 lb weight of the car. Why? The vehicle is sitting on a slope. Only the cosine of the weight vector acts to produce load on the axles. Thus, the weight on the axles should only add up to 3,246 lb times $\cos 3.433^\circ = 3,240$ lb.

3. You are planning to buy a new mini-van to pull your boat trailer (see below). Although you like the new front-wheel-drive (FWD) vans available, you are not sure it will be able to pull the boat out of the water on some of the steep access ramps you must use.

- Derive the expressions for the maximum grade the vehicle can climb without wheel slippage (traction-limited gradeability) when equipped with front-wheel-drive (FWD), rear-wheel-drive (RWD), and four-wheel-drive (4WD) powertrain configurations.

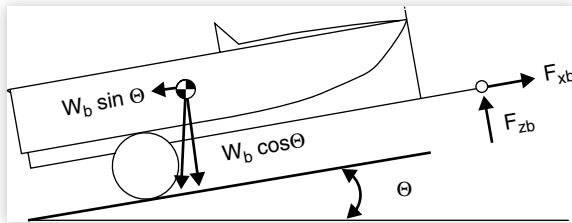
(In the analysis it is reasonable to assume the longitudinal acceleration is zero, neglect rolling resistance, assume the boat is clear of the water so that there are no buoyancy forces on it, ignore any change in hitch height as the forces are applied, and use the small angle approximations.)

- Calculate the maximum gradeability for the three vehicle combinations on a ramp with a coefficient of friction of 0.3, given the following vehicle information.

Van properties	Combined boat/trailer properties
Front axle weight = 1520 lb	Axle weight = 1200 lb
Rear axle weight = 1150 lb	Hitch load = 250 lb
C.G. height = 24.5 in	Wheelbase = 110 in
Hitch height = 14 in	C.G. height = 35 in
Hitch rear overhang = 23 in	
Wheelbase = 120 inches	

Solution:

In order to derive the equations for traction-limited gradeability, first draw a free-body diagram of the boat trailer to find the hitch forces as a function of grade.



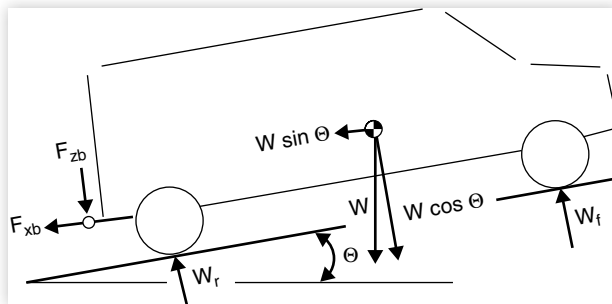
Taking moments about the point where the tire contacts the ground (counterclockwise moments are positive):

$$\sum T_y = 0 = W_b h_3 \sin \Theta + F_{zb} (e + f) - W_b f \cos \Theta - F_{xb} h_2 \quad (1)$$

Also, the force balance along the longitudinal axis of the boat trailer gives:

$$\sum F_x = 0 = F_{xb} - W_b \sin \Theta \quad (2)$$

Next, we perform a similar analysis on the van.



Taking moments about the rear tire contact point:

$$\sum T_y = 0 = Wh_1 \sin \Theta - Wc \cos \Theta + F_{zb} d + F_{xb} h_2 + W_f (b + c) \quad (3)$$

And for moments about the front axle:

$$\sum T_y = 0 = Wh_1 \sin \Theta + Wb \cos \Theta + F_{zb} (b + c + d) + F_{xb} h_2 - W_r (b + c) \quad (4)$$

There are four equations and four unknowns (F_{zb} , F_{xb} , W_f , W_r). We can therefore solve for any one of the unknowns desired. For the case of the FWD, the traction limit will be determined by the load on the front axle times the coefficient of friction, μ . The solution is obtained from [Equation \(3\)](#), using [Equations \(1\)](#) and [\(2\)](#) to eliminate the hitch

forces from the final equation. The tractive force will be equal to the combined weight of the van and boat times the grade angle. That is:

$$\begin{aligned} (W + W_b) \sin \Theta &= F_{xf} = \mu W_f \\ &= \mu \left[W \frac{c}{L} \cos \Theta - W \frac{h_1}{L} \sin \Theta - W_b \frac{h_2}{L} \sin \Theta \right. \\ &\quad \left. + W_b \frac{d}{L L_t} h_3 \sin \Theta - W_b \frac{d}{L L_t} f \cos \Theta - W_b \frac{d}{L L_t} h_2 \sin \Theta \right] \end{aligned} \quad (5)$$

The trigonometric functions in the equation make it complicated to obtain a simplified solution. Using the small angle approximation, $\sin \Theta$ can be replaced with Θ , and $\cos \Theta$ can be treated as 1. It is also convenient to define several alternate variables for use in the solution. These will be:

$L = b + c$ = Wheelbase of the van

$L_t = e + f$ = Wheelbase of the trailer (hitch to wheels)

$\zeta = W_b/W$ = Nondimensional weight of the trailer

Solving the equation for Θ , we obtain the gradeability expression for the case of:

FWD

$$\Theta = \mu \frac{\frac{c}{L} - \zeta \frac{d}{L} \frac{f}{L_t}}{1 + \mu \frac{h_1}{L} + \zeta \left(1 + \mu \frac{h_2}{L} + \mu \frac{d}{L} \frac{h_2 - h_3}{L_t} \right)}$$

The numerator represents the static weight on the front axle, due to the weight of the van diminished by the vertical load of the trailer on the hitch (the hitch load decreases the front axle load, and hence the gradeability). The second term in the denominator reflects the effect of longitudinal transfer of load from the front axle on a grade due to the elevated position of the C.G. on the van. The terms in parentheses in the denominator represent the effects of the trailer. The first term in parentheses is the direct effect of the added weight of the trailer. The next term arises from the longitudinal transfer of load off of the front axle due to the towing force at the hitch. The last term is the effect of the change in vertical load on the hitch due to the tow force.

A similar analysis produces a different solution for the case of:

RWD

$$\Theta = \mu \frac{\frac{b}{L} + \zeta \frac{(L+d)}{L} \frac{f}{L_t}}{1 - \mu \frac{h}{L} + \zeta \left(1 - \mu \frac{h_2}{L} - \mu \frac{(L+d)}{L} \frac{h_2 - h_3}{L_t} \right)}$$

For the rear-wheel drive case, the static load of the trailer (second term in the numerator) increases gradeability because it increases load on the drive wheels. In the denominator, the terms representing longitudinal load transfer are negative (thereby decreasing the magnitude of the denominator and increasing the gradeability).

Finally, in the case of four-wheel drive, the performance that will be obtained depends on the type of drive system. The most effective utilizes a limited-slip differential on each axle and a limited-slip interaxle differential, such that the torque is distributed

to all the wheels in proportion to their traction. This allows the van to develop a traction force that is the coefficient of friction times its weight.

$$(W + W_b) \tan \Theta = \mu W$$

or:

$$\Theta = \mu \frac{W}{W + W_b} = \mu \frac{1}{1 + \zeta}$$

For four-wheel-drive systems that do not have full limited-slip features, the solution would require a more complex treatment based on an analysis of the drive forces that would be available from the individual axles.

Example calculations:

For the parameters given in the problem, the solutions are:

$$\text{FWD } \Theta = 0.1018 = 10.18\% \text{ slope} = 5.84 \text{ deg}$$

$$\text{RWD } \Theta = 0.1142 = 11.42\% \text{ slope} = 6.51 \text{ deg}$$

$$\text{4WD } \Theta = 0.1944 = 19.44\% \text{ slope} = 11.0 \text{ deg}$$

Despite the fact that the assumed vehicle has a greater static load on the front axle (57% of the weight), the RWD configuration has better gradeability because of the longitudinal transfer of load on the grade.

References

1. Roberts, P., *Collector's History of the Automobile* (New York, N.Y.: Bonanza Books, 1978), 320pp.
2. *Encyclopedia Americana*, Vol. 2 (1966), 645pp.
3. *American Cars Since 1775* (New York: Automobile Quarterly, Inc., 1971), 504pp.
4. Olley, M., "Reminiscences - Feb 16/57," Unpublished, 1957, 17pp.
5. Lanchester, F.W., "Some Reflections Peculiar to the Design of an Automobile," *Proceedings of the Institution of Automobile Engineers* 2 (1908): 187-257.
6. Segel, L., "Some Reflections on Early Efforts to Investigate the Directional Stability and Control of the Motor Car," Unpublished, 1990, 7pp.
7. Broulhiet, G., "La Suspension de la Direction de la Voiture Automobile: Shimmy et Dandinement," *Societe des Ingénieurs Civils de France Bulletin* 78 (1925).
8. Lanchester, F.W., "Automobile Steering Gear—Problems and Mechanism," *Proceedings of the Institution of Automobile Engineers* 22 (1928): 726-741.
9. Becker, G. et al., *Schwingungen in Automobilfahrt* (Berlin: Krayn Berlag, 1931).
10. Lanchester, F.W., "Motor Car Suspension and Independent Springing," *Proceedings of the Institution of Automobile Engineers* 30 (1936): 668-762.
11. Olley, M., "Independent Wheel Suspensions Its Whys and Wherefores," *Society of Automotive Engineers Journal* 34, no. 3 (1934): 73-81.
12. Rieckert, P., and Schunk, T.E., "Zur Fahrmechanik des Gummibereiften Kraftfahrzeugs," *Ingenieur Archiv* 11 (1940).

13. Rocard, Y., "Les Mefaits du Roulement, Auto-Oscillations et Instabilite de Route," *La Revue Scientifique* 84, no. 45 (1946).
14. Segel, L., "Research in the Fundamentals of Automobile Control and Stability," *Transactions of the Society of Automotive Engineers* 65 (1956): 527-540.
15. Ellis, J.R., *Vehicle Dynamics*, (London: Business Books Limited, 1969), 243pp.
16. Ellis, J.R., *Road Vehicle Dynamics* (Akron, OH: John R. Ellis, Inc., 1988), 294pp.
17. Wong, J.Y., *Theory of Ground Vehicles* (New York: John Wiley & Sons, 2008), 592pp.
18. Mola, S., *Fundamentals of Vehicle Dynamics*, (Flint, MI: General Motors Institute, 1986).
19. Cole, D., "Elementary Vehicle Dynamics," *Course Notes in Mechanical Engineering*, The University of Michigan, Ann Arbor, MI, 1972.
20. Fitch, J.W., *Motor Truck Engineering Handbook*, 3rd ed. (Anacortes, WA: James W. Fitch, 1984), 288pp.
21. Newton, K., Steeds, W., and Garrett, T.K., *The Motor Vehicle*, 10th ed. (London: Butterworths, 1983), 742pp.
22. *Automotive Handbook*, 2nd ed. (Stuttgart: Robert Bosch GmbH, 1986), 707pp.
23. Bastow, D., *Car Suspension and Handling*, 2nd ed. (London: Pentech Press), 1990, 300pp.
24. Goodsell, D., *Dictionary of Automotive Engineering* (London: Butterworths, 1989), 182pp.
25. "Vehicle Dynamics Terminology," SAE J670, Society of Automotive Engineers, Warrendale, PA.
26. Den Hartog, J.P., *Mechanics* (New York, NY: McGraw-Hill Book Company, Inc., 1948), 174.



Acceleration Performance

Reprinted with permission from © General Motors



Cadillac's 3.0L Twin Turbo

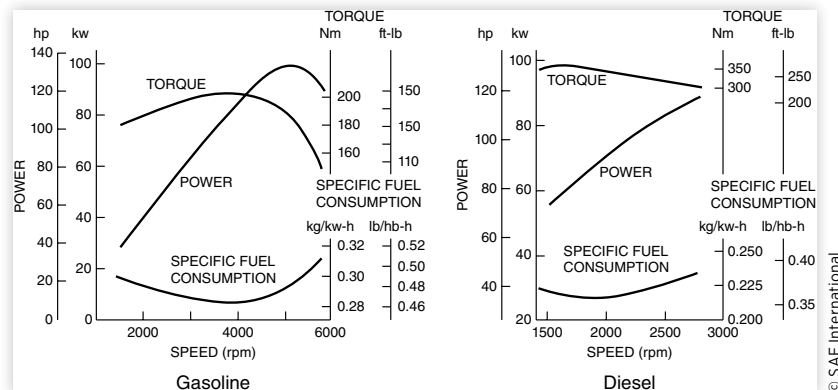
Maximum performance in longitudinal acceleration of a motor vehicle is determined by one of two limits—engine power or traction limits on the drive wheels. Which limit prevails may depend on vehicle speed. At low speeds tire traction may be the limiting factor, whereas at high speeds engine power may account for the limits.

Power-Limited Acceleration

The analysis of power-limited acceleration involves examination of the engine characteristics and their interaction through the powertrain.

Engines

The source of propulsive power is the engine. Engines may be characterized by their torque and power curves as a function of speed. [Figure 2.1](#) shows typical curves for gasoline and diesel engines. Gasoline engines typically have a torque curve that peaks

FIGURE 2.1 Performance characteristics of gasoline and diesel engines.

© SAE International

in the mid-range of operating speeds controlled by the induction system characteristics. In comparison, diesel engines may have a torque curve that is flatter or even rises with decreasing speed. This characteristic, controlled by the programming of the injection system, has led to the high-torque-rise heavy-duty engines commonly used in commercial vehicles. (In some cases the torque rise may be so great as to provide nearly constant power over much of the engine operating speed range.)

The other major difference between the two types of engines is the specific fuel consumption that is obtained. At their most efficient, gasoline engines may achieve specific fuel consumption levels in the range near 0.4 lb/hp-hr, whereas diesels may be near 0.2 or lower.

Power and torque are related by the speed. Specifically,

$$\begin{aligned} P \text{ (ft-lb/sec)} &= T \text{ (ft-lb)} \times \omega_e \text{ (rad/sec)} \\ HP &= T \text{ (ft-lb)} \times \omega_e \text{ (rad/sec)} / 550 = T \text{ (ft-lb)} \times RPM / 5252 \end{aligned} \quad (2.1)$$

where:

P = Power

T = Torque

ω_e = Engine angular velocity

HP = Horsepower

RPM = Revolutions per minute

Also,

$$P \text{ (kW)} = 0.746 \times HP \quad 1 \text{ HP} = 550 \text{ ft-lb/sec} \quad (2.2)$$

The ratio of engine power to vehicle weight is the first-order determinant of acceleration performance. At low to moderate speeds, an upper limit on acceleration can be obtained by neglecting all resistance forces acting on the vehicle. From Newton's Second Law:

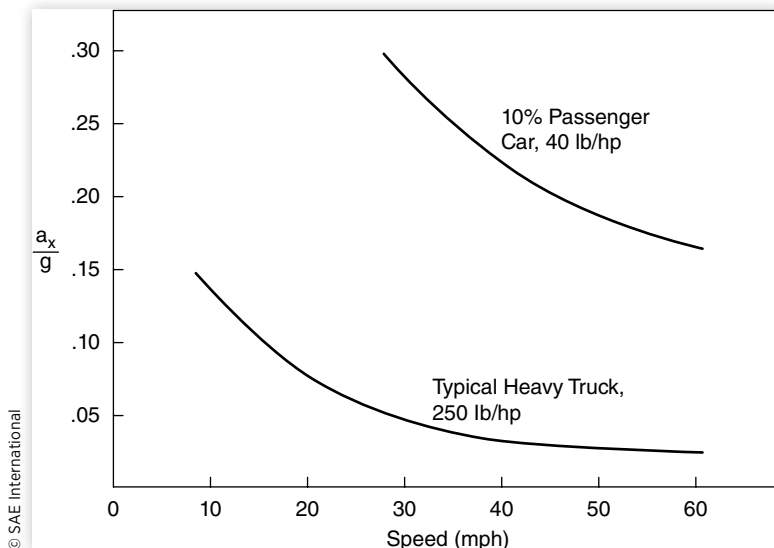
$$Ma_x = F_x \quad (2.3)$$

here:

M = Mass of the vehicle, W/g

a_x = Acceleration in the forward direction

F_x = Tractive force at the drive wheels

FIGURE 2.2 Effect of velocity on acceleration capabilities of cars and trucks [2].

Since the drive power is the tractive force times the forward speed, [Equation \(2.3\)](#) can be written as:

$$a_x = \frac{1}{M} F_x = 550 \frac{g \text{ HP}}{V \text{ W}} \left(\text{ft/sec}^2 \right) \quad (2.4)$$

where:

g = Gravitational constant (32.2 ft/sec²)

V = Vehicle forward speed (ft/sec)

HP = Engine horsepower

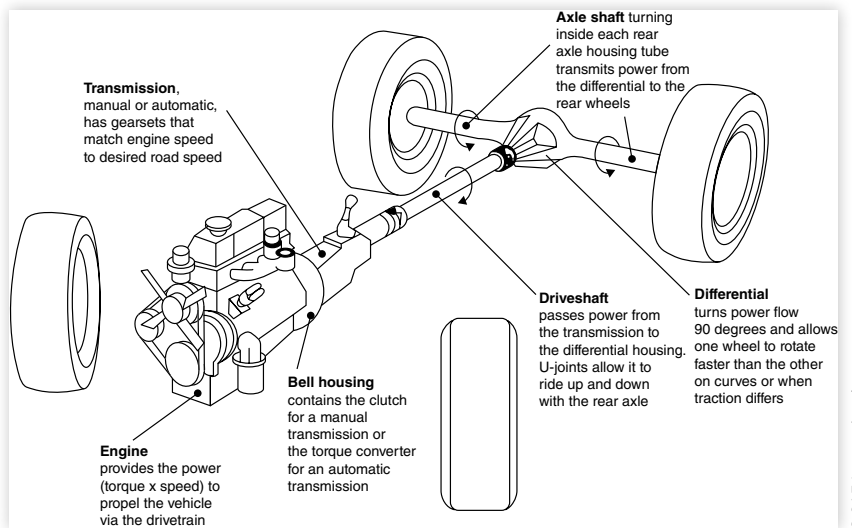
W = Weight of the vehicle (lb)

Because of the velocity term in the denominator, acceleration capability must decrease with increasing speed. The general relationship of the above equation is shown in [Figure 2.2](#) for cars and trucks. As might be expected, heavy trucks will have much lower performance levels than cars because of the less favorable power-to-weight ratio. Although this is a very simple representation of acceleration performance, it is useful to highway engineers responsible for establishing highway design policies with respect to the needs for climbing lanes on long upgrades, sight distances at intersections, and acceleration areas on entrance ramps [1].

Powertrain

More exact estimation of acceleration performance requires modeling the mechanical systems by which engine power is transmitted to the ground. [Figure 2.3](#) shows the key elements.

Starting with the engine, it must be remembered that engine torque is measured at steady speed on a dynamometer; thus, the actual torque delivered to the drivetrain is reduced by the amount required to accelerate the inertia of the rotating components (as well as accessory loads not considered here). The torque delivered through the clutch as input to the transmission can be determined by application of Newton's Second Law as:

FIGURE 2.3 Primary elements in the power train.

© SAE International

$$T_c = T_e - I_e \alpha_e \quad (2.5)$$

where:

 T_c = Torque at the clutch (input to the transmission) T_e = Engine torque at a given speed (from dynamometer data) I_e = Engine rotational inertia α_e = Engine rotational acceleration

The torque delivered at the output of the transmission is amplified by the gear ratio of the transmission but is decreased by inertial losses in the gears and shafts. If the transmission inertia is characterized by its value on the input side, the output torque can be approximated by the expression:

$$T_d = (T_c - I_t \alpha_e) N_t \quad (2.6)$$

where:

 T_d = Torque output to the driveshaft N_t = Numerical ratio of the transmission I_t = Rotational inertia of the transmission (as seen from the engine side)

Similarly, the torque delivered to the axles to accelerate the rotating wheels and provide tractive force at the ground is amplified by the final drive ratio with some reduction from the inertia of the driveline components between the transmission and final drive. The expression for this is:

$$T_a = F_x r + I_w \alpha_w = (T_d - I_d \alpha_d) N_f \quad (2.7)$$

where:

 T_a = Torque on the axles F_x = Tractive force at the ground r = Radius of the wheels I_w = Rotational inertial of the wheels and axles shafts α_w = Rotational acceleration of the wheels I_d = Rotational inertia of the driveshaft α_d = Rotational acceleration of the driveshaft N_f = Numerical ratio of the final drive

Now the rotational accelerations of the engine, transmission, and driveline are related to that of the wheels by the gear ratios.

$$\alpha_d = N_f \alpha_w \quad \text{and} \quad \alpha_e = N_t \alpha_d = N_t N_f \alpha_w \quad (2.8)$$

Equations (2.5) to (2.8) can be combined to solve for the tractive force available at the ground. Recognizing that the vehicle acceleration, a_x , is the wheel rotational acceleration, α_w , times the tire radius, yields:

$$F_x = \frac{T_e N_{tf}}{r} - \left\{ (I_e + I_t) N_{tf}^2 + I_d N_f^2 + I_w \right\} \frac{a_x}{r^2} \quad (2.9a)$$

where N_{tf} is the combined ratio of the transmission and final drive.

Thus far the inefficiencies due to mechanical and viscous losses in the driveline components (transmission, driveshaft, differential, and axles) have not been taken into account. These act to reduce the engine torque in proportion to the product of the efficiencies of the individual components [3]. The efficiencies vary widely with the torque level in the driveline because viscous losses occur even when the torque is zero. As a rule of thumb, efficiencies in the neighborhood of 80% to 90% are typically used to characterize the driveline [4]. The effect of mechanical losses can be approximated by adding an efficiency value to the first term on the right-hand side of the previous equation, giving:

$$F_x = \frac{T_e N_{tf} \eta_{tf}}{r} - \left\{ (I_e + I_t) N_{tf}^2 + I_d N_f^2 + I_w \right\} \frac{a_x}{r^2} \quad (2.9b)$$

where η_{tf} is the combined efficiency of the transmission and final drive.

Thus, Equation (2.9b) provides an expression for the tractive force that can be obtained from the engine. It has two components:

1. The first term on the right-hand side is the engine torque multiplied by the overall gear ratio and the efficiency of the drive system, then divided by tire radius. This term represents the steady-state tractive force available at the ground to overcome the road load forces of aerodynamics and rolling resistance, to accelerate, or to climb a grade.
2. The second term on the right-hand side represents the “loss” of tractive force due to the inertia of the engine and drivetrain components. The term in brackets indicates that the equivalent inertia of each component is “amplified” by the square of the numerical gear ratio between the component and the wheels.

Knowing the tractive force, it is now possible to predict the acceleration performance of a vehicle. The expression for the acceleration must consider all the forces that were shown in Figure 1.6. The equation takes the form:

$$Ma_x = \frac{W}{g} a_x = F_x - R_x - D_A - R_{hx} - W \sin \Theta \quad (2.10)$$

where:

M = Mass of the vehicle = W/g

a_x = Longitudinal acceleration (ft/sec^2)

F_x = Tractive force at the ground (Equation 2.9b)

R_x = Rolling resistance forces

D_A = Aerodynamic drag force

R_{hx} = Hitch (towing) forces

F_x includes the engine torque and rotational inertia terms. As a convenience, the rotational inertias from Equation (2.9b) are often lumped in with the mass of the vehicle to obtain a simplified equation of the form:

$$(M + M_r) a_x = \frac{W + W_r}{g} a_x = \frac{T_e N_{tf} \eta_{tf}}{r} - R_x - D_A - R_{hx} - W \sin \Theta \quad (2.11)$$

where M_r is the equivalent mass of the rotating components.

The combination of the two masses is an “effective mass,” and the ratio of $(M + M_r)/M$ is the “mass factor.” The mass factor will depend on the operating gear, with typical values as below [5]:

Vehicle	Gear:	Mass factor			
		High	Second	First	Low
Small car		1.11	1.20	1.50	2.4
Large car		1.09	1.14	1.30	-
Truck		1.09	1.20	1.60	2.5

A representative number is often taken as [5,6]:

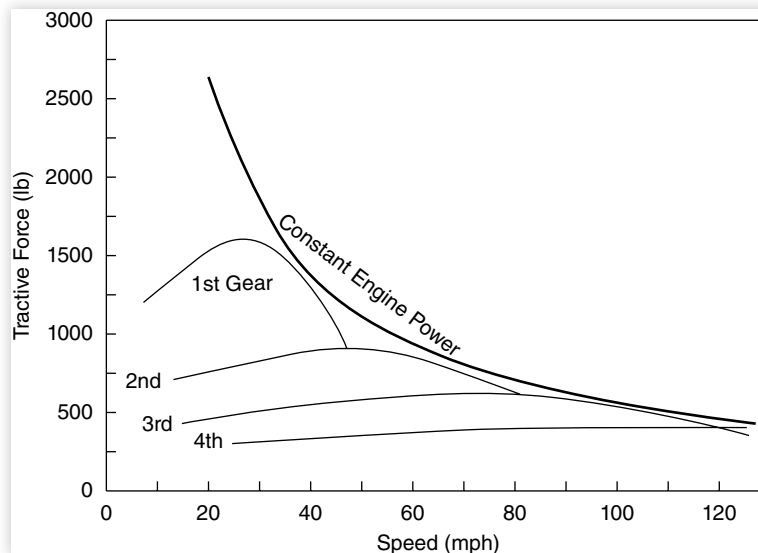
$$\text{Mass Factor} = 1 + 0.04N_{tf} + 0.0025N_{tf}^2 \quad (2.12)$$

In the complete form of [Equation \(2.11\)](#), there are no convenient explicit solutions for acceleration performance. Except for the grade term, all other forces vary with speed, and must be evaluated at each speed. The equation as shown above can be used to calculate acceleration performance by hand for a few speeds, but when repeated calculations are required (for example, to calculate acceleration from zero to a high speed), the use of computing tools is the preferred method [7–9].

The tractive force generated by the engine/powertrain (the first term on the right side of [Equation 2.11](#)) is the effort available to overcome road load forces and accelerate the vehicle. This is shown for a four-speed manual transmission in [Figure 2.4](#).

The “Constant Engine Power” line is equal to the maximum power of the engine, which is the upper limit of tractive effort available, less any losses in the driveline. It is only approached when the engine reaches the speed at which it develops maximum power.

FIGURE 2.4 Tractive effort-speed characteristics for a manual transmission.



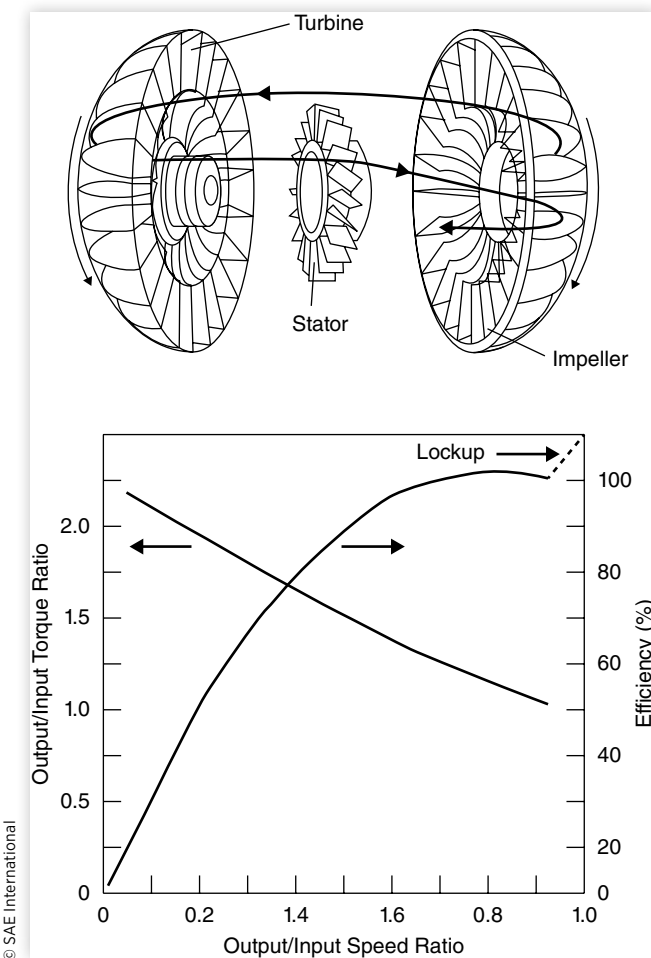
The tractive force line for each gear is the image of the engine torque curve multiplied by the ratios for that gear. The curves illustrate visually the need to provide a number of gear ratios for operation of the vehicle. Low gears are necessary for getting the vehicle moving from rest and driving low speeds, providing high tractive effort but have a limited speed range. In contrast, higher gears expand the speed range but reduce the available tractive effort.

For maximum acceleration performance the optimum shift point between gears is the point where the lines cross. The area between the lines for the different gears and the constant power curve is indicative of the deficiencies of the transmission in providing maximum acceleration performance.

Automatic Transmissions

Automatic transmissions provide somewhat different performance, more closely matching the ideal because of the torque converter on the input. Torque converters are fluid couplings that utilize hydrodynamic principles to amplify the torque input to the transmission at the expense of speed. **Figure 2.5** shows the torque ratio and efficiency characteristics of a typical torque converter as a function of speed ratio (output/input speed). At zero output speed (speed ratio of zero) the output torque will be several times

FIGURE 2.5 Characteristics of a typical torque converter.



that of the input. Thus the torque input to the transmission will be twice the torque coming out of the engine when the transmission is stalled, providing for good “off-the-line” acceleration performance. As speed builds up and the transmission input approaches engine speed, the torque ratio drops to unity.

Figure 2.5 also shows the three main components of a torque converter:

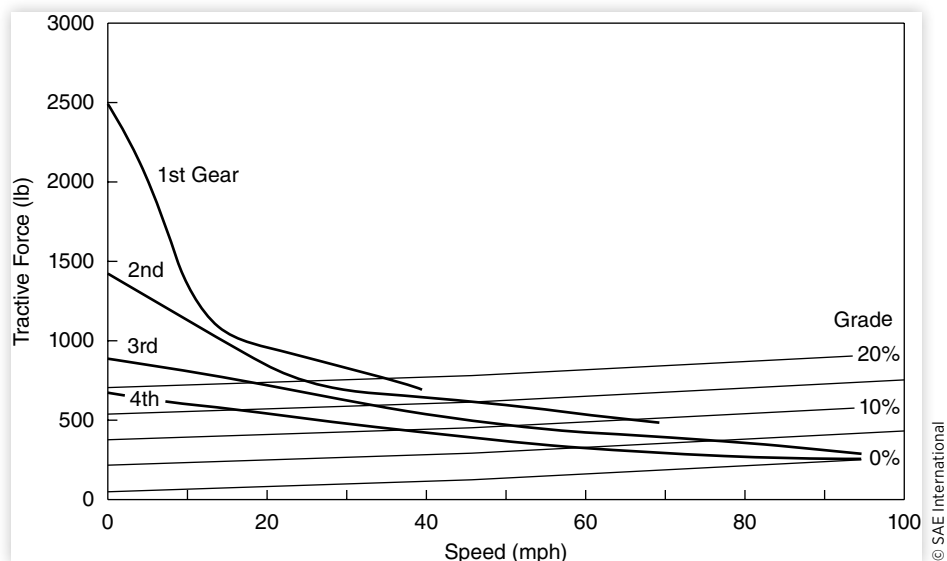
- Impeller (input from engine)
- Stator
- Turbine (output to transmission)

The Stator deflects the return flow in the direction of, and adds torque to, the impeller. As a result, the turbine torque will be larger than the engine torque that is input to the impeller. In general, the torque converter is characterized by the torque capacity (K). When engine braking is taken into account K approaches infinity as the speed ratio (output speed / input speed) approaches one. Therefore it is common to use $1/K$, or the Inverse Capacity Factor.

Compared to a manual transmission, the torque amplification characteristics of a torque converter provide for a more favorable tractive effort-speed performance envelope. [Figure 2.6](#) shows the tractive effort-speed characteristics for a 4-speed automatic transmission. The initial part of the tractive force curve is dominated by the torque amplification from the torque converter. From there, the force curves blend into the engine torque curve. The intersections of the tractive force curves with the road load curves (straight lines) represent the maximum steady state speed in each transmission gear.

Because of the slip possible with the fluid coupling, the torque curves in each gear can extend down to zero speed without stalling the engine. At low speed in first gear the effect of the torque converter is especially evident as the tractive effort rises down toward the zero speed condition. In general the torque converter is characterized by the torque capacity (K). When engine braking is taken into account K approaches infinity as the speed ratio (output speed / input speed) approaches 1. Therefore it is common to use $1/K$, or the Inverse Capacity Factor.

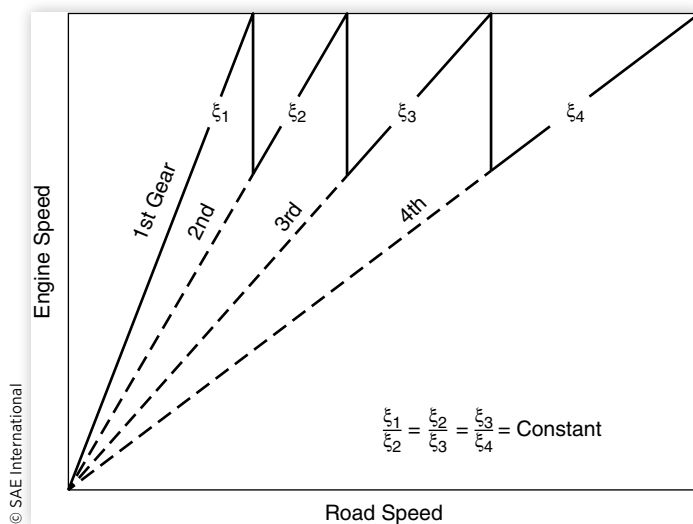
FIGURE 2.6 Tractive effort-speed characteristics for an automatic transmission.



Also shown on this figure are the road load forces arising from rolling resistance, aerodynamic drag, and road grade (0, 5, 10, 15, and 20%). At a given speed and gear the difference between the tractive effort curve and the appropriate road load curve is the tractive force available to accelerate the vehicle (and its rotating components). The intersection between the road load curves and any of the tractive effort curves is the maximum speed that can be sustained in that gear.

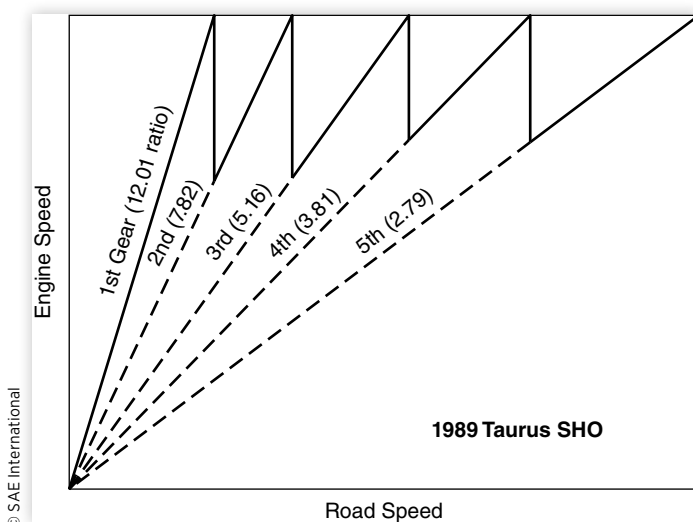
The actual ratios selected for a transmission may be tailored for performance in specific modes—an optimal first gear for starting, a second or third gear for passing, and a high gear for fuel economy at road speeds. The best gear ratios usually fall close to a geometric progression, in which the ratios change by a constant percentage from gear to gear. [Figure 2.7](#) illustrates the relationship of engine speed to road speed obtained with geometric progression. [Figure 2.8](#) shows the engine-road speed relationship for an actual production car. Note that although it is close to geometric progression, some variation occurs.

FIGURE 2.7 Selection of gear ratios based on geometric progression.



© SAE International

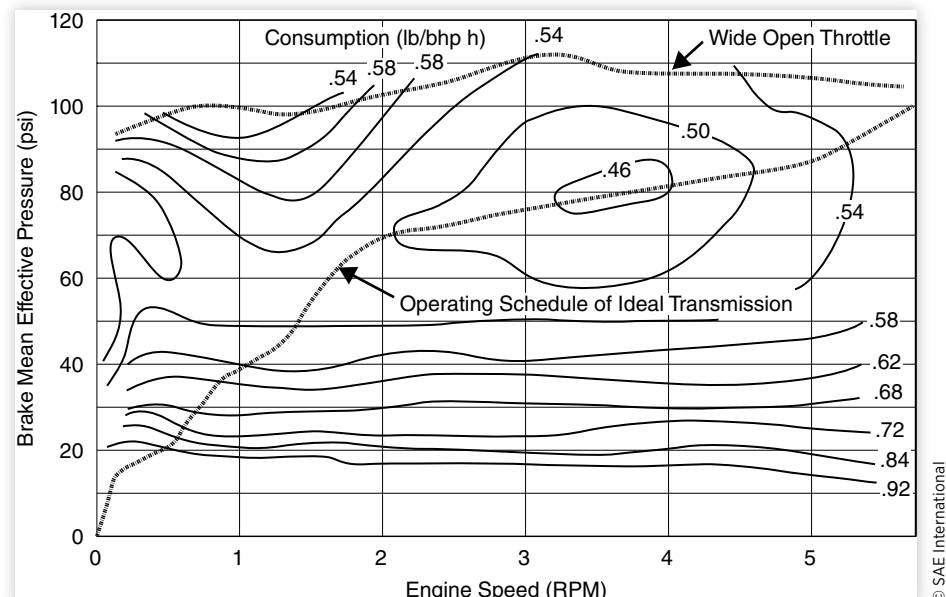
FIGURE 2.8 Gear ratios on a typical passenger car.



© SAE International

Selection of transmission gear ratios must also reflect the realities of the pressures for fuel economy and emissions. The engine performance in both of these respects is quantified by mapping its characteristics. An example of a fuel consumption map for a V-8 engine is shown in [Figure 2.9](#). The figure shows lines of constant fuel consumption (pounds per brake-horsepower-hour) as a function of brake-mean-effective-pressure (indicative of torque) and engine speed. Near the boundaries the specific fuel consumption is highest. In the middle is a small island of minimum fuel consumption at the rate of 0.46 lb/bhp-hr. To maximize highway fuel economy the vehicle and driveline should be designed to operate in this region. For best economy over the full driving range, the transmission should be designed to operate along the bold line which stays within the valleys of minimum fuel consumption over the broadest range of engine speeds.

FIGURE 2.9 Specific fuel consumption map of a V-8 engine (300 in.³).



© SAE International

For emissions purposes, similar maps of engine performance can be developed to characterize the emissions properties, and a similar logic would be used to identify transmission characteristics that would minimize emissions.

Example Problems

1. We are given the following information about the engine and drivetrain components for a passenger car:

Engine inertia	0.8 in-lb-sec ²					
RPM/torque (ft-lb)	800	120	2400	175	4000	200
	1200	132	2800	181	4400	201
	1600	145	3200	190	4800	198
	2000	160	3600	198	5200	180

Transmission data, gear	1	2	3	4	5
Inertias	1.3	0.9	0.7	0.5	0.3 in-lb-s ²
Ratios	4.28	2.79	1.83	1.36	1.00
Efficiencies	0.966	0.967	0.972	0.973	0.970
Final drive	Inertia		1.2 in-lb-sec ²		
	Ratio		2.92		
	Efficiency		0.99		
Wheel inertias	Drive 11.0 in-lb-sec ²		Non-drive 11.0 in-lb-sec ²		
Wheel size	801 rev/mile \Rightarrow 6.59 ft circumference \Rightarrow 12.59 in radius				

(a) Calculate the effective inertia of the drivetrain components in first gear.

Solution:

The effective inertia is given by the second term on the right-hand side of [Equation \(2.9b\)](#), which had the following form:

$$F_x = \frac{T_e N_{tf} \eta_{tf}}{r} - \left\{ (I_e + I_t) N_{tf}^2 + I_d N_f^2 + I_w \right\} \frac{a_x}{r^2} \quad (2.9b)$$

The term in the brackets is the effective inertia. It is calculated as follows:

$$\begin{aligned} I_{eff} &= \left\{ (I_e + I_t) (N_{tf})^2 + I_d N_f^2 + I_w \right\} \\ &= (0.8 + 1.3) \text{ in-lb-sec}^2 (4.28 \times 2.92)^2 + 1.2 \times 2.92^2 + 2 \times 11.0 \text{ in-lb-sec}^2 \\ &= 328 + 10.2 + 22 = 360.2 \text{ in-lb-sec}^2 \end{aligned}$$

Notes:

1. The engine and first gear components are the largest inertia when operating in first gear. In fifth gear, the inertia of these components is about 9.7 in-lb-sec².
2. Only the inertia of the drive wheels was included in this solution because only they subtract from the tractive force available at the ground at the drive wheels. We must keep in mind that the non-driven wheels contribute an additional inertia when the vehicle is accelerated. The inertia of the non-driven wheels should be lumped in with the inertia (mass) of the total vehicle.
3. The rotational inertia, in units of in-lb-sec², is converted into translational inertia (mass) when divided by r² in Equation (2.9). We can see its magnitude as follows:

$$M_{eff} = I_{eff}/r^2 = 360.2 \text{ in-lb-sec}^2 / 12.59^2 \text{ in}^2 = 2.27 \text{ lb-sec}^2/\text{in}$$

Perhaps the more familiar form is the effective weight:

$$W_{eff} = M_{eff} g = 2.27 \text{ lb-sec}^2/\text{in} \times 386 \text{ in/sec}^2 = 877 \text{ lb}$$

Comparing this figure to the weight of a typical passenger car (2500 lb), we see that it adds about 35% to the effective weight of the car during acceleration in first gear. The inertia of the non-driven wheels will add another 27 lb to the effective weight (1%).

2. Calculate the maximum tractive effort and corresponding road speed in first and fifth gears of the car described above when inertial losses are neglected.

Solution:

Maximum tractive effort will coincide with maximum torque, which occurs at 4400 rpm. So the problem reduces to finding the tractive effort from the first term in Equation (2.9) for that value of torque.

$$\begin{aligned} F_x &= T_c N_{tf} \eta_{tf} / r \\ &= 201 \text{ ft-lb} (4.28 \times 2.92) (0.966 \times 0.99) / 12.59 \text{ in} \times 12 \text{ in} / \text{ft} \\ &= 2290 \text{ lb} \end{aligned}$$

The road speed is determined by the use of relationships given in [Equation \(2.8\)](#). Although the equation is written in terms of acceleration, the same relationships hold true for speed. That is:

$$\omega_d = N_f \omega_w \quad \text{and} \quad \omega_e = N_t \omega_d = N_t N_f \omega_w \quad (2.8a)$$

The wheel rotational speed will be:

$$\begin{aligned} \omega_w &= \omega_e / (N_t N_f) = 4400 \text{ rev/min} \cdot 2\pi \text{ rad/rev} \cdot 1 \text{ min/60 sec} / (4.28 \times 2.92) \\ &= 36.87 \text{ rad/sec} \end{aligned}$$

The corresponding ground speed will be found by converting the rotational speed to translational speed at the circumference of the tire.

$$V_x = \omega_w \cdot r = 36.87 \text{ rad/sec} \times 12.59 \text{ in} = 464.2 \text{ in/sec} = 38.7 \text{ ft/sec} = 26.4 \text{ mph}$$

The same method is used to calculate performance in high gear as well:

$$\begin{aligned} F_x &= T_e N_{tf} \eta_{tf} / r \\ &= 201 \text{ ft-lb} (1.0 \times 2.92) (0.99 \times 0.97) / 12.59 \text{ in} \times 12 \text{ in} / \text{ft} \\ &= 537 \text{ lb} \end{aligned}$$

$$\begin{aligned} \omega_w &= \omega_e / (N_t N_f) = 4400 \text{ rev/min} \cdot 2\pi \text{ rad/rev} \cdot 1 \text{ min/60 sec} / (1.0 \times 2.92) \\ &= 157.8 \text{ rad/sec} \end{aligned}$$

$$V_x = \omega_w \cdot r = 157.8 \text{ rad/sec} \times 12.59 \text{ in} = 1987 \text{ in/sec} = 165 \text{ ft/sec} = 113 \text{ mph}$$

Traction-Limited Acceleration

Presuming there is adequate power from the engine, the acceleration may be limited by the coefficient of friction between the tire and road. In that case F_x is limited by:

$$F_x = \mu W \quad (2.13)$$

where:

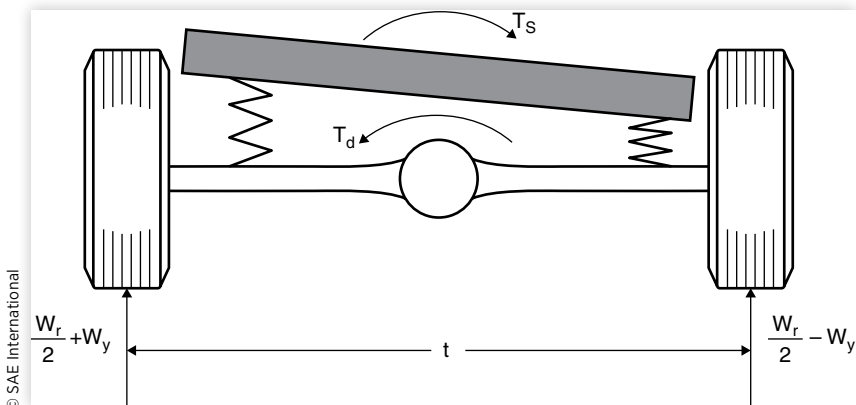
μ = Peak coefficient of friction

W = Weight on drive wheels

The weight on a drive wheel then depends on the static plus the dynamic load due to acceleration, and on any transverse shift of load due to drive torque.

Transverse Weight Shift due to Drive Torque

Transverse weight shift occurs on all solid drive axles, whether on the front or rear of the vehicle. The basic reactions on a rear axle are shown in [Figure 2.10](#). The driveshaft

FIGURE 2.10 Free-body diagram of a solid drive axle.

into the differential imposes a torque T_d on the axle. As will be seen, the chassis may roll compressing and extending springs on opposite sides of the vehicle such that a torque due to suspension roll stiffness, T_s , is produced. Any difference between these two must be absorbed as a difference in weight on the two wheels. If the axle is of the non-locking type, then the torque delivered to both wheels will be limited by the traction limit on the most lightly loaded wheel.

Writing Newton's Second Law for rotation of the axle about its centerpoint allows the reactions to be related. When the axle is in equilibrium:

$$\sum T_O = (W_r / 2 + W_y - W_r / 2 + W_y) t / 2 + T_s - T_d = 0 \quad (2.14)$$

or

$$W_y = (T_d - T_s) / t$$

In the above equation, T_d can be related to the drive forces because:

$$T_d = F_x r / N_f \quad (2.15)$$

where:

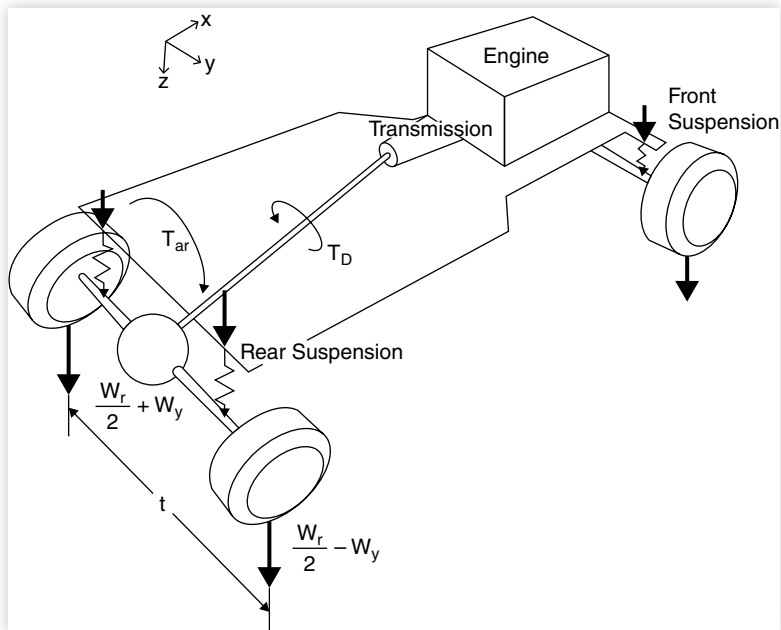
F_x = Total drive force from the two rear wheels

r = Tire radius

N_f = Final drive ratio

However, it is necessary to determine the roll torque produced by the suspension, which requires an analysis of the whole vehicle because the reaction of the drive torque on the chassis attempts to roll the chassis on both the front and rear suspensions. The entire system of interest is illustrated in [Figure 2.11](#) for the case of a rear-wheel-drive car.

The drive torque reaction at the engine/transmission is transferred to the frame and distributed between the front and rear suspensions. It is generally assumed that the roll torque produced by a suspension is proportional to the roll angle (Hooke's Law) of the chassis. Then:

FIGURE 2.11 Diagram of drive torque reactions on the chassis.

© SAE International

$$T_{sf} = K_{\phi f} \phi \quad (2.16a)$$

$$T_{sr} = K_{\phi r} \phi \quad (2.16b)$$

$$K_\phi = K_{\phi f} + K_{\phi r} \quad (2.16c)$$

where:

T_{sf} = Roll torque on the front suspension

T_{sr} = Roll torque on the rear suspension

$K_{\phi f}$ = Front suspension roll stiffness

$K_{\phi r}$ = Rear suspension roll stiffness

K_ϕ = Total roll stiffness

The roll torque on the rear suspension, T_{sr} can be related to the roll angle, and the roll angle can be related to the drive torque as follows. The roll angle is simply the drive torque divided by the total roll stiffness:

$$\phi = T_d / K_\phi = T_d / (K_{\phi f} + K_{\phi r}) \quad (2.17)$$

Therefore, substituting in Equation (2.16b),

$$T_{sr} = K_{\phi r} T_d / (K_{\phi f} + K_{\phi r})$$

This in turn can be substituted into Equation (2.14), along with the expression for T_d obtained from Equation (2.15):

$$W_y = \frac{F_x r}{N_f t} \left[1 - \frac{K_{\phi r}}{K_{\phi r} + K_{\phi f}} \right] \quad (2.18a)$$

The term in the brackets collapses to yield:

$$W_y = \frac{F_x r}{N_f t} \frac{K_{\phi f}}{K_\phi} \quad (2.18b)$$

This equation gives the magnitude of the lateral load transfer as a function of the tractive force and a number of vehicle parameters such as the final drive ratio, track width of the axle, tire radius, and suspension roll stiffnesses. The net load on the rear axle during acceleration will be its static plus its dynamic component (see Equation 1.7). For a rear axle:

$$W_r = W \left(\frac{b}{L} + \frac{a_x h}{g L} \right) \quad (2.19)$$

Neglecting the rolling resistance and aerodynamic drag forces, the acceleration is simply the tractive force divided by the vehicle mass.

$$W_r = W \left(\frac{b}{L} + \frac{F_x h}{M g L} \right) \quad (2.20)$$

Then the weight on the right rear wheel, W_{rr} will be $W_r/2 - W_y$ or:

$$W_{rr} = \frac{Wb}{2L} + \frac{F_x h}{2L} - \frac{F_x r}{N_f t} \frac{K_{\phi f}}{K_\phi} \quad (2.21)$$

and

$$F_x = 2\mu W_{rr} = 2\mu \left(\frac{Wb}{2L} + \frac{F_x h}{2L} - \frac{F_x r}{N_f t} \frac{K_{\phi f}}{K_\phi} \right) \quad (2.22)$$

Traction Limits

Solving for F_x gives the final expression for the maximum tractive force that can be developed by a solid rear axle with a non-locking differential:

$$F_{x \max} = \frac{\mu \frac{Wb}{L}}{1 - \frac{h}{L} \mu + \frac{2\mu r}{N_f t} \frac{K_{\phi f}}{K_\phi}} \quad (2.23)$$

For a solid rear axle with a locking differential, additional tractive force can be obtained from the other wheel up to its traction limits such that the last term in the denominator of the above equation drops out. This would also be true in the case of an independent rear suspension because the driveline torque reaction is picked up by the chassis-mounted differential. In both of these cases the expression for the maximum tractive force is:

$$F_{x \max} = \frac{\mu \frac{Wb}{L}}{1 - \frac{h}{L} \mu} \quad (2.24)$$

Finally, in the case of a front axle, the fore/aft load transfer is opposite from the rear axle case. Since the load transfer is reflected in the second term of the denominator, the opposite direction yields a sign change. Also, the term “ $W b/L$ ” arose in the earlier

equations to represent the static load on the rear drive axle. For a front-wheel-drive vehicle, the term becomes “W c/L.” For the solid front drive axle with non-locking differential:

$$F_{x\max} = \frac{\mu \frac{W_c}{L}}{1 + \frac{h}{L} \mu + \frac{2\mu r}{N_f t} \frac{K_{\phi_r}}{K_\phi}} \quad (2.25)$$

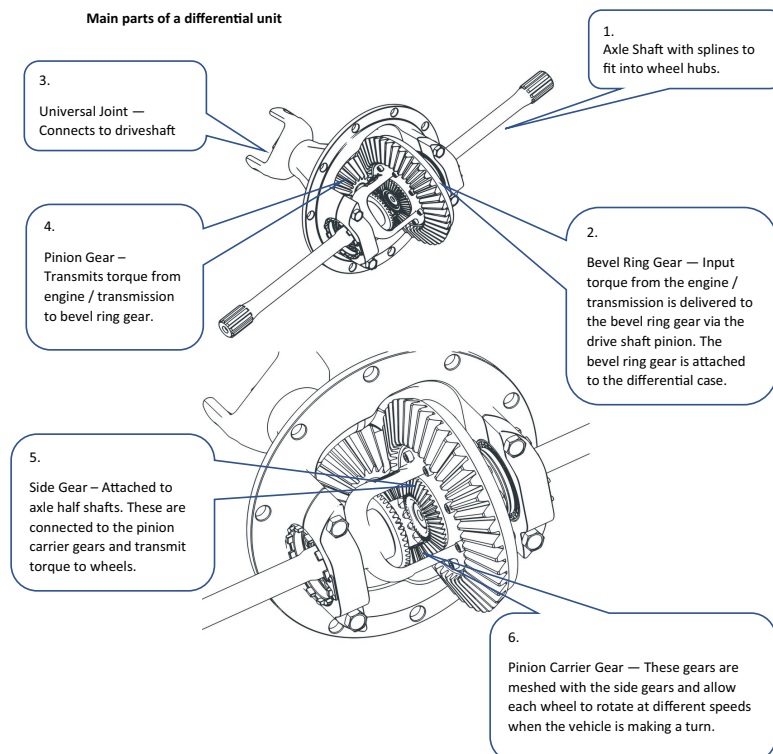
And for the solid front drive axle with locking differential, or the independent front drive axle as typical of most front-wheel-drive cars today:

$$F_{x\max} = \frac{\mu \frac{W_c}{L}}{1 + \frac{h}{L} \mu} \quad (2.26)$$

PARTS OF A DIFFERENTIAL (FIGURE 2.12)

1. Axle Shaft, with splined ends to connect to wheel hubs — The splines allow the shaft to transmit torque to the drive wheels while also being able to slide within the hub as the wheel moves in jounce and rebound.
2. Bevel Ring Gear — Also called a Crown Wheel. Input torque from the engine / transmission is delivered to the bevel ring gear via the drive shaft pinion. The ring gear rotates at a speed equal to the mean speed of the left and right wheels.

FIGURE 2.12 Main parts of a differential unit.



3. Universal Joint — Connects to drive shaft.
4. Pinion Gear — Transmits torque from engine / transmission via the drive shaft to bevel ring gear.
5. Side Gears — Also called Sun Gears. Attached to axle half shafts, these are connected to the pinion carrier gears and transmit torque to the wheels.
6. Pinion Carrier Gears —Also called Planet Pinion Gears or Spider Gears. These gears are meshed with the side gears and allow each wheel to rotate at different speeds when the vehicle is making a turn.

DIFFERENTIAL RULES

Rules for Free Differentials

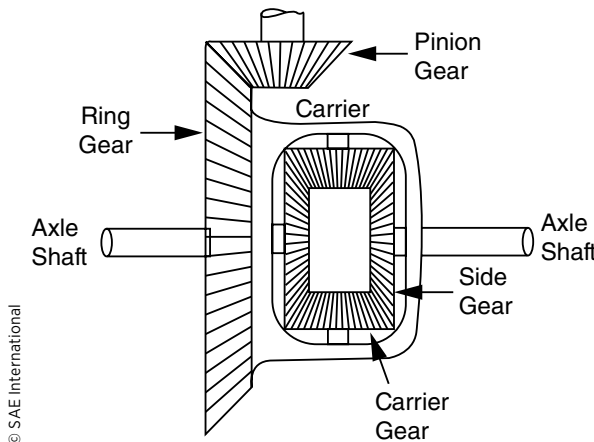
$$T_{\text{left}} = T_{\text{right}} = \frac{T_{\text{carrier}}}{2}$$

$$\frac{\omega_{\text{left}} + \omega_{\text{right}}}{2} = \omega_{\text{carrier}}$$

Rules for Locking Differentials

$$T_{\text{left}} + T_{\text{right}} = T_{\text{carrier}}$$

$$\omega_{\text{left}} = \omega_{\text{right}} = \omega_{\text{carrier}}$$



Example Problems

1. Find the traction-limited acceleration for the rear-drive passenger car with and without a locking differential on a surface of moderate friction level. The information that will be needed is as follows:

Weights	Front, 2100 lb	Rear, 1850 lb; Total, 3950 lb
C.G. height	21.0 in	Wheelbase, 108 in
Coefficient of friction	0.62	Tread, 59.0 in
Final drive ratio	2.90	Tire size, 13.0 in
Roll stiffnesses	Front, 1150 ft-lb/deg	Rear, 280 ft-lb/deg

Solution:

The equation for the maximum tractive force of a solid axle rear-drive vehicle with a non-locking differential was given in [Equation \(2.23\)](#):

$$F_{x\max} = \frac{\mu \frac{Wb}{L}}{1 - \frac{h}{L}\mu + \frac{2\mu r}{N_f t} \frac{K_{\phi f}}{K_\phi}} \quad (2.23)$$

In this equation, $W b/L$ is just the rear axle weight, which is known; therefore we do not have to find the value for the parameter “b.” Likewise, all the other terms are known and can be substituted into the equation to obtain:

$$\begin{aligned} F_{x\max} &= \frac{(0.62)1850 \text{ lb}}{1 - \frac{21}{108}0.62 + \frac{2(0.62)}{2.9} \frac{13 \text{ in}}{59 \text{ in}} \frac{1150}{1430}} \\ &= \frac{1147 \text{ lb}}{1 - 0.121 + 0.0758} = \frac{1147}{0.9548} = 1201 \text{ lb} \\ a_x &= \frac{F_{x\max}}{Mg} = \frac{1201 \text{ lb}}{3950 \text{ lb}} = 0.3041 \text{ g's} = 9.79 \frac{\text{ft}}{\text{sec}^2} \end{aligned}$$

With a locking differential the third term in the denominator disappears ([Equation 2.24](#)) so that we obtain:

$$\begin{aligned} F_{x\max} &= \frac{(0.62)1850 \text{ lb}}{1 - \frac{21}{108}0.62} = \frac{1147 \text{ lb}}{1 - 0.121} = \frac{1147}{0.879} = 1305 \text{ lb} \\ a_x &= \frac{F_{x\max}}{Mg} = \frac{1305 \text{ lb}}{3950 \text{ lb}} = 0.330 \text{ g's} = 10.64 \frac{\text{ft}}{\text{sec}^2} \end{aligned}$$

Notes:

- For both cases the numerator term is the weight on the drive axle times the coefficient of friction which is equivalent to 1147 lb of tractive force.
- Similarly, the dynamic load transfer onto the rear (drive) axle from acceleration is accounted for by the second term in the denominator which diminishes the magnitude of the denominator by 12.1%, thereby increasing the tractive force by an equivalent percentage.
- The lateral load transfer effect appears in the third term of the denominator, increasing its value by approximately 7.6%, which has the effect of decreasing the tractive force by about the same percentage. Comparing the two answers, the loss from lateral load transfer on the drive axle with a nonlocking differential is 104 lb. On higher friction surfaces a higher loss would be seen.

2. Find the traction-limited performance of a front-wheel-drive vehicle under the same road conditions as the problem above. The essential data are:

Weights	Front, 1950	Rear, 1150	Total, 3100
C.G. height	19.0 in	Wheelbase, 105 in	
Coefficient of friction	0.62	Tread, 60 in	
Final drive ratio	3.70	Tire size, 12.59 in	
Roll stiffnesses	Front, 950 ft-lb/deg	Rear, 620 ft-lb/deg	

Solution:

Most front-wheel-drive vehicles have an independent front suspension. Thus the equation for maximum tractive effort is given by [Equation \(2.26\)](#), and we notice that all the data required to calculate lateral load transfer on the axle are not needed. The maximum tractive force is calculated by substituting in the equation as follows:

$$F_{x\max} = \frac{\mu \frac{W_c}{L}}{1 + \frac{h}{L}\mu} \quad (2.26)$$

$$F_{x\max} = \frac{(0.62)1950 \text{ lb}}{1 + \frac{19}{105}0.62} = \frac{1209 \text{ lb}}{1 + 0.1122} = 1087 \text{ lb}$$

$$a_x = \frac{F_{x\max}}{Mg} = \frac{1087 \text{ lb}}{3100 \text{ lb}} = 0.3506 \text{ g's} = 11.29 \frac{\text{ft}}{\text{sec}^2}$$

Note:

- Even though the front-wheel-drive vehicle has a much higher percentage of its weight on the drive axle, its performance is not proportionately better. The reason is the loss of load on the front (drive) axle due to longitudinal weight transfer during acceleration.

References

- Gillespie, T.D., "Methods of Predicting Truck Speed Loss on Grades," The University of Michigan Transportation Research Institute, Report No. UM-85-39, November 1986, 169pp.
- St. John, A.D., and Kobett, D.R., "Grade Effects on Traffic Flow Stability and Capacity," Interim Report, National Cooperative Highway Research Program, Project 3-19, December 1972, 173pp.
- Marshall, H.P., "Maximum and Probable Fuel Economy of Automobiles," SAE Technical Paper [800213](#), 1980, doi:[10.4271/800213](#).
- Smith, G.L., "Commercial Vehicle Performance and Fuel Economy," SAE Paper [700194](#), 1970, doi:[10.4271/700194](#).
- Taborek, J.J., *Mechanics of Vehicles* (Cleveland, OH: Tommotor Corporation, 1957), 93pp.
- Cole, D., "Elementary Vehicle Dynamics," *Course Notes in Mechanical Engineering*, The University of Michigan, Ann Arbor, MI, 1972.
- Buck, R.E., "A Computer Program (HEVSIM) for Heavy Duty Vehicle Fuel Economy and Performance Simulation," U.S. Department of Transportation, Research and Special Projects Administration, Transportation Systems Center, Report No. DOT-HS-805-912, September 1981, 26pp.
- Zub, R.W., "A Computer Program (VEHSIM) for Vehicle Fuel Economy and Performance Simulation (Automobiles and Light Trucks)," U.S. Department of Transportation, Research and Special Projects Administration, Transportation Systems Center, Report No. DOT-HS-806-040, October 1981, 50pp.
- Phillips, A.W., Assanis, D.N., and Badgley, P., "Development and Use of a Vehicle Powertrain Simulation for Fuel Economy and Performance Studies," SAE Technical Paper [900619](#), 1990, doi:[10.4271/900619](#).



Braking Performance

© Yauhen_D / Shutterstock.com



ABS test drive.

Basic Equations

The general equation for braking performance may be obtained from Newton's Second Law written for the x-direction. Considering the free-body diagram shown in Figure 1.6, we can write Equation (3.1) as:

$$Ma_x = -\frac{W}{g}D_x = -F_{xf} - F_{xr} - D_A - W \sin \Theta \quad (3.1)$$

where:

- W = Vehicle weight
- g = Gravitational acceleration
- $D_x = -a_x$ = Linear deceleration
- F_{xf} = Front axle braking force
- F_{xr} = Rear axle braking force
- D_A = Aerodynamic drag
- Θ = Uphill grade angle

The front and rear braking force terms arise from the torque of the brakes along with rolling resistance effects, bearing friction, and driveline drags. A comprehensive analysis of the deceleration requires detailed knowledge of all these forces acting on the vehicle.

Constant Deceleration

Simple and fundamental relationships can be derived for the case where it is reasonable to assume that the forces acting on the vehicle will be constant throughout a brake application. The simple equations that result provide an appreciation for the basic relationships that govern braking maneuvers. From [Equation \(3.1\)](#),

$$D_x = \frac{F_{xt}}{M} = -\frac{dV}{dt} \quad (3.2)$$

where:

F_{xt} = Total of all longitudinal deceleration forces on the vehicle (+)

V = Forward velocity

This equation can be integrated (because F_{xt} is constant) for a deceleration from initial velocity, V_o , to final velocity, V_f :

$$\int_{V_o}^{V_f} dV = -\frac{F_{xt}}{M} \int_0^{t_s} dt \quad (3.3)$$

$$V_o - V_f = \frac{F_{xt}}{M} t_s \quad (3.4)$$

where:

t_s = Time for the velocity change.

Because velocity and distance are related by $V = dx/dt$, we can substitute for “ dt ” in [Equation \(3.2\)](#), integrate, and obtain the relationship between velocity and distance:

$$\frac{V_o^2 - V_f^2}{2} = \frac{F_{xt}}{M} X \quad (3.5)$$

where:

X = Time traveled during the deceleration.

In the case where the deceleration is a full stop, V_f is zero, and X is the stopping distance, SD. Then:

$$SD = \frac{V_o^2}{2 \frac{F_{xt}}{M}} = \frac{V_o^2}{2 D_x} \quad (3.6)$$

and the time to stop is:

$$t_s = \frac{V_o}{\frac{F_{xt}}{M}} = \frac{V_o}{D_x} \quad (3.7)$$

Thus, all other things being equal, the time to stop is proportional to the velocity, whereas the distance is proportional to the velocity squared (i.e., doubling the velocity doubles the time to stop, but quadruples the distance required).

Deceleration with Wind Resistance

The aerodynamic drag on a vehicle is dependent on vehicle drag factors and the square of the speed. To determine stopping distance in such cases, a more complicated expression is necessary but can still be integrated. To analyze this case:

$$\Sigma F_x = F_b + CV^2 \quad (3.8)$$

where:

F_b = Total brake force of front and rear wheels

C = Aerodynamic drag factor

Therefore:

$$\int_0^{SD} dx = M \int_{V_0}^0 \frac{V dV}{F_b + CV^2} \quad (3.9)$$

This may be integrated to obtain the stopping distance:

$$SD = \frac{M}{2C} \ln \left[\frac{F_b + CV_o^2}{F_b} \right] \quad (3.10)$$

Energy/Power

The energy and/or power absorbed by a brake system can be substantial during a typical maximum-effort stop. The energy absorbed is the kinetic energy of motion for the vehicle, and is thus dependent on the mass.

$$\text{Energy} = \frac{M}{2} (V_o^2 - V_f^2) \quad (3.11)$$

The power absorption will vary with the speed, being equivalent to the braking force times the speed at any instant of time. Thus, the power dissipation is greatest at the beginning of the stop when the speed is highest. Over the entire stop, the average power absorption will be the energy divided by the time to stop:

$$\text{Power} = \frac{M}{2} \frac{V_o^2}{t_s} \quad (3.12)$$

Calculation of the power is informative from the standpoint of appreciating the performance required from a brake system. A 3000 lb car in a maximum-effort stop from 80 mph requires absorption of nearly 650,000 ft-lb of energy. If stopped in 8 seconds (10 mph/sec), the average power absorption of the brakes during this interval is 145 HP. An 80,000 lb truck stopped from 60 mph typically involves dissipation at an average rate of several thousands of horsepower!

Braking Forces

The forces on a vehicle producing a given braking deceleration may arise from a number of sources. Though the brakes are the primary source, others will be discussed first.

Rolling Resistance

Rolling resistance always opposes vehicle motion; hence, it aids the brakes. The rolling resistance forces will be:

$$R_{xf} + R_{xr} = f_r (W_f + W_r) = f_r W \quad (3.13)$$

The parameter “ f_r ” is the rolling resistance coefficient and will be discussed in the next chapter. Note that the total force is independent of the distribution of loads on the axles (static or dynamic). Rolling resistance forces are nominally equivalent to about 0.01 g deceleration (0.3 ft/sec^2).

Aerodynamic Drag

The drag from air resistance depends on the dynamic pressure and is therefore proportional to the square of the speed. At low speeds, however, it is negligible. At normal highway speeds, aerodynamic drag may contribute a force equivalent of about 0.03 g (1 ft/sec^2). More discussion of this topic is presented in the next chapter.

Driveline Drag

The engine, transmission, and final drive contribute both drag and inertia effects to the braking action. As discussed in the previous chapter on Acceleration Performance, the inertia of these components adds to the effective mass of the vehicle, and warrants consideration in brake sizing on the drive wheels. The drag arises from bearing and gear friction in the transmission and differential, as well as engine braking. Engine braking is equivalent to the “motoring” torque (observed on a dynamometer) arising from internal friction and air pumping losses. It is worth noting that the pumping losses disappear if the engine is driven to a speed high enough to float the valves. Thus, engine braking disappears when an engine over-revs excessively. This can be a serious problem on low-speed truck engines where valve float may occur above 4000 rpm, and has been the cause of runaway accidents on long grades. For a manual transmission with the clutch engaged during braking, the engine braking is multiplied by the currently selected gear ratio. Automatic transmissions with torque converters are designed for power transfer from the engine to the driveline, but are relatively ineffective in the reverse direction; hence, engine drag does not contribute substantially to braking on vehicles so equipped.

Whether or not driveline drag aids in braking depends on the rate of deceleration. If the vehicle is slowing down faster than the driveline components would slow down under their own friction, the drive wheel brakes must pick up the extra load of decelerating the driveline during the braking maneuver. On the other hand, during low-level decelerations the driveline drag may be sufficient to decelerate the rotating driveline components and contribute to the braking effort on the drive wheels as well.

Grade

Road grade will contribute directly to the braking effort, either in a positive sense (uphill) or negative (downhill). Grade is defined as the rise over the run (vertical over horizontal distance). The additional force on the vehicle arising from grade, R_g , is given by:

$$R_g = W \sin \Theta \quad (3.14)$$

For small angles typical of most grades:

$$\Theta(\text{rad}) \cong \text{Grade} = \text{Rise/run}$$

$$R_g = W \sin \Theta \cong W\Theta$$

Thus a grade of 4% (0.04) will be equivalent to a deceleration of $\pm 0.04 \text{ g}$ (1.3 ft/sec^2).

Brakes

Automotive brakes in common usage today are of two types—drum and disc [1, 2, 3] as shown in [Figure 3.1](#).

Historically, drum brakes have seen common usage in the U.S. because of their high brake factor and the easy incorporation of parking brake features. On the negative side, drum brakes may not be as consistent in torque performance as disc brakes. The lower brake factors of disc brakes require higher actuation effort, and development of integral parking brake features has been required before disc brakes could be used for all wheel positions.

Brake Factor

The brake factor is a mechanical advantage that can be utilized in drum brakes to minimize required actuation effort. The mechanism of a common drum brake is shown in simplified form in [Figure 3.2](#). The brake consists of two shoes pivoted at the bottom. The application of an actuation force, P_a , pushes the lining against the drum generating a friction force whose magnitude is the normal load times the coefficient of friction (μ) of the lining material against the drum. Taking moments about the pivot point for shoe A:

$$\Sigma M_p = eP_a + n\mu N_A - mN_A = 0 \quad (3.15)$$

where:

e = Perpendicular distance from actuation force to pivot

N_A = Normal force between lining A and drum

n = Perpendicular distance from lining friction force to pivot

m = Perpendicular distance from the normal force to the pivot

FIGURE 3.1 Drum brake and disc brake.

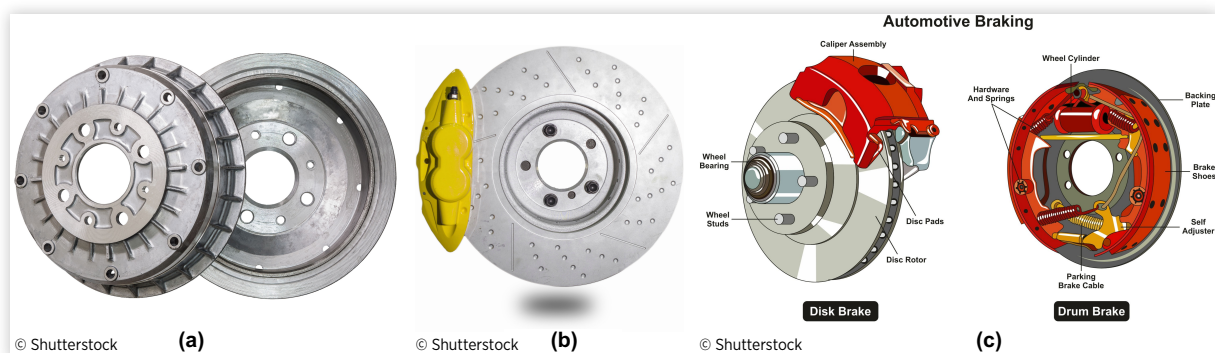
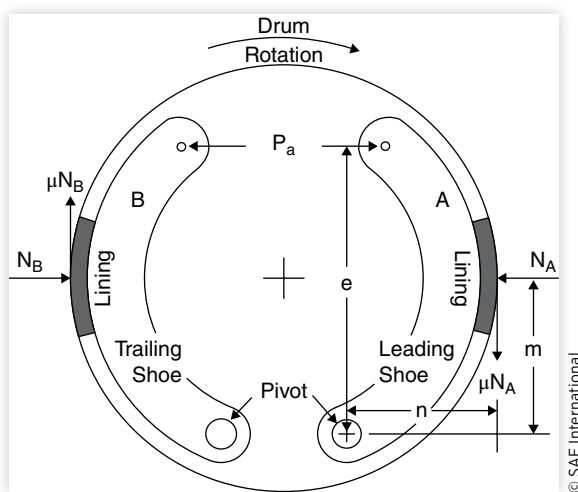


FIGURE 3.2 Forces acting on the shoes of a simple drum brake.



Shoe B is a trailing shoe configuration on which the friction force acts to reduce the application force. The brake factor is much lower, and higher application forces are required to achieve the desired braking torque.

By using two leading shoes, two trailing shoes, or one of each, different brake factors can be obtained. The duo-servo brake has two leading shoes coupled together to obtain a very high brake factor. The consequences of using high brake factors is sensitivity to the lining coefficient of friction, and the possibility of more noise or squeal. Small changes in μ due to heating, wear, or other factors cause the brake to behave more erratically. Since disc brakes lack this self-actuation effect they generally have better torque consistency, although at the cost of requiring more actuation effort.

The difference between the two types of brakes can usually be seen in their torque properties during a stop. Brake torque performance can be measured in the laboratory using an inertial dynamometer, which is simply a large rotating mass attached to the drum with provisions to measure the torque obtained. The brake is applied with a constant actuation force to stop a rotating inertia nominally equivalent to the mass carried at the wheel on which it might be used. The torque measured during the stop typically looks like that shown in [Figure 3.3](#).

The friction force developed by each brake shoe is:

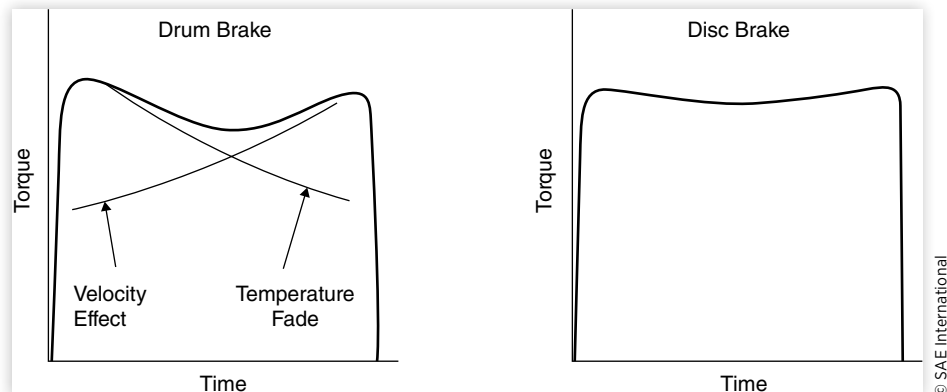
$$F_A = \mu N_A \quad \text{and} \quad F_B = \mu N_B$$

[Equation \(3.15\)](#) can be manipulated to obtain:

$$\frac{F_A}{P_a} = \frac{\mu e}{(m - \mu n)} \quad \text{and} \quad \frac{F_B}{P_a} = \frac{\mu e}{(m + \mu n)} \quad (3.16)$$

The shoe on the right is a “leading” shoe. The moment produced by the friction force on the shoe acts to rotate it against the drum and increase the friction force developed. This “self-servo” action yields a mechanical advantage characterized as the “brake factor.” The brake factor is not only proportional to μ in the numerator, but is increased by its influence in the denominator. (The expressions become more complicated with lining distributed over a larger arc, but show the same effect.) Clearly, if μ gets too large, the term “ μn ” may equal “ m ” and the brake factor goes to infinity, in which case the brake will lock on application.

FIGURE 3.3 Inertia dynamometer torque measurements.



On drum brakes, the torque will often exhibit a “sag” in the intermediate portion of the stop. It has been hypothesized that this effect is due to the combination of temperature fade and velocity effects (torque increases as velocity decreases). Disc brakes normally show less torque variation in the course of a stop. With an excess of these variations during a brake application, it can be difficult to maintain the proper balance between front and rear braking effort during a maximum-effort stop. Ultimately this can show up as less consistent deceleration performance in braking maneuvers resulting in longer stopping distances [4].

The torque from the brake can be modeled from the curves such as shown in [Figure 3.3](#), but can be difficult to predict accurately over all conditions of operation. The torque normally increases almost linearly with the actuation effort, P_a , but to levels that vary with the speed and the energy absorbed (through the temperatures generated). This relationship can be represented as:

$$T_b = f(P_a, \text{Velocity, Temperature}) \quad (3.17)$$

Efforts to model brakes by a general equation including each of the independent factors and the interrelated effects results in a torque equation which may require up to 27 coefficients. Because the equation depends on the brake temperature which increases during a brake application, it is necessary to incorporate a thermal model of the brake in the calculation process [5]. Experience at The University of Michigan in trying to model brake torque performance in this fashion has been only partially successful. For moderate-level applications, good predictions can be obtained. However, a high-energy application (in which the temperature gets above 650°F) will permanently change the brake such that a new set of 27 coefficients must be determined.

The torque produced by the brake acts to generate a braking force at the ground and to decelerate the wheels and driveline components. Then:

$$F_b = \frac{(T_b - I_w \alpha_w)}{r} \quad (3.18)$$

where:

r = Rolling radius of the tires

I_w = Rotational inertia of wheels (and drive components)

α_w = Rotational deceleration of wheels

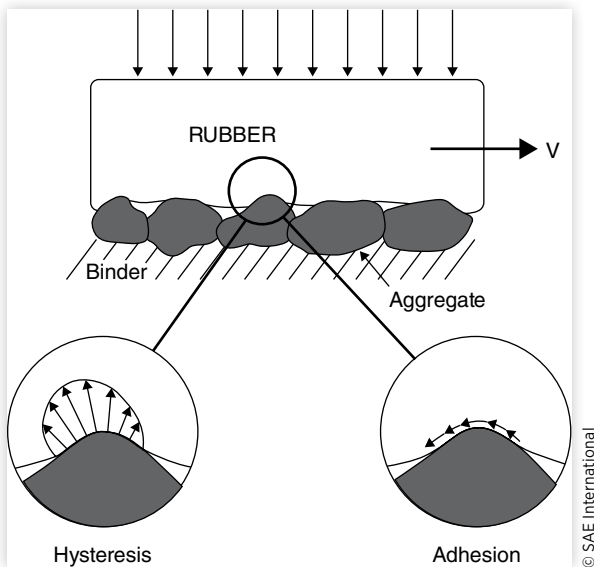
Except during a wheel lockup process, α_w is related to the deceleration of the vehicle through the radius of the wheel ($\alpha_w = a_x/r$), and I_w may be simply lumped in with the vehicle mass for convenience in calculations. In that case the torque and brake force are related by the relationship:

$$F_b = \frac{T_b}{r} \quad (3.19)$$

Tire-Road Friction

As long as all wheels are rolling, the braking forces on a vehicle can be predicted using [Equation \(3.19\)](#). However, the brake force can only increase to the limit of the frictional coupling between the tire and road.

There are two primary mechanisms responsible for friction coupling, as illustrated in [Figure 3.4](#). Surface adhesion arises from the intermolecular bonds between the rubber and the aggregate in the road surface. The adhesion component is the larger of the two mechanisms on dry roads, but is reduced substantially when the road surface is contaminated with water. This is the source of friction loss on wet roads.

FIGURE 3.4 Mechanisms of tire-road friction [6].

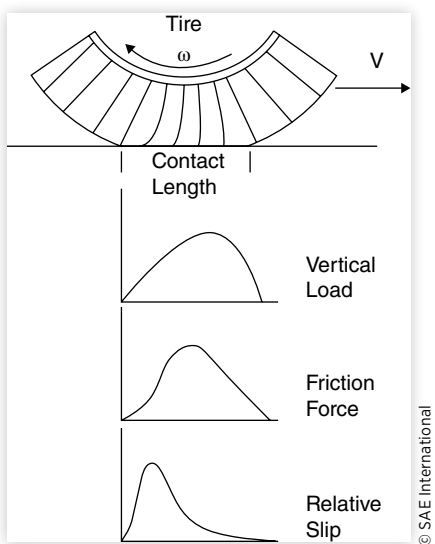
Because of these mechanisms, brake force and slip coexist. Brake force (expressed as a coefficient F_x/F_z) is shown as a function of slip in [Figure 3.6](#). Slip of the tire is defined by the ratio of slip velocity in the contact patch (forward velocity - tire circumferential speed) to forward velocity:

$$\text{Slip} = \frac{V - \omega r}{V} \quad (3.20)$$

where:

V = Vehicle forward velocity

ω = Tire rotational speed (rad/sec)

FIGURE 3.5 Braking deformations in the contact patch.

The bulk hysteresis mechanism represents energy loss in the rubber as it deforms when sliding over the aggregate in the road. Bulk (or hysteretic) friction is not so affected by water on the road surface. As a result, better wet traction is achieved with tires that have high hysteresis rubber in the tread.

Both adhesive and hysteretic friction depend on some small amount of slip occurring at the tire-road interface. Additional slip is observed as a result of the deformation of the rubber elements of the tire tread as they deform to develop and sustain the braking force. This mechanism is illustrated in [Figure 3.5](#). As the element enters the tire contact patch, it is undeformed. As the element proceeds into the center of tire contact, deformation must occur for the tire to sustain a friction force. The deformation increases from the front to the back of the tire contact patch, and the force developed by each element increases proportionately from front to back. At high braking levels, the elements in the rear extreme of the contact patch begin to slide on the surface, and the braking force from the tire may begin to decrease.

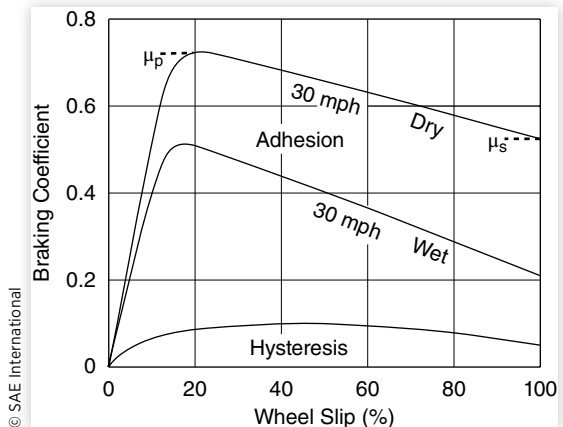
The brake coefficient deriving from adhesive and hysteretic friction increases with slip up to about 10 to 20% in magnitude depending on conditions. Under wet road conditions, the adhesive friction contribution is diminished such that the overall coefficient is lower. The peak coefficient is a key property, usually denoted by μ_p . It establishes the maximum braking force that can be obtained from the particular tire-road friction pair. At higher slip the coefficient diminishes, reaching its lowest value at 100% slip, representing the full lock condition and denoted by μ_s . In a braking situation, μ_p corresponds to the highest brake force that can be generated, and is only theoretically possible to achieve because the system is unstable at this point. For a given brake torque output level, once the wheel is decelerated to achieve μ_p , any disturbance about this condition results in an excess of brake torque, causing further deceleration of the wheel. The increased slip reduces the brake force such that the wheel deceleration continues and the wheel goes to lock. Only a brake release (as in an anti-lock control) can return the wheel to operation at μ_p .

In addition to the tire and the road as key elements in determining the friction coupling available, other variables are important, as described in the following sections.

Velocity

On dry roads, both peak and slide friction decrease with velocity. Under wet conditions, even greater speed sensitivity prevails because of the difficulty of displacing water in the contact patch at high speeds. When the speed and water film thickness are sufficient, the tire tread will lift from the road, creating a condition known as hydroplaning.

FIGURE 3.6 Braking coefficient versus slip [6].



Inflation Pressure

On dry roads, peak and slide coefficients are only mildly affected by inflation pressure. On wet surfaces, inflation pressure increases are known to significantly improve both coefficients.

Vertical Load

Increasing vertical load is known to categorically reduce normalized traction levels (F_x/F_z) under both wet and dry conditions. In other words, as the load increases, the peak and slide friction forces do not increase proportionately. In the vicinity of a tire's rated load, both coefficients will decrease on the order of 0.01 for a 10% increase in load.

Example Problems

- Consider a light truck weighing 3635 lb, performing a full stop from 60 mph on a level surface with a brake application that develops a steady brake force of 2000 lb. Determine the deceleration, stopping distance, time to stop, energy dissipated, and the brake horsepower at initial application and averaged over the stop. Neglect aerodynamic and rolling resistance forces.

Solution:

The deceleration may be calculated from Newton's Second Law:

$$D_x = \frac{F_x}{M} = \frac{F_b}{M} = \frac{(2000 \text{ lb}) 32.2 \text{ ft/sec}^2}{3635 \text{ lb}} = 17.72 \frac{\text{ft}}{\text{sec}^2}$$

The deceleration can be computed directly in terms of g's by using the form:

$$D_x(g) = \frac{F_x}{W} = \frac{F_b}{W} = \frac{2000 \text{ lb}}{3635 \text{ lb}} = 0.55 \text{ g} = 12.08 \frac{\text{mph}}{\text{sec}}$$

Now that the deceleration is known, the stopping distance may be computed using Equation (3.6):

$$\begin{aligned} SD &= \frac{V_o^2}{F_{xt}} = \frac{V_o^2}{2D_x} \\ &= \frac{(88 \text{ ft/sec})^2}{2(17.72 \text{ ft/sec}^2)} = 218.51 \text{ ft} \end{aligned} \quad (3.6)$$

The time to stop comes from Equation (3.7):

$$t_s = \frac{V_o}{F_{xt}/M} = \frac{88 \text{ ft/sec}}{17.72 \text{ ft/sec}^2} = 4.966 \text{ sec}$$

The energy dissipated comes from Equation (3.11):

$$\begin{aligned} \text{Energy} &= \frac{M}{2}(V_o^2 - V_f^2) = \frac{3635 \text{ lb}}{2(32.2 \text{ ft/sec}^2)} (88 \text{ ft/sec})^2 \\ &= 437,103 \text{ ft-lb} \end{aligned}$$

The power dissipation at the point of brake application is simply the brake force times the forward velocity, which is:

$$\text{Power (initial)} = (2000 \text{ lb})88 \text{ ft/sec} = 176,000 \text{ ft-lb/sec}$$

$$\text{HP(initial)} = \left(176,000 \frac{\text{ft-lb}}{\text{sec}} \right) \frac{1 \text{ hp}}{550 \text{ ft-lb/sec}} = 320 \text{ hp}$$

On average over the stop, the power may be computed using Equation (3.12) is:

$$\begin{aligned} \text{Power} &= \frac{M V_o^2}{2 t_s} = \frac{3635 \text{ lb}}{2(32.2 \text{ ft/sec}^2)} \frac{(88 \text{ ft/sec})^2}{4.966 \text{ sec}} \\ &= \frac{437,103 \text{ ft-lb}}{4.966 \text{ sec}} = 88,019 \frac{\text{ft-lb}}{\text{sec}} = 160 \text{ hp} \end{aligned}$$

2. For the vehicle described in the previous problem, calculate the stopping distance taking aerodynamic drag into account. The aerodynamic drag force will be given by:

$$F_a = CV^2 = 0.00935 \left(\frac{\text{lb-sec}^2}{\text{ft}^2} \right) V^2 \left(\frac{\text{ft}^2}{\text{sec}^2} \right)$$

The stopping distance may be computed from Equation (3.10):

$$\begin{aligned} SD &= \frac{M}{2C} \ln \left[\frac{(F_b + CV_o^2)}{F_b} \right] \\ &= \frac{3635 \text{ lb}}{2 \left(0.00935 \frac{\text{lb-sec}^2}{\text{ft}^2} \right) \left(32.2 \frac{\text{ft}}{\text{sec}^2} \right)} \ln \frac{2000 \text{ lb} + 0.00935 \frac{\text{lb-sec}^2}{\text{ft}^2} \left(88 \frac{\text{ft}}{\text{sec}} \right)^2}{2000 \text{ lb}} \\ &= 214.69 \text{ ft} \end{aligned} \quad (3.10)$$

Thus, roughly 4 ft will be cut from the stopping distance when aerodynamic drag is included in the calculation. The drag itself is only 74.4 lb at the beginning of the stop and decreases with the square of the velocity, so its contribution decreases over the course of the stopping maneuver.

Federal Requirements for Braking Performance

Out of the public concern for automotive safety in the 1960s, the Highway Safety Act of 1965 was passed establishing the National Highway Traffic Safety Administration (NHTSA), charged with promulgating performance standards for new vehicles such that safety on highways would be increased. Among the many standards that have been imposed are Federal Motor Vehicle Safety Standard (FMVSS) 105 [7], establishing braking performance requirements for vehicles with hydraulic brake systems, and FMVSS 121 [4], establishing braking performance requirements for vehicles with air brake systems.

FMVSS 105 defines service brake and parking brake performance requirements over a broad range of conditions, such as:

- Lightly loaded to fully loaded at gross vehicle weight rating (GVWR)
- Preburnish to full burnish conditions
- Speeds from 30 to 100 mph
- Partially failed systems tests
- Failure indicator systems
- Water recovery
- Fade and recovery
- Brake control force limits

Although the standard is quite detailed and complex, the requirements for stopping distance performance can be summarized into five tests:

1. First effectiveness—A fully loaded passenger car with new, unburnished brakes must be able to stop from speeds of 30 and 60 mph in distances that correspond to average decelerations of 17 and 18 ft/sec², respectively.
2. Second effectiveness—A fully loaded passenger car with burnished* brakes must be able to stop from 30, 60, and 80 mph in distances that correspond to average decelerations of 17, 19 and 18 ft/sec², respectively.
3. Third effectiveness—A lightly loaded passenger car with burnished brakes must be able to stop from 60 mph in a distance that corresponds to an average deceleration of 20 ft/sec².
4. Fourth effectiveness—A fully loaded passenger car with burnished brakes must be able to stop from 30, 60, 80, and 100 mph in distances that correspond to average decelerations of 17, 18, 17, and 16 ft/sec², respectively.
5. Partial failure—A lightly loaded and fully loaded passenger car with a failure in the brake system must be able to stop from 60 mph in a distance that corresponds to an average deceleration of 8.5 ft/sec².

* Burnish refers to a process in which new brakes are “worn in” by repeated brake applications according to a procedure defined in the standard.

It is notable that the hydraulic brake standard (FMVSS 105) has stopping distance requirements only for dry surfaces of an 81 Skid Number. Skid Number is the tire-road friction coefficient measured by the American Society for Testing and Materials Method E-274-85 [8]. Although the Skid Number is measured with a special, standard tire, the Skid Number and coefficient of friction are generally assumed to be equivalent. The air brake vehicle standard (FMVSS 121) has stopping distance performance requirements on both wet surfaces (30 Skid Number) and dry surfaces (81 Skid Number). Obviously, the prudent brake system engineer considers a range of surface friction conditions, from at least 30 to 81 SN, regardless of any gaps in the Federal performance standards.

Brake Proportioning

The braking decelerations achievable on a vehicle are simply the product of application level and the brake gains (torque/pressure) up to the point where lockup will occur on one of the axles. Lockup reduces the brake force on an axle and results in some loss of ability to control the vehicle. It is well recognized that the preferred design is to bring both axles up to the lockup point simultaneously. Unfortunately, this is not possible over the complete range of operating conditions to which a vehicle will be exposed. Balancing the brake outputs on both the front and rear axles is achieved by “proportioning” the pressure appropriately for the foundation brakes installed on the vehicle. Proportioning then adjusts the brake torque output at the front and rear wheels in accordance with the peak traction forces possible.

The first-order determinants of peak traction force on an axle are the instantaneous load and the peak coefficient of friction. During braking, a dynamic load transfer from the rear to the front axle occurs such that the load on an axle is the static plus the dynamic load transfer contributions. Thus for a deceleration, D_x :

$$W_f = \frac{c}{L} W + \frac{h}{L} \frac{W}{g} D_x = W_{fs} + W_d \quad (3.21)$$

and

$$W_r = \frac{b}{L} W - \frac{h}{L} \frac{W}{g} D_x = W_{rs} - W_d \quad (3.22)$$

where:

W_{fs} = Front axle static load

W_{rs} = Rear axle static load

$W_d = (h/L)(W/g)D_x$ = Dynamic load transfer

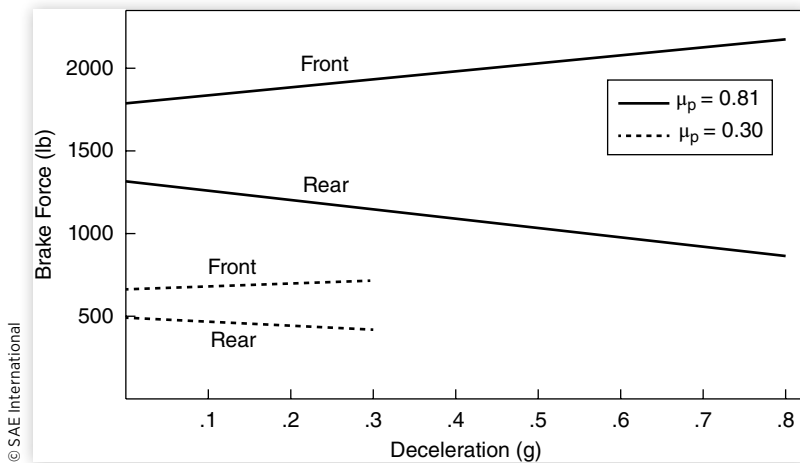
Then, on each axle the maximum brake force is given by:

$$F_{xmf} = \mu_p W_f = \mu_p \left(W_{fs} + \frac{h}{L} \frac{W}{g} D_x \right) \quad (3.23)$$

and

$$F_{xmr} = \mu_p W_r = \mu_p \left(W_{rs} - \frac{h}{L} \frac{W}{g} D_x \right) \quad (3.24)$$

where μ_p is the peak coefficient of friction.

FIGURE 3.7 Maximum brake forces as a function of deceleration.

The maximum brake force is dependent on the deceleration, varying differently at each axle. **Figure 3.7** shows graphically the maximum brake forces according to the above equations for a typical passenger car on both a high and low coefficient surface. The deceleration is shown in units of g's (equivalent to D/g). Attempts at braking on an axle above the boundary value results in brake lockup on that axle.

Inasmuch as the equations above contain the deceleration as a variable, they do not provide an explicit solution for the maximum braking forces on an axle. These can be obtained by recognizing that the deceleration is a function of the total braking force imposed on the vehicle (neglecting for simplicity the other forces that may be present). To solve for F_{xmf} , we can use the relationship:

$$D_x = \frac{(F_{xmf} + F_{xr})}{M} \quad (3.25)$$

and for F_{xmr} :

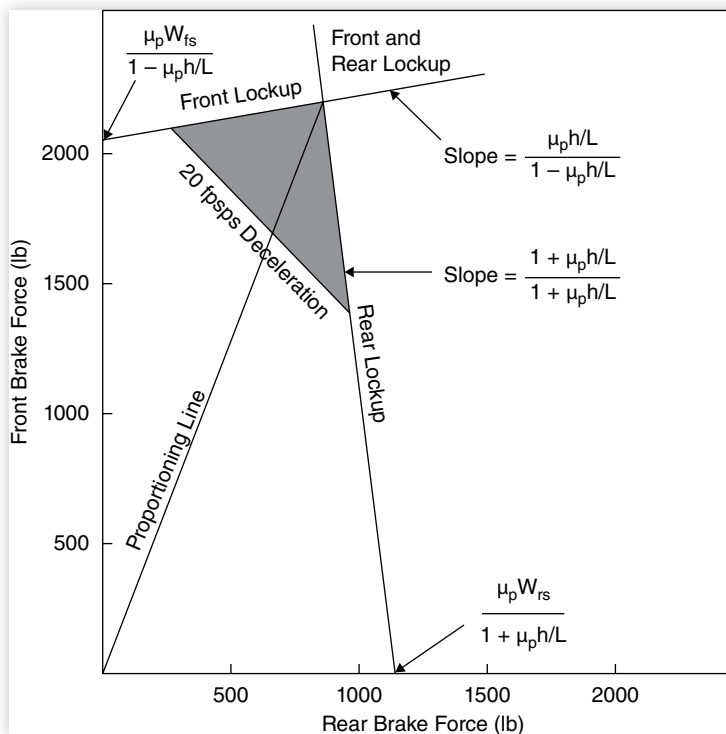
$$D_x = \frac{(F_{xmr} + F_{xf})}{M} \quad (3.26)$$

Substituting into Equations (3.23) and (3.24) yields the following equations for the maximum braking force on each axle:

$$F_{xmf} = \frac{\mu_p \left(W_{fs} + \frac{h}{L} F_{xr} \right)}{1 - \mu_p \frac{h}{L}} \quad (3.27)$$

$$F_{xmr} = \frac{\mu_p \left(W_{rs} - \frac{h}{L} F_{xf} \right)}{1 + \mu_p \frac{h}{L}} \quad (3.28)$$

This tells us that the maximum braking force on the front axle is dependent on the (1) braking forces on the rear axle throughout the course of the deceleration maneuver, as well as (2) any forward load transfer resulting from the application of the rear brakes.

FIGURE 3.8 Maximum braking forces on the front and rear axles.

© SAE International

Conversely, the same effect is evident on the rear axle. These relationships can best be visualized by plotting the rear versus front brake forces as shown in [Figure 3.8](#).

The horizontal axis represents rear brake force and is generally proportional to the rear brake pressure (related by the torque-to-pressure relationship for that foundation brake). The vertical axis is front brake force, again proportional to front brake pressure in accordance with the brake gain. The origin of each line is obtained from [Equations \(3.27\)](#) and [\(3.28\)](#) by setting the brake force of the opposite brake to zero.

Lines for the maximum front axle brake force slope upward and to the right (positive) at the slope of $\mu_p h/L/(1 - \mu_p h/L)$. Lines for the rear axle maximum brake force slope downward and to the right (negative) with a slope that is equal to $-\mu_p h/L/(1 + \mu_p h/L)$. Increasing the surface coefficient or the vehicle C.G. height increases the slopes of the maximum brake force lines on the graph. Varying the load condition on the vehicle translates the origin of each of the lines on the graph. The intersection point for the front and rear brake boundaries can be determined by manipulating [Equations \(3.27\)](#) and [\(3.28\)](#). Designating the points as F_{xfi} and F_{xri} , it can be shown that these coordinates are:

$$F_{xfi} = \mu \left(W_{fs} + \mu W \frac{h}{L} \right) \quad (3.29)$$

$$F_{xri} = \mu \left(W_{rs} - \mu W \frac{h}{L} \right) \quad (3.30)$$

An attempt to brake the vehicle to a level that goes above the front brake force boundary will cause front wheel lockup to occur, and steering control will be lost. Likewise, braking effort that falls to the right of the rear brake boundary causes rear

wheel lockup, placing the vehicle in an unstable condition. The instability has safety implications and therefore warrants careful consideration in the design of the brake system. This issue is discussed in more detail in a later section.

In a graph of the form of [Figure 3.8](#), the deceleration is proportional to the sum of the front and rear brake forces. Thus 2,000 lb of front brake force with zero rear force, 1,000 lb front with 1,000 lb rear, and zero front with 2,000 lb rear brake force, all correspond to the same deceleration level, and a line of constant deceleration can be plotted by connecting these points. If the same scale is used for the front and rear brake forces, lines of constant deceleration plot as 45-deg. diagonals on the graph.

If a deceleration capability of 20 ft/sec^2 is required on the 0.81μ surface, any combination of front to rear brake force would satisfy that requirement so long as it falls in the triangle bounded by the deceleration line and the maximum brake force lines for the 0.81μ surface.

"Brake proportioning" describes the relationship between front and rear brake forces determined by the pressure applied to each brake and the gain of each. It is represented by a line on the graph starting at the origin and extending upward and to the right. A fixed, or constant, proportioning is represented by a straight line.

The primary challenge in brake system design is the task of selecting a proportioning ratio (the slope of a line on the graph) that will satisfy all design goals despite the variabilities in surface friction, front/rear weight distribution, vehicle C.G. height, and brake condition. A number of these objectives are defined by the FMVSS 105 braking standard in the various effectiveness tests, although performance objectives for low coefficient surfaces should be included by the brake engineer as well. To date, low coefficient performance has only been specified in FMVSS 121, which defines braking performance requirements for air-braked trucks.

The primary factor determining brake proportioning is the gain of the brakes used on the front and rear wheels. The brake force on individual wheels can be described by the equation:

$$F_b = \frac{T_b}{r} = G \frac{P_a}{r} \quad (3.31)$$

where:

F_b = Brake force

T_b = Brake torque

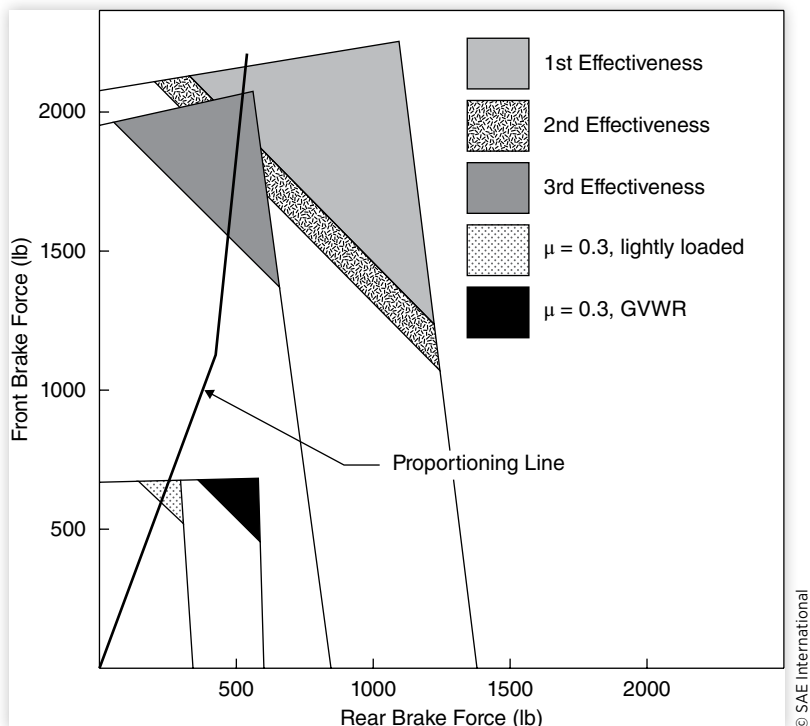
r = Tire rolling radius

G = Brake gain (in-lb/psi)

P_a = Application pressure

Achieving good performance over the full range of conditions under which a vehicle operates can be difficult. As an example of the complexity that can be experienced in trying to identify appropriate brake proportioning, consider the case shown in [Figure 3.9](#). The figure illustrates the range of variations that arise from vehicle loading (lightly loaded and GVWR) and surface friction (30 and 81 SN). On the graph the brake force boundaries and deceleration requirements have been plotted for the FMVSS 105 dry surface tests conditions. In addition, similar boundaries have been plotted for wet road conditions assuming a friction coefficient of 30 SN. Under the wet conditions, a deceleration performance goal of 8 ft/sec^2 (0.25 g) has been assumed.

To achieve all performance goals, a proportioning design must be selected that passes through all of the triangles shown. This cannot be achieved with a straight line providing a constant relationship between front and rear brake force. A solution to this problem is to incorporate a valve in the hydraulic system that changes the pressure going

FIGURE 3.9 Front/rear brake force graph for multiple braking conditions.

to the rear brakes over some portion of the operating pressure range. Such a valve is known as a pressure proportioning valve. Most pressure proportioning valves in common use today provide equal pressure to both front and rear brakes up to a certain pressure level, and then reduce the rate of pressure increase to one of the brakes thereafter. A proportioning valve identified as a “500/0.3” means that the pressure to the front and rear brakes is equal up to 500 psi. Above this level the pressure proportioned to the rear brakes increases at only 30% of the rate going to the front brakes. That is:

$$P_f = P_r = P_a = \text{Application pressure} \quad \text{for } P_a < 500 \text{ psi} \quad (3.32a)$$

$$P_f = P_a \quad \text{and} \quad P_r = 500 + 0.3(P_a - 500) \quad \text{for } P_a > 500 \text{ psi} \quad (3.32b)$$

With this proportioning we can see that it is possible to achieve a front/rear brake balance satisfying all dry surface conditions as evidenced by the fact that the proportioning line passes through all of the performance triangles. The only exception is the fully loaded vehicle (GVWR) on the low coefficient surface, where the brake proportioning will not quite achieve 0.25 g. In every case, the plot indicates that front lockup will occur first.

Achieving good proportioning is especially difficult on trucks because of the disparity between loaded and empty conditions. Typically, the performance triangles do not overlap in those cases, so no choice of proportioning will satisfy all goals. Several solutions are available. In Europe, load-sensing proportioning valves have been used on trucks for some years. These valves, installed on the axle(s), sense the load condition and adjust the brake proportioning appropriately. Less commonly used is the inertia-proportioning valve which senses the deceleration rate and can adjust proportioning in

accordance with the deceleration level. Finally, anti-lock brake systems offer a versatile method of automatically proportioning brakes that is becoming well accepted in the automotive industry.

Anti-lock Brake Systems

Rather than attempt to adjust the proportioning directly, anti-lock systems (ABS) sense when wheel lockup occurs, release the brakes momentarily on locked wheels, and reapply them when the wheel spins up again. Modern anti-lock brake systems are capable of releasing the brakes before the wheel goes to full lockup, and modulating the level of pressure on reapplication to momentarily hold the wheel near peak slip conditions.

The concept of ABS dates back to the 1930s but has only become truly practical with electronics available on modern vehicles. An ABS consists of an electronic control unit (ECU), a solenoid for releasing and reapplying pressure to a brake, and a wheel speed sensor. The ECU normally monitors vehicle speed through the wheel speed sensors, and upon brake application begins to compute an estimate of the diminishing speed of the vehicle. Actual wheel speeds can be compared against the computed speed to determine whether a wheel is slipping excessively, or the deceleration rate of a wheel can be monitored to determine when the wheel is advancing toward lockup. Different ABS designs use different combinations of these variables to determine when lockup is imminent and brake release is warranted. At that point a command signal is sent to the solenoid to release the brake pressure, allowing the wheel to spin back up. Once the wheel regains speed, the pressure is increased again. Depending on the refinement of the control algorithms, the pressure rise rate and the final pressure may be controlled to minimize cycling of the brakes.

Figure 3.10 shows a typical plot of wheel speed cycling during the stop of a vehicle with ABS. When the brakes are first applied, wheel speeds diminish more or less in accordance with the vehicle speed in the first region of the plot (point 1). If the brakes are applied to a high level, or the road is slippery, the speed of one or more wheels begins to drop rapidly (point 2), indicating that the tire has gone through the peak of the μ -slip

FIGURE 3.10 Wheel speed cycling during ABS operation.

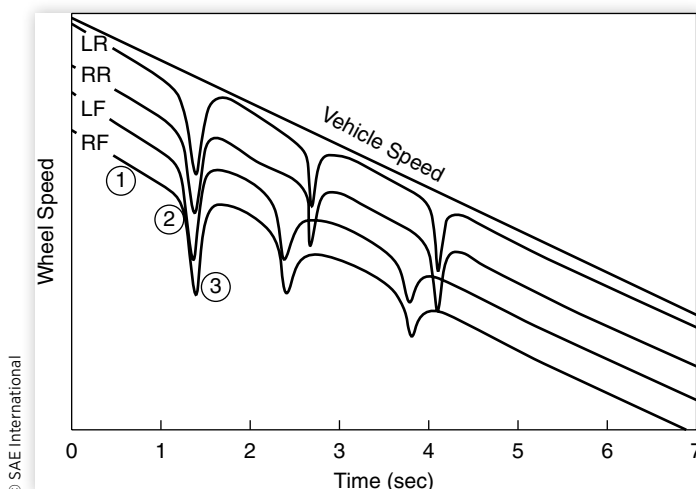
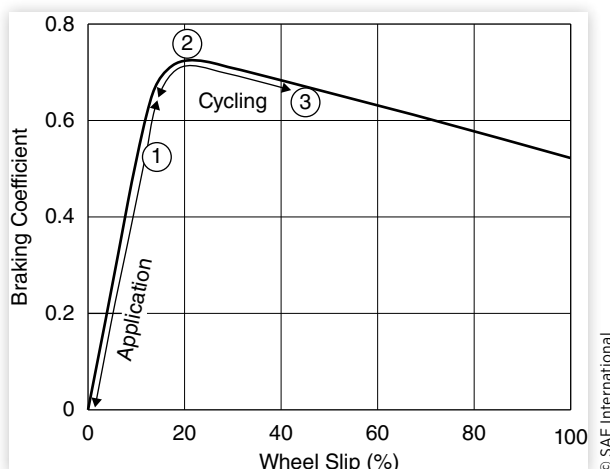


FIGURE 3.11 ABS operation to stay at the peak braking coefficient.



curve and is heading toward lockup. At this point the ABS intervenes and releases the brakes on those wheels before lockup occurs (point 3). Once the wheel speed picks up again, the brakes are reapplied. The objective of the ABS is to keep each tire on the vehicle operating near the peak of the μ -slip curve for that tire. This is illustrated in [Figure 3.11](#).

Braking Efficiency

Recognizing that braking performance of any vehicle will vary according to the friction of the road surface on which it is attempted, the concept of braking efficiency has been developed as a measure of performance. Braking efficiency, η_b , may be defined as the ratio of actual deceleration achieved to the “best” performance possible on the given road surface. It can be shown with the use of the equations presented earlier that the best

performance any vehicle can achieve is a braking deceleration (in g's) equivalent to the coefficient of friction between the tires and the road surface. That is:

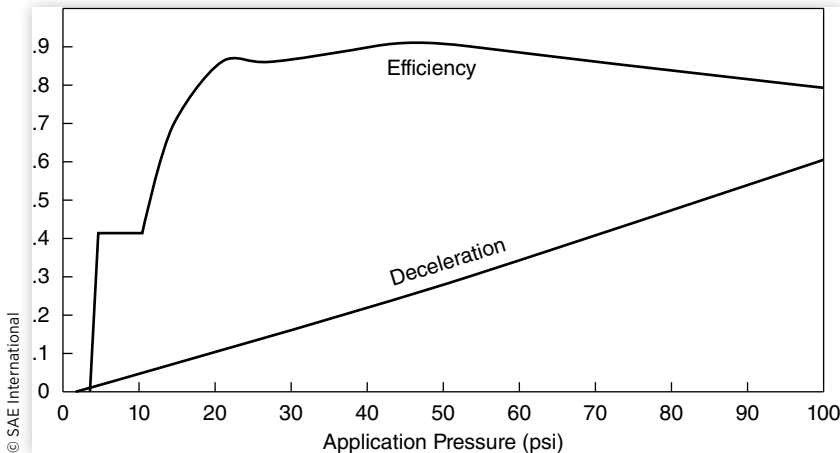
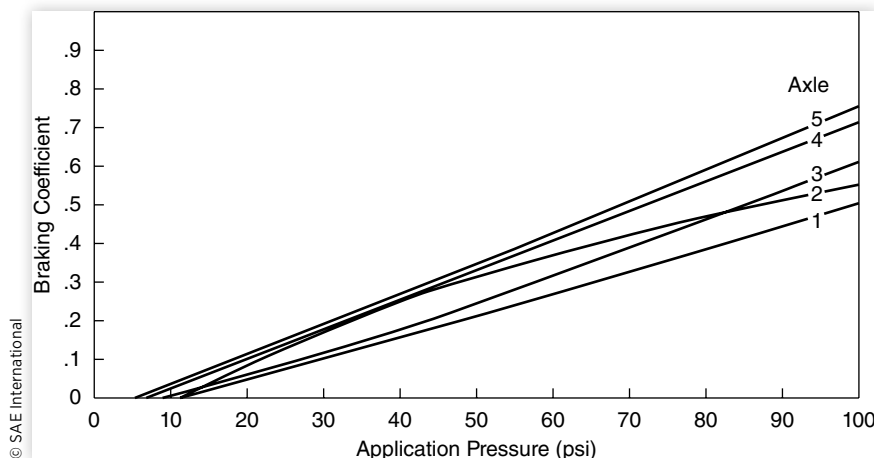
$$\eta_b = \frac{D_{act}}{\mu_p} \quad (3.33)$$

The braking efficiency concept is useful as a design tool for the engineer to assess success in optimizing the vehicle braking system [9]. Yet implementation of braking standards using the braking efficiency approach (to avoid the problems of designating surfaces with standard friction levels via the ASTM Skid Number [8]) has been unsuccessful. The main problem has been the difficulty of defining an effective friction level for a tire-road surface pair because of the variations in friction with velocity, wheel load, tire type, and other factors.

Braking efficiency is determined by calculating the brake forces, deceleration, axle loads, and braking coefficient on each axle as a function of application pressure. The braking coefficient is defined as the ratio of brake force to load on a wheel or axle. The braking efficiency at any level of application pressure is the deceleration divided by the highest braking coefficient of any axle. Since the axle with the highest braking coefficient defines the required level of road friction, the braking efficiency is also equal to the ratio of deceleration to the required road surface coefficient.

Braking efficiency is a useful method for evaluating the performance of brake systems, especially on heavy trucks where multiple axles are involved. [Figure 3.12](#) shows the braking efficiency calculated for a five-axle tractor-semitrailer.

Contributions to braking from individual axles are better assessed by examining the braking coefficient developed on each. A plot of these curves (sometimes known as a friction utilization plot) is shown in [Figure 3.13](#). Five curves representing the five axles of the combination are shown. Brake coefficient is defined for an axle as the ratio of brake force to load. Ideally, all axles would have the same braking coefficient at a given application pressure, indicating that they all brake in proportion to their load. However, the diverse load conditions, longitudinal load transfer during braking, and the shifting of load between tandem axles due to brake reactions (inter-axle load transfer) preclude

FIGURE 3.12 Efficiency plot for a tractor-semitrailer.**FIGURE 3.13** Braking coefficient on five axles of a tractor-semitrailer.

perfect harmony of the system. This is the reason the braking efficiency falls below the maximum theoretical value of 1. In the case of the tractor-semitrailer shown here, the braking efficiency rises quickly to a value of 0.9 at low brake application pressures, but drops off again at higher pressure due to the spread in braking coefficient among the axles at high deceleration conditions.

Rear Wheel Lockup

In the discussion so far, wheel lockup has been considered only as a boundary on braking performance. However, it has great impact on the handling behavior of the vehicle as well and must be considered by the brake engineer. Once a wheel locks up it loses its ability to generate the cornering forces needed to keep the vehicle oriented on the road.

Lockup of front wheels causes loss of the ability to steer the vehicle, and it will generally continue straight ahead despite any steering inputs, drifting to the side in response to road cross-slope, side winds, and/or lateral asymmetries in the vehicle that result in unequal load conditions (i.e., yaw moment generation factors).

It is well recognized that rear wheel lockup places a motor vehicle in an unstable condition. Once the wheels lock up, any yaw disturbances (which are always present) will initiate a rotation of the vehicle. The front wheels, which yaw with the vehicle, develop a cornering force favoring the rotation, and the yaw angle continues to grow. Only when the vehicle has completely spun around is it again stable. On long vehicles (some trucks and buses) the rotational accelerations are usually slow enough that the driver can apply corrective steer and prevent the full rotation. However, on smaller passenger cars, it is generally accepted that the average driver cannot readily control the vehicle in such a driving situation. As a result, there is a philosophy among automotive engineers that a front brake bias constitutes the preferred design.

The preference for front brake lockup first cannot easily be achieved in a brake system design under all circumstances because of in-use variations in brake gain, vehicle C.G. height (particularly on light trucks), pavement friction, and parking brake requirements. The potential consequences in the hands of the motorist have been estimated using the braking efficiency as the measure of performance [10]. The basis for it arises from studies of driver behavior that show that brake applications occur on the average about 1.5 times per mile. Though most of the brake applications are executed at a moderate level, high decelerations are required in a certain percentage of the brake applications. Braking level demands of motorists are shown in [Figure 3.14](#), which plots the percent of decelerations exceeding given deceleration levels. Twenty percent of all brake applications exceed 0.2 g, while only 1% exceed 0.35 g, and less than 0.1% go up to 0.5 g.

FIGURE 3.14 Distribution of braking decelerations with passenger cars.

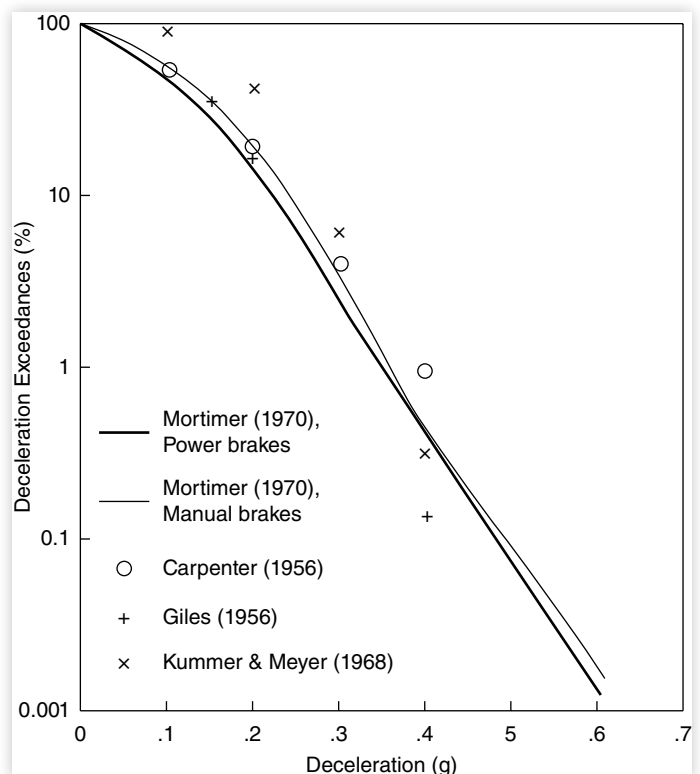
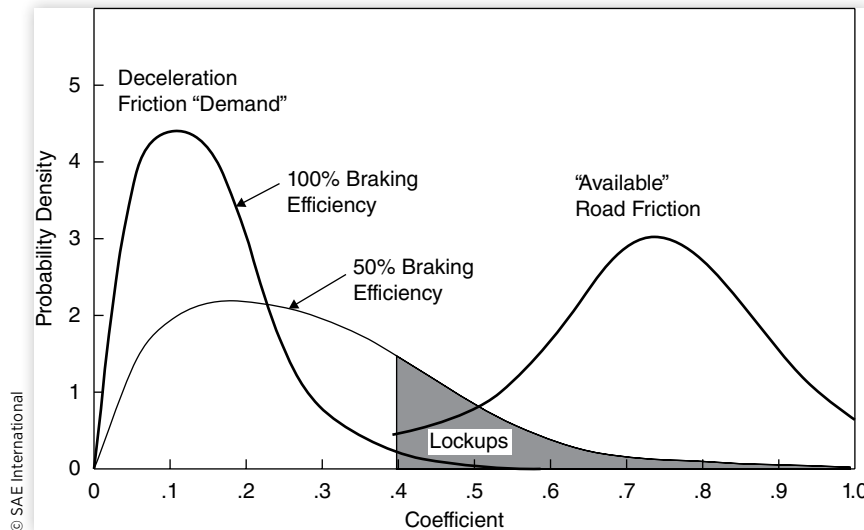


FIGURE 3.15 Comparison of friction demand and availability.

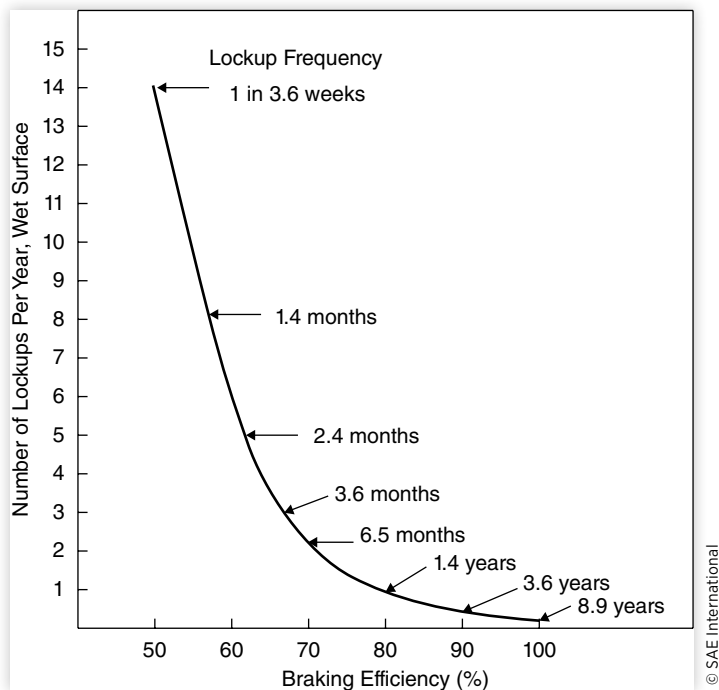


The comparison of deceleration demands in normal driving to the available friction level of roads is shown in [Figure 3.15](#). The distribution of road friction coefficients is estimated from numerous surveys of “skid resistance” routinely made by many highway departments. By and large, most roads have friction levels sufficient to accommodate the deceleration demands of the motorists if the friction is efficiently utilized. That is, if the brake systems on all vehicles were 100% efficient under all conditions, little overlap would occur in the braking “demand” and friction “available” curves, and there would be few braking instances in which wheel lockup occurs.

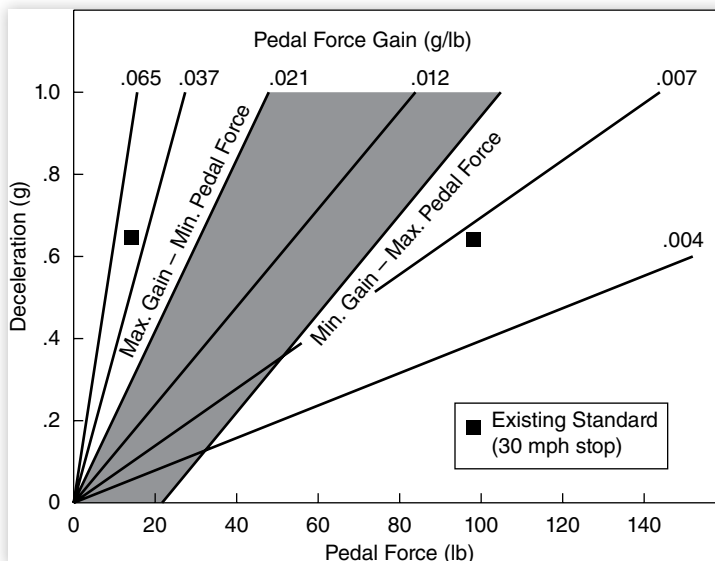
However, when braking efficiency is less than 100%, higher friction is required to achieve a desired deceleration level. With lower efficiency the “friction demand” curve shifts to the right. Thus the overlap and frequency at which braking demand will exceed the friction available will increase. Using the average value of 1.5 brake applications per mile and 10,000 miles per year for a typical passenger car, the frequency of wheel lockup in braking can be estimated for different braking system efficiencies as shown in [Figure 3.16](#). Clearly, it illustrates the acute sensitivity of lockup frequency to braking efficiency. If the inefficiency is due to a rear bias in the brake force distribution, the lockups will occur on the rear axle, and directional instability will result. Most occurrences will be on roads with lower friction levels, which are normally wet road conditions. Since the majority of these instances will occur on roads with friction coefficients in the range of 0.4 to 0.6, particular emphasis should be placed on obtaining good braking system efficiency in this road friction range.

Pedal Force Gain

Ergonomics in the design of a brake system can play an important role in the ease with which the driving public can optimally use the braking capabilities built into a vehicle. Aside from positioning of the brake pedal, the effort and displacement properties of the pedal during braking are recognized as influential design variables. In the 1950s when power brake systems first came into general use, there was little uniformity among manufacturers in the level of effort and pedal displacement properties of the systems.

FIGURE 3.16 Predicted frequency of lockup events.

In 1970 the National Highway Traffic Safety Administration sponsored research to determine ergonomic properties for the brake pedal that would give drivers the most effective control [11]. The research identified an optimum range for pedal force gain—the relationship between pedal force and deceleration. [Figure 3.17](#) shows the results from the NHTSA study indicating the optimal gain values by the shaded area.

FIGURE 3.17 Optimal pedal force gain properties.

Example Problem

Calculate the braking coefficients and braking efficiency for a passenger car in 100 psi increments of application pressure up to 700 psi, given the following information:

Wheelbase = 108.5 in CGH = 20.5 in Tire radius = 12.11 in
 Weight: $W_f = 2210 \text{ lb}$ $W_r = 1864 \text{ lb}$ Total = 4074 lb
 Front brake gain = 20 in-lb/psi Rear brake gain = 14 in-lb/psi
 Proportioning valve design = 290/0.3

Solution:

The easiest way to visualize the answer is to tabulate data in columns as shown below. The calculation steps are as follows:

1. The front application pressure is the reference, so we list values from 100 and up.
2. The rear application pressure is calculated from the front using the relationship similar to that given in Equation (3.32). Namely,

$$P_r = P_a \quad \text{for } P_a < 290 \text{ psi} \quad (3.32a)$$

$$P_r = 290 + 0.3(P_a - 290) \quad \text{for } P_a > 290 \text{ psi} \quad (3.32b)$$

3. The front and rear brake forces are the product of the application pressure on that brake, times the torque gain, times two brakes per axle, then divided by tire radius.

$$F_{xf} = 2G_f \frac{P_f}{r} \quad \text{and} \quad F_{xr} = 2G_r \frac{P_r}{r}$$

4. The deceleration is the sum of the brake forces divided by the total vehicle weight (this results in deceleration in units of g).

$$D_x = \frac{F_{xf} + F_{xr}}{W}$$

5. The front and rear axle loads are calculated from Equations (3.21) and (3.22).

$$W_f = W_{fs} + (h/L)(W/g)D_x \quad (3.21)$$

and

$$W_r = W_{rs} - (h/L)(W/g)D_x \quad (3.22)$$

where "D_x" is in units of ft/sec².

6. The braking coefficients (μ_f and μ_r) are the ratio of axle brake force to axle load.

$$\mu_f = \frac{F_{xf}}{W_f} \quad \text{and} \quad \mu_r = \frac{F_{xr}}{W_r}$$

7. The braking efficiency, η_b , is the deceleration divided by the highest of the two braking coefficients from the axles.

p_f	P_r	F_f	F_r	D_x	W_f	W_r	μ_f	μ_r	η_b
100 psi	100 psi	330 lb	231 lb	.138 g	2316 lb	1758 lb	.142	.131	97%
200	200	661	462	.276	2422	1652	.273	.280	99
300	293	991	677	.409	2525	1549	.393	.437	94
400	323	1321	747	.508	2601	1473	.508	.507	100
500	353	1651	816	.606	2676	1398	.617	.583	98
600	383	1982	886	.704	2752	1322	.720	.670	98
700	413	2312	955	.802	2827	1247	.818	.766	98

Notes:

- (a) The braking efficiency starts high (97%-99%) by the match of the brake gains and axle loads, but begins to diminish with deceleration because of the decreasing load on the rear axle.
- (b) When the application pressure reaches 290 psi, the proportioning valve “kicks in” reducing the pressure rise rate on the rear axle. This brings things back into balance providing 100% efficiency at 400 psi.

References

1. Newcomb, T.P. and Spurr, R.T., *Braking of Road Vehicles* (London, England: Chapman and Hall, Ltd., 1967), 292pp.
2. Limpert, R., “Analysis and Design of Motor Vehicle Brake Systems,” The University of Michigan, May 1971, 466pp.
3. *Engineering Design Handbook, Analysis and Design of Automotive Brake Systems*, DARCOM-P706-358, US Army Material Development and Readiness Command, Alexandria, VA, December 1976, 252pp.
4. “Standard No. 121; Air Brake Systems,” Code of Federal Regulations, Title 49, Part 571.121, October 1, 1990, 366-382.
5. Johnson, L., Fancher, P.S., and Gillespie, T.D., “An Empirical Model for the Prediction of the Torque Output of Commercial Vehicle Air Brakes,” Highway Safety Research Institute, University of Michigan, Report No. UM-HSRI-78-53, December 1978, 83pp.
6. Meyer, W.E. and Kummer, H.W., “Mechanism of Force Transmission between Tire and Road,” SAE Technical Paper [620407](#), 1962, doi:[10.4271/620407](#).
7. “Standard No. 105; Hydraulic Brake Systems,” Code of Federal Regulations, Title 49, Part 571.105, October 1, 1990, 199-215.
8. “Test Method for Skid Resistance of Paved Surfaces Using a Full-Scale Tire,” *Method E274-85, 1986 Annual Book of ASTM Standards*, American Society for Testing and Materials, Philadelphia, PA.
9. Gillespie, T.D. and Balderas, L., “An Analytical Comparison of a European Heavy Vehicle and a Generic U.S. Heavy Vehicle,” The University of Michigan Transportation Research Institute, Report No. UMTRI-87-17, August 1987, 374pp.
10. Ervin, R.D. and Winkler, C.B., “Estimation of the Probability of Wheel Lockup,” *IAVD Congress on Vehicle Design and Components*, Geneva, March 3-5, 1986, D145-D165.
11. Mortimer, R.E., Segel, L., Dugoff, H., Campbell, J.O. et al., “Brake Force Requirement Study: Driver Vehicle Braking Performance as a Function of Brake System Design Variables,” The University of Michigan Highway Safety Research Institute, Report No. HuF-6, April 1979, 22pp.



Road Loads

© Shutterstock



Virtual Reality technology simulates aerodynamic properties

Aerodynamics

Aerodynamics makes its major impact on modern cars and trucks through its contribution to “road load.” Aerodynamic forces interact with the vehicle causing drag, lift (or downforce), lateral forces, moments in roll, pitch and yaw, and noise. These impact fuel economy, dynamic handling, and NVH.

The aerodynamic forces produced on a vehicle arise from two sources—form (or pressure) drag, and viscous friction. In this chapter we will first examine the mechanics of air flow to explain the nature of the flow around the body of the vehicle. Then, vehicle design features will be examined to show the qualitative influence on aerodynamic performance.

Mechanics of Air Flow around a Vehicle

The gross flow over the body of a car is governed by the relationship between velocity and pressure and is expressed by Bernoulli's equation [1, 2]. (Bernoulli's equation assumes incompressible flow and is reasonable for automotive aerodynamics; the equivalent relationship for compressible flow is the Euler Equation.) Bernoulli's equation can be written as:

$$\begin{aligned} P_{\text{static}} + P_{\text{dynamic}} &= P_{\text{total}} \\ P_s + 1/2\rho V^2 &= P_t \end{aligned} \quad (4.1)$$

where:

ρ = Density of air

V = Velocity of air (relative to the car)

This relationship is derived by applying Newton's Second Law to an incremental body of fluid flowing in a well-behaved fashion. For purposes of explanation, "well-behaved" simply means that the flow is moving smoothly and is experiencing negligible friction—conditions that apply reasonably to the air stream approaching a motor vehicle. In deriving the equation, the sum of the forces brings in the pressure effect acting on the incremental area of the body of fluid. Equating this to the time rate of change of momentum brings in the velocity term.

Bernoulli's equation states that the static plus the dynamic pressure of the air will be constant (P_t) as it approaches the vehicle. Visualizing the vehicle as stationary and the air moving (as in a wind tunnel), the air streams along lines, appropriately called "streamlines." A bundle of streamlines forms a streamtube. The smoke streams used in a wind tunnel allow streamtubes to be visualized as illustrated in [Figure 4.1](#).

At a distance from the vehicle the static pressure is simply the ambient, or barometric, pressure (P_{atm}). The dynamic pressure is produced by the relative velocity, which is constant for all streamlines approaching the vehicle. Thus the total pressure, P_t , is the same for all streamlines and is equal to $P_s + 1/2 \rho V^2$.

As the flow approaches the vehicle, the streamtubes split, some going above the vehicle while others go below it. By inference, one streamline must go straight to front of the body and stagnate (i.e., the air contacting the front of the bumper on a car or the leading edge of a wing on an airplane). At that point the relative velocity has gone to zero. With the velocity term zero, the static pressure observed at that point on the vehicle will be P_t . That is, if a pressure tap is placed on the vehicle at this point, it will record the total pressure.

FIGURE 4.1 Streamtubes flowing over an aerodynamic body.

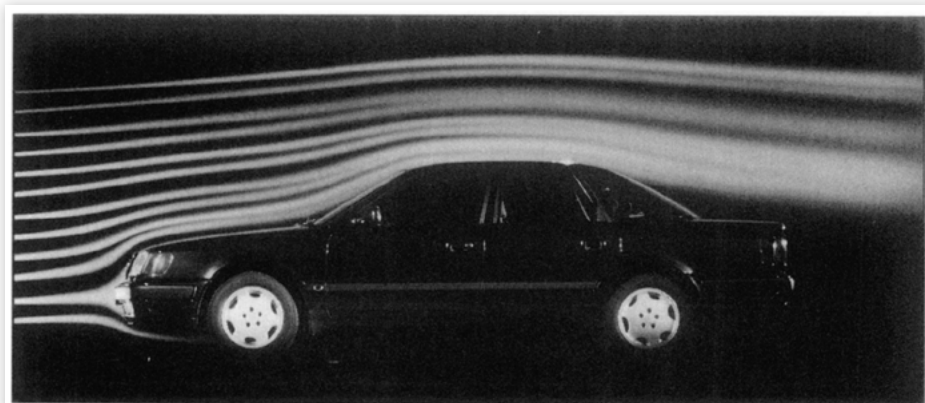
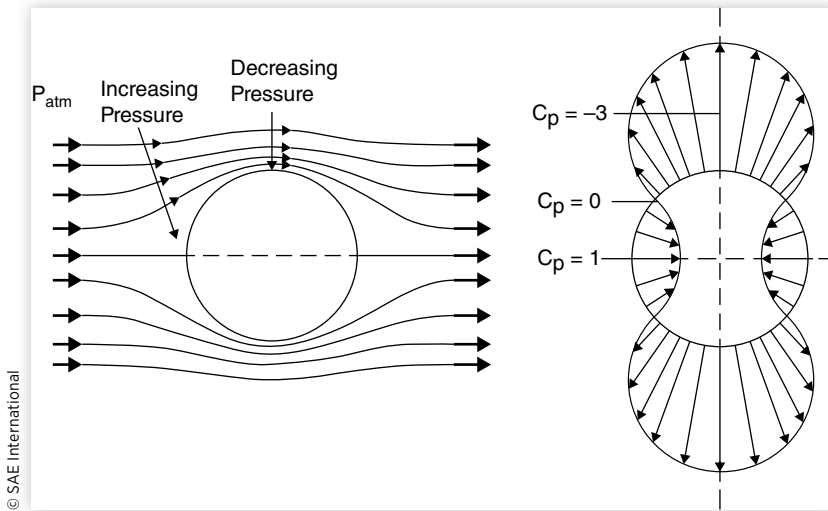


FIGURE 4.2 Pressure and velocity gradients in the air flow over a body.

Consider what must happen to the streamlines flowing above the hood. As they first turn in the upward direction, the curvature is concave upward. At a distance well above the vehicle where the streamlines are still straight, the static pressure must be the same as the ambient. In order for the air stream to be curved upward, the static pressure in that region must be higher than ambient to provide the force necessary to turn the air flow. If the static pressure is higher, then the velocity must decrease in this region in order to obey Bernoulli's equation.

Conversely, as the flow turns to follow the hood (downward curvature at the lip of the hood) the pressure must go below ambient in order to bend the flow, and the velocity must increase. These points are illustrated in [Figure 4.2](#), showing flow over a cylinder.

Thus Bernoulli's equation explains how the pressure and velocity must vary in the gross air flow over a car body. In the absence of friction the air would simply flow up over the roof and down the back side of the vehicle, exchanging pressure for velocity as it did at the front. In that case, the pressure forces on the back side of the vehicle would exactly balance those on the front, and there would be no drag produced.

We know, however, that drag is produced. The drag is due in part to friction of the air on the surface of the vehicle, and in part to the way the friction alters the main flow down the back side of the vehicle. Its explanation comes about from understanding the action of boundary layers in the flow over an object. Consider a uniform flow approaching a sharp-edged body as shown in [Figure 4.3](#).

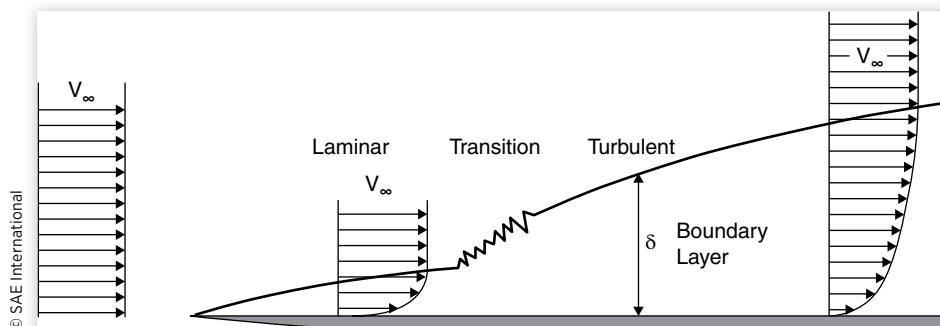
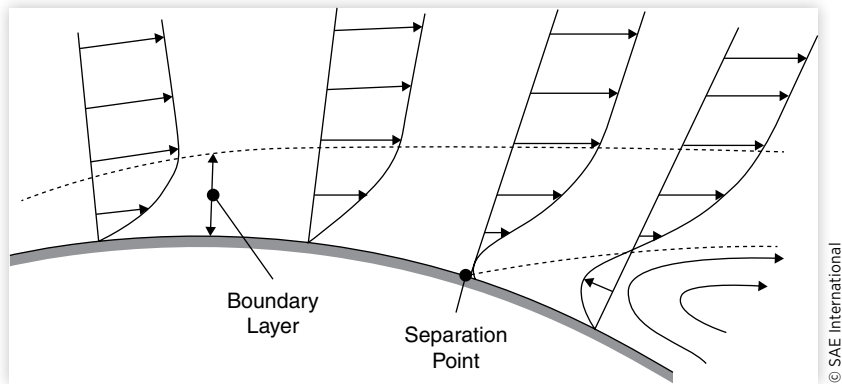
FIGURE 4.3 Development of a boundary layer.

FIGURE 4.4 Flow separation in an adverse pressure gradient.

© SAE International

Approaching the body, all air is traveling at a uniform velocity (and is assumed to be well-behaved, laminar flow). As it flows past the body, the air contacting the surface must drop to zero velocity due to friction on the surface. Thus a velocity profile develops near the surface, and for some distance, δ , the velocity is less than that of the main flow. This region of reduced velocity is known as the “boundary layer.” The boundary layer begins with zero thickness and grows with distance along the body. Initially, it too is laminar flow, but will eventually break into turbulent flow.

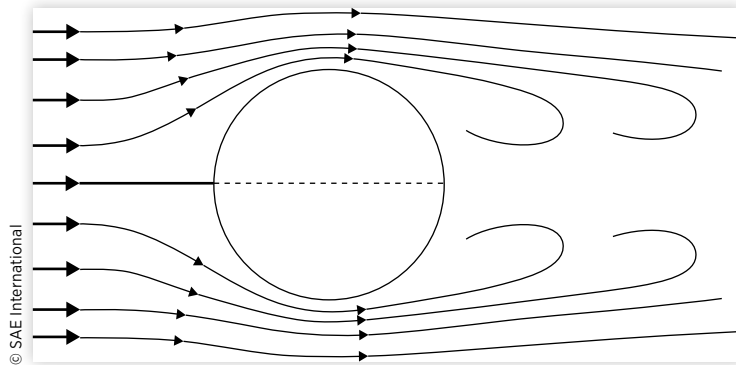
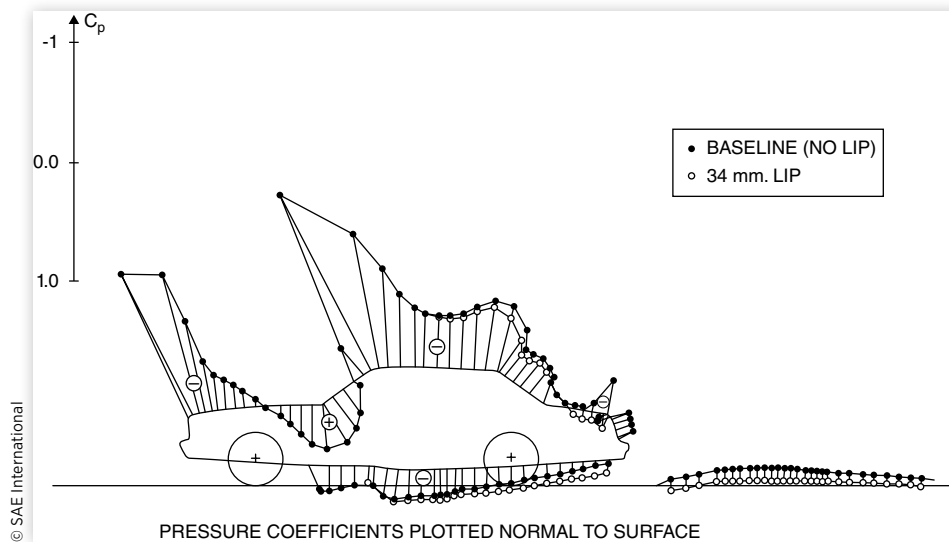
On the front face of a vehicle body, the boundary layer begins at the point where the stagnation streamline hits the surface. In the boundary layer the velocity is reduced because of friction. The pressure at the stagnation point is the total pressure (static plus dynamic) and decreases back along the surface. The pressure gradient along the surface thus acts to push the air along the boundary layer, and the growth of the layer is impeded. Pressure decreasing in the direction of flow is known as a “favorable pressure gradient” because it inhibits the boundary layer growth.

Unfortunately, as the flow turns again to follow the body, the pressure must increase again. The increasing pressure acts to decelerate the flow in the boundary layer, causing it to grow in thickness. This produces what is known as an “adverse pressure gradient.” At some point, the flow near the surface may actually be reversed by the action of the pressure, as illustrated in [Figure 4.4](#). The point where the flow stops is known as the “separation point.” Note that at this point, the main stream is no longer “attached” to the body but is instead able to break free and continue in a more or less straight line. Because it tries to include air from the region behind the body, the pressure in this region drops below the ambient. Vortices form and the flow is very irregular in this region. Under the right conditions, a von-Karman Vortex Street may be formed, which is a periodic shedding of vortices. Their periodic nature can be perceived as aerodynamic buffeting. The vortex action while flowing over a cylinder is shown in [Figure 4.5](#).

The phenomenon of separation prevents the flow from simply proceeding down the back side of a car. The pressure in the separation region is below that imposed on the front of the vehicle, and the difference in these overall pressure forces is responsible for what is known as “form drag.” The drag forces arising from the action of viscous friction in the boundary layer on the surface of the car is the “friction drag.”

Pressure Distribution on a Vehicle

These basic mechanisms account for the static pressure distribution along the body of a car. [Figure 4.6](#) shows experimentally measured pressures [3] plotted perpendicular to

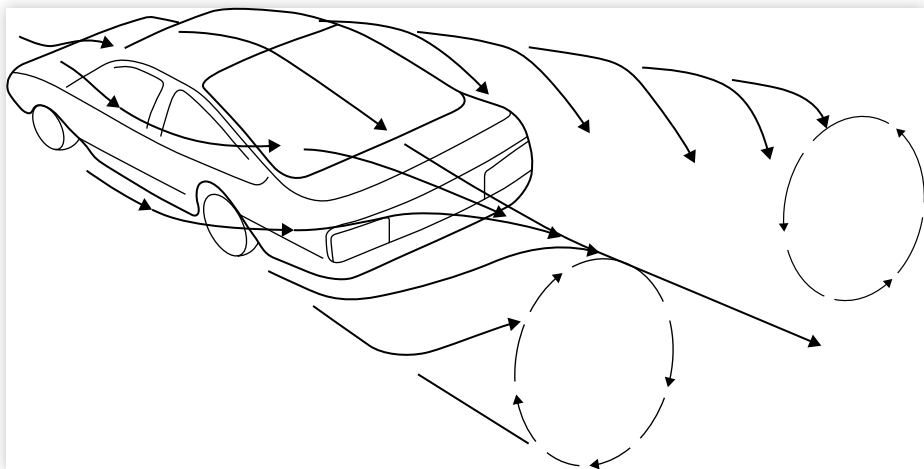
FIGURE 4.5 Vortex shedding in flow over a cylindrical body.**FIGURE 4.6** Pressure distribution along the centerline of a car.

the surface. The pressures are indicated as being negative or positive with respect to the ambient pressure measured some distance from the vehicle.

Note that a negative pressure is developed at the front edge of the hood as the flow rising over the front of the vehicle attempts to turn and follow horizontally along the hood. The adverse pressure gradient in this region has the potential to stall the boundary layer flow creating drag in this area. In recent years, styling detail in the front hood line has been given high priority to avoid separation from the hood and the drag penalty that results.

Near the base of the windshield and cowl, the flow must be turned upward, creating a high pressure region. This high-pressure region is an ideal location for inducing air for climate control systems or the engine intake, and has been used for this purpose in countless vehicles in the past. The high pressures in this region are accompanied by lower velocities, serving as an aid in keeping windshield wipers from being disturbed by aerodynamic forces such that they may lift off the surface of the windshield.

Over the roof line the pressure again goes negative as the air flow tries to follow the roof contour. Evidence of the low pressure in this region is seen in the billowing action of the fabric roof on convertibles. The pressure remains low down over the backlite and

FIGURE 4.7 Vortex systems in the wake of a car.

© SAE International

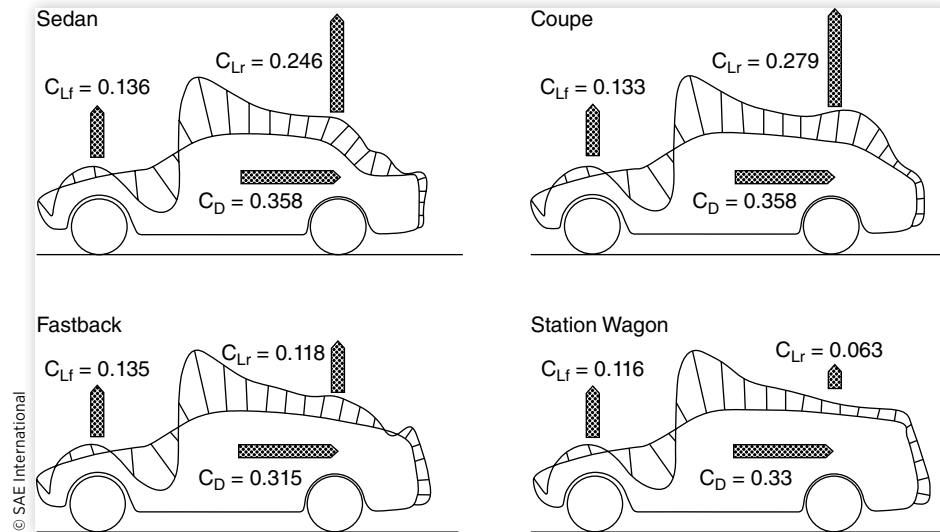
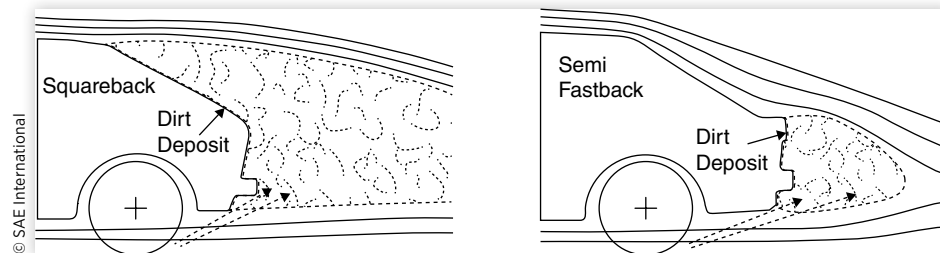
on to the trunk because of the continuing curvature. It is in this area that flow separation is most likely. Design of the angles and details of the body contour in this region are a source of critical concern in regards to the aerodynamics of the vehicle. Because of the low pressure, the flow along the sides of the car will also attempt to feed air into this region [4] and may add to the potential for separation. The general air flow patterns over the top and sides of a car are shown in [Figure 4.7](#). The flow along the sides is drawn up into the low-pressure region in the rear area, combining with flow over the roof to form vortices trailing off the back of the vehicle.

The choice of the backlite angles and deck lid lengths on the back of a car has a direct impact on aerodynamic forces through control of the separation point. Separation must occur at some point, and the smaller the area, generally the lower the drag. Theoretically, the ideal shape from an aerodynamic viewpoint is a teardrop rear shape, i.e., a conical shape that tapers off to a point with shallow angles of 15 degrees or less. It was recognized as early as the 1930s that because the area toward the point of the cone is quite small, the end of the ideally shaped vehicle can be cut off without much penalty of a large separation area [5, 6, 7]. The blunt rear-end shape allows greater head room in the back seat without substantially increasing drag. This characteristic shape has acquired the name “Kamm-back.”

While the size of the separation area affects the aerodynamic drag directly, the extent to which the flow is forced to turn down behind the vehicle affects the aerodynamic lift at the rear. [Figure 4.8](#) illustrates the effect on lift and drag for four styles of vehicle [4]. Flow control that minimizes the separation area generally results in more aerodynamic lift at the rear because of the pressure reduction as the flow is pulled downward.

Another consideration in aerodynamic design at the rear is the potential for dirt deposition on the backlite and tail lights. The high degree of turbulence in the separation zone includes moisture and dirt kicked up from the roadway by the tires. If the separation zone includes these items, dirt will be deposited on these areas and vision will be obstructed. [Figure 4.9](#) illustrates this phenomenon.

Whether separation will occur at the rear edge of the roof line is strongly dependent on the shape at that location and the backlite angle. For the vehicle on the left, the sharp edge at the roof line promotes separation at this point. While a well-defined separation boundary helps minimize aerodynamic buffeting, the inclusion of the backlite in the separation area promotes dirt deposition on the window.

FIGURE 4.8 Aerodynamic lift and drag forces with different vehicle styles.**FIGURE 4.9** Effect of separation point on dirt deposition at the rear.

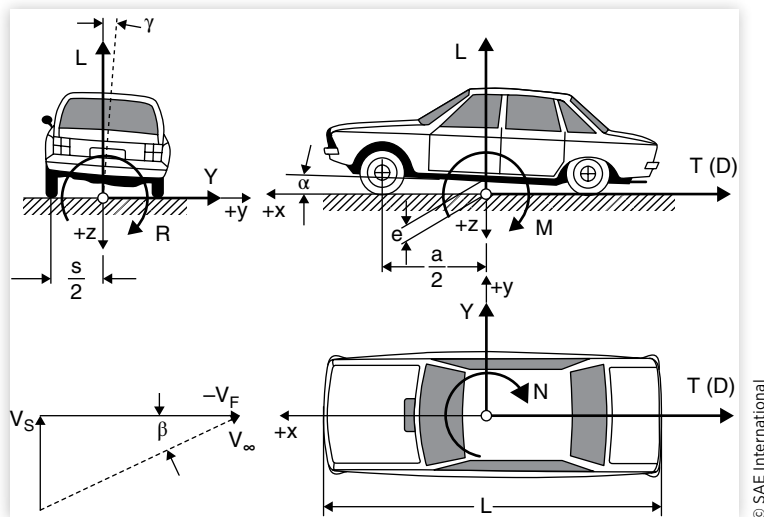
Although the vehicle on the right has a comparable backlite angle, the smooth transition at the rear of the roof and the addition of a modest trunk extension encourages the air stream to follow the vehicle contours down the rear deck. The separation region is well defined by the sharp contours at the end of the deck, helping to stabilize the separation zone and minimize buffeting. Only the tail light region is exposed to road dirt with this design.

Aerodynamic Forces

As a result of the air stream interacting with the vehicle, forces and moments are imposed. These may be defined systematically as the three forces and three moments shown in [Figure 4.10](#), acting about the principal axes of the car [8]. The reactions are as follows:

Direction	Force	Moment
Longitudinal (x-axis, positive rearward)	Drag	Roll moment
Lateral (y-axis, positive to the right)	Side force	Pitch moment
Vertical (z-axis, positive upward)	Lift	Yaw moment

FIGURE 4.10 Aerodynamic forces and moments acting on a car [14].



The origin for the axis system is defined in SAE J1594 [9]. Inasmuch as the aerodynamic reactions on a vehicle are unrelated to its center of gravity location (and the CG location may not be known in wind tunnel tests), the origin for force measurement is in the ground plane at the mid-wheelbase and mid-track position.

Drag Components

Drag is the largest and most important aerodynamic force encountered by passenger cars at normal highway speeds. The overall drag on a vehicle derives from contributions by many sources. Various aids may be used to reduce the effects of specific factors. [Figure 4.11](#) lists the main sources of drag and the potential for drag reductions in these areas estimated for cars produced in the 1970s.

For the vehicle represented in the figure, approximately 65% (.275/.42) of the drag arises from the body (forebody, afterbody, underbody, and skin friction). The major contributor is the afterbody because of the drag produced by the separation zone at the rear. It is in this area that the maximum potential for drag reduction is possible. [Figure 4.12](#) shows the influence of rear end inclination angle on the drag for various lengths of rear extension (beyond the rear edge of the roof line) [10]. Slope angles up to 15 degrees consistently reduce drag. As the angles increase, the drag again increases because of flow separation. (In practice, higher drop angles have been achieved without separation.)

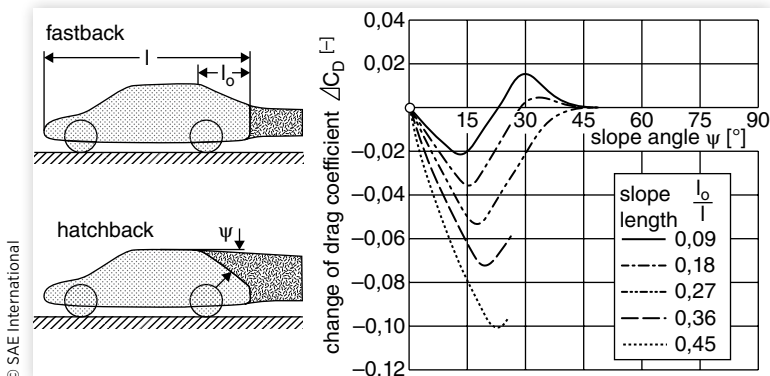
Forebody drag is influenced by design of the front end and windshield angle. Generally the “roundness” of the front end establishes the area over which the dynamic pressure can act to induce drag. [Figure 4.13](#) shows the influence of the height of the front edge of the vehicle [10]. The location of this point determines the location of the streamline flowing to the stagnation point. This streamline is important as it establishes the separation of flow above and below the body. Minimum drag is obtained when the stagnation point is kept low on the frontal profile of the vehicle. A well-rounded shape, in contrast to the crisp lines traditionally given to the frontal/grill treatment of passenger cars, is equally important to aerodynamics. A rounded low hood line can yield reductions of 5 to 15% in the overall drag coefficient [11].

FIGURE 4.11 Main sources of drag on a passenger car.

DRAG COEFFICIENT COMPONENT	TYPICAL VALUE
Forebody	0.05
Afterbody	0.14
Underbody	0.06
Skin Friction	0.025
Total Body Drag	0.275
Wheels and Wheel Wells	0.09
Drip rails	0.01
Window recesses	0.01
External mirrors	0.01
Total Protuberance Drag	0.12
Cooling system	0.025
Total Internal Drag	0.025
Overall Total Drag	0.42 ¹
VEHICLE OF THE 1980s	
Cars	0.30 – 0.35
Vans	0.33 – 0.35
Pickup trucks	0.42 – 0.46

¹ Based on cars of 1970s vintage.

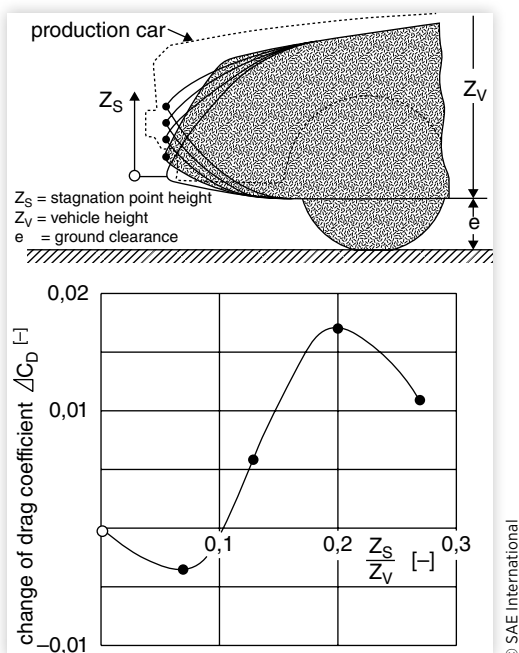
© SAE International

FIGURE 4.12 Influence of rear end inclination on drag.

The windshield establishes the flow direction as it approaches the horizontal roof. Thus its angle has a direct influence on drag, particularly on trucks. Shallow angles reduce drag, but complicate vehicle design by allowing increased solar heating loads and placing more critical demands on the manufacturer of the windshield to minimize distortion at shallow angles. [Figure 4.14](#) shows the change in drag as the windshield angle is increased from the nominal angle of 28 degrees [10]. With a steep angle, the air velocity approaching the windshield is reduced by the high pressure in that region. With a shallow angle, the wind speed will be higher, adding to the aerodynamic loads on the windshield wipers.

© SAE International

FIGURE 4.13 Influence of front end design on drag.



The underbody is a critical area generating body drag. Suspensions, exhaust systems, and other protruding components on the underbody are responsible for the drag. The air flow in this area is a shear plane controlled by zero air speed on the road surface, and induced flow by drag of the underbody components. The recognized fix for minimizing underbody drag is the use of a smooth underbody panel.

Protuberances from the body represent a second area where careful design can reduce drag. The wheels and wheel wells are a major contributor in this class. Significant drag develops at the wheels because of the turbulent, recirculating flow in the cavities. [Figure 4.15](#) illustrates the complex flow patterns that occur around a wheel [13]. The sharp edges of the wheel cutout provide opportunities to induce flow in the horizontal plane, while the rotating wheel tends to induce circulation in the vertical plane. These effects allow the wheel to influence more flow than simply that which is seen because of its frontal area presented to the flow. The obvious improvement is aerodynamic shielding of the wheels and wheel well areas. While this is possible to some extent on rear wheels, rotation of the front wheels about their steering axis complicates the use of such treatment at the front of the vehicle. Experimental research has shown that decreasing the clearance between the underside and the ground and minimizing the wheel cavity decreases the total aerodynamic drag contribution from the wheel [12].

The cooling system is the last major contributor to drag. Air flow passing through the radiator impacts on the engine and the firewall, exerting its dynamic pressure as drag on the vehicle. The air flow pattern inside a typical engine compartment may be very chaotic due to the lack of aerodynamic treatment in this area. [Figure 4.16](#) illustrates this situation [12]. With no attention to the need for air flow management, the air entering through the radiator dissipates much of its forward momentum against the vehicle components in the engine compartment before spilling out through the underside openings. The momentum exchange translates directly into increased drag.

Flow management in the cooling system can affect the drag coefficient by as much as 0.025 [10]. The drag contribution from this source is normally taken to be the difference in drag measured with the cooling system inlets open and covered. As seen in [Figure 4.17](#), careful design to direct the flow (allowing it to maintain its velocity so that the static pressure remains low) can reduce the drag produced. Although these various arrangements may not be feasible within the styling theme of a given car, the potential for aerodynamic improvements is evident in the drag reductions shown. In order to reduce drag on modern cars, cooling inlet size is held to the practical minimum.

FIGURE 4.14 Influence of windshield angle on drag.

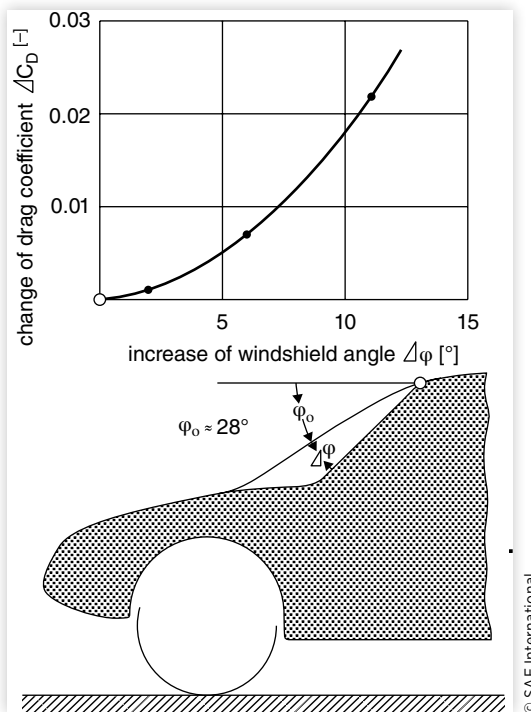
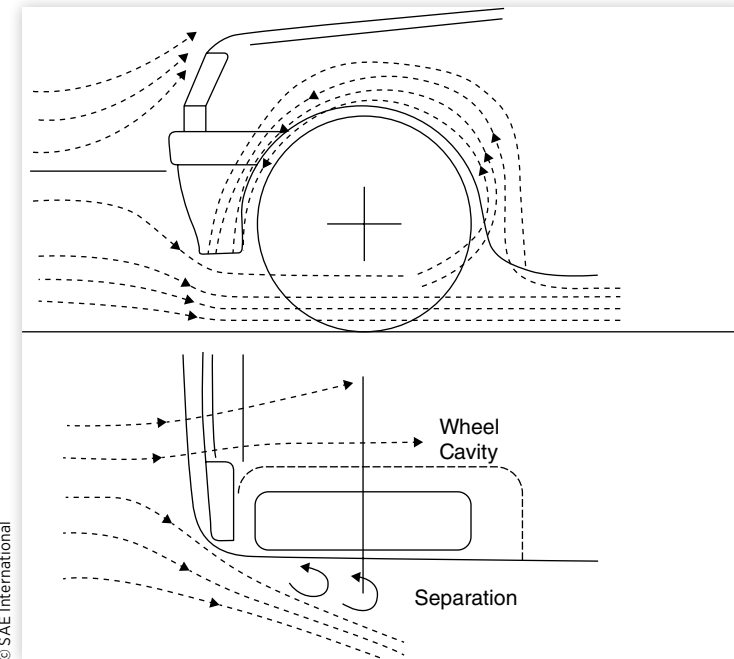
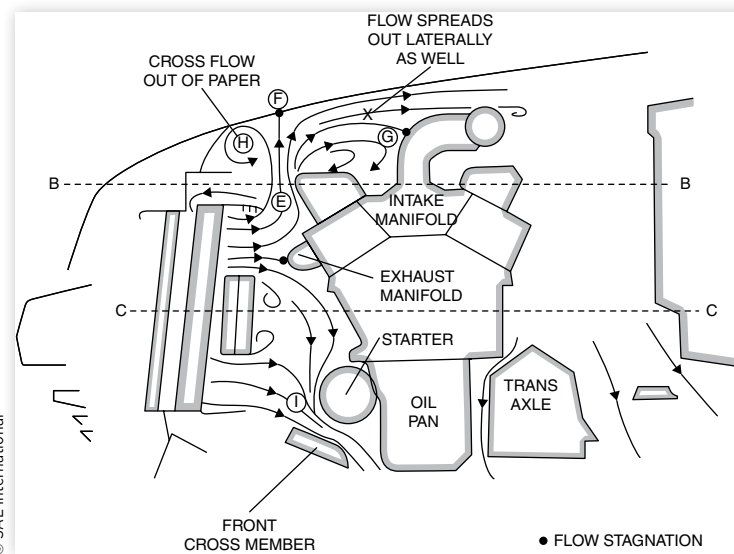


FIGURE 4.15 Air flow recirculation in a wheel well.



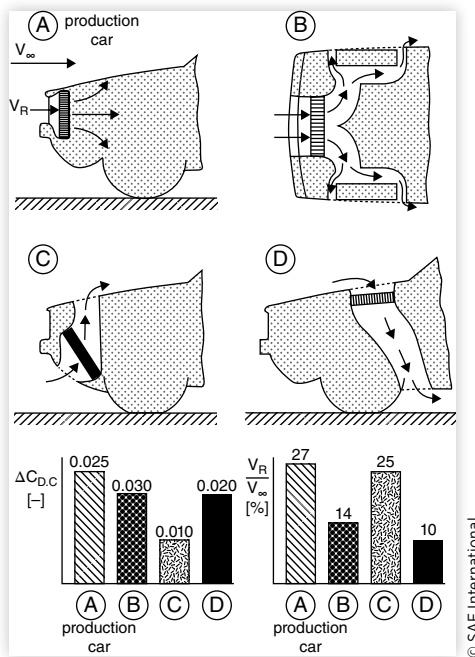
© SAE International

FIGURE 4.16 Air flow pattern inside a typical engine compartment. (Source: Williams, J., Ohler, W., Hackett, J., and Hammar, L., "Water Flow Simulation of Automotive Underhood Air Flow Phenomena," SAE Technical Paper 910307, SP-855, 1991, 31pp.)



© SAE International

FIGURE 4.17 Influence of cooling system on drag.



Aerodynamic Aids

BUMPER SPOILERS

Front bumper spoilers are aerodynamic surfaces extending downward from the bumper to block and redirect the shear flow that impacts on the underbody components. While the spoiler contributes pressure drag, at least with a shallow depth the reduction in underbody drag is more significant. As spoiler depth is increased, eventually the increasing pressure drag outweighs further reduction in underbody drag and the overall drag increases. The low pressure produced also has the effect of reducing front-end lift.

AIR DAMS

Air dams are flow-blocking surfaces installed at the perimeter of the radiator to improve flow through the radiator at lower vehicle speeds. The improvement derives from the decreased pressure behind the radiator/fan, and may reduce drag by reduction of pressure on the firewall.

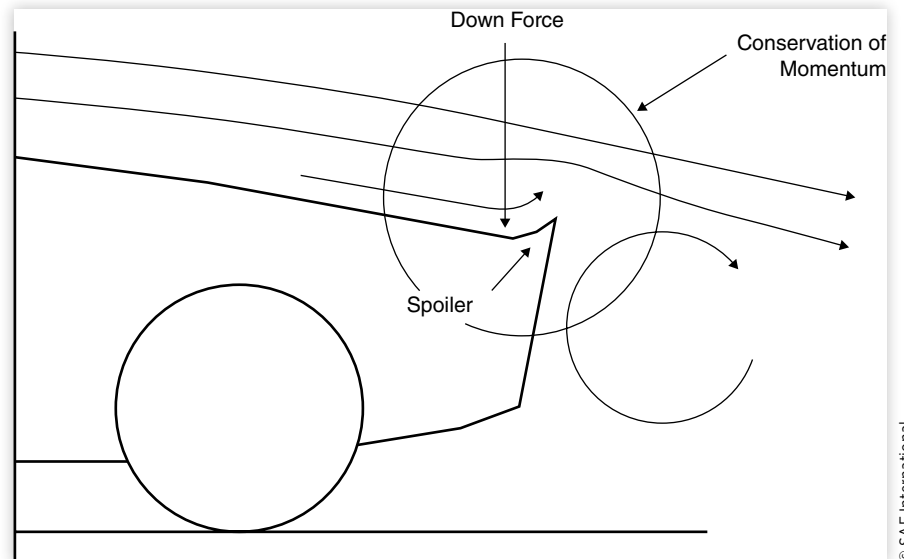
DECK LID SPOILERS

Spoilers and air foils on the rear deck may serve several purposes. By deflecting the air upward, as shown in [Figure 4.18](#), the pressure is increased on the rear deck creating a downforce at the most advantageous point on the vehicle to reduce rear lift. The spoilers may also serve to stabilize the vortices in the separation flow, thus reducing aerodynamic buffeting. In general, deck lid spoilers tend to increase drag.

WINDOW AND PILLAR TREATMENTS

Drip rails and offsets between windows and pillars on a car body are always sources of drag. Disturbance to the air flow in these regions may cause small separation zones.

FIGURE 4.18 Influence of a spoiler on flow over the rear.



The disturbance to the air in the high-velocity air stream causes momentum loss which creates drag. Smooth contours are important not only for drag reduction, but also for reduction of aerodynamic noise.

OPTIMIZATION

The development of automotive aerodynamics has been described as occurring in three stages [14]:

1. Adaptation of streamlined shapes from other disciplines (e.g., shipbuilding) at the turn of the century.
2. Application of the knowledge of fluid mechanics from aircraft aerodynamics around the 1930s.
3. Current efforts to optimize the numerous details of the design to obtain good air flow characteristics.

The optimization is founded on the premise that the styling concept of the car is established and aerodynamic improvement can only be attempted in the form of changes to detail in the styling. An example of the optimization is shown in [Figure 4.19](#). The sketches show minor modifications in detail such as a change in the air dam (A), hood line (B), A-pillar shape (C) and D-pillar shape (D and E). The graph illustrates the magnitude of drag reduction obtained from various combinations of these changes. The power of drag reduction by attention to details is illustrated by the fact that an overall drag reduction of 21% is achieved.

Drag

Because air flow over a vehicle (or any other body for that matter) is so complex, it is necessary to develop semi-empirical models to represent the effect. Therefore, aerodynamic drag is characterized by the equation:

$$D_A = \frac{1}{2} \rho V^2 C_D A \quad (4.2)$$

where:

C_D = Aerodynamic drag coefficient

A = Frontal area of the vehicle

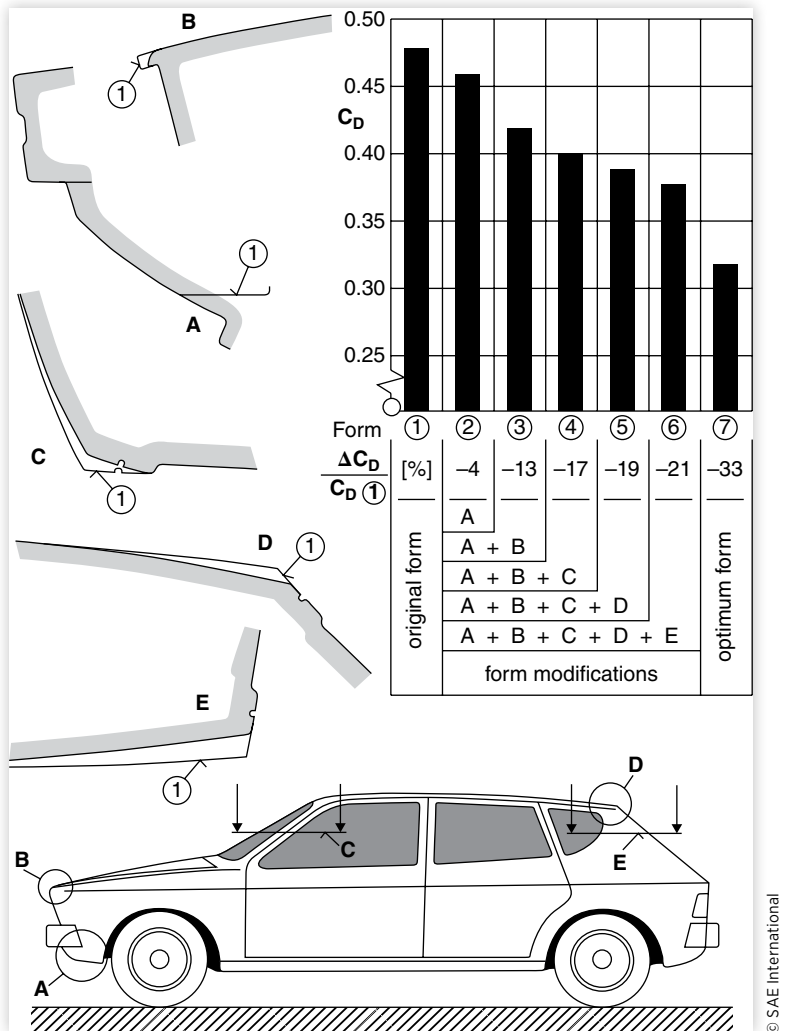
ρ = Air density

(Note: The SAE symbol for drag, "D," is subscripted with an "A" in the text to denote it as aerodynamic drag, distinguishing it from symbols used elsewhere in the text. The same convention will be used with aerodynamic lift and side force.)

The term $1/2\rho V^2$ in the above equation is the dynamic pressure of the air, and is often referred to as the "q," typically expressed in units of pounds per square ft. The drag coefficient, C_D , is determined empirically for the car. The frontal area, A , is the scale factor taking into account the size of the car. (A half-scale model of a car, which has one-fourth of the area, will have one-fourth of the drag.) Because the size of a vehicle has a direct influence on drag, the drag properties of a car are sometimes characterized by the value of " $C_D A$."

AIR DENSITY

The air density is variable depending on temperature, pressure, and humidity conditions. At standard conditions (59°F and 29.92 in of Hg) the density is 0.076 lb/ft³. As used in this equation, the air density must be expressed as mass density, obtained by dividing by the acceleration of gravity; thus the value for standard atmospheric conditions

FIGURE 4.19 Optimization of body detail.

© SAE International

is $\rho = 0.076/32.2 = 0.00236 \text{ lb-sec}^2/\text{ft}^4$. Density at other conditions can be estimated for the prevailing pressure, P_r , and temperature, T_r , as shown by Equations (4.3a and 4.3b):

$$\rho = 0.00236 \left(\frac{P_r}{29.92} \right) \left(\frac{519}{460 + T_r} \right) \quad (4.3a)$$

where:

P_r = Atmospheric pressure in inches of mercury

T_r = Air temperature in degrees Fahrenheit

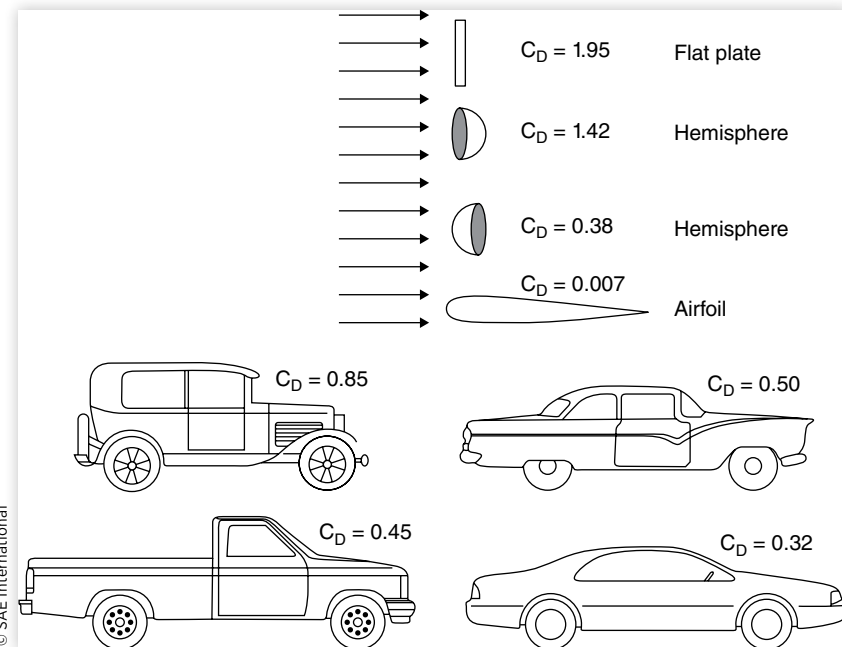
In the metric system the equivalent equation for air density in kg/m^3 is:

$$\rho = 1.225 \left(\frac{P_r}{101.325} \right) \left(\frac{288.16}{273.16 + T_r} \right) \quad (4.3b)$$

where:

P_r = Atmospheric pressure in kilopascals

T_r = Air temperature in degrees Celsius

FIGURE 4.20 Drag coefficients of various bodies.

DRAg COEFFICIENT

The drag coefficient is determined experimentally from wind tunnel tests or coastdown tests. The definition of C_D comes from [Equation \(4.2\)](#):

$$C_D = \frac{D_A}{\frac{1}{2} \rho V^2 A} = \frac{\text{Drag force}}{(\text{Dynamic pressure})(\text{Area})} \quad (4.4)$$

The drag coefficient varies over a broad range with different shapes. [Figure 4.20](#) shows the coefficients for a number of shapes. In each case it is presumed that the air approaching the body has no lateral component (i.e., it is straight along the longitudinal axis of the vehicle). Note that the simple flat plate has a drag coefficient of 1.95. This coefficient means that the drag force is 1.95 times as large as the dynamic pressure acting over the area of the plate. The extreme drag produced by the plate results from the fact that the air spilling around the plate creates a separation area much larger than the plate itself.

In practice, a vehicle driving along a road experiences atmospheric winds in addition to the wind component arising from its speed. Atmospheric winds vary in intensity throughout the United States, with typical mean values of 10-20 mph, and gusty winds in the range of 50-60 mph. The atmospheric wind will be random in direction with respect to the vehicle's direction of travel. Thus the relative wind seen by the vehicle will consist of the large component due to its speed, plus a smaller atmospheric wind component in any direction. [Figure 4.21](#) illustrates how the relative wind will vary randomly.

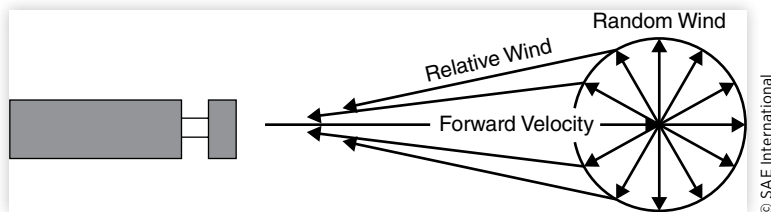
When the atmospheric wind blows toward the vehicle a "headwind" is present, and the total velocity used in [Equation \(4.2\)](#) is:

$$V = V_v + V_w \quad (4.5)$$

where:

V_v = Vehicle speed

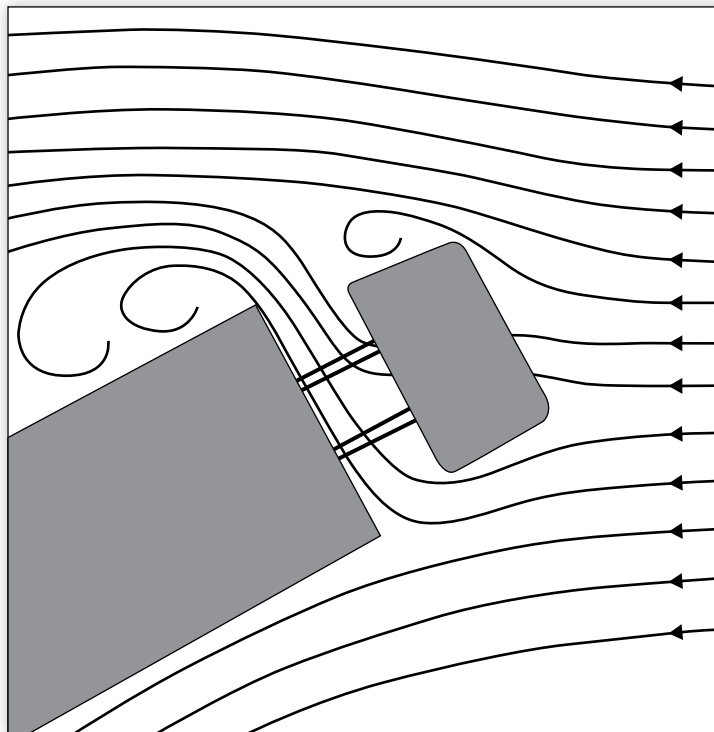
V_w = Wind speed

FIGURE 4.21 Relative wind seen by a motor vehicle on the road.

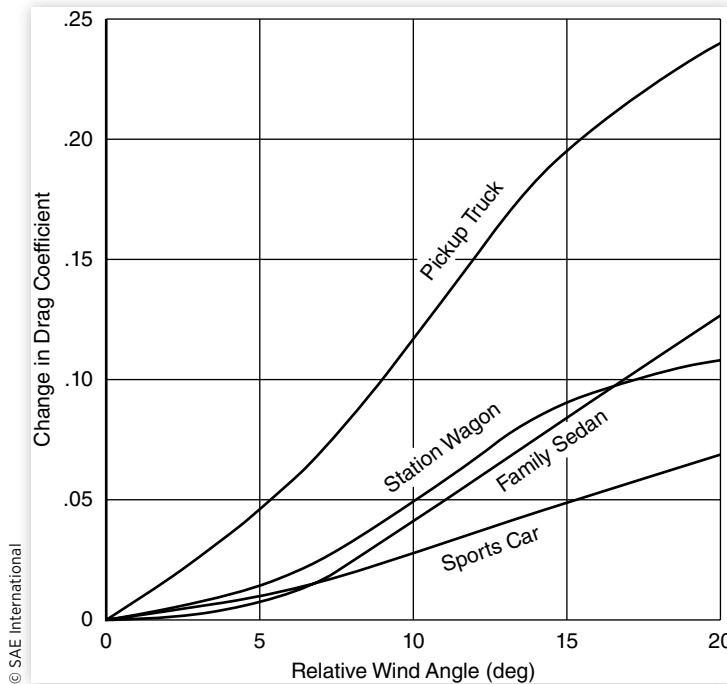
© SAE International

Blowing in the direction of travel is a “tailwind,” and the velocities are subtracted. Because the velocity is squared in [Equation \(4.2\)](#), the increase in drag from a headwind is much greater than the decrease in drag from a tailwind of the same velocity.

In an average sense, the relative wind can be represented as a vector emanating from any point on the perimeter of the circle, and the average drag on the road will not be equivalent to simply the mean speed of the vehicle. Particularly important in this regard is the way in which the drag coefficient varies with a side wind component. On tractor-trailers side winds are particularly important because they disturb the aerodynamic flow field. [Figure 4.22](#) shows the air flow around a tractor-trailer when the relative wind is at a 30-deg. angle. Note that the flow is well attached on the right side of the vehicle, but a huge separation region occurs on the downwind side. In addition to the drag created by the wind impinging on the front of the truck, the large momentum change of the wind hitting the trailer adds another large drag component. Thus with trucks and cars, the change in drag coefficient with yaw angle of the wind is very important.

FIGURE 4.22 Air flow around a tractor-semitrailer with 30-deg. wind angle.

© SAE International

FIGURE 4.23 Influence of yaw angle on drag coefficients of typical vehicle types.

In contrast, with the much better aerodynamic design of cars, their drag coefficient is not as sensitive to yaw angle because the flow will not separate so readily. Normally, the drag coefficient increases by 5 to 10% with yaw angles in the range typical of on-road driving for passenger cars. [Figure 4.23](#) shows the typical influence of yaw angle on the drag coefficients of several different types of vehicles.

Side Force

The lateral wind components will also impose a side force on the vehicle when it is attempting to change its direction of travel. The exact effect depends both on the vehicle and the nature of the wind. In strong crosswinds, the side force is typically greater than the drag force, such that the angle of the overall wind force is much greater than the relative wind angle [15].

When the vehicle first encounters a crosswind condition on the road (a transient crosswind), the lateral force is first imposed on the front of the vehicle and may divert it in the downwind direction. The aerodynamic shape of the vehicle and even the steering system characteristics affect performance in this sense. Crosswind behavior is an important enough aspect of aerodynamics that it is discussed separately in a later section.

Under steady-state wind conditions, the side force imposed on a vehicle in a crosswind is given by:

$$S_A = 1/2\rho V^2 C_s A \quad (4.6)$$

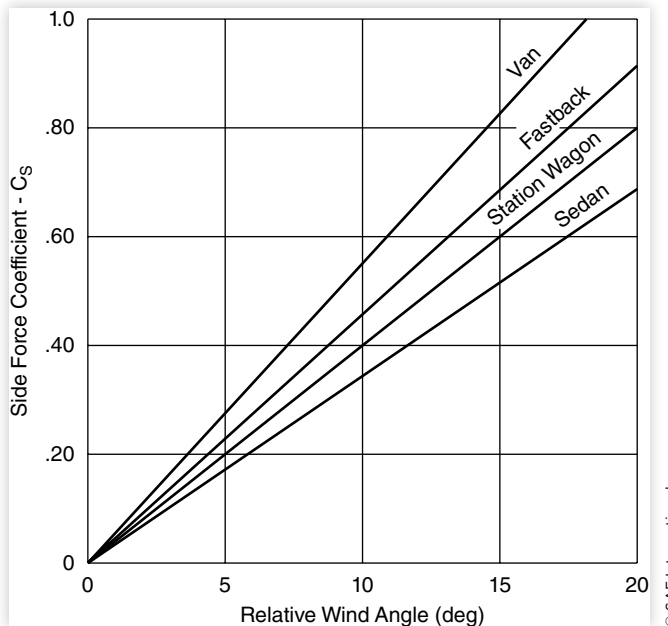
where:

S_A = Side force

V = Total wind velocity

C_s = Side force coefficient (function of the relative wind angle)

A = Frontal area

FIGURE 4.24 Side force coefficient as a function of yaw angle for typical vehicles.

© SAE International

Note that the frontal area, rather than the side area, is used in the equation. **Figure 4.24** shows typical characteristics of C_s as a function of wind angle. The side force coefficient is zero at zero relative wind angle, and grows nearly linearly with the angle for the first 20 to 40 degrees. The slope of the gradient varies somewhat with vehicle type, but will typically be in the range of 0.035/deg to 0.06/deg [16].

The side force acts on the body at the center of pressure, which is normally located ahead of the center of gravity such that the vehicle is turned away from the wind. In wind tunnel measurements the side force is measured in the ground plane at the mid-wheelbase position. The difference between this location and the center of pressure results in an overturning moment and a yaw moment whenever a side force is present.

Lift Force

The pressure differential from the top to the bottom of the vehicle causes a lift force. These forces are significant concerns in aerodynamic optimization of a vehicle because of their influence on driving stability. The lift force is measured at the centerline of the vehicle at the center of the wheelbase. The force, L_A , is quantified by the equation:

$$L_A = 1/2\rho V^2 C_L A \quad (4.7)$$

where:

L_A = Lift force

C_L = Lift coefficient

A = Frontal area

As was seen in **Figure 4.8**, the lift force is dependent on the overall shape of the vehicle. At zero wind angle, lift coefficients normally fall in the range of 0.3 to 0.5 for modern passenger cars [17], while under crosswind conditions the coefficient may increase dramatically, reaching values of 1 or more [18].

In aerodynamic studies the combined effects of lift and the pitching moment may be taken into account simultaneously by determining a lift coefficient for both the front and rear wheels [15]. In that case an equation similar to [Equation \(4.7\)](#) is used to describe the lift effect at each axle.

Lift can have a negative impact on handling through the reduced control forces available at the tires. Front lift, which reduces steering controllability, is reduced by front bumper spoilers and by rearward inclination of front surfaces. Lift at the rear of the vehicle, which also reduces stability, is the most variable with vehicle design. In general, designs that cause the flow to depart with a downward angle at the rear of the vehicle create rear lift. Lift can be decreased by use of underbody pans, spoilers, and a change in the angle of attack of the body (a 3-deg. cant on the body can decrease lift force by 40 percent).

Pitching Moment

While the lift force acts to decrease (or increase) the weight on the axles, the pitching moment acts to transfer weight between the front and rear axles. Aerodynamic pitching moment arises from the fact that the drag does not act at the ground plane (thus it accounts for the elevation of the drag force) and the lifting force may not act exactly at the center of the wheelbase. The aerodynamic pitching moment is described by the equation:

$$PM = 1/2\rho V^2 C_{PM} AL \quad (4.8)$$

where:

PM = Pitching moment

C_{PM} = Pitching moment coefficient

A = Frontal area

L = Wheelbase

Because it is a moment equation, a characteristic length is needed to achieve dimensional consistency in the equation. The vehicle wheelbase is used for this purpose. A moment can be translated without changing its effect, so there is no need for a “point of action” (i.e., the moment is applied to the body rather than at a specific aerodynamic reference point). Most modern cars have an aerodynamic pitching moment in the range of 0.05 to 0.2, and it is quite sensitive to the angle of attack on the vehicle. [Figure 4.25](#) shows how the pitching moment coefficient varies with body pitch angle for several vehicles.

Yawing Moment

The lateral force caused by a side wind does not normally act at the mid-wheelbase position. Thus a yawing moment, YM , is produced. The yawing moment is quantified by the equation:

$$YM = 1/2\rho V^2 C_{YM} AL \quad (4.9)$$

where:

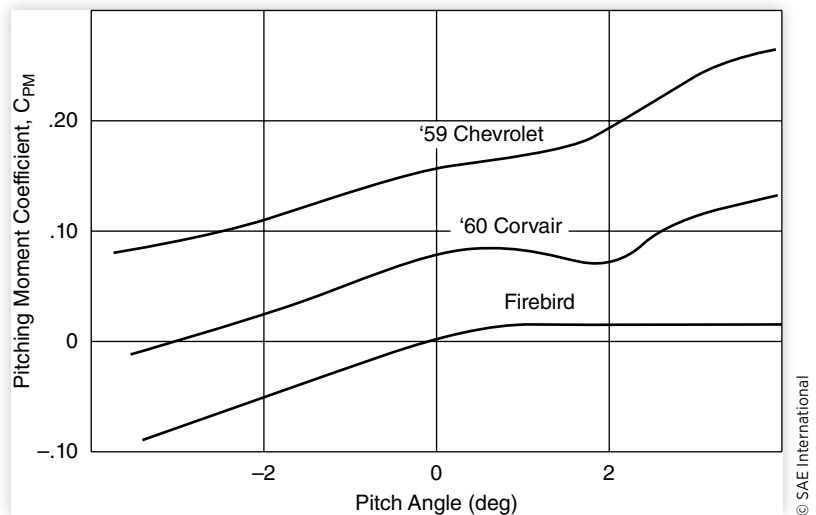
YM = Yawing moment

C_{YM} = Yawing moment coefficient

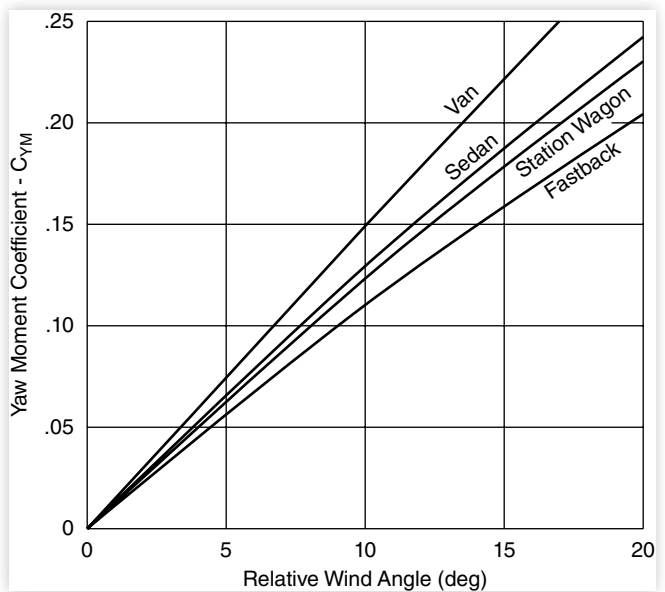
A = Frontal area

L = Wheelbase

The yawing moment coefficient varies with wind direction, starting at zero with zero relative wind angle and growing almost linearly up to 20-deg. of aerodynamic slip angle. [Figure 4.26](#) shows the coefficient for some typical vehicles. The slope of the coefficient at small angles ranges from 0.007/deg to 0.017/deg [18].

FIGURE 4.25 Variation of pitching moment coefficient with body pitch angle [16].

© SAE International

FIGURE 4.26 Yawing moment coefficient for typical vehicles.

© SAE International

Rolling Moment

The lateral force caused by a side wind acts at an elevated point on the vehicle. Thus a rolling moment, RM , is produced. The moment has only a minor influence on vehicle stability, depending largely on the roll steer properties of the suspensions. The rolling moment is quantified by the equation:

$$RM = 1/2\rho V^2 C_{RM} AL \quad (4.10)$$

where:

- RM = Rolling moment
- C_{RM} = Rolling moment coefficient
- A = Rrontal area
- L = Wheelbase

The rolling moment coefficient is sensitive to wind direction much like the yawing moment coefficient, being quite linear over the first 20 degrees of the aerodynamic slip angle. The slope of the rolling moment coefficient ranges from 0.018/deg to 0.04/deg [18].

Crosswind Sensitivity

The growing sophistication of aerodynamic design in motor vehicles in combination with the increased sensitivities to crosswinds often accompanying drag reductions has stimulated interest in understanding and controlling the factors that affect behavior in a crosswind [19, 20, 21, 22]. “Crosswind sensitivity” generally refers to the lateral and yawing response of a vehicle in the presence of transverse wind disturbances which affect the driver’s ability to hold the vehicle in position and on course.

Crosswind sensitivity is dependent on more than just the aerodynamic properties of the vehicle. In the literature [19] the key elements that have been identified are:

- Aerodynamic properties
- Vehicle dynamic properties (weight distribution, tire properties, and suspensions)
- Steering system characteristics (compliances, friction, and torque assist)
- Driver closed-loop steering behavior and preferences

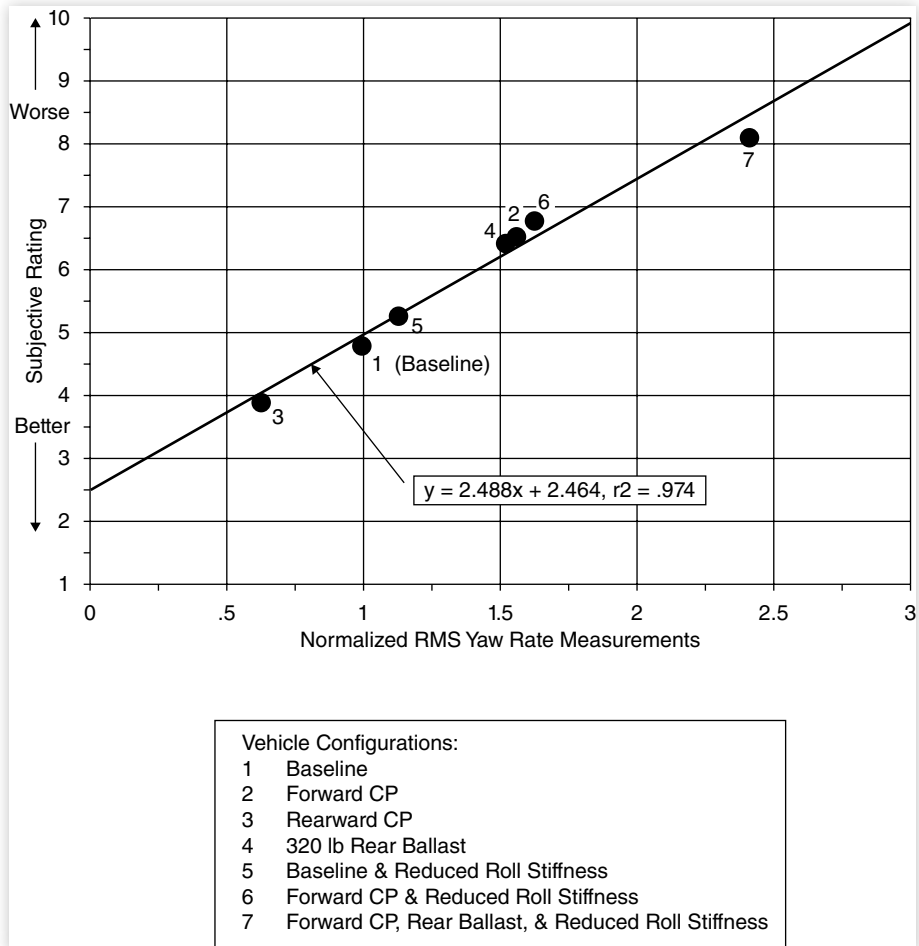
Crosswind behavior is studied using instrumented vehicles in natural random (ambient) wind conditions, under exposure to crosswind generators (fans that produce a crosswind in an experimental test area), and in driving simulators. The primary variables of interest are the yaw response, lateral acceleration response, steering corrections when holding a specified course, and the subjective judgments of test drivers.

Good crosswind behavior is most strongly correlated with yaw rate response. [Figure 4.27](#) illustrates the correlation that has been obtained between subjective ratings in a “gauntlet” crosswind (fans alternately blowing in opposite directions) and yaw rate response [19]. The high degree of correlation in these particular tests suggests that yaw rate response in a crosswind nearly explains all variation in subjective ratings from vehicle to vehicle. Other measures of response that correlate well with subjective ratings in order of importance are lateral acceleration at the driver’s seat headrest, steering wheel displacement, and lateral acceleration.

The aerodynamic property of primary importance to crosswind sensitivity is the center of pressure location and its relative distance ahead of the vehicle’s neutral steer point. The neutral steer point is the point on the vehicle at which a lateral force produces equal sideslip angles at both the front and rear axles.

The center of pressure is the resultant action point of the combined lateral force and yaw moment reactions on the vehicle. In general, more rearward center of pressure locations, which are closer to the neutral steer point, minimize lane deviations in a crosswind and are subjectively more acceptable. The effect of fore/aft center of pressure location is seen in the lateral acceleration responses of three vehicles given in [Figure 4.28](#). A forward center of pressure location induces a large lateral acceleration response because the effective action point is near the front of the vehicle and the vehicle is turned

FIGURE 4.27 Correlation of subjective ratings with normalized RMS yaw rate response [19].



© SAE International

strongly away from the wind. With a rearward center of pressure position, the vehicle yaws less and resists the tendency to be displaced sideways.

Other vehicle dynamic properties come into play in determining how the vehicle responds to a given crosswind force. For example, the weight distribution on the front and rear axles determines the center of gravity location and the neutral steer point location. Tire properties (such as cornering stiffness) also affect the location of the neutral steer point and, hence, the degree to which the vehicle resists the yawing moment disturbance from the aerodynamic side force.

A first estimate of crosswind sensitivity can be obtained from a calculation of static yaw rate response to a steady crosswind with no steering input [19]. Under static conditions, a vehicle's passive crosswind response is given by:

$$\frac{r}{\alpha_{cw}} = \frac{qC_y A}{MV} \left[\frac{d_{ns} + (b - L/2 + LC_{YM})}{d_{ns} + \zeta_d} \right] \quad (4.11)$$

where:

r = Yaw rate

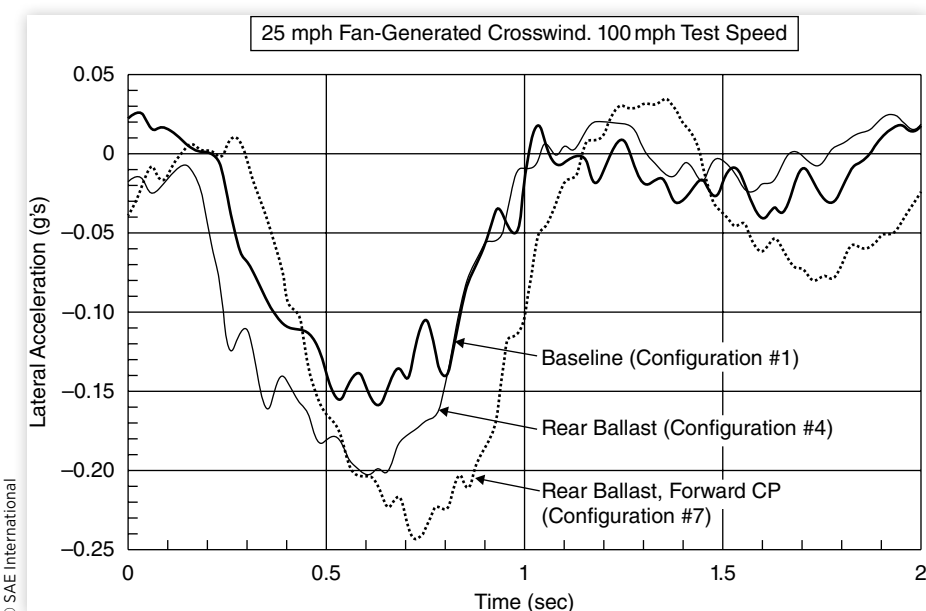
α_{cw} = Aerodynamic wind angle

- q = Dynamic pressure = $\rho V^2/2$
 C_y = Side force coefficient
 C_{YM} = Yawing moment coefficient
 A = Frontal area
 M = Mass of the vehicle
 V = Forward velocity
 d_{ns} = Distance from center of mass to neutral steer point
 b = Distance from front axle to center of mass
 L = Wheelbase
 ζ_d = Moment arm proportional to the tire force yaw damping moment about the neutral steer point = $\frac{L^2}{MV^2} \frac{C_f C_r}{(C_f + C_r)}$
 C_f = Effective total tire cornering stiffness of the front axle
 C_r = Effective total tire cornering stiffness of the rear axle

As noted above, the neutral steer point identifies that fore/aft point on the vehicle where an external side force will not cause the vehicle to yaw. This point is affected by tire force properties, steering system compliance, suspension kinematics, and weight distribution. The numerator in the second term on the right-hand side of [Equation \(4.11\)](#) is the distance from the neutral steer point to the aerodynamic center of pressure. Thus a large distance between these points contributes to crosswind sensitivity.

The denominator in this same term contains the moment arm of the tire force yaw damping moment. This term can be increased to reduce crosswind sensitivity by increasing wheelbase or the effective tire cornering stiffness. Effective tire cornering stiffness is favorably influenced directly by using tires with high cornering stiffness and by eliminating compliances in the steering or suspension which allow the vehicle to yield to the crosswind. However, the moment arm is strongly diminished by forward speed, thereby tending to increase crosswind sensitivity as vehicle speed increases.

FIGURE 4.28 Crosswind lateral acceleration response with variation of CP location [19].



The static analysis discussed above may overlook certain other vehicle dynamic properties that can influence crosswind sensitivity. Roll compliance, particularly when it induces suspension roll steer effects, may play a significant role not included in the simplified analysis. Thus a more comprehensive analysis using computer models of the complete dynamic vehicle and its aerodynamic properties may be necessary for more accurate prediction of a vehicle's crosswind sensitivity.

Rolling Resistance

The other major vehicle resistance force on level ground is the rolling resistance of the tires. At low speeds on hard pavement, the rolling resistance is the primary motion resistance force. In fact, aerodynamic resistance becomes equal to the rolling resistance only at speeds in the range of 50-60 mph. For off-highway, level ground operation, the rolling resistance is the only significant retardation force.

While other resistances act only under certain conditions of motion, rolling resistance is present from the instant the wheels begin to roll. Rolling resistance has another undesirable property—a large part of the power expended in a rolling wheel is converted into heat within the tire. The resulting temperature rise reduces both the abrasion resistance and the flexure fatigue strength of the tire material, and may become the limiting factor in tire performance.

There are at least seven mechanisms responsible for rolling resistance:

1. Energy loss due to deflection of the tire sidewall near the contact area
2. Energy loss due to deflection of the tread elements
3. Scrubbing in the contact patch
4. Tire slip in the longitudinal and lateral directions
5. Deflection of the road surface
6. Air drag on the inside and outside of the tire
7. Energy loss on bumps

Considering the vehicle as a whole, the total rolling resistance is the sum of the resistances from all the wheels:

$$R_x = R_{xf} + R_{xr} = f_r W \quad (4.12)$$

where:

R_{xf} = Rolling resistance of the front wheels

R_{xr} = Rolling resistance of the rear wheels

f_r = Rolling resistance coefficient

W = Weight of the vehicle

For theoretically correct calculations, the dynamic weight of the vehicle, including the effects of acceleration, trailer towing forces, and the vertical component of air resistance, is used. However, for vehicle performance estimation, the changing magnitude of the dynamic weight complicates the calculations without offering significant improvements in accuracy. Furthermore, the dynamic weight transfer between axles has minimal influence on the total rolling resistance (aerodynamic lift neglected). For these reasons, static vehicle weight is sufficiently accurate for computation of rolling resistance in most cases.

All of these considerations apply, in a strict sense, only for straight-line motion. For vehicles subjected to lateral forces (cornering or aerodynamic loading), the direction

of rolling resistance deviates from the direction of actual travel, and the tractive force must overcome the vectorial resultant of the side force and rolling resistance.

Factors Affecting Rolling Resistance

The coefficient of rolling resistance, f_r , is a dimensionless factor that expresses the effects of the complicated and interdependent physical properties of tire and ground. Establishment of standardized conditions for measurement of the effects of variables like the structure of the ground material, composition of the rubber, design elements of the tire, temperature, etc., proves difficult if not impossible. Some of the more important factors are discussed below.

TIRE TEMPERATURE

Because much of the rolling resistance on paved surfaces arises from deflection and energy loss in the tire material, the temperature of the tire can have a significant effect on the resistance experienced. In the typical situation where a tire begins rolling from a cold condition, the temperature will rise and the rolling resistance will diminish over an initial period of travel. [Figure 4.29](#) shows the relative changes in temperature and rolling resistance that will occur [18]. As shown in the figure, the tire must roll a distance of at least 20 miles before the system approaches stable operation. In typical tire tests it is therefore common to warm up the tire for 20 minutes or more before taking measurements that may be affected by the warm-up conditions. For the short trips representing the majority of automotive travel, the tires never warm up to benefit from the lowest possible levels of rolling resistance.

TIRE INFLATION PRESSURE/LOAD

To a large extent, the tire inflation pressure determines the tire elasticity and, in combination with the load, determines the deflection in the sidewalls and contact region. The overall

FIGURE 4.29 Relative tire temperature and rolling resistance during warm-up.

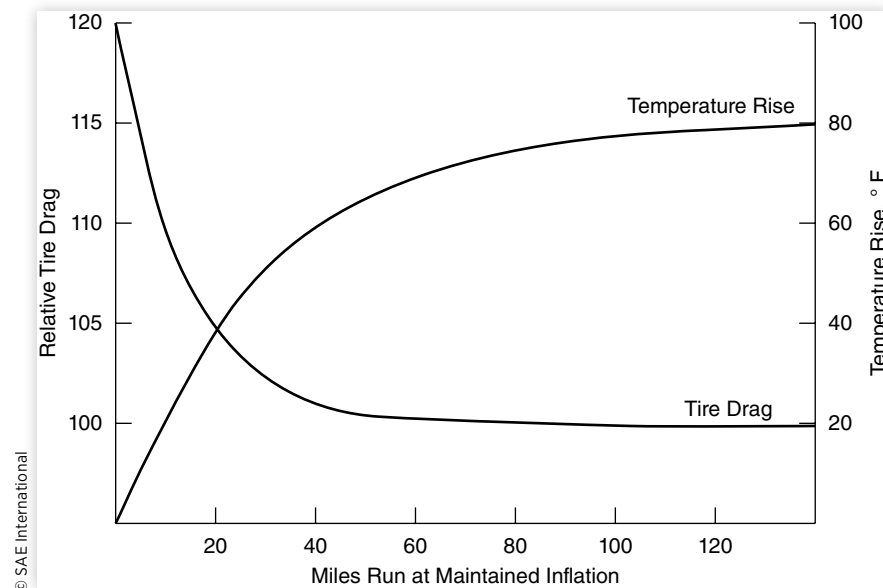
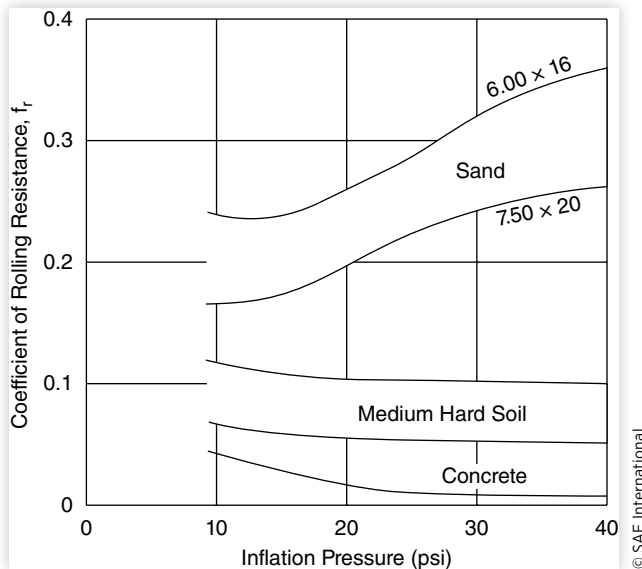


FIGURE 4.30 Coefficient of rolling resistance versus inflation pressure [16].

effect on rolling resistance also depends on the elasticity of the ground. [Figure 4.30](#) shows how the coefficient changes with inflation pressure on different types of surfaces.

On soft surfaces like sand, high inflation pressures result in increased ground penetration work and therefore higher coefficients. Conversely, lower inflation pressure, while decreasing ground penetration, increases tire-flexure work. Thus the optimum pressure depends on the surface deformation characteristics. In general, the “increased traction” obtained by lowering tire pressure on a sand surface is actually achieved through a reduction in rolling resistance.

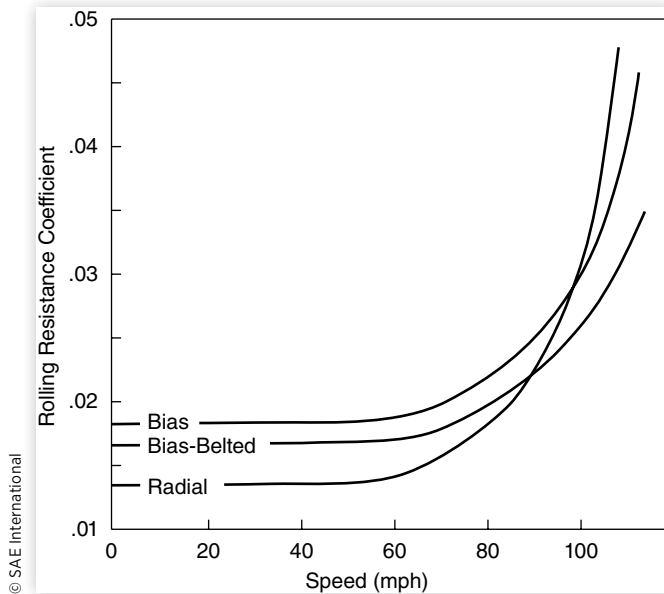
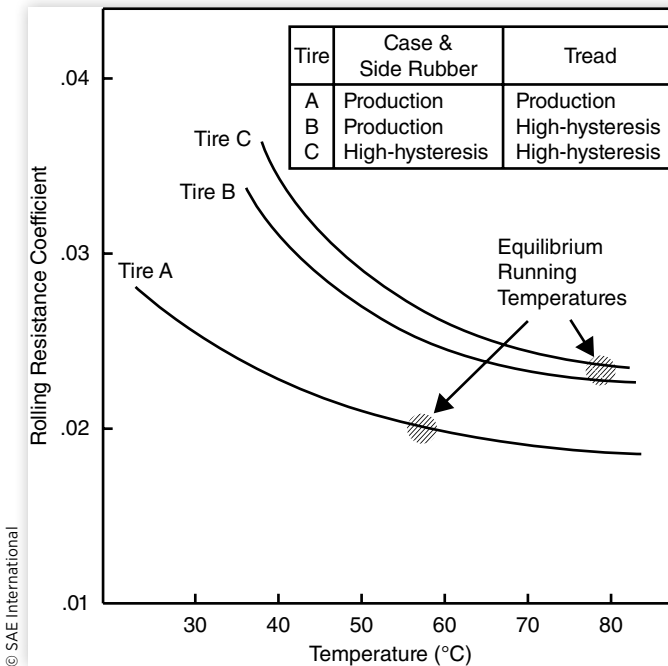
On medium plastic surfaces such as dirt, the effects of inflation pressure on tire and ground approximately balance, and the coefficient remains nearly independent of inflation pressure. On hard (paved) surfaces, the coefficient decreases with higher inflation pressure since flexure work of the tire body will be greatly reduced.

VELOCITY

The coefficient is directly proportional to speed because of increased flexing work and vibration in the tire body, although the effect is small at moderate and low speeds and is often assumed to be constant for calculation purposes. The influence of speed becomes more pronounced when it is combined with lower inflation pressures. [Figure 4.31](#) shows the rolling resistance versus speed for remove radial, bias-belted, and bias-ply tires [23]. The sharp upturn in the coefficients at high speeds is caused by a high-energy standing wave developed in the tire carcass just behind the tire contact patch. If allowed to persist for even moderate periods of time, catastrophic failure can result. Thus formation of a standing wave is one of the primary effects limiting a tire’s rated speed. Modern tires rated for high speed normally include stabilizers in the shoulder area to control the development of standing waves.

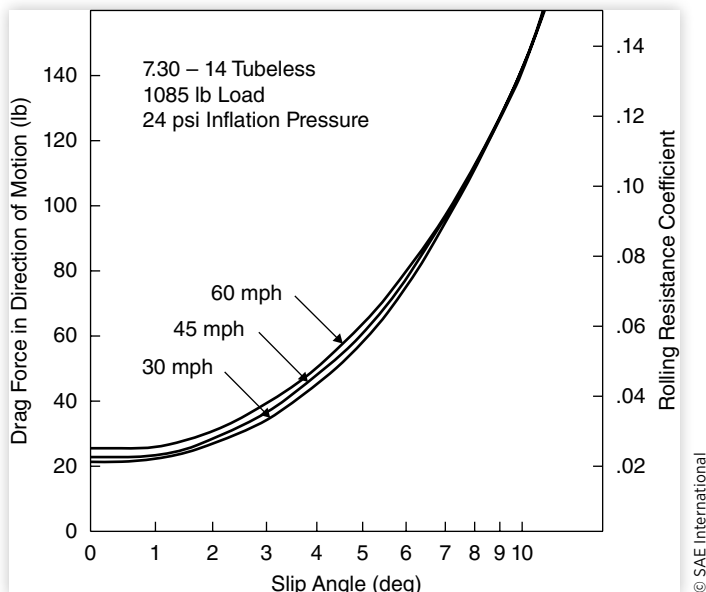
TIRE MATERIAL AND DESIGN

The materials and thickness of both the tire sidewalls (usually expressed in plies) and the tread determine the stiffness and energy loss in the rolling tire. [Figure 4.32](#) shows the rolling resistance of experimental tires constructed using different types of rubber

FIGURE 4.31 Rolling resistance versus speed.**FIGURE 4.32** Rolling resistance versus temperature for tires with different polymers.

in the sidewalls and tread areas [23]. The plot vividly illustrates the losses deriving from hysteresis in the tread material. Although hysteresis in the tread rubber is important for good wet traction, it degrades rolling resistance performance.

Worn-out, smooth-tread tires show coefficient values up to 20 percent lower than new tires. Fine laminations, on the other hand, increase the coefficient as much

FIGURE 4.33 Rolling resistance coefficient versus slip angle.

© SAE International

as 25 percent. The cord material in the sidewall has only a small effect, but the cord angle and tire belt properties (belted versus radial-ply tires) have a significant influence.

TIRE SLIP

Wheels transferring tractive or braking forces show higher rolling resistance due to wheel slip and the resulting frictional scuffing. Cornering forces produce the same effects. **Figure 4.33** shows the rolling resistance effects as a function of slip angle [23]. At a few degrees of slip, equivalent to moderate-high cornering accelerations, the rolling resistance coefficient may nearly double in magnitude. The effect is readily observed in normal driving when the tire will “scrub” off speed in a corner.

Typical Coefficients

The multiple and interrelated factors affecting rolling resistance make it virtually impossible to devise a formula that takes all variables into account. Before a value for rolling resistance coefficient can be chosen for a particular application, the overall degree of accuracy required for the calculations should be established.

Several equations for estimating rolling resistance have been developed over the years. Studies on the rolling loss characteristics of solid rubber tires [23] led to an equation of the form:

$$f_r = \frac{R_x}{W} = C \frac{W}{D} \sqrt{\frac{h_t}{w}} \quad (4.13)$$

where:

R_x = Rolling resistance force

W = Weight on the wheel

C = Constant reflecting loss and elastic characteristics of the tire material

D = Outside diameter

h_t = Tire section height

w = Tire section width

From this formulation, rolling resistance is seen to be load sensitive, increasing linearly with load. Larger tires reduce rolling resistance, as do low aspect ratios (h/w). Some confirmation of the general trends from this equation appear in the literature from studies of the rolling resistance of conventional passenger car tires of different sizes under the same load conditions [23].

Other equations for the rolling resistance coefficient for passenger car tires rolling on concrete surfaces have been developed. The variables in these equations are usually inflation pressure, speed, and load. The accuracy of a calculation is naturally limited by the influence of factors that are neglected.

At the most elementary level, the rolling resistance coefficient may be estimated as a constant. The table below lists some typical values that might be used in that case.

Vehicle type	Concrete	Surface medium hard	Sand
Passenger cars	0.015	0.08	0.30
Heavy trucks	0.012	0.06	0.25
Tractors	0.02	0.04	0.20

At lower speeds the coefficient rises approximately linearly with speed. Thus equations have been developed which include a linear speed dependence. For example, consider Equation (4.14):

$$f_r = 0.01(1 + V/100) \quad (4.14)$$

where V is the speed in mph.

Over broader speed ranges, the coefficient rises in a manner that is closer to a speed-squared relationship. The Institute of Technology in Stuttgart has developed the following equation for rolling on a concrete surface [16]:

$$f_r = f_o + 3.24f_s(V/100)^{2.5} \quad (4.15)$$

where:

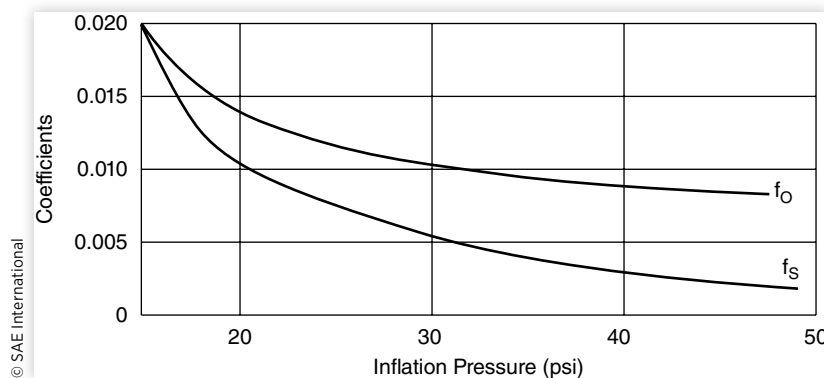
V = Speed in mph

f_o = Basic coefficient

f_s = Speed effect coefficient

The two coefficients, f_o and f_s , depend on inflation pressure and are determined from the graph shown in [Figure 4.34](#).

FIGURE 4.34 Coefficients for Equation (4.15).



At the University of Michigan Transportation Research Institute, similar equations for estimating rolling resistance of heavy truck tires of both the radial and bias-ply types were developed [24]. These are:

$$f_r = (0.0041 + 0.000041V)C_h \quad \text{Radial tires} \quad (4.16a)$$

$$f_r = (0.0066 + 0.000046V)C_h \quad \text{Bias-ply tires} \quad (4.16b)$$

where:

V = Speed in mph

C_h = Road surface coefficient

= 1.0 for smooth concrete

= 1.2 for worn concrete, brick, cold blacktop

= 1.5 for hot blacktop

Rolling resistance is clearly a minimum on hard, smooth, dry surfaces. A worn-out road almost doubles rolling resistance. On wet surfaces, higher rolling resistance is observed probably due to the cooler operating temperature of the tire which reduces its flexibility.

Total Road Loads

The summation of the rolling resistance and aerodynamic forces (and grade forces, if present) constitutes the propulsion load for the vehicle, and is normally referred to as "road load." The road load force is thus:

$$R_{RL} = f_r W + 1/2\rho V^2 C_D A + W \sin \theta \quad (4.17)$$

The sum of these forces is plotted for a typical large vehicle in [Figure 4.35](#). The rolling resistance has been assumed constant with a coefficient of 0.02 and a vehicle weight of 3,650 lb. The aerodynamic drag assumes a vehicle with a frontal area of 23.3 ft² and a drag coefficient of 0.34. The total road load curve rises with the square of the

FIGURE 4.35 Road load plot for a typical passenger car.

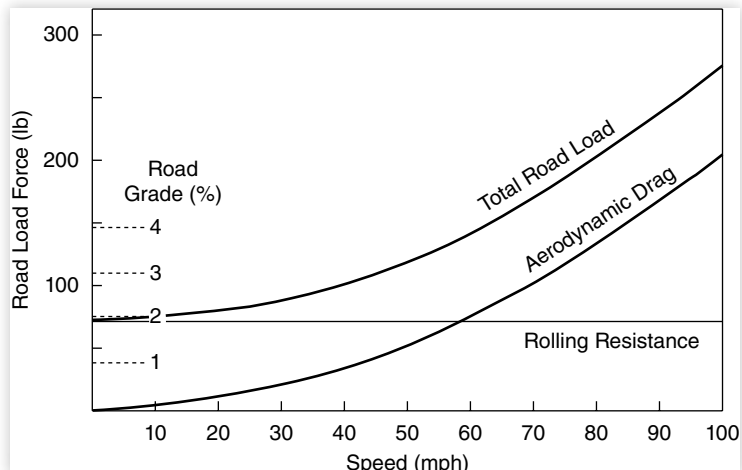
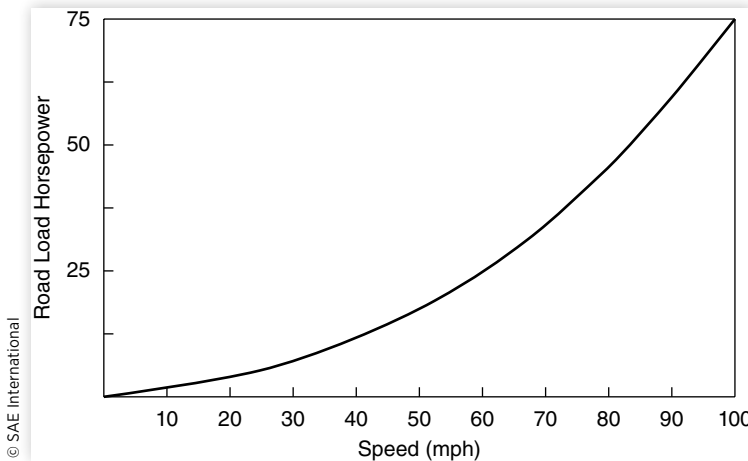


FIGURE 4.36 Road load power plot for a typical passenger car.

speed due to the aerodynamic component. Rolling resistance and grade simply slide the whole curve upward in proportion to their size.

The road load horsepower is computed by multiplying Equation (4.16) by the vehicle velocity and applying the appropriate conversion factor to obtain horsepower. In that case:

$$HP_{RL} = R_{RL} V / 550 = \left(f_r W + 1/2 \rho V^2 C_D A + W \sin \Theta \right) V / 550 \quad (4.18)$$

The road load power corresponding to the road load forces in [Figure 4.35](#) is shown in [Figure 4.36](#) for a level road condition. Note that the power increases much more rapidly with velocity in [Equation \(4.18\)](#). Thus at high speeds a small increase in speed results in a large increase in vehicle power required, with an associated penalty to fuel economy.

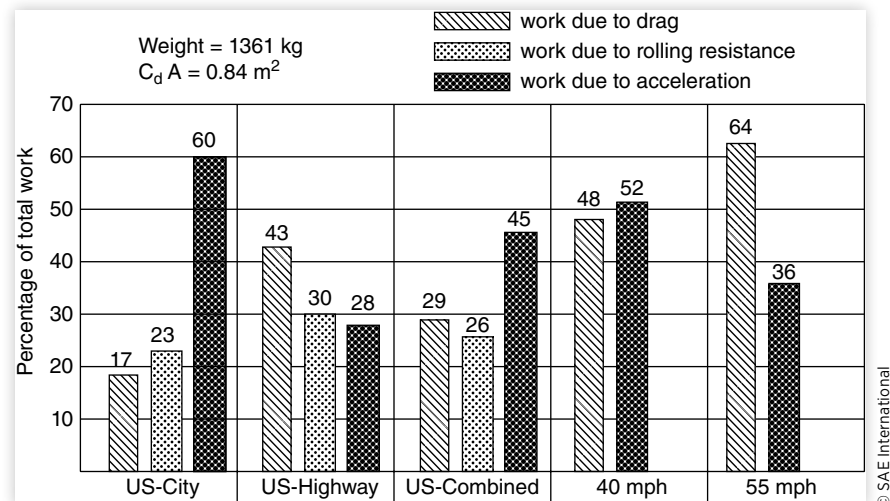
Fuel Economy Effects

Today, aerodynamic and rolling resistance forces are of particular interest for their effect on fuel consumption. Aerodynamic drag, of course, is the most important of the aerodynamic properties. In the decade of the 1970s, drag coefficients of 0.4 to 0.5 were common on relatively large cars. In the 1980s, drag coefficients are commonly less than 0.4 with some cars less than 0.3. In addition, the smaller cross-sectional areas contribute to lower overall drag.

The exact improvements in fuel economy that may be expected from improvements in road loads are difficult to predict because of the uncertainty about the ways in which cars are used and driven. [Figure 4.37](#) shows an estimate of where the energy is used in EPA driving cycles and in steady highway driving [25].

Example Problems

1. A heavy truck weighing 72,500 lb is driving on the highway at a speed of 67 mph. The air temperature is 55°F and the barometric pressure is 26.01 in Hg. The truck is 8' wide by 13.5' high, and has an aerodynamic drag coefficient of 0.65. The truck has

FIGURE 4.37 Subdivision of work of a compact car in driving cycles.

radial-ply tires. Calculate the aerodynamic drag, the rolling resistance (according to the SAE equations), and the road load horsepower under these conditions.

Solution:

The aerodynamic drag may be calculated using [Equation \(4.2\)](#). The temperature and barometric pressure conditions are not standard, so we must first calculate the local air density using [Equation \(4.3a\)](#).

$$\rho = 0.00236 \frac{P_r}{29.92} \frac{519}{460 + T_r}$$

$$\rho = 0.00236 \frac{26.01}{29.92} \frac{519}{(460+55)} = 0.00207 \frac{\text{lb}\cdot\text{sec}^2}{\text{ft}^4} = 0.0667 \frac{\text{lb}}{\text{ft}^3}$$

Now the aerodynamic drag can be calculated:

$$D_A = 0.5 \left(0.00207 \frac{\text{lb}\cdot\text{sec}^2}{\text{ft}^4} \right) \left(\frac{67 \text{ mph}}{0.682 \text{ mph}/\text{ft/sec}} \right)^2 0.65(8 \text{ ft})(13.5') = 702 \text{ lb}$$

The rolling resistance comes from a combination of [Equations \(4.12\)](#) and [\(4.16a\)](#). First from the SAE equation, we calculate the rolling resistance coefficient, assuming a surface coefficient of unity:

$$f_r = [0.0041 + 0.000041(67 \text{ mph})] = 0.00685$$

Then the rolling resistance is:

$$R_x = 0.00685(72,500 \text{ lb}) = 497 \text{ lb}$$

At the speed of 67 mph (98.3 ft/sec) the horsepower required to overcome aerodynamic drag is:

$$HP_A = 702 \text{ lb}(98.3 \text{ ft/sec})1 \text{ hp}/(550 \text{ ft-lb/sec}) = 125 \text{ hp}$$

And the horsepower to overcome rolling resistance is:

$$HP_R = 497 \text{ lb}(98.3 \text{ ft/sec})1 \text{ hp}/(550 \text{ ft-lb/sec}) = 88.8 \text{ hp}$$

Notes:

- a. A total of nearly 215 hp is required to keep the truck rolling at this speed.
 - b. Highway trucks typically have diesel engines rated at 350 to 600 horsepower. These engines are designed to run continuously at maximum power, so it is not unreasonable for them to run at this output level for the majority of their trip.
 - c. At a typical brake specific fuel consumption of 0.35 lb per brake-horsepower-hour, the engine will burn 82.6 lb of diesel fuel per hour (13 gallons/hour), getting about 5.25 miles per gallon. It is not unusual to have a fuel tank capacity of 300 gallons onboard a highway tractor, allowing them to run for nearly 24 hours or 1500 miles without having to stop for fuel.
2. A passenger car has a frontal area of 21 square ft and a drag coefficient of 0.42. It is traveling along at 55 mph. Calculate the aerodynamic drag and the associated horsepower requirements if it is driving into a 25 mph headwind, and separately, with a 25 mph tailwind.

Solution:

The drag can be calculated from [Equation \(4.2\)](#), although the relative velocity must take into account the headwinds and tailwinds as given in [Equation \(4.4\)](#). We will assume that the air temperature and pressure conditions are effectively near standard conditions so that the standard value for air density can be used.

Headwind condition:

$$D_A = 0.5 \left(0.00236 \frac{\text{lb-sec}^2}{\text{ft}^4} \right) \left(\frac{(55+25) \text{ mph}}{0.682 \text{ mph/ft/sec}} \right)^2 0.42 (21 \text{ ft}^2) = 143 \text{ lb}$$

Tailwind condition:

$$D_A = 0.5 \left(0.00236 \frac{\text{lb-sec}^2}{\text{ft}^4} \right) \left(\frac{(55-25) \text{ mph}}{0.682 \text{ mph/ft/sec}} \right)^2 0.42 (21 \text{ ft}^2) = 20 \text{ lb}$$

Notes:

- a. The normal aerodynamic drag on this vehicle in the absence of any headwind or tailwind would be 68 lb.
- b. The headwind more than doubles the drag because the drag increases with the square of the relative headwind velocity, which goes from 55 to 80 mph.
- c. The tailwind reduces the drag considerably due to the speed square effect.

References

1. Li, W.H. and Lam, S.H., *Principles of Fluid Mechanics* (Reading, MA: Addison-Wesley Publishing Company, Inc., 1964), 374pp.
2. Shepherd, D.G., *Elements of Fluid Mechanics* (New York: Harcourt, Brace and World, Inc., 1965), 498pp.
3. Schenkel, F.K., "The Origins of Drag and Lift Reductions on Automobiles with Front and Rear Spoilers," SAE Technical Paper [770389](#), 1977, doi:[10.4271/770389](#).

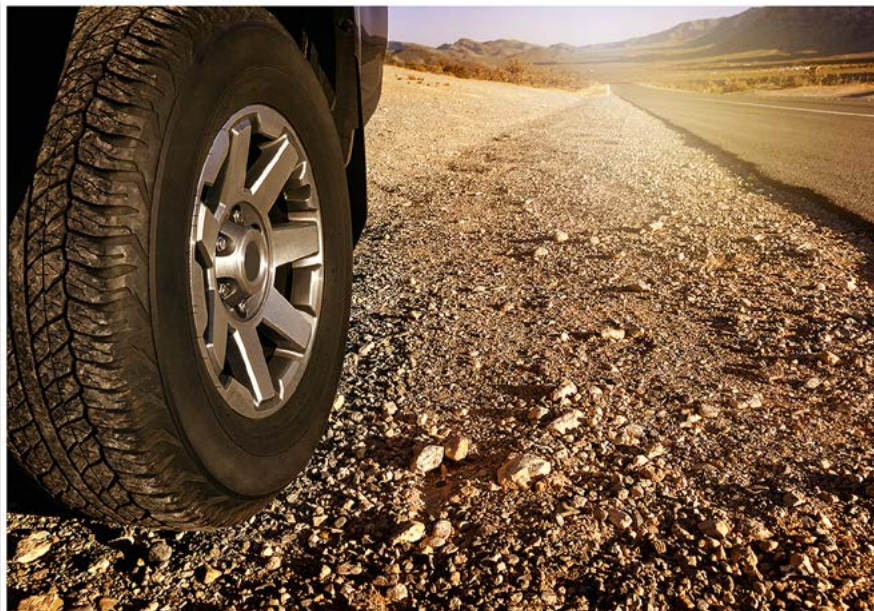
4. Kramer, C., "Introduction to Aerodynamics," Lecture notes for Short Course 1984-01, von Karman Institute for Fluid Dynamics, January 1984, 60pp.
5. Lay, W.E., "Is 50 Miles per Gallon Possible with Correct Streamlining?" SAE Technical Paper [330039](#), 1933, doi:[10.4271/330039](#).
6. Hoerner, S., *Fluid-Dynamic Drag* (Midland Park, NJ: Published by the author, 1965).
7. Kamm, W., "Einfluss der Reichsautobahn auf die Gestaltung von Kraftfahrzeugen," *AIZ* 37 (1943): 341-354.
8. "SAE Vehicle Dynamics Terminology," SAE J670e, Society of Automotive Engineers, Warrendale, PA (see Appendix A).
9. "Vehicle Aerodynamics Terminology," SAE J1594, Society of Automotive Engineers, Warrendale, PA, June 1987, 5pp.
10. Buchheim, R., Deutzenback, K.-R., and Luckoff, H.-J., "Necessity and Premises for Reducing the Aerodynamic Drag of Future Passenger Cars," SAE Technical Paper [810185](#), 1981, doi:[10.4271/810185](#).
11. Hucho, W.-H. and Janssen, L.J., "Beitrag der Aerodynamik im Rahmen einer Scirocco," *AIZ* 77 (1975): 1-5.
12. Scibor-Rylski, A.J., *Road Vehicle Aerodynamics*, 2nd ed. (London: Pentech Press, 1984), 244pp.
13. Max Sardou, M.S.W.T. and Sardou, S.A., "Why to Use High Speed Moving Belt Wind Tunnel for Moving Ground Surface Vehicles Development," Lecture notes for Short Course 1984-01, von Karman Institute for Fluid Dynamics, January 1984, 59pp.
14. Hucho, W.H., Janssen, L.J., and Emmelmann, H.J., "The Optimization of Body Details-A Method for Reducing the Aerodynamic Drag of Road Vehicles," SAE Technical Paper [760185](#), 1976, doi:[10.4271/760185](#).
15. Gilhaus, A.M. and Renn, V.E., "Drag and Driving-Stability-Related Aerodynamic Forces and Their Interdependence-Results of Measurement on 3/8-Scale Basic Car Shapes," SAE Technical Paper [860211](#), 1986, doi:[10.4271/860211](#).
16. Cole, D., "Elementary Vehicle Dynamics," *Course Notes in Mechanical Engineering*, The University of Michigan, Ann Arbor, MI, 1972.
17. Hucho, W.-H. Ed., *Aerodynamics of Road Vehicles* (London: Butterworths, 1987), 566pp.
18. Hogue, J.R., "Aerodynamics of Six Passenger Vehicles Obtained from Full Scale Wind Tunnel Tests," SAE Technical Paper [800142](#), 1980, doi:[10.4271/800142](#).
19. Mac Adam, C.C., Sayers, M.W., Pointer, J.D., and Gleason, M., "Crosswind Sensitivity of Passenger Cars and the Influence of Chassis and Aerodynamic Properties on Driver Performance," *Vehicle Systems Dynamics* 19 (1990): 36.
20. Willumeit, H.P. et al., "Method to Correlate Vehicular Behavior and Driver's Judgment under Side Wind Disturbances," *Dynamics of Vehicles on Roads and Tracks, Proceedings*, Swets and Zeitlinger B.V., Lisse, 1988, 509-524.
21. Uffelmann, F., "Influence of Aerodynamics and Suspension on the Cross-Wind Behaviour of Passenger Cars - Theoretical Investigation under Consideration of the Driver's Response," in Nordstrom, O. Ed., *Dynamics of Vehicles on Roads and Tracks* (Lisse: Swets and Zeitlinger B.V., 1986), 568-581.
22. van den Heme, H. et al., "The Cross-Wind Stability of Passenger Cars: Development of an Objective Measuring Method," *Fourth IAVSD Congress*, 1987.

23. Clark, S.K. et al., "Rolling Resistance of Pneumatic Tires," The University of Michigan, Interim Report No. UM-010654-3-1, July 1974, 65pp.
24. Fancher, P.S. and Winkler, C.B., "Retarders for Heavy Vehicles: Phase III Experimentation and Analysis; Performance, Brake Savings, and Vehicle Stability," U.S. Department of Transportation, Report No. DOT HS 806 672, January 1984, 144pp.
25. Buchheim, R., "Contributions of Aerodynamics to Fuel Economy Improvements of Future Cars," *Fuel Economy Research Conference*, Section 2: Technical Presentations.



Ride

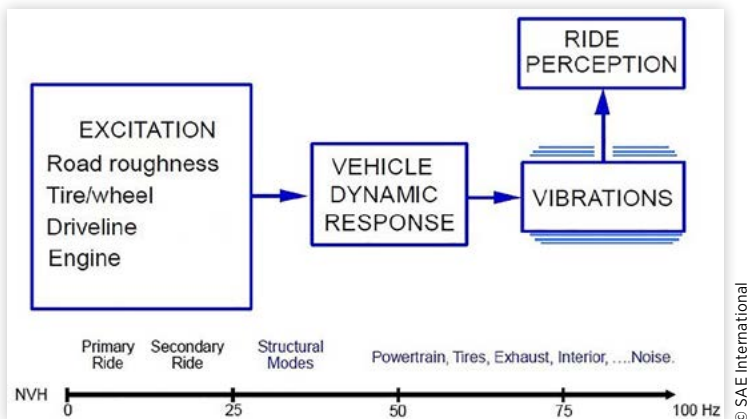
© Shutterstock



Tires over rough terrain.

Automobiles travel at high speed and as a consequence experience a broad spectrum of vibrations. These are transmitted to the passengers either by tactile, visual, or aural paths. The term “ride” is commonly used in reference to tactile and visual vibrations, while the aural vibrations are categorized as “noise.” Alternatively, the spectrum of vibrations may be divided up according to frequency and classified as ride (0–25 Hz) and noise (25–20,000 Hz). The 25 Hz boundary point is approximately the lower frequency threshold of hearing, as well as the upper frequency limit of the simpler vibrations common to all motor vehicles. The different types of vibrations are usually so interrelated that it may be difficult to consider each separately; i.e., noise is usually present when lower-frequency vibrations are excited.

The vibration environment is one of the more important criteria by which people judge the design and construction quality of a car or truck. The subjective nature of

FIGURE 5.1 The ride dynamic system.

these judgments makes it a challenge for engineers to develop objective methods for addressing ride as a performance mode of the vehicle.

The lower-frequency ride vibrations (0 - 25 Hz) are manifestations of dynamic behavior common to all rubber-tired motor vehicles. The study of these modes is therefore an important area of vehicle dynamics and is the focus of this chapter. As an aid in developing a systematic picture of ride behavior, it is helpful to think of the overall dynamic system as shown in [Figure 5.1](#). The vehicle is a dynamic system but only exhibits vibration in response to excitation inputs. The response properties determine the magnitude and direction of vibrations imposed on the passenger compartment, and ultimately determine the passenger's perception of the vehicle. Therefore, an understanding of ride involves the study of three primary topics:

- Ride excitation sources
- Basic mechanics of vehicle vibration response
- Human perception and tolerance of vibrations

Excitation Sources

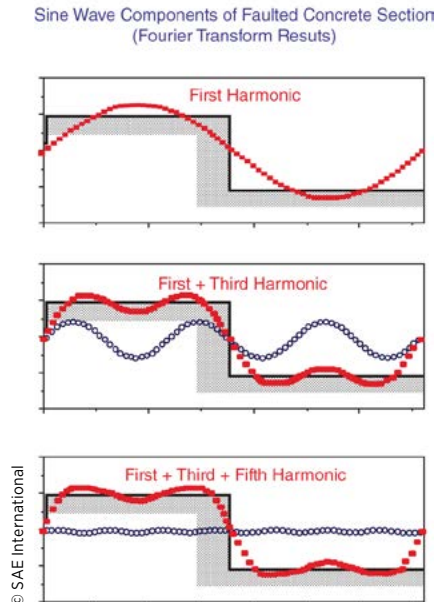
There are multiple sources from which vehicle ride vibrations may be excited. These generally fall into two classes—road roughness and on-board sources. The on-board sources arise from rotating components and include the tire/wheel assemblies, the driveline, and the engine.

Road Roughness

Road roughness encompasses everything from potholes that are the result of localized pavement failures to the ever-present random deviations reflecting the practical limits of precision to which the road surface can be constructed and maintained. Roughness is described by the elevation profile along the wheel tracks over which the vehicle passes. Road profiles fit the general category of “broad-band random signals” and can therefore be described either by the profile itself or by its statistical properties. One of the most useful representations is the Power Spectral Density (PSD) function.

Like any random signal, the elevation profile measured over a length of road can be decomposed by the Fourier Transform process [1] into a series of sine waves varying in their amplitudes and phase relationships. A plot of the amplitudes versus spatial frequency is the PSD. Spatial frequency is expressed as the “wavenumber” with units of cycles/foot (or cycles/meter), and is the inverse of the wavelength of the sine wave on which it is based.

What is a PSD?

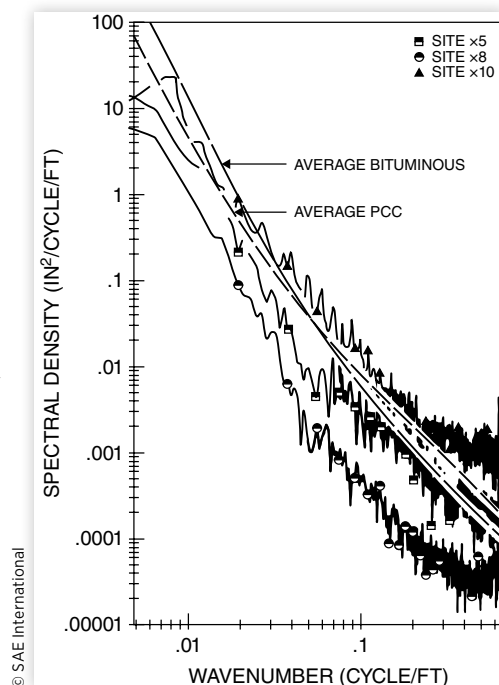


One objective measure of road roughness is established by the International Roughness Index (IRI). With this system, road roughness is measured with a high-speed profilometer resulting in units of m/km or in/mi (i.e., incremental elevation / distance traveled).

As shown in the figure above, roads with an IRI of 100 or less are considered smooth; 150 is typical of many well-maintained road surfaces; and rough roads may have an IRI of around 200. Anything over 200 is considered to be unacceptable to most people.

Road elevation profiles can be measured either by performing close interval rod and level surveys [2] or by high-speed profilometers [3]. When the PSDs are determined, plots such as those shown in [Figure 5.2](#) are typically obtained [4, 5, 6]. Although the PSD of every road section is unique, all roads show the characteristic drop in amplitude with wavenumber. This simply reflects the fact that deviations in the road surface on the order of hundreds of feet in length may have amplitudes of inches, whereas those only a few feet in length are normally only fractions of an inch in amplitude. The general amplitude level of the plot is indicative of the roughness level—higher amplitudes implying rougher roads. The wavenumber range in the figure corresponds to wavelengths of 200 ft (61 m) on the left at 0.005 cycle/ft (0.016 cycle/meter), to about 2 ft (0.6 m) on the right at 0.5 cycle/ft (1.6 cycles/meter).

FIGURE 5.2 Typical spectral densities of road elevation profiles.



The upper PSD in the figure is a deteriorating Portland Cement concrete (often called “rigid pavement” or PCC) road surface. Note a marked periodicity in the range of wavenumber between 0.01 cycle/foot (0.03 cycle/meter) and 0.1 cycle/foot (0.3 cycle/meter), which is related to the fixed slab length used in the construction of the road. The lowest PSD is a similar road overlaid with a bituminous asphalt surface layer yielding a much smoother surface (the PSD amplitude is reduced by an order of magnitude). The reduction is especially pronounced in the high-wavenumber range. The intermediate PSD is a typical asphalt road (often called “flexible pavement”).

Although many ride problems are peculiar to a specific road or road type, the notion of “average” road properties can often be helpful in understanding the response of a vehicle to road roughness. The general similarity in the spectral content of the roads seen in [Figure 5.2](#) (i.e., that elevation amplitude diminishes systematically with increasing wavenumber) has long been recognized as true of most roads [7, 8, 9]. Consequently, road inputs to a vehicle are often modeled with an amplitude that diminishes with frequency to the second or fourth power approximating the two linear segments of the curve shown in the figure. The average properties shown in the figure are derived from recent studies of a large number of roads [4]. The spectral contents are slightly different for bituminous and Portland Cement concrete roads. Other less common road types, such as surface treatment and gravel roads, will have slightly differing spectral qualities [6]. The general level of the elevation of the curve may be raised or lowered to represent different roughness levels, but the characteristic slopes and inflection points are constant. The difference between the bituminous and PCC average curves is the relative magnitude of high-versus low-wavenumber content. For a given overall roughness, more of it is concentrated in the high wavenumber (short wavelength) range with PCC surfaces, resulting in high frequency vibrations. For bituminous surfaces, greater excitation in the low frequency range is due to the low wavenumber range.

The PSD for average road properties shown in [Figure 5.2](#) can be represented by the following equation:

$$G_z(v) = G_o \left[1 + (v_o/v)^2 \right] / (2\pi v)^2 \quad (5.1)$$

where:

- $G_z(v)$ = PSD amplitude ($\text{ft}^2/\text{cycle/ft}$)
- v = Wavenumber (cycles/ft)
- G_o = Roughness magnitude parameter (roughness level)
 - = 1.25×10^5 for rough roads
 - = 1.25×10^6 for smooth roads
- v_o = Cutoff wavenumber
 - = .05 cycle/foot for bituminous roads
 - = .02 cycle/foot for PCC roads

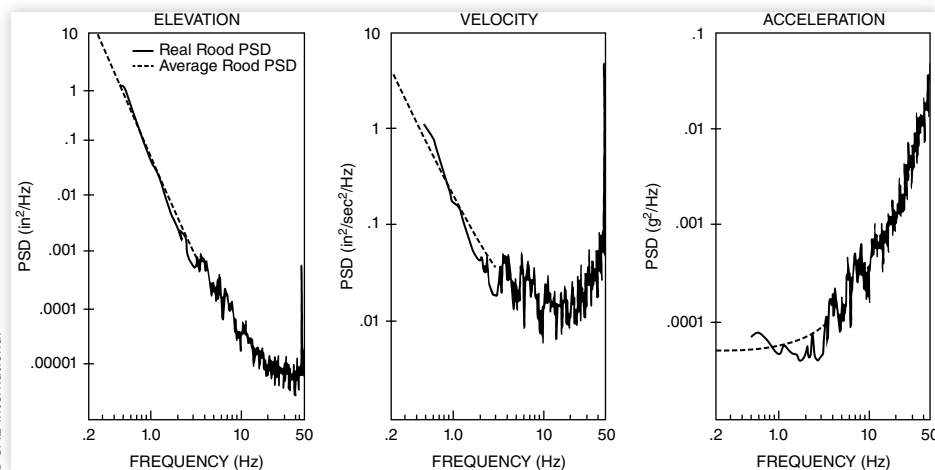
[Equation 5.1](#), in combination with a random number sequence, provides a very useful method to generate road profiles with random roughness that have the spectral qualities of typical roads [4]. This makes it useful in the study of vehicle dynamics.

Since the roughness of a road is the deviation in elevation seen by a vehicle as it moves along the road, it therefore serves as a vertical displacement at the wheels and excites ride vibrations. The most common and meaningful measure of ride vibration is vertical acceleration, therefore a thorough study of vehicle ride dynamics should consider road roughness as an acceleration input at the wheels. To do this, two steps are involved: First, a speed of travel must be assumed such that the elevation profile is transformed to displacement as a function of time. Second, this displacement may be differentiated once to obtain the velocity of the input at the wheels, and then differentiated a second time to obtain an acceleration. [Figure 5.3](#) shows the transformation

of road profile elevation first to a velocity, then to an acceleration input to a vehicle. A vehicle speed of 50 mph has been assumed. The conversion from spatial frequency (cycles/foot) to temporal frequency (cycles/second or Hz) is obtained by multiplying the wavenumber by the vehicle speed in feet/second.

FIGURE 5.3 Elevation, velocity, and acceleration PSDs of road roughness input to a vehicle traveling at 50 mph on a real and average road.

© SAE International



Note that the acceleration spectrum has a relatively constant amplitude at low frequency, but begins increasing rapidly above 1 Hz such that it is an order of magnitude greater at 10 Hz. Viewed as an acceleration input, road roughness presents its largest inputs to the vehicle at high frequency, thereby having the greatest potential to excite high-frequency ride vibrations unless attenuated accordingly by the dynamic properties of the vehicle. As will be seen, the vehicle's ability to attenuate this high frequency input is an important aspect of the "ride isolation" properties for which suspensions are designed.

By considering road roughness as an acceleration input, the primary effect of the vehicle's travel speed can be demonstrated. At any given temporal frequency the amplitude of the acceleration input will increase with the square of the speed. This is illustrated by considering a simple sine wave representation of roughness:

$$Z_r = A \sin(2\pi v X) \quad (5.2)$$

where:

Z_r = Profile elevation

A = Sine wave amplitude

v = Wavenumber (cycles/ft)

X = Distance along the road

Since the distance, X , is equal to the velocity, V , times the time of travel, t , Equation 5.2 can be rewritten as:

$$Z_r = A \sin(2\pi v V t) \quad (5.3)$$

Differentiating twice to obtain acceleration produces:

$$\ddot{Z}_r = -(2\pi v V)^2 A \sin(2\pi v V t) \quad (5.4)$$

As shown in Equation 5.4, the acceleration amplitude coefficient contains the velocity squared term. In general, increasing the assumed speed in Figure 5.3 will cause the acceleration plot to shift upward due to the effect of the speed-squared term. It may also be noted that the curve would shift to the left slightly because of the corresponding change in the temporal frequency represented by each roughness wavenumber. This also adds to the acceleration amplitude, although not as strongly as the speed-squared effect.

Our discussion thus far has focused on the notion that road roughness acts only as a vertical input to the vehicle, exciting the bounce and pitch motions without regard to a roll excitation. This requires that the road profile points in the left and right wheeltracks are averaged before processing in order to obtain the PSD (the PSDs of either wheeltrack will usually appear quite similar to that of the average). If the ride analysis is to remain focused on the pitch and bounce modes, this may be sufficient. The reality, however, is that the road roughness at the left and right wheeltracks are not likely to be equal and therefore at any given location on the road, the difference in elevation between the left and right road profile points represents a roll excitation input to the vehicle. The PSD for the roll displacement input to a vehicle is typically similar to that for the elevation, as was shown in Figure 5.2, although its amplitude is attenuated at wavenumbers below 0.02 to 0.03 cycle/ft. Typical roll excitation characteristics of road roughness are more readily seen by normalizing the roll amplitude (difference between the wheeltracks) by the vertical amplitude (average of the wheeltracks) in each wavenumber band of the PSD. As a result, the roll excitation can be observed in relationship to the vertical excitation present in the road.

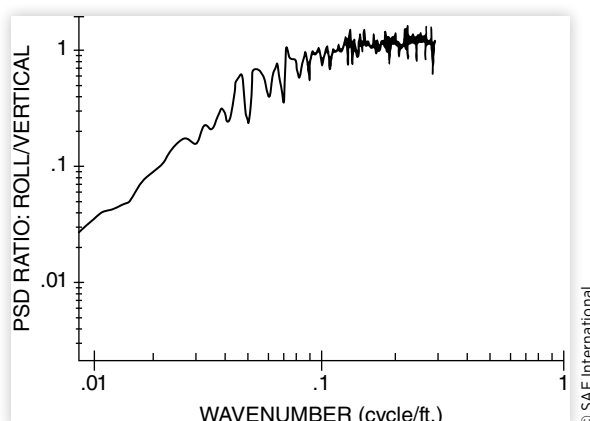
The PSDs obtained have the characteristics as shown in Figure 5.4. At low wavenumbers (long wavelengths) the roll input from a roadway is much lower in its relative magnitude than that of the vertical input to the vehicle; this is due to the fact that the difference in elevation is constrained by civil engineering requirements to maintain the superelevation of the road.

The normalized roll input magnitude grows with wavenumber because of the natural tendency for bumps in the left and right wheeltracks to become less correlated at high wavenumbers (short wavelengths). For most vehicles, resonance in roll occurs at a lower frequency (0.5–1.0 Hz) than resonance in bounce. Thus of the two, bounce is the more dominant response. At higher frequency, where the bounce and roll inputs are more nearly equal in magnitude, vehicles are less responsive to roll.

For example, consider a vehicle with a roll natural frequency of 1.0 Hz traveling at 60 mph (88 ft/sec). Roll excitation in the road at the 88 ft wavelength (0.011 cycle/ft) will therefore directly excite roll motions. Since the roll amplitude at this wavenumber is only 10 percent of the vertical input, the vehicle's occupants will be more conscious of bounce vibrations than those caused by roll motion.

At low speed — e.g., 6 mph — a 1.0 Hz roll resonant frequency would be excited by input from wavenumbers on the order of 0.1 cycle/ft, at which the roll and vertical inputs are essentially equal in magnitude. The roll and bounce motions would therefore be approximately equal as well. The common case where this is observed is in the off-road operation of 4 × 4 vehicles where the exaggerated ride vibrations are often composed of both roll and bounce motions.

FIGURE 5.4 Spectral density of normalized roll input for a typical road.



Tire/Wheel Assembly

Ideally, the tire/wheel assembly is soft and compliant in order to absorb road bumps as part of the ride isolation system. At the same time, it ideally does not exhibit a rotating unbalance or other imperfections that might contribute to an excitation that would be an input to the vehicle. Practically speaking, the imperfections in the manufacture of tires, wheels, hubs, brakes, and other rotating assemblies may result in nonuniformities of three major types:

1. Mass unbalance
2. Dimensional variations
3. Stiffness variations

These nonuniformities all combine in a tire/wheel assembly that cause it to experience variations in the forces and moments at the ground as it rolls on the road surface [10]. In turn, these variations are transmitted to the axles of the vehicle and act as excitation sources for ride vibrations [11]. The force variations may be in the vertical (radial) direction, longitudinal (tractive) direction, and/or the lateral direction [12]. The moment variations in the directions of the overturning moment, aligning torque, and rolling resistance moment generally are not significant as sources of ride excitation, although they can contribute to steering system vibrations.

Dynamic unbalance derives from a nonuniform and asymmetric mass distribution in the individual components of the assembly along or about the axis of rotation [14]. Asymmetry about the axis of rotation is observed as static unbalance. The resultant effect is a force rotating in the wheel plane with a magnitude proportional to the unbalance mass, the radius from the center of rotation, and the square of the rotational speed. Because it is rotating in the wheel plane, this force produces both radial as well as longitudinal excitations. The unbalance force is given by the equation:

$$F_i = (m r) \omega^2 \quad (5.5)$$

where:

F_i = Unbalance force

$m r$ = Unbalance magnitude (mass times radius)

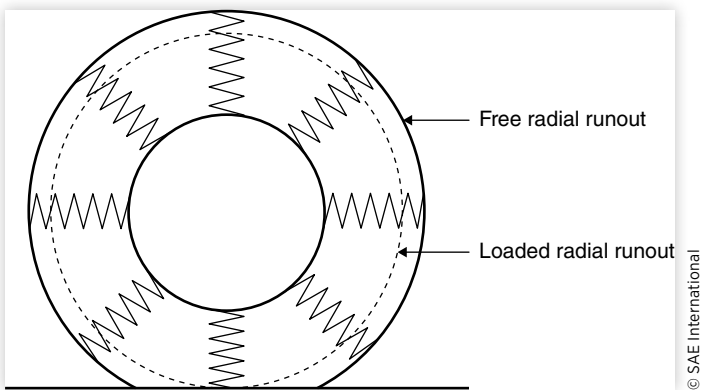
ω = Rotational speed (rad/sec)

Dynamic unbalance creates a rotating torque on the wheel, appearing as variations in the overturning moment and aligning torque at the wheel rotational frequency. Dynamic unbalance has the biggest effect on steered wheels which may experience steering vibrations as a result of the excitation. Note that static unbalance can exist in the absence of dynamic unbalance, and vice versa. The tires, wheels, hubs, and foundation brake components (i.e., discs or drums) may all contribute to the unbalance effects.

The tire, being an elastic body analogous to an array of radial springs, may exhibit variations in stiffness about its circumference. [Figure 5.5](#) illustrates that tire model. The free length of the springs establishes the dimensional nonuniformities (free radial runout), yet the variations in their compressed length at a nominal load determines the rolling nonuniformities (loaded radial runout).

Dimensional runouts in the wheel or hub on which the tire is mounted do not produce stiffness variations directly, but may contribute to the free- or loaded-radial runouts that are observed.

The significant effect of the nonuniformities in a tire/wheel assembly is the generation of excitation forces and displacements at the axle of the vehicle as the wheel rotates.

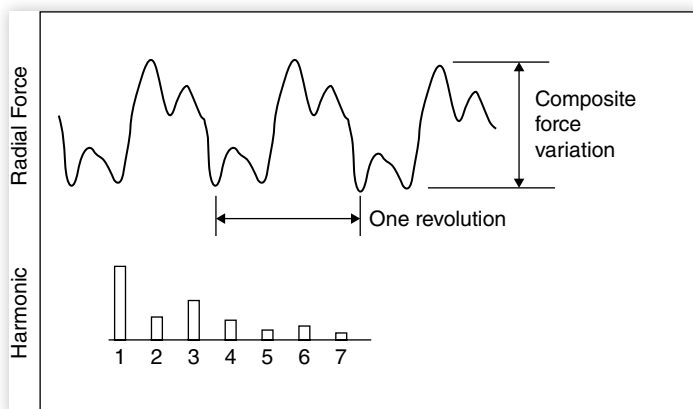
FIGURE 5.5 Tire radial spring model.

© SAE International

The excitation force observed when the wheel is rolled at constant radius and speed repeats with each revolution of the wheel [15].

Radial force variations measured at a constant radius typically take the form illustrated in [Figure 5.6](#). The peak-to-peak magnitude of force variation is called “composite force variation,” were the force signature may be described in more detail by the amplitude of the harmonics of which it is composed. Using a Fourier transform [1], the composition of the signal as a series of sine waves at the fundamental as well as at each multiple frequency can be determined. The amplitude of each harmonic is usually the parameter of primary interest. Although the phase angle of each must also be known to reconstruct the original signal, phase angle information appears to have little relationship to ride phenomena [16].

The first harmonic of the radial force variation tends to be less than that of the composite, with the higher-order harmonics tending to be of diminishing magnitude. For passenger-car tires a decrease of about 30 percent per order has been observed [15], with less of an effect at high speed. Runout of the hub and wheel may also contribute to the radial force variations. The runout may be quantified by finding the point-by-point average radius of the two bead seats around the circumference of the assembled wheel. The first harmonic force variation arising from this source is closely linked to the runout of the wheel. Although the force variation may initially be expected to be equal to the runout times the stiffness of the tire mounted on the wheel, closer inspection and

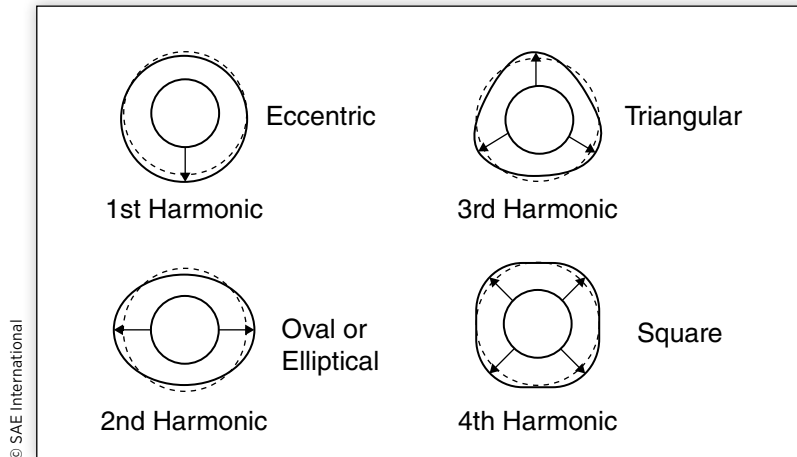
FIGURE 5.6 Tire radial force variations.

© SAE International

consideration of experimental results has shown that the force variation is only about 70 percent of that magnitude, indicating that the tire partially masks runout of the wheel [17]. Higher harmonic runouts in the wheel are not as closely related to radial force variations in the overall assembly.

The various harmonics of radial nonuniformities in a tire/wheel assembly are functionally equivalent to imperfections in the shape as shown in [Figure 5.7](#).

FIGURE 5.7 Radial nonuniformities in a tire.



- 1. Eccentricity — The tires, wheels, and hubs individually may exhibit radial eccentricity, resulting in a first-harmonic nonuniformity which produces both radial and tractive excitation on the axle. Since there is one high point and one low point on the assembly, the excitation occurs at the rotational speed of the wheel (10–15 Hz at normal highway speeds). The overall magnitude of the nonuniformity for the assembly depends on the magnitudes in the individual components and their relative positions when assembled [11]. This means eccentricity in one component may partially compensate for that in others when the high and low points of the different parts are matched during the assembly of the tire and wheel. The “match-mounting” technique is commonly used in the tire/wheel assemblies for passenger cars to minimize first-harmonic nonuniformities of the assembly. In those cases, wheels may be purposely manufactured with an eccentricity equivalent to the average radial runout of the production tires with which they will be used. The tires and wheels are marked for high/low points to facilitate match-mounting.
- 2. Ovality — Tires and wheels may have elliptical variations that add or subtract depending on the mounting positions [11], although match-mounting is not practical for minimizing this nonuniformity. Because the assembly has two high points and two low points on its circumference, radial and tractive force excitation is produced at twice the wheel rotational frequency (20–30 Hz at normal highway speeds).
- 3. Higher-order radial variations — Third- and higher-order variations are predominantly of importance in the tire only. Such variations in the wheel are substantially absorbed by the tire [13]. The third harmonic is analogous to a tire with a triangular shape, the fourth harmonic reflects a square shape, and so on. While tires do not purposely have these shapes, the effects may arise from construction methods. For example, in a tire with four plies of fabric material, the overlaps associated with each ply would normally be distributed around the circumference of the tire. The additional stiffness created at each of the overlap positions will then result in a fourth-harmonic stiffness variation and an

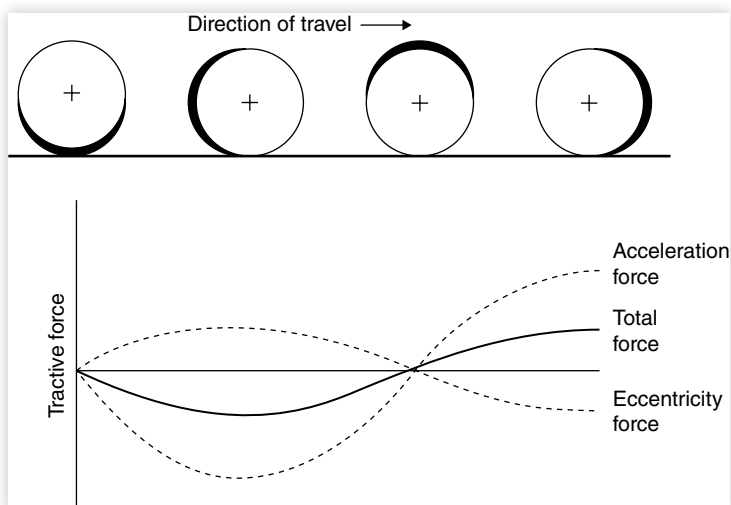
associated fourth-harmonic force variation. The force variations act in the radial and tractive force directions at the multiple of wheel speed equal to the harmonic number.

Because the magnitude of the radial force variation is relatively independent of speed, low-speed measurements of radial force variations at a constant radius (the method commonly used by tire manufacturers to monitor production) indicate the magnitude of the force tending to excite ride vibrations. Only the frequency is changed with speed. The nonuniformity force can be treated as a direct excitation at the axle. As a point of clarity, it should be noted that the excitation force is not equivalent to the actual force variation experienced at the axle, as the dynamic response of the vehicle can greatly amplify the forces [10]. Nevertheless, the measurement of radial force variations described above is the proper and valid means to characterize the radial excitation potential associated with nonuniformities in the tire and wheel components. Alternatively, measurements of loaded radial runout are also valid and can be transformed to radial force variation by simply multiplying by the radial spring rate of the tire.

Tractive force variations arise from dimensional and stiffness nonuniformities as a result of two effects. The causes are best illustrated by considering a simple eccentric wheel model, as shown in [Figure 5.8](#). With eccentricity, even at low speed, the axle must roll up and down the “hill” represented by the variation in radius of the wheel assembly. Thus, a longitudinal force is involved and a tractive force variation is observed. Its magnitude will be dependent on the load carried and the amount of eccentricity [17]; however this magnitude is independent of speed.

On the other hand, at high speed, the wheel must accelerate and decelerate in the course of a revolution because of its varying radius. Thus, a tractive force at the ground, and accordingly at the hub, must appear in order to produce the acceleration. Here, the magnitude of the force will be dependent on the longitudinal stiffness properties of the tire and the rotational moment of inertia of the wheel. The magnitude of the tractive force arising from this mechanism will vary with speed because the acceleration varies with speed, typically increasing by a factor of about 5 over the speed range of 5 to 60 mph. Therefore, the tractive force variation in a tire or tire/wheel assembly can only be measured validly at high speed, and the rotational inertia properties of the wheel assembly must be closely matched to that of the vehicles on which they will be mounted.

FIGURE 5.8 Tractive force variations arising from an eccentric wheel.



Lateral force variations may arise from nonuniformities in the tire but otherwise cannot be readily related to lateral runout effects in the wheel or hub components. They also tend to be independent of speed; thus, measurements of the force magnitudes at low speed are also valid for high speed [11]. First-order lateral variations in the tires or wheels, or in the way in which they are mounted, will result in wobble, affecting the dynamic balance of the assembly. The wobble in the wheel may contribute a minor lateral force variation, but may also result in radial and tractive force variations comparable to the effect of ovality [11] owing to the fact that the wheel is elliptical in the vertical plane.

Higher-order lateral variations are predominantly important in the tire only. Wheel variations are substantially absorbed by the tire [11, 13]. These sources could potentially cause steering vibrations, but otherwise have not been identified as the cause of ride problems.

In general, the imperfections in tires and wheels tend to be highly correlated [18, 19] such that radial variations are usually accompanied by unbalance and tractive force variations. Thus, it may be difficult to cure a tire-related ride problem simply by correcting one condition (such as unbalance) without consideration of the other nonuniformities likely to be present.

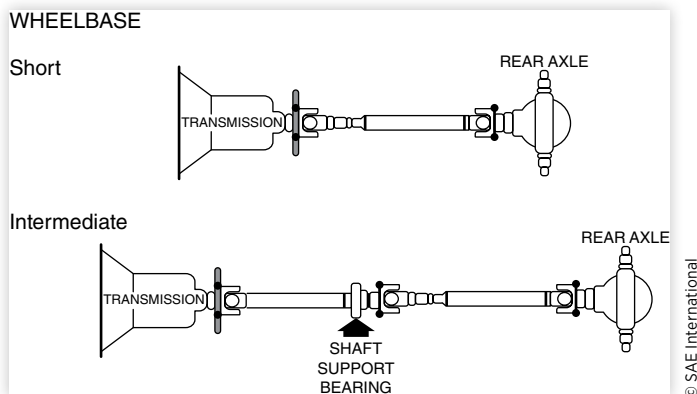
Wrapping up the discussion of the tire/wheel assembly as a source of ride excitation, it must be recognized that the assembly is a dynamic system and as such influences the excitation of the axle. This influence derives from the modal resonance properties of the assembly, which at the low-frequency end are dominated by the tire tread band resonances. The capacity to resonate makes the assembly a vibration absorber at certain modal frequencies, while accentuating the transmissibility properties at the antiresonance frequencies [20]. Ultimately, the tire can play a significant role in noise, vibration, and harshness (NVH) of a motor vehicle, and in the ride development process the vehicle must be properly tuned to avoid various buzzes and booms that can be triggered by tire response. For a detailed presentation on tires, please see Chapter 10.

Driveline Excitation

The third major source of excitation to the vehicle arises from the rotating driveline. While the driveline is often considered to be everything from the engine to the driven wheels, the engine/transmission package will be treated separately in the following discussion.

For the sake of clarity, the driveline consists of the driveshaft, gear reduction, differential in the drive axle, and axle shafts connecting to the wheels. Of these components, the driveshaft with its spline and universal joints has the most potential for exciting ride vibrations. The rear axle gearing and remainder of the driveline are also capable of generating vibrations in the form of noise, a result of the gear mating which can set up torsional vibrations along the drivetrain. These generally occur at frequencies above those considered as ride, however.

Within the driveline, the most frequent ride excitations arise from the driveshaft, normally arranged as shown in [Figure 5.9](#) [21]. On rear-drive passenger cars and short-wheelbase trucks, a single-piece shaft is commonly used, whereas on long-wheelbase trucks and buses a multiple-piece shaft supported by an intermediate bearing is frequently required. Excitations to the vehicle arise directly from two sources: (1) mass unbalance of the driveshaft hardware and secondary couples, or (2) moments imposed on the driveshaft due to angulation of the cross-type universal joints [22, 23].

FIGURE 5.9 Typical driveline arrangements [39].

Mass imbalance — Unbalance of the driveshaft may result from the combination of any of the five following factors:

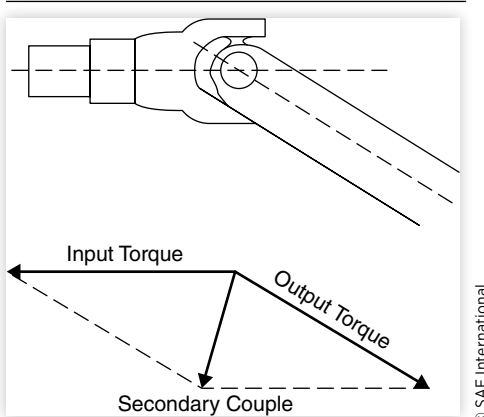
1. Asymmetry of the rotating parts
2. The shaft may be off-center on its supporting flange or end yoke
3. The shaft may not be straight
4. Running clearances may allow the shaft to run off-center
5. The shaft is an elastic member and may deflect

An initial unbalance exists as a result of the asymmetry, runouts, and looseness in the structure. The unbalance creates a rotating force vector, thereby imposing forces on the driveshaft supports in both the vertical and lateral directions. Forces at the front support apply to the transmission, while those in the rear exert forces on the drive axle directly. Where intermediate bearings are employed on trucks, forces may be imposed on the frame via the crossmembers at those locations. The force rotates at the speed of the shaft which is always the wheel speed multiplied by the numerical ratio of the final drive, and is equivalent to engine speed when in direct drive. Altogether, this unbalance appears like a harmonic of the wheel, equal to a value that is the numerical ratio of the rear axle.

In general, the magnitude of the excitation force is equivalent to the product of the unbalance and the square of the rotating speed. Because the shaft is elastic, however, it may bend in response to the unbalance force, allowing for additional asymmetry, as well as an increase in the “dynamic” unbalance. As a result, the apparent magnitude of the unbalance may change with speed. In theory [23], the shaft can only be dynamically balanced for one speed.

Secondary couples — The use of universal joints in a driveline opens the way for the generation of ride excitation forces when they are operated at an angle, due to the secondary couple that is produced. The magnitude and direction of the secondary couple can be determined by a simple vector summation of torques on the universal joint as illustrated in [Figure 5.10](#).

The magnitude of this secondary couple is proportional to the torque applied to the driveline and the angle of the universal joint. When the torque varies during rotation due to engine torque pulsations and/or nonconstant-velocity joints, the secondary

FIGURE 5.10 Torque reactions causing a secondary couple.

couple will vary accordingly. The secondary couple reacts as forces at the support points of the driveline on the transmission, crossmembers supporting the driveline intermediate bearings, and at the rear axle. Hence, these forces vary with driveline rotation and impose excitation forces on the vehicle [22].

When cross-type (Cardan or Hooke) universal joints are used and operate at an angle, they are a direct source of torque pulsations in the driveline [40]. Although these joints do not have a constant relationship between input and output velocity when operated at an angle, they must satisfy the following equation:

$$\frac{\omega_o}{\omega_i} = \frac{\cos \theta}{1 - \sin^2 \beta \sin^2 \theta} \quad (5.6)$$

where:

ω_o = Output speed

ω_i = Input speed

θ = Angle of the U-joint

β = Angle of rotation of the driving yoke

Because of the “ $\sin^2 \beta$ ” term in the denominator, the speed variation reaches a maximum of twice per revolution (at 90 deg. and 270 deg.). Thus, a second-harmonic speed variation occurs as a result of the symmetry of the cross around each arm. It can be shown from the above equation that the maximum speed variation changes with joint angle as:

$$\left| \frac{\omega_o}{\omega_i} \right|_{\max} = \frac{1}{\cos \theta} \quad (5.7)$$

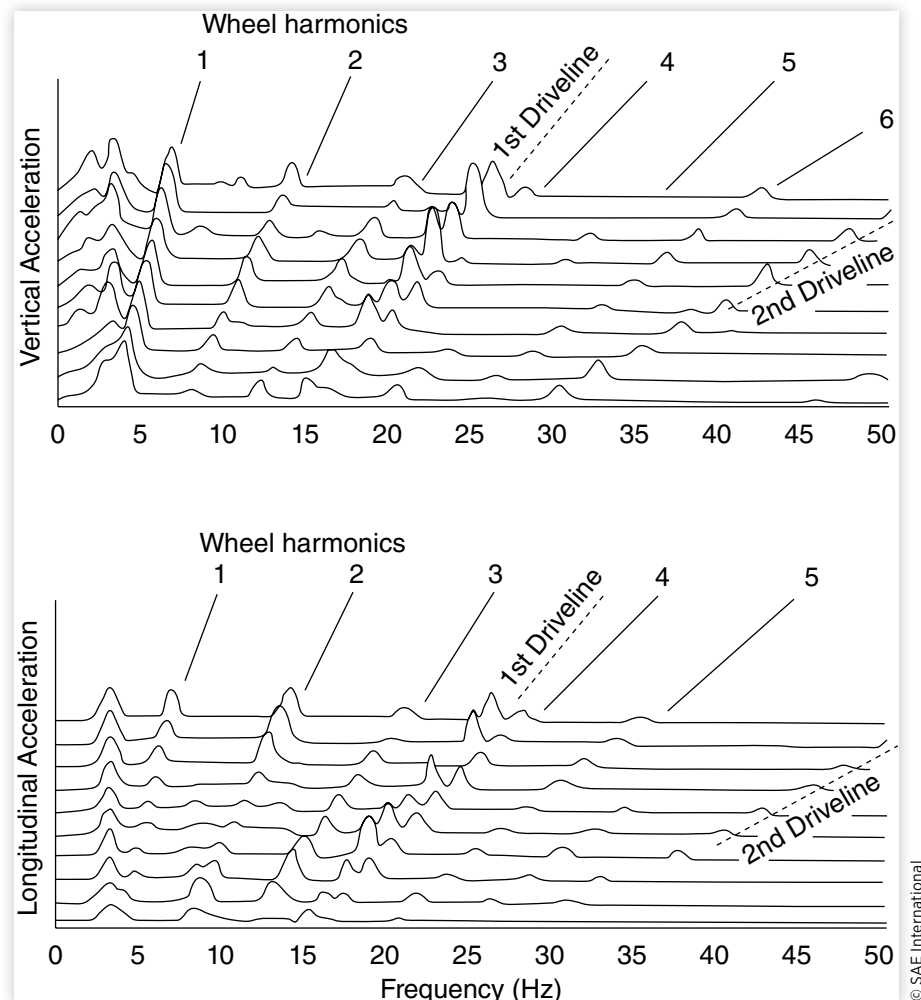
Because of the stiffness of the driveline and the accelerations it experiences, torque variations will necessarily arise from the speed variation. These may cause excitation of torsional vibrations in the driveline, as well as be the source of ride excitation forces on the vehicle. The excitation occurs at the second harmonic of the driveline speed and will vary with the level of torque applied to the driveline. Excitation from the secondary couple can be minimized by proper design of the driveline—maintaining parallel axes on the transmission output shaft and rear axle input shaft, proper phasing of the joints, and keeping angles within the limits recommended by the manufacturers [21, 22, 23].

The torque variations may also act directly at the transmission and the rear axle. Torque variations at the axle will vary the drive forces at the ground and thus may act directly to generate longitudinal vibrations in the vehicle. The torque variations at the transmission produce excitation in the roll direction on the engine/transmission assembly. In part, these variations must be reacted in the mounting points on the body and thus have a direct path to the interior.

[Figure 5.11](#) illustrates the nature of the vibrations that may be produced as a result of driveline and tire/wheel nonuniformities. In this case the accelerations were measured in a truck cab under carefully controlled conditions (i.e., the vehicle was operated on a smooth road to suppress background vibrations that would mask the desired effects, and all of the tire/wheel assemblies, except for one, were carefully match-mounted to achieve consistency in the tire/wheel excitation).

The figure shows a map of the vibration spectra measured at different vehicle speeds. Excitation from tire/wheel inputs appear as ridges in the spectra moving to higher frequency as the speed increases. The first, second, and higher harmonics of the tire/wheel assemblies are evident in the spectra. The ridge at 3.7 times the wheel rotational speed corresponds to the first harmonic of the driveline; this is due to unbalance of the driveshaft and other

FIGURE 5.11 Spectral map of vibrations arising from driveline and tire/wheel nonuniformities.



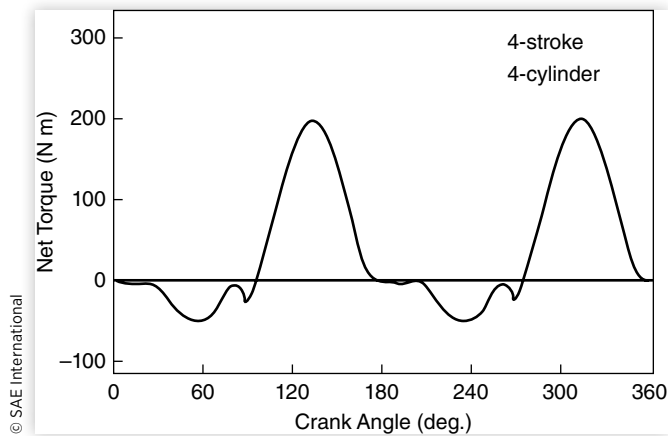
components rotating at this speed. The second harmonic of the driveline at 7.4 times the wheel speed is the result of torque variations in the driveshaft and arise from speed variations caused by the operating angles of the cross-type universal joints.

These or comparable vibrations from the wheels and drivelines will always be present on a vehicle, but are often difficult to recognize in a complex spectrum that includes substantial road roughness excitation. Nevertheless, they constitute one of the factors contributing to the overall ride vibration spectrum and represent one of the areas in which careful design can improve the ride environment of the vehicle.

Engine and Transmission

The engine serves as the primary power source on a vehicle. The fact that it rotates and delivers torque to the driveline opens the possibility that it may be a source for vibration excitation on the vehicle. Further, the mass of the engine in combination with that of the transmission is a substantial component of the chassis and, if used correctly, can act as a vibration absorber.

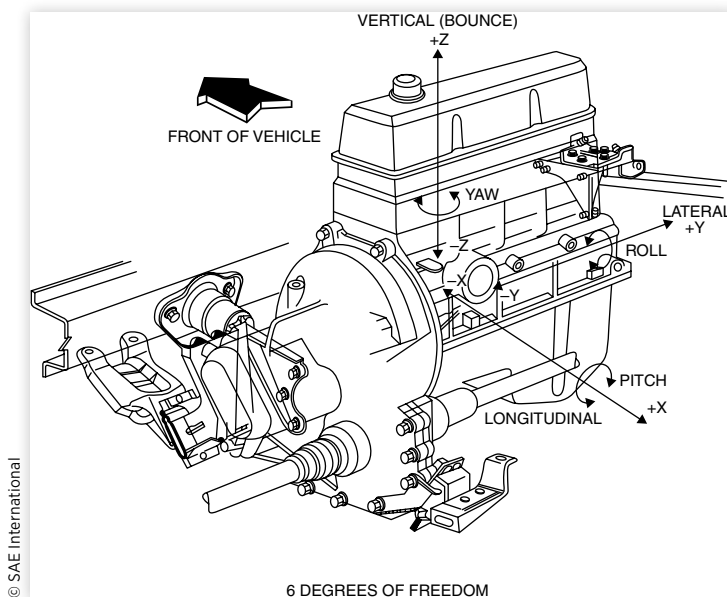
FIGURE 5.12 Torque variations at the output of a four-stroke, four-cylinder engine.



Piston engines deliver power in a cyclic manner; this means the torque delivered by the engine is not constant in magnitude [24]. The torque delivered at the crankshaft consists of a series of pulses corresponding to each power stroke of a cylinder (see [Figure 5.12](#)), and the flywheel acts as an inertial damper along with the inertias and compliances in the transmission. As a result, the torque output to the driveshaft consists of a steady-state component with superimposed torque variations. Those torque variations acting through the driveline may result in excitation forces on the vehicle similar to those produced by the secondary couple from the cross-type universal joints explained in the previous sections.

Because of compliance in the engine and transmission mounts, the system will vibrate in six directions: three translational directions and three rotational directions around the translational axes. The axis system for a transverse-mounted front-engine configuration is shown in [Figure 5.13](#). The figure also shows a three-point mount typical of those used with most transverse engines today.

FIGURE 5.13 Typical transverse engine and mounting hardware. (Photo courtesy of Ford Motor Company.)



Of all the directions of motion, the most important to vibration is the engine roll direction (i.e., about the lateral axis of a transverse-mounted engine or about the longitudinal axis of an engine mounted in the north-south direction), which is excited by drive torque oscillations. Torque oscillations occur at the engine firing frequency as well as at sub-harmonics of that frequency due to cylinder-to-cylinder variations in the torque profile.

A key to isolating these excitations from the vehicle body is to design a mounting system with (1) a roll axis that aligns with the engine inertial roll axis, and (2) provide a resonance about this axis at a frequency that is below the lowest firing frequency of the engine. By so doing, torque variations which occur above the resonant frequency are attenuated. In effect, the torque is absorbed by the inertial motion of the engine rather than being transmitted to the vehicle body and therefore into the passenger cabin.

The inertial axis of four-cylinder engines will generally be inclined downward toward the transmission because of the contribution from the mass of the transmission. This requires the mounting system to be low at the transmission end and high at the front of the engine. On V-type engines (six- and eight-cylinder) the inertial axis is lower in the front and permits a mounting system that is more closely aligned with the crankshaft.

The worst-case scenario is the isolation of the idle speed torque variations for a four-cylinder engine with the transmission in drive, which may have a firing frequency of 20 Hz or below. Successful isolation therefore requires a roll axis resonance of 10 Hz or below. Because the system acts like a simple second-order mass spring dynamic system [14], torque variations at frequencies below the resonant frequency will be felt directly at the mounts. When the system is operating close to the torsional resonant frequency, excitation amplitudes that are much greater than the torque variations will occur.

Engines may produce forces and moments in directions other than roll as a result of the inherent imbalances in the reciprocating/rotating masses [24]. These take the form of forces or couples at the engine rotational frequency or its second harmonic, and must be isolated in the same manner as for the roll mode described above. For the more commonly used engine configurations the balance conditions are as follows:

1. Four-cylinder inline — Vertical force at twice engine rotational frequency; can be balanced with counter-rotating shafts.
2. Four-cylinder, opposed, flat — Various forces and moments at rotational frequency and twice rotational frequency depending on crankshaft arrangement.
3. Six-cylinder inline, four cycle — Inherently balanced in all directions.
4. Six-cylinder inline, two-cycle — Vertical couple generating yaw and pitch moments at the engine rotational frequency; can be balanced.
5. Six-cylinder, 60-deg. V — Generates a counter-rotating couple at rotational frequency that can be balanced with counter-rotating shaft.
6. Six-cylinder, 90-deg. V (uneven firing) — Generates yaw moment of twice rotational frequency; can be balanced with counter-rotating shaft.
7. Six-cylinder, 90-deg. V (even firing) — Generates yaw and pitching moments at crankshaft speed; can be balanced. Also generates complex yaw and pitching moments at twice rotational speed which are difficult to balance.
8. Eight-cylinder inline — Inherently balanced in all directions.
9. Eight-cylinder, 90-deg. V — Couple at primary rotational speed; can be balanced with counter-rotating shafts.

With proper design of the mounting system the mass of the engine-transmission combination can be utilized as a vibration absorber attenuating other vibrations to which

the vehicle is prone. Most often it is used to control vertical shake vibrations arising from the wheel excitations. For this purpose the mounting system is designed to provide a vertical resonance frequency near that of the front wheel hop frequency (12-15 Hz), allowing the engine to act as a vibration damper for this mode of vehicle vibration.

Vehicle Response Properties

A systematic treatment of the vehicle as a dynamic system best starts with the basic properties of a vehicle on its suspension system—i.e., the motions of the body and axles. At low frequencies the body, which is considered to be the sprung mass portion of the vehicle, moves as an integral unit on the suspensions. This is rigid-body motion. The axles and associated wheel hardware, which form the unsprung masses, also move as rigid bodies and consequently impose excitation forces on the sprung mass. Beyond this, one must look to structural modes of vibration and resonances of sub-systems on the vehicle. In addition, there are many individual variables of design and operating conditions that are known to affect the vibration response on the vehicle.

The dynamic behavior of a vehicle can be characterized most meaningfully by considering the input-output relationships. The input may be any of the excitations discussed in the preceding section, or combinations thereof. The output most commonly of interest will be the vibrations on the body. The ratio of output and input amplitudes represents a “gain” for the dynamic system, and the term “transmissibility” is often used to denote the gain. Transmissibility is the nondimensional ratio of response amplitude to excitation amplitude for a system in steady-state forced vibration. The ratio may be one of forces, displacements, velocities, or accelerations. The magnitude ratio of the transfer function is sometimes used in a similar fashion to denote the gain, although this term is normally reserved for use with linear systems.

Suspension Isolation

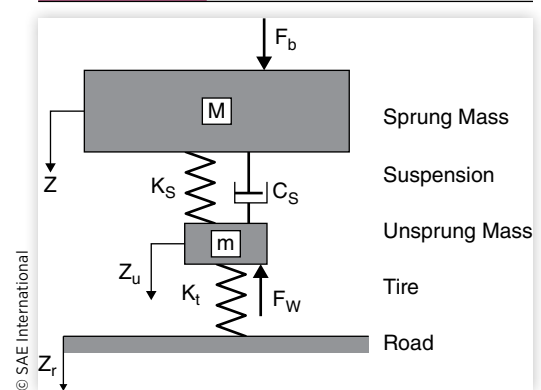
At the most basic level, all highway vehicles share the “ride isolation” properties common to a sprung mass supported by primary suspension systems at each wheel. The dynamic behavior of this system is the first level of isolation from the roughness of the road. The essential dynamics can be represented by a quarter-car model, as shown in [Figure 5.14](#).

It consists of a sprung mass supported on a primary suspension, which in turn is connected to the unsprung mass of the axle. The suspension has both stiffness and damping properties, and the tire is represented as a simple spring. In some cases, a damper is included in the representation of the tire to represent the small amount of damping inherent to its visco-elastic nature [25]. A more detailed discussion of this model is provided in the SAE Ride and Vibration Data Manual [26].

The sprung mass resting on the suspension and tire springs is capable of motion in the vertical direction. The effective stiffness of the suspension and tire springs in series is called the “ride rate” and is determined as follows:

$$RR = \frac{K_s K_t}{K_s + K_t} \quad (5.8)$$

FIGURE 5.14 Quarter-car model.



where:

RR = Ride rate

K_s = Suspension stiffness

K_t = Tire stiffness

In the absence of damping, the bounce natural frequency at each corner of the vehicle can be determined from:

$$\omega_n = \sqrt{\frac{RR}{M}} \quad (\text{rad/sec}) \quad (5.9a)$$

or

$$f_n = 0.159 \sqrt{\frac{RR}{W/g}} \quad (\text{cycles/sec}) \quad (5.9b)$$

where:

M = Sprung mass

$W = M * g$ = Weight of the sprung mass

g = Acceleration due to gravity

When damping is present, as it is in the suspension, the resonance occurs at the “damped natural frequency,” ω_d , given by:

$$\omega_d = \omega_n \sqrt{1 - \zeta_s^2} \quad (5.10)$$

where:

ζ_s = Damping ratio

The damping ratio can be defined according to [Equation 5.11](#) as:

$$= C_s / \sqrt{4K_s M} \quad (5.11)$$

where:

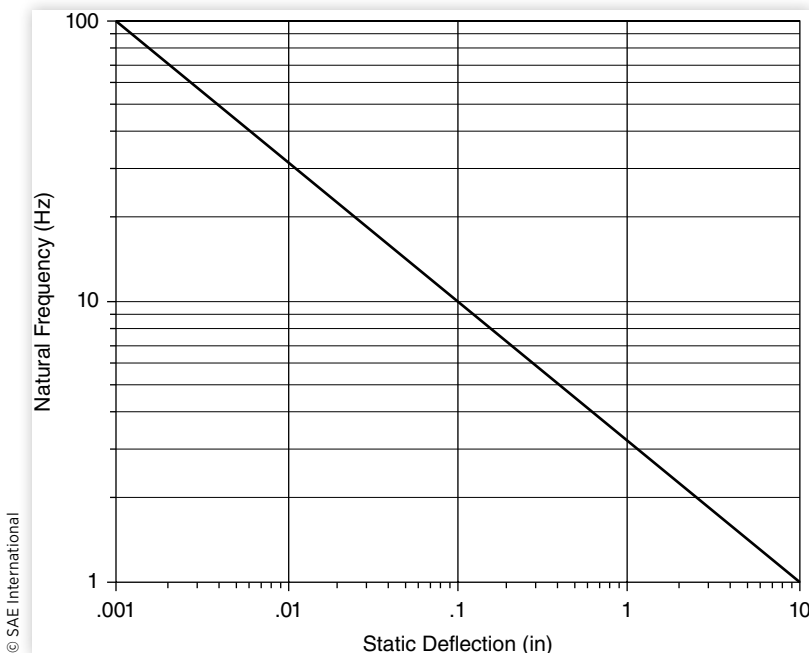
C_s = Suspension damping coefficient

The denominator of [Equation \(5.11\)](#) is the critical damping, C_{crit} .

For ride to be considered to be good, the suspension damping ratio on modern passenger cars usually falls between 0.2 and 0.4. Because of the manner in which damping influences the resonant frequency in the equation above (i.e., under the square root sign), it is usually quite close to the natural frequency. With a damping ratio of 0.2, the damped natural frequency is 98% of the undamped natural frequency, and even at 0.4 damping, the ratio is about 92%. Due to this small difference between the damped and undamped natural frequencies, the undamped natural frequency, ω_n , is commonly used to characterize the vehicle.

The ratio of W/K_s represents the static deflection of the suspension due to the weight of the vehicle. Because the “static deflection” predominates in determining the natural frequency, it is a straightforward and simple parameter indicative of the lower bound on the isolation of a system. [Figure 5.15](#) provides a nomograph relating the natural frequency to static deflection.

A static deflection of 10 in (254 mm) is necessary to achieve a 1 Hz natural frequency—a design considered to be optimum for highway vehicles. A 5-in (127 mm) deflection results in a 1.4 Hz frequency, and 1 in (25 mm) equates to a 3.13 Hz frequency. While it is not necessary for the suspension to provide a full 10 in (254 mm) of travel to achieve the 1 Hz frequency, in general, provisions for larger deflections are necessary with lower frequencies.

FIGURE 5.15 Undamped natural frequency versus static deflection of a suspension.

For example, with a spring rate low enough to yield a 1 Hz frequency, at least 5 in of stroke must be available in order to absorb a bump acceleration of one-half "g" without hitting the suspension jounce stops. Most large cars have a usable suspension stroke in the range of 7 to 8 in. On small, compact cars the stroke may be in the range of 5 or 6 in.

The dynamic behavior for the complete quarter-car model in steady-state vibration can be obtained by writing Newton's Second Law for the sprung and unsprung masses. By considering a free-body diagram for each, the following differential equations are obtained for the sprung and unsprung masses, respectively:

$$M\ddot{Z} + C_s \dot{Z} + K_s Z = C_s \dot{Z}_u + K_s Z_u + F_b \quad (5.12)$$

$$m\ddot{Z}_u + C_s \dot{Z}_u + (K_s + K_t)Z_u = C_s \dot{Z} + K_s Z + K_t Z_r + F_w \quad (5.13)$$

where:

Z = Sprung mass displacement

Z_u = Unsprung mass displacement

Z_r = Road displacement

F_b = Force on the sprung mass

F_w = Force on the unsprung mass

While the two equations mean solving for the unknowns can be complicated, closed-form solutions can be obtained for the steady-state harmonic motion by methods found in classical texts. The solutions of primary interest are those for the sprung mass motion in response to road displacement inputs, forces at the axle, and forces applied directly to the sprung mass. The amplitude ratios for these cases are as follows:

$$\frac{\ddot{Z}}{\ddot{Z}_r} = \frac{K_1 K_2 + j[K_1 C \omega]}{\left[\chi \omega^4 - (K_1 + K_2 \chi + K_2) \omega^2 + K_1 K_2 \right] + j[K_1 C \omega - (1 + \chi) C \omega^3]} \quad (5.14)$$

$$\frac{\ddot{Z}}{F_w/M} = \frac{K_2\omega^2 + j[C\omega^3]}{[\chi\omega^4 - (K_1 + K_2)\chi + K_2]\omega^2 + K_1K_2] + j[K_1C\omega - (1+\chi)C\omega^3]} \quad (5.15)$$

$$\frac{\ddot{Z}}{F_b/M} = \frac{[\chi\omega^4 - (K_1 + K_2)\omega^2] + j[C\omega^3]}{[\chi\omega^4 - (K_1 + K_2)\chi + K_2]\omega^2 + K_1K_2] + j[K_1C\omega - (1+\chi)C\omega^3]} \quad (5.16)$$

where:

j = Complex operator

$C = C_s/M$

$K_1 = K_t/M$

$K_2 = K_s/M$

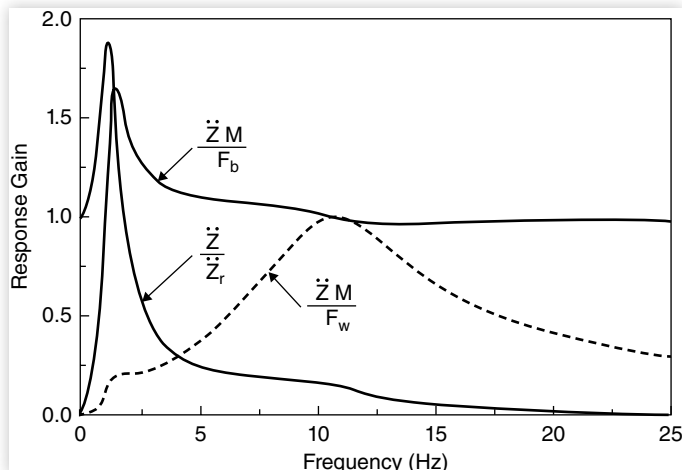
$\chi = m/M$ = Ratio of unsprung to sprung mass

The equations above are complex in form consisting of real and imaginary components, the latter denoted by the “ j ” operator. To obtain the amplitude ratios, the real and imaginary parts of the numerators and denominators must be evaluated at the frequency of interest. The magnitude of the numerator is then determined by taking the square root of the sum of the squares of the real and imaginary parts. The denominator magnitude is determined similarly, and then the ratio of the two may be taken. With appropriate manipulation, the phase angle of the equations may also be determined.

The quarter-car model is limited to the study of the dynamic behavior in the vertical direction only. Yet, using equations such as those developed above, it can be used to examine vibrations produced on the sprung mass as a result of inputs from road roughness, radial forces arising from tire/wheel nonuniformities, or vertical forces applied directly to the sprung mass from onboard sources. The response properties can be presented by examining the response gain as a function of frequency, as shown in [Figure 5.16](#). The gain is defined differently for each type of excitation input.

For road roughness input, the gain is the ratio of sprung mass motion (acceleration, velocity, or displacement) to the equivalent input from the road. Remember that at very low frequency the gain is unity (the sprung mass moves in exact duplication of the road input). By classical design of motor vehicles, the sprung mass is chosen to have its natural

FIGURE 5.16 Quarter-car response to road, tire/wheel, and body inputs.



frequency at or just above 1 Hz. Therefore, at frequencies near 1 Hz the sprung mass is resonating on the suspension and the road inputs are amplified. The amplitude ratio at this peak is very sensitive to the damping level, and on typical passenger cars will be in the range of 1.5 to 3. For typical heavy trucks the amplitude ratio is dependent on the road and operating conditions, but in the worst case may reach levels as high as 5 or 6 [27]. Above resonance, the road inputs are increasingly attenuated. In the range of 10 to 12 Hz, the unsprung mass of the tire/wheel assembly goes into a vertical (hop) resonance mode, adding a small bump to the attenuation curve in this region.

The sprung-mass response to tire/wheel excitation is illustrated by choosing an appropriate nondimensional expression for the gain of the system. The input is an excitation force at the axle due to the tire/wheel assembly. The output—acceleration of the sprung mass—may be transformed to a force by multiplying by the mass. The output is therefore the equivalent force on the sprung mass necessary to produce the accelerations. The gain is zero at zero frequency because the force on the axle is absorbed within the tire spring and no sprung-mass acceleration is produced. It rises with frequency through the 1 Hz sprung mass resonance but continues to climb until wheel resonance occurs in the 10 - 12 Hz range; only then does it diminish. This plot tells much about the sensitivity to radial force variations in tires and wheel components that should be expected with motor vehicles. In particular, it illustrates that vehicles will tend to be the most responsive to excitation from tire and wheel nonuniformities acting near the resonant frequency of the wheel, and at that frequency the nonuniformity force is transmitted directly to the sprung mass (i.e., the response gain of unity).

The response gain for direct force excitation on the sprung mass may be expressed nondimensionally by again using the equivalent force on the sprung mass as the output. The response is similar in this case, but shows greater dominance of the sprung-mass resonance. At high frequencies the gain approaches unity because the displacements become so small that suspension forces no longer change and the force is entirely dissipated as acceleration of the sprung mass. By implication, virtually all extraneous forces that enter into the body of a vehicle are detrimental to ride vibrations.

The basic isolation properties inherent to a quarter-car model combined with typical spectra of road roughness provide an initial picture of the general nature of the ride acceleration spectrum that should be expected to act on a motor vehicle due to road inputs. The sprung-mass acceleration spectrum can be calculated for a linear model by multiplying the road spectrum by the square of the transfer function:

$$G_{zs}(f) = |H_v(f)|^2 G_{zr} \quad (5.17)$$

where:

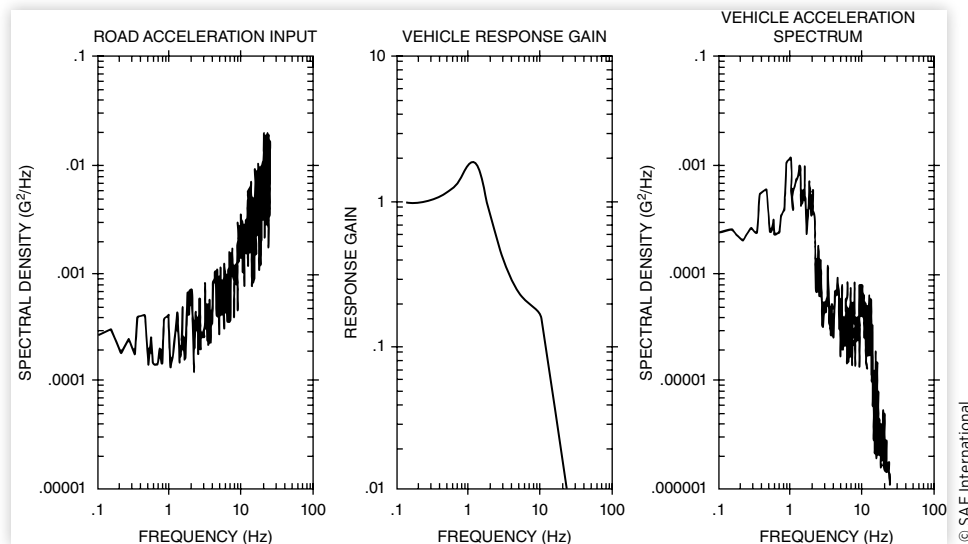
$G_{zs}(f)$ = Acceleration PSD on the sprung mass

$H_v(f)$ = Response gain for road input

G_{zr} = Acceleration PSD of the road input

These results are illustrated in [Figure 5.17](#). While the road represents an input of acceleration amplitude which grows with frequency, the isolation properties of the suspension system compensate by a decrease in the vehicle's response gain.

The net result is an acceleration spectrum on the vehicle with a high amplitude at the sprung-mass resonant frequency, moderate attenuation out through the resonant frequency of the wheel, and a rapid attenuation thereafter. Note that even though the road input amplitude increases with frequency, the acceleration response on the vehicle is qualitatively similar to the vehicle's response gain. Thus the acceleration spectrum provides some idea of the response gain of the system even when the exact properties of the road are not known.

FIGURE 5.17 Isolation of road acceleration by a quarter-vehicle model.

© SAE International

Example Problem

Determine the front and rear suspension ride rates for a mid-size car given the following properties: tire spring rate = 1198 lb/in; front suspension rate = 143 lb/in; rear suspension rate = 100 lb/in. Also estimate the natural frequencies of the two suspensions when the front tires are loaded to 957 lb and the rear tires are loaded to 730 lb.

Solution:

The ride rates can be calculated using [Equation \(5.8\)](#):

$$RR_f = \frac{K_s K_t}{(K_s + K_t)} = \frac{(143)(1198)}{(143 + 198)} = 127 \frac{\text{lb}}{\text{in}}$$

$$RR_r = \frac{K_s K_t}{(K_s + K_t)} = \frac{(100)(1198)}{(100 + 1198)} = 92.3 \frac{\text{lb}}{\text{in}}$$

The natural frequencies for the suspensions can be determined from [Equation \(5.9b\)](#).

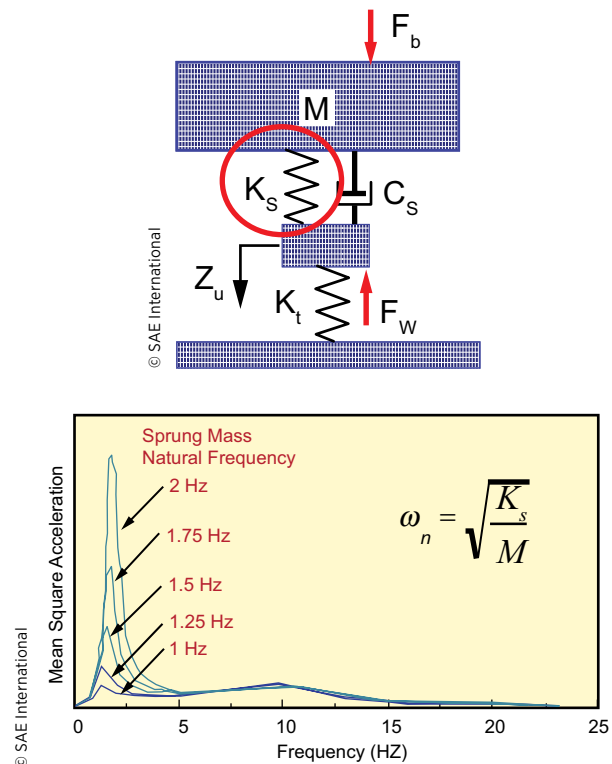
$$f_{nf} = 0.159 \sqrt{\frac{RR_f g}{W}} = 0.159 \sqrt{\frac{127 \text{ lb/in} \times 386 \text{ in/sec}^2}{957 \text{ lb}}} = 1.14 \text{ Hz}$$

$$f_{nr} = 0.159 \sqrt{\frac{RR_r g}{W}} = 0.159 \sqrt{\frac{92.3 \text{ lb/in} \times 386 \text{ in/sec}^2}{730 \text{ lb}}} = 1.11 \text{ Hz}$$

Suspension Stiffness

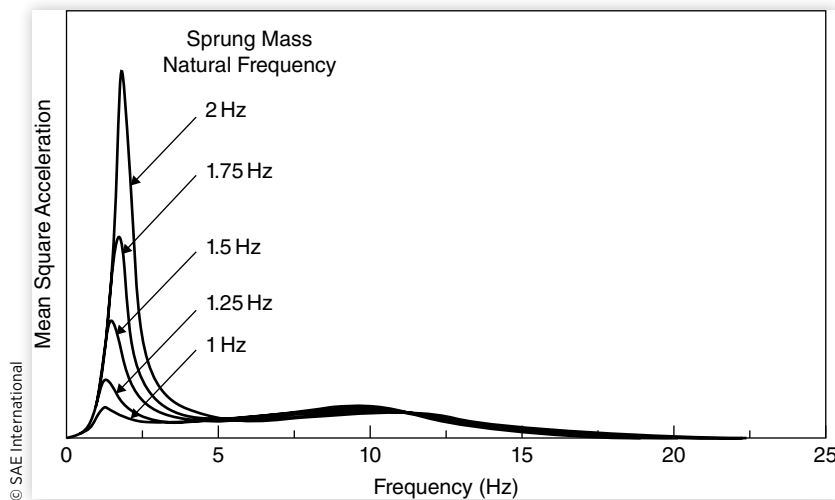
Because the suspension spring is in series with a relatively stiff tire spring, the suspension spring predominates in establishing the ride rate. The natural frequency of the system will therefore be in the bounce (i.e., vertical) mode. Since road acceleration inputs increase in amplitude at higher frequencies, the best isolation is achieved by keeping the natural

frequency as low as possible. For a vehicle with a given weight, it is therefore desirable to use the lowest practical suspension spring rate to minimize the natural frequency.



The effect on accelerations transmitted to the sprung mass can be estimated analytically by approximating the road acceleration input as a function that increases with the square of the frequency. [Equation \(5.17\)](#) can then be used to calculate the mean-square acceleration as a function of frequency. [Figure 5.18](#) shows the acceleration spectra

FIGURE 5.18 On-road acceleration spectra with different sprung mass natural frequencies.



calculated for a quarter-car model in which the suspension spring rate has been varied to achieve natural frequencies in the range of 1 to 2 Hz. Because it is plotted on a linear scale, the area under the curves indicates the relative level of mean-square acceleration over the frequency range shown.

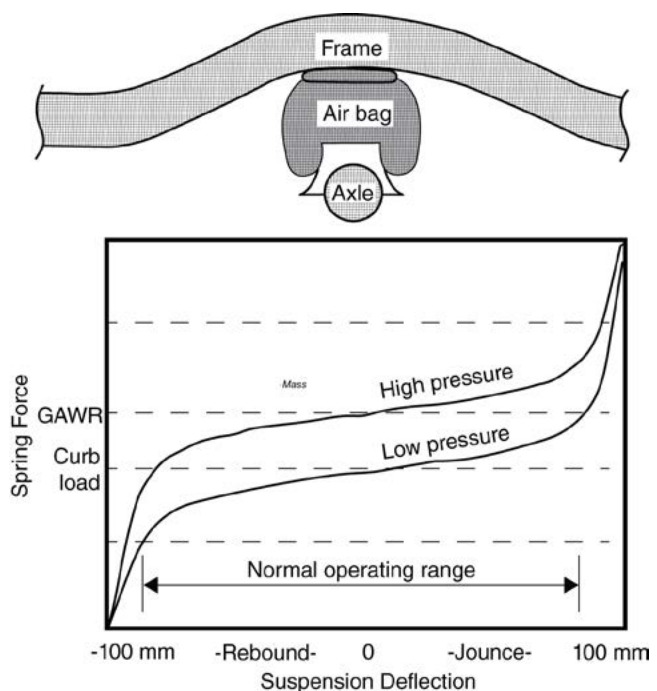
The lowest acceleration occurs at the natural frequency of 1 Hz. At higher values of natural frequency (stiffer suspension springs), the acceleration peak in the 1 to 5 Hz range increases, reflecting a greater transmission of road acceleration inputs. It can also be seen that the mean square acceleration increases by several hundred percent. Further, the stiffer springs elevate the natural frequency of the wheel hop mode near 10 Hz, allowing for more acceleration transmission in the high-frequency range.

While this analysis clearly shows the benefits of keeping the suspension soft for ride isolation, the practical limits of stroke that can be accommodated within a given vehicle size and suspension envelope constrain the natural frequency for most cars to a minimum in the range of 1 to 1.5 Hz. For performance-oriented cars in which ride quality may be sacrificed in order to take advantage of the handling benefits afforded by a stiff suspension, natural frequencies may be in the range of 2 to 2.5 Hz.

AIR SPRING SUSPENSIONS

Advantages:

- Compensates for load changes
- Keeps at the mid-point of travel
- Increases stiffness proportionate to load
- Maintains same natural frequency



© SAE International

Before moving on to the next section, consider the case of an air spring. Relative to coil springs, air springs offer the advantages of load compensation; stiffness is increased in proportion to load; natural frequency is maintained over its operating range; and they can remain at the midpoint of their travel.

Suspension Damping

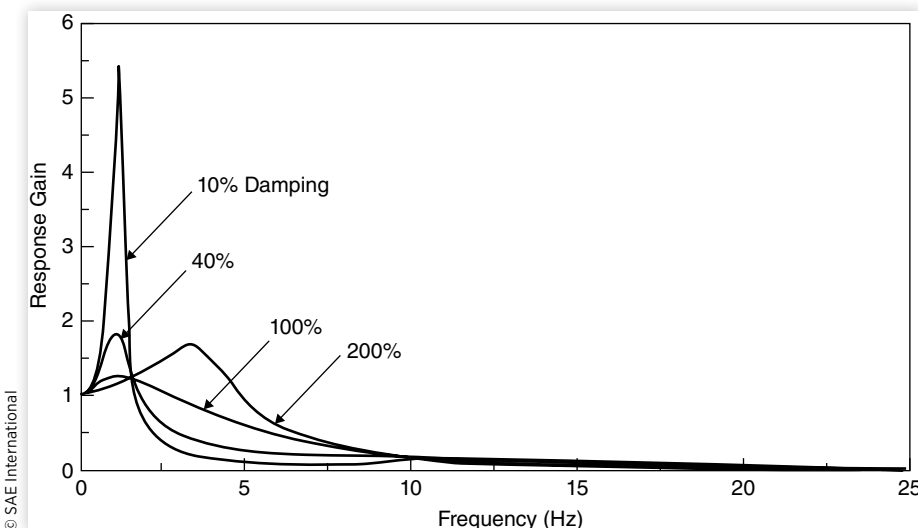
Damping in suspensions comes primarily from the action of hydraulic shock absorbers. Contrary to their name, they do not absorb the shock from road bumps; rather, the suspension absorbs the shock and the shock absorber's function is to dissipate the energy put into the system by the bump.

The nominal effect of damping is illustrated for the quarter-car model by the response gains shown in [Figure 5.19](#). The percent damping is determined from the damping ratio given in [Equation \(5.11\)](#). At very light damping (10%) the response is dominated by a very high response at 1 Hz. This type of response, often referred to as "float," causes the sprung mass to amplify long undulations in the roadway. While this is undesirable, benefit is obtained at all frequencies above the resonant point as a result of the high attenuation achieved.

The 40% damping ratio curve is reasonably representative of most cars, recognizable by the fact that the amplification at the resonant frequency is in the range of 1.5 to 2.0. At 100% (critical) damping, the 1 Hz bounce motions of the sprung mass are well controlled, but with penalties in the isolation at higher frequencies. If damping is pushed beyond the critical, for example, to 200%, the damper becomes so stiff that the suspension no longer moves and the vehicle bounces on its tires, resonating in the 3 to 4 Hz range.

While this analytical treatment provides a simplified illustration of the ride effect of damping in the suspension, the tailoring of shock absorbers to achieve optimum performance is much more complicated in the modern automobile. Shock absorbers must be tailored not only to achieve the desired ride characteristics, but also play a key role in keeping good tire-to-road contact essential for handling and safety. In general, this is achieved by choosing the "valving" in the shock so that it is not a simple linear element (with force proportional to velocity) as has been assumed so far.

FIGURE 5.19 Effect of damping on suspension isolation behavior.

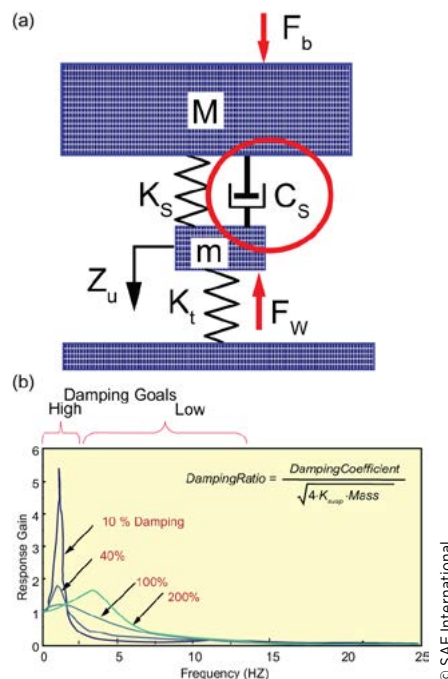


First, the damping in suspension jounce (compression) and rebound (extension) directions is not equal. Damping in the jounce direction adds to the force transmitted to the sprung mass when a wheel encounters a bump, thus making it undesirable to have high damping in this direction. On the other hand, damping in the rebound direction is necessary to dissipate the energy stored in the spring from the encounter with the bump. Consequently, typical shock absorbers are dual-rate with approximately a three-to-one ratio between rebound and jounce damping. Aside from this, the tuning characteristics described below are used for damping control in both directions.

TUNING – DAMPING

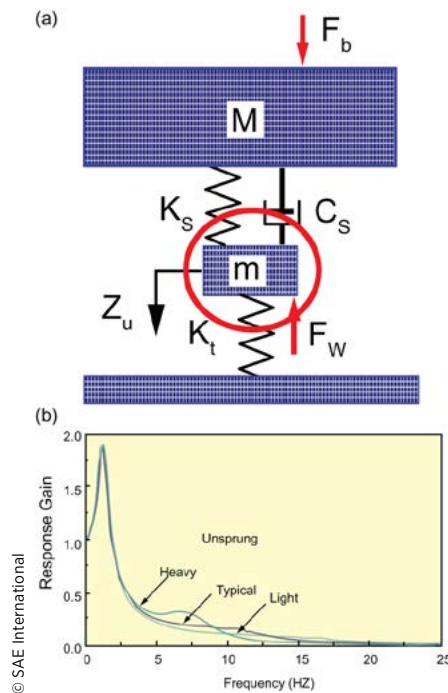
Typical car is about 40% of critical damping.

$$C_{crit} = \sqrt{4 \cdot K_s \cdot M}$$



TUNING – UNSPRUNG MASS

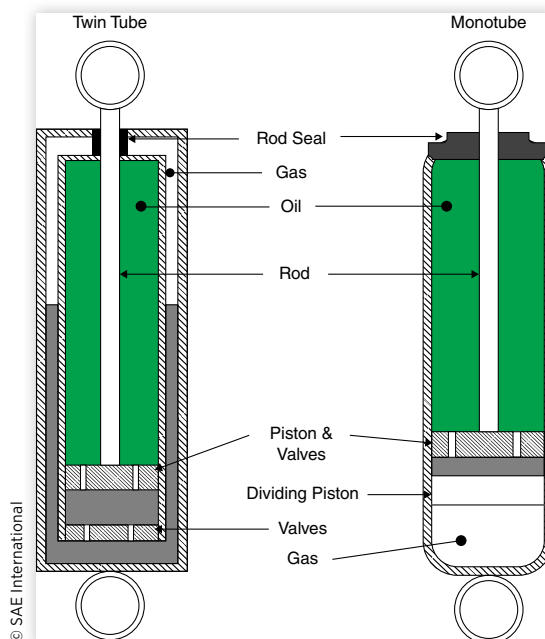
$$f_{n-axle} = \sqrt{\frac{K_{\text{suspension}} + K_{\text{tire}}}{\text{Unsprung Mass}}}$$



© SAE International

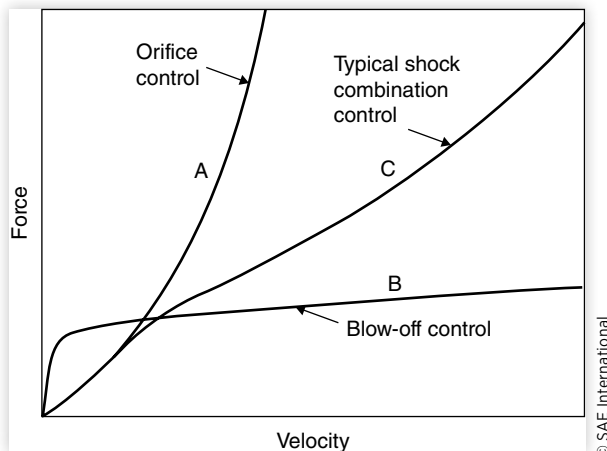
Since the mid-1950s, telescopic shock absorbers have been used almost exclusively for damping in automotive suspensions. Telescopic shocks are a piston-in-tube arrangement with one end connected to the sprung mass and the other to the axle or wheel. There are two types of telescopic shock absorbers—the twin tube and the gas-pressurized monotube—as illustrated in [Figure 5.20](#).

FIGURE 5.20 Twin tube and gas-pressurized monotube shock absorbers.



© SAE International

FIGURE 5.21 Force-velocity properties of shock absorber valving.



flow until a desired pressure is reached, at which point it allows “blow-off” with a damping force as shown in curve B. By combining orifice and blow-off controls in series and parallel arrangements, typical shock damping behavior such as that shown in curve C is obtained.

For a comprehensive treatment of shock absorber damping in ride analysis, the shock must be modeled as a nonlinear element. The force-velocity characteristics like those shown in the Figure 5.21 may be represented by polynomials or straight-line segments approximating the curve. Finally, the elastomer bushings in the end attachments of the shocks constitute a significant compliance in the system for small, high-frequency motions typical of an axle and should be taken into account.

Active Control

In the interest of improving the overall ride performance of automotive vehicles in recent years, suspensions incorporating active components have been developed. Most frequently, the active components are hydraulic cylinders that can exert forces in the suspension on command from an electronic controller tailored to produce the desired ride characteristics. The characteristics that are optimal for ride often compromise performance in other modes, most notably in handling.

The quarter-car model can be used to quantify the comparative ride performance of passive and active systems [41]. The two systems are illustrated in Figure 5.22. For a

Each has its own advantages but they are functionally similar. During compression and extension, the piston moves through the fluid in its bore. Valves in the piston restrict the flow of fluid through the piston, creating the damping force. In the case of the twin tube shock, additional restriction from valving in the base of the tube may be used to further tailor the damping behavior.

Two types of valving may be used in combination to produce the desired characteristics. A simple orifice valve generates a damping force which grows with the square of the velocity as shown by curve A in Figure 5.21. When designed to provide adequate damping to control body motions at low velocities, simple orifice control yields too much damping at the high velocities typical of axle hop motions. A second type of valving is the “blow-off” valve in which the flow passage is blocked by a spring-loaded valve; this prevents

flow until a desired pressure is reached, at which point it allows “blow-off” with a damping force as shown in curve B. By combining orifice and blow-off controls in series and parallel arrangements, typical shock damping behavior such as that shown in curve C is obtained.

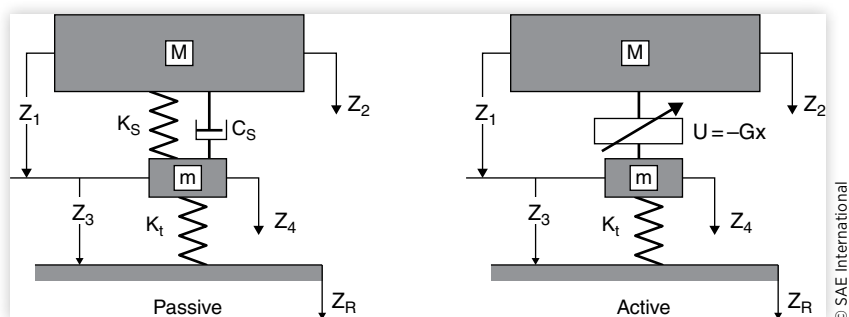
For a comprehensive treatment of shock absorber damping in ride analysis, the shock must be modeled as a nonlinear element. The force-velocity characteristics like those shown in the Figure 5.21 may be represented by polynomials or straight-line segments approximating the curve. Finally, the elastomer bushings in the end attachments of the shocks constitute a significant compliance in the system for small, high-frequency motions typical of an axle and should be taken into account.

Active Control

In the interest of improving the overall ride performance of automotive vehicles in recent years, suspensions incorporating active components have been developed. Most frequently, the active components are hydraulic cylinders that can exert forces in the suspension on command from an electronic controller tailored to produce the desired ride characteristics. The characteristics that are optimal for ride often compromise performance in other modes, most notably in handling.

The quarter-car model can be used to quantify the comparative ride performance of passive and active systems [41]. The two systems are illustrated in Figure 5.22. For a

FIGURE 5.22 Quarter-car model representations of passive and active suspensions.



vehicle traveling at a constant forward velocity over a random road surface, the road excitation can be reasonably well approximated by a constant-slope spectrum (road profile displacement inputs are obtained by integrating a white-noise source). Three performance variables are of interest:

1. Vibration isolation—measured by the sprung mass acceleration (\ddot{Z}_2)
2. Suspension travel —measured by deflection of the suspension (Z_1)
3. Tire load constancy—measured by deflection of the tire (Z_3)

Since the vehicle is modeled as a linear system subjected to white-noise input, the mean square response of any motion variable of interest can be computed using the relationship:

$$E[y^2] = S_o \int_{-\infty}^{\infty} |H_y(\omega)|^2 d\omega \quad (5.18)$$

where:

$E[y^2]$ = Mean square response

S_o = Spectral density of the white-noise input

$H_y(\omega)$ = Transfer function relating the response 'y' to the white-noise input

The transfer functions may be derived from the governing equations, substituted into [Equation \(5.18\)](#), and integrated to obtain the root mean square responses. In the process it is convenient to define certain characteristic parameters, as follows:

$$\chi = m/M \quad \text{Mass ratio} \quad (5.19a)$$

$$r_k = K_t/K_s \quad \text{Stiffness ratio} \quad (5.19b)$$

$$\zeta_s = \frac{C_s}{2\sqrt{K_s M}} \quad \text{Damping ratio} \quad (5.19c)$$

$$\omega_u = \sqrt{\frac{K_t}{m}} \quad \text{Natural frequency of the unsprung mass} \quad (5.19d)$$

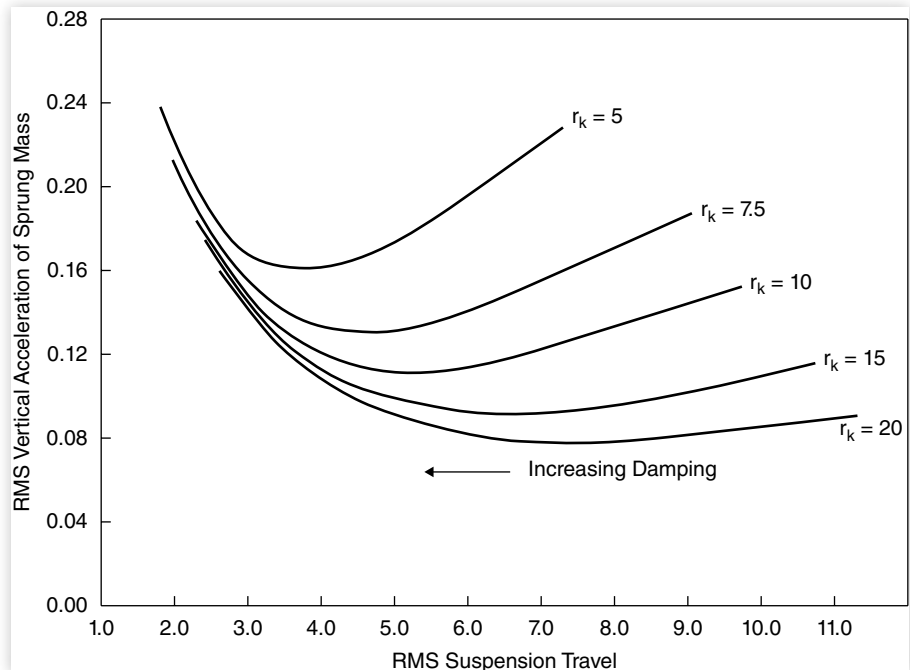
Among these vehicle parameters, the suspension designer is only free to select the stiffness and damping values. The influence of these parameters is displayed in [Figure 5.23](#), where the root-mean-square (rms) vertical acceleration is plotted against the rms suspension travel with different values of stiffness and damping.

The stiffness ratios shown in [Figure 5.23](#) are typical of the range for most production cars. The stiffest suspension, $r_k = 5$, would be representative of sports and performance cars. The softest, $r_k = 20$, would correspond to luxury cars with air suspensions. For any given stiffness ratio the vertical acceleration varies with damping and has an optimum which corresponds to the point of lowest rms acceleration. High levels of damping reduce the rms suspension travel but at the cost of increased acceleration (the greater damping forces transmit more road input across the suspension into the sprung mass). Low levels of damping allow greater suspension travel, but also increase the rms acceleration because of the uncontrolled motions at the sprung mass resonant frequency.

In practice it is not possible to use the entire range of performance shown in the figure. In particular, the low damping levels use suspension strokes that are beyond the range available on most passenger cars, and the low damping is insufficient to control wheel hop oscillations which compromise road-holding behavior. The shaded area in [Figure 5.24](#) indicates the practical range of performance for passive suspensions.

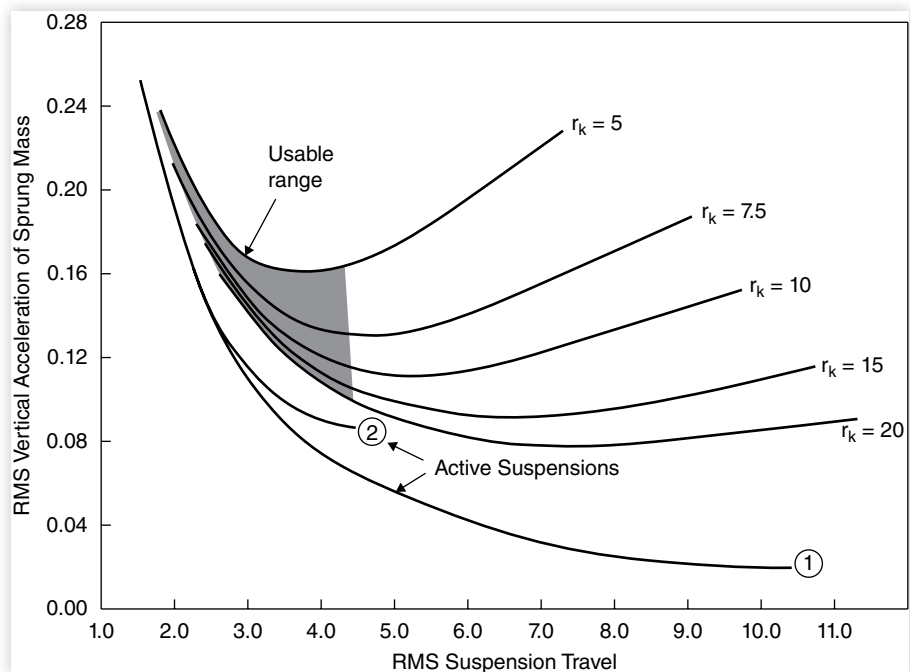
The quarter-car model for an active suspension, shown in [Figure 5.22](#), differs by the presence of a force generator in place of the suspension spring and damper. The force

FIGURE 5.23 Acceleration versus suspension travel for a passive suspension ($\chi = 0.15$).



© SAE International

FIGURE 5.24 Acceleration versus suspension travel for an active suspension.



© SAE International

generator corresponds to a hydraulic cylinder controlled by an electronic system. The electronics can potentially sense accelerations on the sprung and unsprung masses, the suspension displacement and tire radius (or load), and vary the force linearly in proportion to any combination of these state variables.

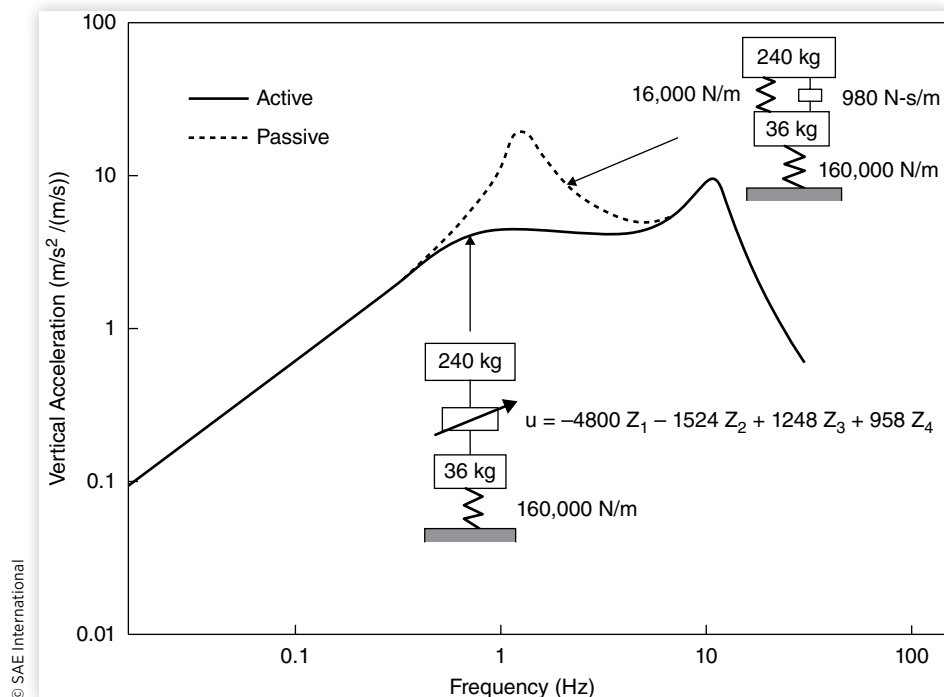
The optimal control algorithm for an active suspension can be determined analytically [41]. Optimization to minimize vertical acceleration and suspension travel results in the performance shown by curve 1 in Figure 5.24. For any given limit of suspension travel, the active suspension always yields better performance. At the upper limit of the usable range for the passive suspension (defined by the shaded area), a ride improvement equivalent to a 30% reduction in rms acceleration is possible with an active suspension.

The optimization for ride (indicated by curve 1) is less than optimal for road-holding because of insufficient damping of the wheel hop resonances. The 30% reduction in vertical acceleration is achieved at the expense of unsprung mass damping, which is only about 5%. If the optimization is constrained to a more reasonable (20%) unsprung mass damping ratio, the best performance for an active suspension becomes curve 2 in Figure 5.24. With this constraint the ride improvement of the active suspension over the best passive suspension is reduced to only about 10 percent.

The benefits of an active suspension are largely obtained by control of the sprung mass motions near its resonant frequency. The vertical acceleration response of the two systems is compared in Figure 5.25.

At the sprung mass resonant frequency the active suspension reduces the response amplitude over that which occurs with the passive suspension. Since the active suspension can sense sprung mass accelerations and exert forces to minimize their amplitude, the system achieves very effective damping of this mode. At the unsprung mass resonant

FIGURE 5.25 Comparison of vertical acceleration response of active and passive systems [42].



frequency the active suspension behaves just like the passive suspension. This occurs because the suspension forces necessary to control wheel hop motions react against the sprung mass, and would necessarily increase sprung mass accelerations. In effect, optimization of ride accelerations on the sprung mass is not achieved when the sprung mass is used as a reaction point for forces to control unsprung mass motions.

Wheel Hop Resonances

Next to the sprung mass of a vehicle, the axles and wheels (which make up the unsprung mass) are the second largest masses capable of separate resonances as rigid bodies. All individually sprung wheels have a vertical bounce (hop) mode which is excited by road and wheel nonuniformity inputs adding to the vibrations present on the vehicle. The influence of the wheel vertical resonance on the sprung mass vibrations was seen in the basic response of the quarter-car model given earlier in [Figure 5.16](#). The response gains for inputs from the road, or at the wheel, would normally attenuate quickly and continuously in the absence of a wheel resonant mode. However, in both cases, the response is accentuated at frequencies above the body resonance point as a result of the wheel motion, with the effect greatest at the resonant frequency of the wheel.

The resonant frequency is determined by the wheel/axle mass suspended against the springs in the suspension, acting along with that of the tires. Characteristically, the unsprung mass will correspond to a weight that is proportional to the gross axle weight rating (GAWR), which, in turn, is indicative of the loads normally carried by the axle. For nondriven axles, the weight, W_a , is typically about 10 percent of the GAWR, whereas for drive axles it will be about 15 percent of the GAWR. Inasmuch as the tires and suspension springs are normally sized in proportion to the GAWR, and the resonant frequency depends on the ratio of the mass to the total spring rate of the tires and suspension springs, the resonant frequencies of most wheels, at least theoretically, would fall in a limited range.

Wheel hop frequencies are much higher than the sprung mass resonance, so the sprung mass remains stationary during wheel hop. Thus both the tire and the suspension springs act in parallel to resist wheel hop motions, and the total spring rate controlling the axle mass is the sum of the two. The resonant frequency may then be calculated as:

$$f_a = 0.159 \sqrt{(K_t + K_s)g / W_a} \quad (5.20)$$

where:

f_a = Wheel hop resonant frequency (Hz)

K_t = Tire spring rate

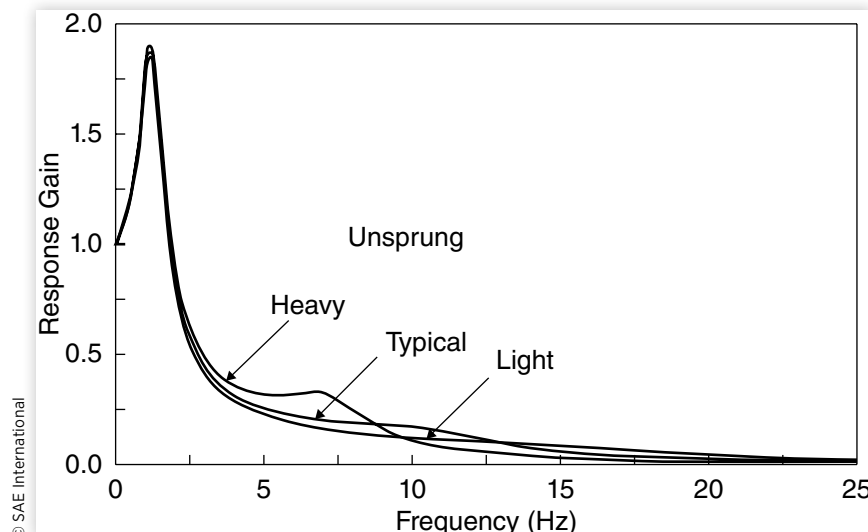
K_s = Suspension spring rate

W_a = Axle weight

For passenger cars the typical unsprung weight at a wheel is on the order of 100 lb, with a tire stiffness of 1000 lb/in and a suspension stiffness of 100 lb/in. With these nominal values the calculated resonant frequency will be approximately 10 Hz. Friction in the suspension will increase the effective spring rate for small ride motions which in turn will increase the resonant frequency to 12–15 Hz.

The magnitude of the unsprung mass arising from the wheels, axle/spindle, brakes, and suspension components influences the transmission of road inputs to the sprung mass. The quarter-car model may be used to examine the road-to-body transmissibility

FIGURE 5.26 Effect of unsprung mass on suspension isolation behavior.



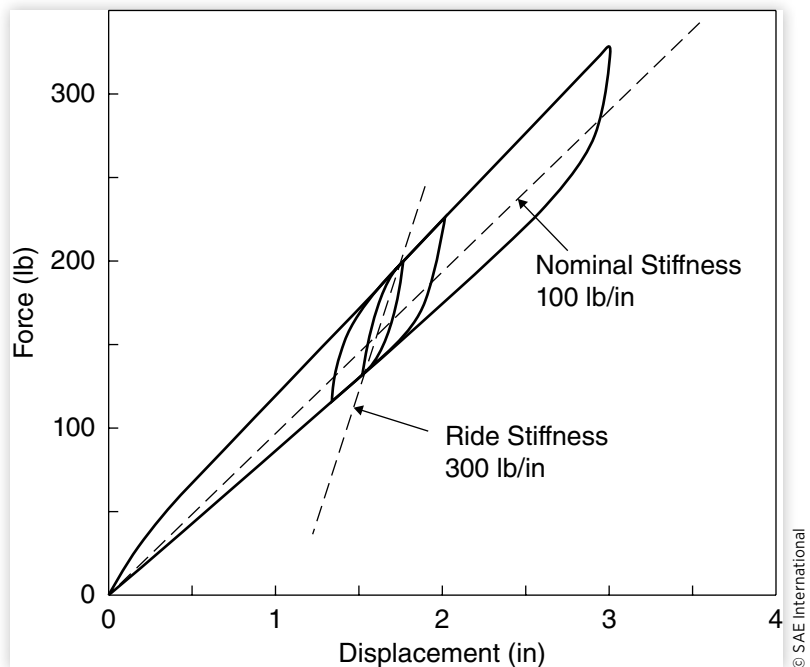
with variations in unsprung mass. [Figure 5.26](#) compares the response gains as the unsprung mass is changed from the typical value (nominally 10% of the sprung mass value) to a magnitude that is twice the value (heavy) and only one-half the value (light). The body resonant behavior near 1 Hz is unaffected by the unsprung mass changes, but above that frequency changes are evident. A heavier mass pulls the wheel hop resonant frequency down near 7 Hz, greatly increasing transmission of road inputs in this range. Inasmuch as these are more objectionable vibrations and are harder to isolate by other means, ride degradation results. With a lighter unsprung mass the wheel-hop resonant frequency is pushed higher and provides better isolation in the mid-frequency range, although there is some penalty above resonance. Since it is easier to isolate high-frequency vibrations elsewhere in the chassis, the lighter unsprung mass will generally produce better ride performance.

Suspension Nonlinearities

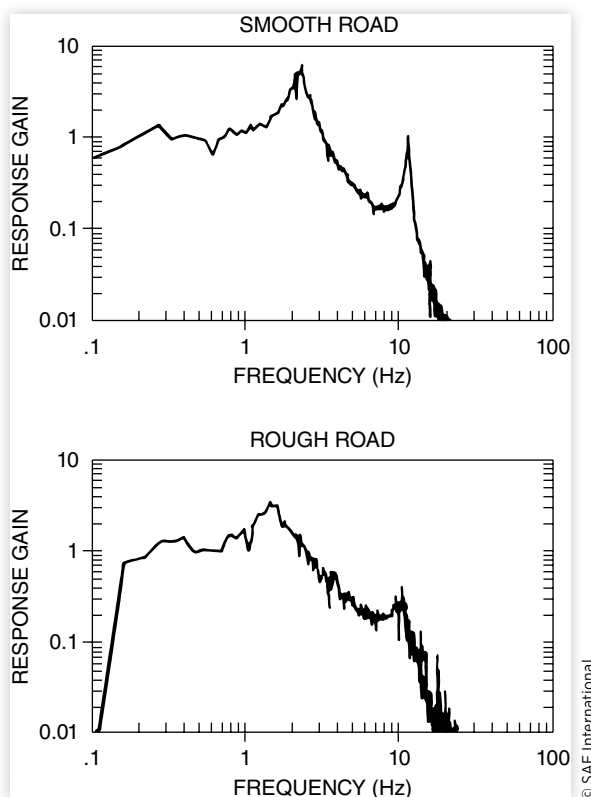
In practice, the suspension systems on many vehicles are not really linear, as assumed above, due to friction (sometimes termed “stiction”) in the struts and bushings, or the interleaf friction in a leaf spring suspension. Rather than a simple linear relationship between force and displacement, the suspension exhibits hysteretic behavior similar to that of the leaf spring shown in [Figure 5.27](#).

Ride motions are typically quite small in amplitude, involving only a fraction of an inch of suspension travel. Thus in the figure, ride motions are represented by excursions on the small inner loops of the spring hysteresis curves. The area enclosed by a hysteresis loop for any given excursion represents the damping energy dissipated by the suspension. The more important effect is the much higher effective stiffness of suspensions undergoing small deflections.

For the leaf spring shown, the effective stiffness for small ride motions is approximately three times greater than the nominal stiffness of the spring. In more extreme cases of suspension friction, the ride stiffness may be nearly an order of magnitude larger. For this reason, it is important to minimize the friction levels in suspension struts and bushings to achieve good ride.

FIGURE 5.27 Load-deflection characteristics of a hysteretic leaf spring.

© SAE International

FIGURE 5.28 Response of a quarter-vehicle model with a hysteretic suspension.

With hysteresis in the suspension, the vehicle response changes with amplitude and spectral content of the excitation. Because of the nonlinearities, a time-based simulation of its response to random road roughness input must be performed to establish the transmissibility properties. Using a quarter-car model with a hysteretic spring, the response gain (ratio of sprung mass acceleration to road acceleration) across the frequency spectrum can be calculated. [Figure 5.28](#) shows calculations of this type for a truck leaf spring suspension [28]. Using the same road at a high (rough) and low (smooth) amplitude illustrates the way in which suspension nonlinearities affect dynamic behavior of a vehicle.

On smooth roads the suspension deflections are small, resulting in a high effective stiffness and very little damping. Hence, the sprung-mass resonance moves up in frequency to 2.5 Hz and, because of low damping, the resonance becomes a high, narrow peak reaching a gain in excess of 5. Likewise, the axle resonance, which occurs at just above 10 Hz, becomes very accentuated. On the rough road the greater suspension deflections produce a lower effective stiffness and greater damping. Hence, the resonances diminish in both their frequency and amplitude. Though the road is rougher, the reduced response of the vehicle compensates somewhat for the greater input. This type of behavior is very characteristic of heavy trucks; thus it is often observed that some heavy trucks ride better on rough roads than on smooth roads.

Rigid Body Bounce/Pitch Motions

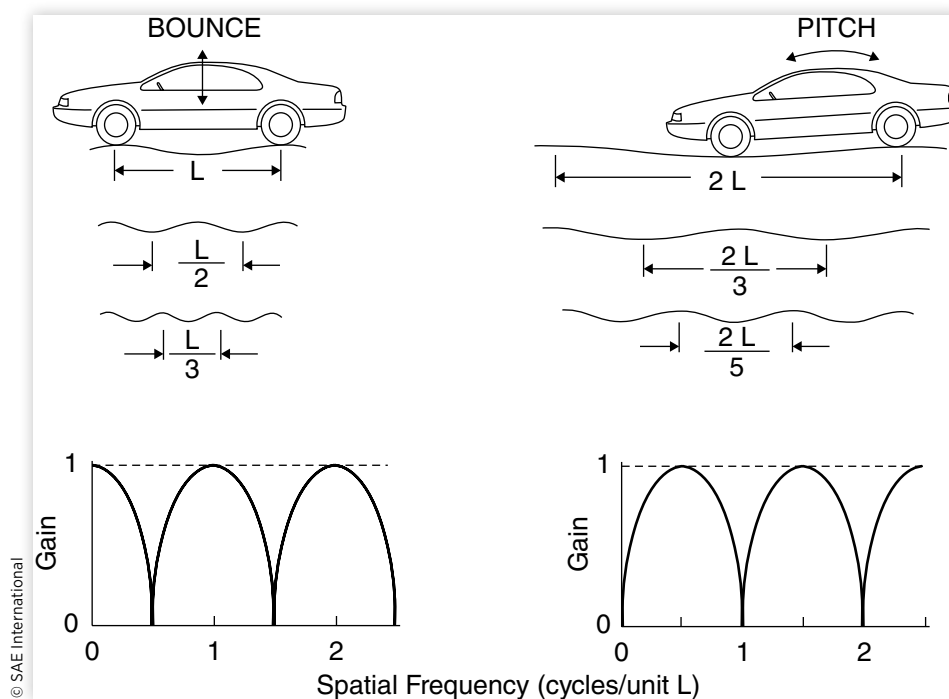
The simple mechanics of the quarter-car model do not fully represent the rigid-body motions that may occur on a motor vehicle. Because of the longitudinal distance between the axles, it is a multi-input system that responds with pitch motions [12] as well as vertical bounce. Depending on the road and speed conditions, one or the other of the motions may be largely absent, or they may not necessarily be observed at the point on the vehicle where the vibration measurements are made. The pitch motions are important because they are generally considered objectionable and are the primary source of longitudinal vibrations at locations above the center of gravity. Understanding the pitch and bounce motions is essential because it is their combination that determines the vertical and longitudinal vibrations at any point on the vehicle.

As the vehicle traverses a road, the roughness excitation at the different axles is not independent. The rear wheels see nearly the same input profile as the front wheels, only delayed in time. The time delay is equal to the wheelbase divided by the speed of travel. The time delay acts to filter the bounce and pitch excitation amplitude, and has been called “wheelbase filtering” [29].

In order to understand the influence of wheelbase filtering, it is convenient to think of the vehicle as having independent pitch and bounce modes. Consider a two-axle vehicle as illustrated in **Figure 5.29**. As the vehicle moves along the road, the roughness input at the front wheels acts subsequently on the rear wheels, delayed in time by the interval equal to the wheelbase divided by speed. Inasmuch as the road contains roughness at all wavelengths, one can examine the response of the vehicle to individual wavelengths.

Only bounce motion input occurs at a wavelength equal to the wheelbase of the vehicle. The same is true for wavelengths much, much longer than the wheelbase, and also for short wavelengths which have an integer multiple equal to the wheelbase.

FIGURE 5.29 The wheelbase filtering mechanism.



In a similar fashion, only pitch motion input will be seen on a wavelength that is twice the wheelbase, or on any shorter wavelength that has an odd-numbered integer multiple equal to twice the wheelbase. As a consequence the vehicle will be unresponsive in either bounce or pitch to certain wavelengths in the road with the filtering qualities shown in [Figure 5.29](#).

The influence may be seen better in the response gain for a simple vehicle with a 1.25 Hz natural frequency at both front and rear axles (the bounce and pitch vibration modes are uncoupled). The gray line in the top plot of [Figure 5.30](#) shows the vertical response gain that would result at each axle as calculated from the quarter-car model. When the road input is applied with that at the rear axle delayed from that of the front, the response at the passenger positions midway between the wheels will be altered by wheelbase filtering. Assuming a 9-ft (2.7-m) wheelbase and a speed of 50 mph (80 km/h), response nulls occur at approximately 4, 12, 20 Hz, etc. The null points are equal to the velocity divided by twice the wheelbase and odd multiples thereof. Thus at high speeds a passenger car tends to experience vertical bounce vibrations more or less as predicted

FIGURE 5.30 Effect of wheelbase filtering on bounce and pitch response.

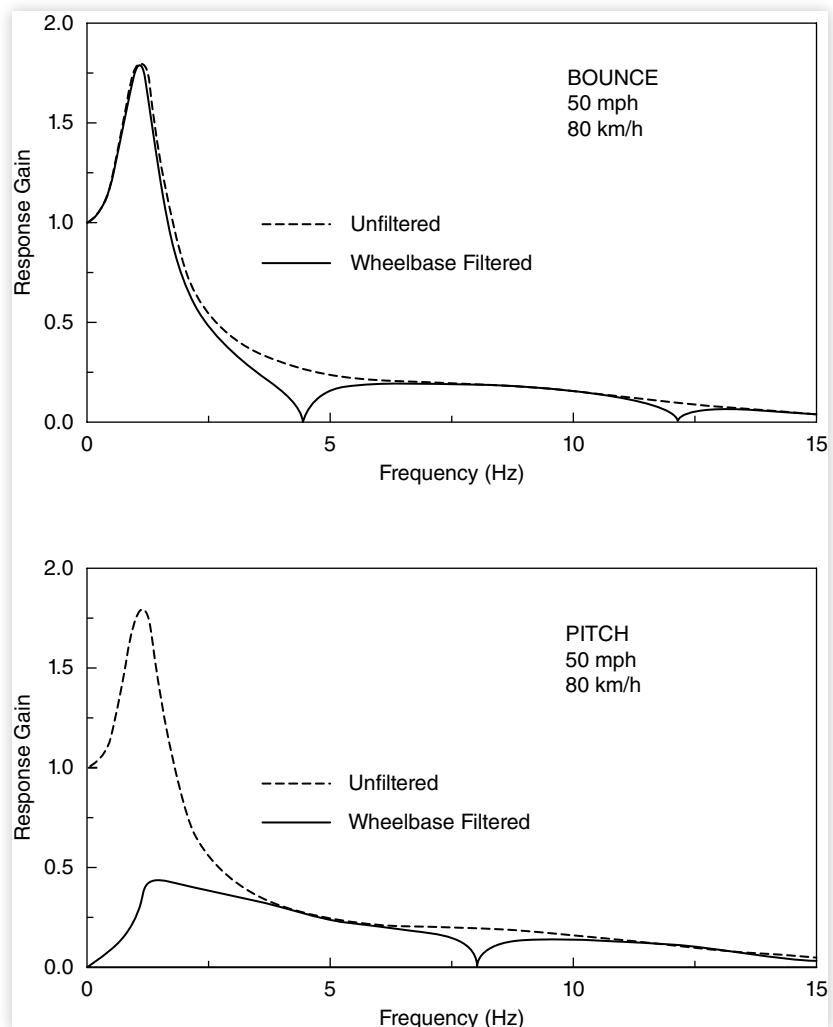
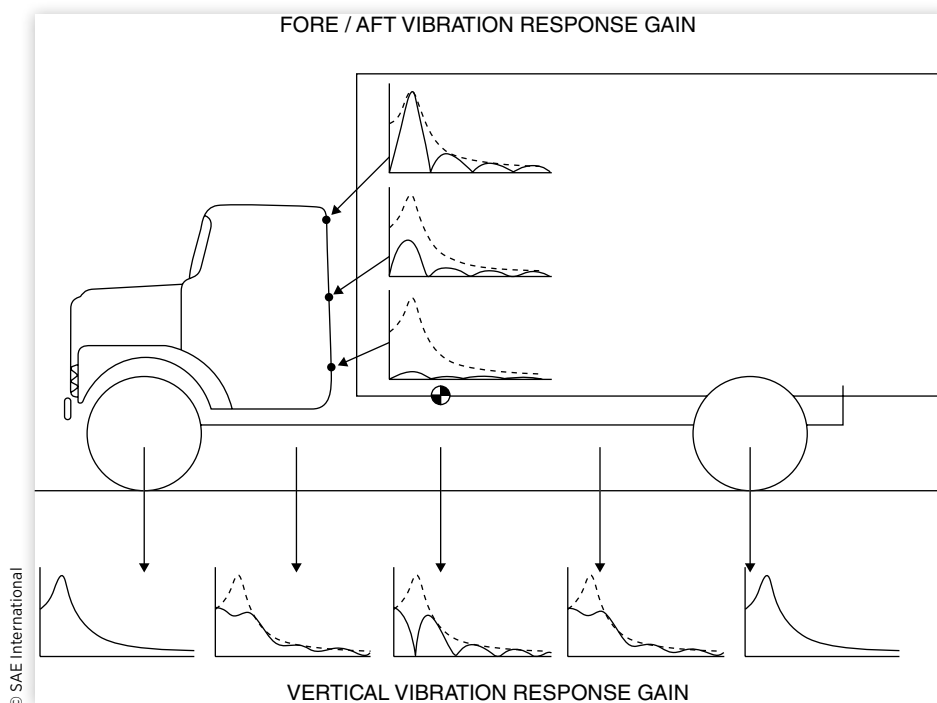


FIGURE 5.31 Effect of wheelbase filtering on vertical and longitudinal response gain of a truck [44].



by a quarter-car model with the exception of the null points indicated. At lower speeds the null points shift proportionately to lower frequencies.

The pitch response of the vehicle has similar qualities as given in the bottom plot of the figure. The pitch resonance frequency will typically be close to the bounce frequency, so the same resonant frequency has been assumed in the figure. The null frequencies in pitch for this same vehicle will be at 8, 16, 24 Hz, etc. Consequently, there will be little pitch of the vehicle at normal highway speeds. Only at low speed is the pitch mode readily excited by road inputs.

The bounce and pitch vibration behavior of heavy trucks presents a somewhat different picture because of the higher resonant frequencies and longer wheelbases of these vehicles. Because of the stiffer suspensions the natural frequencies of bounce and pitch tend to be closer to 2.5-3 Hz. With wheelbases in the range of 12-15 ft (3.7-4.6 meters), just the reverse behavior occurs at high speed. Namely, the bounce response will have a null at the resonant frequency and the pitch response will be at full amplitude. Consequently, wheelbase filtering will affect the vibration response on a heavy truck as illustrated in [Figure 5.31](#).

The vertical vibration response due to rigid-body motions will vary with location along the length of the vehicle, depending on the relative actions of the bounce and pitch motions. Near the midpoint of the vehicle the vertical vibrations are affected only by bounce, hence, the response properties at this point reflect the wheelbase filtering phenomenon directly. The vertical acceleration spectra measured at this point will show the characteristic decreases at the bounce null frequencies. At points toward the extremes of the vehicle both pitch and bounce will contribute to the vertical accelerations and the effect of wheelbase filtering will become less evident. Over the axles some combination of bounce and pitch will be present at each frequency, such that wheelbase filtering will

have no effect on the response; rather, the vertical response will be equivalent to that seen in the quarter-vehicle model earlier.

The pitch action is the predominant source for fore/aft vibrations that are seen on trucks at locations above the center of gravity. Thus the spectrum of fore/aft vibrations will be affected by the wheelbase filtering influence on pitch response, and the amplitude of the vibrations will be dependent on the elevation of the driver's seat above the center of gravity. The fact that fore/aft vibration spectra show periodic reductions at the pitch null frequencies should not be confused as an indication of a multi-resonant system.

Bounce/Pitch Frequencies

The tuning of the bounce and pitch vibration modes on a vehicle has a direct impact on the acceptability of the ride. On most vehicles there is a coupling of motions in the vertical and pitch directions, such that there are no "pure" bounce and pitch modes. The behavior, in terms of natural frequencies and motion centers, for a vehicle with coupled motions in the vertical and pitch directions can be readily determined analytically from the differential equations of motion. Consider a vehicle as shown in [Figure 5.32](#). For simplicity in analysis, the tire and suspension will be considered as a single stiffness (the ride rate), and damping and unsprung masses will be neglected.

For convenience in the analysis, the following parameters are defined:

$$\alpha = (K_f + K_r) / M \quad (5.21)$$

$$\beta = (K_r c - K_f b) / M \quad (5.22)$$

$$\gamma = (K_f b^2 + K_r c^2) / Mk^2 \quad (5.23)$$

where:

K_f = Front ride rate

K_r = Rear ride rate

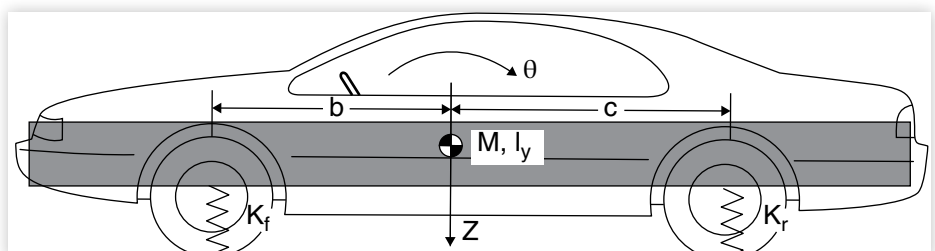
b = Distance from the front axle to the C.G.

c = Distance from the rear axle to the C.G.

I_y = Pitch moment of inertia

k = Radius of gyration = $\sqrt{I_y / M}$

FIGURE 5.32 Pitch plane model for a motor vehicle.



The differential equations for the bounce, Z , and pitch, θ , motions of a simple vehicle can be written as:

$$\ddot{Z} + \alpha Z + \beta \theta = 0 \quad (5.24)$$

$$\ddot{\theta} + \beta Z / k^2 + \gamma \theta = 0 \quad (5.25)$$

Of the several coefficients in these equations, only β appears in both and is appropriately called the coupling coefficient. When $\beta = 0$ no coupling occurs, and the spring center is at the center of gravity. For this condition, a vertical force at the C.G. produces only bounce motion, and a pure torque applied to the chassis will produce only pitch motion.

Without damping, the solutions to the differential equations will be sinusoidal in form. The vertical motion will be:

$$Z = Z_0 \sin \omega t \quad (5.26)$$

and the pitch motion will be:

$$\theta = \theta_0 \sin \omega t \quad (5.27)$$

When these are differentiated twice and substituted into Equation (5.22), we obtain:

$$-Z\omega^2 \sin \omega t + \alpha Z \sin \omega t + \beta \theta \sin \omega t = 0 \quad (5.28)$$

Since the terms must always equal zero regardless of the instantaneous value of the sine function:

$$(\alpha - \omega^2)Z + \beta \theta = 0 \quad (5.29)$$

or,

$$Z/\theta = -\beta / (\alpha - \omega^2) \quad (5.30)$$

The same analysis applied to Equation (5.25) yields:

$$Z/\theta = -k^2 (\gamma - \omega^2) / \beta \quad (5.31)$$

The above equations define conditions under which the motions can occur. The constraints are that the ratio of amplitudes in bounce and pitch must satisfy Equations (5.30) and (5.31).

Equating the right sides of Equations (5.30) and (5.31) yields the expressions for the natural frequencies of the two modes of vibration.

$$(\alpha - \omega^2)(\gamma - \omega^2) = \beta(\beta/k^2) \quad (5.32)$$

Then

$$\omega^4 - (\alpha + \gamma)\omega^2 + \alpha\gamma - \beta^2/k^2 = 0 \quad (5.33)$$

The values of ω satisfying this equation are the roots representing the frequency of the vibration modes. Two of the roots will be imaginary and can be ignored. The others are obtained from the equations as follows:

$$\begin{aligned} (\omega_{1,2})^2 &= \frac{(\alpha + \gamma)}{2} \pm \sqrt{\frac{(\alpha + \gamma)^2}{4} - (\alpha\gamma - \beta^2/k^2)} \\ &= \frac{(\alpha + \gamma)}{2} \pm \sqrt{\frac{(\alpha + \gamma)^2}{4} + \beta^2/k^2} \end{aligned} \quad (5.34)$$

$$\omega_1 = \sqrt{\frac{(\alpha + \gamma)}{2} + \sqrt{(\alpha + \gamma)^2/4 + \beta^2/k^2}} \quad (5.35)$$

$$\omega_2 = \sqrt{\frac{(\alpha + \gamma)}{2} - \sqrt{(\alpha + \gamma)^2/4 + \beta^2/k^2}} \quad (5.36)$$

These frequencies always lie outside the uncoupled natural frequencies.

The oscillation centers can be found using the amplitude ratios of Equations (5.30) and (5.31) with the two frequencies ω_1 and ω_2 in Equations (5.35) and (5.36). When substituted it will be found that $Z/\theta(\omega_1)$ and $Z/\theta(\omega_2)$ will have opposite signs.

When Z/θ is positive, both Z and θ must be both positive or negative. Thus the oscillation center will be ahead of the C.G. by a distance $x = Z/\theta$. Similarly, for the root with a negative value for Z/θ , the oscillation center will be behind the C.G. by a distance $x = Z/\theta$. Likewise, one distance will be large enough that the oscillation center will fall outside the wheelbase, and the other will be small enough that the center falls within the wheelbase. When the center is outside the wheelbase, the motion is predominantly bounce, and the associated frequency will be the bounce frequency. For the center within the wheelbase the motion will be predominantly pitch, and the associated frequency is the pitch frequency. These cases are illustrated in Figure 5.33.

The locations of the motion centers are dependent on the relative values of the natural frequencies of the front and rear suspensions, where those frequencies are defined by the square root of the ride rate divided by the mass:

$$f_f = \frac{1}{2\pi} \sqrt{\frac{K_f g}{w_f}} \quad (5.37)$$

$$f_r = \frac{1}{2\pi} \sqrt{\frac{K_r g}{w_r}} \quad (5.38)$$

FIGURE 5.33 The two vibration modes of a vehicle in the pitch plane.

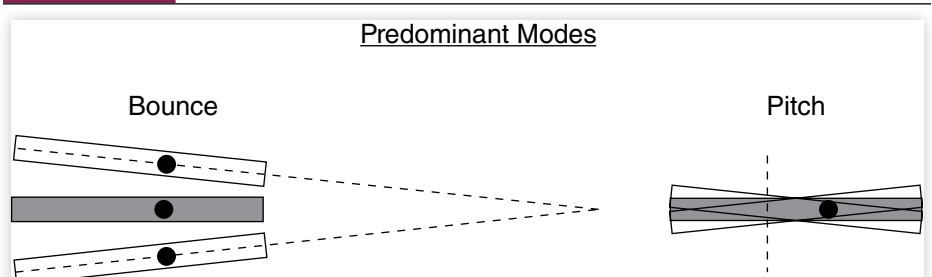


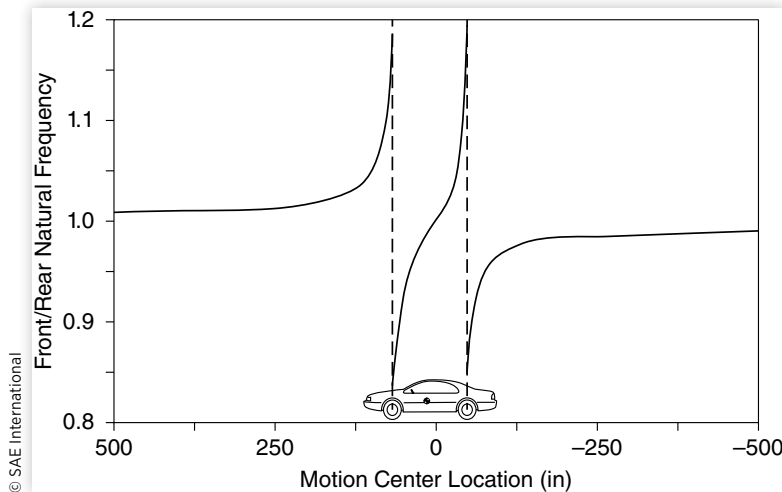
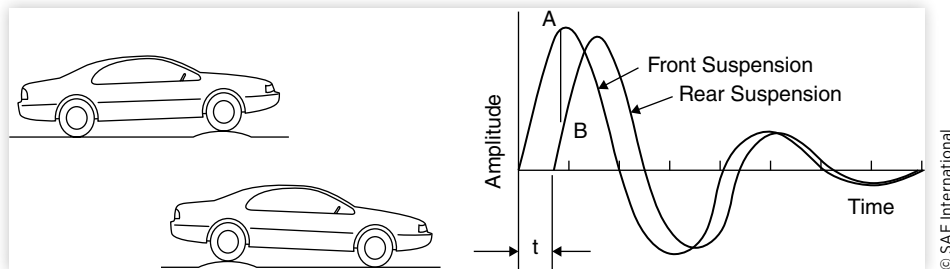
FIGURE 5.34 Effect of natural frequency ratio on position of motion centers.

Figure 5.34 shows the locus of motion centers as a function of front/rear natural frequency. With equal frequencies, one center is at the C.G. location and the other is at infinity. Equal frequencies correspond to decoupled vertical and pitch modes, and “pure” bounce and pitch motions result. With a higher front frequency the motion is coupled with the bounce center ahead of the front axle and the pitch center toward the rear axle. A lower front frequency puts the bounce center behind the rear axle and the pitch center forward near the front axle. This latter case was recognized by Maurice Olley in the 1930s as best for achieving good ride.

Maurice Olley, one of the founders of modern vehicle dynamics, established guidelines back in the 1930s for designing vehicles with good ride (at least for the low-frequency, rigid-body modes of vibration). These were derived from experiments with a car modified to allow variation of the pitch moment of inertia (his famous “*k*” rig) [43]. Although the measure of ride was strictly subjective, those guidelines are considered valid rules of thumb even for modern cars. The Olley Criteria are:

1. *The front suspension should have a 30% lower ride rate than the rear suspension, or the spring center should be at least 6.5% of the wheelbase behind the C.G.* Although this does not explicitly determine the front and rear natural frequencies, since the front-rear weight distribution on passenger cars is close to 50-50, it will generally assure that the rear frequency is greater than the front.
2. *The pitch and bounce frequencies should be close together: the bounce frequency should be less than 1.2 times the pitch frequency. For higher ratios, “interference kicks” resulting from the superposition of the two motions are likely.* In general, this condition will be met for modern cars because the dynamic index is near unity with the wheels located near the forward and rearward extremes of the chassis.
3. *Neither frequency should be greater than 1.3 Hz, which means that the effective static deflection of the vehicle should exceed roughly 6 in.* The value of keeping natural frequencies below 1.3 Hz was demonstrated in [Figure 5.18](#).
4. *The roll frequency should be approximately equal to the pitch and bounce frequencies.* In order to minimize roll vibrations the natural frequency in roll needs to be low just as for the bounce and pitch modes.

The rule that rear suspensions should have a higher spring rate (higher natural frequency) is rationalized by the observation that vehicle bounce is less annoying as

FIGURE 5.35 Oscillations of a vehicle passing over a road bump.

© SAE International

a ride motion than pitch. Since excitation inputs from the road to a car affect the front wheels first, the higher rear to front ratio of frequencies will tend to induce bounce.

To illustrate this concept, consider a vehicle encountering a bump in the road. The time lag between the front and rear wheel road inputs at a forward speed, V , and a car wheelbase, L , will be:

$$t = L / V \quad (5.39)$$

The oscillations at the front and rear of the car for an input of this type are illustrated in **Figure 5.35**. Note that soon after the rear wheels have passed over the bump the vehicle is at the worst condition of pitching, indicated by the points A and B in the figure. Point A corresponds to the front end of the car being in a maximum upward position, whereas the rear end (point B) is just beginning to move. Therefore, the car is pitching quite heavily.

With a higher rear frequency, after about one and one-half oscillations of the rear suspensions, both ends of the car are moving in phase. That is, the body is now merely bouncing up and down until the motion is almost fully damped. At different speeds and for different road geometries, the vehicle response will change. Thus the optimum frequency ratio of the front and rear ends of the car has to be determined experimentally.

Special Cases

1. Most modern vehicles with substantial front and rear overhang exhibit a dynamic index close to unity. That is:

$$DI = k^2 / bc = 1 \quad (5.40)$$

When the equality holds, the front and rear suspensions are located at conjugate centers of percussion (an input at one suspension causes no reaction at the other). In this case the oscillation centers are located at the front and rear axles. This is a desirable condition for good ride if Olley's ride criteria are also satisfied. There is no interaction between the front and rear suspensions [43].

2. Spring center at the C.G. — This condition corresponds to the case of uncoupled pitch and bounce motions ($\beta = 0$). The pitch and bounce oscillations are totally independent. Poor ride results because the motions can be very irregular. Coupling tends to even out the ride [43].
3. Dynamic index greater than unity — This occurs when there is substantial overhang at the front and/or rear of the car. The bounce center is in front of the C.G. (beyond the front axle) and the pitch center is between the C.G. and the rear axle. The natural frequency of pitch is now less than the bounce frequency and

flat ride will still result if the spring center is located far enough behind the C.G. (front ride rate less than rear ride rate) [43].

4. Uncoupled motion ($\beta = 0$) and dynamic index equal to one — This condition results in equal bounce and pitch frequencies. The ride is inferior because there is essentially no pattern to the road-generated motion; it is quite unpredictable [43].

Example Problem

1. Calculate the pitch and bounce centers and their frequencies for a car with the following characteristics:

Front ride rate	= 127 lb/in per wheel
Rear ride rate	= 92.3 lb/in per wheel
Wheelbase	= 100.6 in
Front tire load	= 957 lb per wheel
Rear tire load	= 730 lb per wheel
Dynamic index (DI)	= 1.1

Solution:

The starting point is to find the values for the three parameters given in Equations (5.21), (5.22), and (5.23), but first we must determine the mass, b, c, and k.

$$M = W / g = (957 + 957 + 730 + 730) \text{ lb} / (386 \text{ in/sec})^2 = 8.74 \text{ lb-sec}^2 / \text{in}$$

We can find "b" and "c" from the weight distribution:

$$b = LW_r / W = (100.6 \text{ in}) 1460 \text{ lb} / 3374 \text{ lb} = 43.53 \text{ in}$$

$$c = 100.6 - 43.53 = 57.07 \text{ in}$$

Then:

$$k^2 = b c D I = (43.53 \text{ in})(57.07 \text{ in}) 1.1 = 2,732 \text{ in}^2$$

Now we can solve for each of the parameters.

$$\alpha = (K_f + K_r) / M = [2(127) + 2(92.3)] \text{ lb/in} / (8.74 \text{ lb-sec}^2 / \text{in}) = 50.18 \text{ sec}^{-2}$$

$$\begin{aligned} \beta &= (K_r c - K_f b) / M = [184.6(57.07) - 254(43.53)] \text{ lb/in} / (8.74 \text{ lb-sec}^2 / \text{in}) \\ &= -59.67 \text{ in/sec}^2 \end{aligned}$$

$$\begin{aligned} \gamma &= (K_f b^2 + K_r c^2) / Mk^2 \\ &= [254(43.53^2) + 184.6(57.07^2)] \text{ lb-in} / [8.74 \text{ lb-sec}^2 / \text{in}(2732 \text{ in}^2)] = 45.34 \text{ sec}^{-2} \end{aligned}$$

Then from Equations (5.35) and (5.36) we can solve for the two frequencies.

$$\begin{aligned} \omega_1 &= \sqrt{\frac{(50.18 + 45.34)}{2 \text{ sec}^2} + \sqrt{\frac{(50.18 - 45.34)^2}{4 \text{ sec}^4} + \frac{(59.67 \text{ in/sec}^2)^2}{2,732 \text{ in}^2}}} \\ &= 7.10 \text{ rad/sec} = 1.13 \text{ Hz} \end{aligned}$$

$$\omega_2 = \sqrt{\frac{(50.18 + 45.34)}{2 \text{ sec}^2}} - \sqrt{\frac{(50.18 - 45.34)^2}{4 \text{ sec}^4} + \frac{(59.67 \text{ in/sec}^2)^2}{2,732 \text{ in}^2}}$$

$$= 6.71 \text{ rad/sec} = 1.07 \text{ Hz}$$

Now from Equation (5.30) we can solve for Z/θ for each frequency.

$$Z/\theta_1 = -\beta / (\alpha - \omega_1^2) = 59.67 \text{ in/sec}^2 / (50.18 \text{ sec}^{-2} - 50.41 \text{ sec}^{-2}) = -259 \text{ in/rad}$$

$$Z/\theta_2 = -\beta / (\alpha - \omega_2^2) = 59.67 \text{ in/sec}^2 / (50.18 \text{ sec}^{-2} - 45.02 \text{ sec}^{-2}) = 11.57 \text{ in/rad}$$

Thus the car has a motion center 259 in behind the C.G. with a frequency of 7.1 rad/sec (1.13 Hz). Since it is the most distant from the C.G. it is predominantly vertical and would be the bounce center. The second motion center at 6.71 rad/sec (1.07 Hz) is 11.57 in forward of the C.G. and therefore will be the pitch center.

2. Find the pitch and bounce centers and their frequencies for a car with the following characteristics:

Front ride rate = 132 lb/in

Rear ride rate = 93 lb/in

Wheelbase = 112 in

Front tire load = 1035 lb

Rear tire load = Varying from 567 to 1,000 lb

Dynamic index = 1.05

Solution:

Set up a spreadsheet to perform the calculations while the rear axle load is varied over the specified range. The relevant parameters are shown in the table below for rear wheel load of 567 lb and increments above that value.

W_r	b	c	k²	α	β	γ	ω₁	Z/θ₁	ω₂	Z/θ₂
567	39.64	72.36	3011.8	54.21	360.7	55.55	1.25	49.6	1.11	-60.7
600	41.10	70.90	3059.7	53.12	275.8	53.28	1.21	54.5	1.11	-56.2
625	42.17	69.83	3091.9	52.32	215.8	51.76	1.19	59.8	1.10	-51.7
650	43.20	68.80	3120.9	51.54	159.2	50.39	1.17	68.3	1.10	-45.7
675	44.21	67.79	3146.9	50.79	105.8	49.16	1.15	85.3	1.10	-36.9
700	45.19	66.81	3170	50.06	55.4	48.05	1.13	137.9	1.10	-23.0
725	46.14	65.86	3190.6	49.35	7.7	47.04	1.12	957.3	1.09	-3.4
750	47.06	64.94	3208.9	48.66	-37.2	46.13	1.11	-231.4	1.08	13.9
775	47.96	64.04	3224.9	47.98	-79.8	45.30	1.11	-132.8	1.06	24.3
800	48.83	63.17	3238.8	47.33	-120.0	44.54	1.11	-105.8	1.05	30.6
825	49.68	62.32	3250.8	46.69	-158.0	43.86	1.11	-93.3	1.03	34.9
850	50.50	61.50	3261.1	46.07	-194.0	43.23	1.11	-85.9	1.02	38.0
875	51.31	60.69	3269.7	45.47	-228.1	42.65	1.11	-80.9	1.00	40.4
900	52.09	59.91	3276.8	44.88	-260.3	42.13	1.11	-77.2	0.99	42.5
925	52.86	59.14	3282.4	44.31	-290.9	41.64	1.11	-74.3	0.98	44.2
950	53.60	58.40	3286.8	43.75	-319.8	41.20	1.10	-71.9	0.96	45.7
975	54.33	57.67	3289.9	43.21	-347.2	40.80	1.10	-69.9	0.95	47.1
1000	55.04	56.96	3291.8	42.68	-373.2	40.43	1.10	-68.2	0.94	48.3

- For the base vehicle (567 lb rear wheel load) there is no clear pitch or bounce frequency because both centers are relatively near the wheels. The first frequency, ω_1 , has a center 49.6 in ahead of the C.G., placing it just in front of the front wheels. The second frequency, ω_2 , has its center 60.7 in behind the C.G., placing it just ahead of the rear wheels.
- At 725 lb the ω_1 becomes almost pure bounce (the center is 957 in ahead of the C.G.), while ω_2 is almost pure pitch as its center is only 3.4 in behind the C.G.
- As the rear load continues to increase, the bounce center (ω_1) moves behind the C.G. and the pitch center continues to move forward. At the highest loads the centers are in close proximity to the wheel positions and it is no longer possible to associate a pitch or bounce with each.

Perception of Ride

In the final section of this chapter, we must address how ride is perceived by the vehicle's occupants. As a (subjective) perception, ride is normally associated with the level of comfort experienced while the vehicle is traveling on a given road surface. In its broadest sense, perceived ride is the cumulative product of many factors and include the tactile vibrations transmitted to the occupants through the seat, to the feet via the floor, and to the hands via the steering wheel. It can be difficult to separate the influences of acoustic vibrations (i.e., noise) when considering the perception of ride, especially since noise types and levels are usually highly correlated with other vehicle vibrations. Although not directly associated with ride per se', it is worth noting that the general comfort level within a vehicle can be influenced by other factors such as the seat design and its fit to the passengers, the temperature and ventilation within the cabin, and the spaciousness and organizational layout of the interior. Collectively, these factors may all contribute to what some have described as the "ride quality" of the vehicle.

While factors such as vibrations can be measured and therefore serve as objective criteria from which engineering decisions can be made, other factors such as seat comfort are still heavily dependent on subjective evaluation methods. Complicating matters is the fact that interactions between objective and subjective measurements are typically not well established.

For example, it is the author's experience that tolerance for vibration in a truck is often drastically reduced if the cabin space does not allow room for the occupant's body movement without contacting hard surfaces within the vehicle interior.

Tolerance to Seat Vibrations

As a starting point it is instructive to look at research findings from the scientific community relating to human tolerance for vibration. A brief state-of-the-art review of the vibration limits for human comfort covering work back to the 1920s is presented in the SAE Ride and Vibration Data Manual [26] published in 1965. Major works by Lee and Pradko [30], the International Organization for Standardization [31], Oborne [32], Miwa [33], Parsons [34], Fothergill [35], Leatherwood [36], and others, have made substantial contributions to the database of information related to vibration tolerance. These studies tend to focus on tolerance as it relates to discomfort in a seated position in an effort to sort out the frequency sensitivity of the human body. Pure sinusoidal inputs are often used in attempts to establish quantified levels of discomfort, or equal levels of sensation,

as a function of frequency. Regardless, no universally accepted standard exists for the judgment of ride vibrations due to variables such as:

- seating position
- influence of hand and foot vibration input
- single- versus multiple-frequency input
- multi-direction input
- comfort scaling
- duration of exposure
- sound and visual vibration inputs

Despite these concerns, certain common factors can be observed in the results from much of the recent work. When examining the tolerances for vertical and fore / aft vibrations on seated passengers, it is common practice for the researchers to observe comparable sensitivity curves.

[Figure 5.36](#) shows lines of constant comfort as determined by a number of researchers. Because of the different interpretations of comfort in each study, the nominal level of one curve is neither comparable to the others, nor is it especially meaningful. Nevertheless, note that the majority show a minimum tolerance (maximum sensitivity) of the human body to vertical vibration in the frequency range between 4 and 8 Hz. This sensitivity is well recognized as the result of vertical resonances of the abdominal cavity. At frequencies above and below this range the tolerance increases in proportion to frequency. The actual shape of the boundaries will often show small inflections in the 10 to 20 Hz range due to other organ resonances, especially head resonance near 10 Hz.

As indicated by the plots of the ISO curves in the figure, the duration of the vibration exposure also affects the maximum tolerable level. Hence, two boundaries are shown, one for one minute of exposure, and the second for one hour of exposure. General rules for determining boundaries appropriate to arbitrary exposure levels are available in the ISO Standard [31], and in the work of Lee and Pradko [30].

Very interesting findings were obtained by NASA [37] in research on comfort in mass transport vehicles, notably airplanes. The constant comfort lines for vertical vibration taken from that work are shown in [Figure 5.37](#). The significant point observed is that the sensitivity as a function of frequency is dependent on the acceleration level. At high levels of vibration, the tolerance curves generally match those of other researchers. At low amplitudes, however, the horizontal nature of the curves implies that the discomfort is rather independent of frequency. Therefore, low levels of vibration are equally objectionable regardless of their frequency over the indicated range.

FIGURE 5.36 Human tolerance limits for vertical vibration.

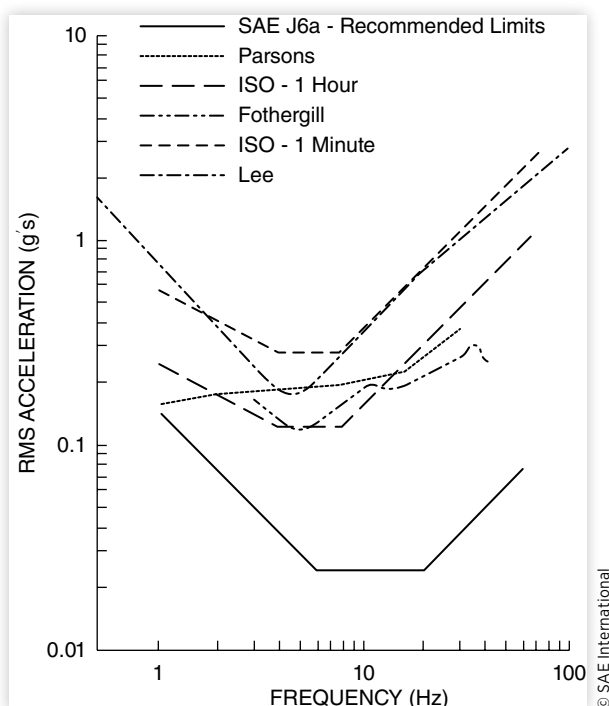
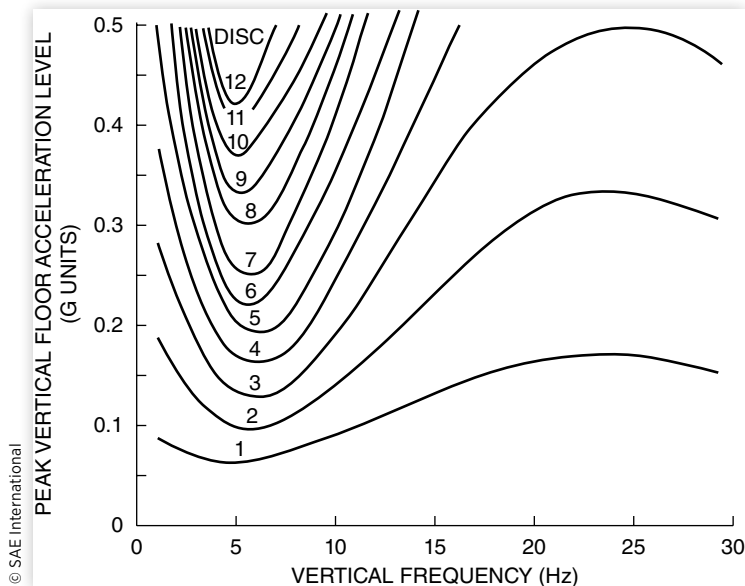


FIGURE 5.37 NASA Discomfort Curves for vibration in transport vehicles.



Human sensitivity to fore/aft vibration is somewhat different from that of the vertical. **Figure 5.38** shows tolerance limits for fore/aft vibration as determined from a number of sources. Again the nominal level of each curve is not especially meaningful, but similar sensitivities are indicated. The most remarkable difference seen is that the region of maximum sensitivity occurs in the 1 to 2 Hz range. This sensitivity is generally recognized to result from the fore/aft resonance of the upper torso. Note also that when the vertical and fore/aft boundaries from individual researchers are compared, the minimum tolerance is observed in the fore/aft direction.

The tolerance curves shown in the figures are generally derived from pure sinusoidal inputs to the subjects, whereas the ride environment in a motor vehicle contains all frequencies over a broad spectrum. In order to apply this information to objective measurements of ride vibration on the seat of a car or truck, it is necessary to resolve this incompatibility. One method commonly used is to filter the acceleration data in inverse proportion to the amplitude of the selected tolerance curve. The inverse filtering allows the resulting acceleration spectrum to be viewed as if all frequencies were equally important. However, this method requires that the vertical and fore / aft vibrations be evaluated separately. To overcome this problem, the weighted root-mean-square (rms) accelerations in each direction are then sometimes combined by various formulas to obtain an overall rms value.

A more fundamental method for combining vertical and fore/aft vibrations emerged from the work of Lee and Pradko [30]. The level of discomfort was related to the level of vibration power being dissipated in the subject's body, whether from vertical, fore/aft, or lateral inputs. By this

FIGURE 5.38 Human tolerance limits for fore/aft vibrations.

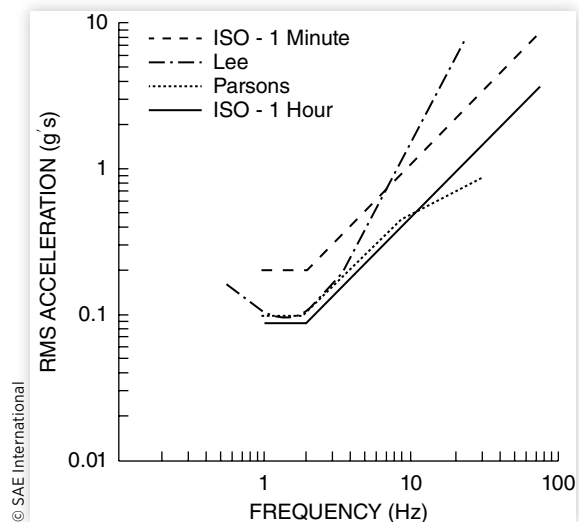
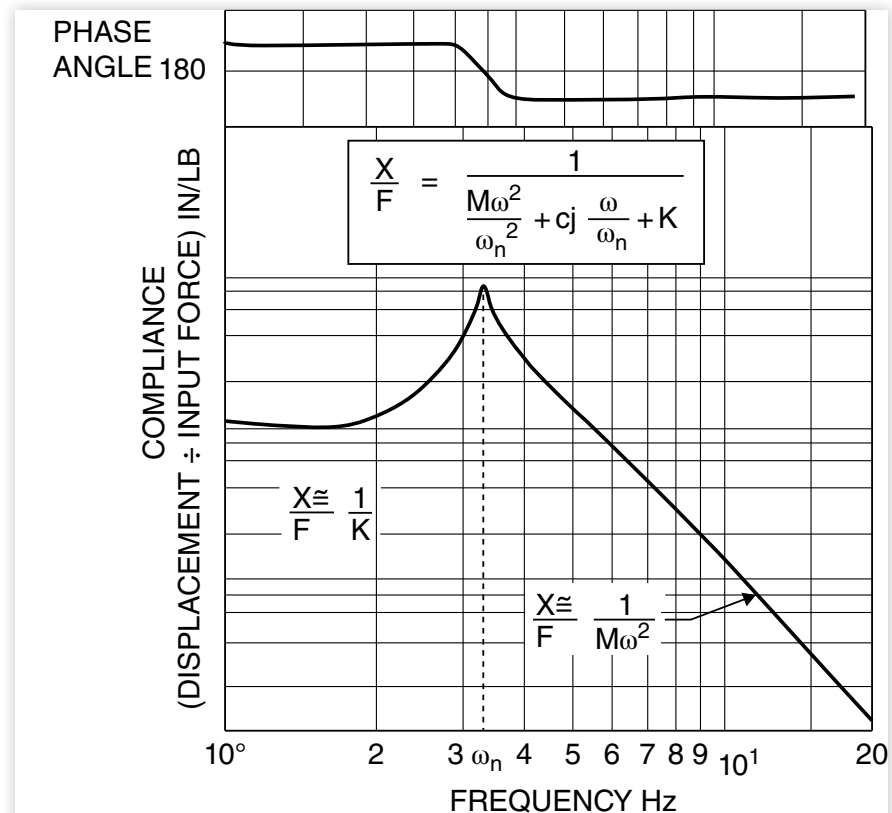
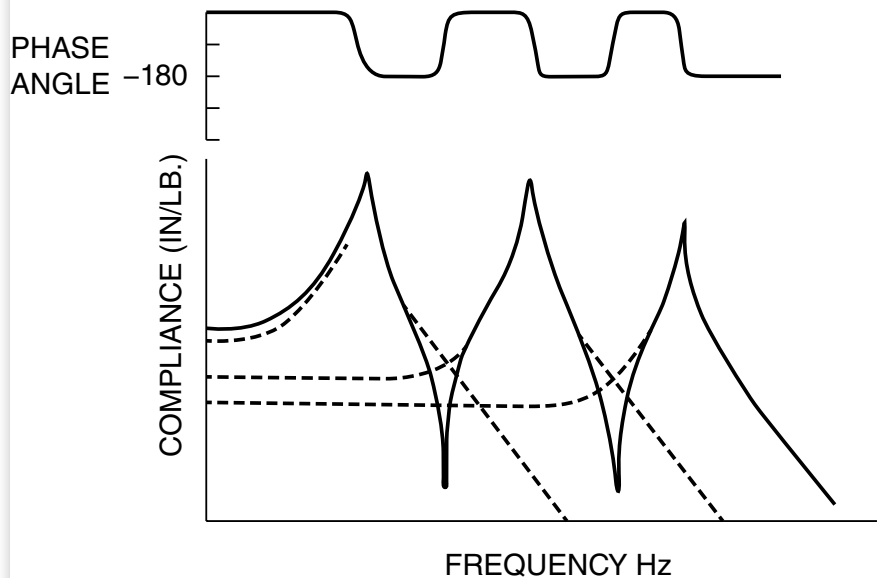


FIGURE 5.39 Representing the response of a dynamic system using log-log plots.

Frequency response plot for one degree of freedom



Frequency response plot showing three modes

method the tolerance curves could be used to weight accelerations so as to arrive at an absorbed power for each direction, and the power quantities are simply added.

The ISO tolerance curves are one of the popular weighting functions used to assess the significance of an acceleration spectrum. However, it should be recognized that the proper method for application of ISO tolerance curves is to evaluate the exposure in one-third octave bands and critique the vibration based on the worst-case band in the spectrum.

When all is said and done, the tolerance curves determined by researchers are instructive to the ride engineer as background in evaluating the vibrations that are imposed on a passenger through the seat. It has often been found that measurements of these vibrations, even weighted in accordance with the selected tolerance curves, bear little correlation to the subjective ratings that will be obtained in a jury during physical vehicle testing. For example, Healey [38] concluded that a simple measure of rms acceleration in a passenger car is as closely correlated to subjective ratings as any combination of weighted accelerations he could devise.

Whether or not a frequency weighting function is used to adjust the relative importance of specific vibration frequencies, there are formats in which the acceleration spectra can be presented that are more meaningful for ride purposes. In the science of dynamics, it is common practice to present frequency domain information in log-log format as shown at the top of [Figure 5.39](#). In this format, the modal response of a system asymptotically approaches straight lines, and the behavior of complex systems (with multiple modes) can be combined as shown in the bottom of the figure. Thus it has great utility in analysis of dynamic systems. For ride purposes, however, this greatly distorts the relative importance of vibrations at the various frequencies. Presentation of ride acceleration spectra in linear-linear format is more meaningful because the area under the plot is indicative of mean-square or root-mean-square accelerations, depending on the units used on the ordinate axis. (Units of acceleration²/Hertz correspond to mean-square values, whereas its square root corresponds to the root-mean-square value.)

[Figure 5.40](#) contrasts these two means of data presentation. Although the log-log format provides more information for understanding the dynamic systems involved, the linear-linear format allows the engineer to see the relative importance of vibrations in any frequency range by the area involved. While the log-log format creates the impression that the vibrations are generally of equal importance across the entire the spectrum, the linear-linear format makes it clear ([Figure 5.40](#)) that the major portion of the mean-square vibration is concentrated in the low frequency range of 5 Hz and below.

FIGURE 5.40 Seat vibrations displayed in linear-linear and log-log format.

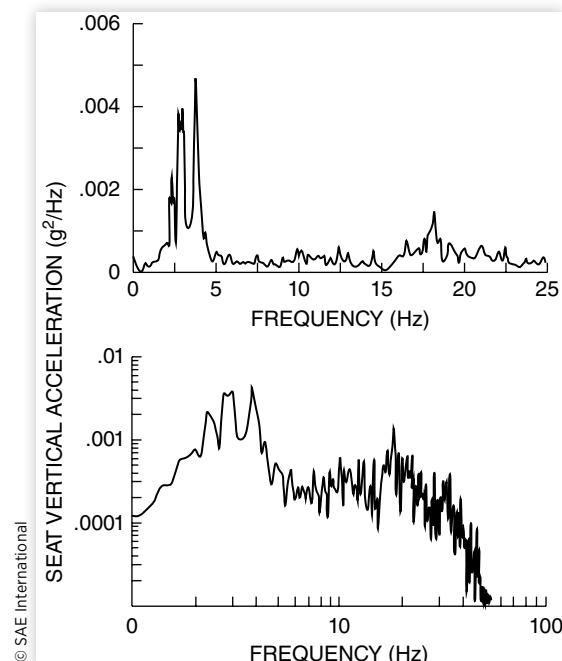
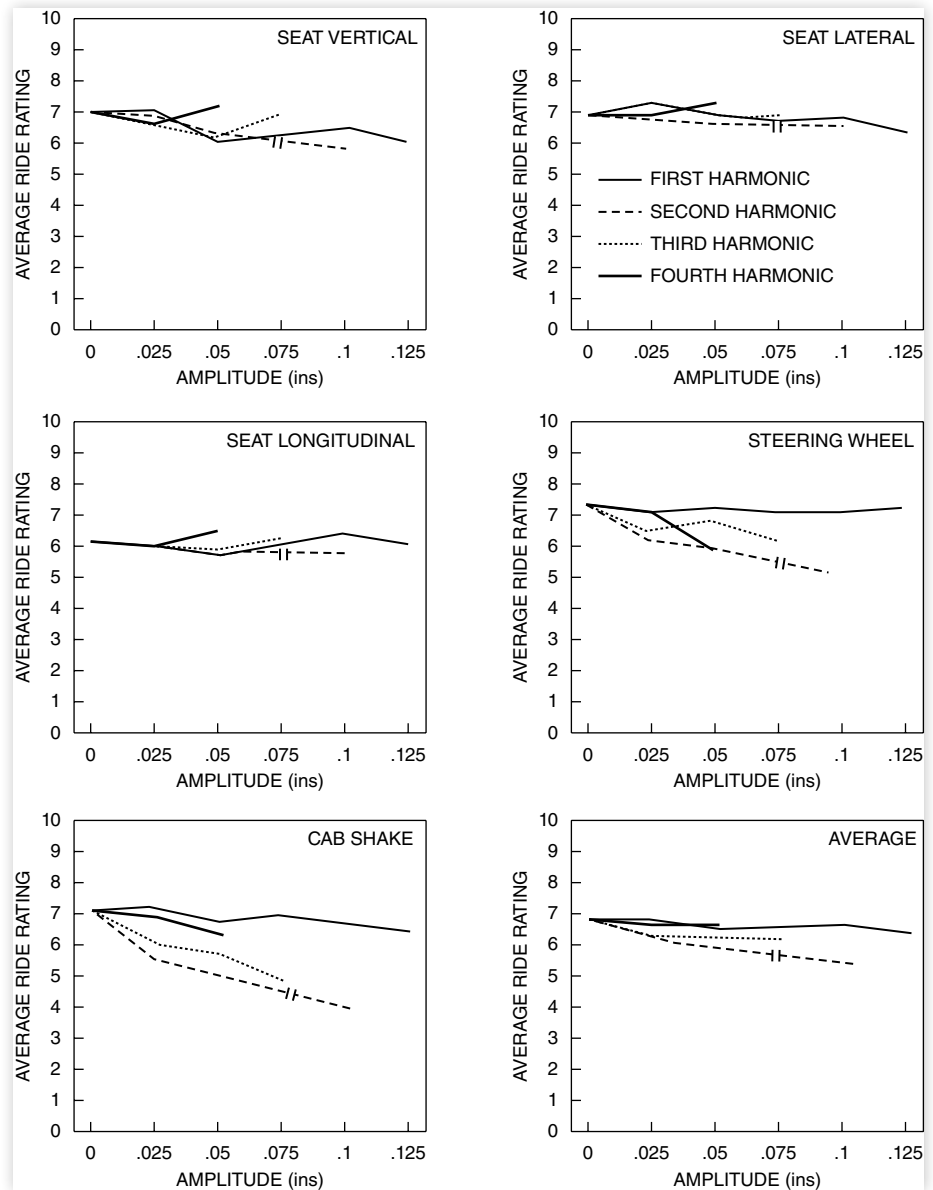


FIGURE 5.41 Effect on ride rating of nonuniformities on the left front wheel of a highway tractor.



© SAE International

Other Vibration Forms

One reason why seat vibration measurements are inadequate as objective measures of ride is that the driver's judgment of the vibration in the vehicle includes far more than what comes through the seat. The point was well demonstrated in studies of the influence of tire/wheel nonuniformities on the ride perception on a highway tractor [17], in which a jury of ten industry engineers rated the ride acceptability of the tractor under varying conditions of tire nonuniformity excitation. The ten-interval scale was used for rating the following vibrations: seat

vertical, seat fore / aft, seat lateral, steering wheel, and cab shake. Sample results from these tests for left front nonuniformity inputs are shown in [Figure 5.41](#).

A significant point observed in the results was the tendency to degrade the ride due to steering-wheel and cab-shake vibrations. Note that the ratings of seat vibrations showed little sensitivity to nonuniformity input; yet the ratings for cab shake and steering wheel were profoundly affected, especially for the second and third harmonics. The steering-wheel rating reflects vibration inputs to the hands of the driver, while the cab-shake category represents inputs at the feet, as well as visual effects from shake of the A-pillar, rear view mirrors, sun visors, etc.

Note since the participants in these tests were asked to rate the acceptability of the vehicle, the ratings necessarily reflect the engineers' judgment with regard to the acceptability of the vehicle as a product. Results of tests such as these bring to light the significance of the question being asked in the context of the factor or factors being studied. Consider, for example, studies involving the rating of roads for their roughness conditions. Highway engineers have found that the questions "How is the ride?" vs. "How is the road?" elicit very different responses from the respective juries. As one might expect, the question "How is the ride?" produces ratings that tend to be dependent on the type of vehicle being used; higher ratings tend to be the norm with a luxury car vs. lower ratings when the vehicle is small and possibly lacks some refinement. When the alternative question "How is the road?" is posed, the results tend to show that the jurists reports are unaffected by the choice of vehicle. As with all engineering studies, the ride development engineer should be sensitive to such issues and work to ensure the correct questions are being asked before executing any experiments involving ride ratings.

Conclusion

As a final note, one might suggest that the goal of the ride engineer is to eliminate all vibrations from the vehicle. Despite the fact that this will never be possible, it nevertheless provides some direction to the development effort. Generally speaking there are two competing phenomena that must be addressed, each with its own goals and objectives. First, the elimination of one vibration will inevitably expose a lesser annoyance. In one such example, the total elimination of vibrations made it possible to hear the ticking of the clock, to the point that that became the major concern. Second, and certainly the more critical of the two from the standpoint of vehicle dynamics, is the fact that elimination of all vibrations would adversely affect the driver's ability to receive proper feedback from the road, critical in cases of limit handling maneuvers.

References

1. Bendat, J.S. and Piersol, A.G., *Random Data: Analysis and Measurement Procedures* (John Wiley & Sons, New York, 1971), 407pp.
2. Sayers, M. and Gillespie, T.D., "Guidelines for Conducting and Calibrating Road Roughness Measurements," *World Bank Technical Paper*, 46, 1986, 87pp. ISSN0253-7494.
3. Spangler, E.B. et al., "GMR Profilometer Method for Measuring Road Profile," General Motors Research Publication GMR-452, 1964, 44pp.
4. Gillespie, T.D., Sayers, M., and Segel, L., "Calibration of Response-Type Road Roughness Measuring Systems," Final Report, NCHRP Project 1-18, NCHRP Rept. No. 228, December 1980, 70pp.

5. LaBarre, R.P., et al, "The Measurement and Analysis of Road Surface Roughness," Report 1970/5, Motor Industry Research Association, December 1969, 31pp.
6. Sayers, M., Gillespie, T.D., and Queiroz, C.A., "The International Road Roughness Experiment: Establishing Correlation and a Calibration Standard for Measurements," *World Bank Technical Paper*, 45, 1986, 453pp. ISSN 0253-7494
7. Van Dusen, B.D., "Truck Suspension Optimization," SAE Technical Paper [710222](#), 1971, doi:[10.4271/710222](#).
8. Kropac, D. and Sprinc, J., "Identification of the System Vehicle-Road Parameters," *Vehicle Systems Dynamics*, II, no. 4, (1982): 241-249.
9. Ribarits, J.L., et al. "Ride Comfort Aspects of Heavy Truck Design," SAE Technical Paper [781067](#), 1978, doi:[10.4271/781067](#)
10. Gillespie, T.D., "The Dynamic Behavior of Nonuniform Tire/Wheel Assemblies," Special Rept., MVMA Project #1163, Transportation Res. Inst., Univ. of Mich., Rept. No. UMTRI-83-8, November 1983, 53pp.
11. Gillespie, T.D., "Relationship of Truck Tire/Wheel Nonuniformities to Cyclic Force Generation," Final Report, MVMA Project No. 1162, Transportation Res. Inst., Univ. of Mich., Rept. No. UMTRI-84-18, April 1984, 136pp.
12. SAE J670, "Vehicle Dynamics Terminology," Society of Automotive Engineers, Warrendale, PA, 2008 (see Appendix A).
13. Luders, A. et al. "Contributions to the Problem of Irregular Running of Vehicle Wheels," *A7Z*, 73 (1971), 1-8 (in German).
14. Thomson, W.T., *Mechanical Vibrations*, 2nd ed. (Prentice Hall, Englewood Cliffs, NJ, June 1959), 252pp.
15. Klamp, W.K. et al. "Higher Orders of Tire Force Variations and Their Significance," SAE Technical Paper [720463](#), 1972, doi:[10.4271/720463](#).
16. Gillespie, T.D., "Influence of Tire/Wheel Nonuniformities on Heavy Truck Ride Quality," Final Rept., MVMA Project #1163, Highway Safety Res. Inst., Univ. of Mich., Rept. No. UM-HSRI-82-30, September 1982, 109pp.
17. Gillespie, T.D., "Tire and Wheel Nonuniformities: Their Impact on Heavy Truck Ride," presentation at the *Meeting of the American Chemical Society*, Denver, CO, October 1984, 21pp.
18. Lippmann, S.A., "Forces and Torques Associated with Roughness in Tires," SAE Technical Paper [610544](#), 1961, doi:[10.4271/610544](#).
19. Morrish, L.M. et al. "The Effect of Loaded Radial Runout on Tire Roughness and Shake," SAE Technical Paper [610545](#), 1961, doi:[10.4271/610545](#).
20. Potts, G.R., et al. "Tire Vibrations," *Tire Science and Technology*, 5, no. 4 (1977), 202-225.
21. Wagner, E.R., "Driveline and Driveshaft Arrangements and Constructions," in *Universal Joint and Driveshaft Design Manual*, Chapter 1, SAE AE-7 (1979), 3-10.
22. Joyner, R.G., "The Truck Driveline as a Source of Vibration," SAE Technical Paper [760843](#), 1976, doi:[10.4271/760843](#).
23. Mazziotti, P.J., "Dynamic Characteristics of Truck Driveline Systems," *11th L. Ray Buckendale Lecture*, SAE SP-262, January 1965.
24. Patterson, D., "Engine Torque and Balance Characteristics," SAE Technical Paper [821575](#), 1982, doi:[10.4271/821575](#).
25. Dahlberg, T., "Optimization Criteria for Vehicles Traveling on a Randomly Profiled Road-A Survey," *Vehicle Systems Dynamics*, 8, no. 4 (1979), 239-252.

26. SAE J6a, "Ride and Vibration Data Manual," Society of Automotive Engineers, Warrendale, PA, December 1965 (see Appendix B).
27. Gillespie, T.D. et al., "Truck Cab Vibrations and Highway Safety," Final Report, FHWA Contract No. DTFH-61-81-C-00083, Highway Safety Research Institute, University of Michigan, Report No. UMHSRI-82-9-1/2, March 1982, 203pp.
28. Sayers, M. and Gillespie, T.D., "The Effect of Suspension System Nonlinearities on Heavy Truck Vibration," *The Dynamics of Vehicles on Roads and Tracks, Proceedings*, A. H. Wickens, Ed., Swets and Zeitlander, Lisse, 1982, 154-166.
29. Butkunas, A.A., "Power Spectral Density and Ride Evaluation," SAE Technical Paper [660138](#), 1966, doi:[10.4271/660138](#).
30. Lee, R.A., and Pradko, F., "Analytical Analysis of Human Vibration," SAE Technical Paper [680091](#), 1968, doi:[10.4271/680091](#).
31. International Standard ISO 26311 978(E), *Guide for the Evaluation of Human Exposure to Whole-Body Vibration*, 2nd ed. (International Organization for Standardization, 1978), 15pp.
32. Oborne, D.J., "Techniques Available for the Assessment of Passenger Comfort," *Applied Ergonomics*, 9, no. 1 (1978), 45-49.
33. Miwa, T., "Evaluation Methods for Vibration Effect. Part 8 - The Vibration Greatness of Random Waves," *Industrial Health*, 87 (1969), 89-115.
34. Parsons, K.C., Whitham, E.M., and Griffin, M.J., "Six Axis Vehicle Vibration and Its Effects on Comfort," *Ergonomics*, 22, no. 2 (1979), 211-225.
35. Fothergill, L.C., et al., "The Use of an Intensity Matching Technique to Evaluate Human Response to Whole-Body Vibration," *Ergonomics*, 20, 3, 1977, 249-261.
36. Leatherwood, J.D. and Dempsey, T.K., "Psychophysical Relationships Characterizing Human Response to Whole-Body Sinusoidal Vertical Vibrations," NASA TN D-8188, NASA Langley Research Center, June 1976, 34pp.
37. Leatherwood, J.D., Dempsey, T.K., and Clevenson, S.A., "A Design Tool for Estimating Passenger Ride Comfort within Complex Ride Environments," *Human Factors*, 22 no. 3 (1980), 291-312.
38. Healey, A.J., et al., "An Analytical and Experimental Study of Automobile Dynamics with Random Roadway Inputs," *Transactions of the ASME*, 99 (1977), 284-292.
39. Wagner, E.R., "Driveline and Driveshaft Arrangements and Constructions," *Universal Joint and Driveshaft Design Manual*. Chapter 1, SAE AE-7 (1979), 440pp.
40. Wagner, E.R., and Cooney, C.E., "Cardan or Hooke Universal Joint," *Universal Joint and Driveshaft Design Manual*, Section 3.1.1, SAE AE-7 (1979), 440pp.
41. Chalasani, R.M., "Ride Performance Potential of Active Suspension Systems - Part I: Simplified Analysis Based on a Quarter-Car Model," Proceedings, *Symposium on Simulation and Control of Ground Vehicles and Transportation Systems*, AMD-Vol. 80, DSC Vol 2, American Society of Mechanical Engineers, 1986, 187-204.
42. Chalasani, R.M., "Ride Performance Potential of Active Suspension Systems - Part II: Comprehensive Analysis Based on a Full-Car Model," Proceedings, *Symposium on Simulation and Control of Ground Vehicles and Transportation Systems*, AMD-Vol. 80, DSC Vol 2, American Society of Mechanical Engineers, 205-226.
43. Cole, D., "Elementary Vehicle Dynamics," course notes in *Mechanical Engineering* (The University of Michigan, Ann Arbor, MI, 1972).
44. Gillespie, T.D., "Heavy Truck Ride, SP-607," Society of Automotive Engineers, Inc., 1985, 68pp.



Steady-State Cornering



Test drive on handling test track.

Introduction

The cornering behavior of a motor vehicle is an important performance mode often equated with handling. “Handling” is a loosely used term meant to imply the responsiveness of a vehicle to driver inputs or the ease of control. As such, handling is an overall measure of the vehicle-driver combination. The driver and vehicle is a “closed-loop” system—meaning that the driver observes the vehicle direction or position, and corrects his/her input to achieve the desired motion. For purposes of characterizing only the vehicle, “open-loop” behavior is used. Open loop refers to vehicle response to specific steering inputs, and is more precisely defined as “directional response” behavior [1].

The most commonly used measure of open-loop response is the understeer gradient [2]. Understeer gradient is a measure of performance under steady-state conditions, although the measure can be used to infer performance properties under conditions that are not quite steady state (quasi-steady-state conditions).

Open-loop cornering, or directional response behavior, will be examined in this section. The approach is to first analyze turning behavior at low speed, and then consider the differences that arise under high-speed conditions. The importance of tire properties will appear in the high-speed cornering case and provide a natural point for systematic study of the suspension properties influential to turning.

Low-Speed Turning

The first step to understanding cornering is to analyze the low-speed turning behavior of a motor vehicle. At low speeds (parking lot maneuvers) the tires need not develop lateral forces. Thus they roll with no slip angle, and the vehicle must negotiate a turn as illustrated in [Figure 6.1](#). If the rear wheels have no slip angle, the center of the turn must lie on the projection of the rear axle. Likewise, the perpendicular from each of the front wheels should pass through the same point i.e., the center of the turn. If they do not pass through the same point, the front tires will “fight” each other in the turn, with each experiencing some scrub (sideslip) in the turn. The ideal turning angles of the front wheels are established by the geometry seen in the figure, and define the steering angles for the turn.

For proper geometry in the turn (assuming small angles), the steer angles are given by:

$$\delta_o = \tan^{-1} \frac{L}{R + t/2} = \frac{L}{R + t/2} \quad (6.1)$$

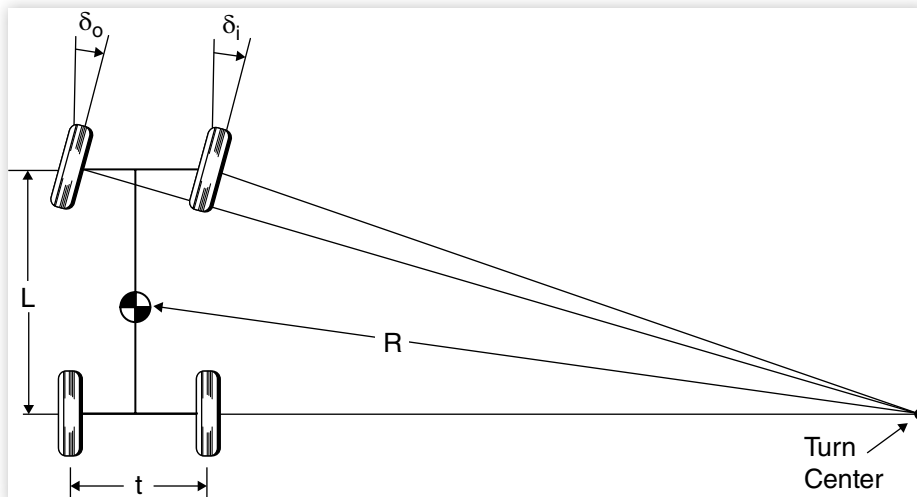
$$\delta_i = \tan^{-1} \frac{L}{R - t/2} = \frac{L}{R - t/2} \quad (6.2)$$

The average angle of the front wheels (again assuming small angles) is defined [2] as the [Ackerman Angle](#):

$$\delta = L/R \quad (6.3)$$

The terms “Ackerman Steering” or “Ackerman Geometry” are often used to denote the exact geometry of the front wheels shown in [Figure 6.1](#). The correct angles are

FIGURE 6.1 Geometry of a turning vehicle.



dependent on the wheelbase of the vehicle and the angle of the turn [3]. Deviations (i.e., error) from the Ackerman geometry in the left-right road wheel steer angles can have a significant influence on front tire wear. Such deviations do not have a significant influence on directional response [4]; however, they do affect the centering torques in the steering system [5]. With correct Ackerman geometry, the steering torque tends to increase consistently with steering wheel angle, thus providing the driver with a natural feel in the feedback through the steering wheel. If we consider the case of parallel steer — i.e., the road wheel steer angles are equal for the left and right wheels — the steering torque grows with the steering wheel angle initially, but is likely to diminish beyond a certain point. Such cases may result in a negative handwheel torque, substantially reducing the quality of the response. This type of steering system behavior is undesirable.

The other significant aspect of low-speed turning is the off-tracking that occurs at the rear wheels. The off-tracking distance, Δ , may be calculated from simple geometry relationships as:

$$\Delta = R \left[1 - \cos(L/R) \right] \quad (6.4a)$$

Using the expression for a series expansion of the cosine, namely:

$$\cos z = 1 - \frac{z^2}{2!} + \frac{z^4}{4!} - \frac{z^6}{6!} \dots$$

Δ can be written as:

$$\Delta \approx \frac{L^2}{2R} \quad (6.4b)$$

Off-tracking is a primary concern in the design and operation of long wheelbase vehicles such as straight trucks, buses, and trailers. For articulated trucks, the geometric equations become more complicated and are known as “tractrix” equations.

High-Speed Cornering

At high speed, the turning equations differ because lateral acceleration will be present. To counteract the lateral acceleration, the tires must develop lateral forces and slip angles will be present at each wheel.

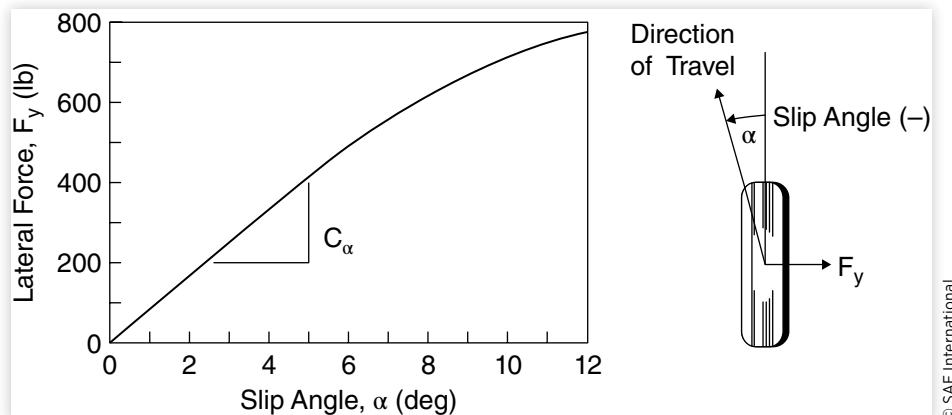
Tire Cornering Forces

Under cornering conditions in which the tire must develop a lateral force, the tire will also experience lateral slip as it rolls. The angle between its direction of heading and its direction of travel is known as slip angle, α [2]. These are illustrated in [Figure 6.2](#).

The lateral force, denoted by F_y , is called the “cornering force” when the camber angle is zero. At a given tire load, the cornering force grows with slip angle. At low slip angles (5 degrees or less), the relationship is linear, hence, allowing the cornering force to be described by the following relationship:

$$F_y = C_\alpha \alpha \quad (6.5)$$

The proportionality constant, C_α , is known as the “cornering stiffness,” and is defined as the slope of the curve for F_y versus α at $\alpha = 0$. A positive slip angle produces a negative force (to the left) on the tire, implying that C_α must be negative; however, SAE defines cornering stiffness as the negative of the slope, such that C_α takes on a positive value [2].

FIGURE 6.2 Tire cornering force properties.

The cornering stiffness is dependent on many variables [6]. Tire size and type (radial-versus bias-ply construction), number of plies, cord angles, wheel width, and tread are significant variables. For a given tire, the load and inflation pressure are the main variables. The plots in [Figure 6.3](#) illustrate the influence of many of these variables.

Because of the strong dependence of cornering force on load, tire cornering properties may also be described by the “cornering coefficient,” which is the cornering stiffness divided by the load. Thus the cornering coefficient, CC_α , is given by:

$$CC_\alpha = C_\alpha / F_z \quad (\text{lb}_y / \text{lb}_z / \text{deg}) \quad (6.6)$$

The cornering coefficient is usually largest at light loads, diminishing continuously as the load reaches its rated value (Tire & Rim Association rated load [7]). At 100% load, the cornering coefficient is typically in the range of 0.2 (lb cornering force per lb load per degree of slip angle).

Cornering Equations

The steady-state cornering equations are derived from the application of Newton’s Second Law along with the equation describing the geometry in turns (modified by the slip angle conditions necessary on the tires). For purposes of analysis, it is convenient to represent the vehicle by the bicycle model shown in [Figure 6.4](#). At high speeds the radius of turn is much larger than the wheelbase of the vehicle. Small angles can be assumed, and the difference between road wheel steer angles on the outside and inside front wheels can become negligible. For convenience, the two front wheels may be represented by a single wheel at a steer angle, δ , with a cornering force equivalent to both tires. The same assumption is made for the rear wheels.

For a vehicle traveling forward with a speed of V , the sum of the forces in the lateral direction from the tires must equal the mass times the centripetal acceleration.

$$\sum F_y = F_{yf} + F_{yr} = MV^2 / R \quad (6.7)$$

where:

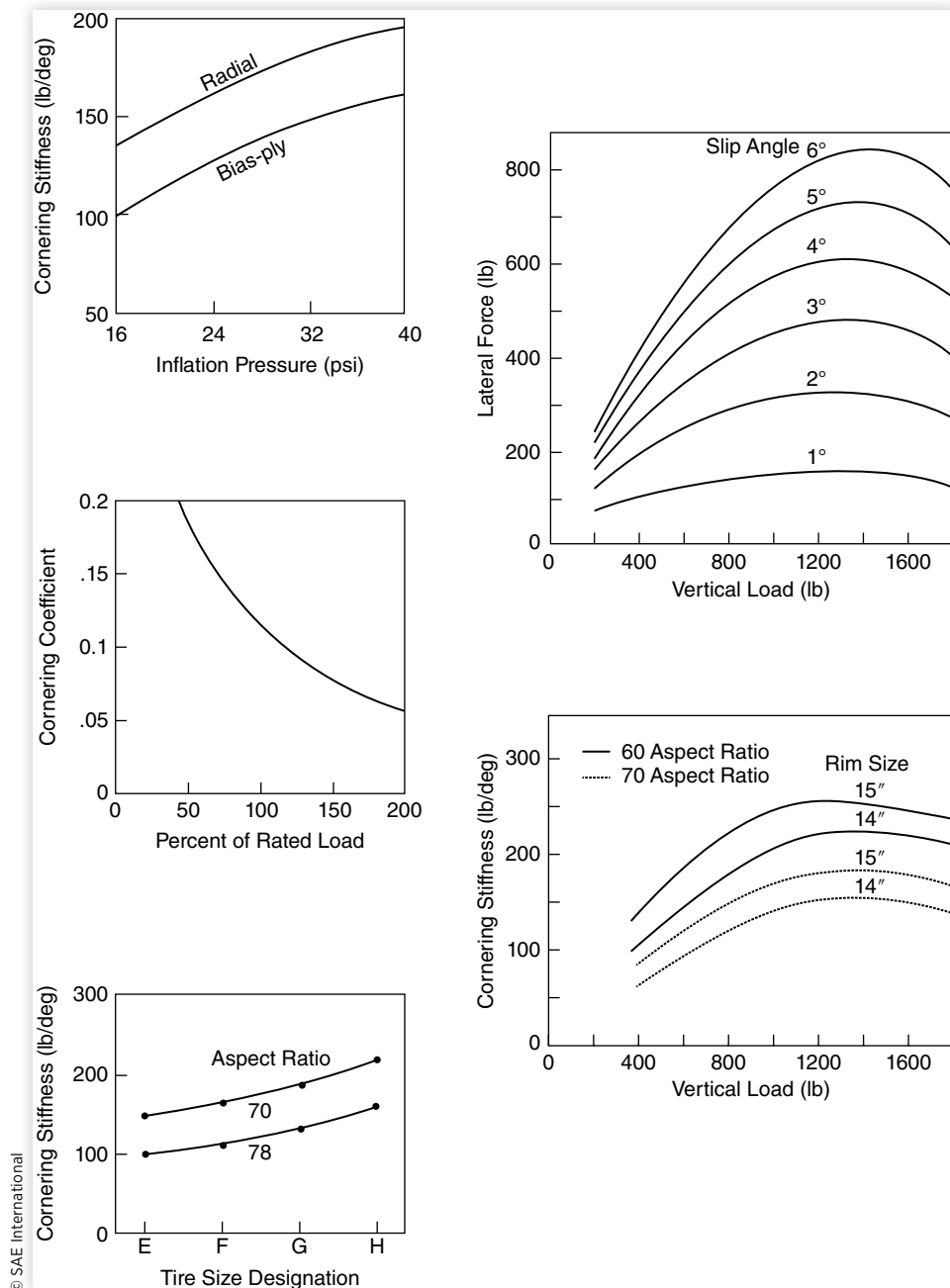
F_{yf} = Lateral (cornering) force at the front axle

F_{yr} = Lateral (cornering) force at the rear axle

M = Mass of the vehicle

V = Forward velocity

R = Radius of the turn

FIGURE 6.3 Variables affecting tire cornering stiffness.

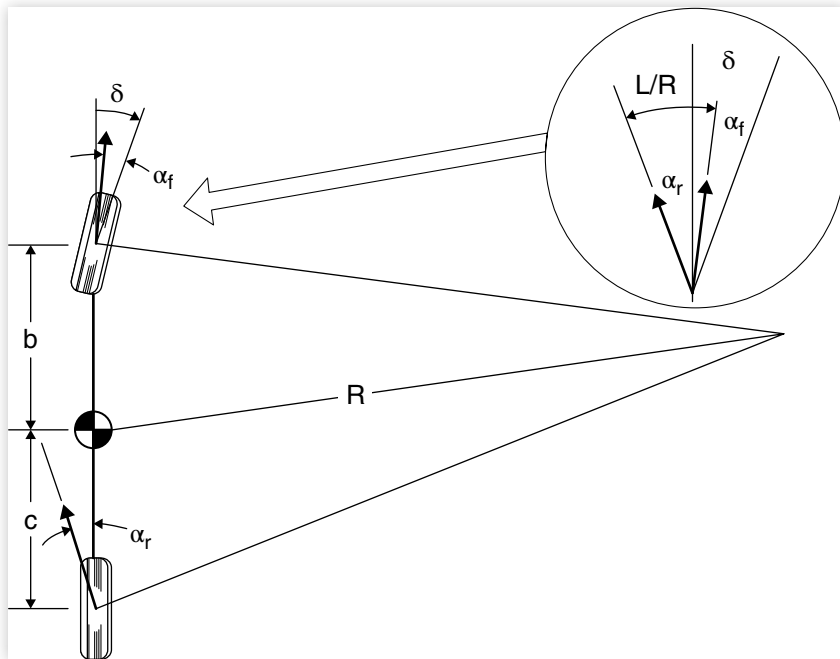
© SAE International

Also, for the vehicle to be in a moment equilibrium about the center of gravity, the sum of the moments from the front and rear lateral forces must be zero.

$$F_{yf} b - F_{yr} c = 0 \quad (6.8)$$

Thus

$$F_{yf} = F_{yr} c / b \quad (6.9)$$

FIGURE 6.4 Cornering of a bicycle model.

© SAE International

Substituting back into [Equation \(6.7\)](#) yields:

$$MV^2 / R = F_{yr} (c / b + 1) = F_{yr} (b + c) / b = F_{yr} L / b \quad (6.10)$$

$$F_{yr} = Mb / L (V^2 / R) \quad (6.11)$$

The term $M b / L$ is simply the portion of the vehicle mass carried on the rear axle (i.e., W_r/g); thus [Equation \(6.11\)](#) simply tells us that the lateral force developed at the rear axle must be W_r/g times the lateral acceleration at that point. Solving for F_{yr} in the same fashion will indicate that the lateral force at the front axle must be W_f/g times the lateral acceleration.

With the required lateral forces known, the slip angles at the front and rear wheels are also established from [Equation \(6.5\)](#). That is,

$$\alpha_f = w_f V^2 / (C_{af} g R) \quad (6.12)$$

and

$$\alpha_r = w_r V^2 / (C_{ar} g R) \quad (6.13)$$

We must now look to the geometry of the vehicle in the turn to complete the analysis. With a little study of [Figure 6.4](#), it can be seen that:

$$\delta = 57.3 L / R + \alpha_f - \alpha_r \quad (6.14)$$

Now substituting for α_f and α_r from [Equations \(6.12\)](#) and [\(6.13\)](#) gives:

$$\delta = 57.3 \frac{L}{R} + \frac{W_f V^2}{C_{af} g R} - \frac{W_r V^2}{C_{ar} g R}$$

$$\delta = 57.3 \frac{L}{R} + \left(\frac{W_f}{C_{af}} - \frac{W_r}{C_{ar}} \right) \frac{V^2}{gR} \quad (6.15)$$

where:

- δ = Steer angle at the front wheels (deg)
- L = Wheelbase (ft)
- R = Radius of turn (ft)
- V = Forward speed (ft/sec)
- g = Gravitational acceleration constant = 32.2 ft/sec²
- W_f = Load on the front axle (lb)
- W_r = Load on the rear axle (lb)
- C_{af} = Cornering stiffness of the front tires (lb_y/deg)
- C_{ar} = Cornering stiffness of the rear tires (lb_y/deg)

Understeer Gradient

The equation is often written in a shorthand form as:

$$\delta = 57.3 \frac{L}{R} + K a_y \quad (6.16)$$

where:

- K = Understeer gradient (deg/g)
- a_y = Lateral acceleration (g)

Equation (6.15) is very important to the turning response properties of a motor vehicle. It describes how the steer angle of the vehicle must be changed with the radius of turn, R , or the lateral acceleration, $V^2/(g R)$. The term $[W_f/C_{af} - W_r/C_{ar}]$ determines the magnitude and direction of the steering inputs required. It consists of two terms, each of which is the ratio of the load on the axle (front or rear) to the cornering stiffness of the tires on the axle. It is called the “Understeer Gradient,” and will be denoted by the symbol, K , which has units of degrees/g. Three possibilities exist:

1. **Neutral Steer:** $W_f/C_{af} = W_r/C_{ar} \rightarrow K = 0 \rightarrow \alpha_f = \alpha_r$

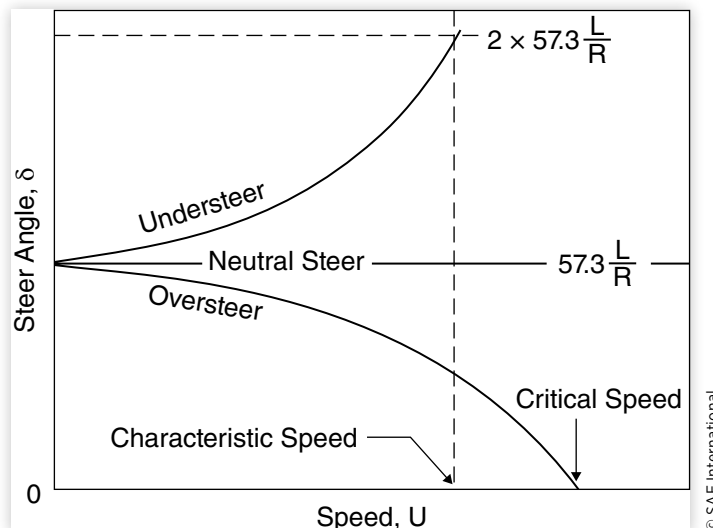
On a constant-radius turn, no change in steer angle will be required as the speed is varied. Specifically, the steer angle required to make the turn will be equivalent to the Ackerman Angle, $57.3 L/R$. Physically, the neutral steer case corresponds to a balance on the vehicle such that the “force” of the lateral acceleration at the C.G. causes an identical increase in slip angle at both the front and rear wheels.

2. **Understeer:** $W_f/C_{af} > W_r/C_{ar} \rightarrow K > 0 \rightarrow \alpha_f > \alpha_r$

On a constant-radius turn, the steer angle will have to increase with speed in proportion to K (deg/g) times the lateral acceleration in g's. Therefore the steer angle increases linearly with the lateral acceleration and with the square of the speed. In the understeer case, the lateral acceleration at the C.G. causes the front wheels to slip sideways to a greater extent than at the rear wheels. In order to develop the lateral force at the front wheels necessary to maintain the radius of turn, the front wheels must be steered to a greater angle.

3. **Oversteer:** $W_f/C_{af} < W_r/C_{ar} \rightarrow K < 0 \rightarrow \alpha_f < \alpha_r$

On a constant-radius turn, the steer angle will have to decrease as the speed (and lateral acceleration) is increased. In this case, the lateral acceleration at the C.G. causes the slip angle on the rear wheels to increase more than at the front. The outward drift at the rear of the vehicle turns the front wheels inward, thus diminishing the radius of the turn. The increase in lateral acceleration that follows causes the rear to drift out even further and the process continues unless the steer angle is reduced to maintain the radius of the turn.

FIGURE 6.5 Change of steer angle with speed.

© SAE International

The way in which steer angle changes with speed on a constant-radius turn for each of these cases is illustrated in [Figure 6.5](#). With a neutral steer vehicle, the steer angle to follow the curve at any speed is simply the Ackerman Angle. With understeer, the angle increases with the square of the speed, reaching twice the initial angle at the characteristic speed. In the oversteer case, the steer angle decreases with the square of the speed and becomes zero at what is known as the critical speed value.

Characteristic Speed

For an understeer vehicle, the understeer level may be quantified by a parameter known as the characteristic speed [8]. Characteristic speed is simply the speed at which the steer angle required to negotiate any turn is twice the Ackerman Angle. This can be seen in [Equation \(6.16\)](#) when:

$$K_a_y = 57.3 \frac{L}{R} \quad (6.17)$$

Since a_y is a function of speed squared, the characteristic speed is:

$$V_{\text{char}} = \sqrt{57.3 \frac{Lg}{K}} \quad (6.18)$$

Critical Speed

In the oversteer case, a critical speed will exist above which the vehicle will be unstable. The critical speed is given by the expression:

$$V_{\text{crit}} = \sqrt{-57.3 \frac{Lg}{K}} \quad (6.19)$$

It must be remembered that K is negative such that the expression under the square root is positive and has a real value. Note that the critical speed is dependent on the wheelbase of the vehicle; for a given level of oversteer, long-wheelbase vehicles have a higher critical speed than short-wheelbase vehicles. An oversteer vehicle can be driven

at speeds less than the critical, but becomes directionally unstable at and above the critical speed. The significance of critical speed becomes more apparent through its influence on the lateral acceleration gain and yaw rate gain as discussed in the next sections.

Lateral Acceleration Gain

Inasmuch as one of the purposes for steering a vehicle is to produce lateral acceleration, the turning [equation \(6.16\)](#) can be used to examine performance from this perspective. [Equation \(6.16\)](#) can be solved for the ratio of lateral acceleration, a_y , to the steering wheel angle, δ . The ratio is the lateral acceleration gain, given by:

$$\frac{a_y}{\delta} = \frac{\frac{V^2}{57.3Lg}}{1 + \frac{KV^2}{57.3Lg}} \quad (\text{g / sec}) \quad (6.20)$$

Note that when K is zero (neutral steer), the lateral acceleration gain is determined only by the numerator and is directly proportional to speed squared. When K is positive (understeer), the gain is diminished by the second term in the denominator and is always less than that of a neutral steer vehicle. Finally, when K is negative (oversteer), the second term in the denominator subtracts from 1, increasing the lateral acceleration gain. The magnitude of the term is dependent on the square of the speed, and subsequently approaches one when the vehicle speed reaches the critical speed. Therefore, the critical speed of [Equation \(6.19\)](#) corresponds to the denominator becoming zero (infinite gain) in [Equation \(6.20\)](#).

Yaw Velocity Gain

A second reason for steering a vehicle is to change the heading angle by developing a yaw velocity (sometimes called “yaw rate”). The yaw velocity, r , is the rate of rotation in heading angle and is given by:

$$r = 57.3V/R \quad (\text{deg/sec}) \quad (6.21)$$

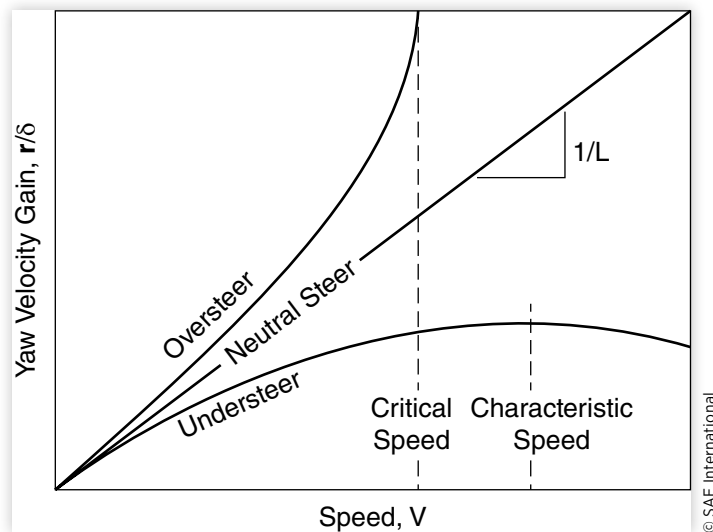
Substituting this expression into [Equation \(6.16\)](#) and solving for the ratio of yaw velocity to steering angle produces:

$$\frac{r}{\delta} = \frac{V/L}{1 + \frac{KV^2}{57.3Lg}} \quad (6.22)$$

The ratio represents a “gain” which is proportional to velocity in the case of a neutral steer vehicle. This is illustrated in [Figure 6.6](#). In accordance with [Equation \(6.19\)](#), we see that in the oversteer case the yaw velocity gain becomes infinite when the vehicle speed reaches the critical speed. In the case of the understeer vehicle, the yaw velocity increases with speed up to the characteristic speed, then begins to decrease thereafter. Thus the characteristic speed has significance as the speed at which the vehicle is most responsive in yaw.

Sideslip Angle

From the discussion of turning behavior, it is evident that when the lateral acceleration is negligible, the rear wheel tracks inboard of the front wheel. As lateral acceleration

FIGURE 6.6 Yaw velocity gain as a function of speed.

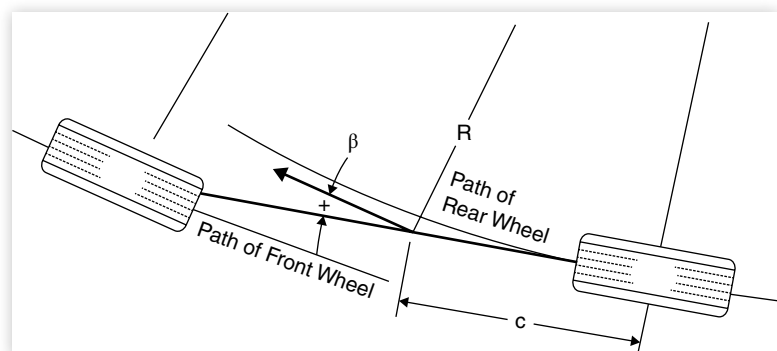
© SAE International

increases, however, the rear of the vehicle must drift outboard to develop the necessary slip angles on the rear tires. At any point on the vehicle a sideslip angle may be defined as the angle between the longitudinal axis and the local direction of travel. In general, the sideslip angle will be different at every point on a car during cornering.

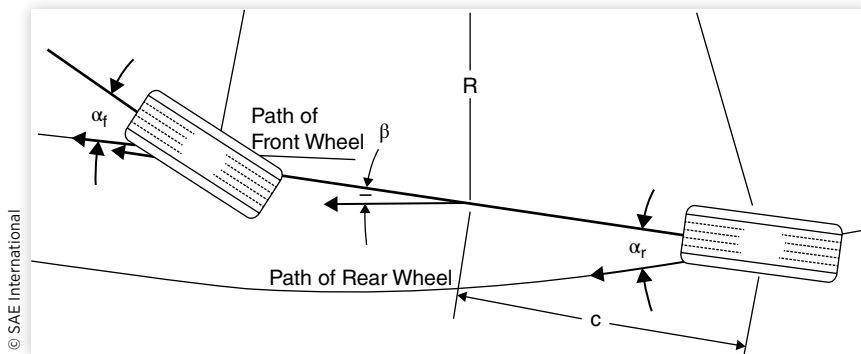
Taking the center of gravity as a case in point, the sideslip angle is defined as shown in **Figure 6.7**. The sideslip angle is defined as positive for this case because the direction of travel (the local velocity vector) is oriented clockwise from the longitudinal axis (clockwise angles viewed from above are positive in SAE convention. See Chapter 1, Figure 1.4a.). At high speed the slip angle on the rear wheels causes the sideslip angle at the C.G. to become negative, as illustrated in **Figure 6.8**.

For any speed the sideslip angle, β , at the C.G. will be:

$$\begin{aligned}\beta &= 57.3 c / R - \alpha_r \\ &= 57.3 c / R - W_r V^2 / (C_{ar} g R)\end{aligned}\quad (6.23)$$

FIGURE 6.7 Sideslip angle in a low-speed turn.

© SAE International

FIGURE 6.8 Sideslip angle in a high-speed turn.

© SAE International

Note that the speed at which the sideslip angle becomes zero is:

$$V_{\beta=0} = \sqrt{57.3 g c C_{ar} / W_r} \quad (6.24)$$

and is independent of the radius of the turn.

Static Margin

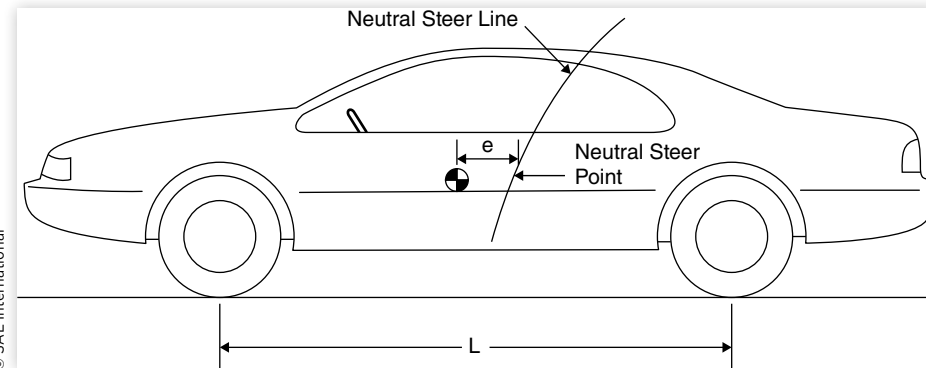
A term often used in discussions of handling is the static margin and, like understeer gradient or characteristic speed, provides a measure of the steady-state handling behavior.

Static margin is determined by the point on the vehicle where a side force will produce no steady-state yaw velocity (i.e., the neutral steer point). We may go one step further and define a neutral steer line as shown in [Figure 6.9](#). The neutral steer line is the locus of points in the x-z plane along which external lateral forces produce no steady-state yaw velocity.

The static margin is defined as the distance the neutral steer point falls behind the C.G., normalized by the wheelbase. This relationship can be expressed as:

$$\text{Static margin} = e / L \quad (6.25)$$

When the point is behind the C.G. the static margin is positive and the vehicle is understeer. At the C.G. the margin is zero and the vehicle is neutral steer. When ahead

FIGURE 6.9 Neutral steer line on a vehicle.

© SAE International

of the C.G., the vehicle is oversteer. For passenger cars the static margin falls in the range of 0.05 to 0.07.

Suspension Effects on Cornering

Thus far the analysis of turning has shown that the behavior is dependent on the ratios of load/cornering stiffness on the front and rear axles (W_f/C_{af} and W_r/C_{ar}). The ratios have the engineering units of deg/g, and have been called the “cornering compliance” [9]. The name arises from the fact that the ratio indicates the number of degrees of slip angle at an axle per “g” of lateral force imposed at that point. Inasmuch as the lateral force in a turn is actually a “D’ Alembert” force at the C.G., it is distributed at the axles in exact proportions to the weight (as the gravitational force is distributed).

Although the understeer gradient was derived for the case of a vehicle in a turn, it can be shown that the gradient determines vehicle response to disturbances in straight-ahead driving. In particular, an analysis by Rocard [10] demonstrates that oversteer vehicles have a stability limit at the critical speed due to normal disturbances in straight-ahead travel.

When the front axle is more compliant than the rear (understeer vehicle), a lateral disturbance produces more sideslip at the front axle; hence, the vehicle turns away from the disturbance. This is illustrated in Olley’s definitions for understeer and oversteer [11] shown in [Figure 6.10](#). If the rear axle exhibits more cornering compliance (oversteer), the rear of the vehicle drifts out and turns into the disturbance. The lateral acceleration acting at the C.G. adds to the disturbance force, further increasing the turning response and precipitating instability.

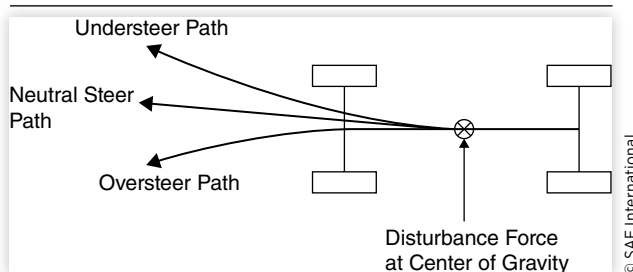
Although tire cornering stiffness was used as the basis for developing the equations for understeer/oversteer, there are multiple factors in vehicle design that may influence the cornering forces developed in the presence of a lateral acceleration. Any design factor that influences the cornering force developed at a wheel will have a direct effect on directional response. The suspensions and steering system are the primary sources of these influences. In this section the suspension factors affecting handling will be discussed.

Roll Moment Distribution

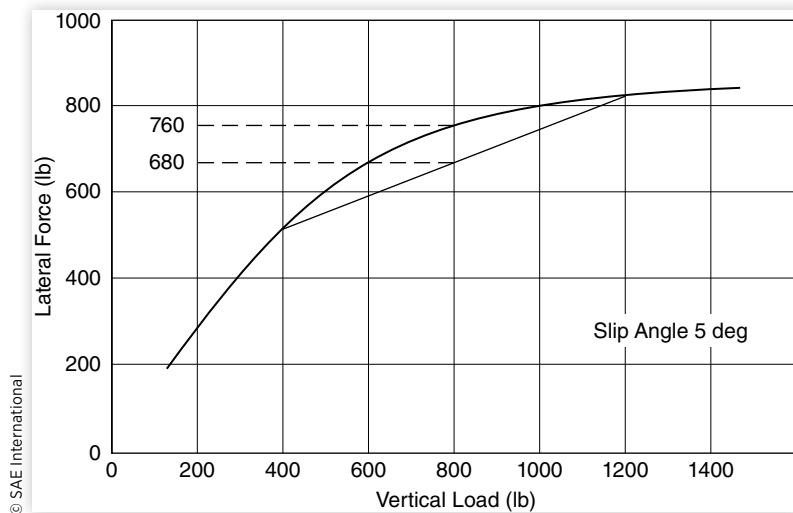
For virtually all pneumatic tires the cornering forces are dependent on, and nonlinear with, load. This is important because load is transferred in the lateral direction during

cornering due to the elevation of the vehicle C.G. above the ground plane. [Figure 6.11](#) shows a typical example of how lateral force varies with vertical load.

FIGURE 6.10 Olley’s definitions for understeer/oversteer.



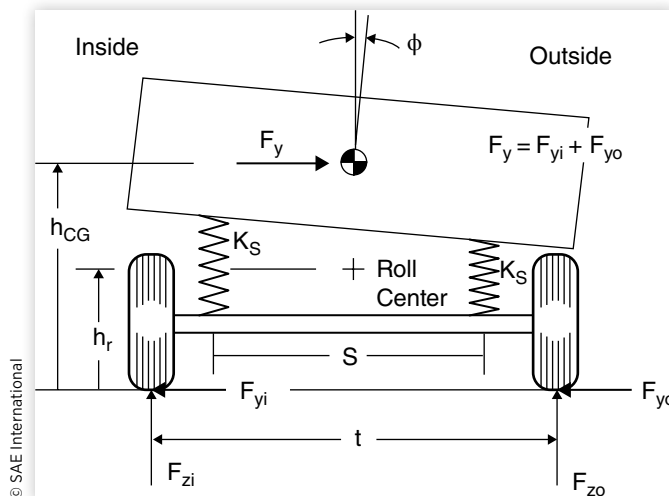
For a vehicle with 800 lb of load on each wheel, about 760 lb of lateral force will be developed by each wheel at the 5-deg. slip angle (see [Figure 6.11](#)). In hard cornering, if the lateral load transfer reduced the vertical load in the inside wheel to 400 lb while increasing it to 1200 lb on the outside wheel, we can see from [Figure 6.11](#) that the average lateral force from both tires would be reduced to about 680 lb. Consequently, the tires will have to assume a greater

FIGURE 6.11 Lateral force-vertical load characteristics of tires.

slip angle to maintain the lateral force necessary for the turn. If these are front tires, the front will plough out and the vehicle will understeer. If on the rear, the rear will slip out and the vehicle will oversteer.

Actually, this mechanism is at work on both axles of all two-axle vehicles. Whether it contributes to understeer or oversteer depends on the balance of roll moments distributed on the front and rear axles. More roll moment on the front axle contributes to understeer, whereas more roll moment on the rear axle contributes to oversteer. Auxiliary roll stiffeners (stabilizer bars) alter handling performance primarily through this mechanism—applied to the front axle for understeer, and to the rear for oversteer.

The mechanics governing the roll moment applied to an axle are shown in the model of [Figure 6.12](#). All suspensions are functionally equivalent to the two springs. The lateral

FIGURE 6.12 Force analysis of a simple vehicle in cornering.

separation of the springs causes them to develop a roll resisting moment proportional to the difference in roll angle between the body and the axle. The roll stiffness is given by:

$$K_\phi = 0.5 K_s s^2 \quad (6.26)$$

where:

K_ϕ = Roll stiffness of the suspension

K_s = Vertical rate of each of the left and right springs

s = Lateral separation between the springs

In the case of an independent suspension, the above expression can be used by substituting the rate at the wheel for K_s and using the track width as the separation distance. When a stabilizer bar is present, the roll stiffness of the bar must be added to the stiffness calculated above.

The suspension is further characterized by a “roll center,” the point at which the lateral forces are transferred from the axle to the sprung mass. The roll center can also be thought of as the point on the body at which a lateral force application will produce no roll angle, and it is the point around which the axle rolls when subjected to a pure roll moment.

By writing Newton’s Second Law for moments on the axle, we can determine the relationship between wheel loads and the lateral force and roll angle. In addition to the vertical forces imposed at the tires, there is a net lateral force, F_y (the sum of the lateral forces on the inside and outside wheels), acting to the right on the axle at its roll center. The body roll acting through the springs imposes a torque on the axle proportional to the roll stiffness, K_ϕ , times the roll angle, ϕ . This results in an equation for the load difference from side to side of the form:

$$F_{zo} - F_{zi} = 2F_y h_r / t + 2K_\phi \phi / t = 2\Delta F_z \quad (6.27)$$

where:

F_{zo} = Load on the outside wheel in the turn

F_{zi} = Load on the inside wheel in the turn

F_y = Lateral force = $F_{yi} + F_{yo}$

h_r = Roll center height

t = Track width

K_ϕ = Roll stiffness of the suspension

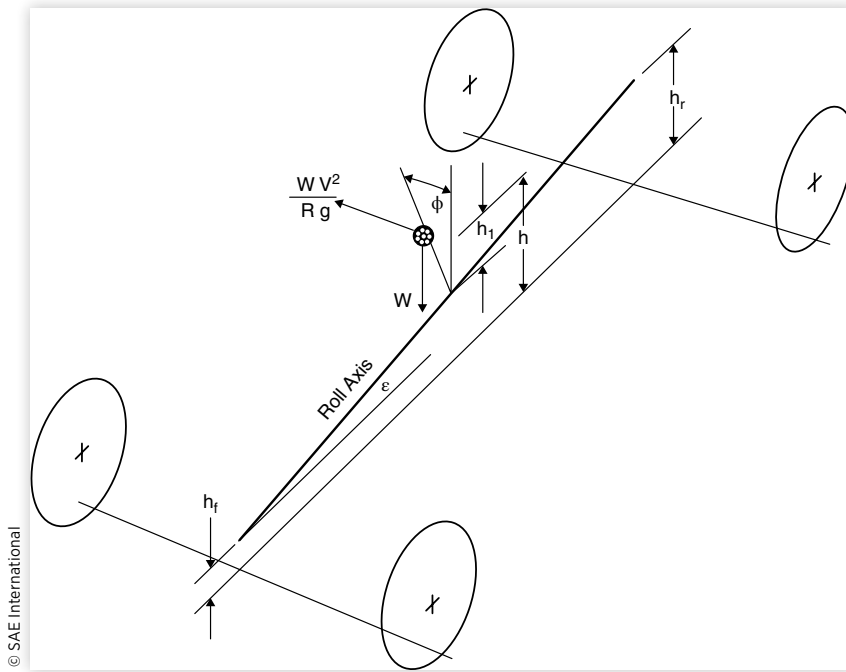
ϕ = Roll angle of the body

Note that lateral load transfer arises from two mechanisms:

1. $2 F_y h_r / t$ —Lateral load transfer due to cornering forces. This mechanism arises from the lateral force imposed on the axle, and is thus an instantaneous effect. It is independent of the roll angle of the body and the roll moment distribution.
2. $2 K_\phi \phi / t$ —Lateral load transfer due to vehicle roll. The effect depends on the roll dynamics, and thus may lag the changes in cornering conditions. It is directly dependent on front/rear roll moment distribution.

The total vehicle must be considered to obtain the expression for the roll moment distribution on the front and rear axles. In this case, we define a roll axis as the line connecting the roll centers of the front and rear suspensions, as shown in [Figure 6.13](#). Now the moment about the roll axis in this case is:

$$M_\phi = [W h_i \sin \phi + W V^2 / (Rg) h_i \cos \phi] \cos \varepsilon \quad (6.28)$$

FIGURE 6.13 Force analysis for roll of a vehicle.

© SAE International

For small angles, $\cos \phi$ and $\cos \epsilon$ may be assumed as unity, and $\sin \phi = \phi$.
Then:

$$M_\phi = Wh_1 \left[V^2 / (Rg) + \phi \right] \quad (6.29)$$

However:

$$M_\phi = M_{\phi f} + M_{\phi r} = (K_{\phi f} + K_{\phi r})\phi \quad (6.30)$$

Equations (6.29) and (6.30) can be solved for the roll angle, ϕ :

$$\phi = \frac{Wh_1 V^2 / (Rg)}{K_{\phi f} + K_{\phi r} - Wh_1} \quad (6.31)$$

The derivative of this expression with respect to the lateral acceleration produces an expression for the roll rate of the vehicle:

$$R_\phi = d\phi / da_y = Wh_1 / [K_{\phi f} + K_{\phi r} - Wh_1] \quad (6.32)$$

The roll rate is usually in the range of 3 to 7 degrees/g for typical passenger cars.

Combining the expression for ϕ from Equation (6.31) with Equation (6.29) allows solution for the roll moments on the front and rear axles:

$$M'_{\phi f} = K_{\phi f} \frac{Wh_1 V^2 / (Rg)}{K_{\phi f} + K_{\phi r} - Wh_1} + W_f h_f V^2 / (Rg) = \Delta F_{zf} t_r \quad (6.33)$$

$$M'_{\phi r} = K_{\phi r} \frac{Wh_1 V^2 / (Rg)}{K_{\phi f} + K_{\phi r} - Wh_1} + W_r h_r V^2 / (Rg) = \Delta F_{zr} t_r \quad (6.34)$$

where:

$$\begin{aligned}\Delta F_{zf} &= F_{zfo} - W_f / 2 = -(F_{zi} - W_f / 2) \\ \Delta F_{zf} &= F_{zro} - W_r / 2 = -(F_{zri} - W_r / 2)\end{aligned}$$

In general, the roll moment distribution on vehicles tends to be biased toward the front wheels due to a number of factors:

1. Relative to load, the front spring rate is usually slightly lower than that at the rear (for flat ride), which produces a bias toward higher roll stiffness at the rear. However, independent front suspensions used on virtually all cars enhance front roll stiffness because of the effectively greater spread between the front suspension springs.
2. Designers usually strive for higher front roll stiffness to ensure understeer at the limits of cornering.
3. Stabilizer bars are often used on the front axle to obtain higher front roll stiffness.
4. If stabilizer bars are needed to reduce body lean, they may be installed on either the front, or both the front and rear. Caution should be used when adding a stabilizer bar only to the rear because of the potential to induce unwanted oversteer.

We now have the solution for roll moments front and rear, and can calculate the difference in load between the left and right wheels on the axle. To translate the lateral load transfer into an effect on understeer gradient, it is necessary to have data which relates the tire cornering force to slip angle and load. At the given conditions, the slip angle on each axle will change when the load transfer is taken into account. The difference between the change on the front and rear (normalized by the lateral acceleration) represents the understeer effect. The effect can be modeled by expressing the tire load sensitivity as a polynomial. In the first analysis, the cornering characteristics of the tires on an axle were described simply by a constant called the cornering stiffness, C_α . The cornering force developed on the axle was given by:

$$F_y = C_\alpha \alpha \quad (6.35)$$

where:

F_y = Lateral force developed on the axle

C_α = Cornering stiffness of two tires, each at one-half the axle load

α = Slip angle

To represent load sensitivity effect, the two tires (inside and outside, relative to the turn) must be treated separately. The cornering stiffness of each tire can be represented by a second- or higher-order polynomial, and the lateral force developed by either will be given by:

$$F'_y = C'_\alpha \alpha = (aF_z - bF_z^2)\alpha \quad (6.36)$$

where:

F'_y = Lateral force of one tire

C'_α = Cornering stiffness of one tire

a = First coefficient in the cornering stiffness polynomial ($lb_y/lb_z/\text{deg}$)

b = Second coefficient in the cornering stiffness polynomial ($lb_y/lb_z^2/\text{deg}$)

F_z = Load on one tire (assumed equal on both tires in previous analysis)

For a vehicle cornering as shown in Figure 6.12, the lateral force of both tires, F_y , is given by:

$$F_y = (aF_{zo} - bF_{zo}^2 + aF_{zi} - bF_{zi}^2)\alpha \quad (6.37)$$

Now, let the load change on each wheel be given by ΔF_z .

$$F_{zo} = F_z + \Delta F_z \quad F_{zi} = F_z - \Delta F_z \quad (6.38)$$

Then:

$$F_y = \left[a(F_z + \Delta F_z) - b(F_z + \Delta F_z)^2 + a(F_z - \Delta F_z) - b(F_z - \Delta F_z)^2 \right] \alpha \quad (6.39)$$

This equation reduces to:

$$F_y = \left[2aF_z - 2bF_z^2 - 2b\Delta F_z^2 \right] \alpha \quad (6.40)$$

Further simplifications can be made if we recognize that the first two terms in the brackets are equivalent to the cornering stiffness of the tires at their static load conditions (as defined in the previous analysis). Namely:

$$C_\alpha = 2aF_z - 2bF_z^2 \quad (6.41)$$

or:

$$F_y = [C_\alpha - 2b\Delta F_z^2] \alpha \quad (6.42)$$

Recall that the steer angle necessary to maintain a turn is given by:

$$\delta = 57.3 L / R + \alpha_f - \alpha_r \quad (6.43)$$

For the two tires on the front axle we can write:

$$F_{yf} = [C_{\alpha f} - 2b\Delta F_{zf}^2] \alpha_f = W_f V^2 / (Rg) \quad (6.44)$$

and on the rear:

$$F_{yr} = [C_{\alpha r} - 2b\Delta F_{zr}^2] \alpha_r = W_r V^2 / (Rg) \quad (6.45)$$

Substituting to eliminate the slip angles in Equation (6.43):

$$\delta = 57.3 \frac{L}{R} + \frac{W_f V^2 / (Rg)}{\left(C_{\alpha f} - 2b\Delta F_{zf}^2 \right)} - \frac{W_r V^2 / (Rg)}{\left(C_{\alpha r} - 2b\Delta F_{zr}^2 \right)} \quad (6.46)$$

This equation can be simplified by utilizing the fact that $C_\alpha \gg 2b\Delta F_z^2$.

Then:

$$\frac{1}{\left(C_\alpha - 2b\Delta F_z^2 \right)} = \frac{1}{C_\alpha \left(1 - \frac{2b\Delta F_z^2}{C_\alpha} \right)} \approx \frac{1}{C_\alpha} \left(1 + \frac{2b\Delta F_z^2}{C_\alpha} \right) \quad (6.47)$$

Equation (6.46) can be rewritten in the form:

$$\delta = 57.3 \frac{L}{R} + \left[\left(\frac{W_f}{C_{\alpha f}} - \frac{W_r}{C_{\alpha r}} \right) + \left(\frac{W_f}{C_{\alpha f}} \frac{2b\Delta F_{zf}^2}{C_{\alpha f}} - \frac{W_r}{C_{\alpha r}} \frac{2b\Delta F_{zr}^2}{C_{\alpha r}} \right) \right] \frac{V^2}{Rg} \quad (6.48)$$

Term number 1 inside the brackets is simply the understeer gradient arising from the nominal cornering stiffness of the tires, K_{tires} , as was developed earlier. Term number 2 represents the understeer gradient arising from lateral load transfer on the tires; i.e.:

$$K_{\text{lt}} = \frac{W_f}{C_{\alpha f}} \frac{2b\Delta F_{zf}^2}{C_{\alpha f}} - \frac{W_r}{C_{\alpha r}} \frac{2b\Delta F_{zr}^2}{C_{\alpha r}} \quad (6.49)$$

The values for ΔF_{zf} and ΔF_{zr} can be obtained from Equations (6.33) and (6.34) as a function of lateral acceleration. Since all the variables in the above equation are positive, the contribution from the front axle is always understeer, while the contribution from the rear axle is always negative, meaning it is an oversteer effect.

Camber Change

The inclination of a wheel outward from the body is known as the camber angle [2]. Camber on a wheel will produce a lateral force known as “camber thrust.” Figure 6.14 shows a typical camber thrust curve.

Camber angle produces much less lateral force than slip angle. About 4 to 6 degrees of camber are required to produce the same lateral force as 1 deg. of slip angle on a bias-ply tire. Camber stiffness of radial tires is generally lower than that for bias-ply tires; hence, as much as 10 to 15 degrees are required on a radial tire. Nevertheless, camber thrust is additive to the cornering force from slip angle and therefore affects understeer. Camber thrust of bias-ply tires is strongly affected by inflation pressure, although not so for radial tires, and it is relatively insensitive to load and speed for both radial and bias tires.

Camber angles are small on solid axles, and at best only change the lateral forces by 10% or less. On independent suspensions, however, camber can play an important role in cornering. Camber changes both as a result of body roll as well as the normal camber change in suspension jounce/rebound. Figure 6.15 illustrates the mechanisms of camber change as a vehicle rolls while cornering.

FIGURE 6.14 Lateral force caused by camber of a tire.

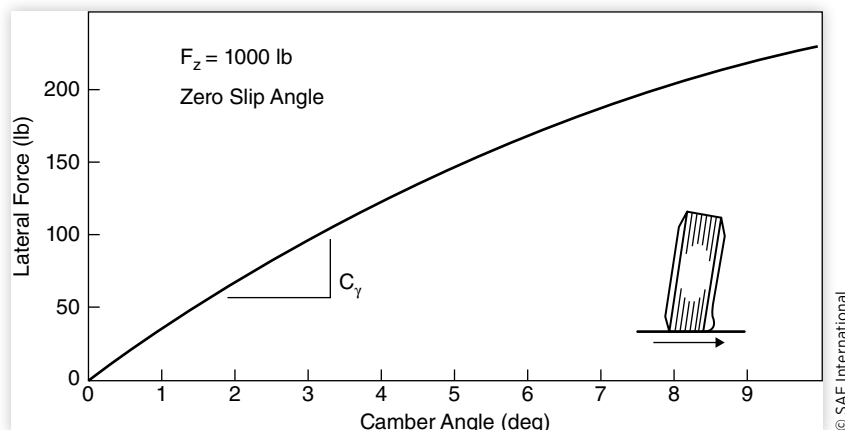
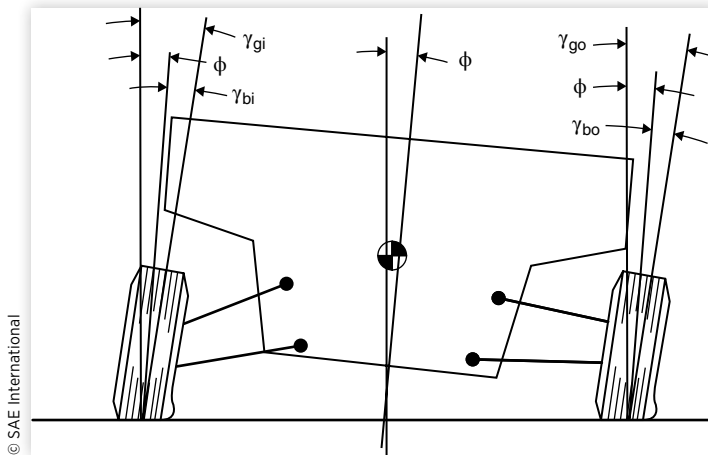


FIGURE 6.15 Camber change in cornering of a vehicle.

The total camber angle during cornering will be:

$$\gamma_g = \gamma_b + \phi \quad (6.50)$$

where:

γ_g = Camber angle with respect to the ground

γ_b = Camber angle of the wheel with respect to the body

ϕ = Roll angle of the vehicle

The camber angle arising from the suspension is a function of the roll angle because the jounce on the inside wheel and the rebound on the outside wheel relate directly to roll angle. Thus we can obtain the derivative of camber angle with respect to roll angle from an analysis of the suspension kinematics. The relationship is dependent on the geometry of the suspension, but for every suspension a kinematic analysis can be performed to develop a camber gradient of the form:

$$\partial\gamma / \partial\phi = f_\gamma \text{ (track width, suspension geometry, roll angle)} \quad (6.51)$$

In turn, the roll angle can be related to lateral acceleration through [Equation \(6.31\)](#) obtained earlier.

The influence on cornering comes about from the fact that the lateral force results not only from slip angle of the tire, but also its camber angle. That is:

$$F_y = C_\alpha \alpha + C_\gamma \gamma \quad (6.52)$$

Thus:

$$\alpha = \frac{F_y}{C_\alpha} - \frac{C_\gamma}{C_\alpha} \gamma \quad (6.53)$$

Now both F_y and γ are related to the lateral acceleration— F_y through [Equation \(6.11\)](#) and γ through [Equation \(6.52\)](#). Thus the equations for α_f and α_r take the forms:

$$\alpha_f = \frac{W_f}{C_\alpha} a_y - \frac{C_\gamma}{C_\alpha} \frac{\partial\gamma_f}{\partial\phi} \frac{\partial\phi}{\partial a_y} a_y \quad \text{and} \quad \alpha_r = \frac{W_r}{C_\alpha} a_y - \frac{C_\gamma}{C_\alpha} \frac{\partial\gamma_r}{\partial\phi} \frac{\partial\phi}{\partial a_y} a_y \quad (6.54)$$

When these are substituted into the turning equation (6.14), it takes the form:

$$\delta = 57.3 \frac{L}{R} + \left[\left(\frac{W_f}{C_{af}} - \frac{W_r}{C_{ar}} \right) + \left(\frac{C_{\gamma f}}{C_{af}} \frac{\partial \gamma_f}{\partial \phi} - \frac{C_{\gamma r}}{C_{ar}} \frac{\partial \gamma_r}{\partial \phi} \right) \frac{\partial \phi}{\partial a_y} \right] \frac{V^2}{Rg} \quad (6.55)$$

Therefore, the understeer deriving from camber angles on each axle is given by:

$$K_{\text{camber}} = \left(\frac{C_{\gamma f}}{C_{af}} \frac{\partial \gamma_f}{\partial \phi} - \frac{C_{\gamma r}}{C_{ar}} \frac{\partial \gamma_r}{\partial \phi} \right) \frac{\partial \phi}{\partial a_y} \quad (6.56)$$

Roll Steer

When a vehicle rolls in cornering, the suspension kinematics may be such that the wheels steer. Roll steer is defined as the steering motion of the front or rear wheels with respect to the sprung mass that is due to the rolling motion of the sprung mass. Consequently, roll steer effects on handling lag the steer input, awaiting roll of the sprung mass.

The steer angle directly affects handling as it alters the angle of the wheels with respect to the direction of travel. Let “ ϵ ” be the roll steer coefficient on an axle (degrees steer/degree roll). Using techniques similar to what was used in the previous section, we can derive the understeer gradient contribution from roll steer as:

$$K_{\text{roll steer}} = (\epsilon_f - \epsilon_r) \frac{\partial \phi}{\partial a_y} \quad (6.57)$$

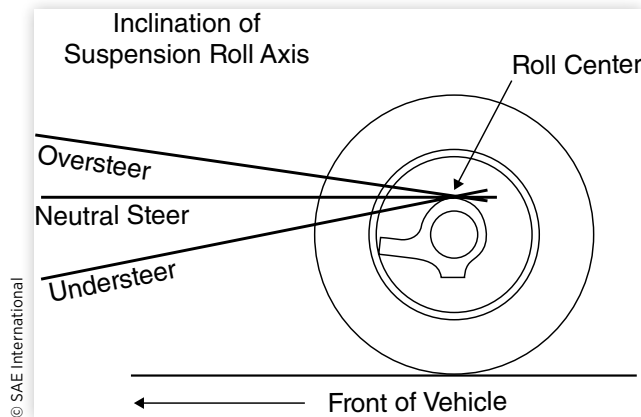
Following the SAE vehicle coordinate system convention established in Figure 1.4a, a positive roll steer coefficient causes the wheels to steer to the right in a right-hand roll. Inasmuch as a right-hand roll occurs when the vehicle is turning to the left, positive roll steer on the front axle steers out of the turn and is understeer. Conversely, positive roll steer on the rear axle is oversteer.

On solid axles the suspension will allow the axle to roll about an imaginary axis which may be inclined with respect to the longitudinal axis of the vehicle. The kinematics of the suspension, regardless of design, may be envisioned as functionally equivalent to leading or trailing arm systems, meaning the roll axis inclination is equal to that of the arms. Given an initial inclination angle, β , on the arms, as the body rolls, the arm on the inside wheel rotates downward while the arm on the outside wheel rotates upward as illustrated in [Figure 6.16](#).

If the initial orientation of a rear axle trailing arm is angled downward, the effect of the trailing arm angle change is to pull the inside wheel forward while pushing the outside wheel rearward. This produces roll steer of the solid axle contributing to oversteer. The roll steer coefficient is equal to the inclination angle ($\epsilon = \beta$ in radians) of the trailing arms. On a rear trailing arm system, roll understeer is achieved by keeping the transverse pivots of the trailing arms below the wheel center. [Figure 6.17](#) illustrates the effect of trailing arm angle on understeer.

FIGURE 6.16 Roll steer with a solid axle.

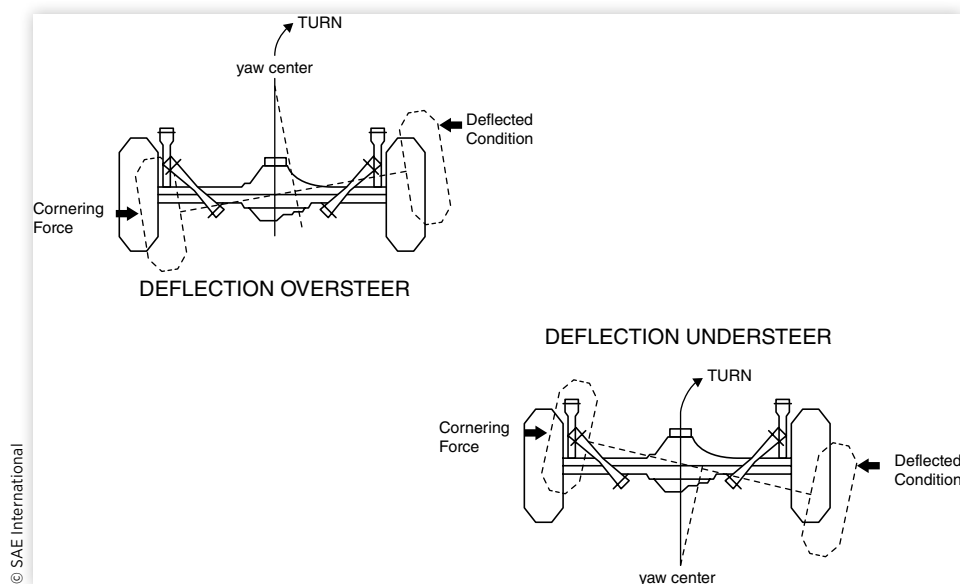


FIGURE 6.17 Influence of rear axle trailing arm angle on understeer.

With independent suspensions the roll steer coefficient must be evaluated from the kinematics of the suspension. On steered wheels, the interactions with the steering system must also be taken into account.

Lateral Force Compliance Steer

With the soft bushings used in suspension linkages for NVH reasons, there is the possibility of steer arising from lateral compliance in the suspension. With the simple solid axle, compliance steer can be represented as rotation about a yaw center as illustrated in [Figure 6.18](#).

FIGURE 6.18 Steer due to lateral compliance in the suspension.

With a forward yaw center on a rear axle, the compliance allows the axle to steer toward the outside of the turn, resulting in oversteer. Conversely, a rearward yaw center results in understeer. On a front axle, just the opposite is true—a rearward yaw center is oversteer, and a forward yaw center is understeer.

The handling influence of lateral force compliance steer can be quantified by defining an appropriate coefficient as follows:

$$A = \delta_c / F_y \quad (\text{degrees steer / unit lateral force}) \quad (6.58)$$

where:

δ_c = Steer angle

F_y = Lateral force

The lateral force experienced on an axle is simply the load on the axle times the lateral acceleration. Thus on the front axle:

$$\delta_{cf} = A_f W_f a_y \quad (6.59)$$

Since the understeer effect is directly related to the steer angles produced on the front and rear axles, the understeer arising from lateral force compliance steer is:

$$K_{lfcs} = A_f W_f - A_r W_r \quad (6.60)$$

Of course, the kinematics of linkages must be analyzed and taken into account to determine the coefficients on independent wheel suspensions and on steered wheels.

Aligning Torque

The aligning torque experienced by the tires on a vehicle always resists the attempted turn, making it the source of an understeer effect. Aligning torque is the manifestation of the fact that the lateral forces are developed by a tire at a point behind the tire center. This distance is known as the “pneumatic trail (p).”

The direct handling influence can be determined by deriving the turning equations with the assumption that the lateral forces are developed not at the wheels, but at a distance “p” behind each wheel. The understeer term obtained is:

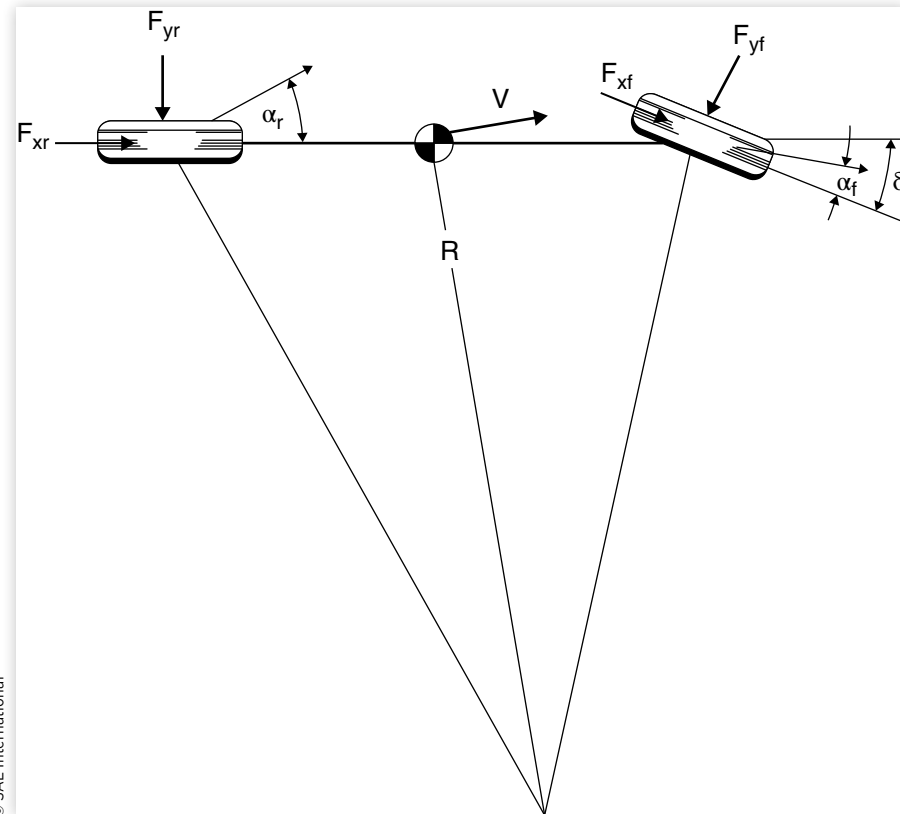
$$K_{at} = W \frac{p}{L} \frac{C_{af} + C_{ar}}{C_{af} C_{ar}} \quad (6.61)$$

Because the C_α values are positive, the aligning torque effect is positive (understeer) and cannot ever be negative (oversteer).

The understeer due to this mechanism is normally less than 0.5 deg/g. However, aligning torque is indirectly responsible for additional, and more significant, understeer mechanisms through its influence on the steering system. These mechanisms will be discussed with the steering system.

Effect of Tractive Forces on Cornering

The turning analysis developed at the outset of this chapter does not consider the potential effects of drive forces present at the wheels. We will now look at the case of drive forces present at front and rear wheels to develop the general equation showing their influence.

FIGURE 6.19 Cornering model with tractive forces.

© SAE International

With drive forces, the “bicycle” model for turning is shown in [Figure 6.19](#). The application of Newton’s Second Law in the lateral direction takes the form:

$$W_f V^2 / (Rg) = F_{yf} \cos(\alpha_f + \delta) + F_{xf} \sin(\alpha_f + \delta) \quad (6.62)$$

$$W_r V^2 / (Rg) = F_{yr} \cos \alpha_r + F_{xr} \sin \alpha_r \quad (6.63)$$

where:

W_f, W_r = Load on the front and rear axles

V = Forward speed

R = Radius of turn

F_{yf}, F_{yr} = Cornering forces on front and rear axles

F_{xf}, F_{xr} = Traction forces on the front and rear axles

α_f, α_r = Slip angles at front and rear wheels

Now the lateral forces, F_{yf} and F_{yr} , are simply the cornering stiffness on the axle times the slip angle. When that substitution is made in [Equations \(6.62\)](#) and [\(6.63\)](#), the right-hand side contains only the tractive forces and the slip angles. Assuming small angles, $\cos \alpha = 1$ and $\sin \alpha = \alpha$, we can then solve for α_f and α_r using substitution into the geometry equation:

$$\delta = 57.3 \frac{L}{R} + \alpha_f - \alpha_r \quad (6.64)$$

On substitution, δ occurs on both the left- and right-hand sides of the equation, and it is necessary to manipulate to get it only on the left-hand side.

$$\delta = \frac{57.3 L / R}{1 + F_{xf} / C_{af}} + \frac{\frac{W_f}{C_{af}} \frac{V^2}{Rg}}{1 + F_{xf} / C_{af}} - \frac{\frac{W_r}{C_{ar}} \frac{V^2}{Rg}}{1 + F_{xr} / C_{ar}} \quad (6.65)$$

The equation can be simplified into a somewhat more convenient form when we realize that F_{xf}/C_{af} and F_{xr}/C_{ar} are much less than one. In that case,

$$\frac{1}{1 + F_{xf} / C_{af}} \approx 1 - F_{xf} / C_{af} \quad (6.66)$$

The same is true for the rear axle.

Equation (6.65) can be manipulated into the form:

$$\delta = \frac{57.3 L / R}{1 + F_{xf} / C_{af}} + \left[\left(\frac{W_f}{C_{af}} - \frac{W_r}{C_{ar}} \right) - \left(\frac{W_f}{C_{af}} \frac{F_{xf}}{C_{af}} - \frac{W_r}{C_{ar}} \frac{F_{xr}}{C_{ar}} \right) \right] \frac{V^2}{Rg} \quad (6.67)$$

This is the final turning equation for the case where tractive forces are taken into account. Though it appears more complicated than what was developed earlier, it contains the same basic terms. The three terms on the right-hand side are as follows:

Term 1: This is the Ackerman steer angle altered by the tractive force on the front axle (rear tractive force does not show up here).

- If F_{xf} is positive (drive force applied in a FWD) it reduces the required steer angle for low-speed maneuvers, and accounts for the sense that FWD “pulls” a vehicle around in low-speed maneuvers.
- If F_{xf} is negative (equivalent to rolling resistance on a RWD or engine drag on a FWD) it tends to increase the required steer angle for turning.
- When front wheels spin on snow or ice, tractive force is still produced but C_{af} goes to zero. In that case the denominator of the term becomes infinite, suggesting that turns of zero radius can be made with virtually no steer angle. This accounts for the “trick” of turning a FWD vehicle within its own length on an icy surface by turning the wheel sharply and making them spin.

Term 2: This is the understeer gradient, unchanged from its earlier form.

Term 3: This term represents the effect of tractive forces on the understeer behavior of the vehicle.

- If F_{xf} is positive it causes an oversteer influence (pulls the front of the vehicle into the turn). This mechanism is an oversteer influence with a FWD in the throttle-on case.
- If F_{xr} is positive it causes an understeer influence by the same reasoning on a RWD.
- On a 4WD vehicle these mechanisms would suggest that the rear axle should “over drive” the front axle to ensure understeer behavior.

Anyone familiar with a FWD vehicle may be aware that the throttle-on oversteer mechanism described here is not evident with most vehicles. In discussion of the effects

of FWD in the steering section, it will be seen that the modification of tire cornering properties caused by traction forces has a stronger influence on handling than the direct action of the forces on the vehicle.

Summary of Understeer Effects

The understeer coefficient, K, for a vehicle is the result of tire, vehicle, and steering system parameters. Its total value is computed as the sum of a number of effects as summarized in the following table.

Understeer component	Source
$K_{\text{tires}} = \frac{W_f}{C_{af}} - \frac{W_r}{C_{ar}}$	Tire cornering stiffness
$K_{\text{camber}} = \left(\frac{C_{\gamma f}}{C_{af}} \frac{\partial \gamma_f}{\partial \phi} - \frac{C_{\gamma r}}{C_{ar}} \frac{\partial \gamma_r}{\partial \phi} \right) \partial a_y$	Camber thrust
$K_{\text{roll steer}} = (\varepsilon_f - \varepsilon_r) d\phi / da_y$	Roll steer
$K_{\text{lfc}} = A_f W_f - A_r W_r$	Lateral force compliance steer
$K_{\text{at}} = W \frac{p}{L} \frac{C_{af} + C_{ar}}{C_{af} C_{ar}}$	Aligning torque
$K_{\text{lft}} = \frac{W_f}{C_{af}} \frac{2b\Delta F_{zf}^2}{C_{af}} - \frac{W_r}{C_{ar}} \frac{2b\Delta F_{zr}^2}{C_{ar}}$	Lateral load transfer
$K_{\text{strg}} = W_f \frac{rv + p}{K_{ss}}$	Steering system

Experimental Measurement of Understeer Gradient

Understeer gradient is defined by SAE [2] as “The quantity obtained by subtracting the Ackerman steer angle gradient from the ratio of the steering wheel angle gradient to the overall steering ratio.” Methods for experimental measurement of understeer gradient [12, 13, 14] are all based on the definition of the gradient reflected in [Equation \(6.16\)](#). Namely,

$$\delta = 57.3 L/R + K a_y \quad (6.16)$$

The derivation of this equation assumes the vehicle to be in a steady-state operating condition; therefore, understeer is defined as a steady-state property. For experimental measurements, the vehicle must be placed into a steady-state turn with appropriate measures of the quantities in the above equation so that the value of K can be determined. Four test methods have been suggested as a means to measure this property—constant radius, constant speed, constant steer angle and constant throttle. Only the first two reasonably reflect normal driving circumstances, hence, the discussion will be limited to these two.

Constant Radius Method

Understeer can be measured by operating the vehicle around a constant radius turn and observing steering wheel angle versus lateral acceleration. The method closely replicates vehicle operation in many highway situations, such as the constant radius turns in off-ramps from limited access highways. At a minimum, instrumentation must be available to measure steering wheel angle and lateral acceleration. Given the radius of the turn and some measure of vehicle velocity (from the speedometer, fifth wheel, or by lap time), lateral acceleration can be computed using the relationship:

$$a_y = V^2 / (Rg) \quad (6.68)$$

The recommended procedure is to drive the vehicle around the circle at very low speed, for which the lateral acceleration is negligible, and note the steering wheel angle (Ackerman steer angle) required to maintain the turn. (The experimenter is challenged to develop good technique for this process as cross-slope on the test surface, bumps, etc., will cause the vehicle to drift in and out as it proceeds, complicating the determination of the average steer angle.) Vehicle speed is then increased in steps that will produce lateral accelerations at reasonable increments (typically 0.1 g), noting the steering wheel angle at each speed. The steering wheel angle (divided by the steering ratio to obtain the road wheel angle) is then plotted as a function of lateral acceleration as illustrated in [Figure 6.20](#).

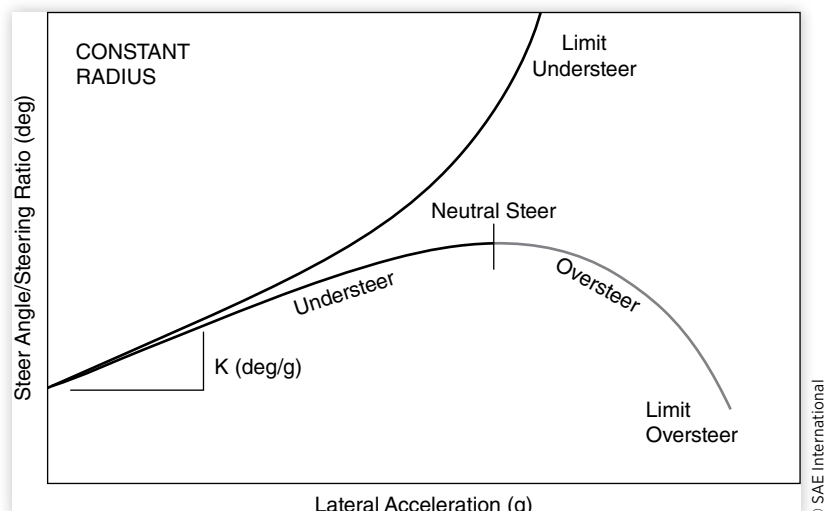
The meaning of this plot can be seen by taking the derivative of [Equation \(6.16\)](#):

$$\frac{\partial \delta}{\partial a_y} = \frac{\partial}{\partial a_y} \left(57.3 \frac{L}{R} \right) + K \frac{\partial a_y}{\partial a_y} \quad (6.69)$$

Since the radius of the turn is constant, the Ackerman steer angle is also constant and its derivative is zero. Thus:

$$K = \frac{\partial \delta}{\partial a_y} \quad (6.70)$$

FIGURE 6.20 Example measurements of understeer gradient by constant radius method.



The slope of the steer angle curve is the understeer gradient. A positive slope (upward and to the right) indicates understeer, zero slope is neutral steer, and a negative slope is oversteer. Typical measurements will take one of the forms shown in [Figure 6.20](#). Some vehicles will be understeer over the entire operating range, remaining so to the limit. Others may be understeer at low lateral acceleration levels but change to oversteer at high lateral acceleration levels and exhibit limit oversteer.

Note that the implied road wheel steer angle (obtained by dividing the steering wheel angle by the steering ratio) is used for characterizing the understeer gradient. While understeer is measured at the steering wheel, it is described by the degrees per g of steer required at the road wheel. As will be seen in the discussion of steering systems, the steering ratio is not a constant because of compliance in the system. This does not invalidate the measurement method, but rather recognizes that those properties in the steering system are a legitimate source of understeer on the vehicle. In cases where the road wheel steer angle is measured directly, a different understeer gradient will be obtained because the steering system effects will not be included. While this method is not incorrect, it fails to fully characterize the understeer properties of the vehicle by excluding contributions from the steering system. Recognizing that the driver must control the vehicle from the steering wheel, the steering system effects should be included to fully characterize understeer.

The constant radius method has the advantage that minimal instrumentation is required, but has the disadvantage that it is difficult to execute in an objective fashion. Determination of a precise steering wheel angle is difficult because of the deviations necessary to keep the vehicle on the selected radius of turn. This aspect of test technique is not readily controlled.

The minimum radius of turn for this test procedure is normally 30 m (≈ 100 ft). For two-axle vehicles the understeer gradient is not affected by the radius of the circle. The gradient for multi-axle straight trucks (three axles or more), however, is sensitive to turn radius in this range.

Constant Speed Method

Understeer can be measured at constant speed by varying the steering wheel angle. Measurements by this method closely duplicate many real driving situations since vehicles are normally driven at near constant speed. With this method, the radius of turn will vary continuously requiring more extensive data collection to determine the gradient. In addition to measuring speed and steer angle, the radius of turn must be determined for each condition as well. The most practical means to measure radius of turn is either by measuring lateral acceleration or yaw rate. The radius of turn is derived from the measurements using the appropriate form of the relationships below:

$$R = V^2 / a_y = V / r \quad (6.71)$$

where:

V = Forward speed (ft/sec or m/sec)

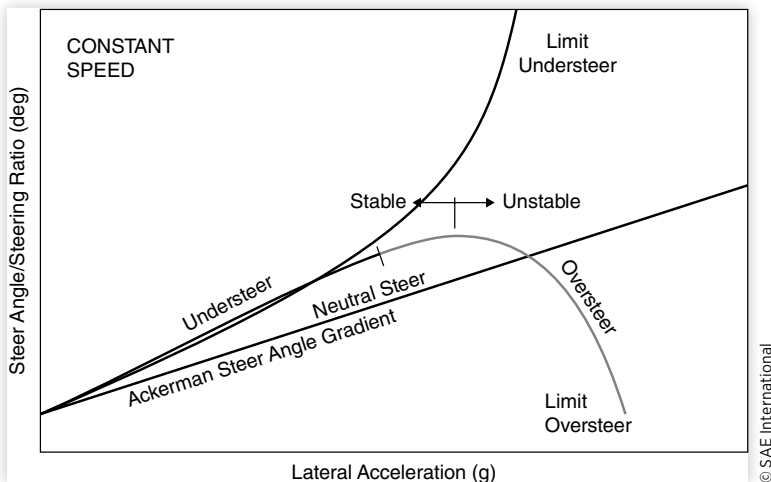
a_y = Lateral acceleration (ft/sec² or m/sec²)

r = Yaw rate (radians/sec)

The Ackerman steer angle gradient for this test procedure is obtained by substituting [Equation \(6.68\)](#) into [Equation \(6.16\)](#), eliminating the radius. This produces the form:

$$\delta = 57.3 L / R + K a_y = 57.3 (L a_y / V^2) + K a_y \quad (6.72)$$

FIGURE 6.21 Example measurements of understeer gradient by constant speed method.



© SAE International

Again taking derivatives with respect to lateral acceleration, we obtain the expression for the understeer gradient:

$$K = \frac{\partial \delta}{\partial a_y} - 57.3 \frac{L}{V^2} \quad (6.73)$$

Since speed and wheelbase are constant, the Ackerman steer angle gradient (the second term on the right-hand side) is a straight line of constant slope and appears in a data plot as shown in [Figure 6.21](#). The Ackerman steer angle gradient is neutral steer. In regions where the steer angle gradient is greater than that of the Ackerman, the vehicle is understeer. A point where the two have the same slope is neutral steer, and where the steer angle gradient is less than the Ackerman, the vehicle is oversteer. For the oversteer vehicle, the point where the slope of the steer angle curve is zero is the stability boundary corresponding to the critical speed.

Example Problems

1. A car has a weight of 1901 lb on the front axle and 1552 lb on the rear with a wheelbase of 100.6 in. The tires have the following cornering stiffness values:

Load	Cornering stiffness	Cornering coefficient
225 lb	67 lb/deg	0.298 lb/lb/deg
450	121	0.269
675	171	0.253
900	225	0.250
1125	257	0.228
1350	300	0.222

Determine the following cornering properties for the vehicle:

- Ackerman steer angles for 500, 200, 100 and 50 ft turn radius
- Understeer gradient

- c. Characteristic speed
- d. Lateral acceleration gain at 60 mph
- e. Yaw velocity gain at 60 mph
- f. Sideslip angle at the C.G. on an 800 ft radius turn at 60 mph
- g. Static margin

Solution:

- a. The Ackerman steer angles are only a function of the wheelbase and radius of turn, and can be found easily from [Equation \(6.3\)](#).

$$\delta_{500} = L/R = 100.6 \text{ in } (1 \text{ ft}/12 \text{ in})/500 \text{ ft} = 0.01677 \text{ rad} = 0.96 \text{ deg}$$

$$\delta_{200} = 100.6 \text{ in } (1 \text{ ft}/12 \text{ in})/200 \text{ ft} = 0.0419 \text{ rad} = 2.4 \text{ deg}$$

$$\delta_{100} = 100.6 \text{ in } (1 \text{ ft}/12 \text{ in})/100 \text{ ft} = 0.0838 \text{ rad} = 4.8 \text{ deg}$$

$$\delta_{50} = 100.6 \text{ in } (1 \text{ ft}/12 \text{ in})/50 \text{ ft} = 0.1677 \text{ rad} = 9.6 \text{ deg}$$

- b. In order to find the understeer gradients we must know the cornering stiffness of the tires at the prevailing loads. On the front axle the tire load is 950 lb per tire. Interpolating the cornering stiffness data between the loads of 900 and 1125 lb leads to a stiffness of 232 lb/deg at 950 lb. On the rear axle the load is 776 lb per tire. Again interpolating between the appropriate loads in the tire data, we obtain a cornering stiffness of 195 lb/deg. Now from [Equation \(6.15\)](#), we get:

$$K = \frac{W_f}{C_{af}} - \frac{W_r}{C_{ar}} = \frac{950 \text{ lb}}{232 \text{ lb/deg}} - \frac{776 \text{ lb}}{195 \text{ lb/deg}} = (4.09 - 3.98) \text{ deg} = 0.11 \text{ deg/g}$$

- c. The characteristic speed is determined from [Equation \(6.18\)](#):

$$V_{char} = \sqrt{57.3Lg/K} = \sqrt{57.3 \frac{\text{deg}}{\text{rad}} \frac{110.6 \text{ in.}}{12 \text{ in./ft}} \frac{32.2 \text{ ft/sec}^2}{0.11 \text{ deg/g}}} = 393 \text{ ft/s} = 268 \text{ mph}$$

- d. The lateral acceleration gain comes from [Equation \(6.20\)](#):

$$\begin{aligned} \frac{a_y}{\delta} &= \frac{\frac{V^2}{57.3Lg}}{1 + \frac{KV^2}{57.3Lg}} = \frac{\frac{(88 \text{ ft/sec})^2}{57.3 \text{ deg/rad}(8.38 \text{ ft})(32.2 \text{ ft/sec}^2)}}{1 + \frac{0.11 \text{ deg/g}(88 \text{ ft/sec})^2}{57.3 \text{ deg/rad}(8.38 \text{ ft})(32.2 \text{ ft/sec}^2)}} \\ &= \frac{0.501 \text{ g/deg}}{1.055} = 0.475 \text{ g/deg} \end{aligned}$$

- e. The yaw rate gain comes from [Equation \(6.22\)](#):

$$\begin{aligned} \frac{r}{\delta} &= \frac{\frac{V/L}{8.38 \text{ ft}}}{1 + \frac{KV^2}{57.3Lg}} = \frac{\frac{10.5/\text{sec}}{8.38 \text{ ft}}}{1 + \frac{0.11 \text{ deg/g}(88 \text{ ft/sec})^2}{57.3 \text{ deg/rad}(8.38 \text{ ft})(32.2 \text{ ft/sec}^2)}} \\ &= \frac{10.5/\text{sec}}{1.055} = 9.95 \frac{\text{deg/sec}}{\text{deg}} \end{aligned}$$

- f. The sideslip angle is obtained from [Equation \(6.23\)](#), but first we must find the value for “c,” the distance from the C.G. to the rear axle. This is obtained from a simple moment balance about the front axle.

$$c = \frac{100.6 \text{ in}}{12 \text{ in / ft}} \frac{1901 \text{ lb}}{(1901 + 1552) \text{ lb}} = 4.62 \text{ ft}$$

$$\begin{aligned} \beta &= 57.3 \frac{c}{R} - \frac{W_r V^2}{C_{\alpha r} R g} = 57.3 \text{ deg/rad} \frac{4.62 \text{ ft}}{800 \text{ ft}} - \frac{1552 \text{ lb} (88 \text{ ft/sec})^2}{390 \text{ lb/deg} (32.2 \text{ ft/sec}^2) (800 \text{ ft})} \\ &= (0.331 - 1.196) \text{ deg} = -0.865 \text{ deg} \end{aligned}$$

- g. To find the static margin, it is necessary to find the neutral steer point. This is the point on the side of the vehicle where one can push laterally and produce the same slip angle at both the front and rear tires. In the solution for part “a,” we determined that the cornering stiffnesses of the front and rear tires are 232 and 195 lb/deg, respectively. From a moment balance in the plan view, we can show that the distance from the neutral steer point to the rear axle (c') must be:

$$c' = L \frac{C_{\alpha f}}{C_{\alpha f} + C_{\alpha r}} = 8.38 \text{ ft} \frac{232}{232 + 195} = 4.55 \text{ ft}$$

Since c was 4.62 ft, therefore the neutral steer point is 0.07 ft (0.8% of the wheelbase) behind the C.G.

Note:

The calculated cornering properties for this vehicle (understeer gradient and static margin) are very close to neutral steer. However, this is a consequence of only the tire properties. Many other systems on the vehicle, particularly the steering and suspension systems, will contribute to the understeer gradient.

2. A passenger car has an equal arm (parallel) independent front suspension and a conventional solid rear axle with leaf spring suspension. The front suspension has a roll stiffness, $K_{\phi f}$, of 1500 in-lb/deg. The leaf springs have a rate of 115 lb/in and a lateral separation of 40 in.

- What is the rear suspension roll stiffness?
- If the sprung mass is 2750 lb at a C.G. height of 10 in above the roll axis, what is the roll rate?
- Assuming a camber stiffness that is 10 percent of the cornering stiffness, estimate the understeer gradient due to camber effects.
- The rear leaf springs have an effective trailing arm angle of -7 degrees (the negative sign means that the pivot of the arms is below the wheel center). What is the understeer gradient due to rear roll steer?

Solution:

- a. The rear suspension roll stiffness can be computed from [Equation \(6.26\)](#):

$$K_{\phi} = 0.5 K_s s^2 = 0.5 (115 \text{ lb/in}) (40 \text{ in})^2 = 92,000 \text{ in-lb/rad} = 1606 \text{ in-lb/deg}$$

- b. The roll rate can be calculated from Equation (6.32):

$$\begin{aligned} d\phi / da_y &= Wh_1 / [K_{\phi f} + K_{\phi r} - Wh_1] \\ &= \frac{2750 \text{ lb} (10 \text{ in})}{\left(1500 \frac{\text{in-lb}}{\text{deg}} + 1606 \frac{\text{in-lb}}{\text{deg}} - \frac{2750 \text{ lb}}{57.3 \text{ deg/rad}} \right)} = \frac{27500 \text{ in-lb}}{(1500 + 1606 - 480)} = 10.5 \text{ deg/g} \end{aligned}$$

- c. The understeer gradient due to camber effects can be estimated from Equation (6.56):

$$K_{\text{camber}} = \left(\frac{C_{\gamma f}}{C_{\alpha f}} \frac{\partial \gamma_f}{\partial \phi} - \frac{C_{\gamma r}}{C_{\alpha r}} \frac{\partial \gamma_r}{\partial \phi} \right) \frac{\partial \phi}{\partial a_y}$$

Although we know the ratio of camber stiffness to cornering stiffness (given as 0.1), the camber gradients must be determined. For an independent front suspension with parallel equal arms, the wheel does not incline with jounce and rebound. Therefore, the camber angle will change exactly with the roll angle and the gradient for the front axle is 1. The rear axle is a solid axle which does not roll significantly. Therefore, its gradient is zero. Finally, we know the roll gradient from part b, where it was calculated as 10.5 deg/g, and the equation can now be solved.

$$K_{\text{camber}} = (0.1 \times 1.0 - 0.1 \times 0) 10.5 \text{ deg/g} = 1.05 \text{ deg/g}$$

- d. The understeer gradient due to roll steer on the rear axle comes from Equation (6.57):

$$K_{\text{roll steer}} = (\varepsilon_f - \varepsilon_r) d\phi / da_y$$

Since we are concerned only with the rear axle, only the second term must be determined. A solid axle will exhibit roll steer dependent on the effective angle of the imaginary trailing arms, which in this case is -7 degrees (-0.122 rad). Then

$$K_{\text{roll steer (rear)}} = +0.122 \text{ rad} (10.5 \text{ deg/g}) = 1.28 \text{ deg/g}$$

By SAE convention, the positive sign means that the wheels steer right as the body rolls to the right (left turn). Since the roll steer turns the rear wheels to the right on a left turn, the rear will swing out more in the turn and oversteer is experienced.

References

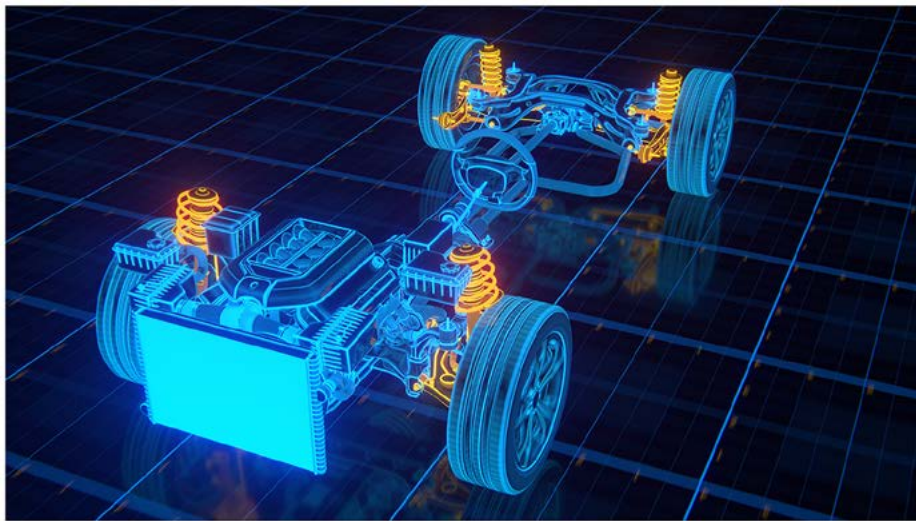
1. Good, M.C., "Sensitivity of Driver-Vehicle Performance to Vehicle Characteristics Revealed in Open-Loop Tests," *Vehicle Systems Dynamics* 6, no. 4 (1977): 245-277.
2. Vehicle Dynamics Standards Committee, "Vehicle Dynamics Terminology," SAE J670, Society of Automotive Engineers, Warrendale, PA (see Appendix A).
3. Durstine, J.W., "The Truck Steering System From Hand Wheel to Road Wheel," SAE Technical Paper [730039](#), 1973, doi:[10.4271/730039](#).
4. Lugner, P. and Springer, H., "Über den Einfluss der Lenkgeometrie auf die stationäre Kurventrfahrt eines LKW, (Influence of Steering Geometry on the Stationary Cornering of a Truck)," *Automobil-Industrie*, November 1974, 21-25.

5. Pitts, S. and Wildig, A.W., "Effect of Steering Geometry on Self-Centering Torque and 'Feel' during Low-Speed Maneuvers," *Automotive Engineer, Institution of Mechanical Engineers*, June-July 1978, 45-48.
6. Nordeen, D.L. and Cortese, A.D., "Force and Moment Characteristics of Rolling Tires," SAE Technical Paper [640028](#), 1963, doi:[10.4271/640028](#).
7. *1991 Yearbook*, The Tire & Rim Association Inc., Copley, OH, 1991.
8. Bundorf, R.T., "The Influence of Vehicle Design Parameters on Characteristic Speed and Understeer," SAE Technical Paper [670078](#), 1967, doi:[10.4271/670078](#).
9. Bundorf, R.T. and Leffert, R.L., "The Cornering Compliance Concept for Description of Vehicle Directional Control Properties," SAE Technical Paper [760713](#), 1976, doi:[10.4271/760713](#).
10. Ellis, J.R., *Vehicle Dynamics*, London: Business Books Limited, 1969, 243pp.
11. Olley, M., "National Influences on American Passenger Car Design," *Proceedings of the Institution of Automobile Engineers* 32 (1938): 509-572.
12. Proposed Recommended Practice, "Passenger Car and Light Truck Directional Control Response Test Procedures," SAE XJ266, Society of Automotive Engineers, Warrendale, PA.
13. Proposed Recommended Practice, "Steady-State Circular Test Procedure for Trucks and Buses," SAE J2181, Society of Automotive Engineers, Warrendale, PA.
14. International Organization for Standardization, "Road Vehicles - Steady-State Circular Test Procedure," International Standard ISO 4138, 1982, 14pp.



Suspensions

© Shutterstock



3D Rendering of Suspension System

With a background understanding of suspension properties that affect ride and directional response provided in the previous chapters, it is now appropriate to examine the various types of suspensions used on modern passenger cars.

The primary functions of a suspension system are to:

- Provide vertical compliance so the wheels can follow the uneven road, isolating the chassis from road roughness.
- Maintain the wheels in the proper steer and camber attitudes to the road surface.
- React to the control forces produced by the tires—longitudinal forces (acceleration and braking), lateral forces (cornering), and braking and drive torques.
- Resist roll of the chassis.
- Keep the tires in contact with the road with minimal load variations.

The properties of a suspension, important to the dynamics of the vehicle, are primarily seen in the kinematic (motion) behavior and its response to the forces and

moments that it must transmit from the tires to the chassis [1–4]. In addition, other characteristics considered in the design process include cost, weight, package space, manufacturability, and ease of assembly.

Suspensions generally fall into one of two groups — solid axles and independent suspensions. Since the suspensions in one group can function quite different from the other, this chapter is broken down by each group.

Solid Axles

Our discussion of suspensions begins with solid axles. A solid axle is one in which the wheels are mounted at either end of a rigid beam so that any movement of one wheel is transmitted to the opposite wheel [5], causing them to steer and camber together. Solid drive (sometimes called “live”) axles are used on the rear of some SUVs and most trucks, and on the front of many four-wheel-drive trucks. Solid beam axles are commonly used on the front of heavy trucks where high load-carrying capacity is required.

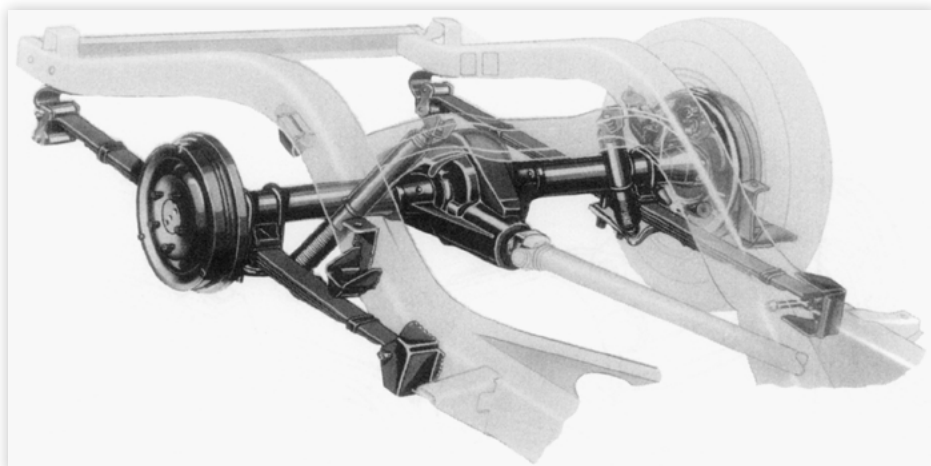
Solid axles have the advantage that wheel camber is not affected by body roll. Thus there is little wheel camber in cornering, except for that which arises from slightly greater compression of the tires on the outside of the turn. In addition, wheel alignment is readily maintained, minimizing tire wear. The major disadvantage of solid steerable axles is their susceptibility to tramp-shimmy steering vibrations.

Hotchkiss

The most familiar form of the solid drive axle is the Hotchkiss drive [5]. The axle is located by semi-elliptic leaf springs as shown in [Figure 7.1](#), and receives its drive torque via a longitudinally mounted driveshaft with universal joints at each end (the forward end connects to the output of the transmission, or possibly a transfer case with four-wheel drive vehicles). The springs, mounted longitudinally, connect to the chassis at their ends with the axle attached near the midpoint.

Leaf springs are perhaps the simplest and least expensive of all suspensions. While compliant in the vertical direction, the leaf is relatively stiff in the lateral and longitudinal

FIGURE 7.1 The Hotchkiss rear suspension. (Photo courtesy of Ford Motor Company.)



directions, thereby reacting the various forces between the sprung and unsprung masses. The Hotchkiss was used widely on the rear axle of passenger cars into the 1960s, and is still used on trucks representing a variety of weight classes, from light to heavy duty. The move away from leaf springs for passenger car applications was due in large part to several factors, namely (1) the inherent friction of the springs (i.e., inter-leaf friction), and (2) the loss in lateral stability of the springs as their lengths were increased to achieve lower spring rates [6]. With softer springs, compliance in the windup direction often required the addition of trailing arms to react brake torques as well as the greater drive torques coincident with high-power engines popular in the post-war decades.

Four Link

In response to the shortcomings of leaf spring suspensions, the four-link rear suspension, shown in [Figure 7.2](#), evolved as the suspension of choice in recent decades for larger passenger cars with solid rear-drive axles. The lower control arms provide longitudinal control of the axle while the upper arms absorb braking/driving torques and lateral forces. Occasionally, the two upper arms will be replaced by a single, triangular arm, but it remains functionally similar to the four-link. The ability to use air or coil springs in lieu of leaf springs provides better ride and NVH characteristics by the elimination of the coulomb friction inherent to stacked leaf springs (i.e., the inter-leaf friction, noted above).

Although more expensive than the leaf spring arrangement, the geometric design properties of the four-link architecture facilitate better control of the roll center location, improved anti-squat and anti-dive characteristics, and more favorable roll steer properties.

De Dion

A cross between the solid axle and an independent suspension is the historically significant but otherwise little-used de Dion system (patented in 1894 by Count de Dion and George Bouton), shown in [Figure 7.3](#). It consists of a cross tube between the two driving wheels with a chassis-mounted differential and half-shafts. As with a solid axle, the de Dion system keeps the wheels upright while the unsprung weight is reduced by virtue of the differential being removed from the axle. Axle control can be provided by a variety

FIGURE 7.2 The four-link rear suspension. (Photo courtesy of Ford Motor Company.)

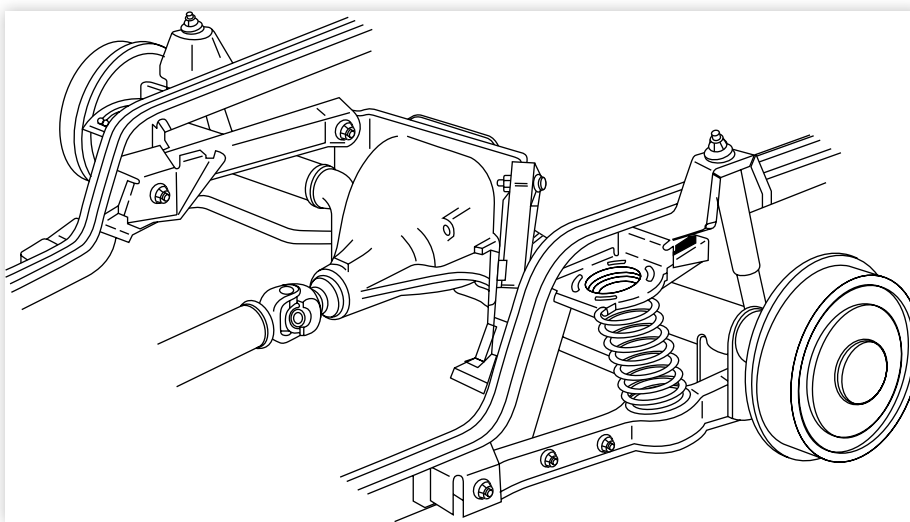
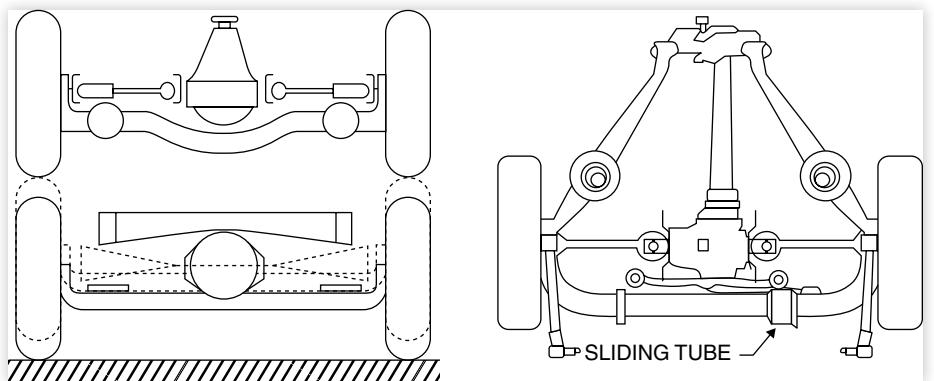


FIGURE 7.3 The de Dion rear suspension.

© SAE International

of linkage arrangements, from leaf springs to trailing arms. Due to the fact that there is no need to provide clearance for a differential housing, space constraints are reduced relative to a driven solid axle. A primary disadvantage is the potential for added friction due to the need for either a sliding tube or splined half-shafts.

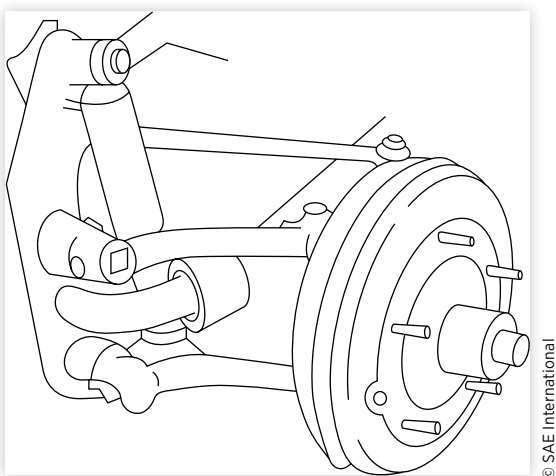
Independent Suspensions

In contrast to the solid axle, independent suspensions allow each wheel at an axle position (i.e., the front or rear) to move in jounce and rebound without directly affecting the wheel on the opposite side. Nearly all passenger cars and light trucks use independent front suspensions for a variety of reasons, not the least of which is providing more room for the engine and therefore allowing it to be placed lower in the chassis. This helps lower the overall C.G. and thus improves the vehicle's dynamics. Relative to solid axles, independent suspensions offer improved resistance to steering vibrations (wobble and shimmy), as well as affording the advantage of having inherently higher.

The first independent suspensions appeared on front axles in the early part of the last century. Maurice Olley [7,8] deserves much of the credit for promoting its virtues, recognizing that by decoupling the wheels and interposing the mass of the car between the two wheels, some of the wobble and shimmy characteristics common to solid axles could be reduced. Further advantages included easy control of the roll center by choice of the geometry of the control arms, the ability to control (track) change with jounce and rebound, larger suspension deflections, and greater roll stiffness for a given suspension vertical rate, as noted above.

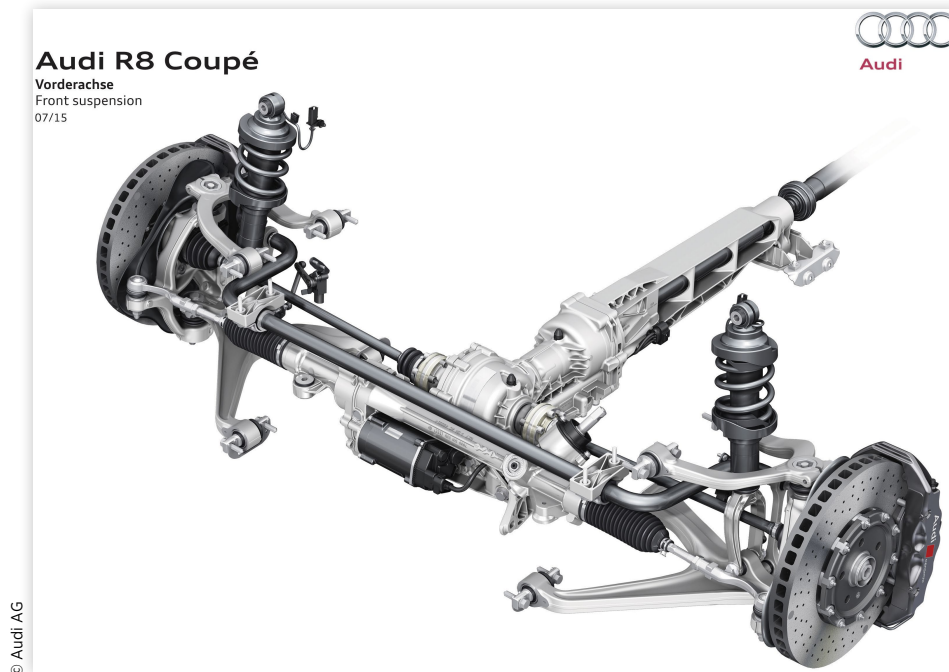
Trailing Arm Suspension

One of the most simple and economical designs of an independent front suspension is the trailing arm used by Volkswagen and Porsche around the time of World War II. This suspension, shown in [Figure 7.4](#), uses parallel, equal length trailing arms which connect to lateral torsion bars at their front ends. These lateral torsion bars provide the spring stiffness. With this design, the wheels remain parallel to the body and camber as the body rolls.

FIGURE 7.4 The trailing arm independent front suspension.

© SAE International

FIGURE 7.5 The A-arm front suspension. (Photo courtesy of Audi.)



SLA Front Suspension

The most common design for the front suspension of American cars following World War II used two lateral control arms to hold the wheel as shown in [Figure 7.5](#). The upper and lower control arms are usually of unequal length from which the acronym SLA (short-long arm) gets its name. The arms are often called “A-arms” in the United States and “wishbones” in Britain. This layout sometimes appears with the upper A-arm replaced by a simple lateral link, or the lower arm replaced by a lateral link and an angled tension strut. Regardless, the suspensions are functionally similar.

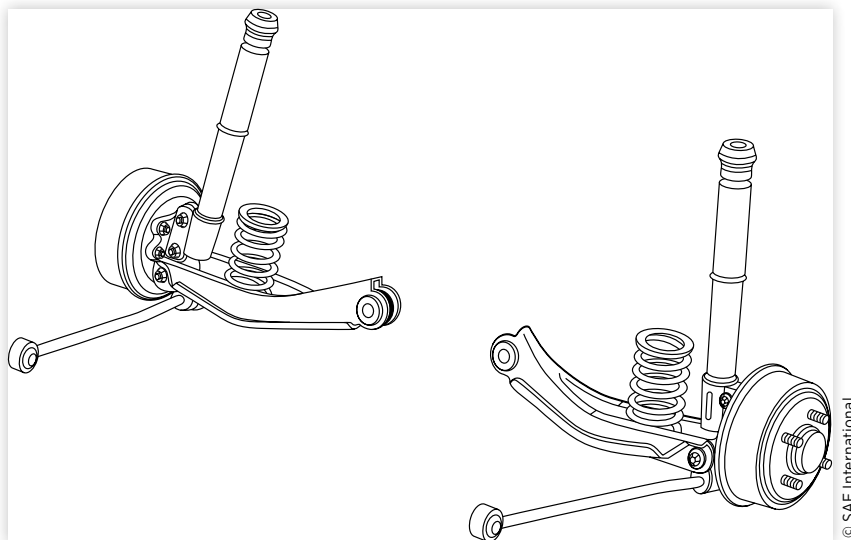
The SLA is well adapted to front-engine, rear-wheel-drive cars because of the package space it provides for the engine oriented in the longitudinal direction. Additionally, it is best suited to vehicles with a sub-frame for mounting the suspension and absorbing the loads.

Design of the geometry for an SLA requires careful refinement to give good performance. The camber geometry of an unequal-arm system can improve camber at the outside wheel by counteracting camber due to body roll, but usually carries with it less-favorable camber at the inside wheel. (Equal-length parallel arms eliminate the unfavorable condition on the inside wheel but at the loss of camber compensation on the outside wheel.) At the same time, the geometry must be selected to minimize track width change in jounce and rebound to avoid excessive tire wear.

MacPherson Strut

Earle S. MacPherson developed a suspension with geometry similar to the unequal length-arm front suspensions by the use of a strut configuration (see [Figure 7.6](#)). The strut is a telescopic member incorporating damping with the wheel rigidly attached at its lower end, such that the strut maintains the wheel in the camber direction. The upper end is fixed to the unibody or chassis, and the lower end is located by linkages which pick up the lateral and longitudinal forces. Due to the need to offset the strut inboard of the wheel, the wheel

FIGURE 7.6 The MacPherson strut suspension. (Photo courtesy of Ford Motor Company.)



© SAE International

loads the strut with an overturning moment which adds friction to the strut itself. This is often counteracted by mounting the coil spring at an angle relative to the strut.

The MacPherson strut provides major advantages in package space for transverse-mounted engines, leading to its widespread use among front-wheel drive cars. Owing to the separation of the connection points on the body, it is well-suited to vehicles with unibody construction. Further advantages a MacPherson Strut arrangement has over an SLA are a lower parts count and the capability to spread the suspension loads to the body structure over a wider area. Disadvantages include the high installed height (i.e., the location of the upper strut mount), which limits the engineer's ability to lower the engine hood height.

Multi-link Rear Suspension

During the mid 1970s, multi-link versions of independent rear suspensions became quite popular (see [Figure 7.7](#)). The multi-link suspension is characterized by ball-joint connections at the ends of the linkages, preventing them from experiencing bending moments. Generally speaking, four links are required to provide longitudinal and lateral control of the wheels while also reacting brake torques. Occasionally five links are used, as in the Mercedes-Benz rear suspensions. The additional link over-constrains the wheel but capitalizes on compliances in the bushings, allowing for more accurate control of the toe angles during cornering maneuvers. Ultimately, the use of linkages affords the engineer greater flexibility to achieve the desired wheel motions.

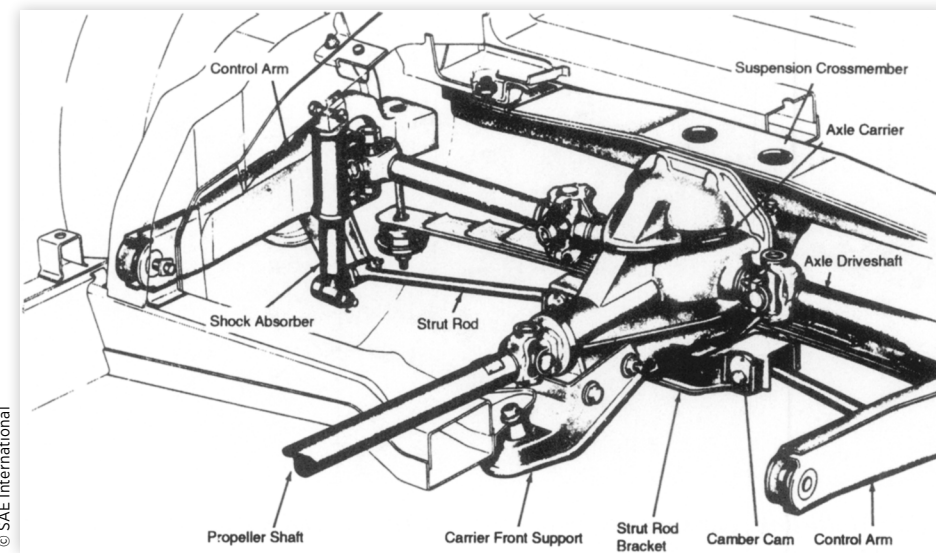
Trailing-Arm Rear Suspension

Suspensions of this type are often used on more expensive and high-performance cars. A popular American car example is the Corvette rear suspension shown in [Figure 7.8](#). The control arms (trailing arms) absorb longitudinal forces and braking moments, and control squat and lift. In the Corvette design the U-jointed half-shafts serve as an upper lateral control arm, while a simple strut rod serves as the lower lateral arm. The independent suspension has the advantage of reducing unsprung weight by mounting the differential to the vehicle body.

FIGURE 7.7 Multi-link rear generic car suspension. (Photo courtesy of Audi.)

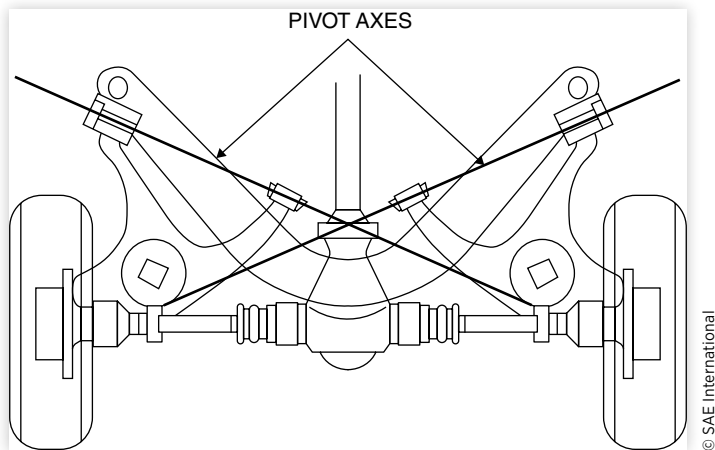


FIGURE 7.8 The Corvette independent rear suspension. (Courtesy of Chevrolet Motor Division.)



Semi-trailing Arm

The semi-trailing arm rear suspension was popularized by BMW and Mercedes-Benz. This design, as shown in [Figure 7.9](#), gives rear wheel camber somewhat between that of a pure trailing arm (no camber change relative to the body) and a swing axle. Its pivot axis is usually about 25 degrees to a line running across the car. The semi-trailing arm produces a steering effect as the wheels move in jounce and rebound. The steer/camber

FIGURE 7.9 The semi-trailing arm rear suspension.

© SAE International

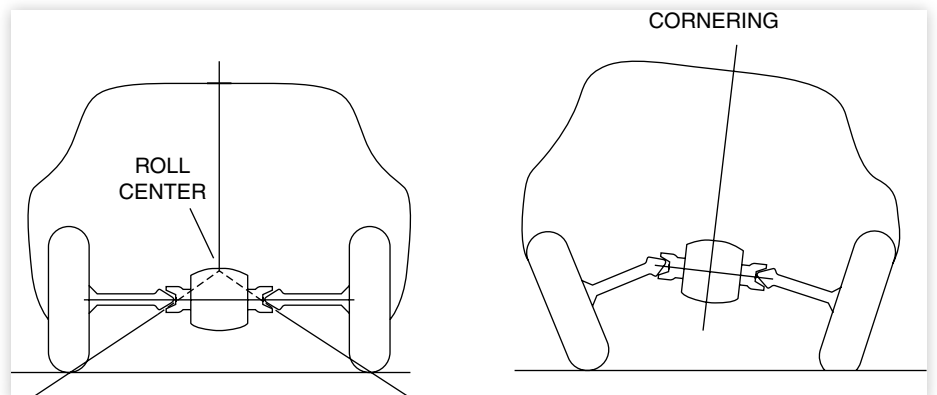
combination on the outside wheel acts against the direction of cornering, thus generating roll understeer on the rear axle. Lateral force compliance steer will contribute oversteer if not controlled.

Swing Axle

The easiest way to achieve an independent rear suspension is by the use of swing axles as shown in [Figure 7.10](#). Edmund Rumpler is credited with inventing this system around the turn of the 20th century, and by 1930 they were used on several European cars, most notably the Volkswagen Beetle.

The camber behavior is established entirely by the axle shafts pivoting at the U-joint adjacent to the differential. The swing radius is small and thus the camber change with jounce and rebound movements can be large. As a result, it is difficult to get consistent cornering performance from swing-axle arrangements.

Critical to any independent suspension, but especially with the swing axle and semi-trailing arm, is a phenomenon known as “jacking.” Jacking occurs during cornering when both tires are developing cornering forces but with the outside (i.e., more heavily loaded tire) contributing the greater cornering force. The inward direction of the cornering force attempts to lift the vehicle such that the wheels “tuck under” the

FIGURE 7.10 The swing-axle rear suspension.

© SAE International

vehicle body. This has the effect of elevating the vehicle body (and therefore reducing its rollover resistance), causing a loss of cornering force on the axle due to camber thrust, and ultimately leading to the possibility that the vehicle will spin out and roll over. Unless an additional control arm is included in the suspension to limit wheel travel under high lateral acceleration conditions, serious directional control problems are likely. This property of swing axle suspensions received much publicity as a result of its use on the Corvair passenger car in the 1960s [9].

Anti-Squat and Anti-Pitch Suspension Geometry

In earlier chapters it was observed that under acceleration the load on the rear wheels increases due to longitudinal weight transfer. The load on the rear axle is:

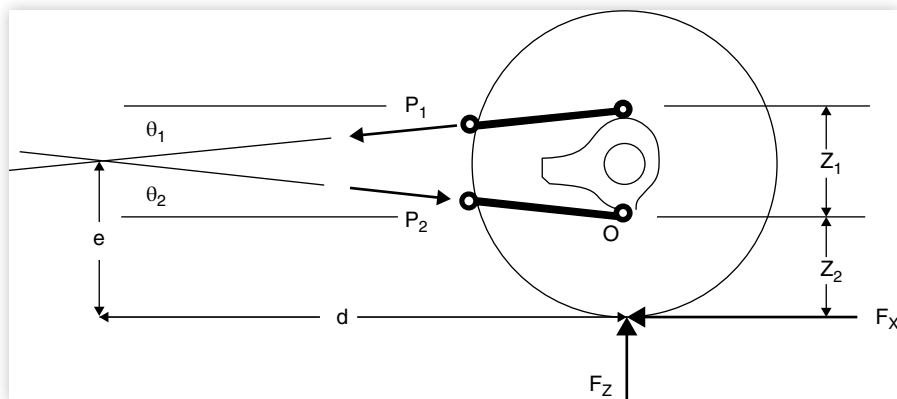
$$W_r = W \left(\frac{b}{L} + \frac{a_x}{g} \frac{h}{L} \right) \quad (7.1)$$

The second term on the right side of this equation is the weight transfer effect. The weight is transferred to the axle and wheels principally through the suspension. Therefore, there is an implied compression in the rear suspension which, in the case of rear-drive vehicles, has been called “Power Squat.” Concurrently, there is an associated rebound in the front suspension. The combination of rear jounce and front rebound deflections result in vehicle pitch. Suspension systems may be designed to counteract the weight transfer and minimize squat and pitch.

Equivalent Trailing Arm Analysis

Anti-squat forces can be generated on a rear-drive axle by the choice of suspension geometry. The mechanics of the system can be understood by recognizing that all suspensions are functionally equivalent to a trailing arm with regard to the reaction of forces and moments onto the vehicle. For analysis purposes consider a drive axle restrained by upper and lower control arms as shown in [Figure 7.11](#). The horizontal drive force at the ground is F_x . The force F_z is the vertical reaction at the ground caused by the vertical

FIGURE 7.11 Forces acting on a drive axle suspension system.



components of the control arm forces. Static vertical loads may be neglected in this analysis. Writing Newton's Second Law for the horizontal and vertical directions and for the moments around the point "o" yields:

$$F_x + P_1 \cos \theta_1 - P_2 \cos \theta_2 = 0 \quad (7.2)$$

$$F_z - P_1 \sin \theta_1 - P_2 \sin \theta_2 = 0 \quad (7.3)$$

$$F_x z_2 - P_1 \cos \theta_1 z_1 = 0 \quad (7.4)$$

From Equation (7.4) we can solve for P_1 :

$$P_1 = \frac{F_x z_2}{z_1 \cos \theta_1} \quad (7.5)$$

Assuming small angles and combining Equations (7.2) and (7.5):

$$P_2 = \frac{F_x (1 + z_2 / z_1)}{\cos \theta_2} \quad (7.6)$$

Then using Equation (7.3) to solve for F_z :

$$F_z = P_1 \sin \theta_1 + P_2 \sin \theta_2 = F_x \frac{z_2}{z_1} \tan \theta_1 + F_x \left(1 + \frac{z_2}{z_1}\right) \tan \theta_2 \quad (7.7)$$

From the geometry it is seen that:

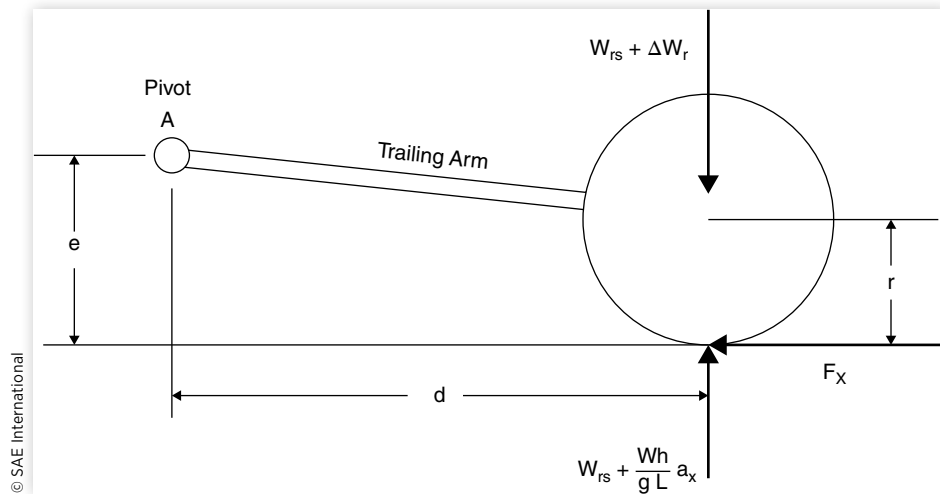
$$\tan \theta_1 = \frac{z_2 + z_1 - e}{d} \quad \text{and} \quad \tan \theta_2 = \frac{e - z_2}{d} \quad (7.8)$$

When this is substituted into Equation (7.7), the ratio of forces is seen to be:

$$\frac{F_z}{F_x} = \frac{e}{d} \quad (7.9)$$

The expression given by Equation (7.9) is identical to that which would be obtained if the control arms were replaced with a single (trailing) arm pivoting on the body at the projected intersection of the control arm axes. The intersection represents a "virtual reaction point" where the torque reaction of the suspension control arms can be resolved into equivalent longitudinal and vertical forces imposed on the vehicle body.

Given that any suspension is functionally equivalent to a trailing arm, the anti-squat performance can be quantified by analyzing the free-body diagram of a rear-drive axle as shown in Figure 7.12. In the figure, point "A" is the imaginary pivot on the vehicle body. Since the arm is rigidly fastened to the axle (resisting axle windup), it has the ability to transmit a vertical force to the sprung mass which can be designed to counteract squat.

FIGURE 7.12 Forces acting on a rear-drive axle during acceleration.

Rear Solid Drive Axle

The system is analyzed by applying Newton's Second Law for the torques around the pivot point "A" (Figure 7.12). The sum of these torques must be zero when the system is in equilibrium. Note that the wheel load is shown as consisting of a static component plus the dynamic component arising from longitudinal load transfer during acceleration. Also, for simplicity in the analysis, the rear axle weight will be neglected. Taking counterclockwise torques to be positive:

$$\sum M_A = W_{rs}d + \frac{W}{g} \frac{h}{L} a_x d - W_{rs}d - \Delta W_r d - F_x e = 0 \quad (7.10)$$

where:

W_{rs} = Static load on the axle = Static load in the suspension

ΔW_r = Change in the suspension load under acceleration

This equation can be solved for the change in rear suspension load.

$$\Delta W_r = \frac{W}{g} \frac{h}{L} a_x - F_x \frac{e}{d} = K_r \delta_r \quad (7.11)$$

where:

K_r = Rear suspension spring rate

δ_r = Rear suspension deflection (positive in jounce)

The front suspension is undergoing a rebound deflection because of the longitudinal load transfer, and has a magnitude of:

$$\Delta W_f = -\frac{W}{g} \frac{h}{L} a_x = K_f \delta_f \quad (7.12)$$

The pitch angle of the vehicle, θ_p , during acceleration is simply the sum of the suspension deflections divided by the wheelbase. Thus we can write:

$$\Theta_p = \frac{\delta_r - \delta_f}{L} = \frac{1}{L} \frac{W}{g} \frac{h}{L} \frac{a_x}{K_r} - \frac{1}{L} \frac{F_x}{K_r} \frac{e}{d} + \frac{1}{L} \frac{W}{g} \frac{h}{L} \frac{a_x}{K_f} \quad (7.13)$$

Since F_x is simply the mass times the acceleration, $(W/g)a_x$, the equation can be rewritten:

$$\begin{aligned}\theta_p &= \frac{1}{L} \frac{W}{g} \frac{h}{L} \frac{a_x}{K_r} - \frac{1}{L} \frac{W}{g} \frac{a_x}{K_r} \frac{e}{d} + \frac{1}{L} \frac{W}{g} \frac{h}{L} \frac{a_x}{K_f} \\ &= \frac{1}{L} \frac{W}{g} a_x \left(\frac{1}{K_r} \frac{h}{L} - \frac{1}{K_r} \frac{e}{d} + \frac{1}{K_f} \frac{h}{L} \right)\end{aligned}\quad (7.14)$$

From this equation, zero pitch angle is achieved when the following condition is satisfied:

$$\frac{e}{d} = \frac{h}{L} + \frac{h}{L} \frac{K_f}{K_r} \quad (7.15)$$

The first term on the right-hand side corresponds to the condition by which anti-squat is achieved on the rear suspension. That is, if $e/d = h/L$, the rear suspension will not deflect (jounce) during acceleration. The degree to which this is achieved is described as the percent anti-squat. For example, if $e/d = 0.5 h/L$, the suspension is said to be 50% anti-squat. Since h/L is in the vicinity of 0.2 for most passenger cars, full anti-squat generally requires an effective trailing arm length of about five times the elevation of “e.”

The anti-squat equation ($e/d = h/L$) defines a locus of points extending from the tire contact point on the ground to the height of the C.G. over the front axle. Locating the trailing arm pivot at any point on this line will provide 100% anti-squat.

Satisfying the equation with inclusion of the second term implies that the rear suspension will lift to compensate for rebound of the front suspension, thereby keeping the vehicle level. The complete equation may be interpreted as the full anti-pitch relationship. Because the ratio of suspension stiffnesses is nominally 1, the anti-pitch condition is approximately:

$$\frac{e}{d} \approx \frac{h}{L} + \frac{h}{L} = 2 \frac{h}{L} \quad (\text{Full anti-pitch}) \quad (7.16)$$

The locus of points for anti-pitch extends from the tire contact point on the ground to the height of the C.G. at the mid-wheelbase position. Anti-pitch is achieved when the trailing arm pivot point is located on the line from the center of tire contact on the ground to the C.G. of the vehicle.

Normally some degree of squat and pitch is expected during vehicle acceleration, so full compensation is unusual. Anti-squat performance cannot be designed without considering other performance modes of the vehicle as well. When the trailing arm is short, the rear axle may experience “power hop” during acceleration near the traction limit. The goals for anti-squat may conflict with those for braking or handling. In this latter case, placing the pivot center above the wheel center can produce roll oversteer.

Independent Rear Drive

In the case of an independent rear-drive configuration, the free-body diagram and the analysis is changed slightly from that above. The difference arises from the fact that there

is a drive torque reaction acting on the free-body system with a magnitude $T_d = r F_x$ (where r is the wheel radius). The differential is mounted on the vehicle body and imposes a drive torque on the system through the half-shafts, as shown in [Figure 7.12](#). This alters [Equation \(7.10\)](#) to the form:

$$\Sigma M_A = W_{rs}d + \frac{W}{L} \frac{h}{g} a_x d - W_{rs}d - \Delta W_r d - F_x(e - r) = 0 \quad (7.17)$$

Carrying this through the analysis alters [Equation \(7.14\)](#) to the form:

$$\theta_p = \frac{1}{L} \frac{W}{g} a_x \left(\frac{1}{K_r} \frac{h}{L} - \frac{1}{K_r} \frac{e-r}{d} + \frac{1}{K_f} \frac{h}{L} \right) \quad (7.18)$$

and it is concluded that full squat compensation is achieved when:

$$\frac{e-r}{d} = \frac{h}{L} + \frac{h}{L} \frac{K_r}{K_f} \quad (7.19)$$

Similarly, 100% anti-squat in the rear suspension corresponds to $(e - r)/d = h/L$.

Front Solid Drive Axle

With a front-drive axle, performing this type of analysis only results in a change of sign on some of the terms in [Equations \(7.14\)](#) and [\(7.15\)](#). The comparable equations obtained are:

$$\theta_p = \frac{1}{L} \frac{W}{g} a_x \left(\frac{1}{K_r} \frac{h}{L} + \frac{1}{K_f} \frac{h}{L} + \frac{1}{K_f} \frac{e}{d} \right) \quad (7.20)$$

and

$$\frac{e}{d} = -\frac{h}{L} - \frac{h}{L} \frac{K_f}{K_r} \quad (7.21)$$

The first term on the right side of [Equation \(7.21\)](#) now corresponds to an anti-lift on the front axle, rather than an anti-squat on the rear axle. The negative signs on the right-hand side of the equation imply that the pivot must be behind the axle, corresponding to an effective leading arm arrangement to obtain the anti-lift behavior.

Independent Front-Drive Axle

The comparable equations for an independent front-drive axle, as is common on most front-drive cars today, are:

$$\theta_p = \frac{1}{L} \frac{W}{g} a_x \left(\frac{1}{K_r} \frac{h}{L} + \frac{1}{K_f} \frac{h}{L} + \frac{1}{K_f} \frac{e-r}{d} \right) \quad (7.22)$$

and

$$\frac{e-r}{d} = -\frac{h}{L} - \frac{h}{L} \frac{K_f}{K_r} \quad (7.23)$$

Four-Wheel Drive

The four-wheel-drive case will be considered assuming independent suspensions on both axles, with the performance depending on how the tractive force is distributed between them. Let ξ represent the fraction of the total drive force developed on the front axle. Then:

$$F_{xf} = \xi F_x \quad \text{and} \quad F_{xr} = (1 - \xi) F_x \quad (7.24)$$

The expressions for the change in load on each axle are:

$$\Delta W_r = \frac{W}{g} \frac{h}{L} a_x - (1 - \xi) F_x \frac{e_r - r}{d_r} = K_r \delta_r \quad (7.25)$$

$$\Delta W_f = \frac{W}{g} \frac{h}{L} a_x + \xi F_x \frac{e_f - r}{d_f} = K_f \delta_f \quad (7.26)$$

Then, using $\theta_p = \frac{\delta_r - \delta_f}{L}$, the pitch equation becomes:

$$\theta_p = \frac{1}{L} \frac{W}{g} a_x \left(\frac{1}{K_r} \frac{h}{L} - \frac{(1 - \xi)}{K_r} \frac{e_r - r}{d_r} + \frac{1}{K_f} \frac{h}{L} + \frac{\xi}{K_f} \frac{e_f - r}{d_f} \right) \quad (7.27)$$

This equation indicates that zero pitch will be obtained when the terms in parentheses sum to zero. The terms included here indicate that the anti-squat and anti-pitch performance depends on a combination of vehicle properties—suspension geometry, suspension stiffness, and tractive force distribution.

In the event one or both of the axles is a solid axle, the pitch expression can be obtained from the above equation by setting “r” equal to zero in the term of the equation applicable to that axle.

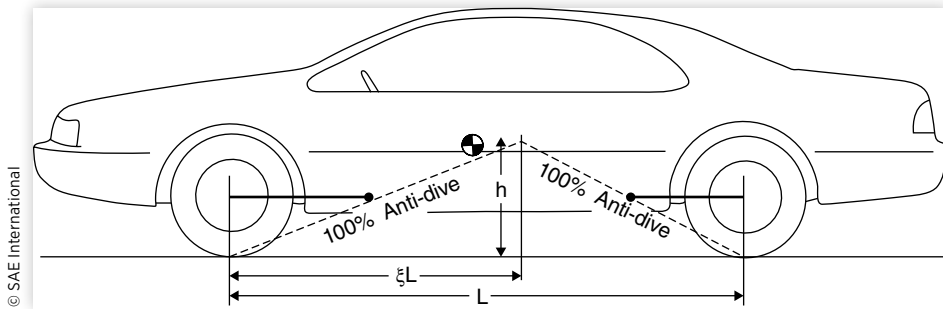
Anti-Dive Suspension Geometry

The longitudinal load transfer incidental to braking acts to pitch the vehicle forward producing “brake dive.” Just as a suspension can be designed to resist acceleration squat, the same principles apply to generation of anti-dive forces during braking. Because virtually all brakes are mounted on the suspended wheel (the only exception is in-board brakes on independent suspensions), the brake torque acts on the suspension and by proper design can create forces which resist dive.

Using an analysis similar to that developed for the four-wheel-drive anti-squat example given previously, it can be shown that the anti-dive is accomplished when the following relationships hold:

Front suspension:

$$\frac{e_f}{d_f} = \tan \beta_f = -\frac{h}{\xi L} \quad (7.28)$$

FIGURE 7.13 Illustration of the conditions for anti-dive.

Rear suspension:

$$\frac{e_r}{d_r} = \tan \beta_r = \frac{h}{(1-\xi)L} \quad (7.29)$$

where:

ξ = Fraction of the brake force developed on the front axle.

Therefore, to obtain 100% anti-dive on the front and 100% anti-lift on the rear, the pivot for the effective trailing arm must fall on the locus of points defined by these ratios. **Figure 7.13** illustrates these conditions. If the pivots are located below the locus, less than 100% anti-dive will be obtained; if above the locus, the front will lift and the rear will squat during braking.

In practice, 100% anti-dive is rarely used. The maximum anti-dive seldom exceeds 50%. A number of reasons for this have been cited:

1. Full anti-dive requires that the pivot be located above the point required for full anti-squat. Thus acceleration lift would be produced on solid drive axles.
2. Flat stops are subjectively undesirable.
3. With full anti-dive, front suspension caster angle changes may increase the steering effort substantially during braking.
4. The required steering system geometry may be quite complex.
5. Excessive variation in rotational speed can occur in the drivetrain as the wheels move in jounce and rebound, causing rattling and noise in the drive gears.
6. In the rear suspension, oversteer problems may be created by the high location of the pivot.
7. Brake hop may be induced if the effective trailing arm is too short. The propensity for brake hop is reduced by a suspension design with a long effective arm.
8. NVH performance may be compromised.

Examples

1. Find the geometry that would be necessary to achieve 100% anti-squat in the rear suspension, and the geometry to achieve full anti-pitch for the solid-axle, rear-wheel-drive vehicle described below. Also, find the pitch rate (degrees pitch/g acceleration) when the geometry is set for 100% anti-squat in the rear suspension.

The front and rear suspension spring rates are 285 and 169 lb/in, respectively (rates are a combination of the left and right sides of each suspension). The C.G. height is 20.5 in and the wheelbase is 108.5 in.

Solution:

Since the vehicle has a rear-drive solid axle, [Equation \(7.15\)](#) applies.

$$\frac{e}{d} = \frac{h}{L} + \frac{h K_r}{L K_f} \quad (7.15)$$

$$\frac{e}{d} = \frac{20.5}{108.5} + \frac{20.5}{108.5} \frac{169}{285} = 0.189 + 0.112 = 0.301$$

If the suspension is to achieve 100% anti-squat, then e/d must equal 0.189. Full pitch compensation would be achieved with $e/d = 0.301$.

The acceleration pitch rate can be calculated using [Equation \(7.18\)](#).

$$\begin{aligned}\theta_p &= \frac{1}{L} \frac{W}{g} a_x \left(\frac{1}{K_r} \frac{h}{L} - \frac{1}{K_r} \frac{e}{d} + \frac{1}{K_f} \frac{h}{L} \right) \\ \frac{\theta_p}{a_x} &= \frac{1}{108.5 \text{ in}} \frac{4074 \text{ lb}}{386 \text{ in/sec}^2} \left(\frac{1}{169 \text{ lb/in}} \frac{20.5}{108.5} - \frac{0.189}{169 \text{ lb/in}} + \frac{1}{285 \text{ lb/in}} \frac{20.5}{108.5} \right) \\ &= 0.0000645 \text{ rad/(in/sec}^2\text{)} = 0.0249 \text{ rad/g} = 1.43 \text{ deg/g}\end{aligned}$$

2. Determine the acceleration pitch rate for the following front-drive vehicle with no anti-lift in the front suspension, and its value if full anti-lift was designed into the suspension. Essential data are—C.G. height of 20.5 in, wheelbase of 108.5 in, a design weight of 4549 lb, and front and rear spring rates of 287 and 174 lb/in, respectively.

Solution:

The pitch equation for a front-wheel drive vehicle comes from [Equation \(7.22\)](#). With no anti-lift the third term on the right side is zero. Thus:

$$\begin{aligned}\frac{\theta_p}{a_x} &= \frac{1}{L} \frac{W}{g} \left(\frac{1}{K_r} \frac{h}{L} + \frac{1}{K_f} \frac{h}{L} \right) \\ &= \frac{1}{108.5 \text{ in}} \frac{4549 \text{ lb}}{386 \text{ in/sec}^2} \left(\frac{1}{174 \text{ lb/in}} \frac{20.5 \text{ in}}{108.5 \text{ in}} + \frac{1}{287 \text{ lb/in}} \frac{20.5 \text{ in}}{108.5 \text{ in}} \right) \\ &= 0.0455 + 0.0276 \text{ rad/g} = 4.2 \text{ deg/g}\end{aligned}$$

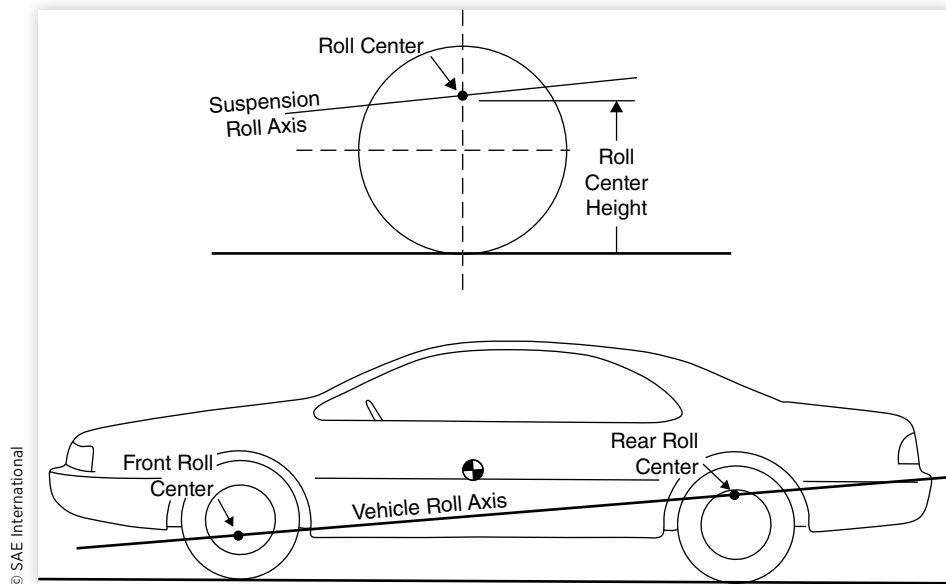
If anti-lift is designed into the suspension it would cancel the second term in this equation, in which case the acceleration pitch rate would be:

$$\frac{\theta_p}{a_x} = 0.0455 \text{ rad/g} = 2.61 \text{ deg/g}$$

Roll Center Analysis

One very important property of a suspension relates to the location at which lateral forces developed by the wheels are transmitted to the sprung mass. This point, which has been referred to as the roll center, affects the behavior of both the sprung and unsprung masses, and thus directly influences cornering.

FIGURE 7.14 Definitions of suspension roll center and roll axis.



© SAE International

Each suspension has a suspension roll center, defined as the point in the transverse vertical plane through the wheel centers at which lateral forces may be applied to the sprung mass without producing suspension roll [10]. It derives from the fact that all suspensions possess a roll axis, which is the instantaneous axis about which the unsprung mass rotates with respect to the sprung mass when a pure couple is applied to the unsprung mass. The roll center is the intersection of the suspension roll axis with the vertical plane through the centers of the two wheels. These definitions are illustrated in **Figure 7.14**. The roll center height is the distance from the ground to the roll center. Once the front and rear suspension roll centers are located, the vehicle roll axis is defined by the line connecting the centers. This axis is the instantaneous axis about which the total vehicle rolls with respect to the ground.

The reference to “instantaneous” axes in these definitions is used to alert the reader to the fact that the location of the axis is only accurate in the absence of roll. As body roll occurs, the change in geometry of most suspensions will cause the roll center to migrate, and thus it is not a true center. Nevertheless, the concept is valid for purposes of establishing where the forces are reacted on the sprung mass, which is necessary for analyzing behavior in the lateral plane.

Solid Axle Roll Centers

The suspension roll axis and roll center can be determined from the layouts of the suspension geometry in the plan and side elevation views. For the analysis, we draw again on the concept of a “virtual reaction point.” (The virtual reaction point is analogous to the “instant center” used in kinematic analysis of linkages, but that term is not used here because of the implication that it defines a center of motion, when in fact this is not the case). Physically, the virtual reaction point is the intersection of the axes of any pair of suspension control arms. Mechanistically, it is the point where the compression/tension forces in the control arms can be resolved into a single lateral force.

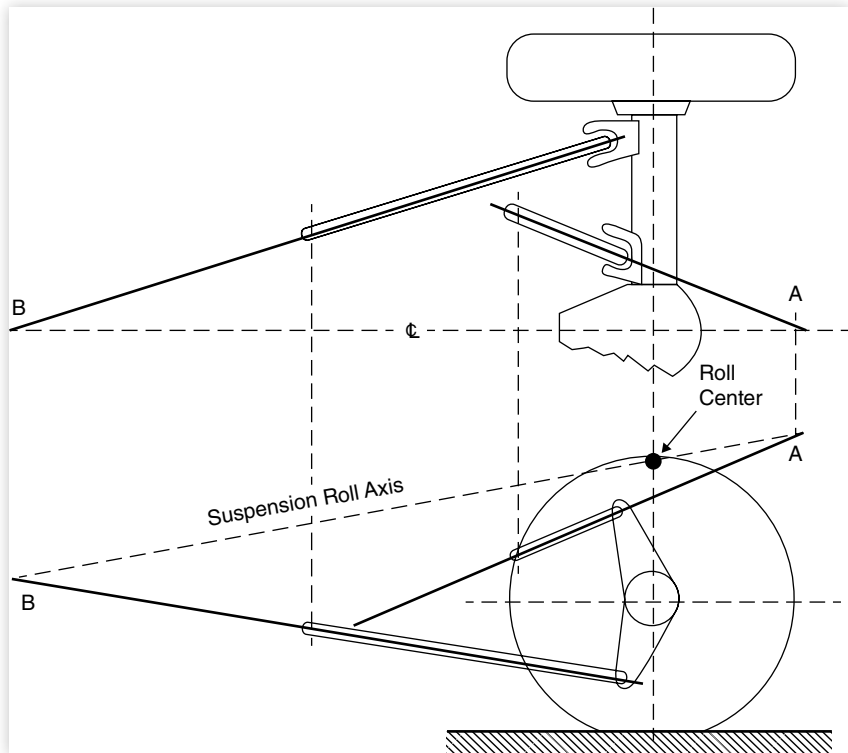
Four-Link Rear Suspension: Consider the case of a four-link suspension with a solid axle, as shown in [Figure 7.15](#). The lateral force acting on the wheel in the top view must react as tension and compression forces in the control arms. The two long arms establish a virtual reaction point ahead of the axle at point B, while the two short arms have a virtual reaction point behind the axle at point A. In effect, each pair of arms acts like a triangular member pivoting at their respective virtual reaction points, with these points establishing the suspension roll axis. Consequently, the lateral force will be distributed between the two points in inverse proportion to the length of the arms in order to achieve moment equilibrium on the axle (i.e., a large force at point A and a small force at point B).

The two forces at points A and B must add up to F_y acting in the transverse vertical plane through the wheel centers. Given that points A and B are at different heights above the ground, their resultant at the axle centerline must be on the line connecting the two. This is the roll center for the axle.

A general procedure for finding roll centers is as follows:

1. In a plan view of the suspension, find the linkages that take the side forces acting on the suspension. Determine the reaction points A and B on the centerline of the vehicle for forces in the links. In the case of paired control arms, this is a virtual reaction point.
2. Locate the points A and B in the side elevation view, thereby identifying the suspension roll axis.
3. The roll center is the point in the side view where the roll axis crosses the vertical centerline of the wheels.

FIGURE 7.15 Roll center analysis of a four-link rear suspension.



In the four-link geometry, the change in slope of the roll axis during cornering is often relatively large compared to other live axles. This means considerable change in roll steer and lateral load transfer, both of which are undesirable effects. Also, the roll center is located relatively high compared to other suspensions, putting excessive roll moment on the rear wheels. On the other hand, the high roll center helps to reduce the tramp and shake of the axle.

Three-Link Rear Suspension: [Figure 7.16](#) shows a three-link suspension consisting of a track bar and two lower control arms. Because the track bar picks up lateral force directly, point A is established at the location where the track bar crosses the centerline of the vehicle. Point B is established as the virtual reaction point for the two lower control arms. Note that the upper link which reacts the axle windup torque does not react lateral forces and is therefore ignored in the analysis.

Due to the location of the track bar, this suspension usually has a roll center that is lower than the four-link geometry. Also, the slope of the roll axis remains relatively unchanged during rolling of the body and with load variations.

Four-Link with Parallel Arms: [Figure 7.17](#) shows a four-link rear suspension with lower control arms that are parallel. This geometry is a special case of the four-link suspension discussed previously. In the top view, the virtual reaction point of the upper links is used to find point A in the usual manner. Because the lower arms are

FIGURE 7.16 Roll center analysis of a three-link rear suspension.

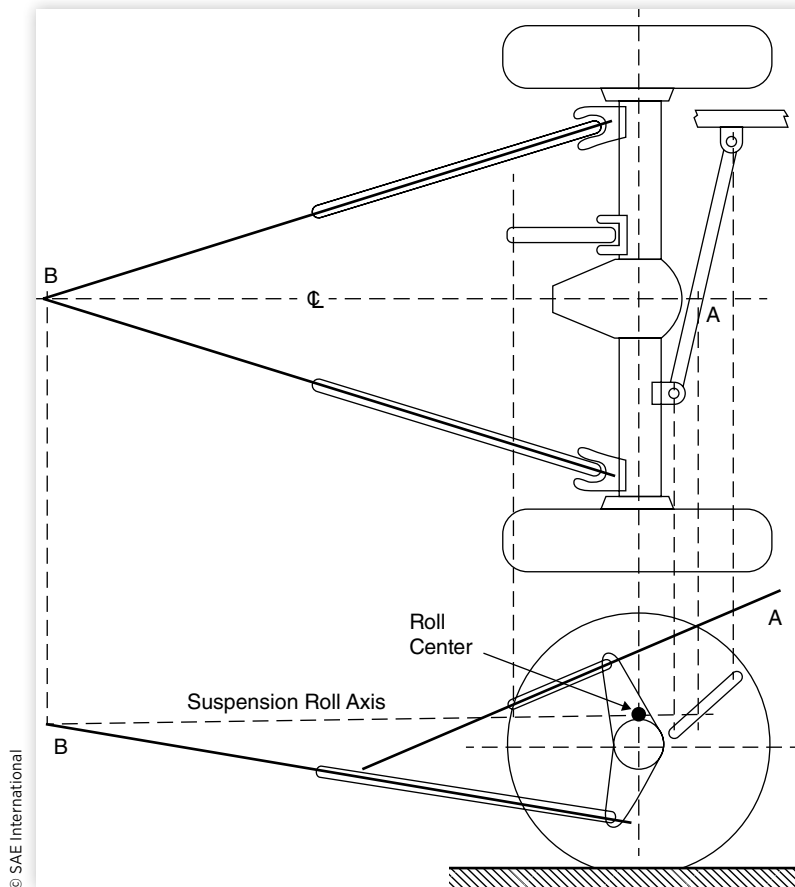
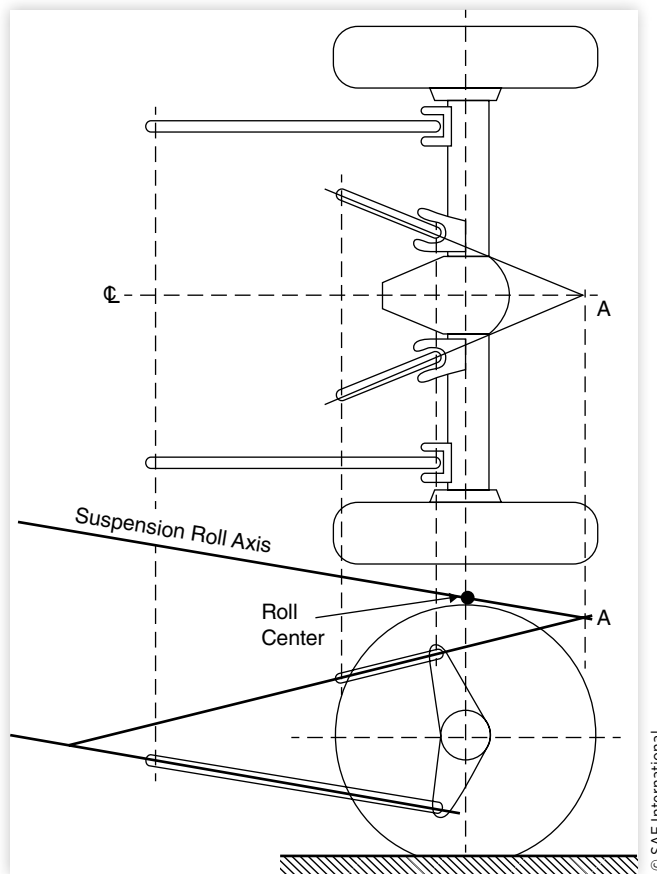
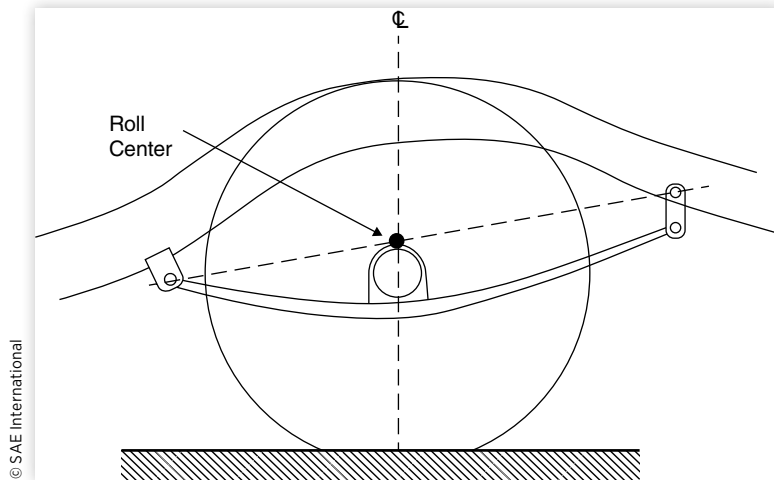


FIGURE 7.17 Roll center analysis of a four-link, parallel lower arm rear suspension.

parallel, their virtual reaction point is at infinity. Although point B is not defined, we know that this point in the side view must lie on the extended lower arm centerline somewhere at infinity. Therefore, the roll axis of this geometry (obtained by connecting points A and B in the side view) must be a line parallel to the lower links as indicated in the figure. The slope of the lower arm is therefore very important in this type of suspension.

Hotchkiss Suspension: The design of this suspension is quite different from those discussed previously, but the general rules for determining the roll axis and roll center still apply. Referring to [Figure 7.18](#), it is seen that the leaf springs are the members that react the side thrust. Because they are parallel to the centerline of the vehicle in the top view, points A and B lie on the centerline of the vehicle, both at infinity.

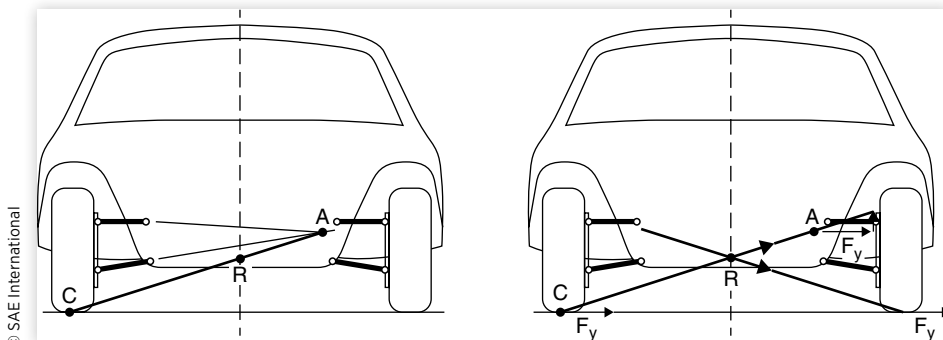
The lateral forces are applied to the body at the front spring eye and the rear shackle attachment point on the frame. The roll axis of the suspension is established by these points and the roll center is found on the line connecting the points. Although this analysis may seem less obvious than those discussed previously, it should be clear that a side force applied at this point will not roll the body, which is the essential definition of the roll center. Experimental measurements of leaf spring suspensions have generally confirmed the validity of this method in establishing the roll center.

FIGURE 7.18 Roll center analysis of a Hotchkiss rear suspension.

Independent Suspension Roll Centers

Determining the roll center of an independent suspension requires a slightly different application of the virtual reaction point concept. Consider the double A-arm suspension shown in [Figure 7.19](#). The virtual reaction point for the A-arms holding the left wheel is located at point A on the right side of the vehicle. Mechanistically, the linkage behaves as if the wheel was held by a rigid side lateral swing arm pinned to the vehicle body at that point. Understanding this behavior is aided by imagining that the swing arm directly connects the tire contact patch (point C) to the pivot point.

A lateral force in the contact patch of the left wheel reacts along the line from the contact patch to the pivot point as illustrated in the left diagram in the figure. Its elevation where it crosses the center plane of the vehicle establishes the roll center, point R. Note that a lateral force from the left-side wheel reacting along that line must have an upward (vertical) force component, thus explaining the source of “jacking” forces inherent to independent suspensions. If the right-hand wheel experiences a lateral force of equal magnitude in the same direction, its reaction will involve a downward force component cancelling the lifting effect from the left wheel. In general, both wheels do not generate equal lateral forces in cornering, so some lifting force is usually present on the suspension.

FIGURE 7.19 Roll center analysis of an independent suspension.

The procedure for finding the roll center of a symmetric independent suspension is as follows:

1. Find the virtual reaction point of the suspension links (point A).
2. Draw a line from the tire-ground contact patch to the virtual reaction point.
3. The point where this line crosses the centerline of the body is the roll center (point R).

Note that this procedure can be used for determining the roll center when the body is rolled; however, the suspensions are no longer symmetrical so both sets must be analyzed.

Positive Swing Arm Geometry: The virtual reaction point of the upper and lower links is first obtained as shown in [Figure 7.20](#). A line is drawn from the tire contact patch to the reaction point. The roll center is established where the line crosses the centerline of the vehicle. This suspension geometry is referred to as the “positive swing arm” because the roll center is located above the ground.

As the vehicle rolls in cornering, the virtual reaction point of the outside wheel moves downward due to jounce of the wheel, while that of the inside wheel moves upward as it goes into rebound. With the loss of symmetry the roll centers for the two wheels no longer coincide. The lateral force from the outside wheel (which usually dominates cornering forces) moves downward on the body, while weaker forces from the inside wheel moves upward. As a consequence, the resultant lateral force reaction on the body moves downward, lowering the effective roll center height.

Negative Swing Arm Geometry: Negative swing arm geometry is shown in [Figure 7.21](#). The virtual reaction point of the links is first obtained and connected to the tire contact patch as shown. The line is then projected downward to the vehicle centerline below the ground. The roll center height is negative; hence, the name “negative swing arm” geometry.

Note that the two independent suspension geometries discussed so far have roll centers either above or below the ground. Consequently, the track width will change

FIGURE 7.20 Positive swing arm independent suspension.

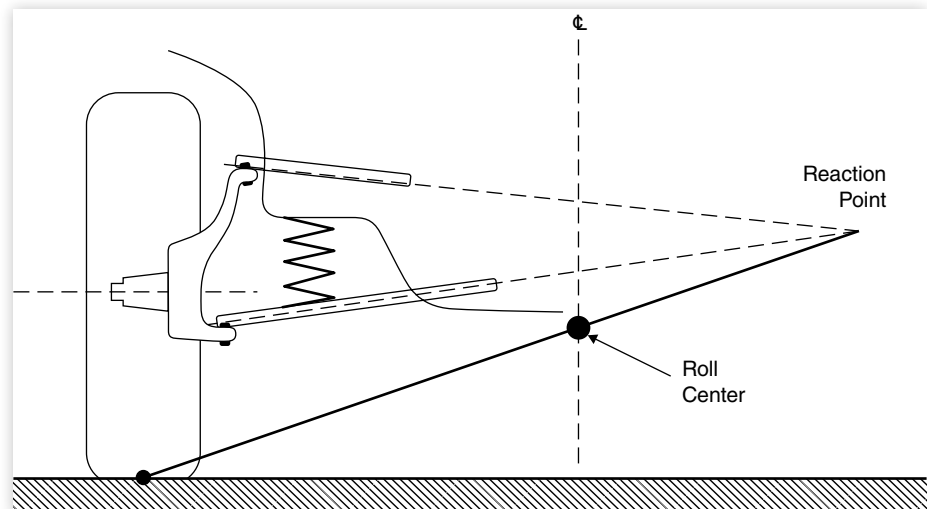
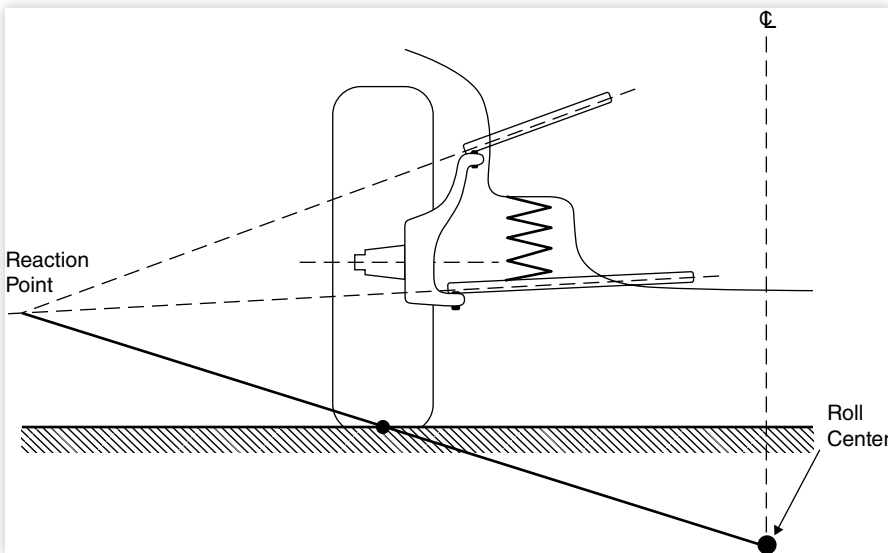


FIGURE 7.21 Negative swing arm independent suspension.

© SAE International



during jounce and rebound. Some lateral scrub of the tire contact patch also occurs. This scrub introduces friction which (in the past) was considered beneficial for reducing the bouncing of the body, but came at the expense of tire wear.

Parallel Horizontal Links: A suspension with parallel links that are horizontal (at design load) is shown in [Figure 7.22](#). The virtual reaction point of the two links is therefore at infinity. Drawing a line from the tire contact patch toward infinity places the roll center in the ground plane.

Inclined Parallel Links: Another possibility is the use of parallel links, which are not horizontal at design load as shown in [Figure 7.23](#). The virtual reaction point is at infinity. The line from the tire contact patch to the roll center is inclined at the

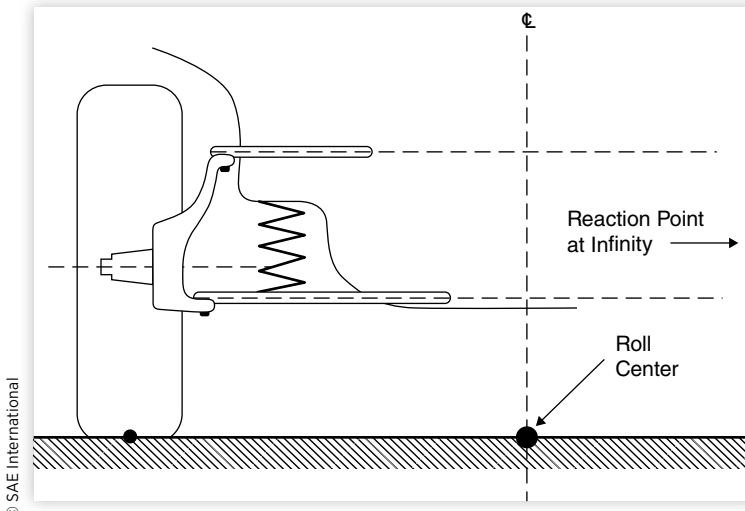
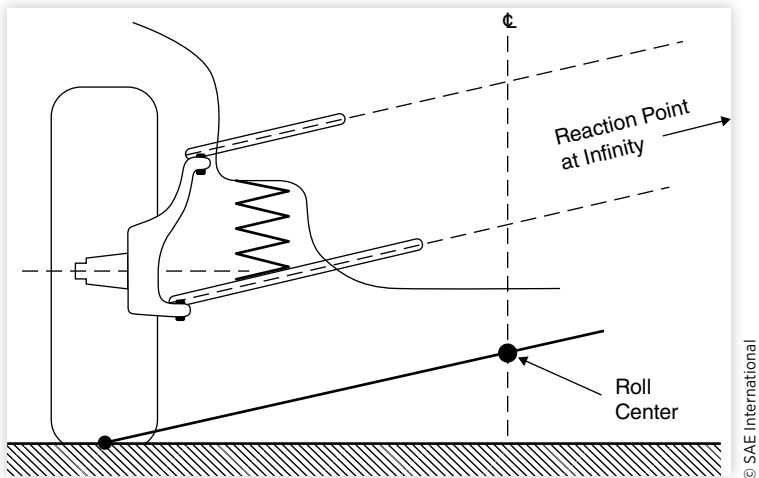
FIGURE 7.22 Parallel horizontal link independent suspension.

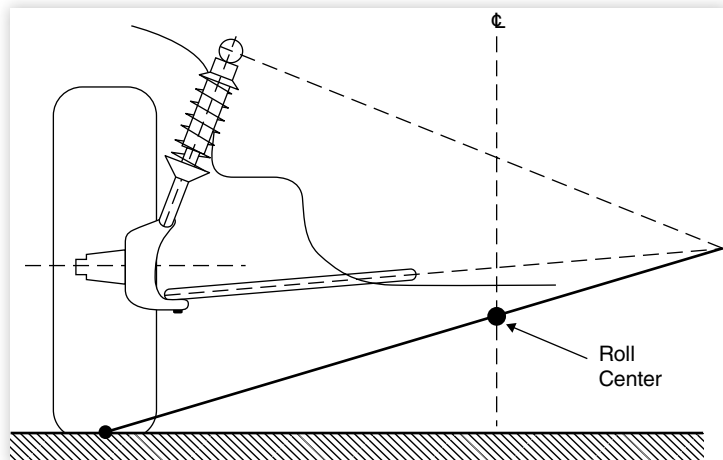
FIGURE 7.23 Inclined parallel link independent suspension.

© SAE International

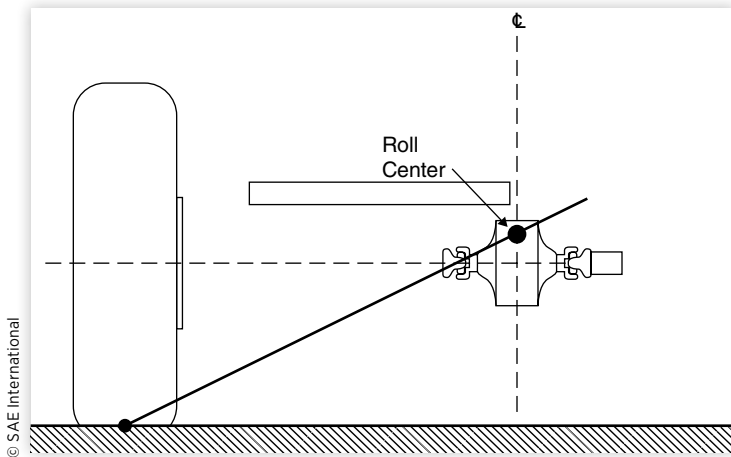
same angle as the control arms. The roll center is elevated above the ground at the vehicle centerline as shown. In this geometry, the roll center moves along the centerline of the vehicle as it rolls because the wheels camber with respect to the body. If the links of the suspension are equal, there will be no camber change with respect to the body and the roll center will remain stationary.

With all of the swing arm geometries the jounce of the outside wheel in cornering lowers the roll center location for that wheel and, consequently, the point at which the lateral force from the wheel is applied to the sprung mass. This reduces the load transfer onto the outside wheel and, with the consequent reduction of cornering force of the wheel, induces an understeer influence on the vehicle.

MacPherson Strut: The MacPherson strut is a combination of a strut with a lower control arm as shown in [Figure 7.24](#). The virtual reaction point must lie at the intersection of the axis of the lower control arm and a line perpendicular to the strut. The roll

FIGURE 7.24 MacPherson strut independent suspension.

© SAE International

FIGURE 7.25 Swing axle independent suspension.

center is located on the centerline of the vehicle at the intersection with the line from the center of tire contact to the virtual reaction point.

Swing Axle: A rear suspension swing axle is generically equivalent to that shown in [Figure 7.25](#). The location of the roll center is easily obtained for this configuration because the virtual reaction point is the actual pivot of the axle. The line from the tire contact passes through the pivot and the roll center is located above the wheel center on the vehicle centerline.

Active Suspensions

In the interest of improving the overall performance of vehicles in recent years, suspensions incorporating active components have been developed. The designs may cover a spectrum of performance capabilities [11], but the active components alter only the vertical force reactions of the suspensions, not the kinematics. Active components that alter suspension kinematic behavior effect the road wheel steer angles and would therefore be covered under steering systems.

Suspension Categories

The various levels of “active” qualities in suspensions may be divided into the categories shown below, listed in order of increasing capabilities.

Passive suspensions consist of components with spring and damping (shock absorber) properties which are time-invariant. Passive elements can only store energy for some portion of a suspension cycle (springs) or dissipate energy (shock absorbers). No external energy is directly supplied to this type of suspension.

Self-leveling suspensions are a variation of the passive suspension in which the primary lift component (usually air springs) can adjust for changes in load. Air suspensions, which are self-leveling, are used on many heavy trucks and on a

few luxury passenger cars. A height control valve monitors the suspension deflection, and when its mean position has varied from normal ride height for a designated period of time (typically more than 5 seconds), the air pressure in the spring is adjusted to bring the deflection within the desired range. The most notable feature of an air suspension is that as the pressure changes with load, the spring stiffness experiences a corresponding change; as a result, the natural frequency of the suspension remains constant.

Semi-active suspensions contain spring and damping elements, the properties of which can be changed by an external control. A signal or external power is supplied to these systems for purposes of changing the properties. There are several sub-categories of semi-active systems:

- Slow-active—Suspension damping and/or spring rate can be switched between several discrete levels in response to changes in driving conditions. Brake pressure, steering angle, or suspension motions are typically used to trigger control changes to higher levels of damping or stiffness. Switching occurs within a fraction of a second giving the system the capability to control pitch, bounce, and roll motions of the sprung mass under more severe road or maneuvering conditions. However, the switch back to softer settings occurs after a time delay. Thus the system does not adjust continuously during individual cycles of vehicle oscillation. Slow-active systems may also be called “adaptive” suspensions.
- Low-bandwidth—Spring rate and/or damping are modulated continuously in response to the low-frequency sprung mass motions (1-3 Hz).
- High-bandwidth—Spring rate and/or damping are modulated continuously in response to both the low-frequency sprung mass motions (1-3 Hz) and the high-frequency axle motions (10-15 Hz).

Full-Active suspensions incorporate actuators to generate the desired forces in the suspension. The actuators are normally hydraulic cylinders and external power is required to operate the system. Full active systems may be classified as low-bandwidth or high-bandwidth according to the definitions given above.

Functions

The interest in active or semi-active suspensions derives from the potential for improvements to vehicle ride performance with no compromise (and perhaps enhancement) in handling. The modes of performance that can be improved by active control are:

Ride Control—Ride improvements can be obtained by several methods. The system may sense and control pitch and bounce motions of the vehicle body directly. Ride improvements are also obtained indirectly when active control is applied to the modes described below. Suspension properties that optimize ride always degrade performance in other modes, thus necessitating a compromise in design. With active suspensions, however, the control can be applied only during the maneuver, and ride performance need not be compromised during other modes of travel. Specifically, the suspension can be tuned for optimal ride performance during steady, straight-ahead travel, and ride isolation properties superior to that obtained with purely passive elements can be achieved without compromise of handling behavior.

Height Control—Automatic control of vehicle height offers several advantages in performance. By adjusting to keep height constant despite changes in load or aerodynamic forces, the suspension can always operate at the design ride height, providing maximum stroke for negotiating bumps, and eliminating changes in handling that

would arise from operation at a position other than the design ride height. A height control can lower the vehicle for reduced drag at high speeds or alter the pitch attitude to modify aerodynamic lift. Height can be elevated for increased ground clearance and suspension stroke on bad roads. Height control can also be convenient for changing tires and to provide clearance for tire chains.

Roll Control—Roll control in cornering is improved by increasing damping or exerting anti-roll forces in the suspension during cornering. Vehicle speed, steer angle, steer rate and/or lateral acceleration may be sensed to determine when roll control is appropriate. With the use of active force-generating components, it is possible to eliminate roll in cornering entirely, and thereby eliminate any roll-induced understeer or oversteer effects from the suspension. In addition, the roll moments may be selectively applied at either the front or rear axles to alter the understeer gradient by action of the change in cornering stiffness due to lateral load transfer.

Dive Control—Control of dive (forward pitch) during braking can be improved by increasing damping or exerting anti-pitch forces in the suspension during braking. Control may be activated by the brake light signal, brake pressure, and/or longitudinal acceleration. Dive control in an active suspension relieves the need to design anti-dive geometry into the suspension linkages.

Squat Control—Control of squat (rearward pitch) during acceleration can be improved by increasing damping or exerting anti-pitch forces in the suspension during acceleration. Control may be activated by the throttle position, gear selection, and/or longitudinal acceleration. Squat control in an active suspension relieves the need to design anti-squat geometry into the suspension linkages of the driven wheels, and can overcome the squat or lift action on the non-driven wheels.

Road Holding—In addition to control of body motions during maneuvers in the modes described above, active suspensions have the potential to improve road holding by reducing the dynamic variations in wheel loads that are caused from road roughness. Generally, cornering performance is improved when dynamic load variations are minimized. The road damage caused by motor vehicles, particularly heavy trucks, is also reduced by minimizing dynamic wheel loads.

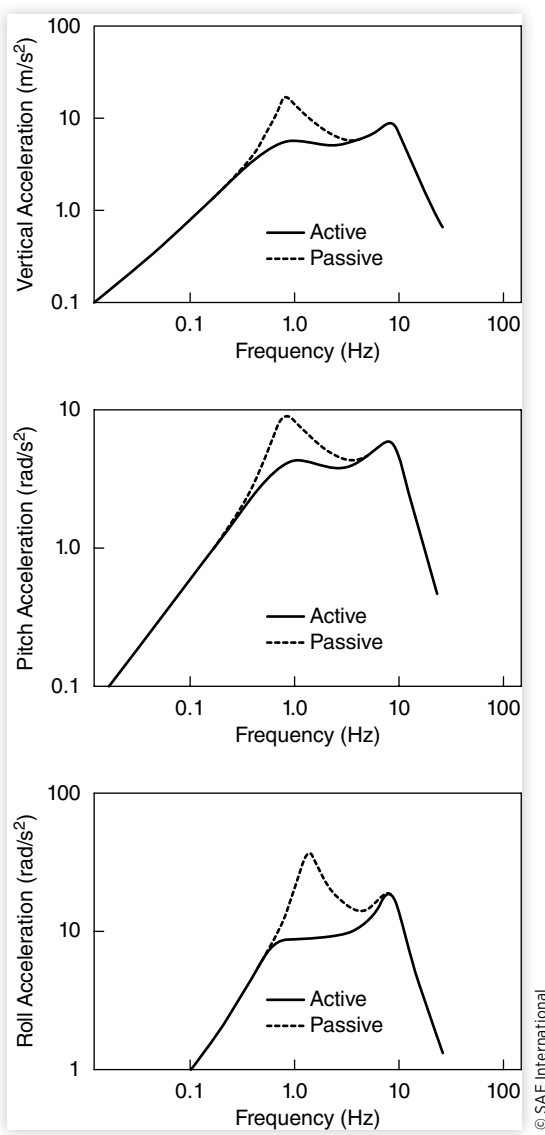
Performance

In general, the semi-active and full-active suspension systems have the greatest capability to achieve optimum performance in the modes described above, but at a penalty in weight, cost, complexity, and reliability. Thus the challenge to vehicle engineers is to achieve the benefits of active control with a minimum of hardware. The table below characterizes the relative performance that can be obtained with each level of sophistication in the design.

Performance potential of various types of suspension systems

Suspension Type	Performance Mode					
	Ride	Height	Roll	Dive	Squat	Road-holding
Passive	Performance is a compromise between all modes					
Self-leveling	High	High	N/A	N/A	N/A	N/A
Semi-active	Medium	N/A	Low	Low	Low	Medium
Full-active	High	High	High	High	High	High

FIGURE 7.26 Comparison of responses for active and passive suspension systems [12].



With semi-active systems, even slow-active variable damping allows improvement in roll, dive, and squat control along with ride and road-holding. Variable stiffness can provide similar benefits, albeit at greater cost due to the need to use air springs or adjustable mechanical springs.

With low-bandwidth stiffness or damping control, a more responsive system can be achieved. High-bandwidth control is effective for maintaining the constant wheel loads beneficial to handling, but there is little additional ride benefit from a high-bandwidth control system. Only with a full-active system can the broadest range of improvements be obtained in all performance modes.

The performance of a full-active system optimized for ride contrasts with that of a passive suspension by much better control of the vertical, pitch, and roll motions at the sprung mass resonant frequencies [12]. **Figure 7.26** compares the response behavior in these three modes for the two types of systems. Whereas the passive system shows sprung mass resonance near 1 Hz in the vertical, pitch, and roll directions, a much reduced response occurs with the active system. In effect, the sprung mass motions in these directions (which are sensed by accelerometers) can be heavily damped by control forces developed in the active suspension system.

With control characteristics optimized for ride, there is no significant change in response at the unsprung mass resonant frequency near 10 Hz. This is rationalized by the fact that for the suspension to exert control forces which will reduce unsprung mass motions, those forces must be reacted against the sprung mass, thereby increasing the ride vibrations. Handling is affected by system response at the wheel hop frequency because of the associated load variations on the tires. Since the performance of the active and passive systems are identical in this region, little handling benefit is realized. To enhance handling, the control system design should be changed to reduce wheel hop response, although some penalty in ride should be expected.

© SAE International

References

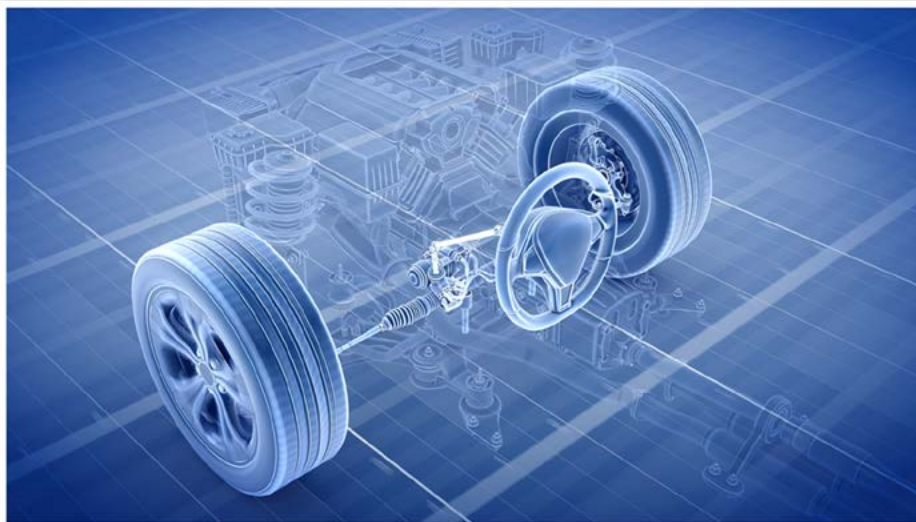
1. Bastow, D., *Car Suspension and Handling*. 2nd ed. (London, Pentech Press, 1990), 300pp.
2. Kami, Y. and Minikawa, M., "Double-Wishbone Suspension for Honda Prelude," SAE Technical Paper [841186](#), 1984, doi:[10.4271/841186](#).
3. Iijima, Y. and Noguchi, H., "The Development of a High-Performance Suspension for the New Nissan 300ZX," SAE Technical Paper [841189](#), 1984, doi:[10.4271/841189](#).

4. Sorsche, J.H., Encke, K., and Bauer, K., "Some Aspects of Suspension and Steering Design for Modern Compact Cars," SAE Technical Paper [741039](#), 1974, doi:[10.4271/741039](#).
5. Goodsell, D., *Dictionary of Automotive Engineering* (London: Butterworths, 1989), 182pp.
6. Leggat, J.W., "Steering and Handling of the Automobile," paper delivered before the Case Institute of Technology, October 21, 1953, 29pp.
7. Olley, M., "Independent Wheel Suspensions-Its Whys and Wherefores," SAE Technical Paper [340080](#), 1934, doi:[10.4271/340080](#).
8. Olley, M., "Road Manners of the Modern Car," *Institution of Automobile Engineers*, 1946, 147-182.
9. Nader, R., *Unsafe at any Speed: the Designed-in Dangers of the American Automobile* (New York: Grossman Publishers, 1965), 365pp.
10. "Vehicle Dynamics Terminology," SAE J670, Society of Automotive Engineers, Warrendale, PA (see Appendix A).
11. Sharp, R.S. and Crolla, D.A., "Road Vehicle Suspension System Design - A Review," *Vehicle Systems Dynamics* 16, no. 3 (1987): 167-192.
12. Chalasani, R.M., "Ride Performance Potential of Active Suspension Systems - Part II: Comprehensive Analysis Based on a Full-Car Model," *Proceedings, Symposium on Simulation and Control of Ground Vehicles and Transportation Systems*. AMO-Vol. 80, DSCVol 2, American Society of Mechanical Engineers, 205-226.



The Steering System

© Shutterstock



3D-rendering of steering system.

Introduction

The function of the steering system is to steer the front wheels in response to driver command inputs in order to provide overall directional control of the vehicle. This directional control is accomplished primarily by steering the front wheels, the contributions of which include not only the kinematics and force and moment reactions within the steering system itself, but also the kinematics and compliances of the suspension system. In the case of front-wheel drive (FWD) vehicles, we must also consider the geometry and reactions from the drivetrain. These phenomena will be examined in this chapter, first as a general discussion of steering systems, followed by a presentation regarding various effects including Ackerman geometry and the forces and moments present within the steering system. We will conclude the chapter by considering influences that are specific to front-wheel drive layouts.

The Steering Linkages

The steering systems used on motor vehicles vary widely in design [1, 2, 3], but are functionally quite similar. [Figure 8.1](#) illustrates some of these systems.

The steering wheel connects — by shafts, universal joints, and vibration isolators — to the steering gearset (i.e., rack-and-pinion or recirculating ball) whose purpose is to transform the rotary motion of the steering wheel to a translational motion necessary to steer the road wheels. The rack-and-pinion system consists of a linearly moving rack with meshed rotating pinion, mounted on the firewall or a forward crossmember, which steers the left and right wheels directly by a tie-rod connection. The tie-rod linkage connects to steering arms at the wheels (i.e., attached to the knuckles), thereby controlling the road wheel steer angles. If the tie rod is located ahead of the wheel center, as shown in [Figure 8.1](#), it is called a forward-steer configuration.

The steering gearbox is an alternative design that used to be common on some passenger cars but is still used for various truck applications. It differs from the rack-and-pinion design in that a frame-mounted steering gearbox rotates a pitman arm, and this arm is mechanically connected to the left and right road wheels through a linkage system that includes tie-rods and potentially a drag link (e.g., heavy truck applications with asymmetric steer linkages). A rear-steer configuration is shown in [Figure 8.1](#), identified by the fact that the tie-rod linkage connects to the steering arm behind the wheel center.

Between these two, the rack-and-pinion system has replaced the steering gearbox design (i.e., sometimes called a recirculating ball or worm-and-sector design) for

FIGURE 8.1 Illustration of typical steering systems.

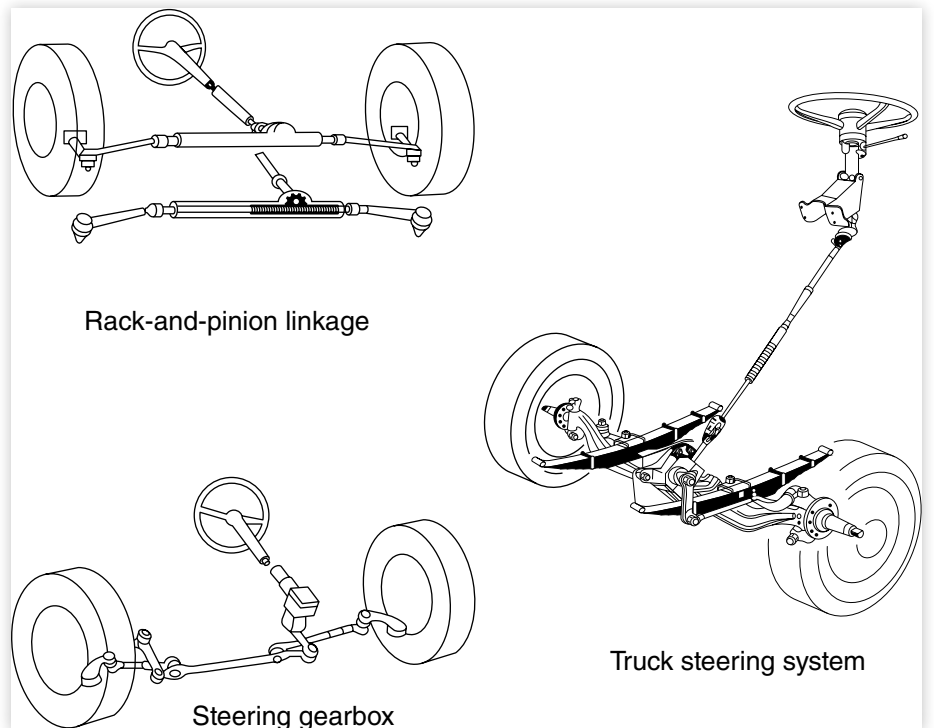
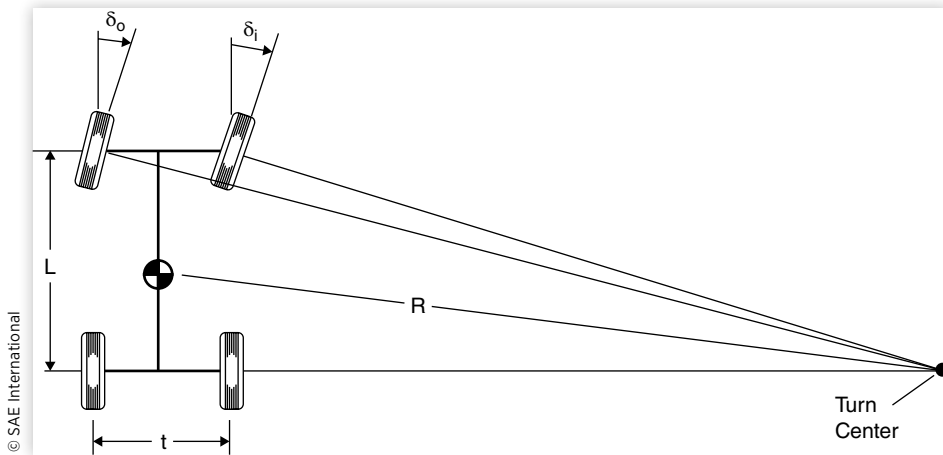


FIGURE 8.2 Ackerman turning geometry.

passenger car applications due to its many advantages, including reduced complexity, easier accommodation of front-wheel drive systems, and its adaptability to vehicles without body-on-frame construction. The primary functional difference in the steering systems used on heavy trucks is the fact that the frame-mounted steering gearbox steers the left road wheel (for left-hand drive vehicles) through a longitudinal drag link, and the right wheel is steered from the left wheel via a tie-rod linkage [1].

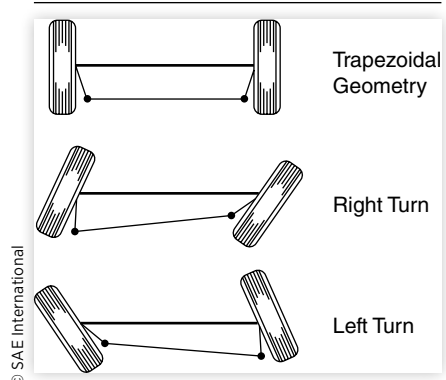
The gearset is the primary means for numerical reduction between the rotational input from the steering wheel and column, and the rotational output about the wheel-end steer axis. The steering wheel to road wheel angle ratios normally vary with angle, but have nominal values on the order of 15 to 1 in passenger cars, and up to as much as 36 to 1 with some heavy trucks. Initially, all rack-and-pinion gearsets had a fixed gear ratio, meaning any variation in ratio with steer angle was achieved through the geometry of the linkages. Today, rack-and-pinion systems are available that vary their gear ratio directly with steer angle.

The lateral translation produced by the steering gearset is relayed through linkages to steering arms located on the left and right wheel-ends. The kinematic geometry of the relay linkages and steering arms is not usually a parallelogram (which would produce equal left and right steer angles, known as parallel steer), but instead is a trapezoid to more closely approximate “Ackerman” geometry. With Ackerman geometry ([Figure 8.2](#) and [Figure 8.3](#)), the inside wheel is steered to a greater angle than the outside wheel due to the fact that for given turn, it has to track a smaller radius. It is worth noting that perfect Ackerman can be difficult to achieve once the vehicle’s design and packaging constraints are taken into account. From an analysis of the triangles it can be shown that correct Ackerman geometry requires the following relationships:

$$\delta_o = \tan^{-1} \frac{L}{(R + t/2)} \approx \frac{L}{(R + t/2)} \quad (8.1)$$

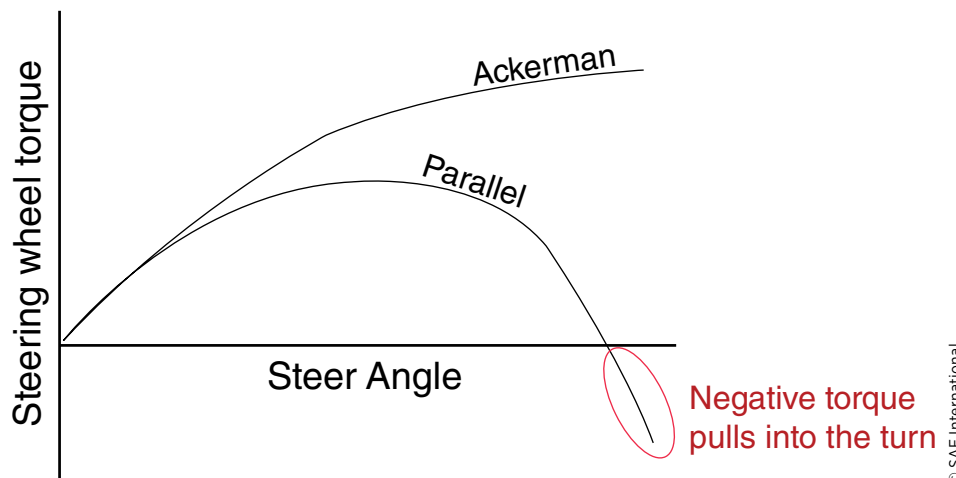
$$\delta_i = \tan^{-1} \frac{L}{(R - t/2)} \approx \frac{L}{(R - t/2)} \quad (8.2)$$

For small angles typical of most turning maneuvers, the arctangent of the angle is very nearly equal to the angle itself (in radians), justifying the approximations shown on the right side of the equations.

FIGURE 8.3 Differential steer from a trapezoidal tie-rod arrangement.

As shown in Figures 8.3 and the one below, when the tie rods are located behind the wheel centers, the steering arm ball joints are located inboard of the steer axis and provide good wheel clearances. If, on the other hand, the steering is designed with the tie rods forward of the wheel centers, the steering arm ball joints must be outboard of the steer rotation axis at the wheels in order to get close to Ackerman geometry. Any resulting interference with the wheel presents a design challenge, making it difficult to achieve good Ackerman geometry.

Steering Torque vs. Steer Angle.



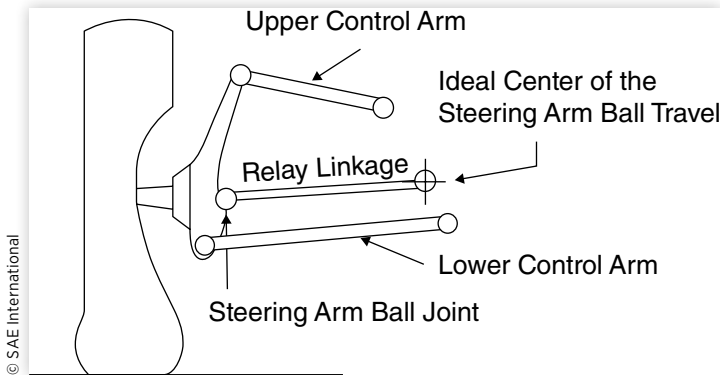
Proper design of the Ackerman geometry is a function of the vehicle wheelbase and the front axle track width. Design methods are straightforward and are available in the literature [1]. The degree to which the Ackerman geometry is achieved on a vehicle has little influence on high-speed directional behavior; however, the same cannot be said for low-speed maneuvers. At low speed, the Ackerman geometry plays an important role in the steering system's self-centering torque [4]. With Ackerman, the steer resisting torque will grow consistently with steer angle. With parallel steer (zero Ackerman) however, the torque will initially grow with angle, but may then diminish (and even become negative) at sufficiently large angles.

Steering Geometry Error

In the typical steering system, the relay linkages transfer the steering action from the gearset mounted on the body of the vehicle to the steering arms on the wheels. The steering action is achieved by translational displacement of the relay linkage in the presence of arbitrary suspension motions. The potential exists for steering actions to arise from the motion of the suspension; these are known as steering geometry errors.

For an ideal steering system, the relay linkage is designed such that the arc described by its ball connection to the steering arm exactly follows the arc of the steering arm during suspension deflections. In that case, no steer action results during the normal ride and handling motions of the suspension. In practice, it is not always possible to achieve this ideal because of packaging constraints, nonlinearities in the motion of the

FIGURE 8.4 Ideal steering geometry for an independent front suspension.



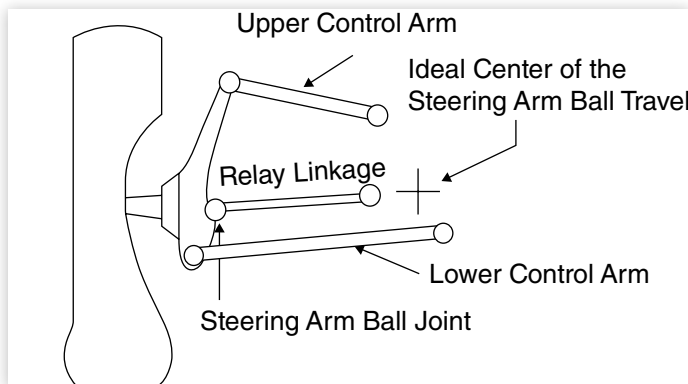
suspension, and geometry changes when the wheels are steered. Consequently, errors will occur that may result in a change in toe angle with suspension deflections, a systematic steer at both wheels, or a combination of both.

The geometry to achieve the “ideal” of no interaction on an independent front suspension is illustrated in [Figure 8.4](#). Regardless of the suspension type used, for the vertical wheel motion around the normal ride point, the motion will be defined by some linkage constraints. For the upper and lower control arm configuration shown, relative to the vehicle body the outboard end of each arm will follow an arc centered at the pivot point on the body. This defines the motion of the upper and lower ends of the steering knuckle and, ultimately, the motion of the steering arm ball at its intermediate location on the knuckle. If the steering arm ball is located in close proximity to one of the control arms, its ideal center will be close to the inboard pivot point of that arm. If located at some intermediate position on the knuckle, its ideal center will be found at a point that is intermediate between the inboard pivots of the two arms. Although the ideal center can be estimated by eye, a geometric study is needed to precisely determine its location. Many of the computer-aided-design (CAD) programs have the capability to identify this point. Alternatively, various geometrical methods (inflection circle, Hartmann’s Construction, or Bobillier’s Construction) may be used to locate the center [5, 6].

It should be noted here that the ideal center for the steering arm ball is determined by the kinematic (motion) behavior of the suspension linkages, the analysis for which is subtly different from that used to model anti-dive and anti-squat suspension behavior. In the analysis of anti-dive and anti-squat, the objective is to determine suspension response to force and torque inputs. The conclusion in that case is that the linkages behave like a single arm pivoted at the virtual center of the upper and lower control arms, located at the intersection of the projections of the control arm axes. However, analysis of the motion of the linkages results in a different center because of the angular changes in the linkages as a result of the motion.

Toe Change

The arc that will be followed by the tie-rod end at the wheel is established by the inboard joint of the relay linkage (tie rod)—the joint being the center of the arc. If the linkage joint is either inboard or outboard of this point, the steering geometry error will cause a steer action as the wheel moves in jounce or rebound. Consider the case illustrated in [Figure 8.5](#) which shows the inboard joint of the tie rod located outboard of the ideal center.

FIGURE 8.5 Geometry error causing toe changes.

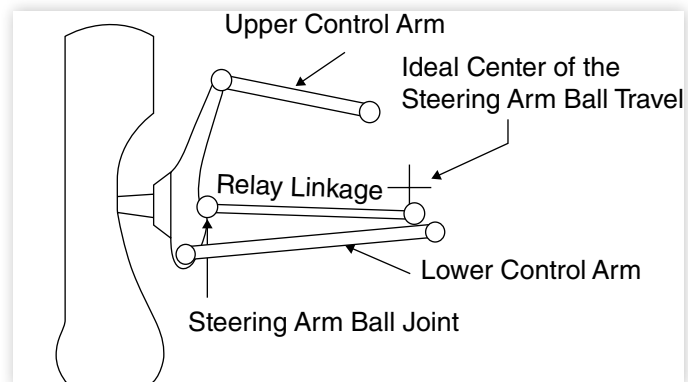
© SAE International

When the left wheel moves in either jounce or rebound, the end of the relay linkage follows an arc which pulls the steering arm to the right as viewed in [Figure 8.5](#). This produces a left-hand steer when the linkage is located behind the wheel centers. By a similar argument, it can be seen that the right wheel will steer to the right in jounce and rebound. Thus, a toe-out error occurs when the wheels are at any position other than the design ride height, and proper toe will be difficult to maintain due to its dependence on front-wheel load condition.

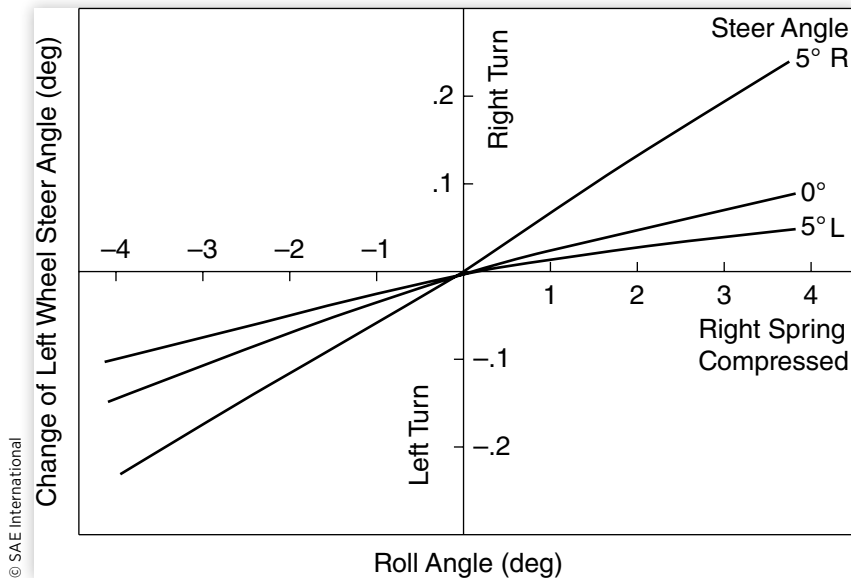
When the relay linkage joint is located too far inboard, the wheels will steer in the opposite direction during jounce and rebound, resulting in a toe-in error. Because of the nature of this error, the toe-out or toe-in conditions will also be experienced when the body rolls in cornering. Inasmuch as these are undesirable effects, these may legitimately be considered to be steering geometry errors.

Roll Steer

A second type of steering geometry error (which is sometimes used intentionally to alter handling behavior) is to locate the inboard joint of the relay linkage either above or below the ideal center. [Figure 8.6](#) illustrates this case, showing a rear view of a left-hand wheel with the inboard joint located below the ideal center. For the case where the linkage is located aft of the wheel, the arc followed by the relay linkage end will produce a left-hand steer on the wheel as it goes into jounce and a right-hand steer when it goes into rebound. Steer in the opposite directions will be produced on the right-side wheel. Thus, toe-in and toe-out will occur with each cycle of bouncing when the vehicle travels down the road.

FIGURE 8.6 Steering geometry error to add understeer.

© SAE International

FIGURE 8.7 Roll steer behavior experimentally measured on a vehicle.

© SAE International

Because of the symmetry of this case, both wheels will steer in the same direction when the body rolls. For example, in a turn to the right (positive steer by the SAE convention) the body rolls to the left inducing jounce on the left wheel and rebound on the right. Thus both wheels steer to the left (out of the turn), contributing an understeer effect to the vehicle's directional response. Conversely, locating the inboard joint of the tie rod above the ideal center produces an oversteer effect.

Figure 8.7 shows the roll steer behavior experimentally measured on a vehicle. Lines sloping upward and to the right reflect a roll steer which is understeer in direction (i.e., in a left-hand turn, as the vehicle body rolls to the right, the wheels steer to the right reducing the severity of turn). At any steer angle, the slope of the curve is the roll steer coefficient, ε . The understeer gradient is given by:

$$K_{\text{roll steer}} = \varepsilon \frac{d\phi}{da_y} \quad (8.3)$$

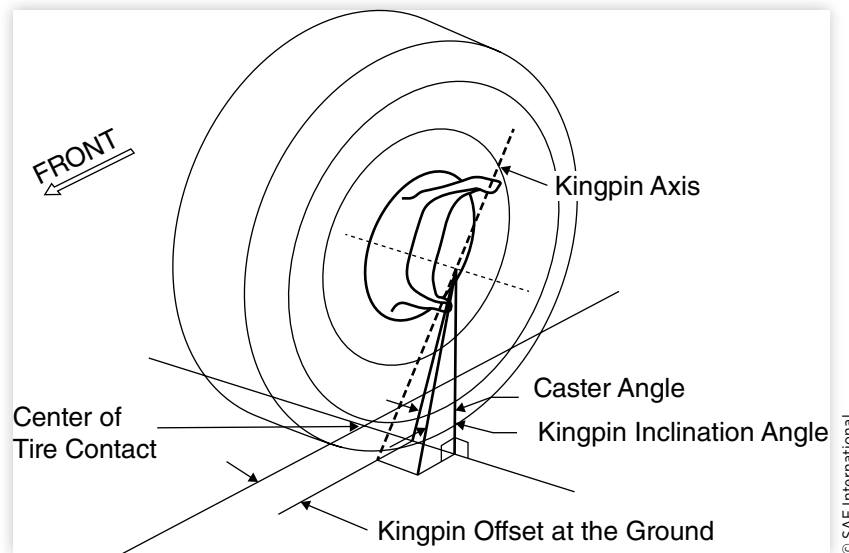
It is worth noting that most suspensions swing in a plane that is skewed with respect to the vehicle's longitudinal axis. The analysis, as illustrated above, should be made in the swing plane and subsequently transferred to the transverse plane.

Front-Wheel Geometry

The important elements of a steering system consist not only of the visible linkages just described, but also the geometry associated with the steer rotation axis at each road wheel. This geometry determines the force and moment reactions in the steering system, affecting its overall performance. The important features of the geometry are shown in **Figure 8.8**.

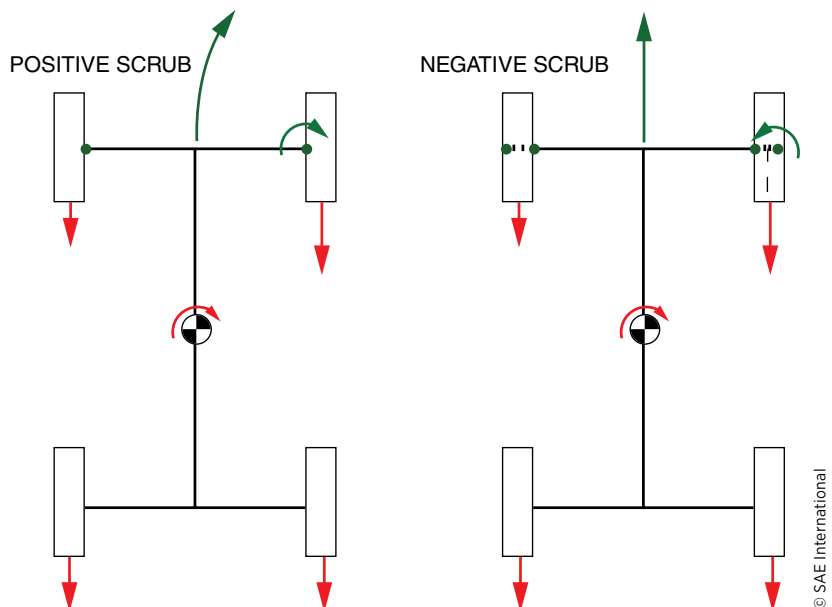
The steer angle is achieved by rotation of the wheel about a steer rotation axis. Historically, this axis has the name "kingpin" axis, although it may be established by ball joints or the upper mounting bearing on a strut. The axis is normally not vertical, but instead may be tipped outward at the bottom, producing a lateral inclination angle (kingpin inclination angle) in the range of 0-5 degrees for trucks and 10-15 degrees on passenger cars.

FIGURE 8.8 Steer rotation geometry at the road wheel.



It is common for the wheel to be offset laterally from the point where the steer rotation axis intersects the ground. The lateral distance from the ground intercept to the wheel centerline is the offset at the ground (sometimes called “scrub”) and is considered positive when the wheel is outboard of the ground intercept. Offset may be necessary to obtain packaging space for brakes, suspension, and steering components. At the same time, it adds “feel of the road” and reduces static steering efforts by allowing the tire to roll around an arc when it is turned [7].

Traction Force Interaction with Scrub.



Caster angle results when the steer rotation axis is inclined in the longitudinal plane. Positive caster places the ground intercept of the steer axis ahead of the center of tire contact. A similar effect is created by including a longitudinal offset between the steer axis and the spin axis of the wheel (spindle), although this is only infrequently used. Caster angle normally ranges from 0–5 degrees and may vary with suspension deflection.

Wheel camber angles and toe-in normally have only secondary effects on steering behavior and high-speed directional response. The typical fractional angles specified for camber are selected to achieve near-zero camber angle for the most common load conditions of the vehicle. The small static toe angles are normally selected to achieve zero angle when driving forces and/or rolling resistance forces are present on the road. The selection of these angles is normally dominated by considerations of front tire wear rather than handling [8, 9].

Steering System Forces and Moments

The forces and moments imposed on the steering system emanate from those generated at the tire-road interface. The SAE has selected a convention by which to describe the forces on a tire, as shown in [Figure 8.9](#). The forces are measured at the center of the contact with the ground and provide a convenient basis by which to analyze steering reactions.

The ground reactions on the tire are described by three forces and moments, as follows:

Normal force	Aligning torque
Tractive force	Rolling resistance moment
Lateral force	Overspinning moment

FIGURE 8.9 SAE tire force and moment axis system.

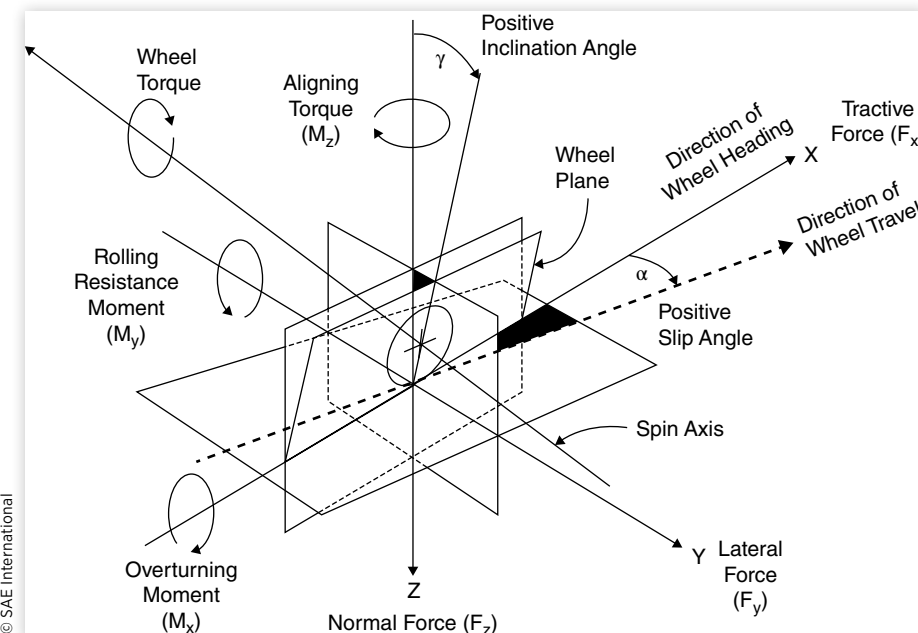
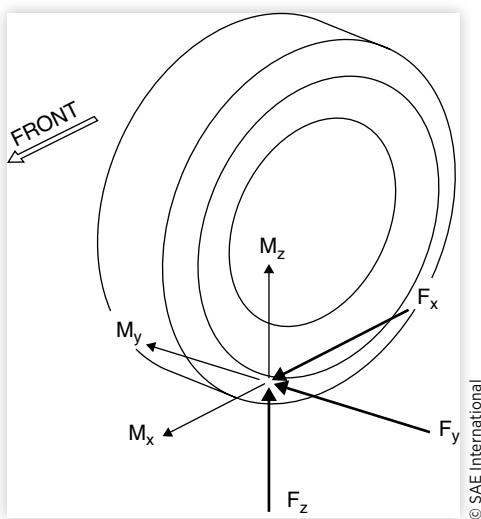


FIGURE 8.10 Forces and moments acting on a right-hand road wheel.



On front-wheel-drive cars, an additional moment is imposed by the drive torque. This will be discussed separately, along with other factors unique to front-wheel-drive cars that affect handling behavior.

The reaction in the steering system is described by the moment produced on the steer axis, which must be resisted to control the road wheel steer angle. Ultimately, the sum of the moments from the left and right wheels acting through the steering linkages with their associated ratios and efficiencies account for the steering-wheel torque feedback felt by the driver at the handwheel.

Figure 8.10 shows the three forces and three moments acting on a right-hand road wheel. Each will be examined separately to illustrate its effect on the steering system.

Vertical Force

The vertical load, F_z , acts vertically upward on the wheel and by SAE convention is considered a positive force. Because the steering axis is inclined, F_z has a component acting to produce a moment attempting to steer the wheel. The moment arises from both the caster and lateral inclination angles. Assuming small angles and neglecting camber of the wheel as it steers, the total moment from the two can be approximated by:

$$M_V = -(F_{zl} + F_{zr})d\sin\lambda\sin\delta + (F_{zl} - F_{zr})d\sin v\cos\delta \quad (8.4)$$

where:

- M_V = Total moment from left and right wheels
- F_{zl}, F_{zr} = Vertical load on left and right wheels
- d = Lateral offset at the ground
- λ = Lateral inclination angle
- δ = Steer angle
- v = Caster angle

The first expression on the right side of [Equation 8.4](#) arises from the lateral inclination angle, and the last from caster angle. The source of each of these moments is most easily visualized by considering the effects of lateral inclination angle and caster angle separately.

The vertical force acting on lateral inclination angle, illustrated in [Figure 8.11](#), results in a sine angle force component, $F_{zr}\sin\lambda$, which nominally acts laterally on the moment arm “ $d \sin \delta$ ” when the wheel is steered. The moment is zero at zero steer angle. With a steer angle, the moments on both the left and right wheels act together to produce a centering moment, as shown in [Figure 8.12](#). The net moment is proportional to the load but independent of left and right load imbalance. When steering, both sides of the vehicle lift, an effect which is often described as the source of the centering moment.

The caster angle results in a sine angle force component, $F_{zr}\sin v$, which nominally acts forward on the moment arm “ $d \cos \delta$ ” as shown in [Figure 8.13](#). The moments on the left and right wheels are opposite in direction, as shown in [Figure 8.14](#), and tend to balance through the relay linkages. The balance depends on equal left and right wheel loads. Hence, load and caster angle may affect wheel toe-in, and imbalances due to load or geometric asymmetry may result in steering pull. With steer angle, one side of the axle lifts and the other drops, such that the net moment that is produced depends also on the roll stiffness of the front suspension as it influences the left and right wheel loads.

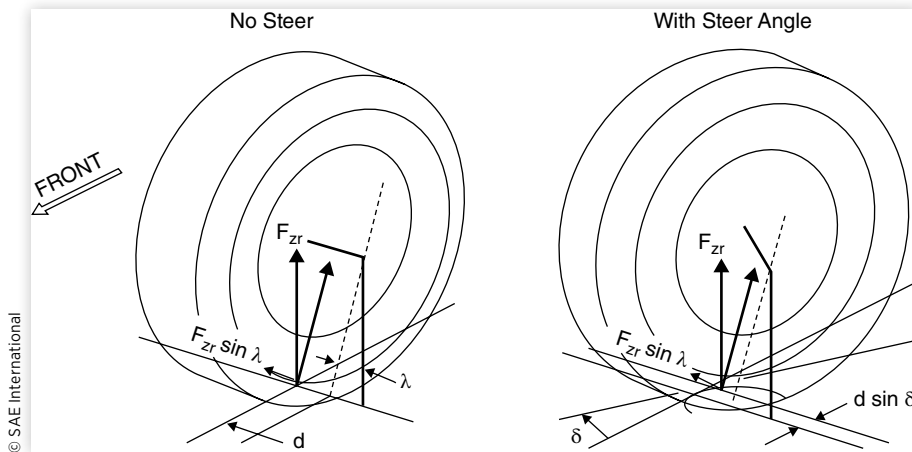
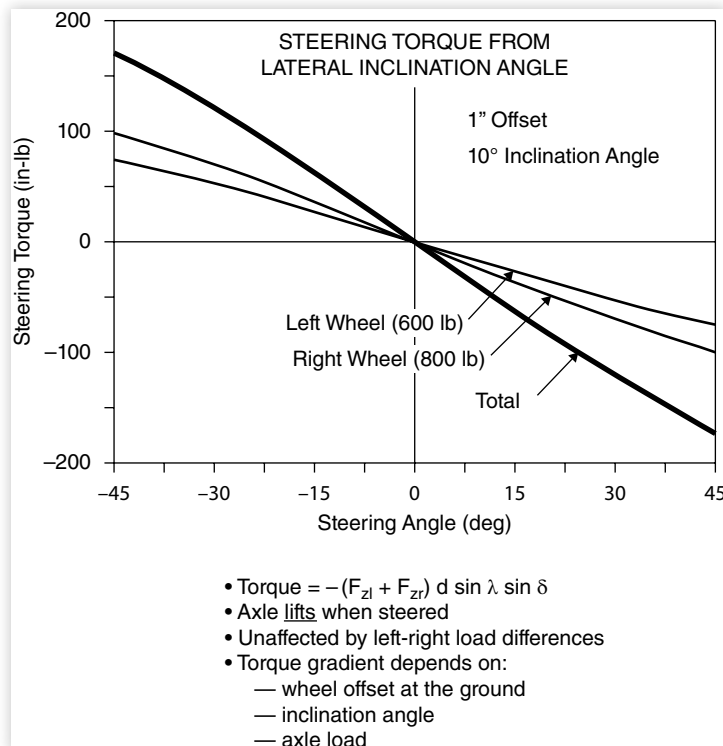
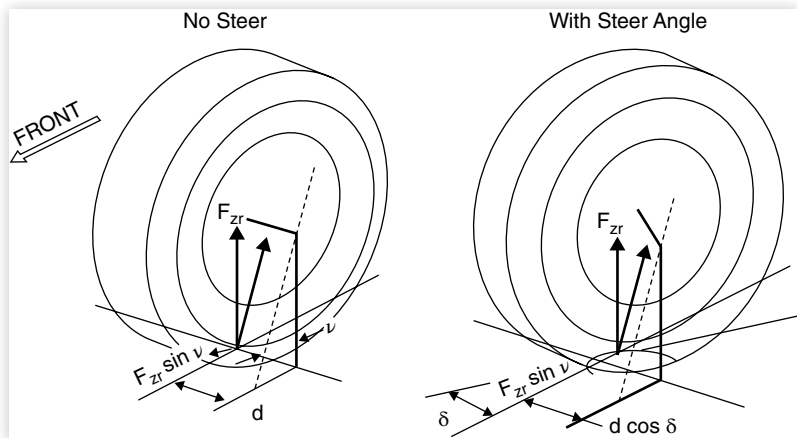
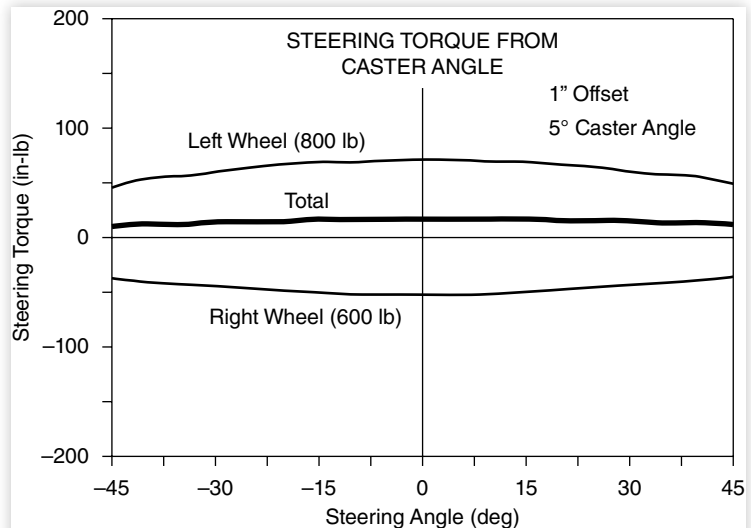
FIGURE 8.11 Moment produced by vertical force acting on lateral inclination angle.**FIGURE 8.12** Steering torques arising from lateral inclination angle.

FIGURE 8.13 Moment produced by vertical force acting on caster angle.

© SAE International

FIGURE 8.14 Steering torques due to caster angle.

© SAE International

- Torque = $(F_{zl} - F_{zr}) d \sin \nu \cos \delta$
- Axle rolls when steered
- sensitive to left-right load imbalance (load or spring asymmetry)
- Torque gradient depends on
 - wheel offset at the ground
 - caster angle
 - left-right load difference in cornering
 - front and rear suspensions roll stiffnesses
 - suspension roll center height
 - center of gravity height
 - lateral acceleration level

Lateral Force

The lateral force, F_y , acting at the tire center produces a moment through the longitudinal offset resulting from caster angle, as shown in [Figure 8.15](#). The net moment produced is:

$$M_L = -(F_{yl} + F_{yr})r \tan \nu \quad (8.5)$$

where:

F_{yl} , F_{yr} = Lateral forces at the left and right wheels (positive to the right)
 r = Tire radius

The lateral force is generally dependent on the steer angle and cornering condition, and with positive caster produces a moment attempting to steer the vehicle out of the turn. Hence, it is a major contributor to understeer.

Tractive Force

The tractive force, F_x , acts on the kingpin offset to produce a moment as shown in [Figure 8.16](#).

The net moment is:

$$M_T = (F_{xl} - F_{xr})d \quad (8.6)$$

where:

F_{xl} , F_{xr} = Tractive forces on the left and right wheels (positive forward).

The left and right moments are opposite in direction and tend to balance through the relay linkage. Imbalances, such as may occur with a tire blowout, brake malfunction, or split the coefficient road surfaces, will tend to produce a steering moment which is dependent on the lateral offset dimension.

FIGURE 8.15 Steering moment produced by lateral force.

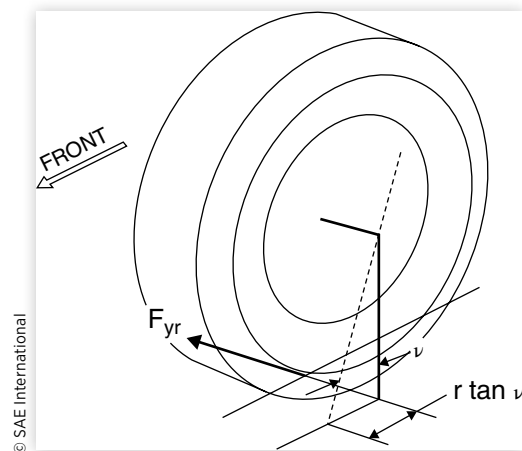
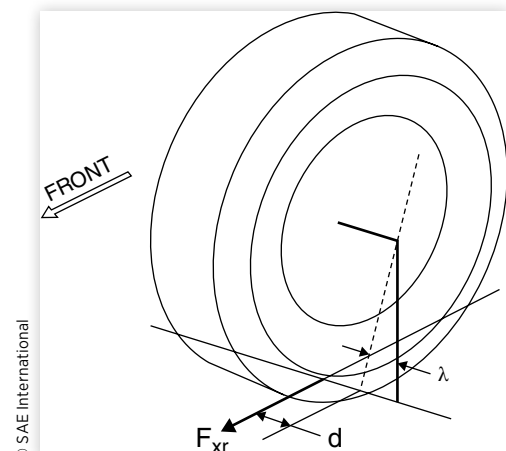


FIGURE 8.16 Steering moment produced by tractive force.



Aligning Torque

The aligning torque, M_z , acts vertically and may be resolved into a component acting parallel to the steering axis. Since moments may be translated without a change in magnitude, the equation for the net moment is:

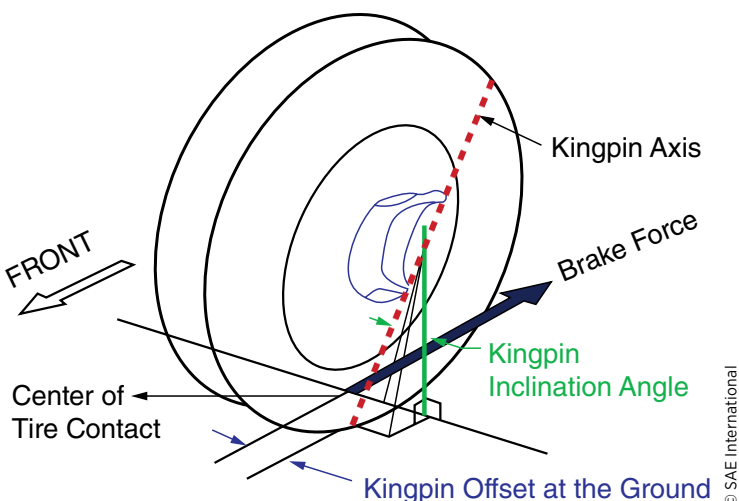
$$M_{AT} = (M_{zl} + M_{zr}) \cos \sqrt{\lambda^2 + v^2} \quad (8.7)$$

where:

M_{zl}, M_{zr} = Aligning torques on the left and right wheels.

Under normal driving conditions, the aligning torques always act to resist any turning motion, thus their effect is understeer. Only under high braking conditions do they act in a contrary fashion (Figure below).

Brake Force.



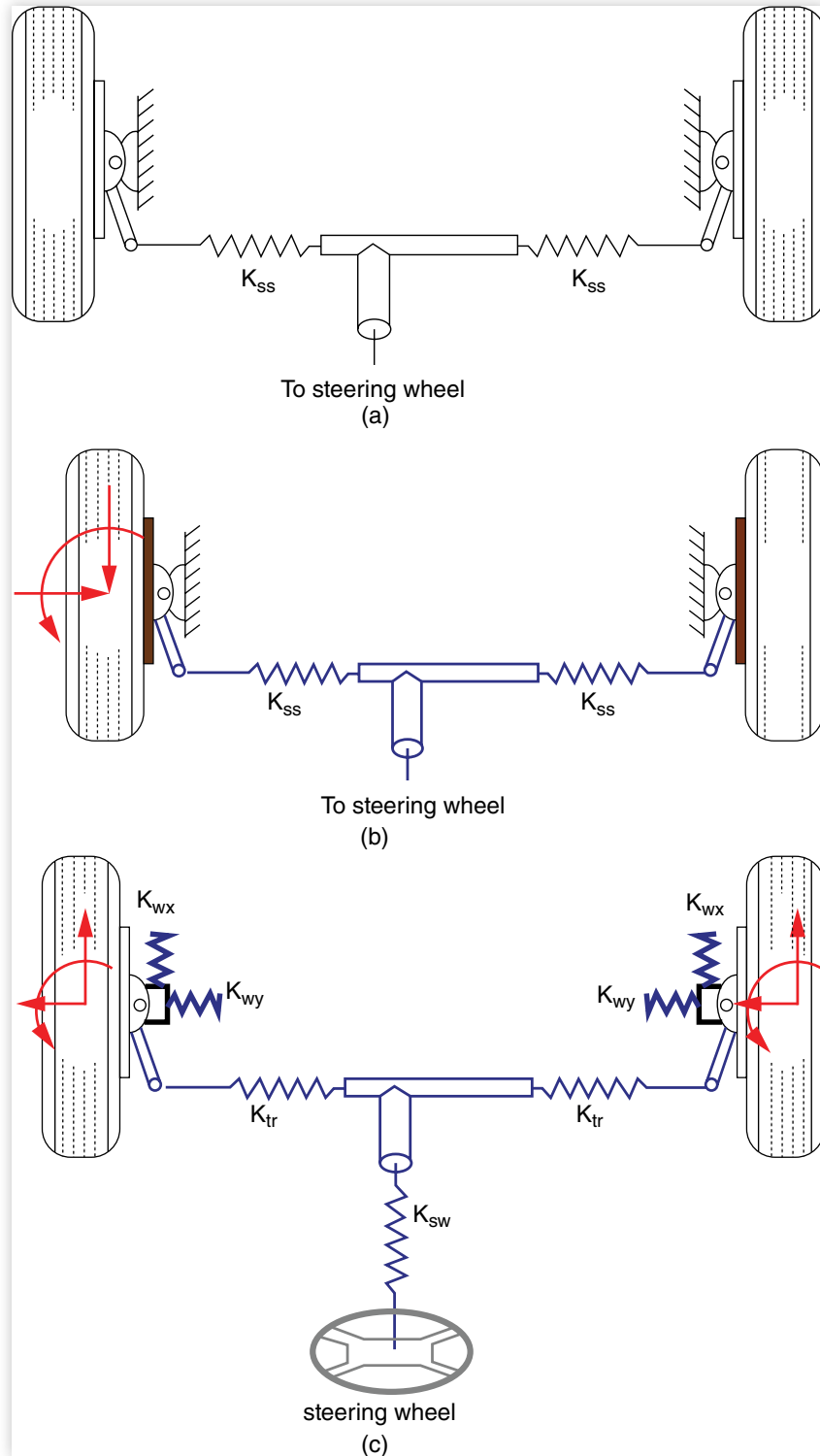
© SAE International

Rolling Resistance and Overturning Moments

These moments at most only have a sine angle component acting about the steer axis. They are second-order effects and are usually neglected in an analysis of steering system torques.

Steering System Models

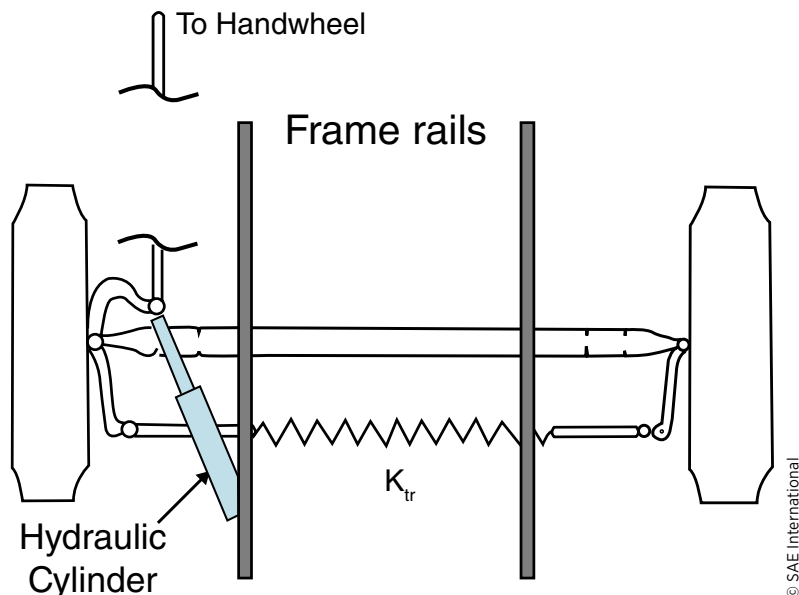
Equations (8.4) through (8.7) from the preceding discussion describe the moments input to the steer axis of each road wheel coming from the forces and moments acting on the tires. The reactions can be summed directly to determine the torque feedback to the steering wheel, if desired. To quantify the influence on open-loop directional response, however, a model of the steering compliances is required [2]. [Figure 8.17](#) shows the simplest model that is suitable for describing low-frequency behavior. The significant properties of the linkages are the stiffnesses shown here as the composite values between the gearset and the road wheels. For various reasons, the front suspensions will also exhibit compliance in the lateral direction that adds to the effective compliance interacting with the steering displacements. These effects can be taken into account by appropriately increasing the “lumped” compliance values of the linkages.

FIGURE 8.17 Steering linkages model.

Depending on the purpose of the analysis, the steering gearset might be represented by the effective steering ratio and by the appropriate input/output torque relationships and efficiencies. Similarly, the model may be expanded by the addition of Ackerman steer angle relationships between the road wheels with nonlinearities if desired.

Power steering systems, common on passenger cars and various truck platforms, are an additional source of forces or moments in the steering system and come in many forms. The power assist may be hydraulic or electric in nature, and the assist force or moment may be applied to the column, the rack, or within the steering gearbox. On such configuration is shown in Figure (PD slide (166 / 184), Linkage Booster Power Steering.)

Linkage Booster Power Steering.



© SAE International

As shown in figure above the steering wheel rotation routes hydraulic pressure through hydraulic cylinder, applying power-assist boost force to the left wheel. In this arrangement, compliance in the column may be bypassed, resulting in the vehicle feeling neutral or oversteer at the handwheel.

The modeling equations for power steering systems are not developed here, but one approach can be to consider the geometric relationships [10] and the application of Hooke's Law to relate forces and displacements across the compliances. Models of steering systems have proved most useful when combined with existing vehicle simulation models such as those from CarSim, ADAMS, and others. The directional response simulations compute the vehicle dynamic motions and the associated force and moment conditions imposed on each tire, needed as input to the steering system model. These are then used as inputs to the model to determine the incremental steer angles produced, in turn altering the turning behavior of the vehicle. This makes it possible to examine the precise influences of steering system properties on the overall vehicle handling behavior.

Examples of Steering System Effects

The specific design of a steering system geometry has a well-recognized influence on steering performance measures such as center feel, returnability, and steering efforts as

normally evaluated by vehicle manufacturers. Additionally, in the systematic study of directional response, other phenomena are observed, ranging from simple influences on steering ratio to cornering and even braking.

Steering Ratio

The steering ratio is defined as the ratio of steering wheel rotation angle to steer angle at the road wheels. Normally these range from 15 or 20 to 1 on passenger cars, and 20-36 to 1 on trucks. Because of the compliance and steer torque gradients with increasing steer angles, the actual steering ratio may be as much as twice the designed ratio. [Figure 8.18](#) shows experimental measurements on a truck which illustrate the phenomenon. While the compliance property is constant on a vehicle, the torque gradient will vary with load on the front tires, tire type, pressure, road coefficient of friction, etc. Hence, the actual steering ratio may vary (always exceeding the design value) and influencing the low-speed maneuverability of the vehicle.

Understeer

The steady-state cornering performance of a vehicle is frequently characterized by the understeer gradient measured at the steering wheel. Because compliance in the steering system allows the road wheels to deviate from the steering wheel input, the results obtained are influenced by the steering system properties. [Figure 8.19](#) shows the steer angle gradient measured at the steering wheel and the left road wheel of a loaded truck with manual steering [11].

The vehicle has a very high understeer gradient at the steering wheel equal to approximately 150 degrees/g (the initial steering wheel gradient on the plot). Corrected for the ratio of the steering system (36 to 1), it is equivalent to an apparent gradient of 4 degrees/g at the road wheel. However, independent measurements of the road wheel angle indicated

FIGURE 8.18 Experimental measurement of steering ratio on a truck.

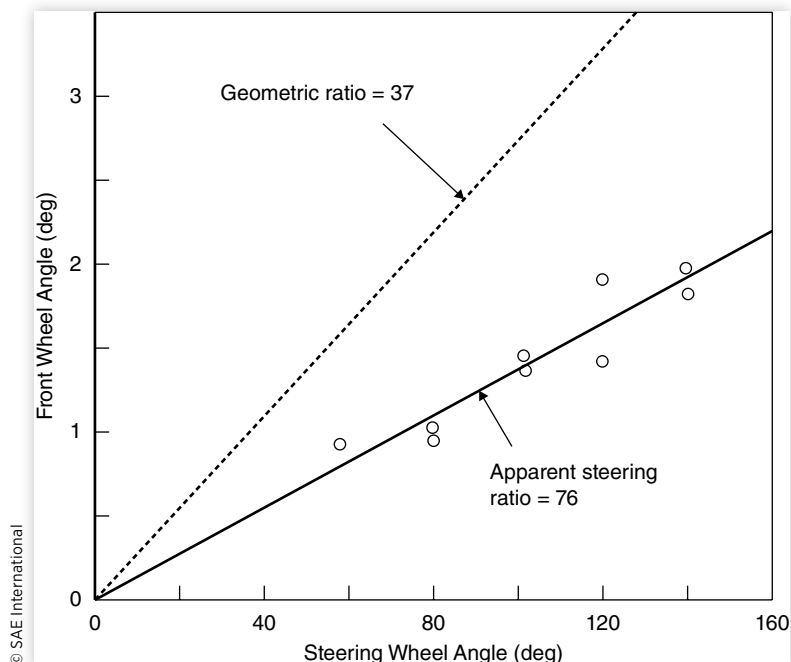
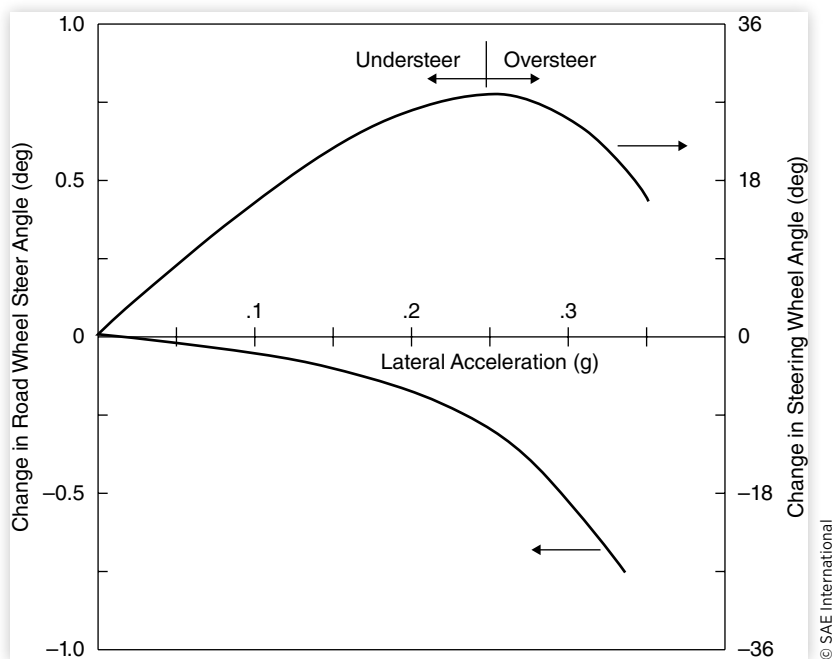


FIGURE 8.19 Understeer gradient measured at the steering wheel and road wheel of a truck.



© SAE International

an initial slope that is nearly horizontal—equivalent to neutral steer at the road wheel. The difference arises from deflections in the steering linkage as the reactions on the road wheels act against the steering compliances.

The magnitude of the steering system contribution is dependent on the front-wheel load and caster angle. From a simple analysis for the understeer influences in which the lateral forces and aligning torques are dominant (neglecting vertical force effects), it can be shown that the understeer gradient is:

$$K_{\text{strg}} = \frac{W_f(rv + p)}{K_{\text{ss}}} \quad (8.8)$$

where:

K_{strg} = Understeer increment (deg/g) due to steering system

W_f = Front wheel load (lb)

r = Wheel radius (in)

p = Pneumatic trail associated with aligning torque (in)

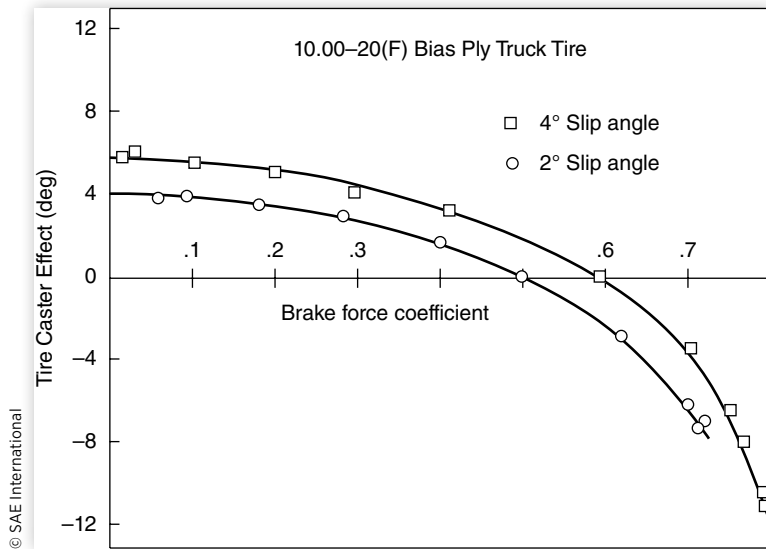
v = Caster angle (rad)

K_{ss} = Steering stiffness (in-lb/deg) between road wheel and steering wheel

As seen here, caster angle and aligning torque effects add to the understeer in the presence of a compliant steering system. For typical values of the above parameters, Equation (8.8) would account for understeer increments on the order of 4-6 deg/g.

Braking Stability

Braking is a special case in which steering system design plays an important role in directional response [2]. Specifically, the design has a direct influence on stability and

FIGURE 8.20 Change of tire aligning torques with braking coefficient.

resistance to brake imbalance effects. It was shown that caster angle influences stability by way of its action to resist steering deviations caused by front brake imbalance. Yet, the benefits of caster angle are particularly vulnerable during braking conditions. Vehicle pitch and front suspension windup may overcome the few degrees of caster angle designed into the system at normal trim conditions. Further, the tire aligning torques, which effectively act like 4-8 degrees of caster angle under free-rolling conditions, can also reverse in direction during braking. This tire effect is illustrated in [Figure 8.20](#) by measurements from a truck tire. The tire caster effect in this plot is obtained by dividing the aligning torque by the lateral force to determine the pneumatic trail at each data point. The pneumatic trail normalized by the tire radius then yields the effective angle at which the lateral force acts under the tire, which is the tire caster effect. While braking on low coefficient of friction road surfaces, the aligning torque acts in the direction to steer the tire in its direction of travel, which on the steered wheels attempts to steer the vehicle out of the turn (an understeer influence). At high braking coefficients, however, the aligning torque reverses direction and may reach elevated negative levels, attempting to steer the tire into the direction of turn (an oversteer influence). As a result, the normal stabilizing effects of positive caster and tire aligning torque may be substantially reduced or eliminated during high-level braking.

Brake force imbalance (due to brake malfunction or a split road surface coefficient) will also act on the compliant steering system, attempting to steer the vehicle. Using the split coefficient surface as an example, the higher brake forces that occur on the high-coefficient surface will attempt to rotate the vehicle onto that surface by virtue of the yaw moment produced on the vehicle. With a positive lateral offset (see Figure 8.9, Equation 8.4), the dominant front wheel brake force on the high-coefficient surface will also attempt to steer the vehicle onto that surface. The brake force “steering” effect may be as much as 2 to 3 times greater than the direct moment on the vehicle in causing the vehicle to veer onto the high-coefficient surface. Negative lateral offsets have been used on certain cars to counteract this mechanism during split coefficient braking, as well as with braking systems that employ a diagonal-split arrangement (i.e., one brake circuit for the left front and right rear wheels, and another brake circuit for the right front and left rear wheels).

Influence of Front-Wheel Drive

It is generally recognized that with front-wheel-drive (FWD) vehicles, the turning behavior varies with the application of engine power. In most cases, throttle-on produces understeer while throttle-off produces oversteer. The turning equation developed in Chapter 6 for FWD vehicles would suggest just the opposite behavior. Therefore, other mechanisms must be at work. Three have been identified and will be covered in this section. What follows focuses on handling influences that are unique to front-wheel drive vehicle configurations. All the other influences considered in earlier sections are still present and act on the vehicle.

Driveline Torque about the Steer Axis

For FWD vehicles in straight-ahead driving, the torque in the driveline produce a moment about the steer axis. This is illustrated in [Figure 8.21](#), where the wheel is in the straight-ahead driving position and a constant-velocity (cv) joint connects the half-shaft to the wheel spindle.

Neglecting the rolling resistance moment and the moments deriving from the normal force between the tire and road, the net moment about the steer axis of one wheel is:

$$M_{SA} = F_x d \cos v \cos \lambda + T_d \sin(\lambda + \zeta) \quad (8.9)$$

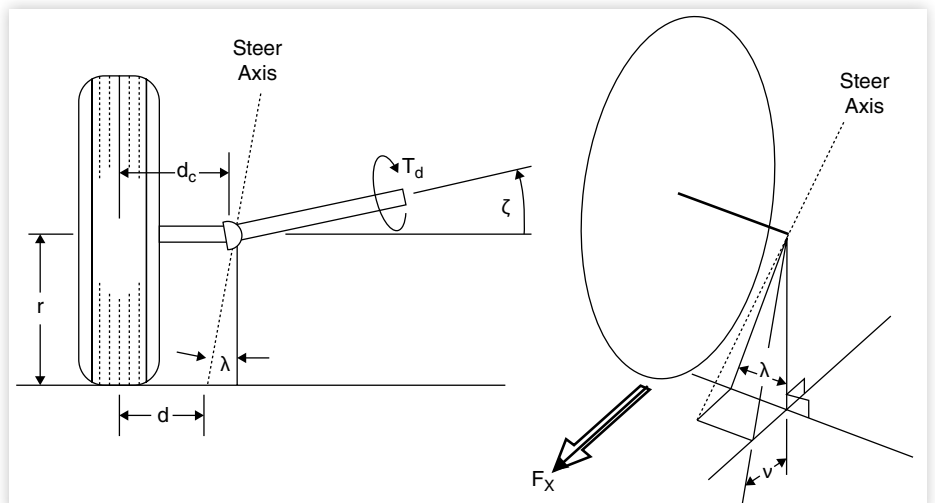
Since

$$T_d = F_x r \quad (8.10)$$

[Equation \(8.9\)](#) can be rewritten:

$$M_{SA} = F_x [d \cos v \cos \lambda + r \sin(\lambda + \zeta)] \quad (8.11)$$

FIGURE 8.21 Drive forces and moments acting on a front wheel.



Normally, the lateral inclination and caster angles (λ and v) are small enough that the cosine function can be assumed unity, in which case:

$$M_{SA} = F_x [d + r \sin(\lambda + \zeta)] \quad (8.12)$$

In effect, the arm about which the drive force acts to create a moment on the steering axis is $[d + r \sin(\lambda + \zeta)]$. As introduced earlier, d is the lateral offset at the ground. The term “ $r \sin(\lambda + \zeta)$ ” is the additional distance out to the perpendicular from the half-shaft at the constant-velocity joint. Envision a plane through the constant-velocity joint which is perpendicular to the half-shaft: the offset that determines the moment arm extends from the tire contact patch to that plane.

When the half-shaft is horizontal (as is most often the case in straight-ahead driving), ζ is zero. Here, the moment arm is $d + r \sin \lambda$, which is the same as the offset at the wheel center, d_c . This is the source of the expression “the drive force acts at the wheel center.” Since the brake torque acts through the suspension, it can be shown that the brake force moment arm is simply the lateral offset at the ground, d . When inboard brakes are used, the moment arm is again $d + r \sin \lambda$.

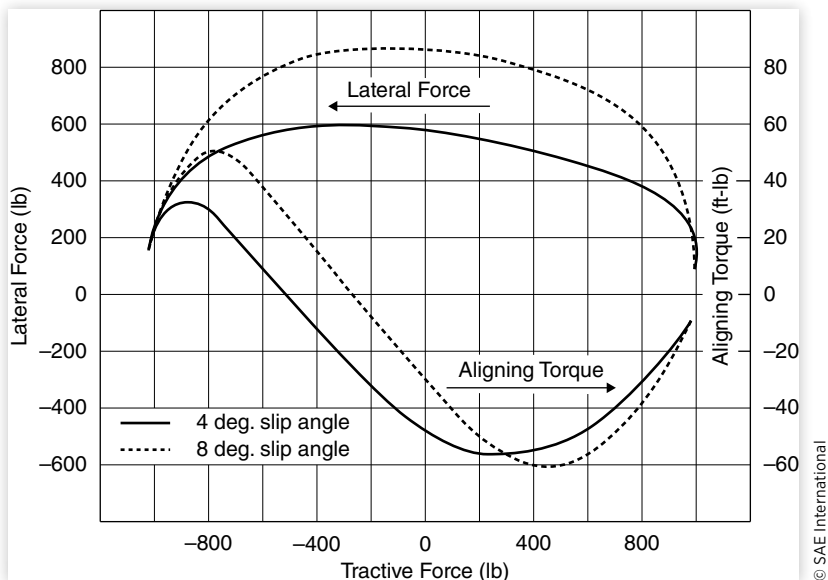
When a vehicle enters a turn, body roll causes the half-shaft on the outside wheel to reduce its inclination angle, ζ (going negative if it were already zero), while the angle on the inside wheel increases. Thus the moment arm about which the drive force acts gets smaller on the outside wheel and larger on the inside wheel. With a drive force (in the forward direction) this imbalance introduces a moment in the steering system which opposes the steer angle, trying to steer the vehicle out of the turn (understeer). The magnitude of the moment is dependent on the following factors: (1) the degree of body roll and how much difference in half-shaft angles that get created; (2) the difference between kingpin inclination angles on the left and right side during body roll; (3) caster angles; and (4) any geometric differences between the left- and right-hand sides (tire radius, etc.).

The understeer influence is proportional to the magnitude of the moment divided by the stiffness of the steering system. Thus minimizing body roll and stiffening the steering system minimizes the effect. Although the influence is specific to each vehicle, the understeer change from throttle-on to throttle-off is estimated to be on the order of 1 deg./g for a typical vehicle [12].

Influence of Tractive Force on Tire Cornering Stiffness

It is well known that a tire loses cornering force when a tractive force is also present. [Figure 8.22](#) shows typical behavior of lateral force as a function of tractive force. The effect presents itself for both bias-ply and radial tires, although it is most pronounced for tires with bias-ply construction. The application of throttle (a demand for drive force) reduces the front tires’ ability to generate lateral force. This trade-off between longitudinal and lateral force means the tires must seek a higher slip angle in an attempt to regain the lateral force that has been lost to the longitudinal force requirement. This phenomena results in an understeer condition.

The magnitude of understeer change will be proportional to the tractive force level. It is estimated [13] that the affect on understeer will be in the range of 0–2 deg / g corresponding to a throttle adjustment that covers the range of 0.2g of acceleration to 0.05 g of deceleration. This effect is lowest with radial-ply tires.

FIGURE 8.22 Effect of tractive force on tire lateral force and aligning moment.

© SAE International

Influence of Tractive Force on Aligning Moment

As seen in Figure 8.22, tractive force demand tends to increase the aligning moment produced by a tire (again less significantly with radial-ply tires). The additional aligning moment tends to steer the vehicle out of the turn, resulting in understeer. The magnitude of the understeer depends on the change in aligning moment divided by the stiffness of the steering system. It has been estimated that this mechanism contributes on the order of 0.5 to 1 deg./g of understeer [12].

Fore/Aft Load Transfer

Understeer is normally characterized only for the case in which the vehicle is subjected to steady speed turns. Nevertheless, for the purposes of describing the influence of FWD on understeer, it has been necessary to consider the differences between accelerating and braking conditions. When the vehicle accelerates, load is dynamically transferred to the rear wheels, the effect being that the rear wheels achieve a higher cornering stiffness while the fronts lose some of their cornering stiffness. This redistribution contributes to understeer. As part of the overall study of FWD vehicle configurations and specifically the effort to characterize the various understeer contributions, it would be worthwhile to understand the degree to which the fore / aft load transfer has on understeer characteristics relative to RWD vehicles subjected to the same test. For a typical car, the understeer influence for the throttle changes described above is on the order of 1 deg/g [12].

Summary of FWD Understeer Influences

In summary, the primary mechanisms responsible for throttle on/off changes in understeer of a FWD vehicle are:

1. The lateral component of drive thrust: While this mechanism is relatively weak (<0.5 deg/g), it is oversteer in direction.

2. Drive torque acting about the steer axis: Highly dependent on driveline geometry and the degree of body roll in cornering, this mechanism is understeer in direction (about 1 deg/g).
3. Loss of lateral force: A tire property which causes understeer (about 1–1.5 deg/g).
4. Increase in aligning moment: A tire property which causes understeer (about 0.5–1 deg/g).
5. Fore/aft load transfer: Although present on FWD and RWD vehicles, it is always understeer in direction (about 1 deg/g).

The total understeer due to these effects is approximately 4–5 deg/g. The mechanisms present in items 2–4 generate torques that feed back into the steering system and are the primary sources of “torque steer” often noted with FWD vehicles. Finally, it is worth mentioning that friction in a differential can be significant (10 to 15%) when a driveline is under load. Although not treated here, under certain circumstances it could be an additional mechanism contributing to throttle-on understeer in FWD vehicles.

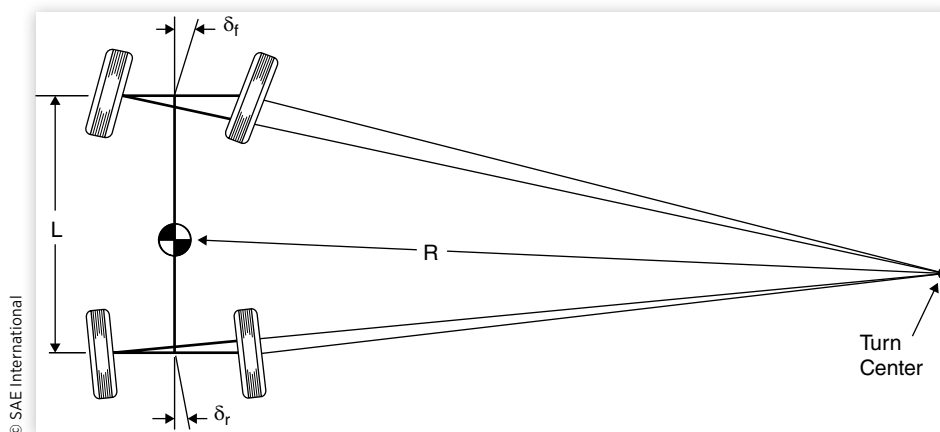
Four-Wheel Steer

Vehicle performance in turning can be enhanced by actively steering both the front and rear wheels, a configuration known as four-wheel steering (4WS). Four-wheel steering may be implemented using one of several means. Active steering is accomplished by steering action applied directly to the rear wheels, in contrast to passive steering in which compliances are purposely designed into the suspension to provide incremental steer deviations that improve cornering [14]. Typical applications of four-wheel steering are to improve low-speed maneuverability and/or high-speed cornering.

Low-Speed Turning

Low-speed turning performance is improved by steering the rear wheels out-of-phase with the front wheels to reduce the turn radius, resulting in improved maneuverability as shown in [Figure 8.23](#). Rear-wheel steer is accomplished by mechanical, hydraulic, or electronic means [14 – 18]. The rear-wheel steer angles are normally only a fraction of what is used on the front steer axle, limited to about 5 degrees of steer. Based on the

FIGURE 8.23 Turning geometry of a four-wheel-steer vehicle.



application, they may be only applied at low speeds [17] or at high steer angles typical of low-speed turns [15]. Analysis of the turning performance is simplified by assuming average angles for the front and rear wheels, analogous to the bicycle model approximation.

With the rear-wheel steer angle proportional to the front-wheel angle, the turning equations are as follows:

$$\delta_r = \xi \delta_f \quad (8.13)$$

$$\delta_f + \delta_r = \delta_f + \xi \delta_f = \delta_f (1 + \xi) = L / R \quad (8.14)$$

The turn radius is:

$$R = \frac{L}{\delta_f (1 + \xi)} \quad (8.15)$$

Equation (8.15) gives the explicit expression for the way in which the turn radius is reduced by the use of rear steer. At 50 percent rear steer, a one-third reduction in turn radius (1/1.5) is achieved. At 100 percent rear steer (steering the rear wheels to the same magnitude as the front wheels), a 50 percent reduction in turn radius (1/2) occurs.

The expression for off-tracking with four-wheel steer is somewhat more complicated than that for two-wheel steer. Recognizing that the front and rear turn radii, R_f and R_r , respectively, are related by the expression:

$$R_f \cos \delta_f = R_r \cos \delta_r = R_r \cos(\xi \delta_f) \quad (8.16)$$

it is possible to obtain an equation in the following form as an approximation of the off-tracking distance:

$$\Delta \approx \frac{L^2 (1 - \xi^2)}{2R (1 + \xi^2)} \quad (8.17)$$

With no rear steer ($\xi = 0$) the off-tracking is the same as developed earlier in Equation (6.4). With the rear wheels steered to the same angle as the front (100 percent), the off-tracking distance becomes zero.

High-Speed Cornering

The out-of-phase rear steer used for low-speed maneuverability would be inappropriate for high-speed turning because the outward movement of the rear wheels would constitute an oversteer influence. Thus an in-phase rear steer is used at high speeds (e.g., 20 mph and above), although limited to a few degrees of steer. The transition between out-of-phase and in-phase steering is accomplished by sensing vehicle speed and changing the steering control algorithm in electronically controlled systems [17], or in mechanical systems by a mechanism that produces in-phase steer at small front wheel angles (0 to 250 degrees at the steering wheel) typical of high-speed driving [15].

The primary advantages of four-wheel steer are derived from the better control of transient behavior in cornering [19–24]. In general, 4WS systems yield a quicker response with better damping of the yaw oscillation that occurs with initiation of a turn. This can be seen in the lateral acceleration response to a step-steer input as shown in Figure 8.24 when the behavior of a “proportional” 4WS is compared to two-wheel steer. Other schemes for improving performance such as adding advances or delays into the steering action at the front or rear wheels can provide additional options to tailor the performance of 4WS vehicles to a specific performance metric.

FIGURE 8.24 Lateral acceleration response with different 4WS systems [20].

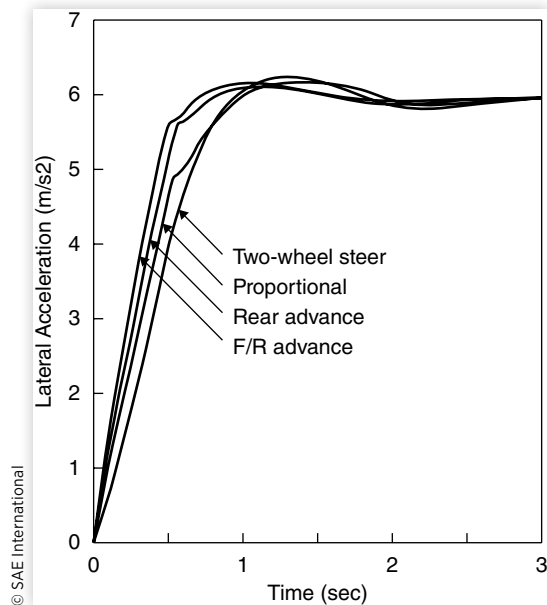
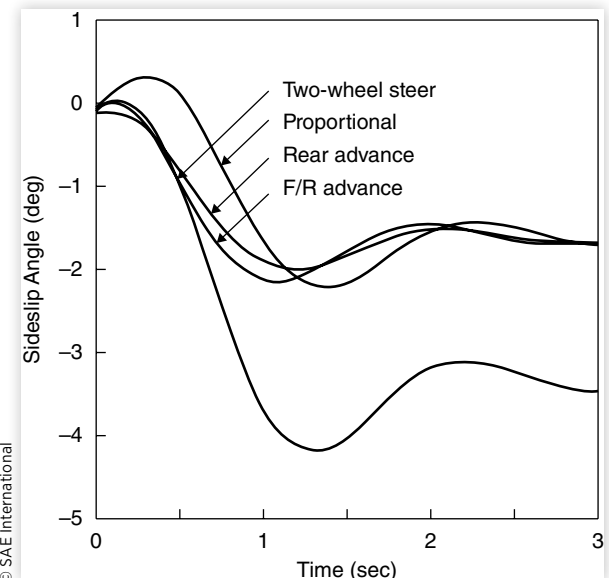


FIGURE 8.25 Body sideslip angle with different 4WS systems [20].



Another picture of the advantages of 4WS can be obtained by examining the response in sideslip angle as a turn is initiated. [Figure 8.25](#) compares the behavior of a two-wheel-steer system to various implementations of four-wheel steer. Depending on the amount of rear-wheel-steer action, the body sideslip angle can be arbitrarily reduced in cornering. The reduced amount of oscillation in sideslip angle with 4WS, as seen in [Figure 8.25](#), adds the general feeling of better stability during transient maneuvers.

Overall, a properly implemented four-wheel steering system can result in a vehicle which is more maneuverable at low speeds, and more responsive and stable in high-speed transient maneuvers. In other high-speed driving (e.g. straight line driving), however, its presence is imperceptible.

References

1. Durstine, J.W., "The Truck Steering System from Hand Wheel to Road Wheel," SAE SP-374, January 1974, 76pp.
2. Gillespie, T.D., "Front Brake Interactions with Heavy Vehicle Steering and Handling During Braking," SAE Technical Paper [760025](#), 1976, doi:[10.4271/760025](#).
3. Dwiggins, B.H., *Automotive Steering Systems* (Albany, NY: Delmar Publisher, 1968), 248pp.
4. Pitts, S. and Wildig, A.W., "Effect of Steering Geometry on Self-Centering Torque and 'Feel' during Low-Speed Maneuvers," *Automotive Engineer, Inst. Mech. Engr.*, July 1978.
5. Hall, A.S., Jr., *Kinematics and Linkage Design* (Englewood Cliffs, NJ: Prentice Hall, Inc., 1961).
6. Dijksman, E.A., *Motion Geometry of Mechanisms* (Cambridge, England: Cambridge University Press, 1976).

7. Taborek, J.J., *Mechanics of Vehicles* (Cleveland, OH: Towmotor Corporation, 1957), 93pp.
8. Lugner, P. and Springer, H., "Über den Einfluss der Lenkgeometrie auf die stationäre Kurvenfahrt eines LKW (Influence of Steering Geometry on the Stationary Cornering of a Truck)," *Automobil-Industrie*, April 1974, 5pp.
9. "Wheel Alignment-Modern Setting for Modern Vehicles," SAE SP-249, December 1963, 13pp.
10. MacAdam, C.C. et al., "A Computerized Model for Simulating the Braking and Steering Dynamics of Trucks, Tractor-Semitrailers, Doubles, and Triples Combinations-User's Manual, Phase 4," Highway Safety Research Institute, University of Michigan, Report No. UM-HSRI-80-58, September 1980, 355pp.
11. Gillespie, T.D., "Validation of the MVMA/HSRI Phase II Straight Truck Directional Response Simulation," Highway Safety Research Institute, University of Michigan, Report No. UM-HSRI-78-46, October 1978, 58pp.
12. Gillespie, T.D. and Segel, L., "Influence of Front-Wheel Drive on Vehicle Handling at Low Levels of Lateral Acceleration," *Road Vehicle Handling*, (London: Mechanical Engineering Publications Ltd., 1983), 61-68.
13. Braess, H.H., "Contributions to the Driving Behavior of Motor Vehicles with Front Wheel Drive Throttle Change during Cornering," Institute of Internal Combustion Machines and Motor Vehicles, Munich, Germany, 1970, 15pp.
14. Sharp, R.S. and Crolla, D.A., "Controlled Rear Steering for Cars - A Review," *Proceedings of the Institution of Mechanical Engineers, International Conference on Advanced Suspensions*, 1988, 149-163.
15. Sano, S. et al., "Operational and Design Features of the Steer Angle Dependent Four Wheel Steering System," *11th International Conference on Experimental Safety Vehicles*, Washington, DC, 1988, 5pp.
16. Nakaya, H. and Oguchi, Y., "Characteristics of the Four-Wheel Steering Vehicle and Its Future Prospects," *Vehicle System Dynamics* 8, no. 3 (1987): 314-325.
17. Takiguchi, T., Yasuda, N., Furutani, S., Kanazawa, H. et al., "Improvement of Vehicle Dynamics by Vehicle-Speed-Sensing Four-Wheel Steering System," SAE Technical Paper [860624](#), 1986, doi:[10.4271/860624](#).
18. Eguchi, T. et al., "Super HICAS" - A New Rear Wheel Steering System with Phase Reversal Control," SAE Technical Paper [891978](#), 1989.
19. Fukui, K., Miki, K., Hayashi, Y., and Hasegawa, J., "Analysis of Driver and a 'Four Wheel Steering Vehicle' System Using a Driving Simulator," SAE Technical Paper [880641](#), 1988, doi:[10.4271/880641](#).
20. Nalecz, A.G. and Bindemann, A.C., "Analysis of the Dynamic Response of Four Wheel Steering Vehicles at High Speed," *International Journal of Vehicle Design* 9, no. 2 (1988): 179-202.
21. Nalecz, A.G. and Bindemann, A.C., "Investigation into the Stability of Four Wheel Steering Vehicles," *International Journal of Vehicle Design* 9, no. 2 (1988): 159-179.
22. Ohnuma, A. and Metz, L., "Controllability and Stability Aspects of Actively Controlled 4WS Vehicles," SAE Technical Paper [891977](#), 1989, doi:[10.4271/891977](#).
23. Whitehead, J., "Four Wheel Steering: Maneuverability and High Speed Stabilization," SAE Technical Paper [880642](#), 1988, doi:[10.4271/880642](#).
24. Whitehead, J.C., "Rear Wheel Steering Dynamics Compared to Front Steering," *Journal of Dynamic Systems, Measurement and Control* 112, no. 1 (March 1990): 88-93.



Rollover

© Exponent®



Roller Coaster Dolly test.

Among the dynamic maneuvers a motor vehicle can experience, rollover is one of the most serious and threatening to the vehicle occupants. Rollover may be defined as any maneuver in which the vehicle rotates 90 degrees or more about its longitudinal axis such that the body makes contact with the ground. Generally speaking, such events occur when the lateral acceleration of a vehicle reaches a level beyond that which can be compensated for by the lateral load transfer on the tires. Rollovers can be classified as either (1) Tripped or (2) Un-tripped.

Tripped rollover may be caused by impacts with fixed road features such as curbs or guardrails, or when the vehicle leaves the road surface and the tires encounter soft ground such as sand or loose soil. Roads with cross-slope or side-slope (i.e., a vehicle driving across a steep hill) are also a source of tripped rollover events.

Un-tripped rollovers are less common but still require a mechanism to generate a roll moment sufficient to tip the vehicle over. One example may be a top-heavy vehicle performing an emergency lane change maneuver on a flat, paved surface.

As we will see in this chapter, there are many ways to estimate the rollover characteristics of a vehicle. The rollover process is one that involves a complex interaction of forces acting on and within the vehicle, as influenced by the maneuver and roadway. The process has been investigated analytically and empirically using models that cover a range of complexities. The process is most easily understood by starting with the fundamental mechanics involved in a quasi-static case (neglecting the inertial terms and accelerations in the roll plane), and progressing to the more complex models.

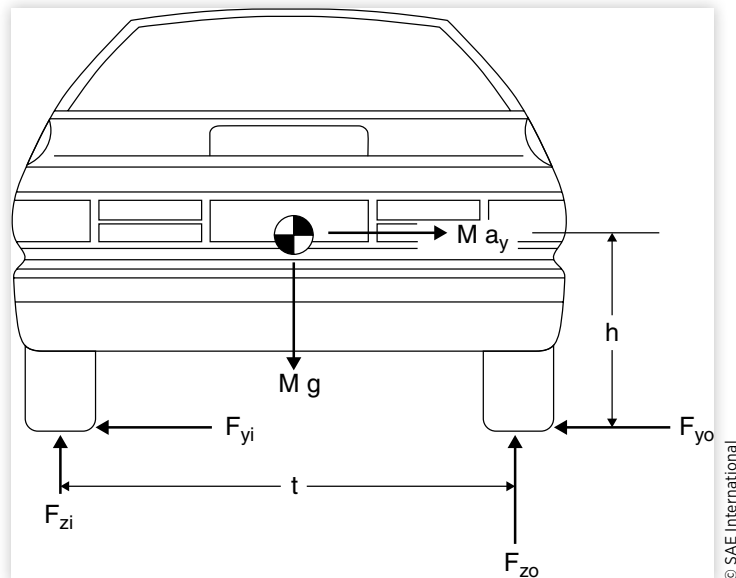
Quasi-Static Rollover of a Rigid Vehicle

Our investigation of rollover can begin by considering the force balance on a rigid vehicle in a cornering maneuver. By a rigid vehicle, we mean that the deflections of the suspensions and tires will be neglected in the analysis.

In the cornering maneuver, the lateral forces act in the ground plane to counterbalance the lateral acceleration acting at the C.G. of the vehicle, as shown in [Figure 9.1](#). The difference in the positions at which these forces act creates a moment on the vehicle and attempts to roll it toward the outside of the turn.

For the purpose of analyzing the behavior, assume the vehicle is in a steady-state turn so that there is no roll acceleration, and let the tire forces shown in [Figure 9.1](#) represent the total for both the front and rear wheels. In many highway situations, it is also appropriate to consider a transverse slope, known as cross-slope or superelevation. For the analysis, the angle will be denoted by the symbol “ φ ,” with a slope downward and to the left, representing a positive angle. A cross-slope in this direction helps to counterbalance the lateral acceleration. Cross-slope angles are normally quite small, justifying the use of small angle approximations ($\sin \varphi = \varphi$, $\cos \varphi = 1$) in the analysis that follows. Taking moments about the center of contact for the outside tires yields:

FIGURE 9.1 Forces acting to roll over a vehicle in a left-hand turn.



$$\sum M_o = 0 = Ma_y h - Mg\phi h + F_{zi}t - Mgt / 2 = 0 \quad (9.1)$$

from which we can solve for a_y to get:

$$\frac{a_y}{g} = \frac{t / 2 + \phi h - \frac{F_{zi}}{Mg} t}{h} \quad (9.2)$$

On a level road ($\phi = 0$) with no lateral acceleration, [Equation \(9.2\)](#) is satisfied when the load on the inside tires, F_{zi} , is one-half of the weight of the vehicle ($M g$). If F_{zi} is assumed to be equal to one half the weight of the vehicle in the presence of lateral acceleration by judicious choice of the cross-slope angle, then the term $F_{zi} t / Mg$ in [Equation \(9.2\)](#) becomes $1/2 Mg t / Mg$. The Mg terms cancel each other out, leaving the numerator of the overall term on the right-hand side of [Equation \(9.2\)](#) as $t/2 - t/2 + (\phi)h$. With an h in both the numerator and denominator, the right-hand side reduces to (ϕ) , resulting in [Equation \(9.3\)](#):

$$\phi = \frac{a_y}{g} \quad (9.3)$$

In highway design, cross-slope is used in curves for exactly this purpose. Given the radius of turn and an intended travel (design) speed, the cross-slope will be chosen to produce a lateral acceleration in the range of zero to 0.1 g's. The speed at which zero lateral acceleration is experienced on a superelevated curve is called the "neutral speed."

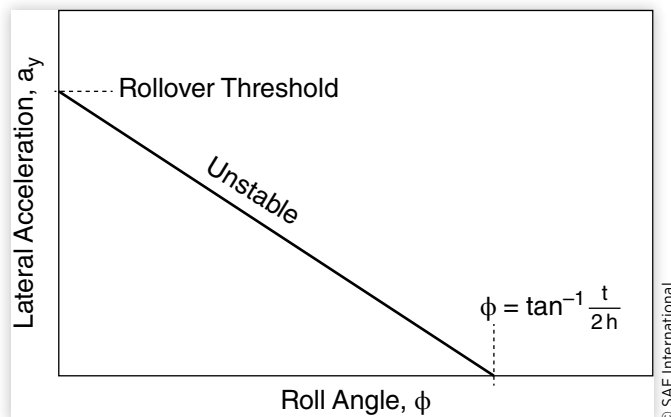
Returning again to [Equation \(9.2\)](#), as the lateral acceleration builds up, the load on the inside wheels must diminish. It is through this process that the vehicle acts to resist, or counterbalance, the roll moment in cornering. The limit cornering condition will occur when the load on the inside wheels reaches zero (all the load has been transferred to the outside wheels). At that point, rollover will begin because the vehicle can no longer maintain equilibrium in the roll plane. The lateral acceleration at which rollover begins is called the "rollover threshold." Applying this condition to [Equation \(9.2\)](#) such that the F_{zi} term set to zero, we have the new expression:

$$\frac{a_y}{g} = \frac{t / 2 + \phi h}{h} \quad (9.4)$$

With no cross-slope the lateral acceleration that constitutes the "rollover threshold" is simply "t over 2h." This simple measure of rollover threshold is often used for a first-order estimate of a vehicle's resistance to rollover. It is especially attractive because it requires knowledge of only two vehicle parameters—the track width and the C.G. height. However, the estimates are very conservative (predicting a threshold that is greater than the actual) and are more useful for comparing vehicles rather than predicting absolute levels of performance. (Some dynamicists use the inverse form of this threshold, "h over t/2" as a measure of rollover propensity, in which case a higher value corresponds to a lower rollover threshold.)

The rollover threshold differs distinctively among the various types of vehicles on the road. As examples, typical values fall in the following ranges [1]:

Vehicle type	C.G. height	Track Width	Rollover threshold
Sports car	18-20 in	50-60 in	1.2-1.7 g
Compact car	20-23	50-60	1.1-1.5
Luxury car	20-24	60-65	1.2-1.6
Pickup truck	30-35	65-70	0.9-1.1
Passenger van	30-40	65-70	0.8-1.1
Medium truck	45-55	65-75	0.6-0.8
Heavy truck	60-85	70-72	0.4-0.6

FIGURE 9.2 Equilibrium lateral acceleration in rollover of a rigid vehicle.

The rigid-vehicle model suggests that the lateral acceleration necessary to reach the rollover of passenger cars and light trucks exceeds the cornering capabilities arising from the friction limits of the tires (typical peak coefficients of friction are on the order of 0.8). That being the case, it is possible for the car to spin out on a flat surface without rolling over. From that, one might conclude that rollover with these types of vehicles should be rare; however, the accident statistics [2] prove otherwise and motivate the more in-depth analysis of rollover phenomena that will be addressed later in this chapter. In the case of heavy trucks, it is possible to reach the rollover threshold within the friction limits of the tires [3]. As a consequence, a heavy vehicle is at risk of rollover if the driver allows the vehicle to spin out on a dry road surface.

Rigid-body rollover can be illustrated more fully by way of a plot of the lateral acceleration as a function of roll angle, ϕ , for equilibrium of the vehicle, as shown in [Figure 9.2](#). Because of the rigid vehicle assumption, while at zero roll angle the lateral acceleration can be any value up to the rollover threshold. Once this threshold is reached, the inside wheels will lift off of the ground. The vehicle begins to roll and the equilibrium lateral acceleration decreases with angle because the center of gravity is lifting and shifting toward the outside wheels.

This region is an inherently unstable roll condition. Consider a vehicle tipped up on two wheels in a turn. In order to be in equilibrium, the vehicle roll angle must be at the precise value as shown in [Figure 9.2](#) where the equilibrium lateral acceleration matches the actual. Any slight disturbance that increases the roll angle reduces the equilibrium lateral acceleration, and the excess lateral acceleration produces a roll acceleration that further increases the angle driving away from the equilibrium point. If allowed to continue, the vehicle roll attitude accelerates rapidly to complete the rollover in a matter of a second or two.

This brings up the issue of defining when rollover begins. Because of the inherent instability of the vehicle when the inside wheels leave the ground, it is appropriate to consider wheel lift-off as the beginning of rollover. Nevertheless, it is possible for a driver to halt the action by quickly steering out of the turn, thereby reducing the lateral acceleration to a level that will return the vehicle to an upright position. Quick response (within a fraction of a second) is necessary because of the speed with which rollover proceeds. Theoretically, rollover becomes irrecoverable only when the roll angle becomes so large that the center of gravity of the vehicle passes outboard of the line of contact of the outside wheels. This limit corresponds to the point in [Figure 9.2](#) where the equilibrium lateral acceleration reaches zero ($\phi = \tan^{-1} (t/2h)$).

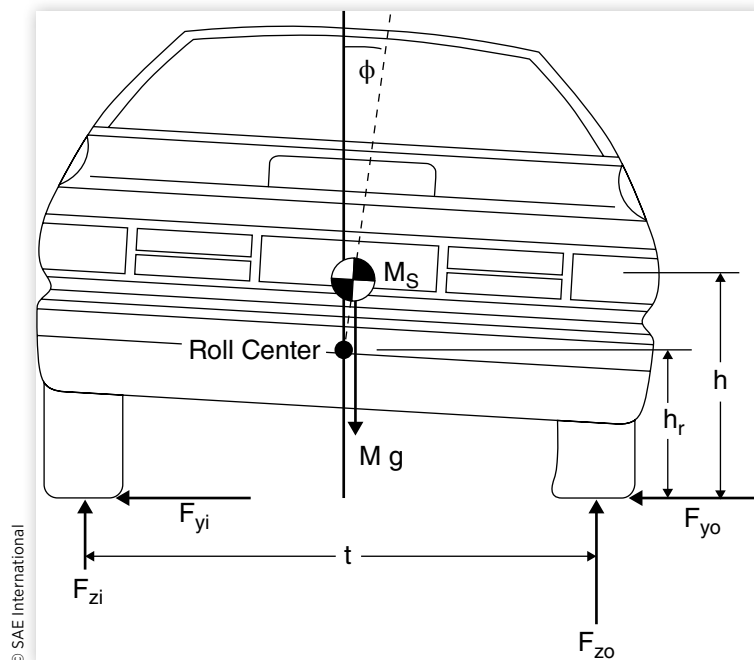
It is well recognized that stunt drivers can take a vehicle up to this point and drive on two wheels for extended distances despite the instability. Yet, it is a rare event for a typical motorist to avoid rollover if the vehicle should end up in this position. Taking a conservative viewpoint, the automotive engineer should assume that the majority of drivers will not have the reflexes or skills to deal with the instability once the wheels on one side of the vehicle leave the ground. Instead, they should focus on optimizing the behavior of the vehicle up to that point. In this regard, electronic chassis controls such as Electronic Stability Control (ESC) and rollover mitigation controls are a common and well-established means of monitoring the vehicle's inputs and responses, and making adjustments to the brakes and drive torque to either prevent, reduce, or eliminate the rollover condition.

Quasi-Static Rollover of a Suspended Vehicle

Neglecting the compliances in the tires and suspensions, as was done in the previous analysis, overestimates the rollover threshold of a vehicle [4]. In cornering, the lateral load transfer unloads the inside wheels of the vehicle and increases load on the outside wheels. Concurrently, the body rolls with a lateral shift of the center of gravity toward the outside of the turn. The offset of the center of gravity reduces the moment arm on which the gravity force acts to resist the rollover.

Figure 9.3 illustrates these mechanisms on a vehicle with a suspension system. The body is represented by its mass, M_s , connected to the axle at an imaginary point known as the roll center. The roll center is the pivot around which body roll occurs, and is also the point at which lateral forces are transferred from the axle to the sprung mass.

FIGURE 9.3 Roll reactions on a suspended vehicle.



A simple analytical solution for the rollover threshold is possible if the mass and roll of the axles are neglected [4, 5]. Taking moments about the point where the right wheel contacts the ground, and assuming the left wheel load has gone to zero gives:

$$\Sigma M_o = 0 = M_s a_y h - M_s g \left[t / 2 - \phi(h - h_r) \right] \quad (9.5)$$

Now the roll angle of the sprung mass, ϕ , is simply the roll rate, R_ϕ , times the lateral acceleration, a_y . The roll rate is the rate of change of roll angle with lateral acceleration expressed in units of radians per g. Substituting to eliminate the roll angle and solving for lateral acceleration yields:

$$\frac{a_y}{g} = \frac{t}{2h} \frac{1}{1 + R_\phi (1 - h_r/h)} \quad (9.6)$$

where:

h = Height of the center of gravity above the ground

h_r = Height of the roll center above the ground at the longitudinal C.G. location

t = Track width

R_ϕ = Roll rate (radians/g)

Thus, taking into account the lateral shift of the C.G., the rollover threshold is “ t over $2h$ ” reduced by the second term on the right-hand side of the above equation. For a passenger car with $h_r/h = 0.5$ and a roll rate of 6 degrees per g (0.1 rad/g), the second term evaluates to approximately 0.95. That is, the rollover threshold is reduced approximately 5 percent due to this mechanism. High performance cars with a low roll rate and low center of gravity experience less of these effects, whereas some luxury cars (i.e., ride comfort-oriented) with a higher roll rate and higher center of gravity may experience more. Solid axles (which tend to have a high roll center) also reduce the effect of lateral shift compared to independent suspensions (which have low roll centers) due to the reduced distance from the C.G. to the roll center.

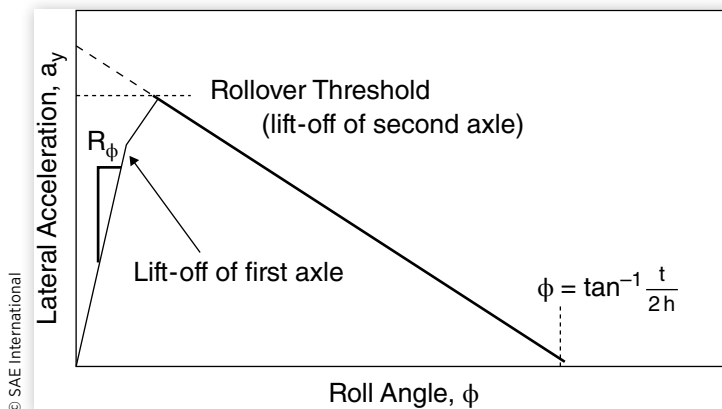
A similar mechanism arises from lateral deflections of the outside tires, which allows the load center under the tires to move inboard during cornering, effectively reducing the track width. For typical passenger cars the lateral shift of the tire contact point may contribute another 5 percent reduction to the threshold.

A more precise analysis of the lateral shift and the effect on the rollover threshold requires detailed modeling of the tires and suspension systems. Among the mechanisms that must be considered are:

- Lateral shift of the sprung mass center of gravity caused directly by roll about the suspension roll center.
- Lateral shift of the suspension roll center with respect to the track width, due to roll of a solid axle or camber of independently sprung wheels.
- Lateral movement of the action point of the tire vertical force due to cornering forces and deflections (these factors being reflected in changes to the overturning moment under combined cornering and camber).
- Differences in behavior of the front and rear suspensions and wheels.

Taking into account all of these effects is less amenable to an analytical solution. Particularly, if the front and rear suspensions are much different in load or roll stiffness, it is necessary to model simultaneous behavior of both the front and rear suspensions. Computer programs [6] are the normal approach to calculating quasi-static rollover threshold when these effects are to be included.

FIGURE 9.4 Equilibrium lateral acceleration in rollover of a suspended vehicle.



When these mechanisms are precisely modeled, the quasi-static roll response of a motor vehicle will take the form shown in [Figure 9.4](#). At low levels of lateral acceleration, the vehicle roll response increases linearly with a slope equal to the roll rate. This proceeds until one of the inside wheels lifts off. Note that both the front and rear wheels will not necessarily leave the ground at precisely the same instant on an actual vehicle due to differences between the front and rear suspensions and their loads. In the case of multi-axle trucks, the slope will change with the lift-off of each inside wheel, resulting in a curve with three or four line segments in this area. At this point, the response changes to a lower slope because the roll rate is reduced to that provided by the one suspension that remains in contact with the ground. When the second inside wheel lifts, the rollover threshold has been reached. Thereafter, the roll response follows the downward sloping line, closely equivalent to that discussed in the case of the rigid vehicle.

The plot indicates that for a vehicle with a given track width and C.G. height, the highest rollover threshold will be achieved by maintaining the sprung mass roll rate at the highest possible level (using suspensions with high roll stiffness), and by designing the front and rear suspensions so as to have the inside wheels lift off at the same roll angle condition.

Experimental methods have been developed to measure the quasi-static rollover threshold by use of a tilt-table. As suggested by the name, the table tilts the vehicle in the lateral, or roll, plane, and from measurement of the angle at which rollover occurs, the threshold is determined. The method is reasonably accurate for heavy trucks which have a high center of gravity and experience rollover at small angles (on the order of 20 to 25 degrees).

For passenger cars, however, the rollover threshold may well be on the order of 45 degrees. At high angles, the component of the vehicle weight acting downward in the vehicle plane is reduced substantially (30 percent at 45 degrees). The reduced loading on the suspensions and tires raises the body above its normal ride position causing premature rollover and invalidating the test. In order to avoid these errors, test procedures must be devised which impose a lateral force at the center of gravity location (the "cable pull" test [5]) or by applying a pure moment to the body of the vehicle.

Transient Rollover

Up to now, the analyses have been quasi-static and focused on the rollover of a vehicle performing a steady-state turn.

Such an assumption is reasonable only when the lateral acceleration is changing much more slowly than the vehicle responds in roll. In order to examine the vehicle's response to rapidly changing lateral acceleration conditions, a transient response model is necessary. A transient response model attempts to represent the way the vehicle roll varies with time. At the most elementary level, a simple roll model may be used to examine the response to analytically simple examples of time-varying lateral accelerations. Alternately, more comprehensive models combining motions in the yaw and roll planes have been developed to examine the roll response associated with specific maneuvering conditions.

Simple Roll Models

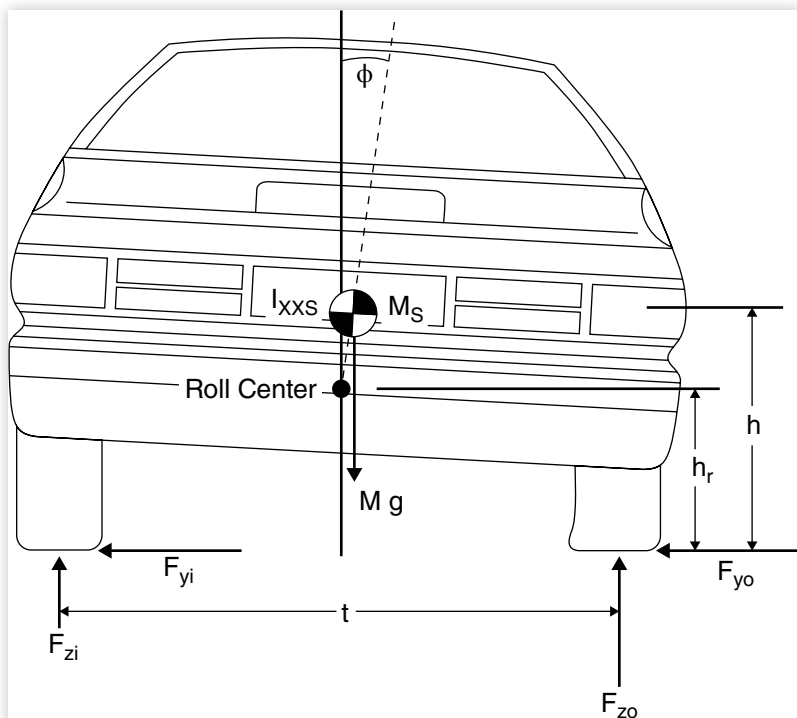
The first and simplest approach for investigating transient roll response is with a model similar to the suspended vehicle discussed previously, to which is added a roll moment of inertia for the sprung mass as shown in [Figure 9.5](#). The sprung mass body is represented by its mass, M_s , and roll moment of inertia, $I_{x\dot{x}s}$. Not shown is the suspension stiffness and damping on the left and right sides of the vehicle. Again, the properties of the front and rear tires and suspensions may be combined to simplify the analysis.

This model can be useful for examining the vehicle's response to suddenly applied lateral accelerations in the nature of a step input. It is also representative of the transient that occurs when a vehicle goes into a slide with the brakes locked and then experiences a sudden return of the cornering forces when the brakes are released. It may also simulate the effects of sliding from a low-friction surface onto one of a high-friction level.

The differential equations of motion in the roll plane can be written and solved analytically for the case of a step input [4]. The response of the system will be similar to that of a damped single-degree-of-freedom system exposed to a step input as shown in [Figure 9.6](#).

With the sudden acceleration input, the roll angle responds like a second-order system. When the damping is below the critical value, the roll angle rises towards the

FIGURE 9.5 Model for transient roll behavior.



equilibrium point. However, because there is roll velocity when equilibrium is reached, the sprung mass roll angle overshoots relative to the steady state roll angle value. Thereafter, the roll angle reverses and may oscillate before settling to a steady-state angle at the equilibrium position.

The fact that the roll angle can overshoot means that wheel lift-off may occur at lower levels of lateral acceleration input in transient maneuvers than for the quasi-static case. A step steer maneuver that produces a lateral acceleration level just below the quasi-static threshold can result in rollover in the transient case because of the overshoot. Thus the rollover threshold is lower in transient maneuvers.

The extent to which overshoot occurs is dependent on roll damping. [Figure 9.7](#) shows the calculated rollover threshold as a function of the damping ratio for a passenger car, SUV, and a heavy truck when subjected to a step-steer input. The lowest rollover threshold occurs when there is no damping. It rises with the damping ratio but at a diminishing rate. Even so, the benefits of roll damping are evident. The rollover threshold of the automobile increases by nearly one-third in going from zero to 50 percent of critical damping. For the automobile and the SUV the transient in a step steer maneuver will reduce the rollover threshold by about 30 percent from the “ $t > 2h$ ” value, compared to only about 10 percent for the quasi-static suspended vehicle. For the heavy truck, the reduction is nearly 50 percent [4].

Exercising this model with a sinusoidal acceleration input illustrates the effect of roll resonance on the rollover threshold. A sinusoidal acceleration is similar to the input that would be experienced in a slalom course.

Under a sinusoidal lateral acceleration, the response of the vehicle will be dependent on the frequency of the input. [Figure 9.8](#) shows the frequency dependence of the lateral acceleration threshold at which rollover (wheel lift-off) occurs for an automobile, SUV and a heavy truck. At zero frequency, the thresholds approach the steady-state values

FIGURE 9.6 Roll response to a step input.

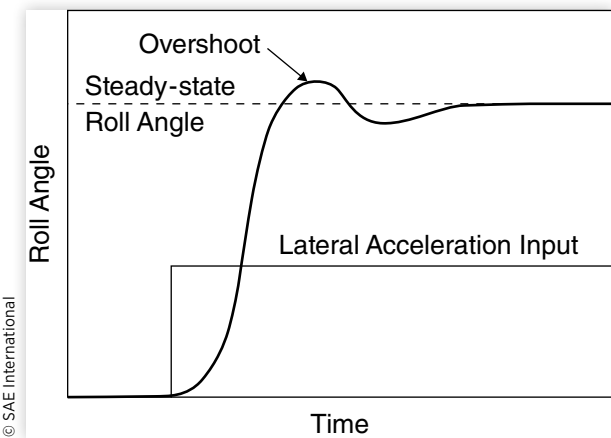


FIGURE 9.7 Effect of damping ratio on rollover threshold in a step steer [4].

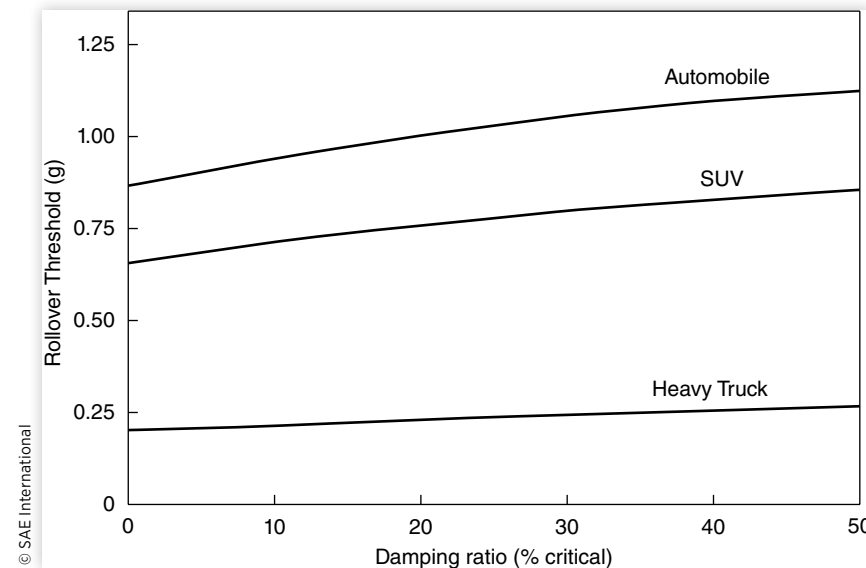
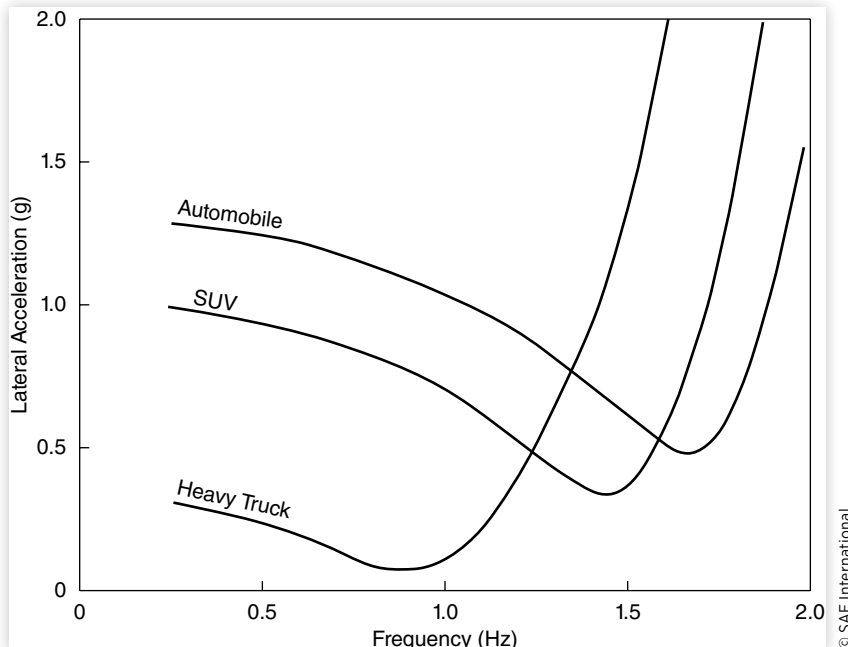


FIGURE 9.8 Rollover threshold as a function of frequency in a sinusoidal steer [4].

© SAE International

that would be obtained from the quasi-static model of the suspended vehicle. With increasing frequency the thresholds drop, going through a minimum which corresponds to the roll resonant frequency.

The roll resonant frequency for a heavy truck, which is less than one cycle per second because of its high center of gravity, makes it especially vulnerable to these dynamics. Experience has shown that “lane-change type” maneuvers executed over two seconds (one-half Hz) are well capable of exciting roll dynamics that can precipitate the rollover of heavy trucks [7]. The two-second timing is easily accomplished by the driver [8] and corresponds to the steering frequency necessary to move 8 to 10 ft laterally to avoid a road obstacle at normal highway speeds. As a result, lane change maneuvers have been identified as a common cause of heavy-truck rollover accidents [7].

The SUV and automobile, which by comparison have a lower C.G. height to track width ratio than heavy trucks, have roll resonant frequencies of 1.5 Hz and greater. In order to tune into roll resonance, a very rapid steer oscillation is necessary. Studies of driver behavior have shown that steering inputs at these frequencies are normally of low amplitude [8]. Further, they produce only minor deviations in the vehicle’s lateral position because of the attenuation of yaw response at these frequencies. (Even a relatively high-amplitude steer oscillation at 2 Hz will only cause the vehicle to move about one foot laterally.) Thus, a logical conclusion is that simple roll resonance is of less significance to rollover with passenger cars and SUVs. In order to perform lane change maneuvers or negotiate slalom courses, the timing of side-to-side oscillations is much slower (on the order of 4 seconds). Exciting frequencies below 1 Hz elicit vehicle roll response that is close to the quasi-static behavior. Therefore, from the rollover perspective, the step steer input actually represents a more challenging maneuver to these vehicles than the sinusoidal steer input.

Yaw-Roll Models

To develop the most complete and accurate picture of vehicle roll behavior, it is necessary to rely on more comprehensive vehicle models which simulate both yaw and roll responses. Yaw motions produce the lateral accelerations causing roll motions, and roll motion in turn alters yaw response through the modification of tire cornering forces arising from lateral load transfer and suspension action. A number of computer models have been developed by the vehicle dynamics community to investigate this behavior [2, 10, 11].

Using a more comprehensive model to examine sinusoidal steer reveals an additional phenomenon of importance to vehicle roll response—the phasing of front and rear tire forces. On vehicles steered by the front wheels only, a steering action causes the front tires to develop lateral force rather immediately (delayed only by the relaxation lengths of the tires), but the rear tires do not develop a force until a sideslip angle builds up. As a result, the rear tire forces exhibit a phase lag when the vehicle is subjected to a sinusoidal steer input. The phenomenon is illustrated for a passenger car in [Figure 9.9](#).

In the one-cycle-per-second sinusoidal steer maneuver shown, the lateral forces on the rear tires lag the fronts by approximately 0.2 seconds, corresponding to about a 70-deg. phase lag. The lateral acceleration, which depends on the sum of the forces, is diminished by the phase lag. If the lateral force from both front and rear tires peaked simultaneously, the lateral acceleration would reach 0.8 g rather than 0.5 g in this maneuver. At higher frequencies, the attenuation is even greater.

The effect of the phase lag is to allow the vehicle to yaw and change direction while moderating the level of lateral acceleration by spreading the acceleration over a longer time period. With passenger cars, this effect contributes to a perception of lack of responsiveness (or sluggishness) in transient cornering. Since the time lag increases with the wheelbase of the vehicle, large cars do not feel as responsive in these maneuvers as small cars. Four-wheel-steer cars invariably steer the rear wheels in the same direction as the front wheels (albeit at a lesser steer angle) to eliminate the phase lag, thereby improving responsiveness in transient cornering. It could be argued that four-wheel steer—like any other feature that enhances cornering response—may therefore contribute to behavior that increases the potential for rollover. Keeping in mind that the roll resonance frequency of passenger cars

FIGURE 9.9 Phasing of tire forces and lateral acceleration in a sinusoidal steer maneuver [4].

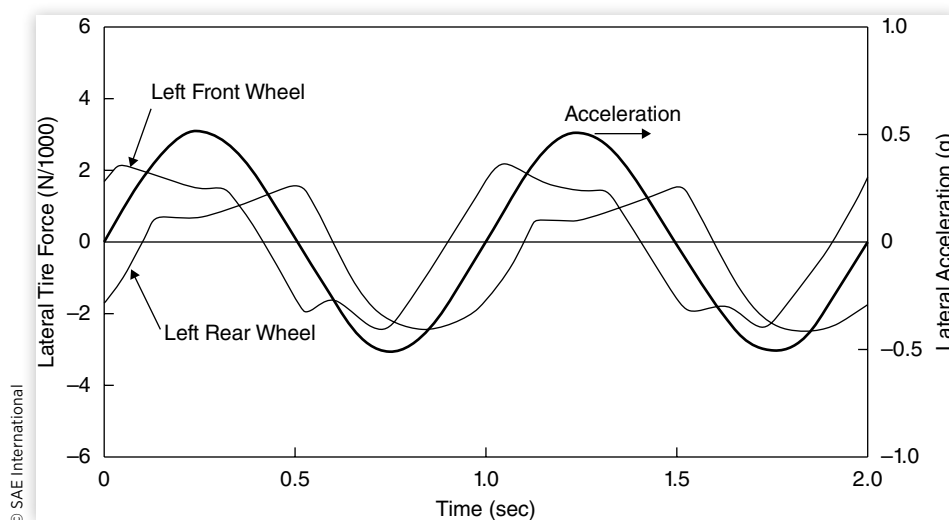
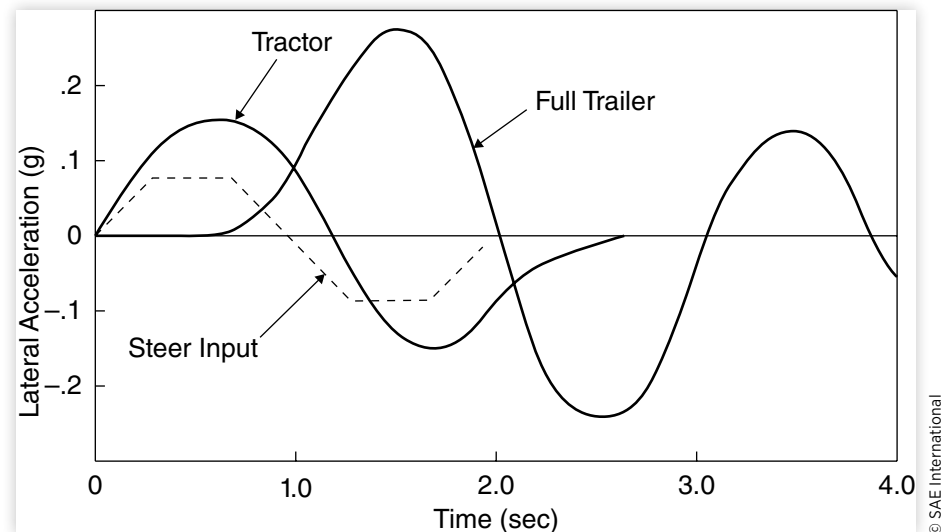


FIGURE 9.10 Lateral accelerations on a tractor and full trailer [3].

© SAE International

is in the range of 1.5 to 2 Hz, the absence of the phase lag with four-wheel steer makes it easier for a motorist to inadvertently excite roll resonance in an evasive maneuver.

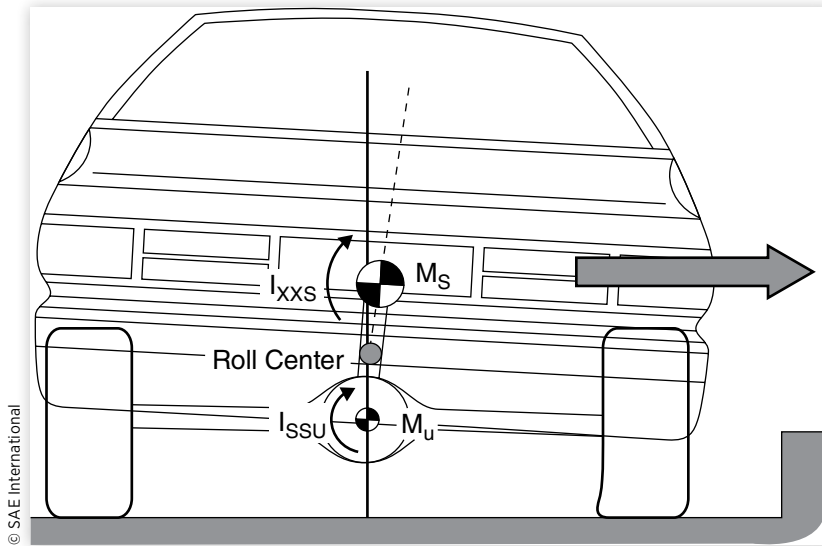
On long vehicles like school buses, trucks, and tractor-trailers, the phase lag may be very pronounced. [Figure 9.10](#) shows the lateral accelerations experienced on the tractor and full trailer of a doubles combination. (A “doubles” vehicle combination is a tractor-semitrailer pulling one or more trailers. Examples include A-doubles and B-doubles).

A sinusoidal steer input lasting two seconds in duration excites both a rearward amplification of the yaw response and roll resonance of the full trailer, such that the full trailer experiences a much larger lateral acceleration than the tractor. Because of the vehicle length, the lateral acceleration on the full trailer is almost exactly 180 degrees out of phase with the tractor. The rearward amplification, which amounts to “cracking the whip,” is recognized as very detrimental to the safety performance of doubles combinations because low-level maneuvers on the tractor are amplified and can cause the full trailer to roll over. One way to prevent this is to use a hitch arrangement between the tractor-semitrailer and the full trailer which provides roll coupling. With roll coupling, the out-of-phase lateral acceleration allows the full trailer to help the tractor-semitrailer resist rollover during the beginning of the maneuver, and the tractor-semitrailer helps the full trailer during the end of the maneuver. This feature is being used in the new generation of hitches for doubles combinations.

Tripping

A final class of rollover accidents that requires special modeling is the case where a vehicle skids laterally and impacts an object such as a curb or soft ground, resulting in a tripped rollover event. Engineering models for this phenomenon have been developed [12], with the understanding of the phenomenon under continuous development. A nonlinear eight-degree-of-freedom simulation model was developed which utilizes simple linear sub-systems to model tires, suspensions, and impact forces. The vehicle is represented by a sprung mass and an unsprung mass (combining the front and rear suspensions), as shown in [Figure 9.11](#). The masses have degrees of freedom in roll as well as lateral and

FIGURE 9.11 Vehicle approaching a tripped rollover.



vertical translation, while vehicle yaw and pitch are analyzed using a single lumped mass. The impact force for lateral wheel/curb impact is modeled using both plastic and elastic deformations. Damping effects are included through energy dissipative forces in the tires, the lateral bushing between the sprung and unsprung masses, the shock absorbers in the suspension, and the wheel/curb impact force. This model was developed for the National Highway Traffic Safety Administration (NHTSA) with public funds, and therefore should be available to anyone by request to the Administration.

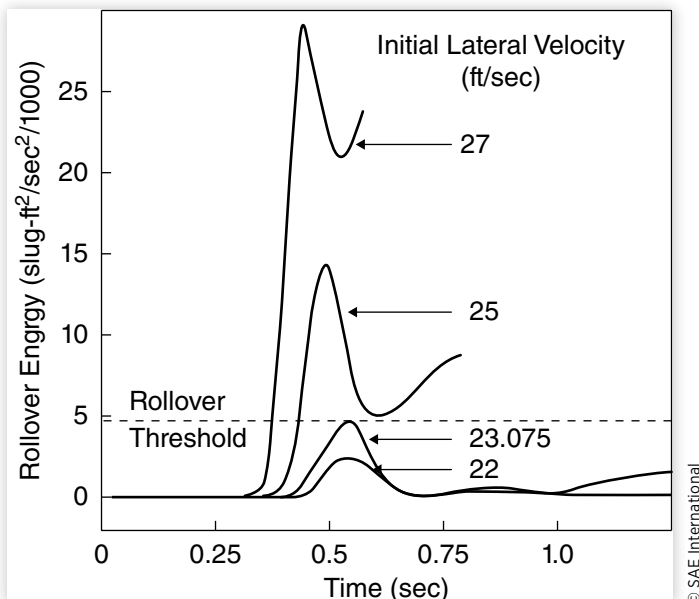
Models of this type have been used to investigate the conditions under which vehicles can experience tripped rollover, focusing on whether sufficient energy is developed in the curb impact to raise the C.G. of the vehicle to the rollover point [13]. Upon impact with the curb, roll rotation of the vehicle produces kinetic energy equal to one-half times the moments of inertia of the sprung and unsprung masses about their rotation points, times their respective rotational velocities squared. Concurrently, the lifting of the vehicle C.G. adds potential energy equal to the mass times the increase in C.G. height. If the total of these two exceeds the potential energy necessary to lift the C.G. over the outside wheels, rollover is predicted.

From an engineering perspective, this energy approach has many weaknesses because of the assumption that all of the kinetic energy is transformed to potential energy, raising the C.G. to the rollover point. It neglects additional energy input or dissipation from wheel contact with the ground during the process, and energy storage or dissipation in the tires.

Figure 9.12 shows typical examples of the results from an energy analysis of the curb impact process. The vertical axis plots the net rollover energy, which is the instantaneous total of the rotational kinetic energy plus the potential energy of the elevated C.G. The rollover threshold is the potential energy level associated with the C.G. passing over the outside wheels. If the rollover energy exceeds the threshold, rollover will occur.

In the analysis, the simulated vehicle is given an initial lateral velocity while still 7.5 ft from the curb. With a 22 ft/sec initial velocity, the impact causes a brief rise in the rollover energy level due to the kinetic energy of rotation and potential energy from elevation of the C.G. However, the net energy always remains well below the threshold, meaning rollover does not occur. With time, the energy is damped out by the suspension system.

The velocity of 23.075 ft/sec represents the case just sufficient to take the vehicle to rollover. The rollover energy rises to the rollover point, where the kinetic energy

FIGURE 9.12 Rotational energy during curb impact.

© SAE International

component nearly reaches zero. Thereafter, the energy drops as the vehicle completes the rollover. At the higher initial speeds of 25 and 27 ft/sec, rollover occurs.

This methodology was used to examine the effect of vehicle parameters on the propensity for rollover. Not surprisingly, the geometric parameters of track width and C.G. height were found to be most influential. The second most important variable is the deformation characteristics of the vehicle at impact. By spreading the impact deformation over a large distance, the energy dissipated when vehicle components are crushed reduces the amount of energy which can contribute to the vehicle's rolling motion. The weight of the vehicle appears to have little effect except as it affects the ride height, i.e., greater weight lowering the C.G. height. Likewise, the suspension stiffness and damping properties were found to be of little influence.

Accident Experience

The primary motivation for giving attention to the mechanics of rollover in vehicle design is to reduce or prevent rollover accidents. In recent years, analysts have examined accident records in an effort to identify those characteristics of vehicles that appear to be most closely correlated with rollover experience—the presumption being that the frequency of rollover accidents can be reduced by altering those correlated properties of the vehicles.

It is common practice in these studies to stratify the analyses both in the types of accidents and the types of vehicles. In the simplest treatment, the frequency of rollover in all accidents of a given make of vehicles might be considered on the assumption that all vehicles are exposed to the same general spectrum of accident types. Therefore, any atypical characteristics of those vehicles are potential causes of rollover and good design practice would argue that they should be eliminated. A flaw in this approach, however, becomes evident when it is recognized that utility vehicles experience more off-road rollover accidents than passenger cars, in part because they operate more frequently in this environment. Improving

their rollover experience by making them lower and wider can only be achieved with a penalty in off-road mobility. In the interest of normalizing accident statistics, it is then necessary to distinguish between (1) on-road and off-road accidents, (2) rollovers as the first or only event of an accident, (3) rollovers as a subsequent event, and (4) the use or exposure factors for the class of vehicle. With regard to vehicle types, they are often classified as passenger cars, utility vehicles (high C.G. four-wheel-drive vehicles used for personal transport), light trucks (used for personal transport and light hauling), and heavy trucks.

Systems Technology, Inc., in the work they have done for NHTSA [14], examined the rollover accident experience of small cars as a function of the rollover potential. A plot of some of their data is shown in [Figure 9.13](#). The rollover rate (fatal accidents per 100,000 new car years) is plotted against rollover threshold for accidents where rollover was the first event or a subsequent event in the accident. The data indicates a trend of decreasing rollover involvement as the threshold increases. However, the degree of scatter in the plot also suggests that more than just the rollover threshold is needed to explain the accident experience. For example, the Mercury Capri has three times as many rollover accidents as the Chevrolet Vega, even though they both have the same rollover threshold. Because of this broad disparity in behavior, there is no guarantee to the automotive engineer that good rollover experience is assured by increasing the rollover threshold.

Observations of this nature are common when examining rollover accident rates and have prompted analysts to hypothesize explanations for the differences in behavior between vehicle makes. A methodical analysis of rollover accident experience for passenger cars and utility vehicles was conducted by Robertson and Kelley [15] in which some of the potential explanatory factors were examined. In their work, a broader range of vehicles was considered. [Figure 9.14](#) shows their data for the number of accidents per 100,000 vehicle-years in which rollover was the “first harmful event.”

As plotted here, the data would appear to show a much more direct relationship between rollover threshold and accident rates. This impression comes about because of the inclusion of the utility vehicles (CJ-5, CJ-7, Blazer, and Bronco) which have much higher accident rates. Among the automobiles, which have thresholds ranging from 1.25 to 1.6, there is no trend evident. The high involvement of the utility vehicles has prompted

FIGURE 9.13 Rollover accident rates of small cars [14].

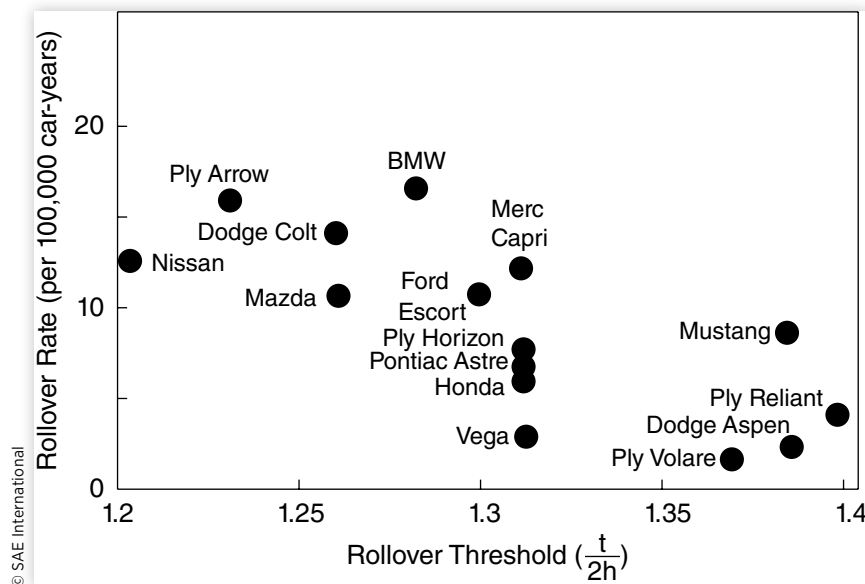
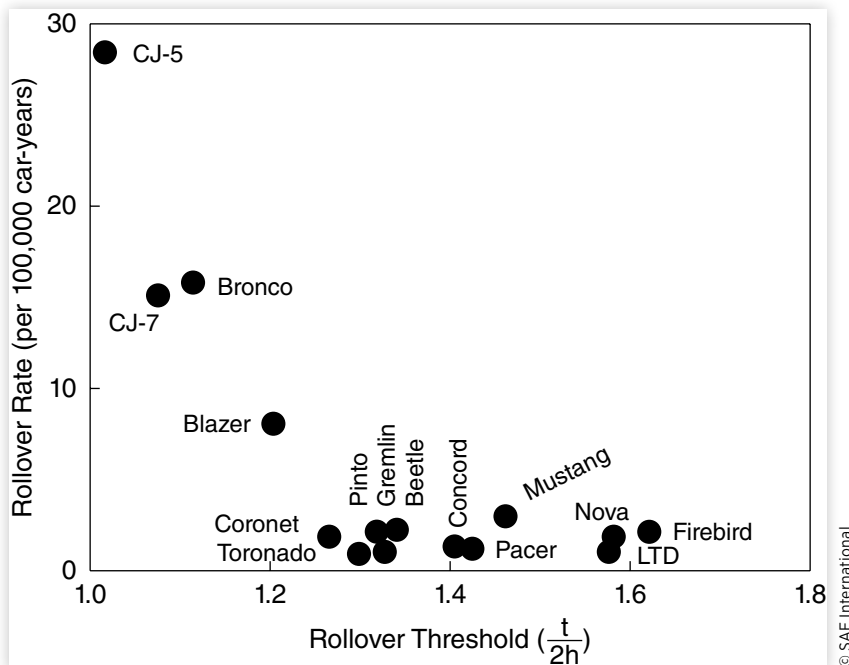


FIGURE 9.14 Rollover rates of cars and utility vehicles [15].

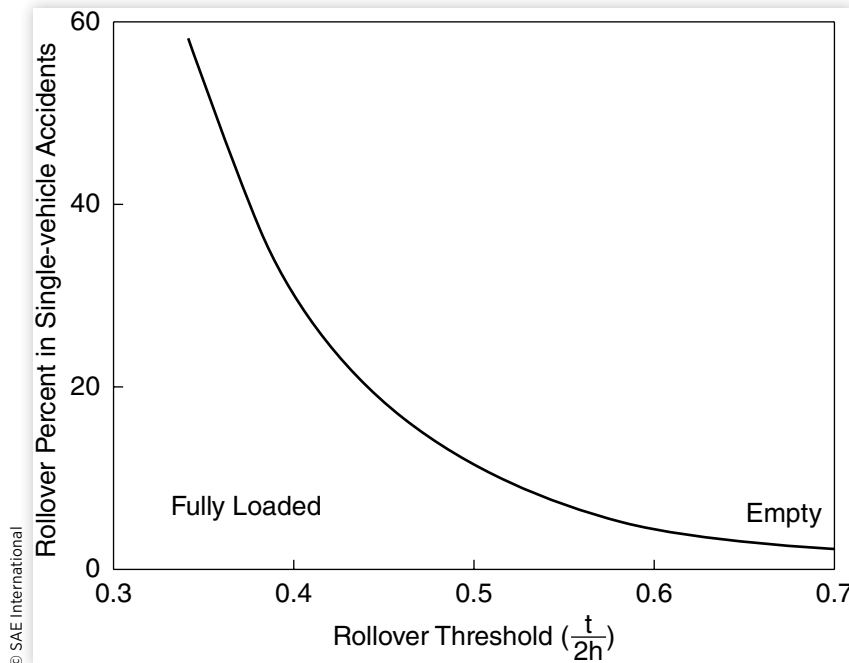
© SAE International

proposals for Federal Motor Vehicle Safety Standards (FMVSS) requiring new vehicles to have a minimum rollover threshold of 1.2. Over-involvement of utility vehicles is not unique to this study, but has been found in other studies [16, 17] as well.

The authors used the accident records to examine other factors which might be peculiar to the use of the different kinds of vehicles, as well as determine if they might be correlated to the accident experience. This allowed other potential explanations for the high frequency of rollover accidents with utility vehicles. For example, it might be argued that the type of driver most attracted to utility vehicles is one willing to take more risks and therefore is more likely to have accidents. However, when the non-rollover fatal accident rates are compared, the SUV rates are seen to be no higher than the passenger cars. When driver characteristics—suspended licenses, history of traffic violations, DWI convictions, or blood alcohol level at the time of the accident—were examined, no explanations were found.

Similarly, the road environment—urban vs. rural, interstate vs. other roads, straight vs. curved, dry vs. wet, etc.—had no correlation. The only significant environmental factor was whether the vehicle crashed on the road or after leaving it. The ratio of fatal rollover crashes on the road relative to those that left the road was substantially higher among the utility vehicles. Finally, the possibility that utility vehicles accumulate higher mileage as a potential explanation of higher rollover accident rates was examined; the conclusion was that the usage rates necessary to account for the higher accident rates were unreasonable.

In general, other reviews of accident experience confirm the conclusions reached above, even though the Robertson study is easily criticized. Numerous studies show conflicting results and interpretations [16, 17, 18] because of the uncertainty in identifying rollover threshold as the most significant variable related to rollover frequency for these classes of vehicles. In particular, the concern that other vehicle factors play a significant role appears justified. Vehicle control and handling stability are identified as important

FIGURE 9.15 Rollover frequency of tractor-semitrailers in single-vehicle accidents [3].

associated variables. Likewise, vehicle wheelbase can be shown to be correlated with rollover experience, suggesting that it is a combination of factors that must be controlled before effective action to reduce rollovers can be taken. Until those factors and interactions are known, it is considered premature to impose an arbitrary limit on rollover threshold on the industry.

Another class of vehicle that has received special attention for rollover accident experience is the heavy truck. For tractor-semitrailer vehicles, the frequency of rollover in single-vehicle accidents has been related to rollover threshold as shown in [Figure 9.15](#). This curve is derived from accident data for three-axle tractors pulling two-axle van-type semitrailers reported to the Bureau of Motor Carrier Safety (BMCS) of the U.S. Department of Transportation. The data were resolved into the illustrated format assuming a rollover threshold for each vehicle combination based on the gross vehicle weight reported to BMCS with each accident. Knowing the gross vehicle weight, the analysis assumed that payload was placed in a fashion representing medium-density freight. Typical values for tire, spring, and geometric properties were then employed to calculate the rollover threshold for each increment of gross weight in the accident file. The relationship shown here has proven to be very useful in heavy truck design for assessing the potential benefits of design alternatives which can reduce rollover experience.

Dynamic Stability Testing

Previous chapters of this book have covered different facets of vehicle dynamics, ranging from physical testing to analytical methods. In the area of dynamic stability testing, continuous effort has been underway for many decades with attempts to not only characterize the vehicles when performing certain maneuvers, but to come up with

agreed-upon methods to facilitate meaningful comparisons and help drive improvements in safety and technology.

Since its founding in the early 1970s, the United States' National Highway Traffic Safety Administration (NHTSA) (along with equivalent organizations in other parts of the world) has been investigating various vehicle dynamics maneuvers useful for evaluating the yaw stability and rollover stability of passenger vehicles and light trucks. These tests include:

- J-Turn
- Evasive Maneuver Test (i.e., moose or elk test)
- Single and Double lane changes
- Fishhook
- Sine with Dwell

Of all the electronic chassis control aids that have been installed on vehicles, the one that has proven to be the most effective at reducing single vehicle accidents is electronic stability control (ESC). According to NHTSA [19], when ESC is installed on passenger cars and light trucks, accident reduction rates for single vehicles are as follows:

- Passenger cars: 34%
- SUVs and light trucks: 59%

All told, this has the potential to save thousands of lives per year, with the following estimates:

- 5,300 - 9,600 lives per year
- 156,000 - 238,000 injuries per year

After careful consideration of these facts, the United States and other countries have mandated ESC on all new passenger cars and light trucks as covered by FMVSS 126 (USA) and UNECE R13H (United Nations Economic Commission for Europe). Under the FMVSS 126 / UNECE R13H mandates, a maneuver known as the 0.7 Hz Sine with Dwell maneuver is used [19].

Electronic Stability Control (ESC)

Although the specifics of an electronic stability control system may differ between suppliers and vehicle implementations, they all work on the same underlying premise: bring an oversteering or understeering vehicle under control by applying a correcting yaw moment (and possibly a correcting roll moment). This is accomplished by doing the following:

- Observe the direction of travel by measuring steering wheel angle, wheel speeds, lateral acceleration, vehicle slip angle, yaw rate, and possibly roll angle and roll rate.
- When metrics such as the vehicle's actual yaw rate do not match the calculated yaw rate for the specified inputs, various actions can be taken that include applying individual wheel brakes and modulating engine output torque.
- For yaw control, the goal is to generate a correcting yaw moment, returning the vehicle to a safe condition by reducing the understeer or oversteer condition.

- For roll control, the goal is to generate a correcting roll moment. This is often accomplished by temporarily locking the outside front tire, thereby reducing the available lateral acceleration that can be generated. Engine torque reduction is also common.

Sine with Dwell: ESC Performance Requirements

The full set of FMVSS 126 test procedure metrics can be found in the NHTSA documentation [19]. A summary of the criteria is shown here, and graphically in [Figure 9.16](#).

- Establish the vehicle's Lateral Stability and Responsiveness
- Run a series of Sine with Dwell tests
- Monitor the vehicle's lateral displacement and yaw rate
- Continue the test until either the vehicle fails the lateral displacement condition or the steering wheel angle input is greater than 270 deg.

[Figure 9.17](#) shows the Steering Wheel Angle input for a simulated Sine with Dwell test series. The two straight lines represent the Slowly Increasing Steer portion of the test, during which the reference steering wheel angle is established that corresponds to a lateral acceleration of +/- 0.3g.

FIGURE 9.16 Flow Chart for a simulated Sine with Dwell test series [20].

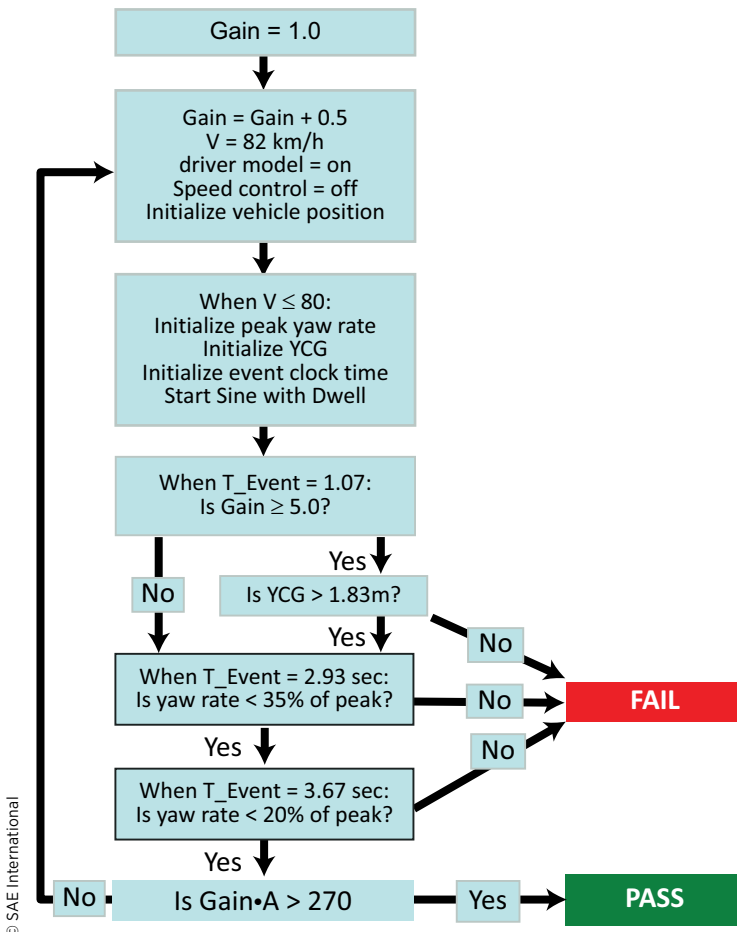
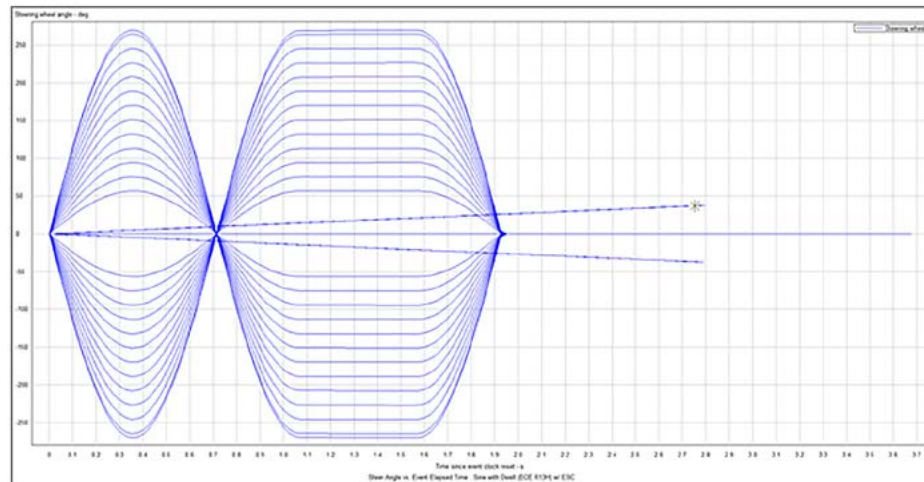
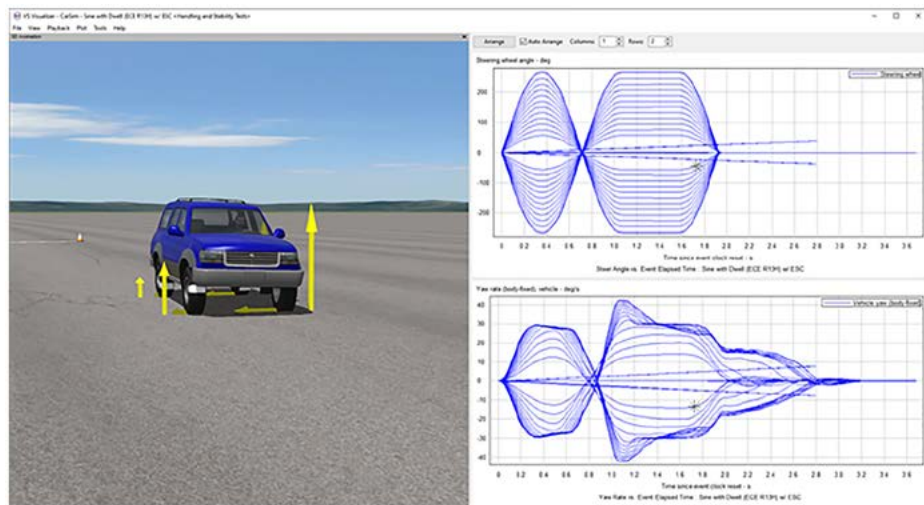


FIGURE 9.17 Steering Wheel Angle input for a Simulated Sine with Dwell test series.

© SAE International

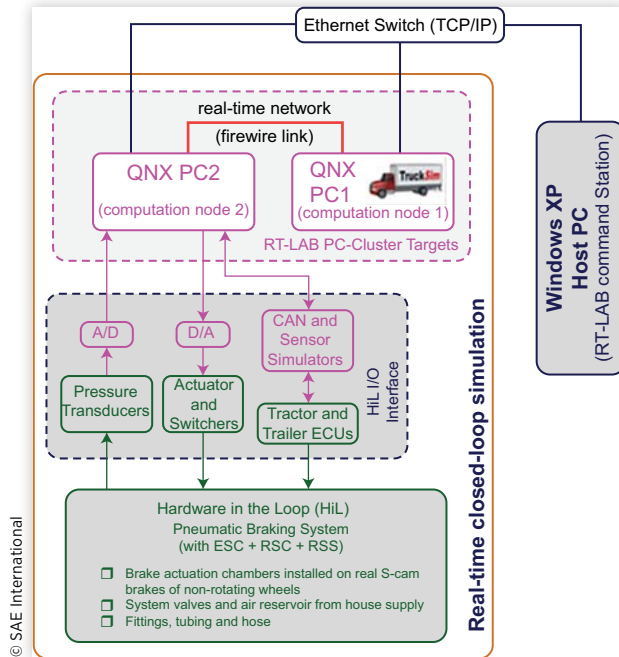
FIGURE 9.18 Simulated Sine with Dwell test series for a vehicle equipped with ESC using CarSim.

© SAE International

Hardware-in-the-Loop Testing of ESC Systems

This chapter thus far has focused on some analytical methods to evaluate the rollover characteristics of vehicles. Due to the number of vehicles to be tested by automotive and commercial vehicle OEMs along with the costs and time-constraints involved, simulation environments are used to ensure a level of coverage that is simply not feasible with physical testing. One such simulation environment is hardware-in-the-loop (HIL), combining hardware (such as physical ESC controllers and vehicle brake components) with software (such as a vehicle plant model). An example of how such a system might be organized is shown in [Figure 9.19](#) [21–22].

FIGURE 9.19 TruckSim-based HIL Platform for Evaluating ESC and Roll Stability Control [Ref. 21-22].



Fishhook Maneuver

As defined by NHTSA, the Fishhook maneuver is a test procedure that evaluates the rollover propensity of a light vehicle [23] by maximizing the roll motion. The procedure consists of one characterization maneuver and one rollover resistance maneuver.

Slowly Increasing Steer

The Slowly Increasing Steer maneuver is used to characterize the lateral dynamics of each vehicle being tested and is based on the “Constant Speed, Variable Steer” test defined in SAE J266 [24]. The goal of the test is to determine the steering input that produces a lateral acceleration of 0.3g, and the handwheel angle required to achieve this lateral acceleration defines the magnitude of the steering input used in the Fishhook maneuver.

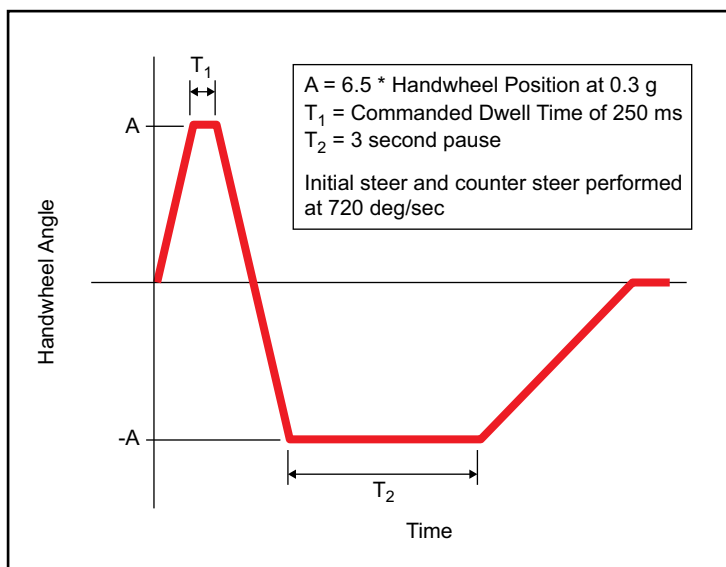
According to the NHTSA documentation [23] there are two approved methods to perform the Slowly Increasing Steer portion of the test. One of them is as follows:

- Straight driving at 50 mph (80.5 km/h)
- Increase handwheel from 0 deg to 270 deg at 13.5 deg/sec
- Hold handwheel at 270 deg for 2 seconds
- Return to 0 deg

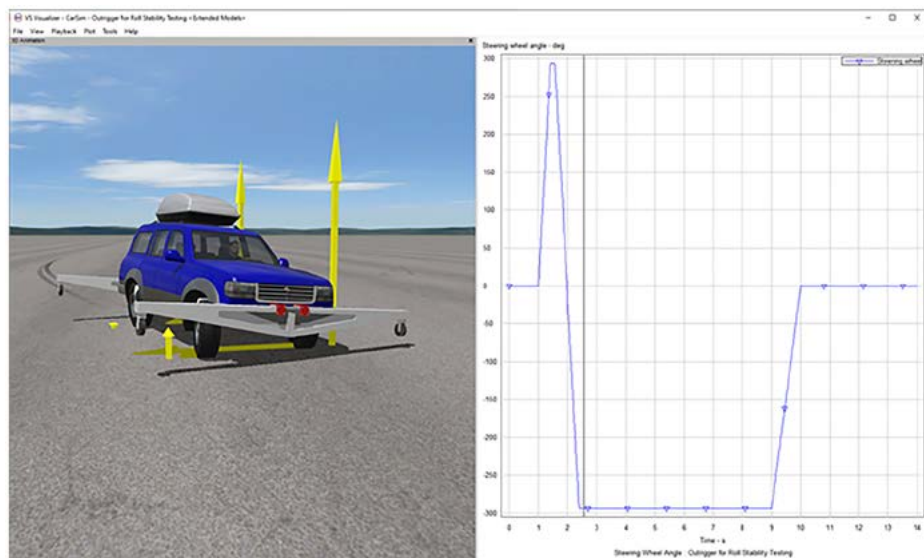
Fishhook Maneuver

The handwheel angle used for the Fishhook maneuver is calculated by taking an average of six Slowly Increasing Steer Tests (three to the left, and three to the right), then multiplied by a scalar of 6.5.

- Various test speeds are used, ranging from 35 - 50 mph (56.3 - 80.5 km/h)

FIGURE 9.20 Steering Wheel Angle Input for Fishhook Test.

© SAE International

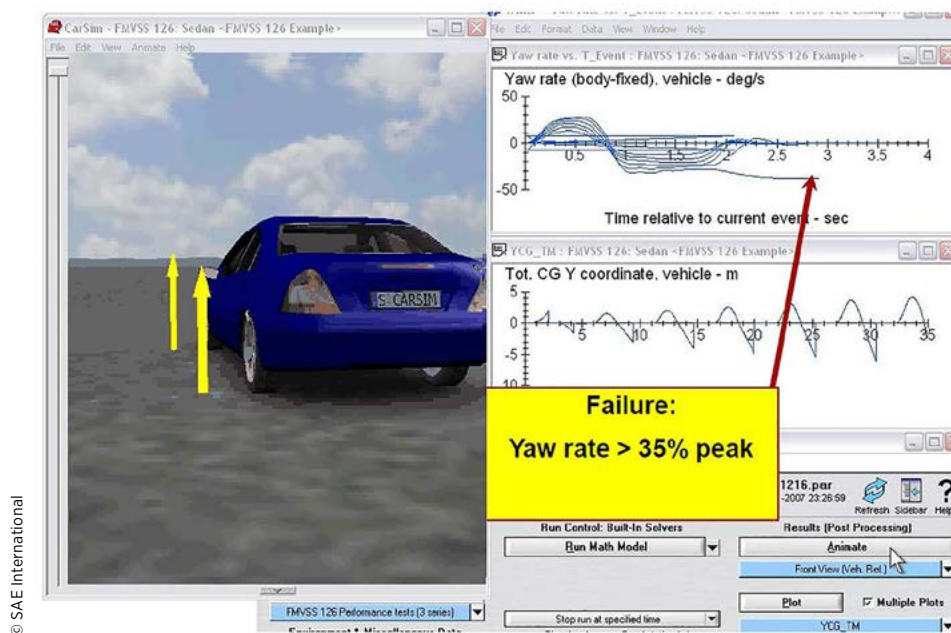
FIGURE 9.21 Simulating a Fishhook Test with CarSim.

© SAE International

- Steering input is 720 deg/sec
- The test is considered failing if two wheels lift off the ground

More detailed information can be found in the NHTSA documentation [23].

In [Figure 9.21](#), we can see the simulation results of an SUV with a rooftop payload performing a fishhook maneuver. Lift-off of the inside front tire is observable as the steering enters the dwell period and the roll momentum of the sprung mass causes it to roll onto the outside tires.



© SAE International

References

1. Gillespie, T.D. and Ervin, R.D., "Comparative Study of Vehicle Roll Stability," The University of Michigan Transportation Research Institute, Report No. UMTRI-83-25, May 1983, 42pp.
2. Ricci, L., Ed., "NCSS for Passenger Cars, January 1977-March 1979," The University of Michigan, Report No. UM-HSRI-80-36, 1980, 102pp.
3. Ervin, R.D., "The Influence of Size and Weight Variables on the Roll Stability of Heavy Duty Trucks," SAE Technical Paper [831163](#), 1983, doi:[10.4271/831163](#).
4. Bernard, J., Shannan, J., and Vanderploeg, M., "Vehicle Rollover on Smooth Surfaces," SAE Technical Paper [891991](#), 1989, doi:[10.4271/891991](#).
5. Bickerstaff, D., "The Handling Properties of Light Trucks," SAE Technical Paper [760710](#), 1976, doi:[10.4271/760710](#).
6. Gillespie, T.D. et al., "Roll Dynamics of Commercial Vehicles," *Vehicle Systems Dynamics* 9 (1980): 1-17.
7. Ervin, R.D. et al., "Ad Hoc Study of Certain Safety-Related Aspects of Double Bottom Tankers," The University of Michigan Transportation Research Institute, Report No. UM-HSRI-78-18, 1978, 78pp.
8. McLean, J.R. and Hoffman, E.R., "The Effects of Restricted Preview on Driver Steering Control and Performance," *Human Factors* 15, no. 4 (1973): 421-430.
9. Gillespie, T.D. and MacAdam, C.C., "Constant Velocity Yaw/Roll Program: User's Manual," The University of Michigan Transportation Research Institute, Report No. UM-HSRI-82-139, October 1982, 119pp.
10. McHenry, R.R., "Research in Automobile Dynamics -A Computer Simulation of General Three-Dimensional Motions," SAE Technical Paper [710361](#), 1971, doi:[10.4271/710361](#).
11. Orlandea, N.V., "ADAMS Theory and Applications," *Proceedings of Advanced Vehicle Systems Dynamics Seminar*, Swets and Zeitlinger, 1987, 121-166.

12. Rosenthal, R.J., et al., "User's Guide and Program Description for a Tripped Roll over Vehicle Simulation," Report No. DOT HS 807 140, Systems Technology Inc., 1987, 76pp.
13. Nalecz, A.G., Bindemann, A.C., and Bare, C., "Sensitivity Analysis of Vehicle Tripped Rollover Model," Final Report, Contract No. DTNH22-8-Z-0762I, University of Missouri-Columbia, July 1988, 100pp.
14. Wade Allen, R. et al., "Validation of Tire Side Force Coefficient and Dynamic Response Analysis Procedures: Field Test and Analysis Comparison of a Front Wheel vs. a Rear Wheel Drive Subcompact," Systems Technology Inc., Working Paper No. 1216-6, Contract No. DTNH22-84-D-17080 - Task 4, February 17, 1986, 50pp.
15. Robertson, L.S. and Kelley, A.B., "Static Stability as a Predictor of Overturn in Fatal Motor Vehicle Crashes," *Journal of Trauma* 29, no. 3 (1988): 313-319.
16. Terhune, K.W., "A Comparison of Light Truck and Passenger Car Occupant Protection in Single Vehicle Crashes (MVMA)," Calspan Corporation, Report No. 7438-1, September 1986, 58pp.
17. Ajluni, K.K., "Rollover Potential of Vehicles on Embankments, Sideslopes, and Other Roadside Features," *Public Roads* 52, no. 4 (March 1989): 107-113.
18. Malliaris, A.C., "Discerning the State of Crash Avoidance in the Accident Experience," *Proceedings, Tenth International Technical Conference on Experimental Safety Vehicles*, Technical Session No. 2, Crash Avoidance, July 1985, 199-220.
19. United States. National Highway Traffic Safety Administration (2007), FMVSS No. 126: Electronic Stability Control Systems. Washington, D.C.: U.S. Dept. of Transportation, National Highway Traffic Safety Administration.
20. Browalski, E., Jogi, S., Waraniak, J., Gillespie, T. et al., "ESC Performance of Aftermarket Modified Vehicles: Testing, Simulation, HIL, and the Need for Collaboration," *SAE Int. J. Passeng. Cars - Electron. Electr. Syst.* 3(2): 204-214, 2010.
21. Gordon, Tim., "HIL tests for truck ESC," *Vehicle Dynamics International*, May 2008, page 66.
22. Svenson, A., Grygier, P., Salaami, M., et al. (2009). Validation of a Hardware In The Loop (HIL) Simulation for Use in Heavy Truck Stability Control System Effectiveness Research. The 21st International Technical Conference on the Enhanced Safety of Vehicles Conference (ESV). Stuttgart, Germany. June 15 – 18, 2009. NHTSA.
23. United States. National Highway Traffic Safety Administration (2013), Laboratory Test Procedure for Dynamic Rollover: The Fishhook Maneuver Test Procedure. Washington, D.C.: U.S. Dept. of Transportation, National Highway Traffic Safety Administration.
24. "Steady-State Directional Control Test Procedures for Passenger Cars and Light Trucks," SAE J266_201811, SAE International, Warrendale, PA.



Tires

Shutterstock



Showroom with tires from multiple manufacturers.

In modern highway vehicles, all the primary control and disturbance forces which are applied to the vehicle, with the exception of aerodynamic forces, are generated in the tire-road contact patch. Thus, it has been said that “the critical control forces that determine how a vehicle person’s, brakes and accelerates are developed in four contact patches no bigger than a person’s hand.” A thorough understanding of the relationship between tires, their operating conditions, and the resulting forces and moments developed at the contact patch is an essential aspect of the dynamics of the total vehicle.

The tire serves essentially three basic functions:

1. It supports the vertical load, while cushioning against road shocks.
2. It develops longitudinal forces for acceleration and braking.
3. It develops lateral forces for cornering.

While the tire is a simple visco-elastic toroid, with modern refinement and optimization of its properties, it is a very complex nonlinear system which is difficult and complex to quantify [1]. Numerous simplified tire models have been developed in the past to approximate various performance properties [2, 3], but for the purposes of understanding their role in vehicle dynamics, it is sufficient to look to empirical data to quantify essential properties.

As a mechanical structure, the elastic torus of a tire is composed of a flexible carcass of high-tensile-strength cords fastened to steel-cable beads that firmly anchor the assembly to the rim. The internal (inflation) pressure stresses the structure in such a way that any external force causing deformation in the carcass results in a tire reaction force. The behavioral characteristics of the tire depend not only on the operating conditions, but on the type of construction as well.

Tire Construction

Two basic types of tire construction are broadly used—radial- and bias-ply tires. The two types are illustrated in [Figure 10.1](#). Bias-ply tires were the standard in the early years of the American automotive industry until about the 1960s when the advantages of radial tires (developed in Europe) became recognized. Over several decades radial tires gradually displaced bias-ply tires on passenger cars, such that they are the standard today. The acceptance on trucks has lagged that of passenger cars, such that radial and bias tires see about equal use today. Bias-belted tires had a brief life as a cross between radial and bias tires during the transition period, but are seen very little today.

Radial construction is characterized by parallel plies (rubberized fabric reinforced by cords of nylon, rayon, polyester or fiberglass) running directly across the tire from one bead to the other at a nominal 90-deg. angle to the circumference. These plies are referred to as the “carcass.” This type of construction makes for an extremely flexible sidewall and a soft ride but otherwise provides little or no directional stability. Directional stability is supplied by a stiff belt of fabric or steel wire that runs around the

FIGURE 10.1 Illustrations of bias and radial tire construction. (Courtesy of Goodyear Tire & Rubber Co.)

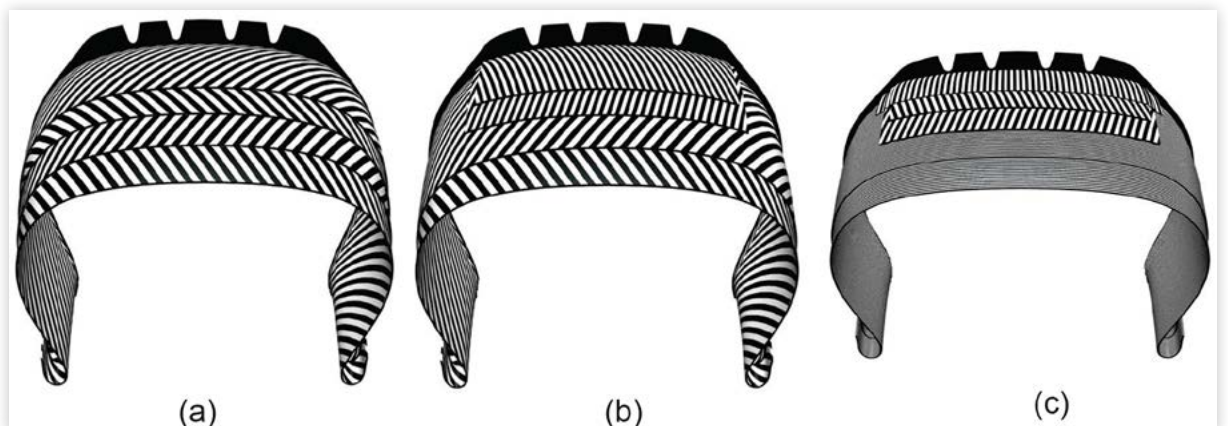
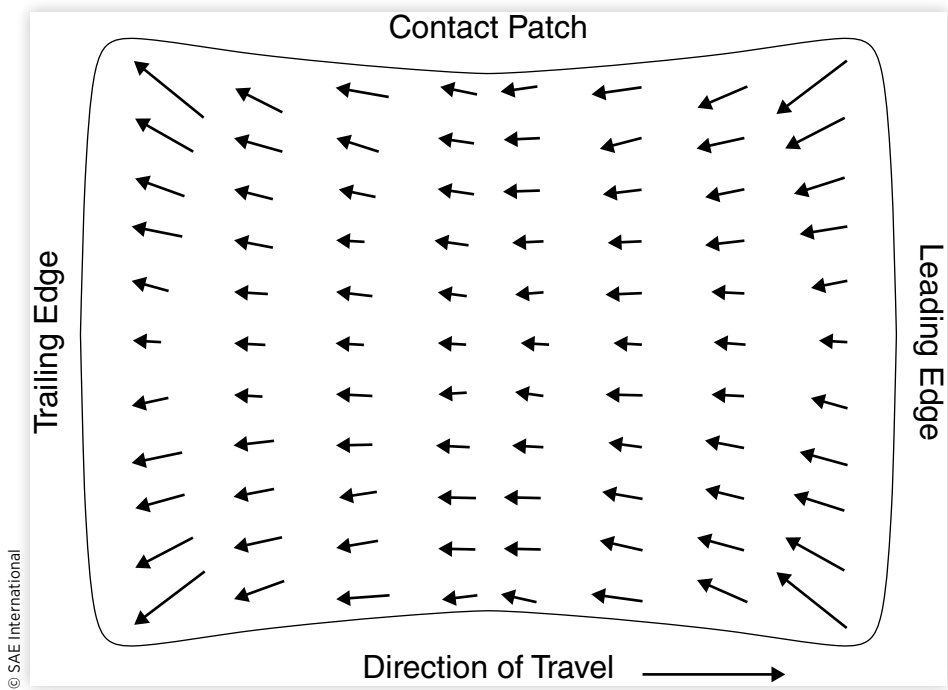


FIGURE 10.2 Squirm in the contact patch of a bias-ply tire.



© SAE International

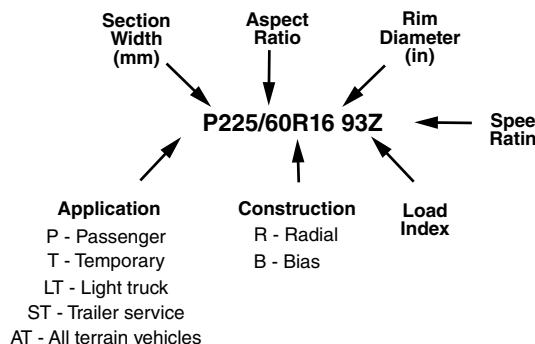
circumference of the tire between the carcass and the tread. The cord angle in the belts is normally within about 20 degrees of the tread. In cornering, the belts help to “stabilize” the tread, keeping it flat on the road despite lateral deflection of the tire. Most radial passenger-car tires have a two-ply fabric sidewall, and either one or two steel belts, or two to six fabric belts.

In bias tire construction the carcass is made up of two or more plies extending from bead to bead with the cords at high angles (35 to 40 degrees to the circumference) and alternating in direction from ply to ply. High angles result in tires which are soft for ride comfort, but low angles are best for directional stability. Although a bias-ply carcass is laterally much stiffer than a radial-ply tire, in cornering, the bias plies allow the tread to roll under, putting more load on the outer ribs. Bias construction also causes more distortion in the contact patch as the toroid deforms into a flat shape, causing the tread to squirm in the contact patch [4] when rolling, as seen in **Figure 10.2**.

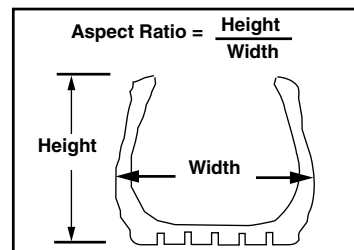
Size and Load Rating

Tire size is denoted by one of several methods, variously including the section height (distance from the bead seat to the outer extreme of the tread), section width (maximum width across the shoulder), aspect ratio (ratio of height to width) and rim diameter [5]. The Tire & Rim Association [6] defines the method of designating tire sizes and the load range for which they should be designed by the manufacturers. Bias tire size (e.g., 6.95–14) denotes the section width with the first number and the rim size with the second, both in units of inches. Radial tire size (e.g., 175R14) denotes the section width in millimeters and the rim diameter in inches. The more recent P-metric designation method (e.g., P175/70R 14) denotes passenger car (P), 175-mm section width, 70 aspect ratio, radial (R-radial, B-belted, D-bias), and a 14-in rim.

Tire Size Designation



Speed Rating	
S	- 180 km/h (112 mph)
T	- 190 km/h (118 mph)
U	- 200 km/h (124 mph)
H	- 210 km/h (130 mph)
V	- 240 km/h (149 mph)
W	- 270 km/h (168 mph)
Y	- 300 km/h (186 mph)
Z	- above 300 km/h

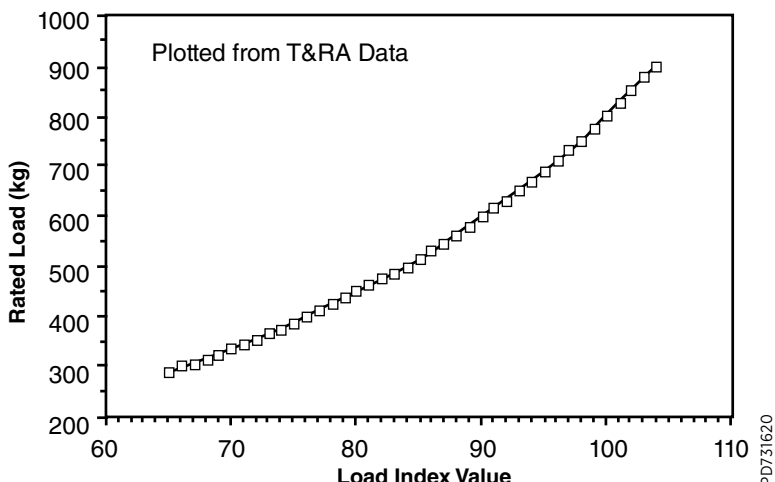


© SAE International

Tire Load Index

The last number in the code on the side of a tire is the Load Index. The Load Index is a number generally in the range of 65 to 104 for passenger car tires. Its purpose is to document the rated load capacity of the tire.

- Numerical value of the Load Index is relative – higher value indicates higher load capacity.
- The Tire & Rim Association publishes a Handbook annually that shows both the Load Index and the rated load of the tire. A plot of that data is shown below.



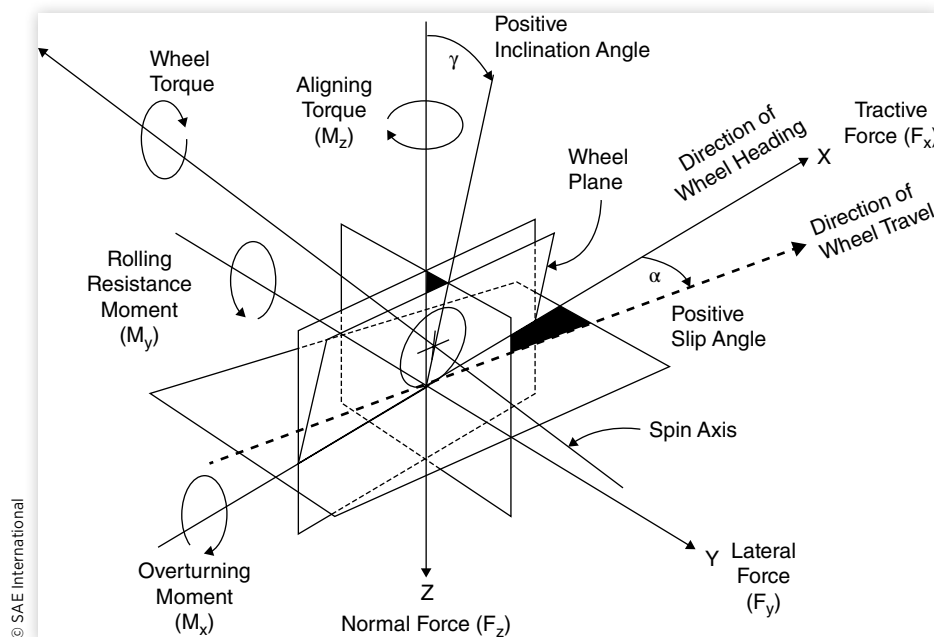
Terminology and Axis System

To facilitate precise description of the operating conditions, forces, and moments experienced by a tire, the SAE [5] has defined the axis system shown in [Figure 10.3](#). The X-axis is the intersection of the wheel plane and the road plane with the positive direction forward. The Z-axis is perpendicular to the road plane with a positive direction downward. The Y-axis is in the road plane, its direction being chosen to make the axis system orthogonal and right-hand.

The following definitions are of importance in describing the tire and its axis system.

- Wheel Plane — central plane of the tire normal to the axis of rotation.
- Wheel Center — intersection of the spin axis and the wheel plane.
- Center of Tire Contact — intersection of the wheel plane and projection of the spin axis onto the road plane.
- Loaded Radius — distance from center of tire contact to the wheel center in the wheel plane.
- Longitudinal Force (F_x) — component of the force acting on the tire by the road in the plane of the road and parallel to the intersection of the wheel plane with the road plane. The force component in the direction of wheel travel (sine component of the lateral force plus cosine component of the longitudinal force) is called tractive force.
- Lateral Force (F_y) — component of the force acting on the tire by the road in the plane of the road and normal to the intersection of the wheel plane with the road plane.
- Normal Force (F_z) — component of the force acting on the tire by the road which is normal to the plane of the road. The normal force is negative in magnitude. The term vertical load is defined as the negative of the normal force, and is thus positive in magnitude.

FIGURE 10.3 SAE tire axis system.



- Overturning Moment (M_x) — moment acting on the tire by the road in the plane of the road and parallel to the intersection of the wheel plane with the road plane.
- Rolling Resistance Moment (M_y) — moment acting on the tire by the road in the plane of the road and normal to the intersection of the wheel plane with the road plane.
- Aligning Moment (M_z) — moment acting on the tire by the road which is normal to the plane of the road.
- Slip Angle (α) — angle between the direction of wheel heading and the direction of travel. Positive slip angle corresponds to a tire moving to the right as it advances in the forward direction.
- Camber Angle (γ) — angle between the wheel plane and the vertical. Positive camber corresponds to the top of the tire leaned outward from the vehicle.

Mechanics of Force Generation

The forces on a tire are not applied at a point, but are the resultant from normal and shear stresses distributed in the contact patch. The pressure distribution under a tire is not uniform but will vary in the X and Y directions. When rolling, it is generally not symmetrical about the Y-axis but tends to be higher in the forward region of the contact patch. Both of these phenomena are shown in [Figure 10.4](#).

Because of the tire's visco-elasticity, deformation in the leading portion of the contact patch causes the vertical pressure to be shifted forward. The centroid of the vertical force does not pass through the spin axis and therefore generates rolling resistance. With a tire rolling on a road, both tractive and lateral forces are developed by a shear mechanism. Each element of the tire tread passing through the tire contact patch exerts a shear stress which, if integrated over the contact area, is equal to the tractive and/or lateral forces developed by the tire.

There are two primary mechanisms responsible for the friction coupling between the tire and the road [4] as illustrated in [Figure 10.5](#).

Surface adhesion arises from the intermolecular bonds between the rubber and the aggregate in the road surface. The adhesion component is the larger of the two mechanisms on dry roads, but is reduced substantially when the road surface is contaminated with water; hence, the loss of friction on wet roads.

FIGURE 10.4 Pressure distributions under a rolling and non-rolling tire.

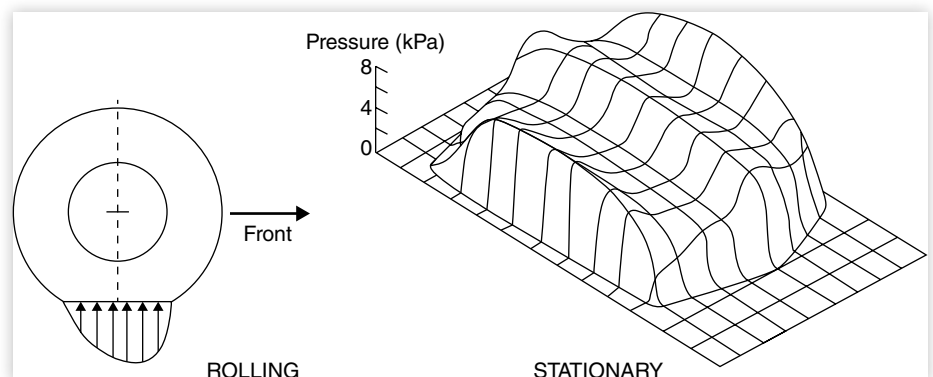
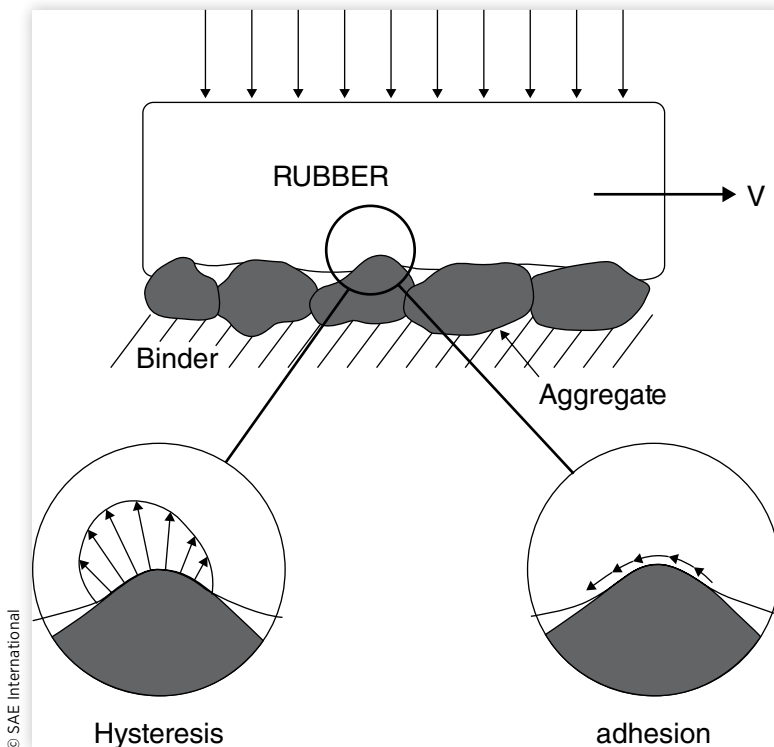


FIGURE 10.5 Mechanisms of tire-road friction.

© SAE International

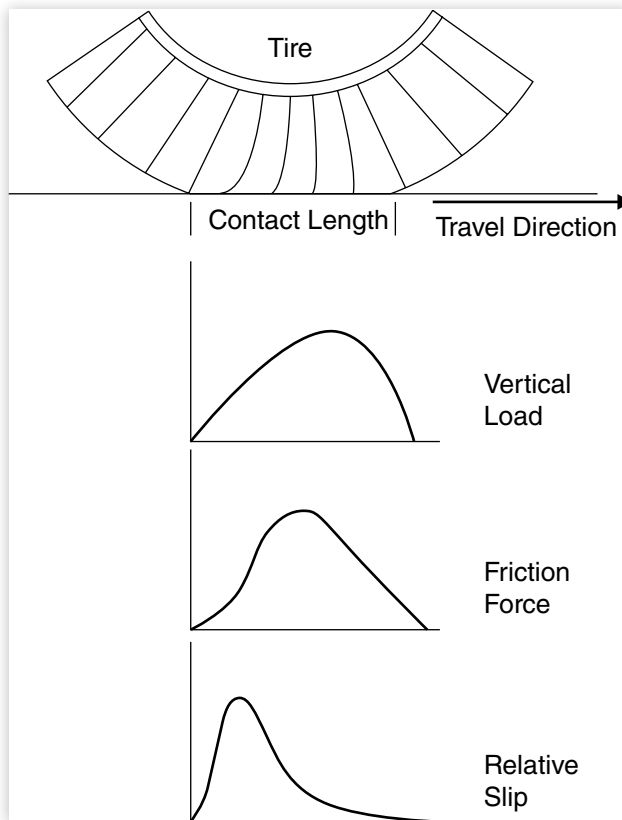
The hysteresis mechanism represents energy loss in the rubber as it deforms when sliding over the aggregate in the road. Hysteresis friction is not so affected by water on the road surface, thus better wet traction is achieved with tires that have high-hysteresis rubber in the tread. Both adhesion and hysteresis friction depend on some small amount of slip occurring at the tire-road interface.

Tractive Properties

Under acceleration and braking, additional slip is observed as a result of the deformation of the rubber elements in the tire tread as they deflect to develop and sustain the friction force. [Figure 10.6](#) illustrates the deformation mechanism in the contact patch under braking conditions.

As the tread elements first enter the contact patch they cannot develop a friction force because of their compliance, i.e., they must bend to sustain a force. This can happen only if the tire is moving faster than the circumference of the tread. As the tread element proceeds back through the contact patch, its deflection builds up concurrently with vertical load and it develops even more friction force. However, approaching the rear of the contact patch the load diminishes and there comes a point where the tread element begins to slip noticeably on the surface such that the friction force drops off, reaching zero as it leaves the road.

Thus acceleration and braking forces are generated by producing a differential between the tire rolling speed and its speed of travel. The consequence is production of

FIGURE 10.6 Braking deformation in the contact patch.

© SAE International

slip in the contact patch. Slip is defined non-dimensionally as a percentage of the forward speed:

$$\text{Slip (\%)} = \left(1 - \frac{r\omega}{V} \right) \times 100 \quad (10.1)$$

where:

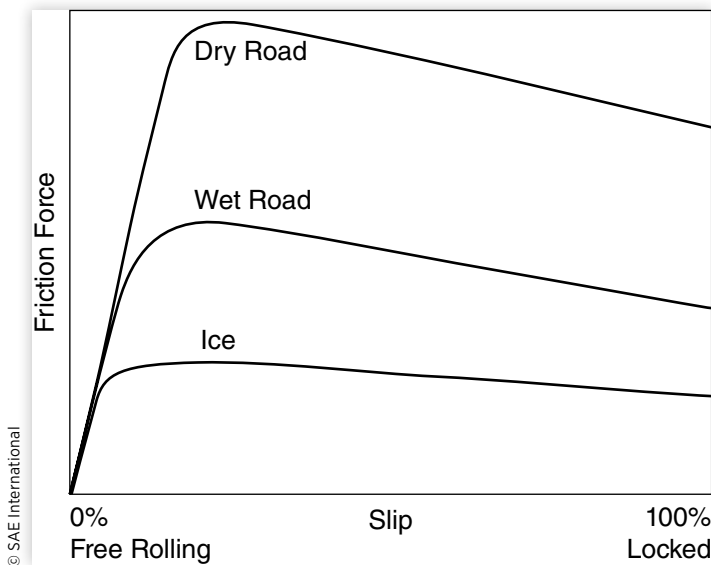
r = Tire effective rolling radius

ω = Wheel angular velocity

V = Forward velocity

Under typical braking conditions, the longitudinal force produced by a tire will vary with slip as shown in [Figure 10.7](#). As slip is applied (e.g., by brake application) the friction force rises with slip along an initial slope that defines a longitudinal stiffness property of the tire. In general, this property is not directly critical to braking performance, except at the detailed level of the design of anti-lock systems where the cycling efficiency may be affected by this property. Longitudinal stiffness tends to be low when the tire is new and has full tread depth, increasing as the tire wears. For the same reasons, rib-type treads produce a higher stiffness than lug (traction) tires.

On a dry road, when the slip approaches approximately 15–20 percent, the friction force will reach a maximum (typically in the range of 70 to 90 percent of the load) as the majority of tread elements are worked most effectively without significant slip. Beyond this point the friction force begins to drop off as the slip region in the rear of the contact

FIGURE 10.7 Brake force versus slip.

patch extends further forward. The force continues to diminish as the tire goes to lockup (100% slip).

Performance on slippery roads is qualitatively similar to dry roads, differing primarily in the peak level of friction force that can be achieved. Since the initial rate at which friction force builds up with slip is dependent on tire stiffness properties, the initial slope is the same. On wet roads, the peak friction force will typically be in the range of 25 to 50 percent of the vertical load. On ice-covered roads, the peak friction will be only 10 to 15 percent of the vertical load and will be reached at only a few percent slip. A part of the treachery of driving on ice is that not only is the friction level low, but the tire is very quick to brake to its maximum friction level.

For purposes of characterizing the traction properties of tires it is common to refer to the coefficient of friction (traction force divided by load) at the peak and slide conditions. These are referred to as μ_p and μ_s , respectively. The peak and slide coefficients are dependent on a number of variables.

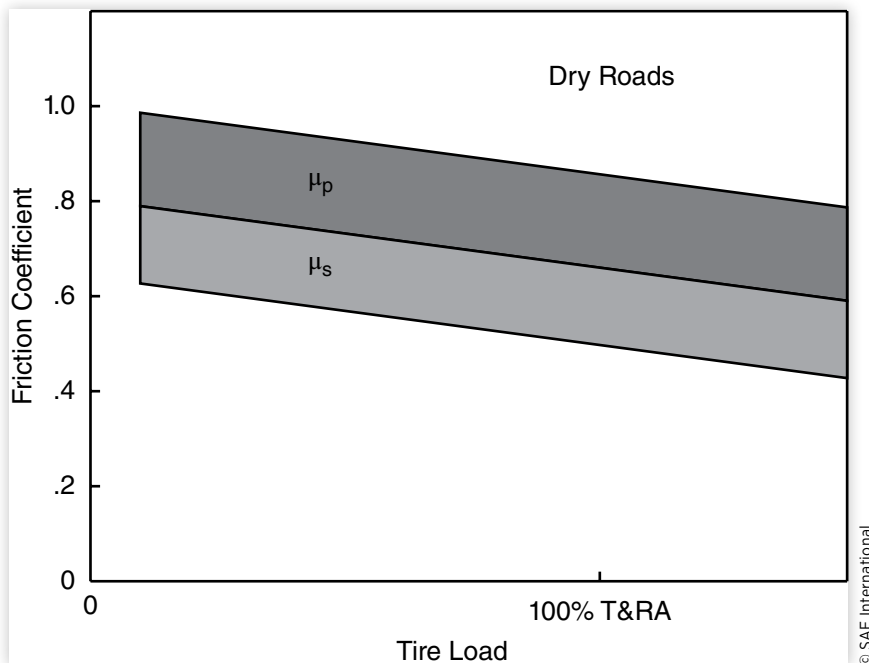
Vertical Load

Increasing vertical load is known categorically to reduce friction coefficients under both wet and dry conditions [7]. That is, as load increases, the peak and slide friction forces do not increase proportionately. Typically, in the vicinity of a tire's rated load, both coefficients will decrease on the order of 0.01 for a 10% increase in load. The general range of the coefficients of friction for passenger-car tires on dry roads as a function of load is shown in [Figure 10.8](#).

Truck tires generally exhibit lower coefficient values because of their higher unit loading in the contact patch and different tread rubber compounds.

Inflation Pressure

On dry roads, peak and slide friction coefficients are only mildly affected by inflation pressure. On wet surfaces, higher inflation pressure is known to significantly improve both coefficients.

FIGURE 10.8 Typical variation of friction coefficient with tire load.

© SAE International

Surface Friction

The road surface and its condition have a direct effect on the friction coefficient that can be achieved. Strictly speaking, a tire alone does not have a coefficient of friction; it is only the tire-road pair that has friction properties. But in the interest of characterizing the relative friction qualities of road surfaces, the highway community has developed a test method in which a “standard” tire is dragged at lockup over the surface.

This method has been standardized by the American Society for Testing and Materials as ASTM Standard Method E-274 using an ASTM Standard E-501 test tire [8]. Equipment for making these measurements is generically referred to as a “skid tester.” The testers are typically configured as a trailer pulled behind a light truck with the capability to brake one wheel of the trailer while measuring the friction force and load. The ratio of friction force to load is a coefficient of friction, which is typically less than 1. For convenience, the coefficient is multiplied by 100 and given the name Skid Number. Thus the Skid Number of 81, which is specified for dry surfaces in government braking regulations, means that the surface should exhibit a 0.81 coefficient of friction when measured with the ASTM E-274 test method. Most clean, dry roads have a Skid Number close to this value.

Skid testers also have the capability to distribute water in front of the locked wheel in a controlled fashion, such that a wet road skid number can be measured. The 30 Skid Number specification for wet road friction in government braking regulations then means that the surface should exhibit a 0.3 coefficient of friction when measured with the ASTM E-274 method under wet conditions. Bituminous asphalt roads with smooth, polished aggregate generally fall in this range when lightly wetted. Portland Cement concrete road surfaces with good texture will have a higher wet Skid Number, in the range of 45 to 50. Road surfaces coated with a bitumen material like driveway sealer (e.g., Jennite) will have Skid Numbers in the range of 20 to 25.

Speed

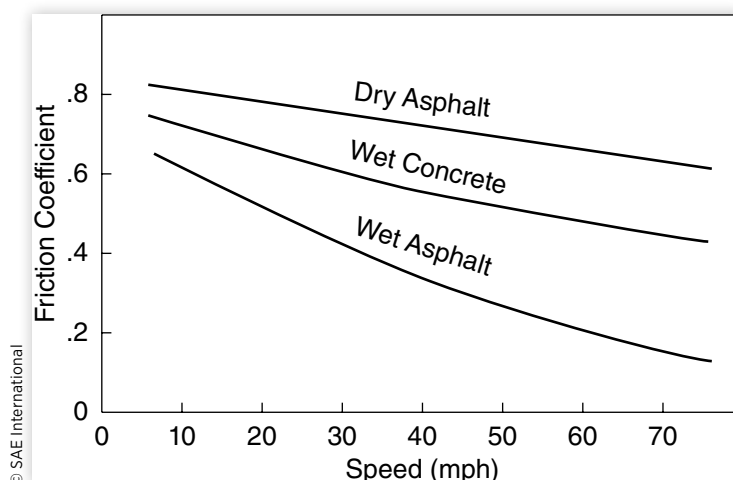
On dry roads, both peak and slide coefficients decrease with velocity as illustrated in [Figure 10.9](#). Under wet conditions, even greater speed sensitivity prevails because of the difficulty of displacing water in the contact patch at high speeds. When the speed and water film thickness are sufficient, the tire tread will lift from the road creating a condition known as hydroplaning.

Relevance to Vehicle Performance

Longitudinal traction properties are the properties of the tire/vehicle system that determine braking performance and stopping distance. The peak coefficient, μ_p , determines the limit for braking when the wheels do not lock up. Because of the weight transfer during deceleration, all wheels cannot be brought to the peak traction condition except by careful design of the braking system so as to proportion the front and rear braking forces in accordance with the prevailing loads under these dynamic conditions. In situations where one or more wheels lock up, the sliding coefficient of friction, μ_s , determines the braking contributions from those wheels. Since it is practically impossible to design a conventional braking system that can achieve exact proportioning for all combinations of load, center of gravity location, and road condition, it is inevitable that the driver will experience occasions of lockup. Therefore, the sliding coefficient of friction is an important tire performance property. With the use of anti-lock braking systems (ABS) the brake system maintains the wheels near the peak of the traction curve and does not allow lockup. Thus with ABS, the dominant tire performance parameter is the peak coefficient.

Longitudinal traction properties may also determine limiting acceleration or hill-climbing performance of a vehicle. Again, the peak coefficient is of primary importance and can be effectively utilized by the skilled driver or a traction control system. The sliding coefficient is only related in an uncontrolled attempt at acceleration. Even then, the sliding coefficient of friction (defined for the wheels-locked condition) is only an approximate indicator of the traction level that can be achieved when uncontrolled wheel spin occurs.

FIGURE 10.9 Sliding coefficient as a function of speed on various surfaces.



Cornering Properties

One of the very important functions of a tire is to develop the lateral forces necessary to control the direction of the vehicle, generate lateral acceleration in corners or for lane changes, and resist external forces such as wind gusts and road cross-slope. These forces are generated either by lateral slip of the tire (slip angle), by lateral inclination (camber angle), or a combination of the two.

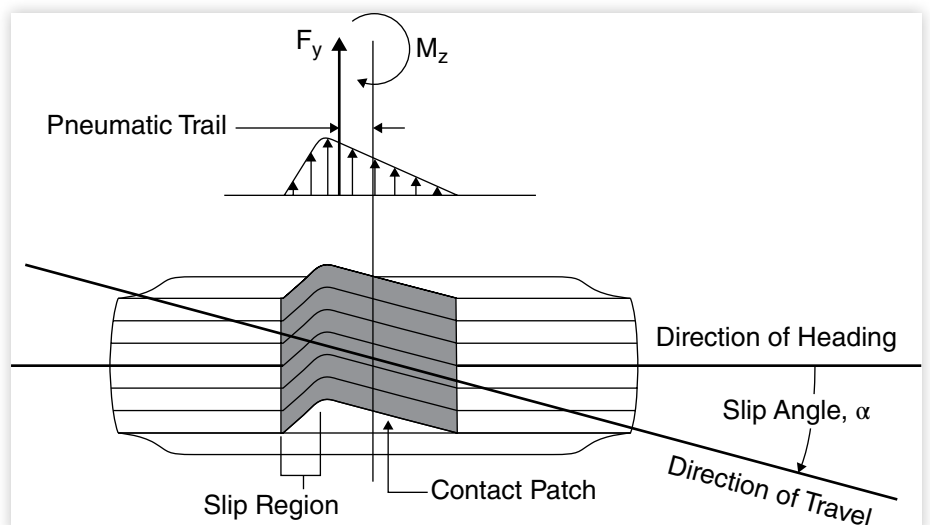
Slip Angle

When a rolling pneumatic tire is subjected to a lateral force, the tire will drift to the side. An angle will be created between the direction of tire heading and the direction of travel. This angle is known as slip angle. The mechanisms responsible can be appreciated by considering the simplified illustration of the tire's behavior as shown in [Figure 10.10](#).

As the tire advances and tread elements come into contact with the road, they are undeflected from their normal position and therefore cannot sustain lateral force. As the tire advances further at the angle of its direction of travel, the tread elements remain in the position of their original contact with the road and are therefore deflected sideways with respect to the tire. By this process, the lateral force builds up as the element moves rearward in the contact patch, up to the point where the lateral force acting on the element overcomes the friction available and slip occurs. Thus, the profile of the lateral force developed throughout the contact patch takes the form shown in [Figure 10.10](#).

The integration of the forces over the contact patch yields the net lateral force with a point of action at the centroid. The asymmetry of the force buildup in the contact patch causes the force resultant to be positioned toward the rear of the contact patch by a distance known as the pneumatic trail. By SAE convention, the lateral force is taken to act at the center of tire contact. At this position, the net resultant is a lateral force, F_y , and an aligning moment, M_z . The magnitude of the aligning moment is equal to the lateral force times the pneumatic trail.

FIGURE 10.10 Rolling tire deformation under a lateral force.



The mechanism is not an instantaneous phenomenon, but lags the actual development of slip angle because of the necessity of deflecting the tire sidewalls in the lateral direction [9]. The lag is closely related to the rotation of the tire, typically taking between one-half and one full revolution of the tire to effectively reach the steady-state force condition. The phenomenon is seen under low-speed test conditions when the tire is given a step change in steer angle. The lateral force response is then similar to that shown in [Figure 10.11](#). With the change in steer angle, the tire must roll through a half-turn or more for the lateral deflection and force to build up. This distance is often referred to as the “relaxation length.” The time lag in development of lateral force necessarily depends on the speed of rotation of the tire. At a highway speed corresponding to 10 revolutions per second of the tire, the time lag will be only about 0.05 (1/20) second, which is imperceptible to many motorists. The effect, however, may be perceptible to expert drivers as a lag or sluggishness in turning response.

The relaxation effect is instrumental in the loss of cornering force when a tire operates on a rough road surface and experiences variations in its vertical load. When the load diminishes, slip occurs over the entire length of the contact patch and the tire sidewalls straighten out. The tire must then roll through its relaxation length in order to again build up a lateral force. As a consequence, the tire is observed to have lower lateral force capability on rough roads. To achieve the best road-holding performance, the suspension should be designed to minimize tire load variations under rough road conditions.

Most commonly, the lateral force behavior of rolling tires is characterized only in the steady state (constant load and slip angle). Experimental measurements invariably exhibit the characteristic relationship to slip angle like that shown in [Figure 10.12](#). When the slip angle is zero (the tire is pointed in its direction of travel), the lateral force is zero. With the first 5 to 10 degrees of slip angle, the lateral force builds rapidly and linearly as the mechanisms shown in the previous figures take effect. In the range of 15 to 20 degrees, the lateral force reaches a maximum (nominally equal to $\mu_p \cdot F_z$) and begins to diminish as the slip region grows in the contact area. At large angles it approaches the behavior of a locked wheel, which has a lateral force equal to the sine angle resultant of the sliding coefficient of friction, μ_s , times the vertical load, F_z .

A property of primary importance to the turning and stability behavior of a motor vehicle is the initial slope of the lateral force curve. The slope of the curve evaluated

FIGURE 10.11 Lateral force response to a step steer.

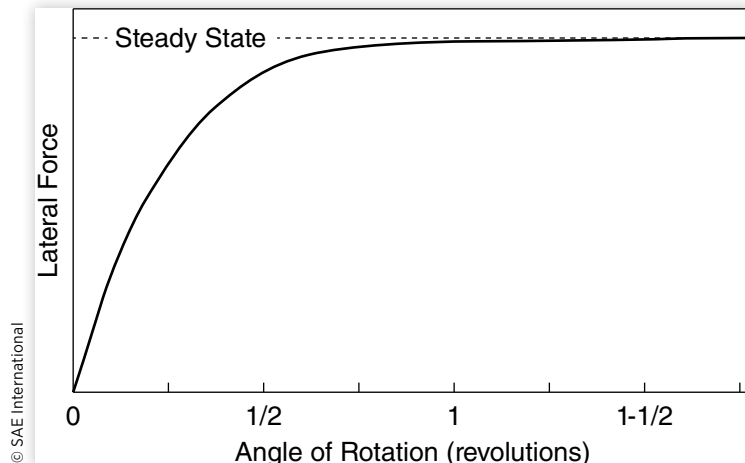
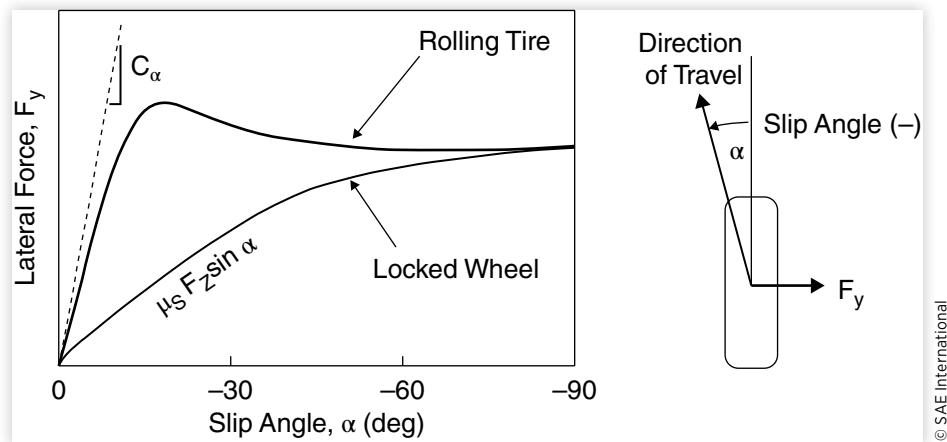


FIGURE 10.12 Tire lateral force properties.

© SAE International

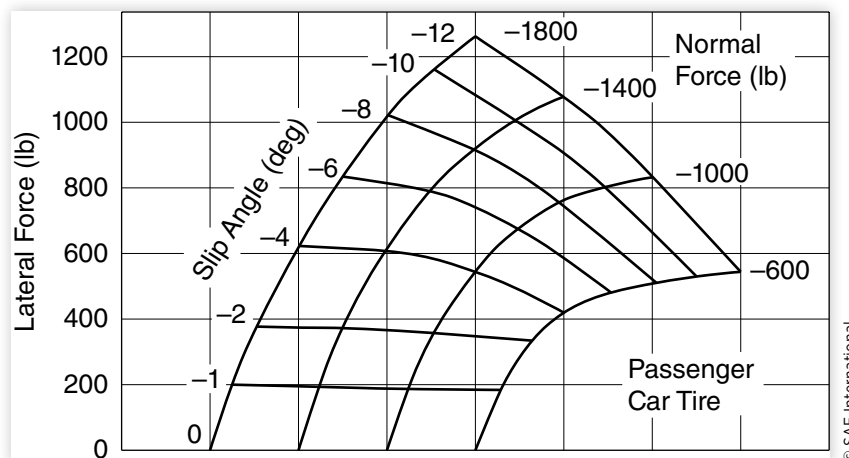
at zero slip angle is known as the “cornering stiffness,” usually denoted by the symbol C_α .

$$C_\alpha = -\left. \frac{\partial F_y}{\partial \alpha} \right|_{\alpha=0} \quad (10.2)$$

It should be noted that by the SAE convention, a positive slip angle produces a negative force (to the left) on the tire, implying that C_α must be negative. For that reason, the slip angles in the figure are labeled with negative angles. In order to get around this problem, the SAE defines cornering stiffness as the negative of the slope, such that C_α takes on a positive value. A positive convention for C_α is used throughout this text.

Tire cornering properties as a function of load and slip angle are often shown in the form of a carpet plot as seen in [Figure 10.13](#).

The vertical axis is the scale of lateral force. The horizontal axis is a scale for both the slip angle and normal force. Note that both the slip angle and normal force are shown as negative numbers—negative slip angle produces a positive lateral force, and negative normal force is a positive vertical load. The load can be shown as positive if it is labeled

FIGURE 10.13 Carpet plot of lateral force due to slip angle for a bias-ply tire.

© SAE International

"vertical load." The carpet plot provides a convenient format for mapping the properties of a tire.

The cornering stiffness is dependent on many variables. Tire size and type (radial versus bias construction), number of plies, cord angles, wheel width, and tread design are significant variables. For a given tire, the load and inflation pressure are the main variables.

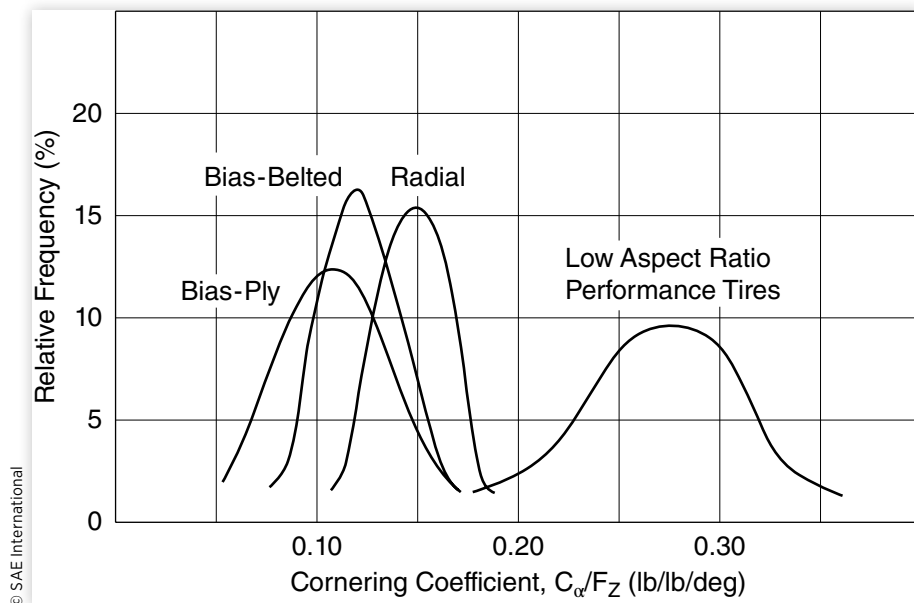
Tire Type

On average, radial tires have a higher cornering stiffness than bias-ply tires. This is illustrated in [Figure 10.14](#), which shows the cornering coefficient for a population of radial, bias, and bias-belted tires used on passenger cars.

The cornering coefficient is the cornering stiffness normalized by the vertical load. For bias-ply tires, the cornering coefficient is about 0.12 lb/lb/deg. This means that at 1 deg. of slip angle, the average bias-ply tire will produce a lateral force that is 10 percent of the vertical load. Radial tires of similar aspect ratio are on average stiffer, producing a lateral force at the same condition that is approximately 15 percent of the vertical load. As seen in [Figure 10.14](#), the properties of bias-belted tires fall between those of radial and bias-ply tires. Although it is a general rule that radial tires have greater cornering stiffness than bias tires, as the distribution illustrates, the opposite may be true among some tires in the population.

By far, one of the greatest influences on tire cornering properties is the aspect ratio—the ratio of section height to section width. For years, the more common passenger-car tires have had aspect ratios from 0.78 down to 0.70, yielding the cornering coefficient properties just described. The trends toward lower-aspect-ratio performance tires (0.60 and lower) on passenger cars have resulted in tires with much higher cornering coefficients. These tires with cornering coefficients in the range of 0.25 to 0.30 and above, have given passenger cars much quicker and precise cornering behavior.

FIGURE 10.14 Frequency distribution of cornering coefficient for passenger-car tires.



Load

Although cornering force at a given slip angle rises with vertical load on the tire, it does not rise proportionately with load. By and large, the maximum cornering force per unit load occurs at the lightest loads. The effect of load can be seen in [Figure 10.15](#) as it affects both the cornering stiffness and the cornering coefficient. Characteristically, the stiffness versus load curve is always concave down, a property that has some significance to the understeer gradient.

Load also decreases the peak coefficient of friction that can be achieved in cornering. Over the range of 50 percent to 125 percent of rated load, the peak friction level may decrease by more than 20 percent.

Inflation Pressure

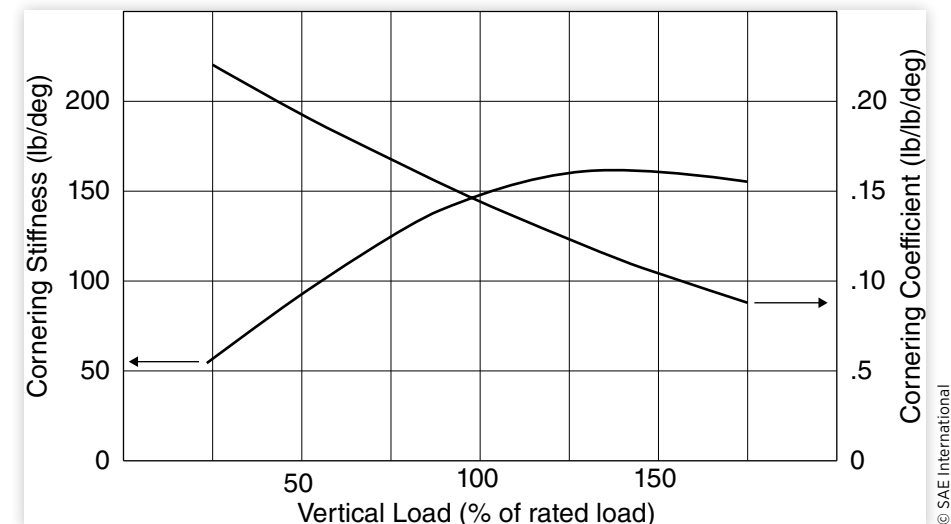
Since inflation pressure increases carcass stiffness but reduces contact length, the net influence on cornering stiffness cannot be generalized across all types of tires [7]. It is generally accepted that increasing inflation pressure results in increasing cornering stiffness for passenger-car tires. Because of the monotonic and rather strong relationship between cornering stiffness and inflation pressure, it was common practice in the past to control the low-g directional behavior of passenger cars through the specification of different inflation pressures for front and rear tires. This practice is no longer common. In the case of truck tires, the influence of inflation pressure on cornering stiffness is varied and dependent on obscure sensitivities to details of the tire carcass design.

Inflation pressure also has a strong influence on the peak traction level that can be achieved under slip angle conditions. Tire inflation pressure has the largest influence on lateral force production at high loads, and tires at reduced inflation pressures arrive at lateral force saturation at substantially higher values of slip angle.

Size and Width

For a given load condition, larger or wider tires exhibit a greater cornering stiffness. This effect is attributable to the contribution of carcass stiffness to cornering stiffness.

FIGURE 10.15 Effect of load on cornering performance.



Larger tires generally have a higher load capacity. Thus, at the same load as a smaller tire, the larger tire will be operating at a lower percentage of its rated load and will in effect have greater cornering stiffness. For tires of the same nominal size but greater width (lower aspect ratio), those with the greater width will generally have a higher carcass stiffness resulting in greater cornering stiffness. The same effect can be accomplished by increasing rim width for a given tire.

Tread Design

The lateral compliance of the tread rubber acts as a series spring in the generation of lateral force response to slip angle; therefore, tread design has a potential influence on cornering stiffness. Among bias-ply tires, it is generally recognized that snow-type tread designs produce lower cornering stiffness levels than do rib-tread designs. It is not clear that this trend holds true for radial tires. In general, changes in the tire's tread design that produce a more open pattern with deeper grooves and less support from one tread block or rib element to another will effect greater lateral compliance in the tread, and therefore see a reduction in the cornering stiffness.

It is not known whether sensitivities of cornering stiffness to tread compound have been demonstrated. Presumably, increases in rubber durometer (i.e., the hardness of the material) produce higher stiffness, and therefore one could expect a stiffness increase with the rubber durometer value. The sensitivity would be expected to be small, however.

Relevance to Vehicle Performance

Cornering stiffness is one of the primary variables affecting steady-state and transient cornering properties of vehicles in the normal driving regime. Understeer gradient, the characteristic commonly used to quantify turning behavior, is directly influenced by the balance of cornering stiffness on front and rear tires, as normalized by their loads. A higher relative cornering stiffness on the rear wheels is necessary to achieve understeer. Higher stiffness on the front wheels will produce oversteer, unless compensated by other factors, and results in a vehicle that has a critical speed above which it becomes unstable.

Camber Thrust

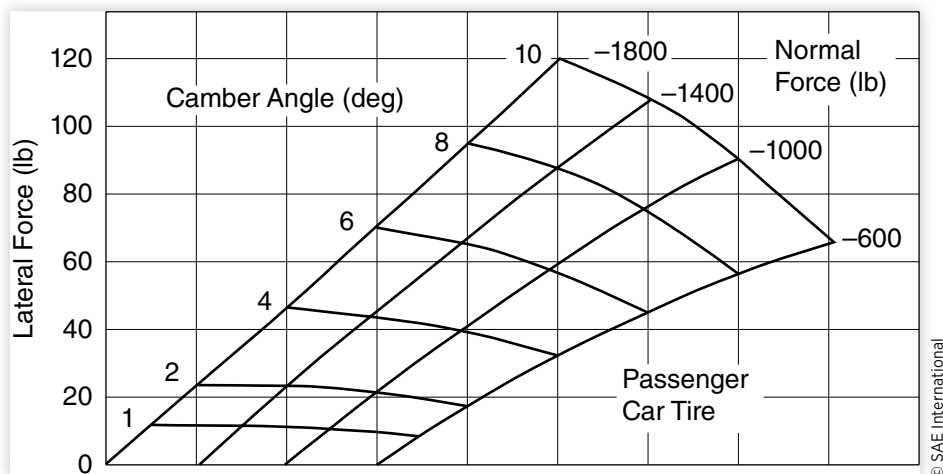
A second means of lateral force generation in a tire derives from rolling at a non-vertical orientation, the inclination angle being known as camber angle. With camber, a lateral force known as "camber thrust" is produced. The inclination angle is defined with respect to the perpendicular from the ground plane such that a positive camber angle corresponds to an orientation in which the top of the wheel is tipped to the right when looking forward, along its direction of travel (see the SAE tire axis system, [Figure 10.3](#)). Note that on a vehicle, positive camber occurs when the wheel leans outward at the top. This means the direction of positive camber differs from side-to-side on a vehicle, and the relationship to a positive lateral force is complicated by that fact. It is sufficient to recognize that the force is always oriented in the direction the tire is inclined.

As with slip angle, the lateral force due to camber angle is characterized by the initial slope of the curve, termed the camber stiffness, C_γ , and is defined in the equation:

$$C_\gamma = -\frac{\partial F_y}{\partial \gamma} \Big|_{\gamma=0} \quad (10.3)$$

As an absolute value, the camber stiffness of a tire is typically in the range of 10 to 20 percent of the cornering stiffness. [Figure 10.16](#) provides a carpet plot of lateral force as a function of camber and load for a typical passenger-car tire.

FIGURE 10.16 Carpet plot of lateral force due to camber angle for a bias-ply tire.



Tire Type

Large changes in camber stiffness are known to accompany differences in tire construction. [Figure 10.17](#) shows the camber stiffness distributions for a population of radial, bias, and bias-belted tires. The camber stiffness for low-aspect-ratio performance tires is in the same range as other radial tires shown. The stiffness for radial passenger-car tires is generally only about 40 to 50 percent of that for bias-ply tires.

The camber coefficient is a particularly important tire property with regard to how a tire responds to surface discontinuities oriented along the direction of travel, such as ruts in the wheelpath, faulting between lanes, shoulder dropoffs, railroad tracks, etc. When a vertically oriented tire operates on a surface with a cross-slope (such as the side of a rut in the wheelpath), the horizontal component of its load acts to push the wheel toward the lowest part of the rut as shown in [Figure 10.18](#).

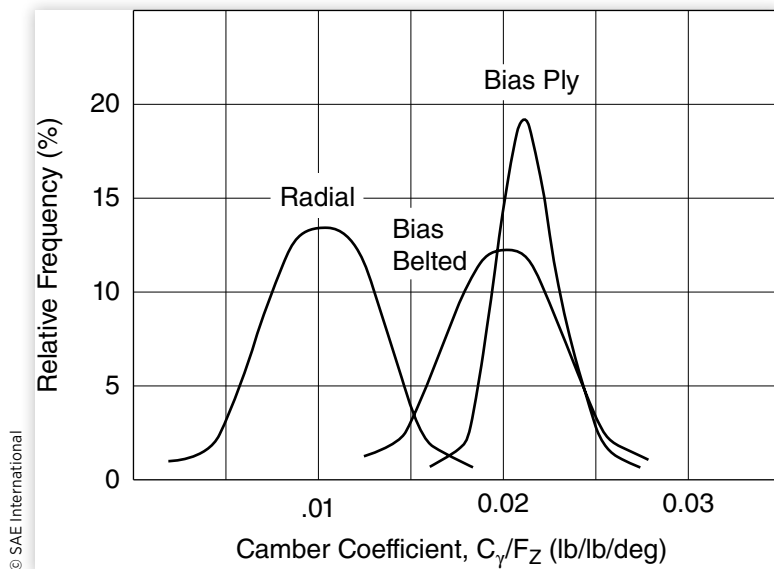
The lateral force per unit load is:

$$\frac{F_y}{W} = \sin \gamma' \approx \gamma' \quad (10.4)$$

where:

W = Weight on the tire

γ' = Inclination angle of the road surface

FIGURE 10.17 Frequency distribution of camber coefficient for passenger-car tires.

At 1 deg. of surface cross-slope angle, a lateral force of $1/57.3 = 0.0175$ lb/lb is produced in the “downhill” direction by the gravitational component. On the other hand, the camber thrust from the tire acts to push the tire “up” the slope in proportion to its camber coefficient. If the camber coefficient is greater than 0.0175 lb/lb/deg, the tire will try to climb out of the rut. If it is less, it will tend to run down to the bottom of the rut and track in that position.

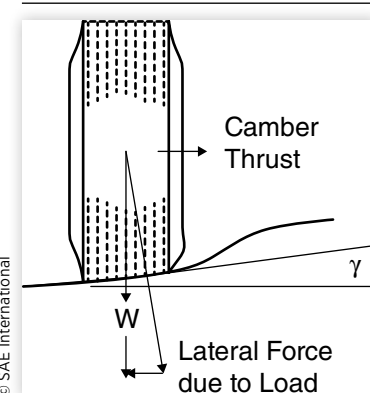
As seen in **Figure 10.17**, radial- and bias-ply tires fall on opposite sides of that boundary, such that radial tires will tend to run in a rut while bias-ply tires will tend to climb out of the rut. With the high proportion of radial tires being used on modern trucks, it has been postulated that this tracking tendency may be one of the primary factors responsible for the dual wheel ruts that frequently develop on asphalt roads.

Load

As indicated by the typical bias-ply car tire in **Figure 10.16**, camber stiffness is only slightly affected by vertical load in the vicinity of the design load. Over the range of 600 to 1800 lb load, the stiffness increases only about 20 percent.

Inflation Pressure

There is no general rule concerning the sensitivity of camber stiffness to inflation pressure. Limited data available tend to show some increase in camber stiffness with inflation

FIGURE 10.18 Forces acting on a tire on a cross-slope surface.

pressure for bias-ply tires (0.25 lb/deg per psi), whereas radial tires are relatively insensitive to changes in pressure [7].

Tread Design

Camber stiffness is sensitive to the gross compliance properties of the tire tread, increasing substantially with tread stiffness. More compliant treads such as those used for open-pattern snow tires will be lower in camber stiffness by factors of 20 to 40 percent. For the same reasons, camber stiffness will go up as the tread wears.

Other Factors

Surface texture has no effect on camber stiffness except as it affects the limiting level of the frictional coupling. Likewise, the presence of water on the surface should have no significant effect. Because of the mechanisms involved, speed should have negligible effect on camber stiffness, except at very high values where centrifugal loading may act to stiffen the tire.

Relevance to Vehicle Performance

Camber thrust is the primary cornering force by which motorcycles and other two-wheeled vehicles are controlled. On passenger cars and trucks, camber thrust contributes to understeer behavior, but normally as a secondary source. On vehicles with independent suspensions where significant camber angles may be achieved, this mechanism may contribute up to about 25 percent of the understeer gradient. On vehicles with solid axles, little camber can occur such that its contribution to turning performance is even less.

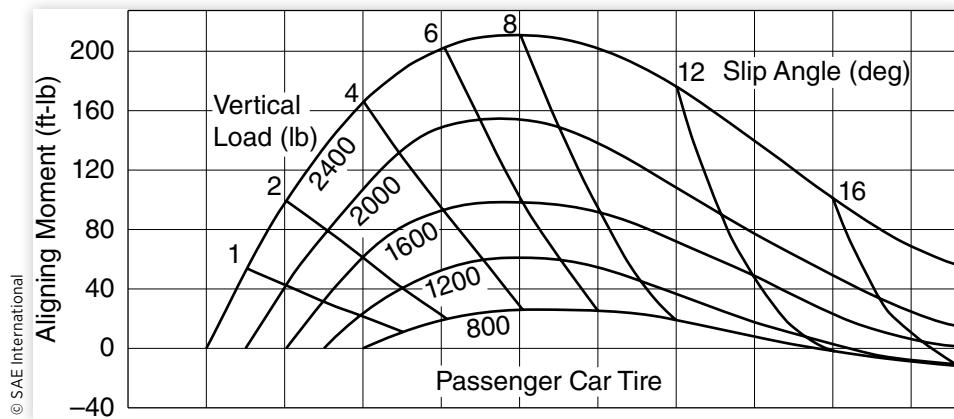
Aligning Moment

Because the shear forces in the contact patch of a tire operating at a slip angle develop with their centroid aft of the tire centerline, an aligning moment or torque is generated about the vertical axis. Although this moment is only a small contribution to the total yaw moments on a vehicle, it nevertheless contributes to reactions in the steering system which may have a more substantial effect overall. It should be noted that positive aligning moment always attempts to steer the tire in the direction it is traveling and therefore has a stabilizing influence on the vehicle.

Slip Angle

A typical carpet plot showing the influence of both slip angle and vertical load on aligning moment is given in [Figure 10.19](#). Both radial and bias-ply tires possess aligning moment characteristics similar to those shown, although on average the moment is larger with radial tires. Typically, bias-ply tires will have an aligning moment coefficient (aligning moment per pound load) of approximately 0.033 ft-lb/lb/deg, whereas radial tires have a coefficient on the order of 0.043 ft-lb/lb/deg.

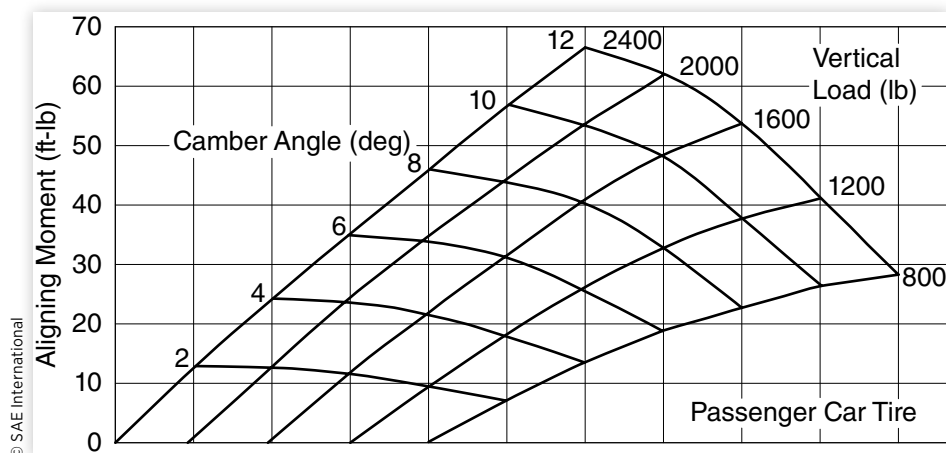
The aligning moment is very sensitive to the size of the contact patch and the growth of the slip region. The shear stress and the torque arm responsible for the moment are both proportional to the distance from the tire center. Thus the major contributors to aligning moment are the tread elements at the extremes of the contact patch. The moment

FIGURE 10.19 Carpet plot of aligning moment versus slip angle and load.

rises with the increasing shear forces up to about 8 degrees of slip angle. At greater angles, however, the growing slip region erodes the extremities and causes a decrease in the aligning moment. At very high slip angles, the slip region advances forward such a distance that the aligning moment can actually become negative.

A high sensitivity to vertical load is seen in the plots. This sensitivity arises from the influence of contact area on the moment. Although doubling the load nominally doubles the contact area, all the increase in area occurs at the extreme regions of the contact patch, i.e., the regions that most affect the aligning moment. As a result, aligning moment increases in an accelerated fashion with load.

An aligning moment is also produced when a tire rolls at a non-zero camber angle. As shown in [Figure 10.20](#), a bias-ply tire produces aligning moments due to camber which are on the order of 10 percent of the magnitude produced in response to slip angle. For radial tires, aligning moments due to camber angle are substantially lower than those measured for bias tires. The aligning moment coefficient (aligning moment per pound load) due to camber will be approximately 0.003 ft-lb/lb/deg for bias-ply tires, versus 0.001 ft-lb/lb/deg for radial tires. With regard to sensitivity to operating variables, as a general rule, influences which increase lateral force level also tend to increase aligning moment due to camber.

FIGURE 10.20 Carpet plot of aligning moment versus camber angle and load.

Path Curvature

Whereas the aligning moments discussed so far arise from a tire generating lateral force by traveling in a straight line with either slip or camber angle, aligning moments are also created when a tire is forced to roll on a curved path regardless of the fact that lateral force is not generated. In effect, a torque must be applied to the tire about the vertical axis to force it to roll on a curve when under load. Such conditions are seen when a vehicle is turned at low speed, or when the wheels are steered with the vehicle stationary such that they are forced to roll on the small-radius path of the scrub radius. Little experimental data is available to quantify behavior under this condition, but [Figure 10.21](#) shows the aligning moment generated by a truck tire on a dry road surface [10]. At zero radius, large torques are required to rotate the tire about the steer axis. The aligning moment goes up disproportionately with load because the increase in contact area that occurs with an increase in load must always occur at the perimeter of the contact patch, and it is the shear in the perimeter region that has the largest contribution to the aligning moment.

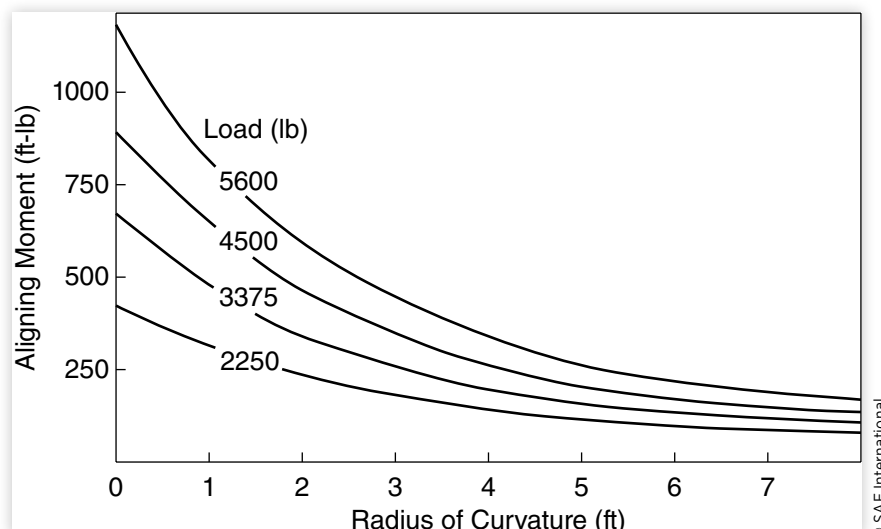
Relevance to Vehicle Performance

Aligning moment, as a torque acting directly on the vehicle, contributes a small component to the understeer of a vehicle. The fact that positive aligning moments attempt to steer the vehicle out of the turn means that they are understeer in direction. Overall, the direct action of the moments contributes only a few percent to the understeer gradient of a vehicle.

The aligning moment has a more direct influence on understeer by its action on the steered wheels. The moment is normally in the direction necessary to turn the steered wheels out of the turn. Even though the steer deflection angles in response to aligning moments may be small (fractions of a degree in normal driving), this is normally an important contribution to understeer gradient.

Aligning moment is also important to steering feel when the vehicle is moving. Its contribution is equal to or greater than caster angle in producing returnability torques—the torques acting to return the steering to the straight-ahead position when cornering.

FIGURE 10.21 Aligning moment as a function of radius of turn.



Aligning moment arising from path curvature is primarily important for static steer and very low-speed maneuvering. The moment is the dominant source of steering torque and may be quite large. Because this represents a condition that places highest torque demand on a steering system, it must be considered in sizing power-steering hardware and in durability testing. By offsetting the tire outside of the steering axis (positive scrub), the tire can be allowed to roll on a radius that will decrease the magnitude of the aligning moment in static steer situations. In operating situations, simply moving the vehicle at low speed while increasing the steering angle greatly increases the radius of curvature and thereby reduces the steering torque required.

Combined Braking and Cornering

When a tire is operated under conditions of simultaneous longitudinal and lateral slip, the respective forces depart markedly from those values derived under independent conditions. The application of longitudinal slip generally tends to reduce the lateral force at a given slip angle condition, and conversely, application of slip angle reduces the longitudinal force developed under a given braking condition. This behavior is shown in [Figure 10.22](#).

Friction Circle

The general effect on lateral force when braking is applied is illustrated in the traction field of [Figure 10.23](#). The individual curves represent the lateral force at a given slip angle. As the brake force is applied, the lateral force gradually diminishes due to the additional slip induced in the contact area from the braking demand.

This type of display of a tire traction field is the basis for the “friction circle” (or friction ellipse) concept [11]. Recognizing that the friction limit for a tire, regardless of direction, will be determined by the coefficient of friction times the load, it is clear that

FIGURE 10.22 Brake and lateral forces as a function of longitudinal slip.

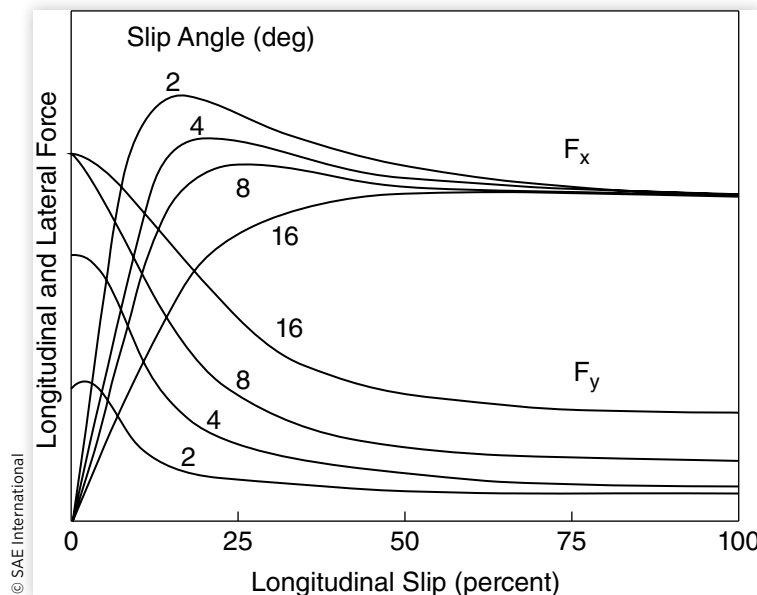
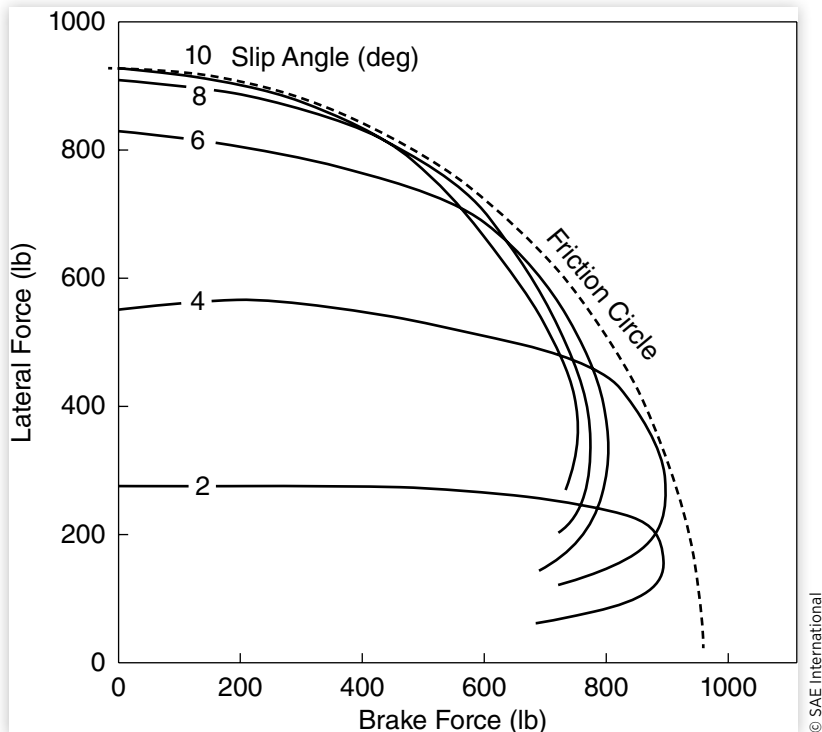


FIGURE 10.23 Lateral force versus longitudinal force at constant slip angles.

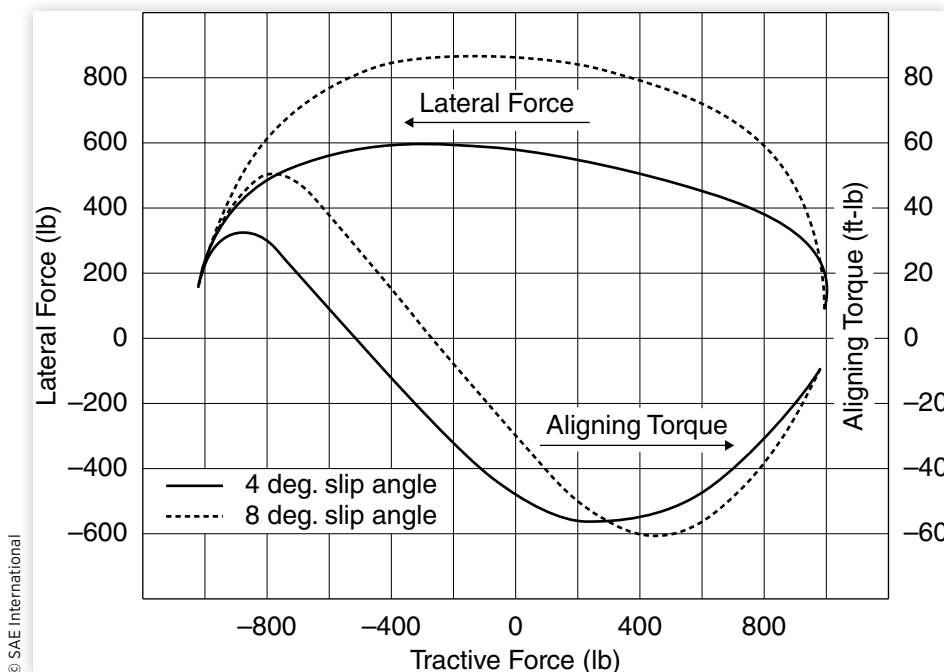
© SAE International

the friction can be used for lateral force, or brake force, or a combination of the two, in either the positive or negative directions. In no case, however, can the vector total of the two exceed the friction limit. The limit is therefore a circle in the plane of the lateral and longitudinal forces. The portion of the circle in the figure is the friction circle for the positive quadrant of the traction field. The limit is characterized as a friction circle for tires which have effectively the same limits for lateral and braking forces. Certain specialized tires, however, may be optimized for lateral traction or braking traction, in which case the limit is not a circle but an ellipse.

The friction circle concept has been used in recent years as a means to evaluate race car drivers by making continuous recordings of the lateral and longitudinal accelerations maintained on a track. For maximum efficiency in getting around a closed course, the tires should be working continuously at either the cornering or braking/acceleration limits. Therefore, the combined lateral and longitudinal accelerations measured on the car should always be pressing the friction limit, and the most effective driver is the one who can most closely maintain this optimum. By plotting the record of the two accelerations on a polar plot similar to Figure 10.23, one gets a visual indication of the performance of the driver by observing the percentage of time spent at the friction limit.

Figure 10.23 illustrates another observation that is frequently made under conditions of combined traction. Note that at intermediate slip angle conditions near 4 degrees, the application of moderate levels of brake force actually increases the lateral force developed at that slip angle. This phenomenon is shown more precisely in the plot of Figure 10.24, which shows the lateral force and aligning moment under tractive forces in both the braking and driving directions [12].

FIGURE 10.24 Lateral force and aligning torque versus tractive force.



© SAE International

Using the free-rolling (zero tractive force) values of lateral force as a reference point, it is seen that when braking (negative) force is applied, the lateral force increases slightly while the aligning moment decreases. In effect, the presence of the braking force acts to stiffen the tire structure (sidewalls and/or tread) with respect to the mechanism that generates lateral force. The reduction of aligning moment implies a significant redistribution of the shear forces in the contact patch. As the braking force increases toward its maximum value, the lateral force diminishes because the friction limits are being approached. Concurrently, the aligning moment decreases to the point where it may actually go negative near the braking limit. A negative aligning moment attempts to steer the wheel to a greater slip angle and may adversely affect stability in braking, particularly through its effects on the steering system [13].

Under a moderate driving (positive) traction force the opposite effects are observed. Lateral force decreases slightly while aligning moment increases markedly. At levels near the friction limit both the lateral force and aligning moment decrease. Unlike braking, however, the aligning moment never goes negative near the limit of driving force.

Variables

Although tire type (radial versus bias-ply) and inflation pressure have significant influences on cornering stiffness, behavior under combined slip is qualitatively similar to that shown above. The behavior is insensitive to velocity and is only affected by surface conditions through the influence on friction limits.

Relevance to Vehicle Performance

The combined slip behavior of tires is only meaningful in the context of braking-in-a-turn maneuvers. When brakes are applied to a vehicle in a steady turn, the increasing

level of tire longitudinal slip produces a loss in tire side force which characteristically serves to disturb the path and/or yaw orientation of the vehicle. Alternatively, if a large steering input is applied while the vehicle is braking, both the braking performance and the cornering performance stand to be degraded in comparison to the performances expected with independent inputs of steering or braking.

Minimal degradation of braking performance occurs with concurrent cornering up to levels of about 0.3 g lateral acceleration. However, as limit braking is approached, the directional or yaw response can be degraded to the point of total loss of control. The nature of the control loss will depend on the order in which the front and rear tires approach the wheel-lock condition. Front-wheel lockup will render the vehicle unsteerable (i.e., an understeer effect), whereas rear-wheel lockup precipitates a spinout (i.e., an oversteer effect).

Conicity and Ply Steer

The behavior of tires in the near-zero lateral slip region has grown more important in recent years with the refinement of high-speed automobiles. The importance derives from the emphasis that is put on the on-center feel of the steering system.

For an ideal tire zero lateral force coincides with zero slip angle, but for actual tires this is not true. For actual tires the behavior of lateral force at small slip angles will be similar to that shown in [Figure 10.25](#). In this plot, the lateral force is plotted as the tire is rolled in both directions, arbitrarily labeled as forward and reverse in the figure. The important observation in the figure is that the lateral force behavior differs with the direction of rotation (forward versus reverse) and may be offset from the origin of the graph.

One mechanism in the tire accounting for this behavior is conicity in the construction. Conicity derives from small side-to-side differences in the tire such as an asymmetrical offset in the positioning of the belt. As the name implies, these variations are manifest in a tire as a bias toward a conical shape as illustrated in [Figure 10.26](#). Because of this shape, a freely rolling tire will want to follow an arc centered about the apex of the cone, shown at the right of [Figure 10.26](#). Forced to follow a straight line, this tire will experience a lateral force toward the right in the figure, regardless of which direction it

FIGURE 10.25 Lateral force behavior around zero slip angle.

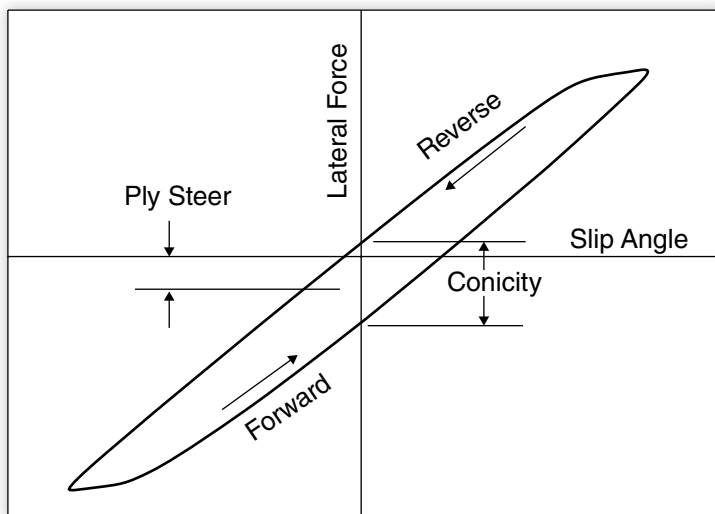
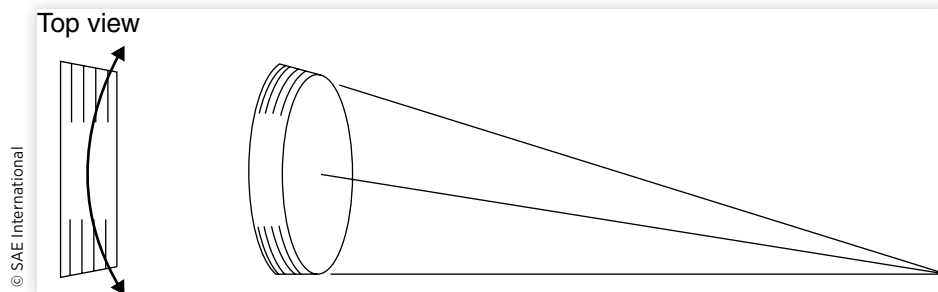


FIGURE 10.26 Conicity in a pneumatic tire.



may roll. By the SAE convention, when the tire rolls upward in the top view, the lateral force is to the right and is positive in direction. Rolling downward, the force will again be to the right, but since the longitudinal axis of the tire is now pointed downward, it is a negative lateral force. Thus conicity is manifest as a difference in the lateral force at zero slip angle when the tire is rolled in opposite directions. Conicity has the character of being random in direction and is dependent on quality control in tire construction. Turning a tire on the rim will change the direction of the lateral force caused by conicity.

The other mechanism that may be present in a tire is ply steer, which arises from the angle of the cords in the belt layers. To avoid this bias in the tire's preferred rolling direction, belts are constructed with alternating belt layers at opposite angles. Unfortunately, a perfect balance is impossible to achieve. Thus a free-rolling tire will exhibit a tendency to drift from its direction of heading. Instead of following an arc as illustrated in Figure 10.26, it will follow a line that is skewed with respect to its center plane. If, then when rolling in one direction, it creates a lateral force to the right in the SAE tire axis system, when rolled in the opposite direction, it will again exhibit a force to the right in the SAE tire axis system. When the tire lateral force properties are measured in the vicinity of zero-degree slip angle, ply steer is manifest as a non-zero offset in the lateral force averaged from both directions of travel. Ply steer is dependent on tire design, and will therefore be nearly equal in magnitude and direction for all tires of a common design. Turning the tire on the rim does not change the direction of the lateral force caused by ply steer.

Both conicity and ply steer force magnitudes are dependent on the vertical load carried by a tire. Conicity is more sensitive to inflation pressure and may therefore be reduced by making pressure adjustments.

Relevance to Vehicle Performance

The effects of conicity and ply steer are to create a "pull" in the steering system or a "drift" in the tracking of the car. Pull refers to a condition where the driver must apply a continuous torque to the steering wheel by holding it off-center to maintain the vehicle's tracking of a straight path. Conversely, with the steering wheel free and in the center position, the vehicle will follow a curved path.

Excess conicity on the front wheels may cause the steering to pull to such a degree that it is fatiguing to the driver and becomes a source of customer dissatisfaction. Conicity on the rear wheels will cause the vehicle to track with the rear wheels offset from the front. It may also affect the centering of the steering wheel in the straight-ahead position.

Since ply steer is likely to act on all wheels in the same direction, a vehicle may exhibit a slight drift due to ply steer forces. This may require some steering wheel offset to compensate and keep the vehicle traveling straight. In this case, no steering pull is likely.

Durability Forces

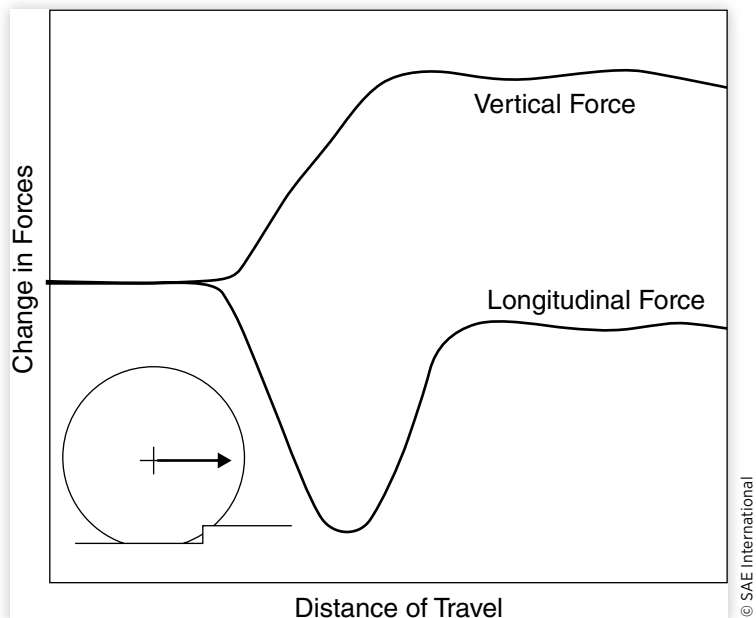
Although tires act as a cushion between the vehicle and the road, the bumps present in most roads transmit forces that are perceptible to the vehicle's occupants and may contribute to the cyclic loading and fatigue of suspension components. Road bump features that have a characteristic length on the same order as the length of the tire contact patch (e.g., tar strips, faults in concrete surfaces, potholes) generate forces that are dependent on the tire's ability to envelop these features. Because these forces, particularly those attributable to encounters with potholes, may be large in magnitude and thus significant to fatigue and durability of a vehicle, they are often referred to as durability forces.

A smooth road surface is seen as a flat plane by a free-rolling tire and generates predominantly vertical force inputs to the tire. Even at high speed, the vertical inputs are slow to change in magnitude relative to the time it takes the tire to advance along the length of its contact patch. However, when a tire encounters an abrupt discontinuity in a road surface, such as the edge of a pothole, the forces may change markedly as the feature passes through the contact patch. Dynamic vertical and longitudinal forces are generated in the process. The shape and magnitude of the force inputs depend on the properties and mechanics of the tire.

Tire performance when enveloping road discontinuities has been studied by examining performance when tires negotiate small step changes in road elevation [14]. (In theory, any shape of bump can be approximated by a well selected combination of small steps.) To understand its behavior, the tire can be thought of as a series of radial springs (sometimes modeled with dampers in parallel with each spring) in contact with the surface. When a tire encounters an upward step in the road surface, the vertical and longitudinal forces on the tire will change abruptly as shown in [Figure 10.27](#).

As the tire contacts the leading edge of the bump, the vertical force begins to rise due to depression of the tread. The force rises more or less continuously until the full contact patch has advanced onto the bump. Performed at high speed, the axle on which

FIGURE 10.27 Vertical and longitudinal tire forces produced by a step in the road.



the tire is mounted is not able to respond and move upward in the time it takes the entire contact patch to move onto the bump. Thus an increase in vertical load occurs that is approximately equal to the bump height times the vertical stiffness of the tire.

The encounter with the bump also creates a longitudinal force as a result of several mechanisms. For the tire to rise onto the bump, a longitudinal force is required. This force must be provided by the axle, thus a negative (i.e., opposite to the direction of travel) force is experienced when the tire first encounters the edge of the bump. Once on the bump, the increased vertical load causes an increase in the rolling resistance of the tire such that the longitudinal force does not immediately return to its original value, but instead must wait for the axle to adjust to a new height representing the balance of vertical forces.

At high speed, a second mechanism is at work as well. With the change in effective radius of the tire on the bump, it must assume a new rotation rate in correspondence with its forward speed. With a smaller radius, the tire must increase its rotational speed. This is accomplished by generating a shear force in the contact patch which is ultimately balanced out by an opposite force reaction at the axle. To speed up the rotation rate of the tire, a second component of negative force is imposed on the axle. The rate at which the tire mounts the bump, the rate at which it must speed up, and the magnitude of the longitudinal force created depends on the forward speed of the wheel. This tells us that this component of longitudinal force depends on the speed of travel.

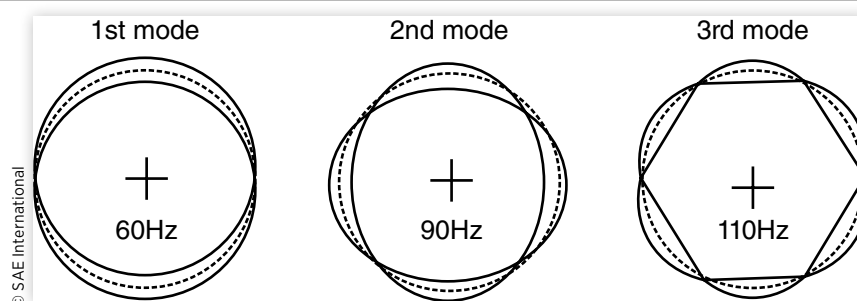
When a tire encounters a downward step in the road surface, similar forces are created differing only in their direction of action. That is, a downward step causes a decrease in vertical force and creates an impulsive force in the forward direction on the axle.

Tire Vibrations

Up till now the tire has been treated as a mechanism for generating forces by which a vehicle may be controlled in braking and turning. With regard to ride dynamics, it is seen to behave primarily as a spring which absorbs the roughness features in the road and interacts with the vertical motions of the body and unsprung masses. The tire, however, is also a dynamic system with resonances that affect the transmission of vibrations to the vehicle and therefore may interact with vehicle resonances [15].

A relatively large portion of the tire mass is concentrated in the tread which is connected to the wheel by the compliant sidewalls. This combination of mass and compliance permits the tread to resonate when excited by road inputs. [Figure 10.28](#) shows examples of the first three modal resonances of the tire in the vertical plane.

FIGURE 10.28 First, second and third modal resonances of a tire.



The first mode, which will occur somewhere near 60 Hz for a passenger-car tire, involves a simple vertical motion of the entire tread band without distortion. The mode is easily excited by vertical input at the proper frequency in the contact patch. Since the entire tread band moves up and down in unison, the force associated with the resonance is transmitted to the wheel and axle.

The second mode contrasts with the first in that the tread band is oscillating in an elliptical fashion, always remaining symmetrical about the vertical and horizontal axes. The top and bottom of the tread are always moving out of phase so that no net vertical force is imposed on the wheel. (Likewise, there is no net fore-aft force.) Although the resonance can be excited by vertical inputs at the contact patch, the tire is very effective at absorbing the inputs without transmitting forces to the axle. In a similar fashion, the third- and higher-order resonances of the tire are very effective in absorbing road inputs without transmitting them to the wheel and axle.

In between these modal resonances, the tire has anti-resonant modes characterized by very asymmetrical tread distortion and little mobility at the contact patch. The asymmetry of the motion results in unbalanced forces being imposed around the circumference of the wheel, such that the resultant force is transmitted to the wheel. The fact that the contact patch is stationary implies that the tire appears as a very stiff, rather than compliant, element with regard to road inputs at this frequency.

From this simple picture of a tire as a resonant system, it is possible to begin building an understanding of the dynamic behavior of the tire in transmitting road vibrations in the chassis of a motor vehicle. The system can be characterized by examining several relevant properties. [Figure 10.29](#) shows experimental measurements on a radial tire mounted on a passenger car exposed to vertical excitation at the contact patch [15].

The transmissibility in this figure is defined as the ratio of acceleration on the axle per unit of road displacement at the contact patch. The first peak just below 20 Hz is axle hop resonance in which the tire acts as the primary stiffness constraining the unsprung mass. More of interest are the several peaks at higher frequencies. Note that they occur

FIGURE 10.29 Tire resonance properties measured on a vehicle.

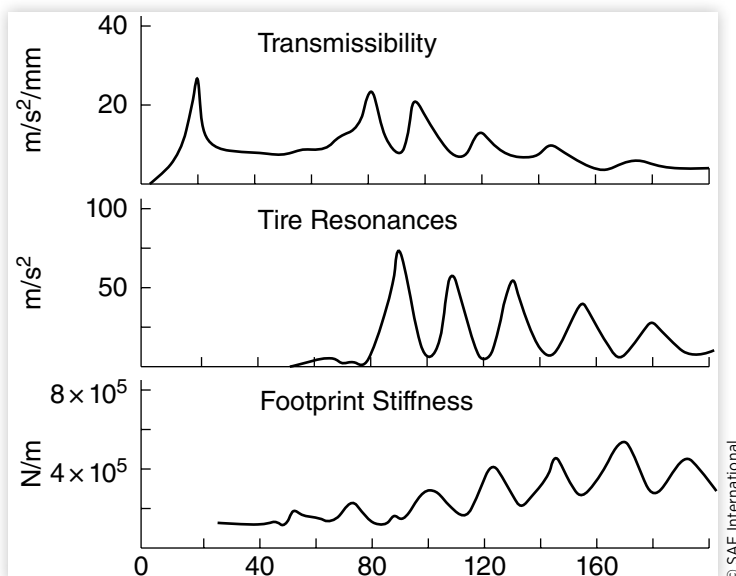
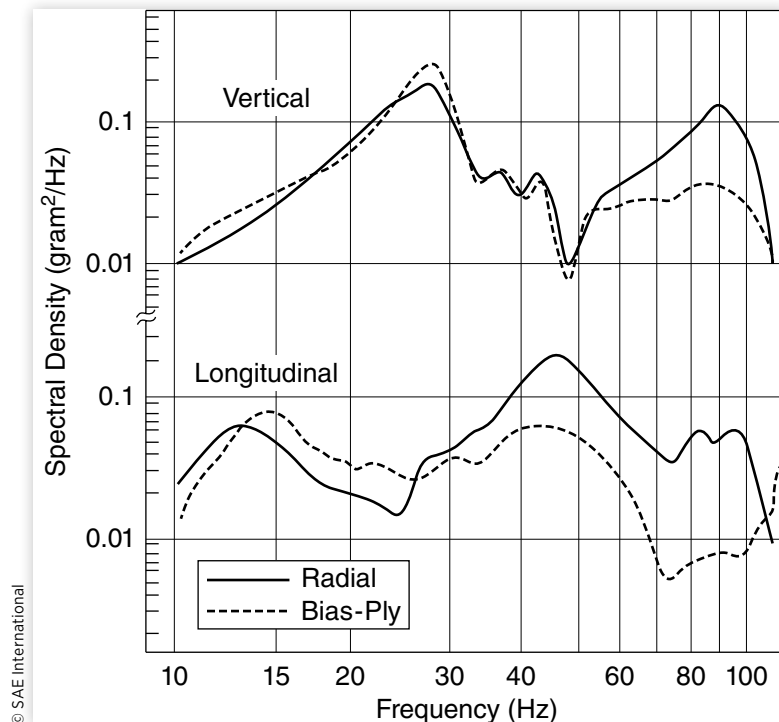


FIGURE 10.30 Spectra of forces measured when a tire encounters an obstacle.



© SAE International

at frequencies in between the tire resonances (i.e., the anti-resonant points), corresponding to the peaks in transmissibility and peaks as well in the footprint stiffness of the tire (tire force per unit of road displacement).

This somewhat simplified picture of tire dynamics hints at the forces that will be input at the wheel of a motor vehicle. **Figure 10.30** shows the spectra of forces measured when a passenger-car tire encounters a small obstacle at a speed of 30 ft per second (20 mph) [16]. Data are shown for both a radial and bias-ply tire and for forces in both the vertical and longitudinal directions.

In the vertical direction, the radial tire is distinguished by the increased amplitude of force in the frequency range of 50 to 100 Hz. From the previous discussion, it would be expected that this behavior is a result of the high transmissibility of the anti-resonant modes in this frequency range for radial-ply tires. Obviously, bias-ply tires are much better in this range.

Perhaps the more important distinction between the two types of tires is seen in the spectra of longitudinal response. Except for a narrow band around 15 to 20 Hz, radial tires are more responsive in the longitudinal direction than bias-ply tires. At the higher frequencies, the greater transmissibility indicates a higher effective stiffness in the longitudinal direction. The higher transmissibility of the radial tire near 10 Hz is one of the key differences that required “ride tuning” when radials were first introduced to the American automotive market. On vehicles historically developed on bias-ply tires, the application of radials produced more suspension fore/aft vibration requiring the addition of more longitudinal compliance in suspensions to prevent these vibrations from being transmitted to the body.

References

1. Clark, S.K., Ed., "Mechanics of Pneumatic Tires," U.S. Department of Transportation National Highway Traffic Administration, U.S. Government Printing Office, Washington, DC, 1981, 931pp.
2. Dugoff, H., Fancher, P.S., and Segel, L., "Tire Performance Characteristics Affecting Vehicle Response to Steering and Braking Control Inputs," The University of Michigan Highway Safety Research Institute, August 1969, 105pp.
3. Sharp, R.S. and El-Nashar, M.A., "A Generally Applicable Digital Computer Based Mathematical Model for the Generation of Shear Forces by Pneumatic Tires," *Vehicle Systems Dynamics* 15, no. 4 (1986): 187-209.
4. Meyer, W.E. and Kummer, H.W., "Mechanisms of Force Transmission Between Tire and Road," SAE Technical Paper 620407, 1962, doi:[10.4271/620407](https://doi.org/10.4271/620407).
5. "Vehicle Dynamics Terminology," SAEJ670e, Society of Automotive Engineers, Warrendale, PA (see Appendix A).
6. *1991 Yearbook*, The Tire & Rim Association Inc., Copley, OH, 1991.
7. Ervin, R.D., "The State of Knowledge Relating Tire Design to Those Traction Properties Which May Influence Vehicle Safety," The University of Michigan Transportation Research Institute, Report No. UM-HSRI-78-31, July 1978, 128pp.
8. *Annual Book of ASTM Standards*, American Society for Testing and Materials, Philadelphia, PA.
9. Loeb, J.S., Guenther, D.A., Chen, H.H., and Ellis, J.R., "Lateral Stiffness, Cornering Stiffness and Relaxation Length of the Pneumatic Tire," SAE Technical Paper 900129, 1990, doi:[10.4271/900129](https://doi.org/10.4271/900129).
10. Pacejka, H.B., "Tire Characteristics and Vehicle Dynamics," Course Notes, University Consortium for Continuing Education, November 2-4, 1988, Washington, DC, 199pp.
11. Radt, H.S. and Milliken, W.F., "MOTIONS OF SKIDDING AUTOMOBILES," SAE Technical Paper 600133, 1960, doi:[10.4271/600133](https://doi.org/10.4271/600133).
12. Nordeen, D.L. and Cortese, A.O., "Force and Moment Characteristics of Rolling Tires," SAE Technical Paper 640028, 1964, doi:[10.4271/640028](https://doi.org/10.4271/640028).
13. Gillespie, T.D., "Front Brake Interactions with Heavy Vehicle Steering and Handling During Braking," SAE Technical Paper 760025, 1976, doi:[10.4271/760025](https://doi.org/10.4271/760025).
14. Lippman, S.A. and Nanny, J., "A Quantitative Analysis of the Enveloping Forces of Passenger Tires," SAE Technical Paper 670174, 1967, doi:[10.4271/670174](https://doi.org/10.4271/670174).
15. Potts, G.R. et al., "Tire Vibrations," *Tire Science and Technology* 5, no. 4 (1977): 202-225.
16. Barson, C.W. and Dodd, A.M., "Vibrational Characteristics of Tyres," Institution of Mechanical Engineers, Paper C94/7n1, 1971, 12pp.

appendix A: (R) Vehicle dynamics terminology

SURFACE VEHICLE
RECOMMENDED PRACTICE

J670 JAN2008

Issued 1952-07

Revised 2008-01

Superseding J670e JUL1976

(R) Vehicle Dynamics Terminology

Table of Contents

Rationale

Foreword

Introduction

1. Scope

2. References

 2.1 Applicable Publications

 2.1.1 SAE Publications

 2.1.2 ISO Publications

 2.2 Related Publications

 2.2.1 SAE Publications

 2.2.2 ISO Publications

 2.2.3 Other Publications

SAE Technical Standards Board Rules provide that: "This report is published by SAE to advance the state of technical and engineering sciences. The use of this report is entirely voluntary, and its applicability and suitability for any particular use, including any patent infringement arising therefrom, is the sole responsibility of the user."

SAE reviews each technical report at least every five years at which time it may be revised, reaffirmed, stabilized, or cancelled. SAE invites your written comments and suggestions.

Copyright © 2019 SAE International

All rights reserved. No part of this publication may be reproduced, stored in a retrieval system or transmitted, in any form or by any means, electronic, mechanical, photocopying, recording, or otherwise, without the prior written permission of SAE.

TO PLACE A DOCUMENT ORDER:

Tel: 877-606-7323 (inside USA and Canada)

Tel: +1 724-776-4970 (outside USA)

Fax: 724-776-0790

Email: CustomerService@sae.org

SAE values your input. To provide feedback

on this Technical Report, please visit

http://standards.sae.org/J2834_201910

SAE WEB ADDRESS:

<http://www.sae.org>

- 3. Axis and Coordinate Systems
- 4. Vehicle
 - 4.1 Geometry and Masses
 - 4.2 Kinematics
 - 4.2.1 Translational Motion Variables
 - 4.2.1.1 Velocities
 - 4.2.1.2 Accelerations
 - 4.2.2 Angular Motion Variables
 - 4.2.2.1 Angles
 - 4.2.2.2 Angular Velocities
 - 4.2.2.3 Angular Accelerations
 - 4.2.3 Vehicle Trajectory Measures
 - 4.3 Forces and Moments
 - 4.3.1 Forces
 - 4.3.2 Moments
- 5. Suspension and Steering
 - 5.1 General Nomenclature
 - 5.2 Suspension Components
 - 5.3 Steering Components
 - 5.4 Masses and Inertias
 - 5.5 Geometry
 - 5.5.1 Steer and Camber Angles
 - 5.5.2 Steering-Axis Geometry
 - 5.6 Suspension Motions
 - 5.7 Kinematics
 - 5.7.1 Ride Kinematics
 - 5.7.2 Roll Kinematics
 - 5.7.3 Steering Kinematics
 - 5.7.4 Anti- Characteristics
 - 5.8 Ride and Roll Stiffness
 - 5.9 Compliances
 - 5.9.1 Camber and Steer Compliances
 - 5.9.2 Other Compliances

6. Brakes

6.1 General Nomenclature

6.2 Brake Components

6.3 Brake Proportioning

7. Tires and Wheels

7.1 Wheel Nomenclature

7.2 Pneumatic Tire Nomenclature

7.3 Wheel Plane Geometry

7.4 Tire Orientation Angles

7.5 Tire Rolling Characteristics

7.6 Wheel Spin and Tire Slip

7.7 Standard Loads and Inflation Pressures

7.8 Wheel Torque

7.9 Tire Forces and Moments

7.10 Pull Forces and Moments

7.11 Properties of Forces in the Road Plane

7.12 Normal Force Properties

7.13 Moment Properties

7.14 Tire/Road Friction

8. States and Modes

8.1 Equilibrium

8.2 Stability

8.3 Control Modes

9. Inputs and Responses

9.1 Inputs

9.2 Responses

10. Vehicle Longitudinal Response

10.1 Longitudinal Load Transfer

10.2 Descriptors of Steady-State Longitudinal Response

10.2.1 Gain Measures

10.2.2 Gradient Measures

10.3 Descriptors of Transient Longitudinal Response

10.4 Descriptors of Transient Brake System Response

10.5 Characterizing Descriptors of Braking Performance

11. Vehicle Lateral Response
 - 11.1 Lateral Load Transfer
 - 11.2 Ranges of Directional Response
 - 11.3 Descriptors of Steady-State Directional Response
 - 11.3.1 Gain or Sensitivity Measures
 - 11.3.2 Gradient Measures
 - 11.3.3 Understeer and Oversteer
 - 11.3.4 Stability Measures
 - 11.3.5 Characterizing Speeds
 - 11.4 Descriptors of Transient Directional Response
 - 11.4.1 Rise-Time Measures
 - 11.4.2 Overshoot Measures
 - 11.4.3 Other Transient Measures
 - 11.5 Descriptors of Limit Response
 - 11.5.1 Directional Response Limits
 - 11.5.2 Rollover Resistance
 - 11.6 Stability and Control Derivatives
 12. Ride Vibration
 - 12.1 Sprung-Mass Vibration
 - 12.2 Unsprung-Mass Vibration
 - 12.2.1 Wheel Vibration Modes
 - 12.2.2 Axle Vibration Modes
 - 12.2.3 Steering-System Vibration Modes
 13. Notes
 - 13.1 Marginal Indicia
- Appendix A Alphabetical Index
- Appendix B Symbols
- Appendix C Superseded Tire Axis System
- Figure 1 Orientations of Axis Systems
- Figure 2 Tire and Wheel Axis Systems
- Figure 3 Yaw, Sideslip, and Course Angles
- Figure 4 Vehicle Sideslip, Reference Steer, and Axle Reference Sideslip Angles
- Figure 5 Rack and Pinion Steering System
- Figure 6 Recirculating-Ball Steering System

Figure 7 Ackermann Geometry

Figure 8 Camber, Inclination, and Vehicle Roll Angles

Figure 9 Nomenclature for Tire and Rim

Figure 10 Tire Force and Moment Nomenclature

Figure 11 Components of Tire Conicity and Plysteer

Figure 12 Tire Residual Lateral Force and Aligning Moment

Figure 13 Tire Conicity Residual Aligning Moment

Figure 14 Steer Properties

Figure C1 Superseded Tire Axis System

Table 1 Vehicle Euler Angles and Standard Order of Rotation

Table 2 Relationships Between Z-Up and Z-Down Tire Axis Systems

Table C1 Relationships Between Superseded Tire Axis System and Z-Down Tire Axis System

Rationale

SAE J670 was last updated over 30 years ago. Since the last revision, the field of vehicle dynamics has changed significantly. New systems such as four-wheel steering and active control have been applied to enhance the performance of vehicles. The terminology for vehicle dynamics needed to be updated to accommodate these new technologies and to make the definitions consistent with current usage in the field. Accordingly, many new terms have been added to the terminology to provide formal definitions for terms that are associated with these new technologies. A number of existing definitions, which were based on front-wheel steer vehicles with passive control, were also revised to accommodate new technologies.

In addition, new SAE and ISO standards have been published since the last revision of SAE J670 that directly relate to topics considered in SAE J670. The content of these new standards also indicated the need to revise SAE J670.

Specifically, in 1987, SAE published J1594, containing aerodynamics terminology previously appearing in SAE J670e. The aerodynamics section of SAE J670e is not included in the revised document, because those terms are now defined in SAE J1594.

In 1991, the International Organization for Standardization (ISO) published a vehicle dynamics vocabulary, ISO 8855. SAE J670e and ISO 8855 are incompatible in several aspects, the most notable being the axis systems defined in the two documents. SAE J670e utilizes an axis system based on aeronautical practice, with positive X forward, positive Y to the right, and positive Z down. ISO 8855 utilizes an axis system with positive X forward, positive Y to the left, and positive Z up. The revised SAE J670 embraces both of these axis orientations. The revised SAE J670 additionally addresses technical shortcomings found in both SAE J670e and ISO 8855 and is a harmonized superset of the two documents.

In 1998, SAE published J2047, containing definitions for tire performance terms that were previously defined in SAE J670e. The revised SAE J670 utilizes many definitions excerpted from SAE J2047, although some of these definitions are revised to enhance their applicability to vehicle dynamics.

Several of the sections of SAE J670e dealing with vibration terminology are not included in the new SAE J670, as the terms that were defined in these sections are commonly defined in engineering textbooks and the definitions are not specific to vehicle dynamics.

Finally, the terminology is extended to include definitions for many suspension and steering components, to enhance communication among vehicle dynamics professionals.

This seventh edition of SAE J670 replaces the preceding edition (SAE J670e) in its entirety.

Foreword

This terminology is intended to be sufficient to allow meaningful communication between vehicle dynamics professionals who need to describe the static and dynamic characteristics of automobiles, light trucks, and trailers. The terminology is to be used for presenting results and findings concerning the longitudinal, lateral, vertical and rotational dynamic performance of the applicable vehicles as predicted by analyses and simulations or as measured in tests and operational situations.

The purpose of this terminology is not to cover all terms in the manner of a dictionary or terms found in a basic engineering textbook. Rather, this document contains compatible definitions that have been carefully selected to aid in conveying ideas with rigor and accuracy in a readily understood and generally acceptable manner.

The terminology draws upon terms and definitions previously appearing in SAE J670e and ISO 8855 and further develops those that are applicable to the subjects covered by this document. For application to the study of vehicle dynamics, the tire terminology in this document contains pertinent definitions extracted from or based upon SAE J2047. Definitions for many chassis components are also provided.

Many of the definitions in the document contain terms appearing in italic font. Definitions for terms in italic may be found elsewhere in the document.

Introduction

ISO 8855:1991 is the international standard corresponding to SAE J670. The scopes of these two standards are different. The scope of SAE J670 is limited to passenger cars and light trucks with two axles, plus those vehicles in combination with single-axle trailers. The scope of ISO 8855 additionally includes heavy commercial vehicles, with multiple axles and multiple units. SAE J670 recognizes axis systems with both Z-Up and Z-Down orientations, while ISO 8855 only recognizes the Z-Up orientation. SAE J670 defines five axis systems: Earth, intermediate, vehicle, tire, and wheel, while ISO 8855 defines four axis systems: Earth, intermediate, vehicle, and wheel (equivalent to the SAE J670 tire system). SAE J670 accommodates four-wheel steering, while ISO 8855 does not. SAE J670 accommodates an inclined road surface that is non-uniform, while ISO 8855 is limited to application on a flat, horizontal road surface. SAE J670 includes definitions

for many suspension and steering components, while component definitions are not included in ISO 8855. SAE J670 also defines many more terms (over 600) than are defined in ISO 8855 (approximately 130).

1. Scope

The vehicle dynamics terminology presented herein pertains to passenger cars and light trucks with two axles and to those vehicles pulling single-axle trailers. The terminology presents symbols and definitions covering the following subjects: axis systems, vehicle bodies, suspension and steering systems, brakes, tires and wheels, operating states and modes, control and disturbance inputs, vehicle responses, and vehicle characterizing descriptors. The scope does not include terms relating to the human perception of vehicle response.

2. References

2.1 Applicable Publications

The following publications form a part of this specification to the extent specified herein. Unless otherwise specified, the latest issue of SAE publications shall apply.

2.1.1 SAE PUBLICATIONS: Available from SAE International, 400 Commonwealth Drive, Warrendale, PA 15096-0001, Tel: 877-606-7323 (inside USA and Canada) or 724-776-4970 (outside USA), www.sae.org.

- | | |
|-----------|------------------------------------------|
| SAE J1594 | Vehicle Aerodynamics Terminology |
| SAE J2047 | Tire Performance Technology |
| SAE J2564 | Automotive Stability Enhancement Systems |

2.1.2 ISO PUBLICATIONS: Available from ANSI, 25 West 43rd Street, New York, NY 10036, Tel: 212-642-4900, www.ansi.org.

ISO 8855:1991 Road vehicles—Vehicle dynamics and road-holding ability—Vocabulary

2.2. Related Publications

2.2.1. SAE PUBLICATIONS: Available from SAE International, 400 Commonwealth Drive, Warrendale, PA 15096-0001, Tel: 877-606-7323 (inside USA and Canada) or 724-776-4970 (outside USA), www.sae.org.

- | | |
|-----------|------------------------------------------------------------------------------------------------------------------|
| SAE J1451 | A Dictionary of Terms for the Dynamics and Handling of Single Track Vehicles (Motorcycles, Mopeds, and Bicycles) |
| SAE J1982 | Nomenclature—Wheels for Passenger Cars, Light Trucks, and Multipurpose Vehicles |
| SAE M-105 | SAE Glossary of Automotive Terms—Second Edition |
| SAE R-159 | Dictionary of Automotive Engineering—Second Edition |

2.2.2 ISO PUBLICATIONS: Available from ANSI, 25 West 43rd Street, New York, NY 10036, Tel: 212-642-4900, www.ansi.org.

- | | |
|-----------|--------------------------------------------------------------------------------------|
| ISO 611 | Road vehicles—Braking of automotive vehicles and their trailers—Vocabulary |
| ISO 612 | Road vehicles—Dimensions of motor vehicles and towed vehicles—Terms and definitions |
| ISO 1176 | Road vehicles—Masses—Vocabulary and codes |
| ISO 3833 | Road vehicles—Types—Terms and definitions |
| ISO 3877 | Tyres, valves and tubes—List of equivalent terms—Part 1: Tyres |
| ISO 3911 | Wheels and rims for pneumatic tyres—Vocabulary, designation and marking |
| ISO 4223 | Definitions of some terms used in the tyre industry—Part 1: Pneumatic tyres |
| ISO 6725 | Road vehicles—Dimensions of two-wheeled mopeds and motorcycles—Terms and definitions |
| ISO 6726 | Mopeds and motorcycles with two wheels—Masses—Vocabulary |
| ISO 7237 | Caravans—Masses and dimensions—Vocabulary |
| ISO 11838 | Motorcycle and motorcycle-rider kinematics—Vocabulary |

2.2.3 OTHER PUBLICATIONS: Bosch Automotive Handbook

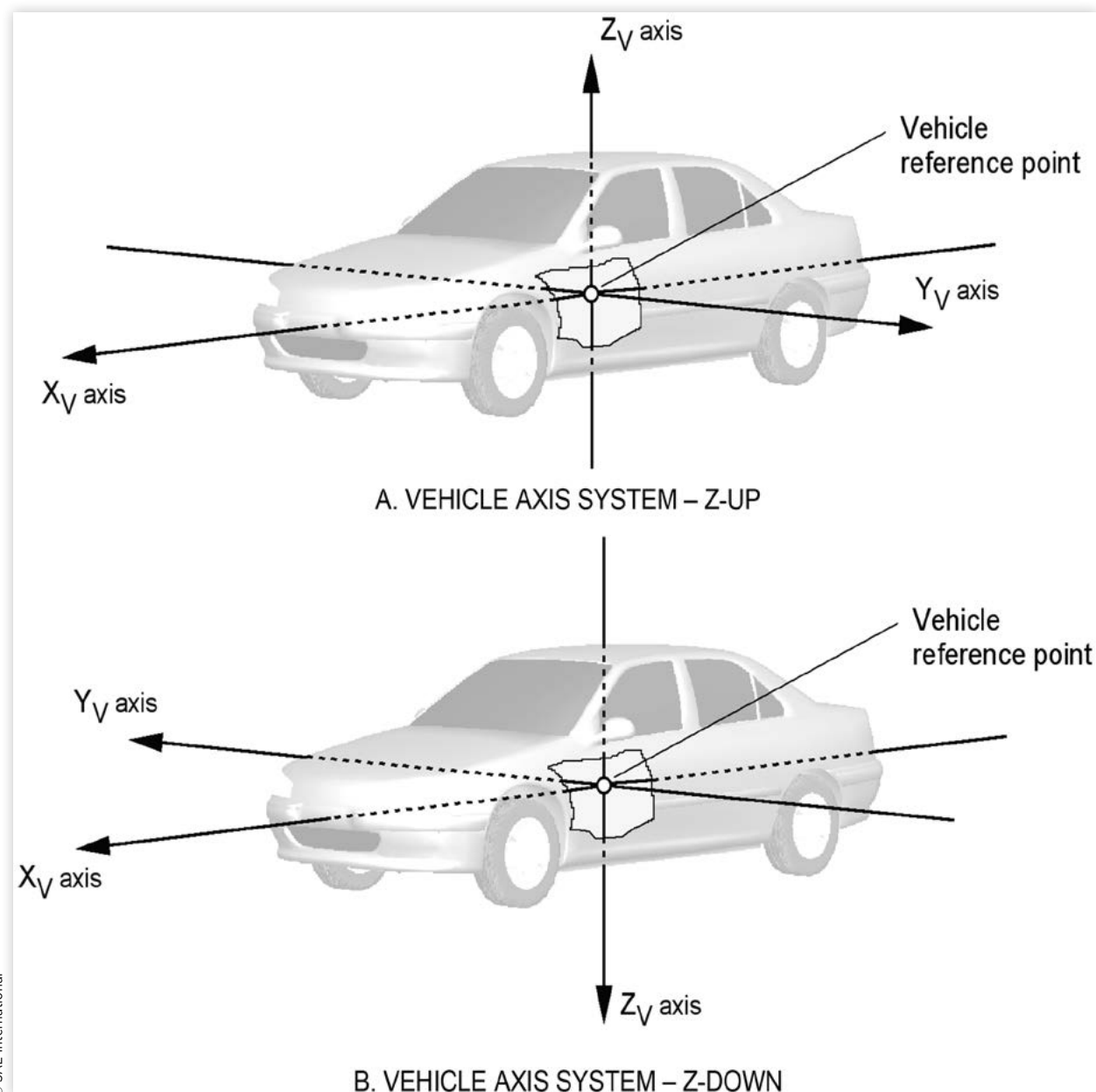
Bosch Automotive Terminology

Tire and Rim Association Year Book

3. Axis and Coordinate Systems

This terminology recognizes axis systems with two existing nominal orientations: the orientation originally defined by SAE J670, which was adopted from aeronautical convention, and the orientation defined in ISO 8855:1991. These axis orientations are equally acceptable, and the selection of the appropriate orientation should be based on the requirements of the analysis or test being performed. The ISO 8855 axis orientation is referred to as the Z-Up orientation, with the traditional SAE J670 axis orientation referred to as the Z-Down orientation. These two axis orientations are shown in [Figure 1](#) below. When definitions are dependent upon the axis orientation, dual definitions are provided, with the definition based on the Z-Up axis orientation appearing first. Many of the terms in this section are also defined in SAE J2047.

The definitions in this section are intended to provide sufficient flexibility to accommodate the broad spectrum of modeling techniques that are currently used to represent the dynamics of vehicles as systems of multiple rigid bodies. Certain commonly used *axis systems* and *coordinate systems* are defined herein. However, there is no intent to limit an analyst or experimentalist to the use of only the *axis systems*, *coordinate systems*, or *reference frames* specifically defined.

FIGURE 1 Orientations of Axis Systems

- 3.1 Reference Frame—A geometric environment in which all points remain fixed with respect to each other at all times.
- 3.2 Inertial Reference (Newtonian Reference)—A reference frame that is assumed to have zero linear and angular acceleration and zero angular velocity. In Newtonian physics, the Earth is assumed to be an inertial reference.
- 3.3 Axis System—A set of three orthogonal directions associated with X, Y, and Z axes. A right-handed axis system is assumed throughout this document, where:

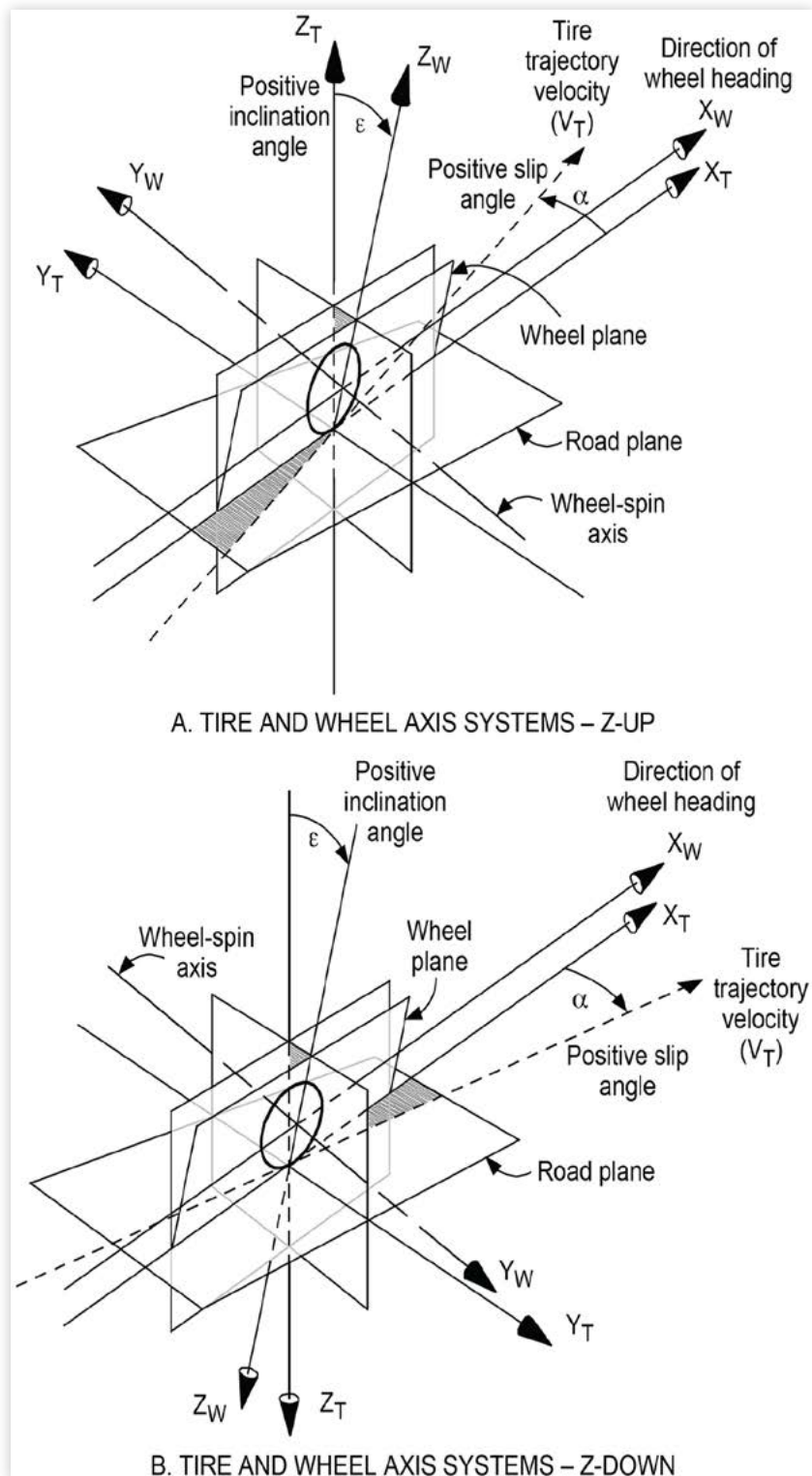
$$\vec{Z} = \vec{X} \times \vec{Y} \quad (\text{Eq.1})$$

- 3.4 Coordinate System—A numbering convention used to assign a unique ordered trio (x, y, z) of values to each point in a *reference frame*. A coordinate system consists of an *axis system* plus an origin point.
- 3.5 Ground Plane—A horizontal plane in the *inertial reference*, normal to the gravitational vector.
- 3.6 Road Surface—The surface, flat, curved, undulated, or other shape, supporting the *tire* and providing friction necessary to generate *tire shear forces* in the *road plane*.
- 3.7 Road Plane—1) A plane representing the *road surface* within each *tire contact patch*. For an uneven road, a different road plane may exist at each *tire contact patch*. 2) The plane formed when the individual road planes at each *tire contact patch* are essentially coplanar.

NOTE—For a planar *road surface*, the *road plane* will be coincident with the *road surface*. For *road surfaces* with surface contours having a wavelength similar to or less than the size of the *tire contact patch*, as in the case of many ride events, an equivalent *road plane* must be determined. Determination of the equivalent *road plane* is dependent on the requirements of the analysis being performed. The equivalent *road plane* may not be coincident with the actual *road surface* at the *tire contact center*.

- 3.8 Vehicle Plane of Symmetry (Longitudinal Plane of Symmetry)—The median plane of a vehicle that is generally laterally symmetric. This plane typically contains the lateral midpoints of the *axles* and the *hitch point*.
- 3.9 Earth-Fixed Axis System (X_E , Y_E , Z_E)—An *axis system* fixed in the *inertial reference*. The X_E and Y_E axes are parallel to the *ground plane*. The Z_E axis is aligned with the gravitational vector. The positive Z_E axis points upward in the Z-Up orientation. The positive Z_E axis points downward in the Z-Down orientation. The orientation of the X_E and Y_E axes is arbitrary and should be based on the needs of the analysis or test.

- 3.10 Earth-Fixed Coordinate System (x_E, y_E, z_E)—A *coordinate system* based on the *Earth-fixed axis system* with an origin that is fixed in the *ground plane*. The location of the origin is generally an arbitrary point defined by the user.
- 3.11 Vehicle Axis System (X_v, Y_v, Z_v)—An *axis system* fixed in the *reference frame* of the vehicle *sprung mass*, so that the X_v axis is substantially horizontal and points forward (with the vehicle at rest), and is parallel to the *vehicle plane of symmetry*. The Y_v axis is perpendicular to the *vehicle plane of symmetry*. The Y_v axis points to the left and the Z_v axis points upward in the *Z-Up* orientation. The Y_v axis points to the right and the Z_v axis points downward in the *Z-Down* orientation. For articulated vehicles, a separate vehicle axis system may be defined for each unit. See [Figure 1](#).
- 3.12 Vehicle Coordinate System (x_v, y_v, z_v)—A *coordinate system* based on the *vehicle axis system* with the origin located at the *vehicle reference point*.
- 3.13 Vehicle Reference Point—A point fixed in the vehicle *sprung mass*. See [Figure 1](#).
- NOTE—The *vehicle reference point* may be defined in a variety of locations, based on the needs of the analysis or test. Commonly used locations include the static *vehicle center of gravity*, the static *sprung-mass center of gravity*, the mid-wheelbase point at the height of the static *vehicle center of gravity*, and the center of the front *axle*.
- 3.14 Intermediate Axis System (X, Y, Z)—A right-handed orthogonal *axis system* whose X and Y axes are parallel to the *ground plane*, with the X axis aligned with the vertical projection of the X_v axis onto the *ground plane*. The Z axis is parallel to the Z_E axis. The positive Z axis points upward in the *Z-Up* orientation. The positive Z axis points downward in the *Z-Down* orientation.
- NOTE—The *intermediate axis system* is used to facilitate angular rotations using the *vehicle Euler angles* and the definition of angular orientation terms, the components of force and moment vectors, and the components of translational and angular motion vectors. See 4.2.2.1, 4.3, 4.2.1, 4.2.2.2, and 4.2.2.3, respectively. An intermediate *coordinate system* is not defined herein.
- 3.15 Tire Axis System (X_T, Y_T, Z_T)—An *axis system* whose X_T and Y_T axes are parallel to the local *road plane*, with the Z_T axis normal to the local *road plane*. The orientation of the X_T axis is defined by the intersection of the *wheel plane* and the *road plane*. The positive Z_T axis points upward in the *Z-Up* orientation. The positive Z_T axis points downward in the *Z-Down* orientation. A local tire axis system may be defined at each *wheel*. See [Figure 2](#).

FIGURE 2 Tire and Wheel Axis Systems

- 3.16 Tire Coordinate System (x_T, y_T, z_T)—A *coordinate system* based on the *tire axis system* with the origin fixed at the *contact center*.

NOTE—The Z-Down orientation of the *tire coordinate system* is equivalent to the orientation of the tire axis system defined in SAE J2047.

- 3.17 Wheel Axis System (X_w, Y_w, Z_w)—An *axis system* whose X_w and Z_w axes are parallel to the *wheel plane*, whose Y_w axis is parallel to the *wheel-spin axis*, and whose X_w axis is parallel to the local *road plane*. The positive Z_w axis points upward in the Z-Up orientation. The positive Z_w axis points downward in the Z-Down orientation. A local wheel axis system may be defined for each *wheel*. See [Figure 2](#).

NOTE—This *axis system* definition is not consistent with the definition of wheel axis system found in ISO 8855:1991 or SAE J2047.

- 3.18 Wheel Coordinate System (x_w, y_w, z_w)—A *coordinate system* based on the *wheel axis system* with the origin fixed at the *wheel center*.

4. Vehicle

4.1 Geometry and Masses

- 4.1.1 Wheelbase L—The distance between the *contact centers* of the *tires* on the same side of the vehicle, measured parallel to the X axis, with the vehicle at rest on a horizontal surface, at a prescribed *load condition*, set of *vehicle trim heights*, or set of *suspension trim heights*, with zero *steer angle*.

NOTE—A vehicle may have a different *wheelbase* on the left and right sides by design. It is common practice to average the left and right *wheelbases*; however, the difference may need to be taken into account in performing some analyses. The *wheelbase* typically changes as the *suspension trim heights* change.

- 4.1.2 Trailer Wheelbase—The distance between the vertical projections of the *articulation point* and the center of the trailer *axle* onto the *ground plane*, with the tow-vehicle/trailer combination at rest on a horizontal surface, at a prescribed *load condition*, set of *vehicle trim heights*, or set of *suspension trim heights*.

- 4.1.3 Track (Track Width, Wheel Track) T—The distance between the *contact centers* of a pair of *tires* on an *axle*, measured parallel to the Y axis, with the vehicle at rest on a horizontal surface, at a prescribed *load condition*, set of *vehicle trim heights*, or set of *suspension trim heights*. For vehicles with dual *tires*, it is the distance between the points centrally located between the *contact centers* of the inner and outer dual *tires*.

NOTE—For vehicles with *independent suspensions*, *track* typically changes as the *suspension trim heights* change.

- 4.1.4 Vehicle Trim Height—A vertical dimension that specifies the location of a fixed point on the vehicle body or chassis relative to ground.

NOTE—A set of congruous *vehicle trim heights* (minimum 3) are necessary to establish the orientation of the vehicle body or chassis relative to ground.

4.1.5 Suspension Trim Height—A vertical dimension that specifies the location of a point on a vehicle *suspension* relative to a point on the vehicle *sprung mass*.

4.1.6 Articulation Point—The instant center of rotation of the trailer relative to the towing vehicle.

NOTE—For trailers with a simple ball hitch, the *articulation point* is coincident with the center of the hitch ball.

4.1.7 Hitch Point(s)—The attachment point(s) of the trailer to the towing vehicle.

4.1.8 Unsprung Weight—All weight that is not carried by the *suspension*, but is supported directly by the *tires*. The unsprung weight includes the weight of the *tires* and *wheels* and all parts that move directly with the *tires* and *wheels*, plus a portion of the weight of the *suspension linkages*, *ride springs*, and driveshafts.

NOTE—It is common practice to include one-half the weight of the *suspension linkage*, *ride springs*, and driveshafts in the *unsprung weight*. For more detailed analyses, the weight distribution of the individual *suspension links* may need to be considered. *Unsprung weight* may also be separately defined for the front and rear *axles* and, further, for *independent suspensions*, for individual *suspension corners*. If *unsprung weight* is defined for subsets of the total unsprung weight, the location being referenced must be explicitly identified (e.g., Left Front Unsprung Weight).

4.1.9 Unsprung Mass—The *unsprung weight* divided by the gravitational constant.

NOTE—*Unsprung mass* may also be separately defined for the front and rear *axles* and, further, for *independent suspensions*, for individual *suspension corners*. If *unsprung mass* is defined for subsets of the total *unsprung mass*, the location being referenced must be explicitly identified (e.g., Left Front Unsprung Mass).

4.1.10 Effective Unsprung Mass—The equivalent mass which reproduces the kinetic energy or inertia forces produced by motion(s) of the unsprung parts while the *sprung mass* is stationary.

NOTE—*Effective unsprung mass* is not the same as the *unsprung mass*, in that it considers effects due to the rotational motion and rotational inertia of the *suspension links*, which usually decreases the apparent *unsprung mass*. This distinction may be important when performing certain dynamic analyses (e.g., ride). The value of *effective unsprung mass* may be different for different directions of excitation. Typically, *effective unsprung mass* is separately defined for the front and rear *axles* and, further, for *independent suspensions*, for individual *suspension corners*. The location being referenced must be explicitly identified (e.g., Left Front Effective Unsprung Mass).

4.1.11 Sprung Weight—All weight that is supported by the *suspension*, including portions of the weight of the *suspension members*. The sprung weight is the *vehicle operating weight* less the *unsprung weight*.

- 4.1.12 Sprung Mass—1) The *sprung weight* divided by the gravitational constant. 2) The portion of the vehicle supported by the *suspension*, frequently treated as a rigid body.
- 4.1.13 Base Vehicle Weight—The total weight of the vehicle, including all fluids necessary for normal operation, without fuel and without a *payload*.
- 4.1.14 Base Vehicle Mass—The *base vehicle weight* divided by the gravitational constant.
- 4.1.15 Curb Weight—The *base vehicle weight* plus a full tank of fuel.
- 4.1.16 Curb Mass—The *curb weight* of the vehicle divided by the gravitational constant.
- 4.1.17 Payload—The weight of the driver, passengers, and cargo at a given *load condition*.
- 4.1.18 Load Condition—A description of the loaded state of the vehicle being analyzed or tested. It includes descriptions of the fuel load and the *payload*, and the location(s) of the *payload*.
- 4.1.19 Vehicle Operating Weight W—The total weight of the vehicle at a given *load condition*, including the *base vehicle weight*, the weight of the fuel load, and the *payload*.
- 4.1.20 Vehicle Operating Mass—The *vehicle operating weight* divided by the gravitational constant.

- 4.1.21 Passenger Mass—The mass representative of a driver or passenger. The conventional mass of a passenger is fixed at 68 kg (150 lb).
- 4.1.22 Vehicle Center of Gravity (C.G.)—The center of gravity of the total vehicle at a given *load condition*.

NOTE—The symbols H or h are commonly used for the height of the *vehicle center of gravity* above ground, with the *suspensions* in equilibrium and the vehicle at rest on a flat, level surface. The symbols a and b are commonly used as the longitudinal distances from the front and rear *axle centerlines*, respectively, to the *vehicle center of gravity*.

- 4.1.23 Sprung-Mass Center of Gravity—The center of gravity of the vehicle *sprung mass* at a given *load condition*.

4.1.24 Mass Moments of Inertia (Total Vehicle)

- 4.1.24.1 Vehicle Roll Moment of Inertia—The moment of inertia of the total vehicle at a given *load condition*, taken about an axis parallel to the X_v axis, that passes through the *vehicle center of gravity*.
- 4.1.24.2 Vehicle Pitch Moment of Inertia—The moment of inertia of the total vehicle at a given *load condition*, taken about an axis parallel to the Y_v axis, that passes through the *vehicle center of gravity*.
- 4.1.24.3 Vehicle Yaw Moment of Inertia—The moment of inertia of the total vehicle at a given *load condition*, taken about an axis parallel to the Z_v axis, that passes through the *vehicle center of gravity*.
- 4.1.24.4 Vehicle Roll-Yaw Product of Inertia—The product of inertia of the total vehicle at a given *load condition*, taken about the axes used to determine the *vehicle roll moment of inertia* and the *vehicle yaw moment of inertia*.

4.1.25 Mass Moments of Inertia (Sprung Mass)

- 4.1.25.1 Sprung-Mass Roll Moment of Inertia—The moment of inertia of the vehicle *sprung mass*, taken about an axis parallel to the X_v axis that passes through the *sprung-mass center of gravity*.
- 4.1.25.2 Sprung-Mass Pitch Moment of Inertia—The moment of inertia of the vehicle *sprung mass*, taken about an axis parallel to the Y_v axis that passes through the *sprung-mass center of gravity*.
- 4.1.25.3 Sprung-Mass Yaw Moment of Inertia—The moment of inertia of the vehicle *sprung mass*, taken about an axis parallel to the Z_v axis that passes through the *sprung-mass center of gravity*.
- 4.1.25.4 Sprung-Mass Roll-Yaw Product of Inertia—The product of inertia of the vehicle *sprung mass*, taken about the axes used to determine the *sprung-mass roll moment of inertia* and the *sprung-mass yaw moment of inertia*.
- 4.1.26 Dynamic Index - Pitch (k_{YY}^2/ab Ratio - Pitch)—The square of the radius of gyration of the *sprung mass* about an axis parallel to the Y_v axis that passes through the *sprung-mass center of gravity*, divided by the product of the two longitudinal distances (a and b) from the *sprung-mass center of gravity* to the front and rear *axle centerlines*.
- 4.1.27 Dynamic Index - Yaw (k_{ZZ}^2/ab Ratio - Yaw)—The square of the radius of gyration of the *vehicle operating mass* about an axis parallel to the Z_v axis that passes through the *vehicle center of gravity*, divided by the product of the two longitudinal distances (a and b) from the *vehicle center of gravity* to the front and rear *axle centerlines*.

4.2 Kinematics

4.2.1 TRANSLATIONAL MOTION VARIABLES: In the following paragraphs, velocity and acceleration are relative to the *Earth-fixed axis system* (X_E, Y_E, Z_E). They are resolved into components in the *intermediate axis system* (X, Y, Z).

NOTE—It is also possible to resolve velocity and acceleration vectors into components in other *axis systems*. For example, velocity and acceleration vectors may be resolved in the *vehicle axis system* (X_v, Y_v, Z_v) to produce v_{Xv}, v_{Yv}, v_{Zv} and a_{Xv}, a_{Yv}, a_{Zv} . Traditionally, v_{Xv}, v_{Yv}, v_{Zv} have been represented by the symbols u, v, w.

4.2.1.1 Velocities

- 4.2.1.1.1 Vehicle Velocity \vec{v} —A vector quantity expressing the velocity of the *vehicle reference point*.
- 4.2.1.1.2 Vehicle Speed—The magnitude of the *vehicle velocity*. In many cases, this is approximated by the *longitudinal velocity*.
- 4.2.1.1.3 Longitudinal Velocity v_x —The scalar value of the component of *vehicle velocity* in the direction of the X axis.

$$v_x = \vec{v} \cdot \hat{X} \quad (\text{Eq. 2})$$

- 4.2.1.1.4 Lateral Velocity v_Y —The scalar value of the component of *vehicle velocity* in the direction of the Y axis.

$$v_Y = \vec{v} \cdot \hat{Y} \quad (\text{Eq. 3})$$

- 4.2.1.1.5 Vertical Velocity v_Z —The scalar value of the component of *vehicle velocity* in the direction of the Z axis.

$$v_Z = \vec{v} \cdot \hat{Z} \quad (\text{Eq. 4})$$

- 4.2.1.1.6 Horizontal Velocity Vector \vec{v}_H —The vector projection of *vehicle velocity* onto the X-Y plane.

$$\vec{v}_H = \vec{v} - (\vec{v} \cdot \hat{Z}) \hat{Z} = v_X \hat{X} + v_Y \hat{Y} \quad (\text{Eq. 5})$$

- 4.2.1.1.7 Horizontal Velocity v_H —The magnitude of the *horizontal velocity vector*.

NOTE—*Horizontal velocity is also the resultant of longitudinal velocity and lateral velocity.*

4.2.1.2 Accelerations

- 4.2.1.2.1 Vehicle Acceleration \vec{a} —A vector quantity expressing the acceleration of the *vehicle reference point*.

- 4.2.1.2.2 Longitudinal Acceleration a_X —The scalar value of the component of *vehicle acceleration* in the direction of the X axis.

$$a_X = \vec{a} \cdot \hat{X} \quad (\text{Eq. 6})$$

- 4.2.1.2.3 Lateral Acceleration a_Y —The scalar value of the component of *vehicle acceleration* in the direction of the Y axis.

$$a_Y = \vec{a} \cdot \hat{Y} \quad (\text{Eq. 7})$$

NOTE—In *steady state, lateral acceleration* is equal to the product of *centripetal acceleration* times the cosine of the vehicle's *sideslip angle*. Since in most test conditions the *sideslip angle* is small, for practical purposes *lateral acceleration* may be considered equal to *centripetal acceleration*.

- 4.2.1.2.4 Vertical Acceleration a_Z —The scalar value of the component of *vehicle acceleration* in the direction of the Z axis.

$$a_Z = \vec{a} \cdot \hat{Z} \quad (\text{Eq. 8})$$

- 4.2.1.2.5 Tangential Acceleration a_T —The scalar value of the component of *vehicle acceleration* in the direction of the *horizontal velocity vector*.

$$a_T = \vec{a} \cdot \hat{v}_H \quad (\text{Eq. 9})$$

- 4.2.1.2.6 Centripetal Acceleration a_c —The scalar value of the component of *vehicle acceleration* in the direction of the horizontal normal to the *horizontal velocity vector*.

$$a_c = \vec{a} \cdot (\hat{Z} \times \hat{v}_H) \quad (\text{Eq. 10})$$

- 4.2.1.2.7 Horizontal Acceleration Vector \vec{a}_H —The vector projection of *vehicle acceleration* onto the X-Y plane.

$$\vec{a}_H = \vec{a} - (\vec{a} \cdot \hat{Z})\hat{Z} = a_x \hat{X} + a_y \hat{Y} \quad (\text{Eq. 11})$$

- 4.2.1.2.8 Horizontal Acceleration a_H —The magnitude of the *horizontal acceleration vector*.

NOTE—*Horizontal acceleration is also the resultant of longitudinal acceleration and lateral acceleration or the resultant of tangential acceleration and centripetal acceleration.*

4.2.2 ANGULAR MOTION VARIABLES

- 4.2.2.1. Angles.** The sign of angles resulting from angular rotations is determined in accordance with the right-hand rule.

- 4.2.2.1.1 Vehicle Angular Orientation—The orientation of the *vehicle axis system* (X_v, Y_v, Z_v) with respect to the *Earth-fixed axis system* (X_E, Y_E, Z_E), for example, as obtained by a sequence of three angular rotations through the *vehicle Euler angles*.

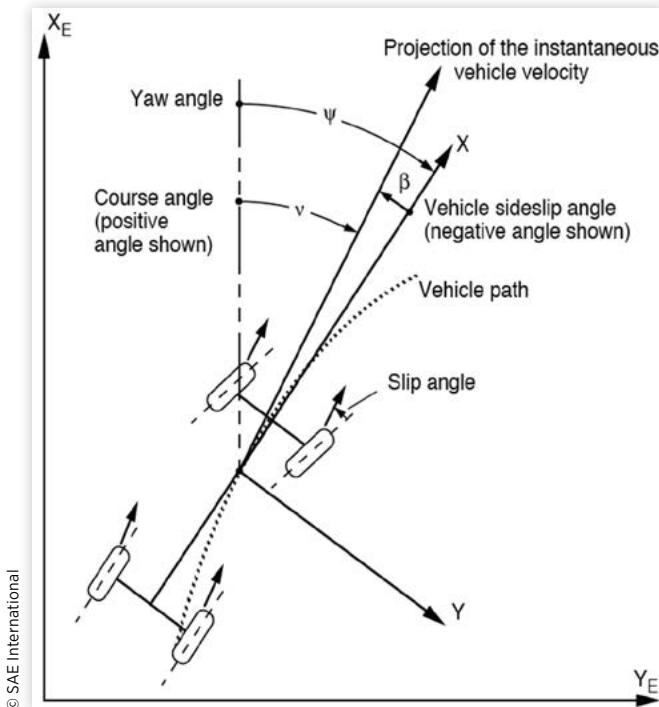
TABLE 1 Vehicle Euler Angles and Standard Order of Rotation

Rotation Order	Angle Produced by Rotation	Rotation Nature
First Rotation	Yaw (ψ)	X_E axis to the X axis about the Z_E axis
Second Rotation	Pitch (θ)	X axis to the X_v axis about the Y axis
Third Rotation	Roll (ϕ)	Y axis to the Y_v axis about the X_v axis

- 4.2.2.1.2 Vehicle Euler Angles (ψ, θ, ϕ)—A sequence of consecutive angular rotations about the Earth-fixed Z_E axis, the intermediate Y axis, and the vehicle X_v axis to obtain the *vehicle angular orientation*. See [Table 1](#).

NOTE—There are other possible sets of orientation angles that can be applied to axis rotations. In choosing a sequence of rotations, the second rotation should ideally span a small angle. The sequence of rotations specified above is preferable for use with the vehicle *sprung mass*, where the magnitude of the *pitch angle* is usually small. Other sets of orientation angles could be chosen for use with individual vehicle components (e.g., rotating *wheels*).

- 4.2.2.1.3 Yaw Angle (Heading Angle) ψ —The angle from the X_E axis to the X axis, about the Z_E axis. See [Figure 3](#).

FIGURE 3 Yaw, Sideslip, and Course Angles (Z-Down Axis Orientation)

- 4.2.2.1.4 **Pitch Angle \$\theta\$**—The angle from the X axis to the \$X_v\$ axis, about the Y axis.

NOTE—The *pitch angle* is not measured relative to the *road plane*, thus a vehicle at rest on an inclined planar *road surface* will have a non-zero *pitch angle*.

- 4.2.2.1.5 **Roll Angle \$\phi\$**—The angle from the Y axis to the \$Y_v\$ axis, about the \$X_v\$ axis.

- 4.2.2.1.6 **Vehicle Roll Angle \$\phi_v\$**—The angle from the *ground plane* to the \$Y_v\$ axis, about the X axis.

NOTE—The *vehicle roll angle* is different from *roll angle* (4.2.2.1.5) if the *pitch angle* is not zero. The *vehicle roll angle* may be computed using the equation:

$$\sin \phi_v = \sin \phi \cos \theta \quad (\text{Eq. 12})$$

The *vehicle roll angle* is not measured relative to the *road plane*; thus, a vehicle at rest on an inclined planar *road surface* will have a non-zero *vehicle roll angle*.

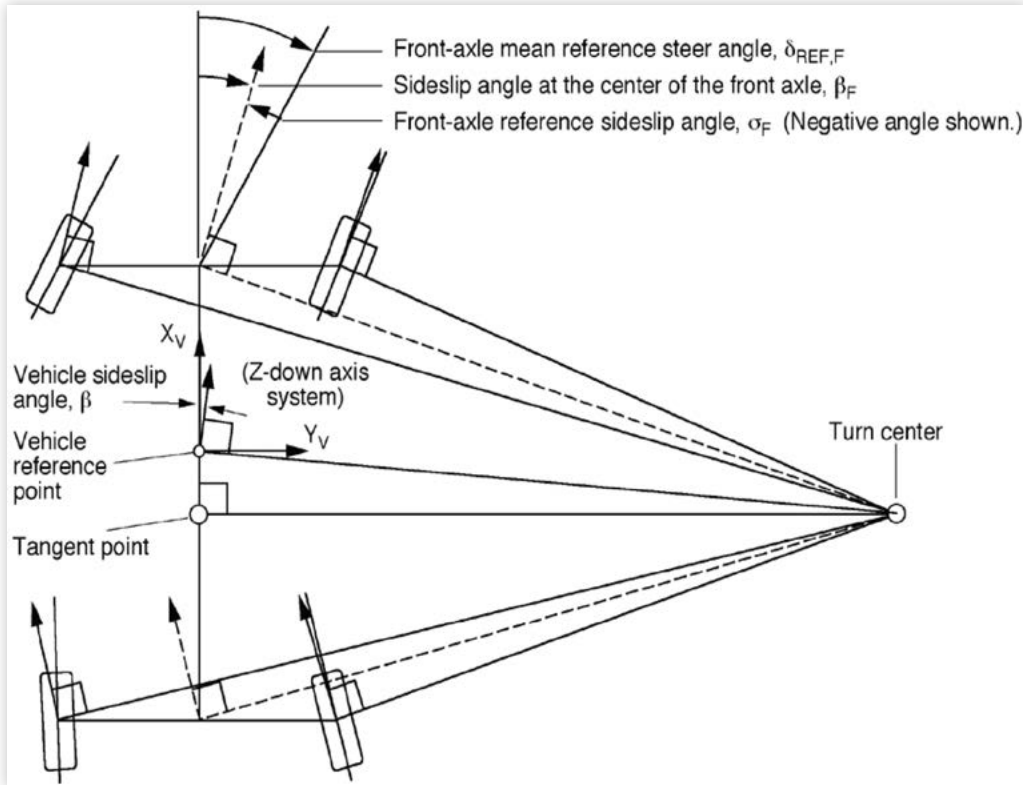
- 4.2.2.1.7 **Sideslip Angle**—At a given point, the angle from the X axis to the vertical projection of the velocity vector of the point onto the *ground plane*, about the Z axis.

4.2.2.1.8 Vehicle Sideslip Angle (Attitude Angle) β —The angle from the X axis to the vertical projection of *vehicle velocity* onto the *ground plane*, about the Z axis. See [Figures 3](#) and [4](#).

NOTE—*Vehicle sideslip angle* may also be calculated from the *longitudinal velocity* v_x and the *lateral velocity* v_y :

$$\beta = \text{Arc tan} \frac{v_y}{v_x} \quad (\text{Eq. 13})$$

FIGURE 4 Vehicle Sideslip, Reference Steer, and Axle Reference Sideslip Angles (Z-Down axis orientation)



© SAE International

4.2.2.1.9 Tangent Point—The point on the X axis whose *sideslip angle* is zero. See [Figure 4](#).

4.2.2.1.10 Axle Reference Sideslip Angle σ_p , σ_r —The *sideslip angle* at the center of a steered *axle* minus the *mean reference steer angle* for the *axle*. See [Figure 4](#).

4.2.2.1.11 Trailer Yaw Articulation Angle Γ ($\Delta\psi$)—The angle from the trailer X_v axis to the normal projection of the tow vehicle X_v axis onto the trailer X_v - Y_v plane, about the trailer Z_v axis. The polarity is determined in the trailer *axis system*.

- 4.2.2.1.12 Trailer Pitch Articulation Angle $\Delta\theta$ —The angle from the trailer X_v axis to the normal projection of the tow vehicle X_v axis onto the trailer X_v – Z_v plane, about the trailer Y_v axis. The polarity is determined in the trailer *axis system*.
- 4.2.2.1.13 Trailer Roll Articulation Angle $\Delta\phi$ —The angle from the trailer Y_v axis to the normal projection of the tow vehicle Y_v axis onto the trailer Y_v – Z_v plane, about the trailer X_v axis. The polarity is determined in the trailer *axis system*.

4.2.2.2 Angular Velocities. In the following paragraphs, angular velocities are relative to the *Earth-fixed axis system* (X_E , Y_E , Z_E). They are resolved into components in the *intermediate axis system* (X , Y , Z).

NOTE—It is also possible to resolve angular velocity vectors into components in other *axis systems*. For example, angular velocity vectors may be resolved in the *vehicle axis system* (X_v , Y_v , Z_v) to produce ω_{Xv} , ω_{Yv} , ω_{Zv} . Traditionally, ω_{Xv} , ω_{Yv} , ω_{Zv} have been represented by the symbols p , q , r .

- 4.2.2.2.1 Vehicle Angular Velocity $\bar{\omega}$ —A vector quantity expressing the angular velocity of the *vehicle axis system*.
- 4.2.2.2.2 Roll Velocity ω_x —The scalar value of the X component of *vehicle angular velocity*.

$$\omega_x = \bar{\omega} \cdot \hat{X} \quad (\text{Eq. 14})$$

- 4.2.2.2.3 Pitch Velocity ω_y —The scalar value of the Y component of *vehicle angular velocity*.

$$\omega_y = \bar{\omega} \cdot \hat{Y} \quad (\text{Eq. 15})$$

- 4.2.2.2.4 Yaw Velocity (Yaw Rate) ω_z —The scalar value of the Z component of *vehicle angular velocity*.

$$\omega_z = \bar{\omega} \cdot \hat{Z} \quad (\text{Eq. 16})$$

4.2.2.3 Angular Accelerations. In the following paragraphs, angular accelerations are relative to the *Earth-fixed axis system* (X_E , Y_E , Z_E). They are resolved into components in the *intermediate axis system* (X , Y , Z). Suggested symbols are not provided for angular accelerations, since the mathematical symbol normally used for angular acceleration (α) is used for tire *slip angle* in vehicle dynamics.

NOTE—It is also possible to resolve angular acceleration vectors into components in other *axis systems*. For example, angular acceleration vectors may be resolved in the *vehicle axis system* (X_v , Y_v , Z_v).

- 4.2.2.3.1 Vehicle Angular Acceleration—A vector quantity expressing the angular acceleration of the *vehicle axis system*.
- 4.2.2.3.2 Roll Acceleration—The scalar value of the X component of *vehicle angular acceleration*.

4.2.2.3.3 Pitch Acceleration—The scalar value of the Y component of *vehicle angular acceleration*.

4.2.2.3.4 Yaw Acceleration—The scalar value of the Z component of *vehicle angular acceleration*.

4.2.3. VEHICLE TRAJECTORY MEASURES

4.2.3.1 Vehicle Trajectory—The path of a selected point on the vehicle in the *Earth-fixed coordinate system*. This point is usually the *vehicle reference point*.

4.2.3.2 Vehicle Path—The vertical projection of the *vehicle trajectory* onto the *ground plane*.

4.2.3.3 Path Radius R—The instantaneous radius of curvature of the *vehicle path*.

NOTE—*Path radius* is the perpendicular distance between the *vehicle path* and the *turn center*. The *path radius* of the *vehicle reference point* may be calculated as:

$$R = \frac{v_h^2}{a_c} \quad (\text{Eq. 17})$$

4.2.3.4 Turn Center—The instantaneous center of curvature of the *vehicle path*.

4.2.3.5 Path Curvature κ —The inverse of *path radius*. Path curvature may be calculated as:

$$\kappa = \frac{1}{R} \quad (\text{Eq. 18})$$

4.2.3.6 Normalized Path Curvature—The *wheelbase* divided by the *path radius* of the *tangent point*.

NOTE—*Normalized path curvature* is the small angle approximation, in radians, of the *included Ackermann steer angle*.

4.2.3.7 Course Angle v —The angle from the X_E axis to the vertical projection of *vehicle velocity* onto the X_E - Y_E plane. See [Figure 3](#). Course angle can be computed from the *yaw angle*, ψ , and the *vehicle sideslip angle*, β :

$$v = \psi + \beta \quad (\text{Eq. 19})$$

4.3 Forces and Moments

External forces and moments acting on the vehicle at any instant may be summed into one resultant force vector and one resultant moment vector. The line of action of the resultant force vector may be moved to any point of interest, providing that the resultant moment vector is altered accordingly. In the following paragraphs, forces and moments are resolved into components in the *intermediate axis system* (X, Y, Z).

NOTE—It is also possible to resolve force and moment vectors into components in other *axis systems*. For example, force and moment vectors may be resolved in the *vehicle axis system* (X_v , Y_v , Z_v) to produce F_{xv} , F_{yv} , F_{zv} and M_{xv} , M_{yv} , M_{zv} . Traditionally, F_{xv} , F_{yv} , F_{zv} have been represented by the symbols X, Y, Z and M_{xv} , M_{yv} , M_{zv} have been represented by the symbols L, M, N.

4.3.1 FORCES

4.3.1.1 Vehicle Force \vec{F} —A vector quantity expressing the sum of the external forces acting on the vehicle at any instant, with its line of action passing through the *vehicle reference point*.

4.3.1.2 Longitudinal Force F_x —The scalar value of the component of *vehicle force* in the direction of the X axis.

$$F_x = \vec{F} \cdot \hat{X} \quad (\text{Eq. 20})$$

4.3.1.3 Lateral Force F_y —The scalar value of the component of *vehicle force* in the direction of the Y axis.

$$F_y = \vec{F} \cdot \hat{Y} \quad (\text{Eq. 21})$$

4.3.1.4 Vertical Force F_z —The scalar value of the component of *vehicle force* in the direction of the Z axis.

$$F_z = \vec{F} \cdot \hat{Z} \quad (\text{Eq. 22})$$

4.3.2 MOMENTS

4.3.2.1 Vehicle Moment \vec{M} —A vector quantity expressing the sum of the external moments acting on the vehicle at any instant, consistent with the line of action of the *vehicle force*.

4.3.2.2 Roll Moment M_x —The scalar value of the component of the *vehicle moment* in the direction of the X axis.

$$M_x = \vec{M} \cdot \hat{X} \quad (\text{Eq. 23})$$

4.3.2.3 Pitch Moment M_y —The scalar value of the component of the *vehicle moment* in the direction of the Y axis.

$$M_y = \vec{M} \cdot \hat{Y} \quad (\text{Eq. 24})$$

4.3.2.4 Yaw Moment M_z —The scalar value of the component of the *vehicle moment* in the direction of the Z axis.

$$M_z = \vec{M} \cdot \hat{Z} \quad (\text{Eq. 25})$$

5. Suspension and Steering

5.1 General Nomenclature

5.1.1 Suspension—A system that provides ride freedom and kinematic control of the motions of the *wheels* at a given longitudinal position on the vehicle.

5.1.1.1 Independent Suspension—A *suspension* utilizing a separate kinematic control mechanism for the *wheel* on each side of the vehicle.

5.1.1.2 Solid-Axle Suspension—A *suspension* utilizing an essentially rigid *axle*.

5.1.1.3 Suspension Corner—For an *independent suspension*: 1) The portion of the *suspension* that controls the kinematic motion of a single *wheel* (left front, right front, left rear, or right rear). 2) The assemblage of the *suspension*, *wheel*, *tire*, *brake*, and all other components that move with a single *wheel*.

5.2 Suspension Components

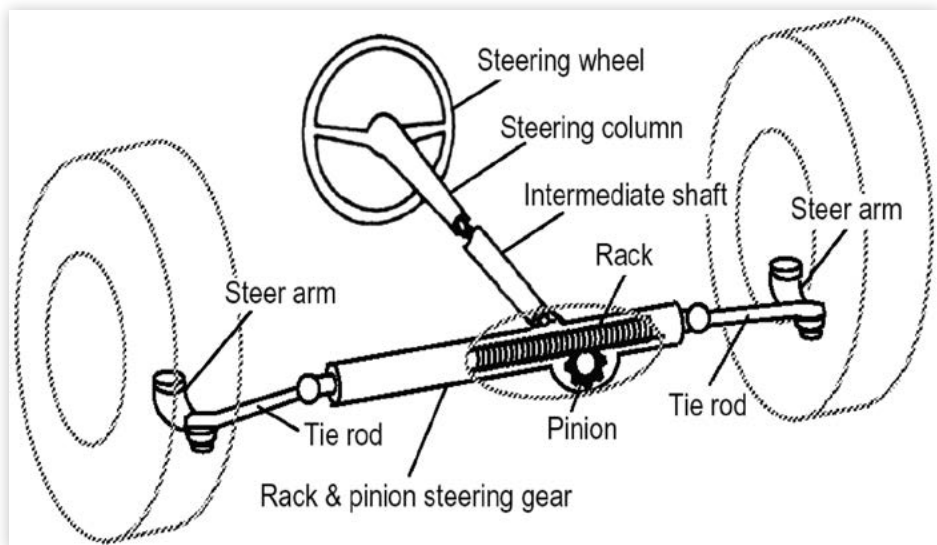
The terms contained in this section and the following section are defined to facilitate communication between vehicle dynamics professionals and engineers involved in the mechanical design of *suspension* and steering systems. Alternative names in common use have been provided for many of these terms. Additional names may be associated with some of these terms due to differences in national or corporate practice.

- 5.2.1 Axle—1) An essentially rigid member used to connect *wheels* on opposite sides of the vehicle at a given longitudinal position. The *axle/wheel* assembly has *suspension ride* and *suspension roll* degrees of freedom relative to the *sprung mass*. 2) The imaginary line connecting the *wheel centers* on opposite sides of the vehicle at a given longitudinal position. 3) Less rigorously, the assemblage of the *suspension*, *wheels*, *tires*, *brakes*, and all other components that move with the *wheels* at a given longitudinal position of the vehicle.
- 5.2.2 Ball Joint (Rod End)—An assemblage of essentially rigid parts, allowing rotational but not translational motion, generally used to connect a *link* or *control arm* to the *knuckle*, or used at each end of a *tie rod*.
- 5.2.3 Bushing—A compliant part that provides primarily rotational motion between a *link* or *control arm* and the body/frame or the *knuckle*. In its most typical form, it is comprised of two (usually steel) concentric cylinders between which is bonded an elastomeric core. Under load, it allows all three linear and all three angular deflections.
- 5.2.4 Control Arm (Wishbone)—A *suspension* part generally used to connect a *knuckle* or *axle* to the *sprung mass*. Kinematically, it consists of a revolute joint at its base and a spherical joint or a revolute joint at its apex. It constrains the motion of the apex to a circular path in a plane perpendicular to the hinge axis at its base. In its most typical form, it is roughly triangular with *bushings* having collinear axes at its base and a *ball joint* at its apex. It may take many forms, with a *bushing* or *ball joint* used at any of the three corners.
- 5.2.5 Damper—A *suspension* part used to provide damping, most commonly in *bounce* and *roll*. A typical damper provides primarily viscous damping, with some attendant Coulomb friction.
 - 5.2.5.1 Shock Absorber—A *damper* that adds negligible kinematic constraint to the *suspension*.
 - 5.2.5.2 Strut—A *damper* that also contributes to rotational constraint of the *knuckle* in camber and caster.
- 5.2.6 Jounce Stop (Jounce Bumper, Bump Stop)—The part that directly limits *jounce* travel of a *suspension*. Jounce stops are usually elastomeric bumpers, but are not limited to this configuration.
- 5.2.7 Rebound Stop—The part that directly limits *rebound* travel of a *suspension*. Rebound stops may be elastomeric bumpers like *jounce stops*, but are often internal stops built into *dampers*.
- 5.2.8 Knuckle (Hub Carrier, Upright)—A *suspension* part that includes the spindle, to which the *control arm(s)*, *link(s)*, *strut*, *ride spring*, and *tie rod* may be attached.

- 5.2.9 Link—An essentially rigid two-force member used to provide kinematic constraint. It typically has a *ball joint* or *bushing* at either end.
- 5.2.9.1 Lateral Link—A *link* used to provide primarily lateral constraint.
 - 5.2.9.2 Leading Link—A *link* used to provide primarily longitudinal constraint whose rearward pivot is attached to the *sprung mass*.
 - 5.2.9.3 Trailing Link—A *link* used to provide primarily longitudinal constraint whose forward pivot is attached to the *sprung mass*.
- 5.2.10 Ride Spring—A spring designed to provide ride compliance for the *suspension*.
NOTE—Commonly used *ride springs* consist of coil springs, leaf springs, torsion bars, and air springs.
- 5.2.11 Stabilizer Bar (Anti-Roll Bar, Anti-Sway Bar)—A torsional spring which is loaded in *suspension roll* to provide additional *suspension roll stiffness*.
NOTE—In its most typical form, a *stabilizer bar* is “U” shaped with the center section orientated laterally and attached to the *sprung mass* with *bushings*. Each end of the “U” attaches to the *control arm*, *knuckle*, or *strut* of an *independent suspension* or the end of an *axle* of a *solid-axle suspension*. Many permutations exist, using *links*, *ball joints* or *bushings* at different locations or with the center section attached to the *unsprung mass*, in the case of a *solid-axle suspension*.
- 5.2.12 Track Bar (Panhard Rod)—A *link* used to provide the primary lateral constraint between the *axle* and the *sprung mass*.
- 5.2.13 Watt Linkage—A four-bar linkage used to provide the primary lateral constraint between the *axle* and the *sprung mass*. It is typically comprised of a vertical member pivoted on the *axle* and two *lateral links*, each attached to it and to the *sprung mass*.

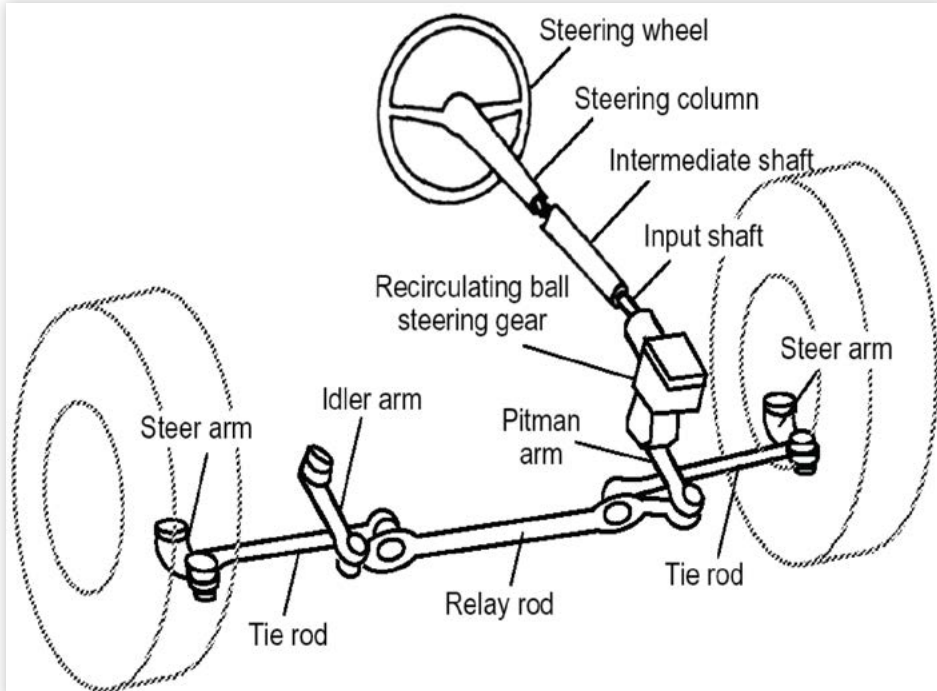
5.3 Steering Components

- 5.3.1 Steering Wheel (Hand Wheel)—The wheel used directly by the driver to steer the vehicle. See [Figures 5](#) and [6](#).
- 5.3.2 Steering Column—A torsional member carrying rotational motion and torsional loads from the *steering wheel* to the *intermediate shaft*. See [Figures 5](#) and [6](#).
- 5.3.3 Intermediate Shaft—A member carrying rotational motion and torsional loads from the *steering column* to the *input shaft*. This component generally contains one or more universal joints or flexible couplings and may also contain a slip joint. See [Figures 5](#) and [6](#).
- 5.3.4 Steering Gear—A gear train and/or mechanism, with housing, carrying steering motion and loads from the *intermediate shaft* to the *tie rods* or *Pitman arm*. A steering gear may have provisions for power assist.
- 5.3.4.1 Rack and Pinion Steering Gear—A *steering gear* employing a rack and pinion gear set. This design transfers rotational motion of the *input shaft* to translational motion of the steering rack. It is used with laterally orientated *tie rods* connected directly to the rack. See [Figure 5](#).

FIGURE 5 Rack and Pinion Steering System

© SAE International

5.3.4.2 Recirculating-Ball Steering Gear (Rotational-Rotational Steering Gear)—A *steering gear* generally employing a ball screw mechanism to transfer rotational motion from the *input shaft* to rotational motion of the *output shaft*. The ball screw mechanism is not required but is widely used and *steering gears* of this general arrangement (rotational-rotational) are so named. See [Figure 6](#).

FIGURE 6 Recirculating-Ball Steering System

© SAE International

NOTE—Many other mechanizations of the *recirculating-ball steering gear* exist (e.g., Acme, worm and sector, worm and roller, cam and peg, etc.), in both manual and power-assisted implementations. These designs are less common in current passenger vehicles, although they are still in use in heavy trucks. The basic mechanical functionality of all these designs is identical, however.

- 5.3.4.3 Input Shaft—A member carrying rotational motion and torsional loads from the *intermediate shaft* into the *steering gear*. The input shaft is considered part of the *steering gear*.
- 5.3.4.4 Output Shaft—A member carrying rotational motion and torsional loads from the *steering gear* to the *Pitman arm*. The output shaft is considered part of a *recirculating-ball steering gear*.
- 5.3.5 Steering Linkage—A kinematic linkage used to transfer motion and loads from the *steering gear* to the *knuckles*.

NOTE—Historically, a wide variety of linkages have been used to perform this function. Currently, common practice on passenger cars and light trucks is the use of lateral *tie rods* acting on longitudinal *steer arms*. *Recirculating-ball steering gears* generally utilize a four-bar linkage (*parallelogram linkage*), of which the *Pitman arm* is one *link*, to transmit motion and loads to the *tie rods*. In systems utilizing *rack and pinion steering gears*, the *tie rods* directly connect the steering rack to the *steer arms*.

- 5.3.5.1 Tie Rod—A lateral *link* connecting the *steer arm* to either the remainder of the *steering linkage* or to the steering rack of a *rack and pinion steering gear*. See [Figures 5 and 6](#).
- 5.3.5.2 Steer Arm (Knuckle Arm)—A crank, usually integral with the *knuckle*, but possibly attached to it, to which the *steering linkage* is attached. See [Figures 5 and 6](#).
- 5.3.5.3 Parallelogram Linkage—A *steering linkage* that is characterized by a four-bar linkage consisting of the *Pitman arm*, *relay rod*, *idler arm*, and the vehicle chassis, that transmits motion and loads to the *tie rods*. See [Figure 6](#).

NOTE—Generally, this *steering linkage* design is not a true parallelogram linkage, due to design considerations that provide *Ackermann geometry* corrections. Typical linkages are actually trapezoidal linkages.

- 5.3.5.3.1 Pitman Arm—A crank that attaches to the *output shaft* of a *recirculating-ball steering gear*. See [Figure 6](#).
- 5.3.5.3.2 Idler Arm—A *link* that provides a motion constraint in a *parallelogram linkage*. The idler arm is the *link* opposite to the *Pitman arm* and connects the *relay rod* to the chassis. See [Figure 6](#).
- 5.3.5.3.3 Relay Rod (Center Link)—A lateral *link* that connects the *tie rods* in a *parallelogram linkage*. The motion of the relay rod is constrained by the motion of the *Pitman arm* and the *idler arm*. See [Figure 6](#).

5.4 Masses and Inertias

- 5.4.1 Unsprung-Mass Center of Gravity—The center of gravity of the *unsprung mass* with a given set of *suspension trim heights*.

NOTE—*Unsprung-mass centers of gravity* may also be separately defined for the front and rear *axles* and, further, for *independent suspensions*, for individual *suspension corners*. If centers of gravity are defined for subsets of the total *unsprung mass*, the location being referenced must be explicitly identified (e.g., Left Front Unsprung Mass Center of Gravity).

- 5.4.2 Unsprung-Mass Moments of Inertia

The following definitions apply to the total inertia of the vehicle *unsprung mass* with a given set of *suspension trim heights*.

NOTE—Moments of inertia may also be separately defined for the front and rear *axles* and, further, for *independent suspensions*, for individual *suspension corners*. If inertias are defined for subsets of the total *unsprung mass*, the moments are taken about axes parallel to the vehicle axes (X_v , Y_v , Z_v) that pass through the center of gravity of the *suspension* components under consideration. The location of the inertia must be explicitly identified (e.g., Left Rear Unsprung Mass Pitch Moment of Inertia).

- 5.4.2.1 Unsprung-Mass Roll Moment of Inertia—The moment of inertia of the *unsprung mass*, taken about an axis parallel to the X_v axis that passes through the *unsprung-mass center of gravity*.

- 5.4.2.2 Unsprung-Mass Pitch Moment of Inertia—The moment of inertia of the *unsprung mass*, taken about an axis parallel to the Y_v axis that passes through the *unsprung-mass center of gravity*.

- 5.4.2.3 Unsprung-Mass Yaw Moment of Inertia—The moment of inertia of the *unsprung mass*, taken about an axis parallel to the Z_v axis that passes through the *unsprung-mass center of gravity*.

- 5.4.3 Spin Moment of Inertia—The moment of inertia of the rotating components at an individual *suspension corner*, taken about the local Y_w axis. The rotating components typically include the *wheel*, *tire*, *brake rotor* or *brake drum*, and the drive axle or half shaft. The location of the inertia must be explicitly identified (e.g., Right Rear Spin Moment of Inertia).

- 5.4.4 Steer Moment of Inertia—The moment of inertia of the steered components at an individual *suspension corner*, taken about the local *steering axis*. The steered components typically include the *knuckle*, *wheel*, *tire*, *brake rotor* or *brake drum*, *brake apply components* (*brake caliper* and *brake pads* or *brake shoes*, *wheel cylinder*, return springs, *brake backing plate*, etc.), and *steering tie rods*. The location of the inertia must be explicitly identified (e.g., Right Front Steer Moment of Inertia).

5.5 Geometry

5.5.1 STEER AND CAMBER ANGLES

- 5.5.1.1 Steer Angle (Road Wheel Steer Angle) δ —For each road *wheel*, the angle from the X_v axis to the *wheel plane*, about the Z_v axis.

NOTE—The sign of the *steer angle* is determined using the right hand rule. For the same physical case, the sign of *steer angle* is reversed in the Z-Up and Z-Down axis orientations.

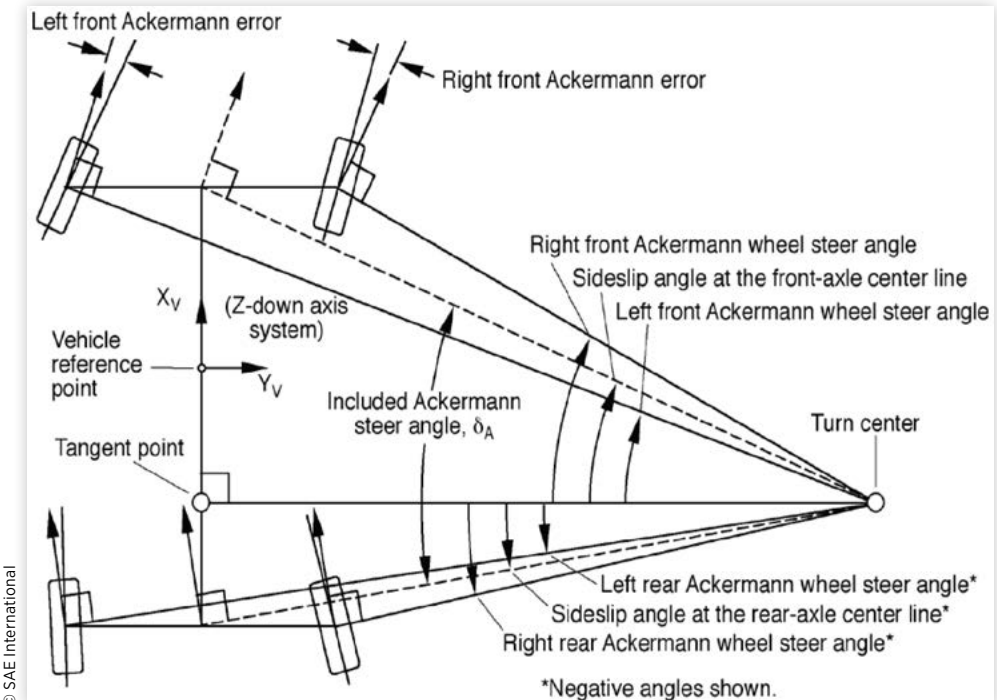
5.5.1.2 Reference Steer Angle—For each steerable *wheel*, the *steer angle* corresponding to a given *steering-wheel angle*, defined by the kinematics of the steering system in the absence of *suspension roll* and *tire forces and moments*, but including static *tire vertical load*, with the vehicle at rest at a specified *load condition*, set of *vehicle trim heights*, or set of *suspension trim heights*.

NOTE—If the kinematic relationship between the *steering-wheel angle* and the *steer angle* is a function of vehicle speed, the *reference steer angle* should be determined at the *speed* of interest. Other factors influencing the relationship between *steering-wheel angle* and *steer angle* (e.g., *yaw velocity*, *lateral acceleration*) are not considered in determining the *reference steer angle*.

5.5.1.3 Ackermann Wheel Steer Angle—For each individual *wheel*, the *steer angle* necessary to cause the local Y_T axis to pass through the vehicle *turn center*. See Figure 7.

NOTE—This definition is more general than the definition used in previous versions of SAE J670 in order to accommodate four-wheel steering. For a front-steer vehicle with the *turn center* lying on a projection of the rear *axle* centerline, this definition accommodates the former definition and defines an *Ackermann wheel steer angle* for both front *wheels*.

FIGURE 7 Ackermann Geometry (Z-Down axis orientation)



5.5.1.4 Mean Reference Steer Angle—The average *reference steer angle* for a pair of *wheels* on an *axle*. See [Figure 4](#).

5.5.1.5 Included Reference Steer Angle δ_{REF} —The *mean reference steer angle* of the front *axle* minus the *mean reference steer angle* of the rear *axle*.

5.5.1.6 Included Ackermann Steer Angle δ_A —The *sideslip angle* of the centerline of the front *axle* minus the *sideslip angle* of the centerline of the rear *axle*. This is the included angle between the line from the *turn center* to the centerline of the front *axle* and the line from the *turn center* to the centerline of the rear *axle*. See [Figure 7](#).

$$\delta_A = \text{Arctan} \frac{L_F}{R} - \text{Arctan} \frac{L_R}{R} \quad (\text{Eq. 26})$$

Where L_F is the signed distance from the *tangent point* to the front *axle*, L_R is the signed distance from the *tangent point* to the rear *axle*, and R is the *path radius* of the *tangent point*.

NOTE—For a *tangent point* located between the *axles*, L_F will be positive and L_R will be negative.

5.5.1.7 Toe Angle—The angle between the X_v axis and the *wheel plane*, about the Z_v axis. The *wheel* has toe-in if the forward portion of the *wheel* is closer to the vehicle centerline than the *wheel center* and has toe-out if it is farther away. By convention, toe-in is considered a positive angle, and toe-out is a negative angle.

NOTE—Static wheel alignment settings for *toe angle*, as well as *static toe*, *camber angle*, *caster angle*, and *steering axis inclination angle*, are normally specified with the vehicle at rest at a given *load condition*, set of *vehicle trim heights*, or set of *suspension trim heights*, with a *steering-wheel angle* of zero, zero *suspension roll angle*, on a horizontal, planar surface.

5.5.1.8 Total Toe Angle (Sum Toe Angle)—The total angle between a pair of *wheels* on an *axle*. The value is equal to the sum of the *toe angles* for the two *wheels*.

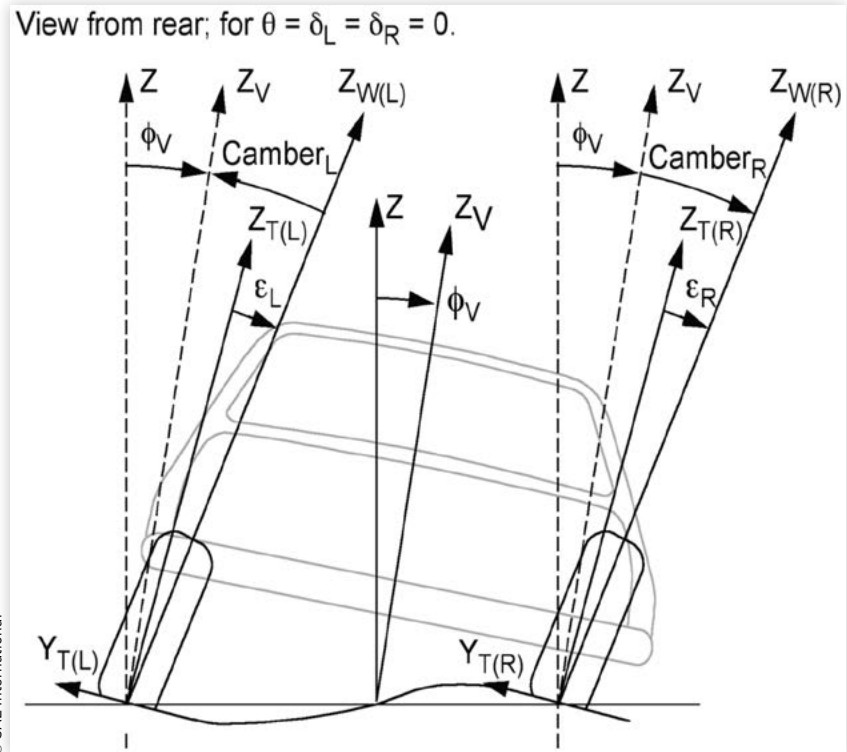
5.5.1.9 Static Toe—The difference in the transverse distances between the *wheel planes* of a pair of *wheels* on an *axle*, taken at the extreme rear and front points of the tire tread or between corresponding points on the *rim*. The measurement location must be specified. When the distance at the rear is greater, the *wheels* have this amount of toe-in, and where smaller, the *wheels* have toe-out.

NOTE—*Static toe* is equal to the product of *total toe angle* in radians and 1) the *tire overall diameter*, if taken at the tire tread; or 2) the *rim diameter*, if taken at the *rim*.

5.5.1.10 Camber Angle—The angle between the Z_v axis and the *wheel plane*, about the X_v axis. It is considered positive when the *wheel* leans outward at the top and negative when it leans inward. See [Figure 8](#).

NOTE—*Camber angle* is a measure of the orientation of the *wheel plane* relative to the vehicle, and is independent of *road plane* geometry. *Camber angle* should not be confused with *inclination angle*, which is a measure of the *wheel plane orientation* relative to the *road plane*. The relation between *camber angle*, *inclination angle*, and *vehicle roll angle* is shown in [Figure 8](#).

FIGURE 8 Camber, Inclination, and Vehicle Roll Angles (Z-Up axis orientation shown, sign of angles is identical for Z-Down axis orientation)



© SAE International

5.5.2 STEERING-AXIS GEOMETRY

5.5.2.1 Steering Axis (Kingpin Axis)—The axis of rotation of the *knuckle* relative to the vehicle *sprung mass* when steered.

NOTE—The *steering axis* is typically determined with the steering system free of any loads except those associated with the static reference condition.

The *steering axis* may shift as the *steer angle* changes, due to *suspension kinematics* and *compliances*.

5.5.2.2 Caster Angle—The angle between the Z_v axis and the normal projection of the *steering axis* onto the X_v-Z_v plane. The angle is positive when the top of the *steering axis* is inclined rearward.

5.5.2.3 Caster Offset at Wheel Center (Spindle Trail)—The distance, measured parallel to the X_v axis, from the normal projection of the *wheel center* onto the X_v-Z_v plane to the normal projection of the *steering axis* onto the X_v-Z_v plane. This distance is positive if the projection of the *steering axis* is forward of the projection of the *wheel center*.

5.5.2.4 Caster Offset at Ground (Caster Trail)—The distance in the X_t direction from the Y_t-Z_t plane to the point where the *steering axis* intersects the X_t-Y_t plane. This distance is positive if the *steering-axis* intersection point is forward of the Y_t-Z_t plane.

- 5.5.2.5 Steering-Axis Inclination Angle (Kingpin Inclination Angle)—The angle between the Z_v axis and the normal projection of the *steering axis* onto the Y_v - Z_v plane. The angle is positive when the top of the *steering axis* is inclined inward.
- 5.5.2.6 Steering-Axis Offset at Wheel Center (Kingpin Offset at Wheel Center)—The distance, measured parallel to the Y_v axis, from the normal projection of the *wheel center* onto the Y_v - Z_v plane to the normal projection of the *steering axis* onto the Y_v - Z_v plane. This distance is positive if the projection of the *steering axis* is inboard of the projection of the *wheel center*.
- 5.5.2.7 Steering-Axis Offset at Ground (Kingpin Offset at Ground, Scrub Radius)—The distance in the Y_T direction between the *wheel plane* and the point where the *steering axis* intersects the X_T - Y_T plane. This distance is positive if the *steering-axis* intersection point is inboard of the *wheel plane*.
- 5.5.2.8 Spindle Length—The distance in the Y_w direction from the *wheel center* to the normal projection of the *steering axis* onto the Y_w - Z_w plane. This distance is positive if the projection of the *steering axis* is inboard of the *wheel center*.

5.6 Suspension Motions

- 5.6.1 Jounce (Compression, Bump)—An upward vertical displacement of the *wheel center* relative to the *sprung mass* from a specified reference *suspension trim height*.
- 5.6.2 Rebound (Extension, Droop)—A downward vertical displacement of the *wheel center* relative to the *sprung mass* from a specified reference *suspension trim height*.
- 5.6.3 Suspension Ride—*Jounce* or *rebound* displacement or velocity of a pair of *wheels* on the same *axle*, which is symmetric with respect to the *vehicle plane of symmetry*.
- 5.6.4 Suspension Roll—*Jounce* or *rebound* displacement or velocity of a pair of *wheels* on the same *axle*, which is antisymmetric with respect to the *vehicle plane of symmetry*.

NOTE—*Suspension ride* and *suspension roll* are qualitative terms describing two special cases of *suspension* vertical motion, which may refer to either displacement or velocity. Any *suspension* displacement or velocity involving *jounce* or *rebound* motion may be viewed as a combination of *suspension ride* and *suspension roll*.

- 5.6.5 Suspension Ride Displacement—The *jounce* or *rebound* displacement produced by *suspension ride*, relative to a pair of reference *suspension trim heights*.
- 5.6.6 Suspension Roll Angle—The angular displacement produced by *suspension roll* relative to a pair of reference *suspension trim heights*. The angular displacement is defined by the normal projection of a line connecting the two *wheel centers* onto the Y_v - Z_v plane.

5.7 Kinematics

Many of the terms defined in this section may be signed. Signs may be assigned based on 1) the direction of the kinematic change and the *axis system* in use, or 2) by the

assumed effect of the kinematic change on the *understeer / oversteer gradient*. The sign convention is dependent on the practices of the organization performing the testing or analysis.

Many of the terms that are defined in this section begin with or include the word “*suspension*” (e.g., Suspension Ride Camber). The definitions of such terms typically make reference to *suspension motion* or displacement. Inclusion of the word “*suspension*” indicates that the relative motion or displacement of interest is that of the *wheel center* in the *vehicle axis system* (i.e., motion of the *suspension* alone and not including *tire deflection*). In most cases, a similar term that does not include the word “*suspension*” (e.g., Ride Camber) could be defined. In this case, the relative motion or deflection of interest would be that of the *tire contact center* in the *vehicle axis system* (i.e., including *tire deflections*).

5.7.1 RIDE KINEMATICS

5.7.1.1 Front- (Rear-) View Swing Center—For *suspension ride* motion, the instant center of the normal projection of the path of the *wheel center* onto the Y_v - Z_v plane. A front-view swing center may be defined at each *suspension trim height*.

5.7.1.2 Front- (Rear-) View Swing-Arm Length—The distance from the *front-view swing center* to the normal projection of the point of interest onto the Y_v - Z_v plane.

NOTE—Commonly used points of interest are the *wheel center* and the *tire contact center*. The point of interest used should be included with the term for clarity (e.g., Front-View Swing-Arm Length to Wheel Center).

5.7.1.3 Front- (Rear-) View Swing-Arm Angle—The angle from the Y_v axis to the line that passes through the *front-view swing center* and the normal projection of the point of interest onto the Y_v - Z_v plane.

NOTE—Commonly used points of interest are the *wheel center* and the *tire contact center*. The point of interest used should be included with the term for clarity (e.g., Front-View Swing-Arm Angle to Wheel Center).

5.7.1.4 Side-View Swing Center—For *suspension ride* motion, the instant center of the normal projection of the path of the *wheel center* onto the X_v - Z_v plane. A side-view swing center may be defined at each *suspension trim height*.

5.7.1.5 Side-View Swing-Arm Length—The distance from the *side-view swing center* to the normal projection of the point of interest onto the X_v - Z_v plane.

NOTE—Commonly used points of interest are the *wheel center* and the *tire contact center*. The point of interest used should be included with the term for clarity (e.g., Side-View Swing-Arm Length to Wheel Center).

5.7.1.6 Side-View Swing-Arm Angle—The angle from the X_v axis to the line that passes through the *side-view swing center* and the normal projection of the point of interest onto the X_v - Z_v plane.

NOTE—Commonly used points of interest are the *wheel center* and the *tire contact center*. The point of interest used should be included with the term for clarity (e.g., Side-View Swing-Arm Angle to Wheel Center).

- 5.7.1.7 Suspension Ride Camber—The change of *camber angle* resulting from a given *suspension ride displacement*.
- 5.7.1.8 Suspension Ride Camber Gradient—The rate of change of *camber angle* with respect to *suspension ride displacement* at a given *suspension ride displacement*.
- 5.7.1.9 Suspension Ride Caster—The change of *caster angle* resulting from a given *suspension ride displacement*.
- 5.7.1.10 Suspension Ride Caster Gradient—The rate of change of *caster angle* with respect to *suspension ride displacement* at a given *suspension ride displacement*.
- 5.7.1.11 Suspension Ride Toe—The change of *toe angle* of a *wheel* resulting from a given *suspension ride displacement*.
- 5.7.1.12 Suspension Ride Toe Gradient—The rate of change of *toe angle* with respect to *suspension ride displacement* at a given *suspension ride displacement*.
- 5.7.1.13 Suspension Ride Steer—The change of *steer angle*, δ , of a *wheel* resulting from a given *suspension ride displacement*.
- 5.7.1.14 Suspension Ride Steer Gradient—The rate of change of *steer angle*, δ , with respect to *suspension ride displacement* at a given *suspension ride displacement*.
- 5.7.1.15 Net (Average) Suspension Ride Steer—The change in *steer angle* for an *axle* resulting from *suspension ride displacement*. It is the average of the *suspension ride steer* changes for the left and right *wheels*.
- 5.7.1.16 Ride Track Change—The change of *track*, T , for an *axle* resulting from a given *suspension ride displacement*.
- 5.7.1.17 Ride Track Change Gradient—The rate of change of *track*, T , for an *axle* with respect to *suspension ride displacement* at a given *suspension ride displacement*.
- NOTE—*Ride track change gradient* exists for a symmetrical *independent suspension* when the *front-view swing centers* are not in the *road plane*. For such a *suspension*, half of the *ride track change gradient* is generally of more interest because it is the tangent of each *front-view swing-arm angle to contact center*, including a slight error due to *tire deflections*. For asymmetrical *independent suspensions*, the *ride track change gradient* is the sum of contributions from each side of the *suspension* and half its value may not be related to the kinematic properties of either side. In this case, half-track change gradients for each side would equal the tangents of the *front-view swing-arm angle to contact center* for each side, again including a slight error due to *tire deflections*. The *ride track change gradient* for solid-*axle suspensions* is zero.

5.7.2 ROLL KINEMATICS

- 5.7.2.1 Suspension Roll Camber—The change of *camber angle* resulting from a given *suspension roll angle*.
- 5.7.2.2 Suspension Roll Camber Gradient—The rate of change of *camber angle* with respect to *suspension roll angle* at a given *suspension roll angle*.
- 5.7.2.3 Suspension Roll Inclination—The change of *inclination angle*, ϵ , resulting from a given *suspension roll angle*.

5.7.2.4 Suspension Roll Inclination Gradient—The rate of change of *inclination angle*, e , with respect to *suspension roll angle* at a given *suspension roll angle*.

NOTE—This definition was applied to the term “roll camber coefficient” in previous editions of SAE J670. The magnitude of the *suspension roll inclination gradient* will be different from the magnitude of the *suspension roll camber gradient* defined above, since the *suspension roll inclination gradient* quantifies the angular change of the *wheel* relative to the *road plane*, while the *suspension roll camber gradient* quantifies the angular change of the *wheel* relative to the *sprung mass*.

5.7.2.5 Suspension Roll Caster—The change of *caster angle* resulting from a given *suspension roll angle*.

5.7.2.6 Suspension Roll Caster Gradient—The rate of change of *caster angle* with respect to *suspension roll angle* at a given *suspension roll angle*.

5.7.2.7 Suspension Roll Steer—The change of *steer angle*, δ , resulting from a given *suspension roll angle*.

5.7.2.8 Suspension Roll Steer Gradient—The rate of change of *steer angle*, δ , with respect to *suspension roll angle* at a given *suspension roll angle*.

5.7.2.9 Roll Center—The point in the transverse vertical plane through the *wheel centers* on an *axle* at which lateral forces may be applied to the *sprung mass* without producing *suspension roll*.

NOTE—The *roll center* constitutes an idealized kinematic concept and does not necessarily represent a true instantaneous center of rotation of the *sprung mass*.

5.7.2.10 Roll Center Height—The height of the *roll center* above a line connecting the *tire contact centers* for an *axle*.

5.7.2.11 Roll Axis—The line joining the front and rear *roll centers*.

5.7.3 STEERING KINEMATICS

5.7.3.1 Steer Camber—The change in *camber angle* resulting from a given *steer angle* displacement.

5.7.3.2 Steer Camber Gradient—The rate of change of *camber angle* with respect to *steer angle* at a given *steer angle*.

5.7.3.3 Steer Caster—The change in *caster angle* resulting from a given *steer angle* displacement.

5.7.3.4 Steer Caster Gradient—The rate of change of *caster angle* with respect to *steer angle* at a given *steer angle*.

5.7.3.5 Ackermann Geometry—Steering-system kinematics which provide for the intersection of the *tire axis system* Y_T axes of the steerable *wheels* at the *turn center*, for non-zero *steering-wheel angles* at negligible *lateral acceleration*. See [Figure 7](#).

NOTE—Ackermann geometry may be achieved at one or more *steering-wheel angles* during steering articulation. For a front steer only vehicle, the

turn center is on the line defined by the rear *wheel centers*. For a four-wheel steer vehicle, the *turn center* is generally not on this line. A steering system with *Ackermann geometry* is said to have 100% Ackermann correction, and one with equal *steer angles* (parallel steer) on the steerable *axle* is said to have 0% Ackermann correction. The Ackermann correction may be less than 0% or greater than 100%.

5.7.3.6 Ackermann Error—The kinematic inconsistency in *steer angle* between two steerable *wheels* on an *axle* with respect to the *turn center*. See [Figure 7](#).

NOTE—For a front steer only vehicle, *Ackermann error* exists if the *tire axis system* Y_T axes of the steerable *wheels* do not intersect on the line defined by the rear *wheel centers*. For a four-wheel steer vehicle, *Ackermann error* exists if the *tire axis system* Y_T axes of the steerable *wheels* do not intersect at a point. If *Ackermann error* exists, an ideal *turn center* may be defined by the intersection of the *tire axis system* Y_T axes of the inner *wheels*. In this case, *Ackermann error* is the difference between the actual outer *wheel steer angle* and the ideal outer *wheel steer angle*, for which the *tire axis system* Y_T axis passes through the ideal *turn center*. *Ackermann error* is defined only at the front *axle* for a front steer only vehicle and at both the front and rear *axles* for a four-wheel steer vehicle.

5.7.3.7 Steering Ratio—The rate of change of *steering-wheel angle* with respect to the *mean reference steer angle* of a pair of steered *wheels* at a given *steering-wheel position*.

5.7.3.8 Overall Steering Ratio—The rate of change of *steering-wheel angle* with respect to *included reference steer angle* at a given *steering-wheel position*.

5.7.3.9 Gear Ratio—The rate of change of *input shaft angle* with respect to *output shaft angle* at a given *input shaft angle*, assuming an infinitely stiff steering gear.

5.7.3.10 Linkage Ratio—The rate of change of *output shaft angle* with respect to the average *steer angle* of a pair of steered *wheels* at a given *output shaft angle*, assuming an infinitely stiff *steering linkage* with no *suspension roll*.

5.7.3.11 C-Factor (Rack Ratio, Rack Speed)—For a *rack and pinion steering gear*, the rate of change of rack position with respect to *input shaft angle* at a given *input shaft angle*, assuming an infinitely stiff steering gear.

NOTE—The *C-Factor* is commonly expressed as the linear rack travel for one complete revolution of the *input shaft*, e.g., 48 mm/rev. For a constant ratio *rack and pinion steering gear*, the *C-Factor* nominally equals the circumference of the pinion pitch circle. This will generally not be true for a variable ratio steering gear.

5.7.4 ANTI- CHARACTERISTICS: *Tire shear forces* acting in the *road plane* are reacted by opposing forces in the vehicle *sprung mass* that act through the instant center of rotation of the *suspension* in side view or through the instant center of rotation of the *suspension corner* in front view. These force pairs form couples in side view or in front view. *Suspension anti- characteristics* are a means of quantifying the kinematic properties of *suspensions* that create opposing couples that reduce changes in *suspension spring*

force, thereby reducing the *suspension motion* that would otherwise occur because of *longitudinal load transfer* or *lateral load transfer*. *Suspension anti-* characteristics may be quantified as the change in *tire normal force* resulting from a unit change in *tire longitudinal force* or *tire lateral force*. *Anti-* characteristics may also be quantified by considering the total amount of *longitudinal load transfer* or *lateral load transfer* reacted through the *suspension* of interest. This representation expresses the strength of the *anti-* property as a percentage, where 0% implies no influence on the change in *suspension spring load* and 100% implies an exact cancellation of the change in *suspension spring load*. The percent *anti-* can be less than 0% or greater than 100%. For longitudinal *anti's*, the configuration of the drivetrain or braking system will determine whether *driving torque* or *braking torque* is reacted through the *suspension* or reacted directly by the *prung mass*, which will affect the magnitude of the *anti-* characteristic.

- 5.7.4.1 Anti-Dive—A property of front *suspension* side-view kinematics whereby *tire braking forces* at the front *wheels* are reacted in a manner that reduces changes in *suspension* spring loads relative to those that would have occurred due to the *longitudinal load transfer*.
- 5.7.4.2 Braking Anti-Lift—A property of rear *suspension* side-view kinematics whereby *tire braking forces* at the rear *wheels* are reacted in a manner that reduces changes in *suspension* spring loads relative to those that would have occurred due to the *longitudinal load transfer*.
- 5.7.4.3 Acceleration Anti-Lift—A property of front *suspension* side-view kinematics whereby *tire driving forces* at the front *wheels* are reacted in a manner that reduces changes in *suspension* spring loads relative to those that would have occurred due to the *longitudinal load transfer*.
- 5.7.4.4 Anti-Squat—A property of rear *suspension* side-view kinematics whereby *tire driving forces* at the rear *wheels* are reacted in a manner that reduces changes in *suspension* spring loads relative to those that would have occurred due to the *longitudinal load transfer*.
- 5.7.4.5 Anti-Roll—A property of *suspension* front-view kinematics whereby *tire lateral forces* are reacted in a manner that reduces changes in *suspension* spring loads relative to those that would have occurred due to *lateral load transfer*.

5.8 Ride and Roll Stiffness

- 5.8.1 Ride Rate—The rate of change of *tire normal force* with respect to displacement of the *tire contact center* in the Z_v direction during *suspension ride* motion, at a specified *suspension trim height*.
- 5.8.2 Suspension Ride Rate (Wheel Rate)—The rate of change of *tire normal force* with respect to displacement of the *wheel center* in the Z_v direction during *suspension ride* motion, at a specified *suspension trim height*.

NOTE—*Ride rate* and *suspension ride rate* apply to a single *tire* or *wheel* and are, therefore, so-called quarter-car properties. Similar terms could apply to the sum of the rates of both *tires* and *wheels* on an *axle* (i.e., Axle Ride Rate and Axle Suspension Ride Rate).

- 5.8.3 Roll Stiffness (Roll Rate)—The rate of change of the restoring couple exerted by a *suspension* on the *sprung mass* with respect to the angular change about the X_v axis of a line connecting the *tire contact centers* of an *axle*, at a specified pair of *suspension trim heights*.
- 5.8.4 Suspension Roll Stiffness (Suspension Roll Rate)—The rate of change of the restoring couple exerted by a *suspension* on the *sprung mass* with respect to *suspension roll angle*, at a specified pair of *suspension trim heights*.
- 5.8.5 Vehicle Roll Stiffness—The sum of the separate *roll stiffnesses*.
- 5.8.6 Roll Stiffness Distribution—The distribution of the *vehicle roll stiffness* between the front and rear *suspensions* expressed as a percentage of the *vehicle roll stiffness*.
- NOTE—The terms *vehicle roll stiffness* and *roll stiffness distribution* are both based on the definition of *roll stiffness*. These concepts therefore include the influence of the compliances of the *tires* as well as the *compliances* of the *suspensions*. Similar terms (and concepts) that would exclude the influence of the *tires* and would depend only on the *compliances* of the *suspension* could be defined by using *suspension roll stiffness* as the basis.

5.9 Compliances

The terms defined in this section may be signed. Signs may be assigned based on 1) the direction of the compliance change and the polarity of the force or moment producing the change, according to the *axis system* in use, or 2) by the assumed effect of the compliance change on the *understeer / oversteer gradient*. The sign convention is dependent on the practices of the organization performing the testing or analysis.

Tire forces and moments produce compliance deflections. When these deflections are separated into components, the force or moment producing the component deflection is prefixed to the name of the compliance, for example *Lateral Force Compliance Camber*.

Compliant deflections produced by *tire longitudinal force* are affected by the manner in which the wheel-spin degree of freedom is constrained (*driveshaft or brakes*).

5.9.1 CAMBER AND STEER COMPLIANCES

- 5.9.1.1 Compliance Camber—The *camber angle* displacement of a *wheel* resulting from compliances in *suspension components*, *steering components*, and vehicle structure, produced by *tire forces and moments*.
- 5.9.1.2 Camber Compliance (Compliance Camber Coefficient)—The rate of change of *inclination angle*, ϵ , with respect to a *tire force or moment*.
- 5.9.1.3 Compliance Steer—The *steer angle* displacement of a *wheel* resulting from compliances in *suspension components*, *steering components*, and vehicle structure, produced by *tire forces and moments*.
- 5.9.1.4 Steer Compliance (Compliance Steer Coefficient)—The rate of change of *steer angle*, δ , with respect to a *tire force or moment*.

5.9.2 OTHER COMPLIANCES

- 5.9.2.1 Lateral Compliance at the Wheel Center—The rate of change of the lateral displacement of the *wheel center* resulting from compliances in *suspension components, steering components*, and vehicle structure, with respect to a *tire force or moment*.
- 5.9.2.2 Lateral Compliance at the Contact Center—The rate of change of the lateral displacement of the *tire contact center* resulting from compliances in *suspension components, steering components*, and vehicle structure, with respect to a *tire force or moment*.
- 5.9.2.3 Longitudinal Compliance—The rate of change of the longitudinal displacement of the *wheel center* resulting from compliances in *suspension components, steering components*, and vehicle structure, with respect to a *tire force or moment*.
- 5.9.2.4 Windup Compliance—The rate of change of the angular displacement of the *wheel* about the *wheel-spin axis* resulting from compliances in *suspension components, steering components*, and vehicle structure, with respect to a *tire force or moment*.
- 5.9.2.5 Axle Windup Compliance—The rate of change of the angular displacement of the *axle* housing of a *solid-axle suspension* about the *wheel-spin axis* resulting from compliances in *suspension components, steering components*, and vehicle structure, with respect to a *tire force or moment*.

6. Brakes

6.1 General Nomenclature

- 6.1.1 Brake—A device whose function is to develop *brake torque* that directly opposes the longitudinal motion of a vehicle.
- 6.1.2 Friction Brake—A *brake* that develops *brake torque* by means of friction between a fixed and rotating member. Dynamically, friction brakes convert mechanical energy into heat. Statically, friction brakes use friction to prevent rotation of the *wheels*.
- 6.1.3 Regenerative Brake—A *brake* that develops *brake torque* by converting mechanical energy into stored energy.
- 6.1.4 Disc Brake—A *friction brake* that develops *brake torque* by clamping a disk-shaped rotating member between non-rotating pieces of *friction material*. The direction of the clamping force application is axial.
- 6.1.5 Drum Brake—A *friction brake* that develops *brake torque* by forcing non-rotating *friction material* radially against a drum-shaped rotating member. In nearly all modern automotive applications, the *friction material* is forced outwardly against the inside surface of a rotating *brake drum*.
- 6.1.6 Anti-Lock Brake System—A closed-loop control system designed to regulate *brake torque* to limit the *tire longitudinal slip ratio* during *brake application*. This is typically accomplished by transducers for sensing *wheel rotation* and an actuation system under control of a computer that regulates *brake pressure*. See also SAE J2564.

- 6.1.7 Brake Pressure—The fluid pressure supplying an individual *brake*.
- 6.1.8 Brake Torque—The torque about the *wheel-spin axis* produced by the *brake*. See also 7.8.2.

6.2 Brake Components

- 6.2.1 Brake Pedal—The pedal used by the driver to actuate the braking system.
- 6.2.2 Master Cylinder—The hydraulic valve assembly used to convert force from the *brake pedal* to hydraulic pressure for *brake* actuation.
- 6.2.3 Proportioning Valve—A hydraulic valve which reduces *brake pressure* supplied to the rear *brakes*, relative to front *brake pressure*, to maintain *brake balance* in the presence of *longitudinal load transfer*.
- 6.2.4 Brake Caliper—The non-rotating part of a *disc brake* which houses the hydraulic cylinder(s) that clamp the *brake pads* against the *brake rotor* during *brake* actuation.
- 6.2.5 Wheel Cylinder—The hydraulic cylinder(s) in a *drum brake* that force the *brake shoes* to press against the *brake drum*.
- 6.2.6 Friction Material (Brake Lining)—The wearing material used to provide frictional effect between the rotating and non-rotating components of a *friction brake*.
- 6.2.7 Brake Pad—The *friction material*, together with a structural substrate, used in *disc brakes*.
- 6.2.8 Brake Shoe—The *friction material*, together with a structural substrate, used in *drum brakes*.
- 6.2.9 Brake Rotor (Brake Disc)—The rotating disc of a *disc brake* upon which the *brake pads* push during *brake* actuation.
- 6.2.10 Brake Drum—The rotating cylinder of a *drum brake* upon which the *brake shoes* push during *brake* actuation.

6.3 Brake Proportioning

- 6.3.1 Brake Balance—A general term used to describe the distribution of *tire braking forces* between the *axles* of a vehicle in relation to the distribution of *tire vertical loads* at a given steady-state *longitudinal acceleration*.

NOTE—A “balanced” brake system provides a distribution of *tire braking forces* that is equal to the distribution of *tire vertical loads* that prevails as the vehicle decelerates. A “front biased” brake system will exhibit a higher ratio of front *tire braking force* to rear *tire braking force* than the ratio of front *tire vertical load* to rear *tire vertical load*. A “rear biased” brake system has the converse *brake balance*.

- 6.3.2 Fixed Proportioning—A braking system that provides a nominally constant ratio of front to rear *brake torque* at all levels of *brake pedal force*.
- 6.3.3 Variable Proportioning—A braking system that alters the ratio of front to rear *brake torque* as a function of a relevant operating condition (e.g., *brake pressure*, *suspension ride displacement*, *longitudinal acceleration*).

7. Tires and Wheels

The information contained in this section is derived from SAE J2047 (1998) and is relevant to vehicle dynamics. This section specifically does not contain information on dynamic forces, tire uniformity characteristics, tire noise and vibration, tire tread wear, tire structural degradation, and tire integrity.

Specific tire and rim dimensions and designations are established by tire and rim standards organizations, for example:

The Tire and Rim Association, 175 Montrose West Ave., Copley, OH 44321

Or

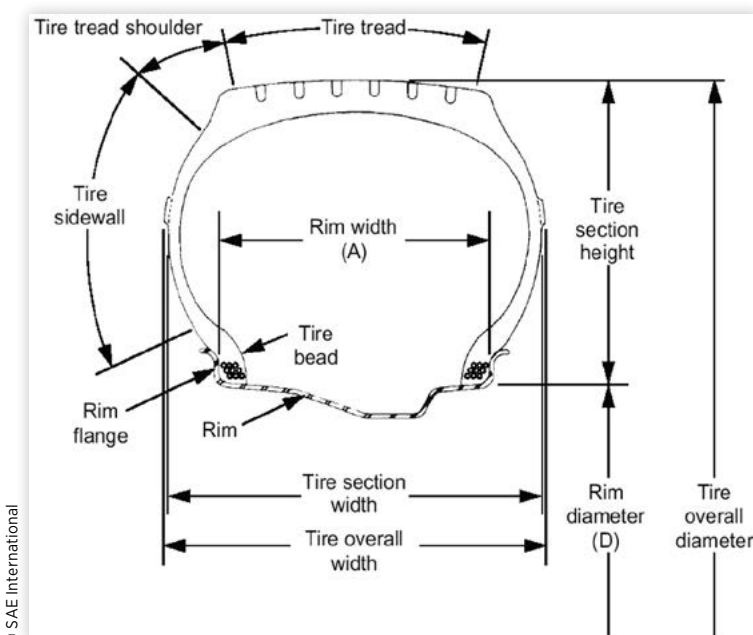
European Tyre and Rim Technical Organization, 32nd Avenue, Brugmann 1060 Brussels, Belgium.

The specific dimensions and designations are available in the tire and rim standards organizations' yearbooks.

7.1 Wheel Nomenclature

- 7.1.1 **Wheel (Road Wheel)**—A rotating, load-carrying member, upon which a *tire* is mounted, whose primary function is to support the vehicle and transmit *tire forces and moments*. It typically consists of two major parts: (a) the *rim* and (b) the wheel disc.
- 7.1.2 **Rim**—The part of the *wheel* on which the *tire* is mounted and supported. See [Figure 9](#).

FIGURE 9 - Nomenclature for Tire And Rim



- 7.1.2.1 Rim Width A—The distance between the inside surfaces of the *rim flanges*.
- 7.1.2.2 Rim Diameter (Specified Rim Diameter) D—The diameter at the intersection of the bead seat and the projection of the vertical portion of the *rim flange*.
- 7.1.2.3 Rim Diameter Designation (Nominal Rim Diameter)—The nominal *rim diameter* assigned for tire/rim matching.
- 7.1.2.4 Rim Contour Designation—A code comprised of numbers and/or letters designating the width and contour (designated shape) of the *rim*.
EXAMPLE—6J, where 6 is the *rim width* expressed in inches, and J is the contour.
- 7.1.2.5 *Rim Size Designation*—*Rim diameter designation by (x) rim contour designation*.
EXAMPLE—15 × 6J has a rim diameter designation of 15, and a rim contour designation of 6J.
- 7.1.2.6 Rim Flange—The part of the *rim* that provides lateral restraint for the *tire*.

7.2 Pneumatic Tire Nomenclature

- 7.2.1 Tire—A flexible, hollow semi-toroid mounted on the *rim* and filled with compressed gas, usually air. [Figure 9](#) includes a cross-sectional view. The purposes of the tire are to attenuate road impact forces and to produce the vehicle control forces.
- 7.2.2 Tire Section Width—The width of an unloaded *tire* measured from sidewall to sidewall, excluding width due to protective ribs, bars, and decorations.
NOTE—This measurement is made on a new *tire* inflated to the recommended pressure 24 hours prior to measurement, to account for inflation growth.
- 7.2.3 Tire Overall Width—The width of an unloaded *tire*, including 24-hour inflation growth, measured from sidewall to sidewall, including width due to protective ribs, bars, and decorations.
- 7.2.4 Tire Overall (Outside) Diameter—The largest diameter of the unloaded *tire*, including 24-hour inflation growth.
- 7.2.5 Tire Section Height—The height of the radial cross-section of the *tire*, including 24-hour inflation growth. Tire section height is usually computed by subtracting the *nominal rim diameter* from the *tire overall diameter* and dividing by two.
- 7.2.6 Tire Aspect Ratio—Ratio of the *tire section height* to the *tire section width* multiplied by 100.
- 7.2.7 Tire Face—The outwardly directed side of a *tire* if mounted on a vehicle according to the vehicle manufacturer's specification or general practice.

- 7.2.8 Tire Load Index—A numerical code associated with the maximum *tire load* a *tire* can carry at the speed indicated by its *tire speed symbol* under specified service conditions.
- 7.2.9 Tire Speed Symbol—An alphabetic code indicating the speed category at which the *tire* can carry a *tire load* corresponding to its *tire load index* under specified service conditions.
- 7.2.10 Contact Patch (Footprint)—The portion of the *tire* touching the *road surface*.
- 7.2.11 Tire Designation—The numbers and/or letters indicating *tire* size and service description.

EXAMPLE—P205/60R15 90H is a specific example for a P-metric passenger *tire*. P denotes a passenger *tire*. 205 is the nominal *tire section width* in millimeters. 60 is the nominal *tire aspect ratio*. R denotes radial ply construction. 15 is the *rim diameter designation*. 90 is the *tire load index*. H is the *tire speed symbol*. For additional detail, refer to the appropriate tire and rim technical organization yearbook.

7.3 Wheel Plane Geometry

- 7.3.1 Tire/Wheel Assembly—The assembly composed of the *tire* and *wheel*.
- 7.3.2 Wheel-Spin Axis—The axis of *wheel* rotation. This axis is coincident with the Y_w axis.
- 7.3.3 Wheel Plane—A plane normal to the *wheel-spin axis*, which is located halfway between the *rim flanges*.
- 7.3.4 Wheel Center—The point at which the *wheel-spin axis* intersects the *wheel plane*.
NOTE—*The wheel center is the origin of the wheel coordinate system*.
- 7.3.5 Contact Line—The intersection of the *wheel plane* and the *road plane*.
- 7.3.6 Contact Center (Center of Tire Contact)—The intersection of the *contact line* and the normal projection of the *wheel-spin axis* onto the *road plane*.
NOTE—*The contact center is the origin of the tire coordinate system*. The *contact center* may not be the geometric center of the *tire contact patch* due to distortion of the *tire* produced by external forces.
- 7.3.7 Loaded Radius R_L —The distance from the *wheel center* to the *contact center* at a specified operating condition.
- 7.3.8 Static Loaded Radius SLR—The *loaded radius* at zero speed.

7.4 Tire Orientation Angles

- 7.4.1 Wheel Plane Orientation—The angular orientation of the *wheel plane* with respect to the *road plane* and the *tire trajectory velocity*. The *wheel* angular orientation is expressed in terms of *inclination angle* and *slip angle*. See [Figures 2, 8 and 10](#).

7.4.2 Slip Angle α —The angle from the X_T axis to the normal projection of the *tire trajectory velocity* onto the X_T - Y_T plane. See [Figure 10](#).

NOTE—The sign of *slip angle* is determined using the right hand rule. For the same physical case, the sign of *slip angle* is reversed in the Z-Up and Z-Down axis orientations. See [Table 2](#).

7.4.3 Inclination Angle ϵ (γ)—The angle from the Z_T axis to the Z_W axis. See [Figures 8](#) and [10](#).

NOTE—The sign of *inclination angle* is determined using the right hand rule. For the same physical case, the sign of *inclination angle* is the same in the Z-Up and Z-Down axis orientations. See [Table 2](#).

TABLE 2 Relationships between Z-Up and Z-Down Tire Axis Systems

	Tire Axis System		
	Z-Up	=	Z-Down
Slip Angle	α	=	$-\alpha$
Inclination Angle	ϵ	=	ϵ
Unit Vectors	i_{XT}	=	i_{XT}
	i_{YT}	=	$-i_{YT}$
	i_{ZT}	=	$-i_{ZT}$
Forces	F_{XT}	=	F_{XT}
	F_{YT}	=	$-F_{YT}$
	F_{ZT}	=	$-F_{ZT}$
Moments	M_{XT}	=	M_{XT}
	M_{YT}	=	$-M_{YT}$
	M_{ZT}	=	$-M_{ZT}$
Velocities	T_W	=	$-T_W$
	V_{XT}	=	V_{XT}
	V_{YT}	=	$-V_{YT}$
	V_{ZT}	=	$-V_{ZT}$
	ω_W	=	$-\omega_W$

7.5 Tire Rolling Characteristics

- 7.5.1 Straight Free-Rolling Tire—A loaded, rolling *tire* moving with zero *braking* or *driving torque* along a linear path with zero *slip angle* and zero *inclination angle*.
- 7.5.2 Tire Trajectory Velocity \bar{v}_T —A vector quantity expressing the velocity of the *contact center* relative to the *Earth-fixed axis system*.

- 7.5.3 Tire Longitudinal Velocity v_{XT} —The scalar value of the component of the *tire trajectory velocity* in the X_T direction.

$$v_{XT} = \vec{v}_T \cdot \hat{X}_T \quad (\text{Eq. 27})$$

- 7.5.4 Tire Lateral Velocity v_{YT} —The scalar value of the component of the *tire trajectory velocity* in the Y_T direction.

$$v_{YT} = \vec{v}_T \cdot \hat{X}_T \quad (\text{Eq. 28})$$

- 7.5.5 Tire Vertical Velocity v_{ZT} —The scalar value of the component of the *tire trajectory velocity* in the Z_T direction.

$$v_{ZT} = \vec{v}_T \cdot \hat{Z}_T \quad (\text{Eq. 29})$$

7.6 Wheel Spin and Tire Slip

- 7.6.1 Wheel-Spin Velocity ω_w —The angular velocity of the *wheel* about the Y_w axis.

NOTE—In previous editions of SAE J670, and in the 1998 edition of SAE J2047, positive *wheel-spin velocity* in the Z-Down axis orientation was defined to be consistent with a positive *tire longitudinal velocity*. In this document, the sign of *wheel-spin velocity* is determined using the right-hand rule for both the Z-Up and Z-Down axis orientations. See [Appendix C](#).

- 7.6.2 Reference Wheel-Spin Velocity ω_{w0} —The *wheel-spin velocity* of the *straight free-rolling tire* at a given set of operating conditions.

NOTE—The effects of *tire longitudinal force* and *tire rolling moment* in the straight free-rolling condition are included.

- 7.6.3 Tire Longitudinal Slip Velocity—The difference between the *wheel-spin velocity* and the *reference wheel-spin velocity*.

- 7.6.4 Tire Longitudinal Slip Ratio S_x —The ratio of *tire longitudinal slip velocity* to the *reference wheel-spin velocity*.

$$S_x = \frac{\omega_w - \omega_{w0}}{\omega_{w0}} \quad (\text{Eq. 30})$$

Where both ω_w and ω_{w0} are determined at the same *tire longitudinal velocity*, *tire load*, and *hot inflation pressure*.

- 7.6.5 Clockwise Tire Rotation (CW)—Clockwise rotation of the *tire face*.

- 7.6.6 Counterclockwise Tire Rotation (CCW)—Counterclockwise rotation of the *tire face*.

7.7 Standard Loads and Inflation Pressures

- 7.7.1 Cold Inflation Pressure—The gauge pressure within a *tire* at prevailing ambient temperature with no pressure build-up caused by tire service.
- 7.7.2 Hot Inflation Pressure (Warm Inflation Pressure)—The equilibrium gauge pressure within a *tire* at a given operating condition.
- 7.7.3 Tire Load—The load or weight supported by the *tire*.
- 7.7.3.1 Tire Load Limit (Tire Load Rating)—The maximum *tire load* recommended by a tire and rim standards organization for a particular tire at a given *cold inflation pressure*.
- 7.8 Wheel Torque T_w —The external torque exerted upon the *wheel* about the *wheel-spin axis*.

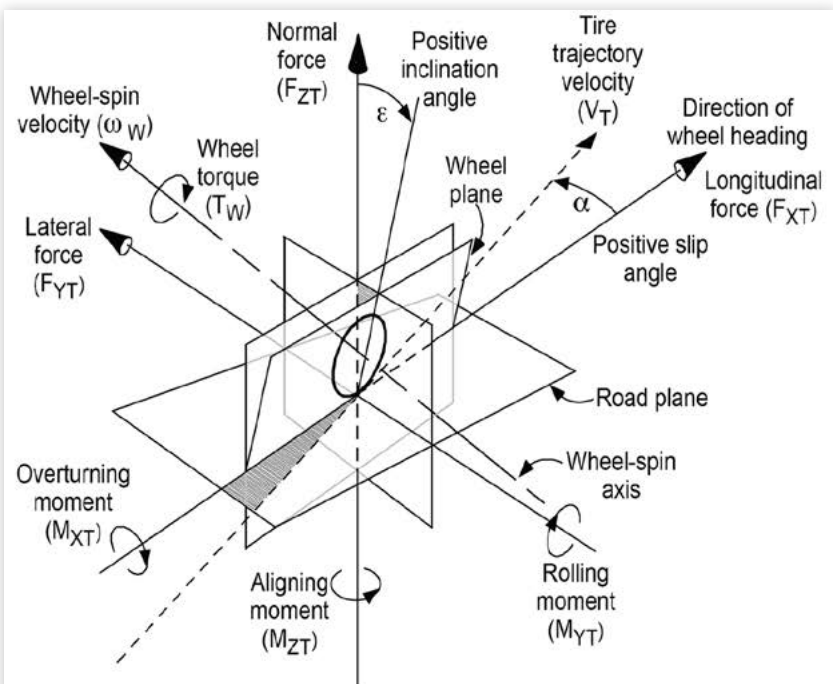
NOTE—In previous editions of SAE J670, and in the 1998 edition of SAE J2047, positive *wheel torque* in the Z-Down axis orientation was defined as a *driving torque* that produced a positive *tire longitudinal force*. In this document, the sign of *wheel torque* is determined using the right-hand rule for both the Z-Up and Z-Down axis orientations. See [Appendix C](#).

- 7.8.1 Driving Torque—A *wheel torque* that produces a *tire driving force*.
- 7.8.2 Braking Torque—A *wheel torque* that produces a *tire braking force*. See also 6.1.8 *brake torque*.

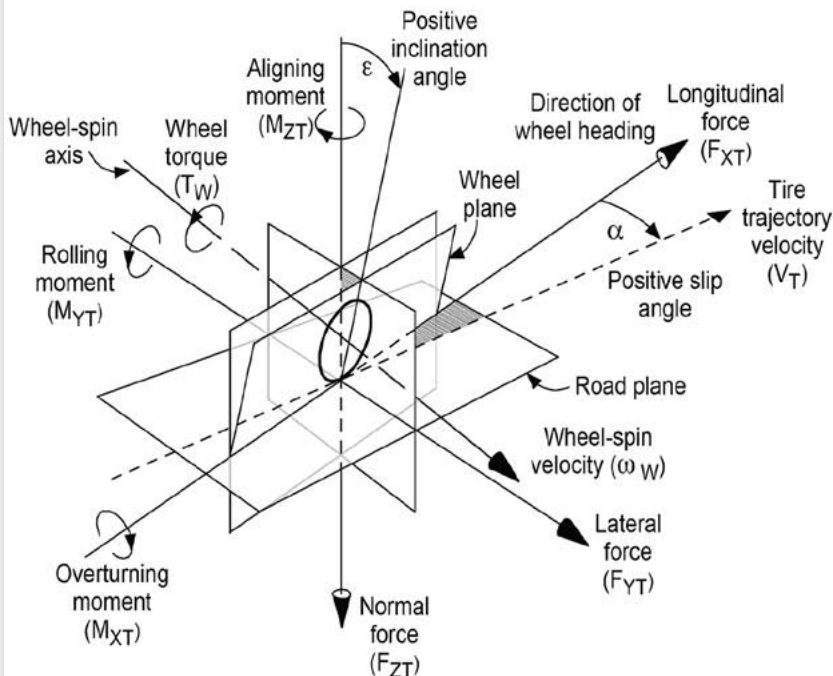
7.9 Tire Forces and Moments

External forces and moments acting on the *tire* at any instant may be summed into one resultant force vector and one resultant moment vector. The line of action of the resultant force vector may be moved to any point of interest, providing that the resultant moment vector is altered accordingly.

The total force and moment exerted on the *tire* by the road can be represented by three force components and three moment components. One force and one moment act in the direction of, and about, each of the three axes in the *tire axis system* described in Section 3. See [Figures 2](#) and [10](#). The three moments and two of the three forces are generally treated as dependent variables. In tire testing and tire modeling, *tire normal force* is generally treated as an independent variable and the magnitudes of the dependent forces and moments typically vary as a function of the *tire normal force*. Additionally, the magnitudes of the dependent forces and moments are somewhat affected by the direction of tire rotation, although this effect is usually neglected.

FIGURE 10 Tire Force And Moment Nomenclature

A. TIRE FORCE AND MOMENT NOMENCLATURE – Z-UP



B. TIRE FORCE AND MOMENT NOMENCLATURE – Z-DOWN

7.9.1 Tire Force \vec{F}_T —A vector quantity expressing the sum of the forces exerted on the *tire* by the road at any instant, with its line of action passing through the *contact center*.

7.9.2 Tire Normal Force (Tire Radial Force) F_{ZT} —The scalar value of the component of the *tire force* in the direction of the Z_T axis.

$$F_{ZT} = \vec{F}_T \cdot \hat{Z}_T \quad (\text{Eq. 31})$$

7.9.3 Tire Vertical Load—The absolute value of *tire normal force*.

7.9.4 Tire Shear Force Vector \vec{F}_{XYT} —The vector projection of the *tire force* onto the X_T - Y_T plane.

$$\vec{F}_{XYT} = \vec{F}_T - (\vec{F}_T \cdot \hat{Z}_T) \hat{Z}_T = F_{XT} \hat{X} + F_{YT} \hat{Y} \quad (\text{Eq. 32})$$

7.9.5 Tire Shear Force F_{XYT} —The magnitude of the *tire shear force vector*.

NOTE—*Tire shear force is also the resultant of tire longitudinal force and tire lateral force.*

7.9.6 Tire Longitudinal Force (Tire Fore-Aft Force) F_{XT} —The scalar value of the component of the *tire force* in the direction of the X_T axis.

$$F_{XT} = \vec{F}_T \cdot \hat{X}_T \quad (\text{Eq. 33})$$

7.9.6.1 Tire Driving Force—The magnitude of a positive *tire longitudinal force*.

7.9.6.2 Tire Braking Force—The magnitude of a negative *tire longitudinal force*.

7.9.7 Tire Lateral Force (Tire Side Force) F_{YT} —The scalar value of the component of the *tire force* in the direction of the Y_T axis.

$$F_{YT} = \vec{F}_T \cdot \hat{Y}_T \quad (\text{Eq. 34})$$

NOTE—For small *slip* and *inclination angles*, *tire lateral force* can be approximated by:

$$F_{YT} = -C_{Ya} \cdot \alpha + C_{Ye} \cdot \varepsilon \quad (\text{Eq. 35})$$

7.9.8 Tire Moment \vec{M}_T —A vector quantity expressing the sum of the external moments acting on the *tire* at any instant, consistent with the line of action of the *tire force*.

7.9.9 Tire Overturning Moment M_{XT} —The scalar value of the component of the *tire moment* in the direction of the X_T axis.

$$M_{XT} = \vec{M}_T \cdot \hat{X}_T \quad (\text{Eq. 36})$$

7.9.10 Tire Rolling Moment (Tire Rolling Resistance Moment) M_{YT} —The scalar value of the component of the *tire moment* in the direction of the Y_T axis.

$$M_{YT} = \vec{M}_T \cdot \hat{Y}_T \quad (\text{Eq. 37})$$

7.9.11 Tire Aligning Moment (Tire Aligning Torque) M_{ZT} —The scalar value of the component of the *tire moment* in the direction of the Z_T axis.

$$M_{ZT} = \vec{M}_T \cdot \hat{Z}_T \quad (\text{Eq. 38})$$

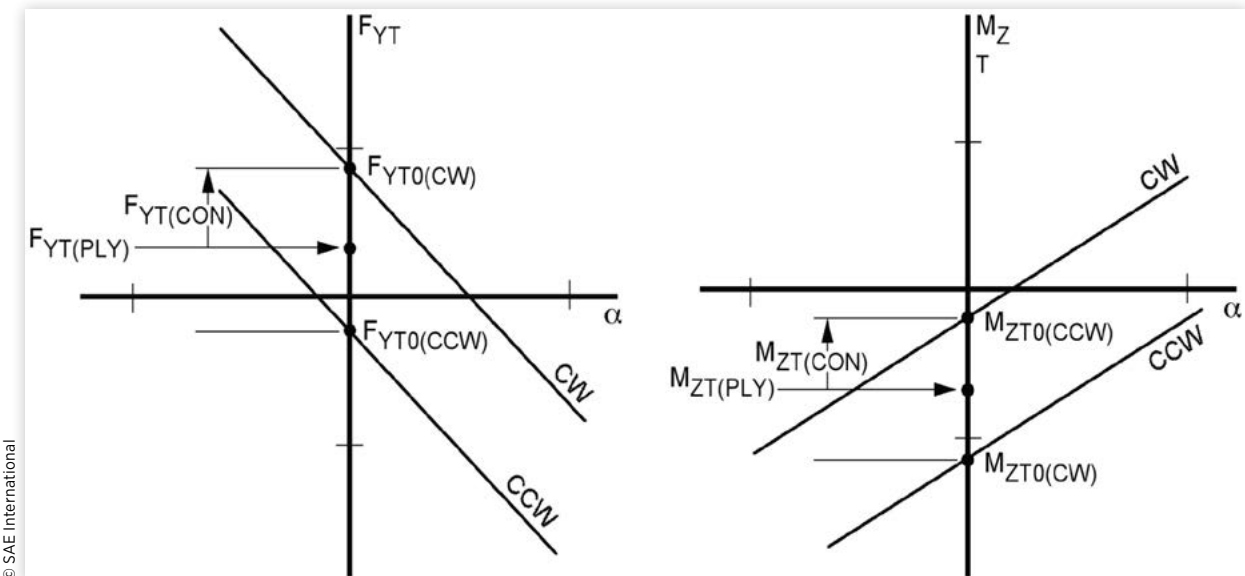
7.10 Pull Forces and Moments

Tire pull forces and moments are intrinsic tire properties arising from asymmetries in tire material, construction, or geometry due to either deliberate design choices, manufacturing irregularities, or both.

- 7.10.1 Lateral Force Offset F_{YT0} —The *tire lateral force* exerted on the *straight free-rolling tire*. It is typically different for *clockwise tire rotation* and *counterclockwise tire rotation*. See [Figures 11](#) and [12](#).

NOTE—The *lateral force offset* is the sum of two components. One, *conicity lateral force*, behaves like a force arising from *inclination angle*. It is directed toward a particular side of the *tire* regardless of the direction of tire rotation. For example, if it were directed from the *wheel plane* toward the *tire face*, *conicity lateral force* has this direction regardless of whether the *tire* is rotating clockwise or counterclockwise. However, in the *tire axis system*, the *conicity lateral force* would change sign depending on the direction of tire rotation. The other component, *plysteer lateral force*, behaves like a force arising from *slip angle*. Its direction relative to the *tire face* depends on the direction of rotation. For example, if the *plysteer lateral force* were directed from the *wheel plane* toward the *tire face* in *clockwise tire rotation*, it would be directed away from the *tire face* in *counterclockwise tire rotation*. In the *tire axis system*, the sign of the *plysteer lateral force* would be independent of the direction of tire rotation.

FIGURE 11 Components of Tire Conicity and Plysteer



- 7.10.1.1 Conicity Lateral Force $F_{YT(CON)}$ —The portion of the *lateral force offset* that is dependent upon the direction of tire rotation. It is illustrated in [Figure 11](#) and can be computed from the *lateral force offsets* in *clockwise* and *cOUNTERCLOCKWISE TIRE ROTATION* according to the following equation, which applies in the *tire axis system*:

$$F_{YT(CON)} = 0.5 \left[F_{YT0(CW)} - F_{YT0(CCW)} \right] \quad (\text{Eq. 39})$$

NOTE—The equation shown above provides the correct magnitude and sign for *conicity lateral force* for a *tire* installed on the right side of the vehicle, with the *tire face* outboard, regardless of the *axis system* being used (Z-Up or Z-Down). For the same *tire* installed on the left side of the vehicle, with the *tire face* outboard, the sign of *conicity lateral force* is reversed.

- 7.10.1.2 Plysteer Lateral Force $F_{YT(PLY)}$ —The portion of the *lateral force offset* that is independent of the direction of tire rotation. It is illustrated in [Figure 11](#) and can be computed from the *lateral force offsets* in *clockwise* and *cOUNTERCLOCKWISE TIRE ROTATION* according to the following equation, which applies in the *tire axis system*:

$$F_{YT(PLY)} = 0.5 \left[F_{YT0(CW)} + F_{YT0(CCW)} \right] \quad (\text{Eq. 40})$$

- 7.10.2 Residual Lateral Force F_{YTR} —The *tire lateral force* at the *slip angle* for which the *tire aligning moment* of the *straight free-rolling tire* at zero *inclination angle* is zero. It is typically different for *clockwise tire rotation* and *cOUNTERCLOCKWISE TIRE ROTATION*. See [Figure 12](#).

- 7.10.2.1 Conicity Residual Lateral Force $F_{YTR(CON)}$ —The portion of the *residual lateral force* that is dependent upon the direction of tire rotation. It is computed from the *residual lateral forces* in *clockwise* and *cOUNTERCLOCKWISE TIRE ROTATION* according to the following equation, which applies in the *tire axis system*:

$$F_{YTR(CON)} = 0.5 \left[F_{YTR(CW)} - F_{YTR(CCW)} \right] \quad (\text{Eq. 41})$$

NOTE—The equation shown above provides the correct magnitude and sign for *conicity residual lateral force* for a *tire* installed on the right side of the vehicle, with the *tire face* outboard, regardless of the *axis system* being used (Z-Up or Z-Down). For the same *tire* installed on the left side of the vehicle, with the *tire face* outboard, the sign of *conicity residual lateral force* is reversed.

- 7.10.2.2 Plysteer Residual Lateral Force $F_{YTR(PLY)}$ —The portion of the *residual lateral force* that is independent of the direction of tire rotation. It is computed from the *residual lateral forces* in *clockwise* and

counterclockwise tire rotation according to the following equation, which applies in the *tire axis system*:

$$F_{YTR(PLY)} = 0.5 [F_{YTR(CW)} + F_{YTR(CCW)}] \quad (\text{Eq. 42})$$

- 7.10.3 Aligning Moment Offset M_{ZT0} —The *tire aligning moment* exerted on the *straight free-rolling tire*. It is typically different for *clockwise tire rotation* and *counterclockwise tire rotation*. See [Figures 11](#) and [12](#).

NOTE—The *aligning moment offset* is the sum of two components. One, *conicity aligning moment*, behaves like a moment arising from *inclination angle*. It tries to turn the *tire* in the direction of the *conicity lateral force*. Thus, in the *tire axis system*, it reverses in sense when the direction of tire rotation reverses. The other component, *plysteer aligning moment*, behaves like a moment arising from *slip angle*. It tries to turn the *tire* to eliminate the *plysteer lateral force*. Its sense is independent of the direction of tire rotation.

- 7.10.3.1 Conicity Aligning Moment $M_{ZT(CON)}$ —The portion of the *aligning moment offset* that is dependent upon the direction of tire rotation. It is illustrated in [Figure 11](#) and can be computed from the *aligning moment offsets* in *clockwise* and *counterclockwise tire rotation* according to the following equation, which applies in the *tire axis system*:

$$M_{ZT(CON)} = 0.5 [M_{ZT0(CW)} - M_{ZT0(CCW)}] \quad (\text{Eq. 43})$$

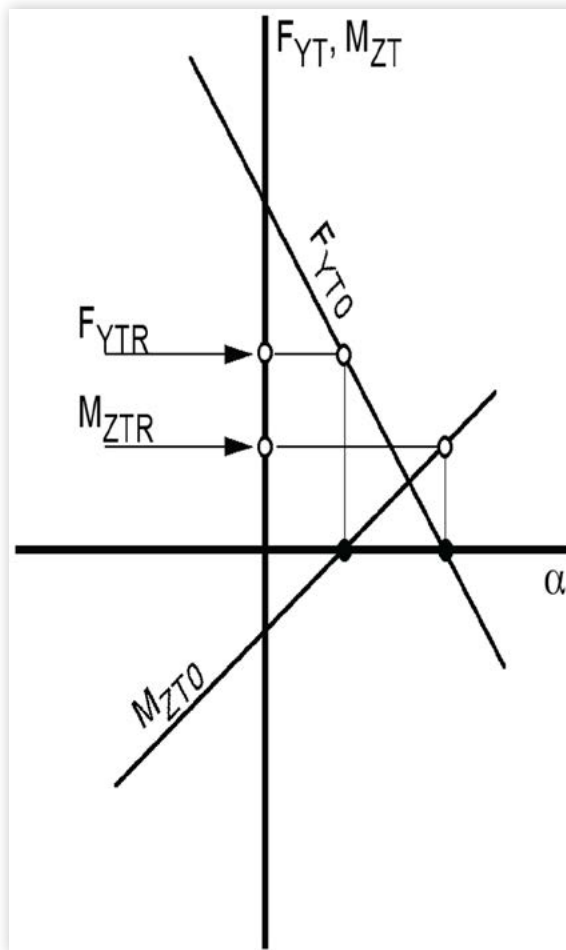
NOTE—The equation shown above provides the correct magnitude and sign for *conicity aligning moment* for a *tire* installed on the right side of the vehicle, with the *tire face* outboard, regardless of the *axis system* being used (Z-Up or Z-Down). For the same *tire* installed on the left side of the vehicle, with the *tire face* outboard, the sign of *conicity aligning moment* is reversed.

- 7.10.3.2 Plysteer Aligning Moment $M_{ZT(PLY)}$ —The portion of the *aligning moment offset* that is independent of the direction of tire rotation. It is illustrated in [Figure 11](#) and can be computed from the *aligning moment offsets* in *clockwise* and *counterclockwise tire rotation* according to the following equation, which applies in the *tire axis system*:

$$M_{ZT(PLY)} = 0.5 [M_{ZT0(CW)} + M_{ZT0(CCW)}] \quad (\text{Eq. 44})$$

- 7.10.4 Residual Aligning Moment M_{ZTR} —The *tire aligning moment* at the *slip angle* for which the *tire lateral force* of the *straight free-rolling tire* at zero *inclination angle* is zero. It is typically different for *clockwise tire rotation* and *counterclockwise tire rotation*. See [Figure 12](#).

NOTE—The *residual aligning moment* is the sum of two components. One, *conicity residual aligning moment*, reverses in sense in the *tire axis system* when the direction of tire rotation reverses. The other component, *plysteer residual aligning moment*, is independent of the direction of tire rotation.

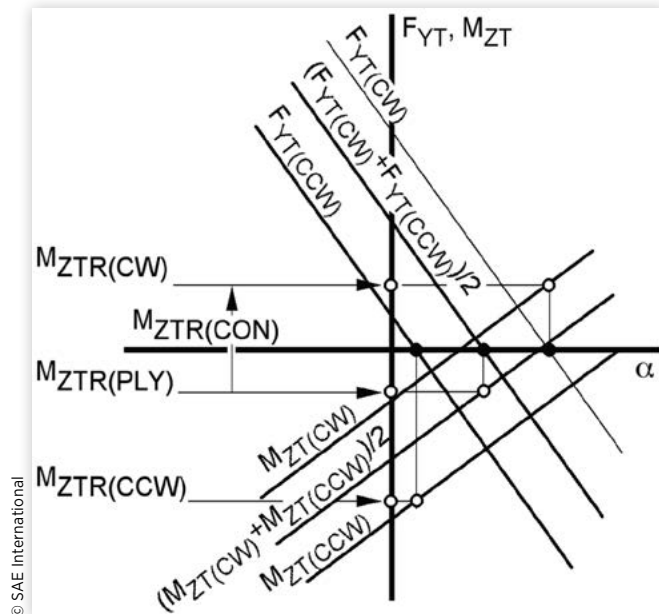
FIGURE 12 Tire Residual Lateral Force and Aligning Moment

© SAE International

7.10.4.1 Conicity Residual Aligning Moment $M_{ZTR(CON)}$ —The portion of the *residual aligning moment* that is dependent upon the direction of tire rotation. It is illustrated in [Figure 13](#) and can be computed using the following equation:

$$M_{ZTR(CON)} = 0.5 \left[M_{ZTR(CW)} - M_{ZTR(CCW)} \right] \quad (\text{Eq. 45})$$

NOTE—The equation shown above provides the correct magnitude and sign for *conicity residual aligning moment* for a *tire* installed on the right side of the vehicle, with the *tire face* outboard, regardless of the *axis system* being used (Z-Up or Z-Down). For the same *tire* installed on the left side of the vehicle, with the *tire face* outboard, the sign of *conicity residual aligning moment* is reversed.

FIGURE 13 Tire Conicity Residual Aligning Moment

- 7.10.4.2 Plysteer Residual Aligning Moment $M_{ZTR(PLY)}$ —The portion of the *residual aligning moment* that is independent of the direction of tire rotation. It is illustrated in [Figure 13](#) and can be computed using the following equation:

$$M_{ZTR(PLY)} = 0.5 \left[M_{ZTR(CW)} + M_{ZTR(CCW)} \right] \quad (\text{Eq. 46})$$

7.11 Properties of Forces in the Road Plane

Force coefficients are determined by dividing a *tire force* by *tire normal force*.

- 7.11.1 Tire Shear Force Coefficient (Tire Normalized Shear Force)—The absolute value of the ratio of *tire shear force* to *tire normal force*.
- 7.11.2 Tire Longitudinal Force Coefficient (Tire Normalized Longitudinal Force)—The ratio of the *tire longitudinal force* to the absolute value of *tire normal force*.
- 7.11.2.1 Tire Driving Force Coefficient (Tire Driving Coefficient, Tire Normalized Driving Force)—The absolute value of the ratio of *tire driving force* to *tire normal force*.
- 7.11.2.2 Tire Braking Force Coefficient (Tire Braking Coefficient, Tire Normalized Braking Force, Adhesion Utilization)—The ratio of the *tire braking force* to the absolute value of *tire normal force*.
- NOTE—The *tire driving force coefficient* is a positive number and the *tire braking force coefficient* is a negative number.
- 7.11.3 Tire Lateral Force Coefficient (Tire Normalized Lateral Force)—The ratio of the *tire lateral force* to the absolute value of the *tire normal force*.

- 7.11.4 Tire Lateral Force Load Sensitivity—The first derivative of *tire lateral force* with respect to the absolute value of *tire normal force* at any given value of *slip angle*.
- 7.11.5 Tire Longitudinal Stiffness (Tire Braking / Driving Stiffness, Tire Longitudinal Force / Longitudinal Slip Gradient) C_{xs} (C_s)—The first derivative of *tire longitudinal force* with respect to *tire longitudinal slip ratio*.
- NOTE—*Tire longitudinal stiffness* is usually determined at zero *slip angle*, zero *inclination angle*, and a *tire longitudinal slip ratio* of zero.
- 7.11.6 Tire Cornering Stiffness C_{ya} (C_a)—The negative of the first derivative of *tire lateral force* with respect to *slip angle*.
- NOTE—*Tire cornering stiffness* is usually determined at zero *slip angle*, zero *inclination angle*, with zero *wheel torque*.
- 7.11.7 Tire Inclination Stiffness (Tire Camber Stiffness) C_{ye} (C_e , C_{Yy} , C_y)—The first derivative of *tire lateral force* with respect to *inclination angle*.
- NOTE—*Tire inclination stiffness* is usually determined at zero *slip angle*, zero *inclination angle*, with zero *wheel torque*.
- 7.11.8 Tire Longitudinal Stiffness Coefficient (Tire Braking / Driving Stiffness Coefficient) C_{xsc} (C_{sc})—The ratio of the *tire longitudinal stiffness* to the absolute value of *tire normal force*.
- 7.11.9 Tire Cornering Stiffness Coefficient (Tire Cornering Coefficient) C_{yaC} (C_{aC})—The ratio of the *tire cornering stiffness* to the absolute value of *tire normal force*. It is the initial slope of the *tire lateral force coefficient* diagram.
- 7.11.10 Tire Inclination Stiffness Coefficient (Tire Camber Stiffness Coefficient, Tire Camber Coefficient) C_{yeC} (C_{eC} , C_{YyC} , C_{yC})—The ratio of the *tire inclination stiffness* to the absolute value of *tire normal force*.
- 7.11.11 Tire Relaxation Length—The distance rolled by a *tire* while *tire lateral force* builds to a particular percentage of the steady-state *tire lateral force*, following a step change in *slip angle* or other independent variable.
- NOTE—*Tire relaxation length* is analogous to the time constant of a first-order system. Common usage refers to the behavior after a step change in *slip angle* from zero. The behavior is typically modeled by an exponential rise. In this model, *tire relaxation length* is the distance rolled associated with the change from the *tire lateral force* at the initiation of the unit-step *slip angle* to 63.2% of the change in steady-state *tire lateral force*.
- 7.11.12 Tire Lateral Force Response Phase Angle—The phase angle between a sinusoidal input of *slip angle* or other independent variable and the sinusoidal *tire lateral force* response.

7.12 Normal Force Properties

- 7.12.1 Tire Deflection—The amount by which the *tire section height* is reduced due to *tire normal force*.

- 7.12.2 Tire Normal Stiffness (Tire Radial Stiffness, Tire Spring Rate) k_{zT} —The first derivative of the absolute value of *tire normal force* with respect to *tire deflection*.

NOTE—This definition is for a static stiffness, which implies stepwise or slowly varying changes in *tire normal force*. The definition is applicable for either a non-rolling or a rolling *tire*. Because the normal stiffness of a non-rolling and a rolling *tire* may be different, the operating condition should be explicitly stated. Other operating conditions influencing *tire normal stiffness* may include tire inflation pressure, *tire longitudinal velocity*, *slip angle*, *inclination angle*, and *wheel torque*.

7.13 Moment Properties

Moment coefficients are determined by dividing a *tire moment* by *tire normal force*.

- 7.13.1 Tire Overturning Moment Coefficient (Tire Normalized Overturning Moment)—The ratio of the *tire overturning moment* to the absolute value of the *tire normal force*.

- 7.13.2 Tire Rolling Moment Coefficient (Tire Normalized Rolling Moment)—The ratio of the *tire rolling moment* to the absolute value of the *tire normal force*.

- 7.13.3 Tire Aligning Moment Coefficient (Tire Normalized Aligning Moment)—The ratio of the *tire aligning moment* to the absolute value of the *tire normal force*.

- 7.13.4 Tire Aligning Moment Load Sensitivity—The first derivative of *tire aligning moment* with respect to the absolute value of *tire normal force* at any given value of *slip angle*.

- 7.13.5 Tire Overturning Stiffness C_{xx_a} —The first derivative of the *tire overturning moment* with respect to *slip angle*.

- 7.13.6 Tire Overturning Inclination Stiffness C_{xx_e} (C_{xy_y})—The first derivative of the *tire overturning moment* with respect to *inclination angle*.

- 7.13.7 Tire Aligning Stiffness C_{zz_a} (C_M)—The first derivative of the *tire aligning moment* with respect to *slip angle*.

NOTE—*Tire aligning stiffness is usually determined at zero slip angle, zero inclination angle, with zero wheel torque.*

- 7.13.8 Tire Aligning Inclination Stiffness C_{zz_e} (C_{zy_y})—The first derivative of the *tire aligning moment* with respect to *inclination angle*.

NOTE—*Tire aligning inclination stiffness is usually determined at zero slip angle, zero inclination angle, with zero wheel torque.*

- 7.13.9 Tire Aligning Stiffness Coefficient $C_{zz_{ac}}$ —The ratio of the *tire aligning stiffness* to the absolute value of the *tire normal force*.

7.14 Tire/Road Friction

In the following definitions, the term “steady-state operating conditions” refers to *road surface*, *tire load*, *tire longitudinal velocity*, temperature, inflation pressure, *slip angle*, *inclination angle*, *tire longitudinal slip ratio*, etc.

7.14.1 Tire Friction Ellipse—The locus of points of a plot of *tire lateral force* versus *tire longitudinal force* (or *tire lateral force coefficient* versus *tire longitudinal force coefficient*) for a *tire* at a particular set of steady-state operating conditions, with all conditions held fixed except one, which is independently varied.

NOTE—Typically, tire measurements to develop a *tire friction ellipse* are performed by independently varying *tire longitudinal slip ratio* while holding all other operating conditions fixed, including *slip angle*. By incrementally changing *slip angle* and repeating the measurement, a series of *tire friction ellipses* may be developed, with each describing the steady-state lateral and longitudinal force generating capability of the *tire* with a given set of operating conditions.

7.14.2 Tire Friction Ellipse Boundary—The locus of points describing the outermost envelope of a series of *tire friction ellipse* plots for a given *tire*, with a given set of steady-state operating conditions. This boundary describes the combined lateral and longitudinal force generation capability limits of the *tire*.

7.14.3 Peak Coefficient of Friction μ_p —The maximum values of the *tire shear force coefficient* attainable by a *tire* with a given set of steady-state operating conditions: 1) during the application of a *braking torque* at zero *slip angle*; 2) during the application of a *driving torque* at zero *slip angle*; or 3) when cornering with zero applied *wheel torque*.

NOTE—Typically, the *peak coefficients of friction* determined in the three pure modes of braking, driving, and cornering will have different values; moreover, the values for cornering may differ for positive and negative *slip angles*. The *peak coefficients of friction* determined in these pure modes define the intersections of the *tire friction ellipse boundary* with the F_{XT} – F_{YT} axes.

7.14.4 Slide Coefficient of Friction μ_s —The values of the *tire shear force coefficient* for a *tire* at a given set of steady-state operating conditions that is: 1) sliding across the surface without angular velocity (locked by braking); 2) spinning because of a heavy *driving torque* application; or 3) skidding sideways at a 90° *slip angle*.

NOTE—While the sliding tire condition is well defined for both braking and cornering (locked *wheel* and 90° *slip angle*, respectively), the spinning tire condition is open-ended. For practical purposes, the *slide coefficient of friction* for the spinning tire condition may be determined at a *tire longitudinal slip ratio* of 1.0 (*tire* spinning so that the *wheel-spin velocity* is twice the *reference wheel-spin velocity*).

7.14.5 Peak-to-Slide Ratio μ_p/μ_s —The ratio of the *peak coefficient of friction* to the *slide coefficient of friction* for a *tire* at a set of steady-state operating conditions in a given operating mode (braking, driving, or cornering).

NOTE—*Peak-to-slide ratio* is often used to characterize a given *road surface*. In reality, it is a property of the *road surface*, *tire*, and the steady-state operating conditions.

8. States and Modes

8.1 Equilibrium

- 8.1.1 Steady State (Trim)—State of a vehicle wherein the sum of the applied external forces and moments, and the inertial forces and moments which balance them, form an unchanging force and moment system in the (X_v, Y_v, Z_v) and (X, Y, Z) *reference frames* over an arbitrarily long time period. Used as the reference state for analysis of dynamic vehicle stability and control characteristics.

NOTE—An arbitrarily long time period as used in the above definition is a time period that is long relative to the longest time constant of the system being examined.

- 8.1.2 Transient State—State of a vehicle wherein the applied external forces and moments, the control positions, or the vehicle motion responses are varying with time.

8.2 Stability

- 8.2.1 Non-Oscillatory Stability (Asymptotic Stability)—Stability characteristic at a prescribed *steady state* if, following any small temporary *disturbance* or *control input*, the vehicle will return to the initial *steady-state* condition without oscillation.
- 8.2.2 Neutral Stability—Stability characteristic at a prescribed *steady state* if, following any small temporary *disturbance* or *control input*, the resulting motion of the vehicle remains close to, but does not return to, the initial *steady-state* condition.
- 8.2.3 Oscillatory Stability—Stability characteristic at a prescribed *steady state* if a small temporary *disturbance* or *control input* causes an oscillatory *vehicle response* of decreasing amplitude and a return to the initial *steady-state* condition.
- 8.2.4 Non-Oscillatory Instability (Divergent Instability)—Stability characteristic at a prescribed *steady state* if a small temporary *disturbance* or *control input* causes an ever-increasing *vehicle response* without oscillation. See [Figure 14](#).
- 8.2.5 Oscillatory Instability—Stability characteristic at a prescribed *steady state* if a small temporary *disturbance* or *control input* causes an oscillatory *vehicle response* of ever-increasing amplitude about the initial *steady-state* condition.

8.3 Control Modes

The following definitions are generic. Typically, they refer to the driver-vehicle interfaces used for the application of *steering*, *braking*, or *acceleration control inputs*.

- 8.3.1 Position Control—The mode of vehicle control wherein *control inputs* or restraints in the form of displacements are placed at some control point in the system, independent of the force required.
- 8.3.2 Fixed Control—The mode of vehicle control wherein the position of some point in the control system is held fixed. This is a special case of *position control*.

- 8.3.3 Force Control—The mode of vehicle control wherein *control inputs* or restraints in the form of forces are placed upon some control point in the system, independent of the displacement required.
- 8.3.4 Free Control—The mode of vehicle control wherein no restraint is placed on the control system. This is a special limit case of *force control*.
- 8.3.5 Closed-Loop Control (Feedback Control)—The mode of vehicle control wherein information about the *vehicle response* is fed back to the input controller (driver or mechanical actuator) for comparison with the desired *vehicle response*, and the *control inputs* are modified to reduce the error between the actual and desired *vehicle response*.
- 8.3.6 Open-Loop Control—The mode of vehicle control wherein *control inputs* are independent of the resulting *vehicle response*.

9. Inputs and Responses

9.1 Inputs

- 9.1.1 Control Input—A positioning of, or application of force to, an element of the vehicle (typically, within the steering, braking or propulsion systems) for the purpose of maintaining, or inducing a change in, motion of the vehicle.

9.1.1.1 Steering Control Input—Positioning of, or application of force to, an element of the steering system (e.g., *steering wheel*, front *wheels*, *Pitman arm*, *steering rack*) for the purpose of maintaining, or inducing a change in, the direction of motion of the vehicle.

9.1.1.1.1 Steering-Wheel Angle (Hand-Wheel Angle) δ_{sw} (δ_H)—The angular displacement of the *steering wheel* measured from a predetermined straight-ahead position. When using the Z-Up axis orientation, counterclockwise rotation of the *steering wheel* is positive. When using the Z-Down axis orientation, clockwise rotation of the *steering wheel* is positive.

NOTE—Straight ahead may be determined as the *steering-wheel angle* that produces zero *yaw velocity* under a given set of initial conditions or as the *steering-wheel angle* that provides a zero net *steer angle*.

9.1.1.1.2 Steering-Wheel Torque (Hand-Wheel Torque) M_{sw} (M_H)—The moment applied to the *steering wheel*, usually by the driver, about its axis of rotation.

9.1.1.1.3 Steering-Wheel Rim Force (Hand-Wheel Rim Force) F_{sw} (F_H)—*Steering-wheel torque* divided by the average value of *steering-wheel radius*, measured to the center of the *steering-wheel rim*.

- 9.1.1.2 Braking Control Input—Positioning of, or application of force to, an element of the braking system (e.g., *brake pedal*, *master cylinder*) for the purpose of maintaining, or inducing a change in, *vehicle speed*.
- 9.1.1.2.1 Brake Pedal Force—The force applied to the *brake pedal*, usually by the driver, tangential to the *brake pedal* pivot axis.
- 9.1.1.2.2 Brake Pedal Displacement (Brake Pedal Travel)—The linear displacement of the center of the *brake pedal* relative to its position with zero *brake pedal force* applied, measured along a chord.
- 9.1.1.3 Acceleration Control Input—Positioning of, or application of force to, an element of the propulsion system (e.g., accelerator pedal, throttle lever) for the purpose of maintaining, or inducing a change in, *vehicle speed*.
- 9.1.1.3.1 Accelerator Pedal Position—The angular displacement of the accelerator pedal relative to its position at idle.
- 9.1.1.3.2 Throttle Position—The angular displacement of the engine throttle lever relative to its position at idle.
- NOTE—*Accelerator pedal position* and *throttle position* are often expressed in percent of wide-open throttle.
- 9.1.1.4 Driver Control Input—A *control input* initiated by actions of the human driver.
- 9.1.1.5 Automatic Control Input—A *control input* initiated by an automatic control system within the vehicle.
- 9.1.2 Control System Input—An event (e.g., approach of another vehicle, change in *yaw velocity*) that induces a change in the signal of a sensor (e.g., a radar range sensor or a *yaw velocity* transducer) that is part of a system that generates *automatic control inputs*.
- 9.1.3 Driver Settings—Parameters of a system that generate *automatic control inputs* and are established by the driver (e.g., cruise control set speed).
- 9.1.4 Disturbance Input—An influence on the vehicle that induces a change in motion of the vehicle.
- 9.1.4.1 Aerodynamic Disturbance Input—A change in wind direction or speed relative to the vehicle, resulting in a change in aerodynamic forces acting on the vehicle.
- 9.1.4.2 Load-Shift Disturbance Input—A shift of mass within a vehicle.
- 9.1.4.3 Road Disturbance Input—A change in road properties (e.g., friction, surface roughness, profile, elevation, gradient), resulting in a change in forces or moments at the tire/road interface.
- 9.1.4.4 Tire/Wheel Disturbance Input—Rotation of a non-uniform or out-of-balance *tire/wheel assembly*, resulting in oscillating forces or moments at the tire/road interface or at the wheel spindle.

9.1.5 Equivalent Time of Initiation—The time at which a *control*, *control system*, or *disturbance input*, in the form of a ramp-step, reaches a user-defined percentage of the difference between the initial and final constant values.

NOTE—This time is considered equivalent to the time of initiation of a true step input and is used as the reference for computing *rise time*, *peak response time*, and *settling time*. Commonly used percentages are 5, 10, and 50.

9.2 Responses

9.2.1 Vehicle Response—The vehicle motion resulting from *control* or *disturbance inputs* to the vehicle.

9.2.2 Control Response—The vehicle motion resulting from a *control input*.

9.2.3 Disturbance Response—The vehicle motion resulting from a *disturbance input*.

9.2.4 Steady-State Response—The *steady state* associated with a set of constant inputs.

9.2.4.1 Gain (Sensitivity)—The rate of change in the *steady-state response* of a motion variable with respect to a *control input* at a given *steady-state* condition.

NOTE—Many *gain* measures may be created using this generic definition. Commonly used *gains* are defined elsewhere in this document. *Gain* measures not in common use should be created by referencing both the output and input in the *gain* name. For example, “Vehicle Roll Angle / Steering-Wheel Angle Gain” would be the rate of change of *vehicle roll angle* with respect to *steering-wheel angle*.

9.2.4.2 Gradient—The rate of change in the *steady-state response* of a variable with respect to a motion variable (typically, lateral acceleration) at a given *steady-state* condition.

NOTE—Many *gradient* measures may be created using this generic definition. Commonly used *gradients* are defined elsewhere in this document. *Gradient* measures not in common use should be created by referencing both the output and input in the *gradient* name. For example, “Steering-Wheel Torque / Lateral Acceleration Gradient” would be the rate of change of *steering-wheel torque* with respect to *lateral acceleration*.

9.2.5 Transient Response—The *transient state* resulting from a set of time-varying inputs.

NOTE—The inputs may include step, ramp-step, sinusoidal, pulse, or other time-varying *control* or *disturbance inputs*. Responses may include *lateral acceleration*, *yaw velocity*, *vehicle speed*, *vehicle roll angle*, *vehicle sideslip angle*, *path curvature*, *yaw angle*, or many others.

9.2.5.1 Dynamic Gain (Dynamic Sensitivity)—The ratio of a measure of the magnitude of the *transient response* of a motion variable to a measure of the magnitude of an input, in a specified transient maneuver.

NOTE—This definition is applicable for periodic or aperiodic inputs, linear or nonlinear responses, and analysis in either the time domain or frequency domain. Many *dynamic gain* measures may be created using this generic definition.

9.2.5.2 Dynamic Gradient—The ratio of a measure of the magnitude of the *transient response* of a motion variable to a measure of the magnitude of another motion variable (typically, *lateral acceleration*), in a specified transient maneuver.

NOTE—This definition is applicable for periodic or aperiodic inputs, linear or nonlinear responses, and analysis in either the time domain or frequency domain. Many *dynamic gradient* measures may be created using this generic definition.

9.2.6 Rise Time (Response Time)—The interval between the *equivalent time of initiation* of a ramp-step input and the time at which the *transient response* of a motion variable first reaches a user-defined percentage of the difference between the final and initial *steady-state* values.

NOTE—A commonly used percentage for determining *rise time* is 90. If a percentage other than 90 is used to determine *rise time*, the percentage should be specified (e.g., 63-Percent Rise Time).

9.2.7 Peak Response Time—The interval between the *equivalent time of initiation* of a ramp-step input and the time at which the *transient response* of a motion variable reaches its peak value, provided there is an *overshoot*.

9.2.8 Settling Time—The interval between the *equivalent time of initiation* of a ramp-step input and the time at which the *transient response* of a motion variable last enters and remains within a user-defined tolerance band around the final *steady-state* value. The band is expressed as a percentage of the difference between the final and initial *steady-state* values.

NOTE—Commonly used percentages for the tolerance band are ± 2 , ± 5 , and ± 10 .

9.2.9 Overshoot—For an underdamped system, the difference between the peak value and the final *steady-state* value of a motion variable in response to a ramp-step input.

9.2.10 Percent Overshoot—The ratio of the *overshoot* to the difference between the final and initial *steady-state* values of a motion variable, expressed as a percentage.

9.2.11 Bandwidth—The frequency at which the response has declined 3 dB from its low-frequency value.

9.2.12 Peak to Steady-State Ratio—The ratio of the peak frequency response to the low-frequency value.

10. Vehicle Longitudinal Response

10.1 Longitudinal Load Transfer

The net *tire vertical load* transferred from one *axle* to the other *axle*. It can be caused by *longitudinal acceleration*, road pitch, drivetrain torque, or other effects.

10.2 Descriptors of Steady-State Longitudinal Response

10.2.1 GAIN MEASURES: Many gain measures may be defined using the generic definition for *gain (sensitivity)* in 9.2.4.1. The following definitions are in common use.

10.2.1.1 Brake Pedal Force Gain—The absolute value of the rate of change of *longitudinal acceleration*, a_x , with respect to *brake pedal force*, on a level road at a given *steady-state longitudinal acceleration* condition.

10.2.1.2 Accelerator Pedal Position Gain—The rate of change of *longitudinal acceleration*, a_x , with respect to *accelerator pedal position*, on a level road at a given *steady-state longitudinal acceleration* condition.

10.2.2 GRADIENT MEASURES: Many gradient measures may be defined using the generic definition for *gradient* in 9.2.4.2. The following definitions are in common use.

10.2.2.1 Pitch Angle Gradient—The rate of change of *pitch angle*, θ , with respect to *longitudinal acceleration*, a_x , on a level road at a given *steady-state longitudinal acceleration* condition.

NOTE—*Pitch angle gradients* determined under acceleration and braking will typically have different magnitudes.

10.2.2.2 Suspension Trim Height Gradient—The mean rate of change of the *suspension trim heights* on an *axle* with respect to *longitudinal acceleration*, a_x , on a level road at a given *steady-state longitudinal acceleration* condition.

NOTE—*Suspension trim height gradients* determined under acceleration and braking will typically have different magnitudes.

10.3 Descriptors of Transient Longitudinal Response

10.3.1 Pitch Angle Overshoot—The difference between the peak value and the final *steady-state value of pitch angle*, θ , in response to a ramp-step *acceleration or braking control input*.

10.4 Descriptors of Transient Brake System Response

10.4.1 Brake Apply Rise Time—The interval between the time at which a ramp-step *braking control input* reaches 50% of its final value and the time at which the *braking control response* reaches 90% of its *steady-state response*.

NOTE—*Brake apply rise time* is a measure of the response speed of braking to a *braking control input* (e.g., *brake pedal force*). Typical control responses include *brake pressure*, *brake torque*, and *vehicle longitudinal acceleration*.

- 10.4.2 Brake Release Time—The interval between the time at which a *braking control input* is removed and the time at which the change in braking *control response* reaches 90% of its *steady-state* magnitude.

NOTE—*Brake release time* is a measure of the response speed of braking to removal of a *braking control input* (e.g., *brake pedal force*). Typical control responses include *brake pressure*, *brake torque*, and *vehicle longitudinal acceleration*.

10.5 Characterizing Descriptors of Braking Performance

- 10.5.1 Adhesion Utilization—See 7.11.2.2 *Tire Braking Force Coefficient*.
- 10.5.2 Braking Efficiency—The absolute value of the maximum steady state *longitudinal acceleration* (in g units) without *wheel lockup* divided by the nominal *peak coefficient of friction* in braking, expressed as a percentage.

NOTE—*Braking efficiency* is a general concept to approximately characterize the adhesion utilization of a vehicle relative to the prevailing *tire/road friction*. Accordingly, the *peak coefficient of friction* used is a representative value for the *tires* on the vehicle. Because *peak coefficient of friction* is often not well known, *braking efficiency* may exceed 100%.

11. Vehicle Lateral Response

11.1 Lateral Load Transfer

The terms in this subsection are most useful in *steady-state* conditions.

- 11.1.1 Tire Lateral Load Transfer—The *tire vertical load* transferred from one *tire* to the other on an *axle*. It can be caused by *lateral acceleration*, road camber, drivetrain torque, or other effects.
- 11.1.2 Total Tire Lateral Load Transfer—The sum of the *tire lateral load transfers* for the front and rear *axles*.
- 11.1.3 Tire Lateral Load Transfer Distribution—The ratio of the *tire lateral load transfer* on the front *axle* to the *total tire lateral load transfer*, usually expressed as a percentage.
- 11.1.4 Overturning Couple—The *roll moment* on the vehicle with respect to a central, longitudinal axis in the *ground plane* due to the effects of *lateral acceleration*, *vertical acceleration*, and *roll acceleration*.
- 11.1.5 Overturning Couple Distribution—The portion of the *overturning couple* reacted by the front *tires* expressed as a percentage of the *overturning couple*.

11.2 Ranges of Directional Response

- 11.2.1 On-Center Range—The *lateral acceleration* range associated with operation on a nearly straight *vehicle path* (typically $\pm 1 \text{ m/s}^2$), over which *vehicle response to steering control inputs* is not proportional.
- 11.2.2 Linear Range—The *lateral acceleration* range over which *vehicle response to steering control inputs* is nearly proportional (beyond the *on-center range*, typically to about $\pm 4 \text{ m/s}^2$).
- 11.2.3 Nonlinear Range—The *lateral acceleration* range over which *vehicle response to steering control inputs* is not proportional (beyond the *linear range*).

11.3 Descriptors of Steady-State Directional Response

Many of the descriptors characterizing vehicle directional stability and control come from classical proving-ground tests or linear analyses using simple vehicle models such as bicycle models. Thus, the definitions that follow may not rigorously include the influences of certain *compliances*, aerodynamics, traction/braking, active directional control systems, etc.

11.3.1 GAIN OR SENSITIVITY MEASURES: Many gain and sensitivity measures may be defined using the generic definition for *gain (sensitivity)* in 9.2.4.1. The following definitions are in common use.

11.3.1.1 Lateral Acceleration Gain (Steering Sensitivity)—The rate of change of *lateral acceleration*, a_y , with respect to *steering-wheel angle*, δ_{sw} , on a level road at a given *steady-state* condition. The value may be determined at either constant radius or constant speed. Values determined at these two conditions will generally differ. This is the reciprocal of *steering-wheel angle gradient*.

NOTE—Steady-state *lateral acceleration* is a function of *longitudinal velocity* v_x and *path radius* R such that a differential change in *lateral acceleration* may, in general, be expressed as:

$$da_y = \frac{\partial a_y}{\partial v_x} dv_x + \frac{\partial a_y}{\partial R} dR \quad (\text{Eq. 47})$$

An incremental change in steady-state *lateral acceleration* may be brought about: 1) by a change of *path radius* at a specified *vehicle speed* ($dv_x = 0$ and $dR \neq 0$) (i.e., the constant-speed method); 2) by a change of *vehicle speed* at a specified *path radius* ($dR = 0$ and $dv_x \neq 0$) (i.e., the constant-radius method); or 3) at least in concept, by changes in both *vehicle speed* and *path radius* according to a specified relationship ($dR = f(dv_x)$). The change in *steer angle* required to produce a given change in *lateral acceleration* (and, therefore, the lateral acceleration gain) may depend on the method. Therefore, the method as well as the nominal *steady-state* condition should always be indicated along with the lateral acceleration gain.

In the *steady-state* condition, *lateral acceleration* is equal to the product of *centripetal acceleration* times the cosine of the *vehicle sideslip angle*. Since in

most test conditions the *vehicle sideslip angle* is small, for practical purposes, the *lateral acceleration* can be considered equal to the *centripetal acceleration*.

- 11.3.1.2 Lateral Acceleration Moment Gain (Control Moment Sensitivity)—The rate of change of *lateral acceleration*, a_y , with respect to *steering-wheel torque*, M_{sw} , on a level road at a given *steady-state* condition. This is the reciprocal of *steering-wheel torque gradient*.
- 11.3.1.3 Yaw Velocity Gain—The rate of change of *yaw velocity*, ω_z , with respect to *steering-wheel angle*, δ_{sw} , on a level road at a given *steady-state* condition.
- 11.3.1.4 Sideslip Angle Gain—The rate of change of *vehicle sideslip angle*, β , with respect to *steering-wheel angle*, δ_{sw} , on a level road at a given *steady-state* condition.
- 11.3.1.5 Path Curvature Gain—The rate of change of *path curvature*, κ , with respect to *steering-wheel angle*, δ_{sw} , on a level road at a given *steady-state* condition.
- 11.3.1.6 Steering-Wheel Torque Gain (Steering Stiffness)—The rate of change of *steering-wheel torque*, M_{sw} , with respect to *steering-wheel angle*, δ_{sw} , on a level road at a given *steady-state* condition.

11.3.2 GRADIENT MEASURES: Many gradient measures may be defined using the generic definition for *gradient* in 9.2.4.2. The following definitions are in common use.

- 11.3.2.1 Steering-Wheel Angle Gradient (Hand-Wheel Angle Gradient)—The rate of change of *steering-wheel angle*, δ_{sw} , with respect to *lateral acceleration*, a_y , on a level road at a given *steady-state* condition. This is the reciprocal of *lateral acceleration gain*.
- 11.3.2.2 Steering-Wheel Torque Gradient (Hand-Wheel Torque Gradient)—The rate of change of *steering-wheel torque*, M_{sw} , with respect to *lateral acceleration*, a_y , on a level road at a given *steady-state* condition. This is the reciprocal of *lateral acceleration moment gain*.
- 11.3.2.3 Reference Steer Angle Gradient—The rate of change of *included reference steer angle*, δ_{ref} , with respect to *lateral acceleration*, a_y , on a level road at a given *steady-state* condition.
- 11.3.2.4 Ackermann Steer Angle Gradient—The rate of change of *included Ackermann steer angle*, δ_A , with respect to *lateral acceleration*, a_y , on a level road at a given *steady-state* condition.
- NOTE—For the conventional four-wheel vehicle with no rear steer, the *Ackermann steer angle gradient* is traditionally defined as $(180/\pi)$ times the *wheelbase* divided by the square of the *vehicle speed*, commonly expressed in degrees per g.
- 11.3.2.5 Roll Angle Gradient—The rate of change of *vehicle roll angle*, ϕ_v , with respect to *lateral acceleration*, a_y , on a level road at a given *steady-state* condition.
- 11.3.2.6 Suspension Roll Angle Gradient—The rate of change of *suspension roll angle* with respect to *lateral acceleration*, a_y , on a level road at a given *steady-state* condition.
- 11.3.2.7 Sideslip Angle Gradient—The rate of change of *vehicle sideslip angle*, β , with respect to *lateral acceleration*, a_y , on a level road at a given *steady-state* condition.

11.3.2.8 Path Curvature Gradient—The rate of change of *path curvature*, κ , with respect to *lateral acceleration*, a_y , on a level road at a given *steady-state* condition.

11.3.2.9 Trailer Yaw Articulation Angle Gradient (Articulation Angle Gradient)—The rate of change of *trailer yaw articulation angle*, $\Delta\psi$, with respect to *lateral acceleration*, a_y , on a level road at a given *steady-state* condition.

11.3.3 UNDERSTEER AND OVERSTEER

11.3.3.1 Understeer / Oversteer Gradient U—The quantity obtained by subtracting the *Ackermann steer angle gradient* from the *reference steer angle gradient*, on a flat, level road at a given *steady-state* condition.

NOTE—In general, in *steady-state* cornering, the *included reference steer angle* may be a function of the *included Ackermann steer angle* and *lateral acceleration*:

$$\delta_{\text{REF}} = f(\delta_A, a_y) \quad (\text{Eq. 48})$$

For a vehicle whose response is linearized about a *steady-state* condition, the *included reference steer angle* would depend on the *included Ackermann steer angle* and *lateral acceleration* according to the following relationship:

$$\delta_{\text{REF}} = \delta_A + U a_y \quad (\text{Eq. 49})$$

It is under these conditions that the *understeer / oversteer gradient* definition is strictly defined.

For a simplified vehicle without aerodynamic forces and moments, without rear steer (except via *suspension compliances*) or with a fixed front/rear steer ratio relationship, and within the *linear range*, the *understeer / oversteer gradient* is a constant, which is independent of speed, *lateral acceleration* and *path radius*. However, aerodynamic forces and moments and certain active directional control systems cause the *understeer / oversteer gradient* to be a function of speed and/or *path radius*, even within the *linear range*.

Different test methods utilize different forms of the above equation. For a constant radius test, the *included Ackermann steer angle* is constant, the *Ackermann steer angle gradient* is zero, and:

$$U = \frac{d\delta_{\text{REF}}}{da_y} \quad (\text{Eq. 50})$$

For a constant steer angle test, the *included reference steer angle* is constant, the *reference steer angle gradient* is zero, and:

$$U = -\frac{d\delta_A}{da_y} \quad (\text{Eq. 51})$$

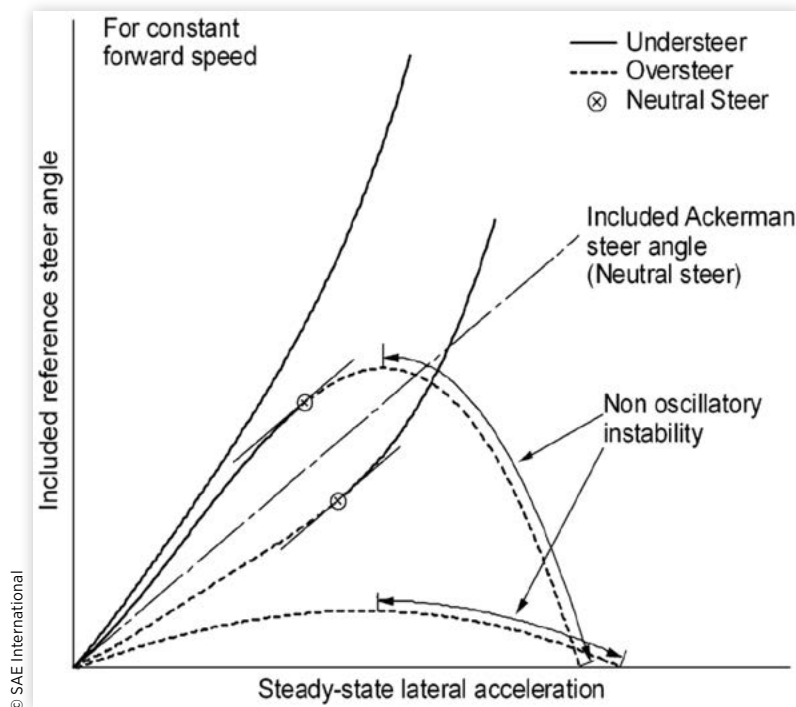
For a constant speed test, neither *reference steer angle gradient* nor *Ackermann steer angle gradient* is zero, and the general format applies:

$$U = \frac{d\delta_{\text{REF}}}{da_y} - \frac{d\delta_A}{da_y} \quad (\text{Eq. 52})$$

It is common practice in both theory and testing to approximate *included Ackermann steer angle* with *normalized path curvature*.

11.3.3.2 Neutral Steer—A vehicle is neutral steer at a given *steady-state* condition, if the *reference steer angle gradient* equals the *Ackermann steer angle gradient*. The *understeer / oversteer gradient* is zero. See [Figure 14](#).

FIGURE 14 Steer Properties



NOTE—As implied by [Figure 14](#), the vehicle is a nonlinear system and may not have the same characteristics at all *steady-state* conditions. Consequently, it is necessary to specify the specific conditions (*vehicle speed, included reference steer angle, lateral acceleration*) when making a determination of the vehicle's *understeer / oversteer* characteristics.

11.3.3.3 Understeer—A vehicle is understeer at a given *steady-state* condition, if the *reference steer angle gradient* is greater than the *Ackermann steer angle gradient*. The *understeer / oversteer gradient* is positive. See [Figure 14](#).

11.3.3.4 Oversteer—A vehicle is oversteer at a given *steady-state* condition, if the *reference steer angle gradient* is less than the *Ackermann steer angle gradient*. The *understeer / oversteer gradient* is negative. See [Figure 14](#).

11.3.3.5 Cornering Compliance D_F , D_R —For an *axle*, the negative of the derivative of the *axle reference sideslip angle* with respect to *lateral acceleration* at a given *steady-state* condition.

$$D_F = -\frac{d\sigma_F}{da_Y} \quad (\text{Eq. 53})$$

$$D_R = -\frac{d\sigma_R}{da_Y} \quad (\text{Eq. 54})$$

NOTE—The *understeer / oversteer gradient* is related to the *cornering compliances* by the relation:

$$U = D_F - D_R \quad (\text{Eq. 55})$$

Where D_F is the front *cornering compliance* and D_R is the rear *cornering compliance*.

11.3.4 STABILITY MEASURES

11.3.4.1 Neutral Steer Line—A set of points in the *vehicle plane of symmetry* at which an arbitrary external *lateral force* applied to the *sprung mass* produces no change in *steady-state yaw velocity*.

11.3.4.2 Static Margin—The horizontal distance from the *vehicle center of gravity* to the *neutral steer line*, divided by the *wheelbase*. It is positive if the *vehicle center of gravity* is forward of the *neutral steer line*.

11.3.4.3 Stability Factor K—The relationship between *path curvature*, κ , *yaw velocity*, ω_z , or *lateral acceleration*, a_y , and *included reference steer angle*, δ_{REF} , for a linear vehicle. The following three relations are equivalent:

$$\frac{\kappa}{\delta_{REF}} = \frac{1/L}{1 + Kv_X^2} \quad (\text{Eq. 56})$$

$$\frac{\omega_z}{\delta_{REF}} = \frac{v_X/L}{1 + Kv_X^2} \quad (\text{Eq. 57})$$

$$\frac{a_y}{\delta_{REF}} = \frac{v_X^2/L}{1 + Kv_X^2} \quad (\text{Eq. 58})$$

Where v_X is the *longitudinal velocity* and L is the *wheelbase*. If $K=0$ the vehicle is *neutral steer*, if $K>0$ the vehicle is *understeer*, and if $K<0$ the vehicle is *oversteer*. The stability factor, K , is related to the *understeer / oversteer gradient* by the relation:

$$K = \frac{U}{Lg} * \frac{\pi}{180} \quad (\text{Eq. 59})$$

11.3.5 CHARACTERIZING SPEEDS

11.3.5.1 Tangent Speed—The *longitudinal velocity* at which the *vehicle sideslip angle* is zero, under *steady-state* operating conditions.

NOTE—Because the *vehicle sideslip angle* is defined at the *vehicle reference point*, *tangent speed* will be affected by the choice of the *vehicle reference point*.

11.3.5.2 **Characteristic Speed v_{CH}** —The *longitudinal velocity* for an *understeer* vehicle at which the *lateral acceleration gain*, at *steady state* and zero *lateral acceleration*, is one-half of the *lateral acceleration gain* of a *neutral steer* vehicle. That is:

$$v_{CH} = \sqrt{\frac{180Lg}{\pi U}} \quad (\text{Eq. 60})$$

NOTE—At the *characteristic speed*, the *yaw velocity gain* is a maximum.

11.3.5.3 **Critical Speed v_{CR}** —The *longitudinal velocity* for an *oversteer* vehicle at which the *lateral acceleration gain*, at *steady state* and zero *lateral acceleration*, is infinite. That is:

$$v_{CR} = \sqrt{-\frac{180Lg}{\pi U}} \quad (\text{Eq. 61})$$

NOTE—Below the *critical speed* the *oversteer* vehicle is stable. Above the *critical speed* the *oversteer* vehicle exhibits *non-oscillatory instability*. No *critical speed* exists for an *understeer* vehicle and the *critical speed* for a *neutral steer* vehicle is infinite.

11.3.5.4 **Zero-Damping Speed v_{ZD}** —The *longitudinal velocity* at which the *trailer yaw articulation angle damping* of a tow vehicle/trailer combination equals zero.

11.4 Descriptors of Transient Directional Response

11.4.1 RISE-TIME MEASURES: Many rise-time measures may be defined using the generic definitions for *rise time* in 9.2.6 and *peak response time* in 9.2.7. The following definitions are in common use.

11.4.1.1 **Lateral Acceleration Rise Time (Lateral Acceleration Response Time)**—The interval between the time at which a ramp-step *steering-wheel angle* input reaches 50% of its final value and the time at which the resulting *lateral acceleration* response reaches 90% of its final *steady-state* value.

11.4.1.2 **Sideslip Angle Rise Time (Sideslip Angle Response Time)**—The interval between the time at which a ramp-step *steering-wheel angle* input reaches 50% of its final value and the time at which the resulting *vehicle sideslip angle* response reaches 90% of its final *steady-state* value.

11.4.1.3 **Yaw Velocity Rise Time (Yaw Velocity Response Time)**—The interval between the time at which a ramp-step *steering-wheel angle* input reaches 50% of its final value and the time at which the resulting *yaw velocity* response reaches 90% of its final *steady-state* value.

11.4.1.4 **Yaw Velocity Peak Response Time**—The interval between the time at which a ramp-step *steering-wheel angle* input reaches 50% of its final value and the time at which the resulting *yaw velocity* response reaches its peak value.

11.4.2 OVERSHOOT MEASURES: Many overshoot measures may be defined using the generic definition for *overshoot* in 9.2.9. The following definitions are in common use.

11.4.2.1 Yaw Velocity Overshoot—The difference between the peak *yaw velocity* response and the final *steady-state* value of *yaw velocity* in response to a ramp-step *steering-wheel angle* input.

11.4.2.2 Roll Angle Overshoot—The difference between the peak *vehicle roll angle* response and the final *steady-state* value of *vehicle roll angle* in response to a ramp-step *steering-wheel angle* input.

11.4.3 OTHER TRANSIENT MEASURES

11.4.3.1 Rearward Amplification—The ratio of the peak amplitude of a given motion variable for the trailer to the peak value of the same variable for the towing vehicle, during a specified maneuver.

11.4.3.2 Minimum Steering Sensitivity—The instantaneous minimum rate of change of *lateral acceleration*, a_y , with respect to *steering-wheel angle*, δ_{sw} , on a level road during a specified maneuver.

11.5 Descriptors of Limit Response

11.5.1 DIRECTIONAL RESPONSE LIMITS

11.5.1.1 Maximum Lateral Acceleration—The highest attainable level of *lateral acceleration* on a horizontal surface, under *steady-state* conditions.

NOTE—Typically, *maximum lateral acceleration* is measured in a constant radius test. It is possible to develop a *lateral acceleration* that is higher than the steady-state *maximum lateral acceleration* in a transient maneuver.

11.5.1.2 Plow—The limit condition for vehicle directional response wherein the front *tires* have reached their cornering limit while the rear *tires* have not reached their limit.

11.5.1.3 Spin—The limit condition for vehicle directional response wherein the rear *tires* have reached their cornering limit while the front *tires* have not reached their limit.

11.5.1.4 Drift—The limit condition for vehicle directional response wherein the front and rear *tires* have both reached their cornering limit.

11.5.2 ROLLOVER RESISTANCE

11.5.2.1 Geometric Stability Ratio (T/2H)—The value obtained by dividing the average vehicle half *track width* by the height of the total *vehicle center of gravity*, at a specified *load condition*.

11.5.2.2 Static Stability Factor SSF—The *geometric stability ratio* at a *load condition* consisting of *curb weight* plus a 50th percentile male (161.4 pound) driver.

NOTE—This load condition is used for evaluation of SSF in the U.S. New Car Assessment Program (NCAP).

11.5.2.3 Static Roll Stability Limit (Static Rollover Threshold)—The maximum *steady-state lateral acceleration* the vehicle can sustain while remaining stable in roll.

11.5.2.4 Static Stability Ratios

The following measures are all approximations of the *static roll stability limit* in g units, derived from specific practical test procedures.

11.5.2.4.1 Centrifuge Ratio—In a centrifuge test, the ratio of the maximum measured *lateral acceleration* at the *vehicle center of gravity* to the gravitational acceleration, that the vehicle can sustain while remaining stable in roll.

11.5.2.4.2 Side-Pull Ratio—In a side-pull test, the ratio of the maximum measured lateral pull force applied through the *vehicle center of gravity* to the *vehicle operating weight*.

NOTE—Typically, the maximum lateral pull force occurs at the moment of two-wheel lift.

11.5.2.4.3 Tilt-Table Ratio—In a tilt-table test, the tangent of the maximum table tilt angle the vehicle can sustain while remaining stable in roll.

11.6 Stability and Control Derivatives

In a simplified horizontal plane model, the unbalanced forces and moments of linear directional stability and control equations in sideslip, yaw, and roll may be written in derivative notation as:

$$\text{Lateral force: } F_Y = f(\beta, \omega_Z, \phi, \delta_{SW}) \quad (\text{Eq. 62})$$

$$F_Y = \left(\frac{\partial F_Y}{\partial \beta} \right) \beta + \left(\frac{\partial F_Y}{\partial \omega_Z} \right) \omega_Z + \left(\frac{\partial F_Y}{\partial \phi} \right) \phi + \left(\frac{\partial F_Y}{\partial \delta_{SW}} \right) \delta_{SW} \quad (\text{Eq. 63})$$

$$\text{Yaw moment: } M_Z = f(\beta, \omega_Z, \phi, \delta_{SW}) \quad (\text{Eq. 64})$$

$$M_Z = \left(\frac{\partial M_Z}{\partial \beta} \right) \beta + \left(\frac{\partial M_Z}{\partial \omega_Z} \right) \omega_Z + \left(\frac{\partial M_Z}{\partial \phi} \right) \phi + \left(\frac{\partial M_Z}{\partial \delta_{SW}} \right) \delta_{SW} \quad (\text{Eq. 65})$$

$$\text{Roll moment: } M_X = f(\omega_X, \phi) \quad (\text{Eq. 66})$$

$$M_X = \left(\frac{\partial M_X}{\partial \omega_X} \right) \omega_X + \left(\frac{\partial M_X}{\partial \phi} \right) \phi \quad (\text{Eq. 67})$$

11.6.1 Stability Derivatives—The partial derivatives of the *force* and *moment* terms with respect to the state variables used in the equations of motion describing the vehicle's dynamics. These partial derivatives are frequently used in linear approximations to the lateral equations of motion.

The following *stability derivatives* may be defined as constants in the linear range:

11.6.1.1 Lateral Force / Sideslip Derivative Y_β —The partial derivative $\frac{\partial F_Y}{\partial \beta}$

11.6.1.2 Lateral Force / Yaw Velocity Derivative Y_r —The partial derivative $\frac{\partial F_Y}{\partial \omega_Z}$

- 11.6.1.3 Lateral Force / Roll Angle Derivative Y_ϕ —The partial derivative $\frac{\partial F_Y}{\partial \phi}$
- 11.6.1.4 Yaw Moment / Sideslip Derivative (Static Directional Stability) N_β —The partial derivative $\frac{\partial M_Z}{\partial \beta}$
- 11.6.1.5 Yaw Moment / Yaw Velocity Derivative (Yaw Damping) N_r —The partial derivative $\frac{\partial M_Z}{\partial \omega_Z}$
- 11.6.1.6 Yaw Moment / Roll Angle Derivative N_ϕ —The partial derivative $\frac{\partial M_Z}{\partial \phi}$
- 11.6.1.7 Roll Moment / Roll Velocity Derivative L_p —The partial derivative $\frac{\partial M_X}{\partial \omega_X}$
- 11.6.1.8 Roll Moment / Roll Angle Derivative L_ϕ —The partial derivative $\frac{\partial M_X}{\partial \phi}$
- 11.6.2 Control Derivatives—The partial derivatives of the *force* and *moment* terms with respect to the vehicle control variables used in the equations of motion describing the vehicle's dynamics. These partial derivatives are frequently used in linear approximations to the lateral equations of motion.

The following *control derivatives* may be defined as constants in the linear range:

- 11.6.2.1 Lateral Force / Steering-Wheel Angle Derivative Y_δ —The partial derivative $\frac{\partial F_Y}{\partial \delta_{SW}}$
- 11.6.2.2 Yaw Moment / Steering-Wheel Angle Derivative (Control Moment) N_δ —The partial derivative $\frac{\partial M_Z}{\partial \delta_{SW}}$
- 11.6.3 Moment Method—An analysis procedure that is concerned with the balanced and unbalanced *forces* and *moments* acting on a vehicle. For the study of lateral dynamics, this method is frequently characterized by a diagram showing *normalized yaw moment* plotted versus *lateral acceleration* along lines of constant *vehicle sideslip angle* and constant *steering-wheel angle* or *included reference steer angle*. The data for constructing this diagram may come from tests of a constrained vehicle or from a computerized model of the vehicle.
- 11.6.3.1 Normalized Yaw Moment C_N —Vehicle *yaw moment* M_Z divided by the quantity *vehicle operating weight* W times *wheelbase* L .
- 11.6.3.2 Normalized Lateral Force C_Y —Vehicle *lateral force* F_Y divided by *vehicle operating weight* W .
- 11.6.3.3 Stability Index—The rate of change of *normalized yaw moment* C_N with respect to *lateral acceleration* a_Y at zero *yaw moment* M_Z , with *steering-wheel angle* δ_{SW} held constant.
- 11.6.3.4 Yaw Moment Reserve—The additional *yaw moment* M_Z that could be developed by an *understeer* vehicle operating at its *maximum lateral acceleration*.

12. Ride Vibration

12.1 Sprung-Mass Vibration

- 12.1.1 Primary Ride—The lower frequency (up to 5 Hz) vibrations of the *sprung mass*, primarily comprised of rigid body motions.
 - 12.1.1.1 Bounce (Heave)—The translational component of ride vibrations at a point of interest in the *sprung mass* in the direction of the Z_v axis.
 - 12.1.1.2 Roll—The angular component of ride vibrations of the *sprung mass* about the X_v axis.
 - 12.1.1.3 Pitch—The angular component of ride vibrations of the *sprung mass* about the Y_v axis.
 - 12.1.1.4 Warp—Twist of the *sprung mass* about the X_v axis.
 - 12.1.1.5 Warp Couple—The difference between the roll couples applied to the *sprung mass* by the front and rear *suspensions*.
- 12.1.2 Secondary Ride (Shake)—The intermediate frequency (5 to 30 Hz) vibrations of the *sprung mass*.
 - 12.1.2.1 Torsional Shake—A mode of vibration characterized by twisting deformations of the *sprung mass* about the X_v axis.
 - 12.1.2.2 Beaming—Modes of vibration characterized by bending deformations of the *sprung mass* about the Y_v axis (Vertical Beaming) or Z_v axis (Lateral Beaming).
- 12.1.3 Harshness—The higher frequency (30 to 100 Hz) vibrations of the *sprung mass*.
- 12.1.4 Hardness—Abrupt, short term forced motion of the *sprung mass* brought about by a transient *road disturbance input*.
- 12.1.5 Boom—A high intensity acoustic vibration (25 to 100 Hz) resulting from a *disturbance input*.

12.2 Unsprung-Mass Vibration

12.2.1 WHEEL VIBRATION MODES

- 12.2.1.1 Wheel Hop—The vertical oscillatory motion of a *wheel* between the *road surface* and the *sprung mass*.
 - 12.2.1.1.1 Parallel Hop—The form of *wheel hop* in which the *wheels* on an *axle* hop in phase.
 - 12.2.1.1.2 Tramp—The form of *wheel hop* in which the *wheels* on an *axle* hop in opposite phase.
 - 12.2.1.1.3 Brake Hop—*Wheel hop* that occurs due to braking.
 - 12.2.1.1.4 Power Hop—*Wheel hop* that occurs due to the application of engine power.

12.2.2 AXLE VIBRATION MODES

- 12.2.2.1 *Axle Hop*—Parallel hop of a solid-axle suspension.
- 12.2.2.2 *Axle Tramp*—Tramp of a solid-axle suspension.
- 12.2.2.3 *Axle Side Shake*—The lateral oscillatory motion of an *axle*.
- 12.2.2.4 *Axle Fore-and-Aft Shake*—The longitudinal oscillatory motion of an *axle*.

12.2.3 STEERING-SYSTEM VIBRATION MODES

- 12.2.3.1 *Wheel Flutter*—Forced oscillation of a steerable *wheel* about its *steering axis*.
- 12.2.3.2 *Wheel Wobble*—A self-excited oscillation of a pair of steerable *wheels* about their *steering axes*, occurring without appreciable *tramp*.
- 12.2.3.3 *Shimmy*—A self-excited, in-phase oscillation of a pair of steerable *wheels* about their *steering axes*, accompanied by appreciable *tramp*.
- 12.2.3.4 *Wheelfight*—A rotational disturbance of the *steering wheel* produced by forces acting on the steerable *wheels*.
- 12.2.3.5 *Wheel Kick*—*Wheelfight* in response to an impulsive input.

13. Notes

13.1 Marginal Indicia

A change bar (I) located in the left margin is for the convenience of the user in locating areas where technical revisions, not editorial changes, have been made to the previous issue of this document. An (R) symbol to the left of the document title indicates a complete revision of the document, including technical revisions. Change bars and (R) are not used in original publications, nor in documents that contain editorial changes only.

PREPARED BY THE SAE VEHICLE DYNAMICS STANDARDS COMMITTEE

APPENDIX A - ALPHABETICAL INDEX

- Acceleration Anti-Lift 5.7.4.3
Acceleration Control Input 9.1.1.3
Accelerations 4.2.1.2
Accelerator Pedal Position 9.1.1.3.1
Accelerator Pedal Position Gain 10.2.1.2
Ackermann Error 5.7.3.6
Ackermann Geometry 5.7.3.5
Ackermann Steer Angle Gradient 11.3.2.4
Ackermann Wheel Steer Angle 5.5.1.3
Adhesion Utilization 7.11.2.2, 10.5.1
Aerodynamic Disturbance Input 9.1.4.1
Aligning Moment Offset 7.10.3
Angles 4.2.2.1
Angular Accelerations 4.2.2.3
Angular Motion Variables 4.2.2
Angular Velocities 4.2.2.2
Anti- Characteristics 5.7.4
Anti-Dive 5.7.4.1
Anti-Lock Brake System 6.1.6
Anti-Roll 5.7.4.5
Anti-Roll Bar 5.2.11
Anti-Squat 5.7.4.4
Anti-Sway Bar 5.2.11
Articulation Angle Gradient 11.3.2.9
Articulation Point 4.1.6
Asymptotic Stability 8.2.1
Attitude Angle 4.2.2.1.8
Automatic Control Input 9.1.1.5
Average Suspension Ride Steer 5.7.1.15
Axis and Coordinate Systems 3
Axis System 3.3
Axe 5.2.1
Axe Fore-and-Aft Shake 12.2.2.4
Axe Hop 12.2.2.1
Axe Reference Sideslip Angle 4.2.2.1.10
Axe Side Shake 12.2.2.3
Axe Tramp 12.2.2.2
Axe Vibration Modes 12.2.2
Axe Windup Compliance 5.9.2.5
Ball Joint 5.2.2
Bandwidth 9.2.11
Base Vehicle Mass 4.1.14
Base Vehicle Weight 4.1.13
Beaming 12.1.2.2
Boom 12.1.5
Bounce 12.1.1.1
Brake 6.1.1
Brake Apply Rise Time 10.4.1
Brake Balance 6.3.1
Brake Caliper 6.2.4
Brake Components 6.2
Brake Disc 6.2.9
Brake Drum 6.2.10
Brake Hop 12.2.1.1.3
Brake Lining 6.2.6
Brake Pad 6.2.7
Brake Pedal 6.2.1
Brake Pedal Displacement 9.1.1.2.2
Brake Pedal Force 9.1.1.2.1
Brake Pedal Force Gain 10.2.1.1
Brake Pedal Travel 9.1.1.2.2
Brake Pressure 6.1.7
Brake Proportioning 6.3
Brake Release Time 10.4.2
Brake Rotor 6.2.9
Brake Shoe 6.2.8
Brake Torque 6.1.8
Brakes 6
Braking Anti-Lift 5.7.4.2
Braking Control Input 9.1.1.2
Braking Efficiency 10.5.2
Braking Torque 7.8.2
Bump 5.6.1
Bump Stop 5.2.6
Bushing 5.2.3
C.G. 4.1.22

Camber and Steer Compliances	5.9.1	Cornering Compliance	11.3.3.5
Camber Angle	5.5.1.10	Counterclockwise Tire Rotation	7.6.6
Camber Compliance	5.9.1.2	Course Angle	4.2.3.7
Caster Angle	5.5.2.2	Critical Speed	11.3.5.3
Caster Offset at Ground	5.5.2.4	Curb Mass	4.1.16
Caster Offset at Wheel Center	5.5.2.3	Curb Weight	4.1.15
Caster Trail	5.5.2.4	Damper	5.2.5
Center Link	5.3.5.3.3	Descriptors of Limit Response	11.5
Center of Tire Contact	7.3.6	Descriptors of Steady-State Directional Response	11.3
Centrifuge Ratio	11.5.2.4.1	Descriptors of Steady-State Longitudinal Response	10.2
Centripetal Acceleration	4.2.1.2.6	Descriptors of Transient Brake System Response	10.4
C-Factor	5.7.3.11	Descriptors of Transient Directional Response	11.4
Characteristic Speed	11.3.5.2	Descriptors of Transient Longitudinal Response	10.3
Characterizing Descriptors of Braking Performance	10.5	Directional Response Limits	11.5.1
Characterizing Speeds	11.3.5	Disc Brake	6.1.4
Clockwise Tire Rotation	7.6.5	Disturbance Input	9.1.4
Closed-Loop Control	8.3.5	Disturbance Response	9.2.3
Cold Inflation Pressure	7.7.1	Divergent Instability	8.2.4
Compliance Camber	5.9.1.1	Drift	11.5.1.4
Compliance Camber Coefficient	5.9.1.2	Driver Control Input	9.1.1.4
Compliance Steer	5.9.1.3	Driver Settings	9.1.3
Compliance Steer Coefficient	5.9.1.4	Driving Torque	7.8.1
Compliances	5.9	Droop	5.6.2
Compression	5.6.1	Drum Brake	6.1.5
Conicity Aligning Moment	7.10.3.1	Dynamic Gain	9.2.5.1
Conicity Lateral Force	7.10.1.1	Dynamic Gradient	9.2.5.2
Conicity Residual Aligning Moment	7.10.4.1	Dynamic Index - Pitch	4.1.26
Conicity Residual Lateral Force	7.10.2.1	Dynamic Index - Yaw	4.1.27
Contact Center	7.3.6	Dynamic Sensitivity	9.2.5.1
Contact Line	7.3.5	Earth-Fixed Axis System	3.9
Contact Patch	7.2.10	Earth-Fixed Coordinate System	3.10
Control Arm	5.2.4	Effective Unsprung Mass	4.1.10
Control Derivatives	11.6.2	Equilibrium	8.1
Control Input	9.1.1	Equivalent Time of Initiation	9.1.5
Control Modes	8.3	Extension	5.6.2
Control Moment	11.6.2.2	Feedback Control	8.3.5
Control Moment Sensitivity	11.3.1.2	Fixed Control	8.3.2
Control Response	9.2.2	Fixed Proportioning	6.3.2
Control System Input	9.1.2		
Coordinate System	3.4		

Footprint 7.2.10	Included Reference Steer Angle 5.5.1.5
Force Control 8.3.3	Independent Suspension 5.1.1.1
Forces 4.3.1	Inertial Reference 3.2
Forces and Moments 4.3	Input Shaft 5.3.4.3
Free Control 8.3.4	Inputs 9.1
Friction Brake 6.1.2	Inputs and Responses 9
Friction Material 6.2.6	Intermediate Axis System 3.14
Front-View Swing Center 5.7.1.1	Intermediate Shaft 5.3.3
Front-View Swing-Arm Angle 5.7.1.3	Jounce 5.6.1
Front-View Swing-Arm Length 5.7.1.2	Jounce Bumper 5.2.6
Gain 9.2.4.1	Jounce Stop 5.2.6
Gain Measures 10.2.1	k_{YY}^2/ab Ratio - Pitch 4.1.26
Gain or Sensitivity Measures 11.3.1	k_{ZZ}^2/ab Ratio - Yaw 4.1.27
Gear Ratio 5.7.3.9	Kinematics 4.2, 5.7
General Nomenclature 5.1, 6.1	Kingpin Axis 5.5.2.1
Geometric Stability Ratio 11.5.2.1	Kingpin Inclination Angle 5.5.2.5
Geometry 5.5	Kingpin Offset at Ground 5.5.2.7
Geometry and Masses 4.1	Kingpin Offset at Wheel Center 5.5.2.6
Gradient 9.2.4.2	Knuckle 5.2.8
Gradient Measures 10.2.2, 11.3.2	Knuckle Arm 5.3.5.2
Ground Plane 3.5	Lateral Acceleration 4.2.1.2.3
Hand Wheel 5.3.1	Lateral Acceleration Gain 11.3.1.1
Hand-Wheel Angle 9.1.1.1.1	Lateral Acceleration Moment Gain 11.3.1.2
Hand-Wheel Angle Gradient 11.3.2.1	Lateral Acceleration Response Time 11.4.1.1
Hand-Wheel Rim Force 9.1.1.1.3	Lateral Acceleration Rise Time 11.4.1.1
Hand-Wheel Torque 9.1.1.1.2	Lateral Compliance at the Contact Center 5.9.2.2
Hand-Wheel Torque Gradient 11.3.2.2	Lateral Compliance at the Wheel Center 5.9.2.1
Hardness 12.1.4	Lateral Force 4.3.1.3
Harshness 12.1.3	Lateral Force / Roll Angle Derivative 11.6.1.3
Heading Angle 4.2.2.1.3	Lateral Force / Sideslip Derivative 11.6.1.1
Heave 12.1.1.1	Lateral Force / Steering-Wheel Angle Derivative 11.6.2.1
Hitch Point 4.1.7	Lateral Force / Yaw Velocity Derivative 11.6.1.2
Horizontal Acceleration 4.2.1.2.8	Lateral Force Offset 7.10.1
Horizontal Acceleration Vector 4.2.1.2.7	Lateral Link 5.2.9.1
Horizontal Velocity 4.2.1.1.7	Lateral Load Transfer 11.1
Horizontal Velocity Vector 4.2.1.1.6	Lateral Velocity 4.2.1.1.4
Hot Inflation Pressure 7.7.2	
Hub Carrier 5.2.8	
Idler Arm 5.3.5.3.2	
Inclination Angle 7.4.3	
Included Ackermann Steer Angle 5.5.1.6	

- Leading Link 5.2.9.2
Linear Range 11.2.2
Link 5.2.9
Linkage Ratio 5.7.3.10
Load Condition 4.1.18
Loaded Radius 7.3.7
Load-Shift Disturbance Input 9.1.4.2
Longitudinal Acceleration 4.2.1.2.2
Longitudinal Compliance 5.9.2.3
Longitudinal Force 4.3.1.2
Longitudinal Load Transfer 10.1
Longitudinal Plane of Symmetry 3.8
Longitudinal Velocity 4.2.1.1.3
Mass Moments of Inertia (Sprung Mass)
 4.1.25
Mass Moments of Inertia (Total Vehicle)
 4.1.24
Masses and Inertias 5.4
Master Cylinder 6.2.2
Maximum Lateral Acceleration 11.5.1.1
Mean Reference Steer Angle 5.5.1.4
Minimum Steering Sensitivity 11.4.3.2
Moment Method 11.6.3
Moment Properties 7.13
Moments 4.3.2
Net Suspension Ride Steer 5.7.1.15
Neutral Stability 8.2.2
Neutral Steer 11.3.3.2
Neutral Steer Line 11.3.4.1
Newtonian Reference 3.2
Nominal Rim Diameter 7.1.2.3
Nonlinear Range 11.2.3
Non-Oscillatory Instability 8.2.4
Non-Oscillatory Stability 8.2.1
Normal Force Properties 7.12
Normalized Lateral Force 11.6.3.2
Normalized Path Curvature 4.2.3.6
Normalized Yaw Moment 11.6.3.1
On-Center Range 11.2.1
Open-Loop Control 8.3.6
Oscillatory Instability 8.2.5
Oscillatory Stability 8.2.3
Other Compliances 5.9.2
Other Transient Measures 11.4.3
Output Shaft 5.3.4.4
Overall Steering Ratio 5.7.3.8
Overshoot 9.2.9
Overshoot Measures 11.4.2
Oversteer 11.3.3.4
Overturning Couple 11.1.4
Overturning Couple Distribution 11.1.5
Panhard Rod 5.2.12
Parallel Hop 12.2.1.1.1
Parallelogram Linkage 5.3.5.3
Passenger Mass 4.1.21
Path Curvature 4.2.3.5
Path Curvature Gain 11.3.1.5
Path Curvature Gradient 11.3.2.8
Path Radius 4.2.3.3
Payload 4.1.17
Peak Coefficient of Friction 7.14.3
Peak Response Time 9.2.7
Peak to Steady-State Ratio 9.2.12
Peak-to-Slide Ratio 7.14.5
Percent Overshoot 9.2.10
Pitch 12.1.1.3
Pitch Acceleration 4.2.2.3.3
Pitch Angle 4.2.2.1.4
Pitch Angle Gradient 10.2.2.1
Pitch Angle Overshoot 10.3.1
Pitch Moment 4.3.2.3
Pitch Velocity 4.2.2.2.3
Pitman Arm 5.3.5.3.1
Plow 11.5.1.2
Plysteer Aligning Moment 7.10.3.2
Plysteer Lateral Force 7.10.1.2
Plysteer Residual Aligning Moment
 7.10.4.2
Plysteer Residual Lateral Force 7.10.2.2
Pneumatic Tire Nomenclature 7.2
Position Control 8.3.1
Power Hop 12.2.1.1.4
Primary Ride 12.1.1
Properties of Forces in the Road Plane 7.11

- Proportioning Valve 6.2.3
Pull Forces and Moments 7.10
Rack and Pinion Steering Gear 5.3.4.1
Rack Ratio 5.7.3.11
Rack Speed 5.7.3.11
Ranges of Directional Response 11.2
Rear-View Swing Center 5.7.1.1
Rear-View Swing-Arm Angle 5.7.1.3
Rear-View Swing-Arm Length 5.7.1.2
Rearward Amplification 11.4.3.1
Rebound 5.6.2
Rebound Stop 5.2.7
Recirculating-Ball Steering Gear 5.3.4.2
Reference Frame 3.1
Reference Steer Angle 5.5.1.2
Reference Steer Angle Gradient 11.3.2.3
Reference Wheel-Spin Velocity 7.6.2
Regenerative Brake 6.1.3
Relay Rod 5.3.5.3.3
Residual Aligning Moment 7.10.4
Residual Lateral Force 7.10.2
Response Time 9.2.6
Responses 9.2
Ride and Roll Stiffness 5.8
Ride Kinematics 5.7.1
Ride Rate 5.8.1
Ride Spring 5.2.10
Ride Track Change 5.7.1.16
Ride Track Change Gradient 5.7.1.17
Ride Vibration 12
Rim 7.1.2
Rim Contour Designation 7.1.2.4
Rim Diameter 7.1.2.2
Rim Diameter Designation 7.1.2.3
Rim Flange 7.1.2.6
Rim Size Designation 7.1.2.5
Rim Width 7.1.2.1
Rise Time 9.2.6
Rise-Time Measures 11.4.1
Road Disturbance Input 9.1.4.3
Road Plane 3.7
Road Surface 3.6
Road Wheel 7.1.1
Road Wheel Steer Angle 5.5.1.1
Rod End 5.2.2
Roll 12.1.1.2
Roll Acceleration 4.2.2.3.2
Roll Angle 4.2.2.1.5
Roll Angle Gradient 11.3.2.5
Roll Angle Overshoot 11.4.2.2
Roll Axis 5.7.2.11
Roll Center 5.7.2.9
Roll Center Height 5.7.2.10
Roll Kinematics 5.7.2
Roll Moment 4.3.2.2
Roll Moment / Roll Angle Derivative 11.6.1.8
Roll Moment / Roll Velocity Derivative 11.6.1.7
Roll Rate 5.8.3
Roll Stiffness 5.8.3
Roll Stiffness Distribution 5.8.6
Roll Velocity 4.2.2.2.2
Rollover Resistance 11.5.2
Rotational-Rotational Steering Gear 5.3.4.2
Scrub Radius 5.5.2.7
Secondary Ride 12.1.2
Sensitivity 9.2.4.1
Settling Time 9.2.8
Shake 12.1.2
Shimmy 12.2.3.3
Shock Absorber 5.2.5.1
Side-Pull Ratio 11.5.2.4.2
Sideslip Angle 4.2.2.1.7
Sideslip Angle Gain 11.3.1.4
Sideslip Angle Gradient 11.3.2.7
Sideslip Angle Response Time 11.4.1.2
Sideslip Angle Rise Time 11.4.1.2
Side-View Swing Center 5.7.1.4
Side-View Swing-Arm Angle 5.7.1.6
Side-View Swing-Arm Length 5.7.1.5
Slide Coefficient of Friction 7.14.4

Slip Angle 7.4.2	Steer Camber Gradient 5.7.3.2
Solid-Axle Suspension 5.1.1.2	Steer Caster 5.7.3.3
Specified Rim Diameter 7.1.2.2	Steer Caster Gradient 5.7.3.4
Spin 11.5.1.3	Steer Compliance 5.9.1.4
Spin Moment of Inertia 5.4.3	Steer Moment of Inertia 5.4.4
Spindle Length 5.5.2.8	Steering Axis 5.5.2.1
Spindle Trail 5.5.2.3	Steering-Axis Geometry 5.5.2
Sprung Mass 4.1.12	Steering-Axis Inclination Angle 5.5.2.5
Sprung-Mass Center of Gravity 4.1.23	Steering-Axis Offset at Ground 5.5.2.7
Sprung-Mass Pitch Moment of Inertia 4.1.25.2	Steering-Axis Offset at Wheel Center 5.5.2.6
Sprung-Mass Roll Moment of Inertia 4.1.25.1	Steering Column 5.3.2
Sprung-Mass Roll-Yaw Product of Inertia 4.1.25.4	Steering Components 5.3
Sprung-Mass Vibration 12.1	Steering Control Input 9.1.1.1
Sprung-Mass Yaw Moment of Inertia 4.1.25.3	Steering Gear 5.3.4
Sprung Weight 4.1.11	Steering Kinematics 5.7.3
Stability 8.2	Steering Linkage 5.3.5
Stability and Control Derivatives 11.6	Steering Ratio 5.7.3.7
Stability Derivatives 11.6.1	Steering Sensitivity 11.3.1.1
Stability Factor 11.3.4.3	Steering Stiffness 11.3.1.6
Stability Index 11.6.3.3	Steering-System Vibration Modes 12.2.3
Stability Measures 11.3.4	Steering Wheel 5.3.1
Stabilizer Bar 5.2.11	Steering-Wheel Torque Gain 11.3.1.6
Standard Loads and Inflation Pressures 7.7	Steering-Wheel Angle 9.1.1.1.1
States and Modes 8	Steering-Wheel Angle Gradient 11.3.2.1
Static Directional Stability 11.6.1.4	Steering-Wheel Rim Force 9.1.1.1.3
Static Loaded Radius 7.3.8	Steering-Wheel Torque 9.1.1.1.2
Static Margin 11.3.4.2	Steering-Wheel Torque Gradient 11.3.2.2
Static Roll Stability Limit 11.5.2.3	Straight Free-Rolling Tire 7.5.1
Static Rollover Threshold 11.5.2.3	Strut 5.2.5.2
Static Stability Factor 11.5.2.2	Sum Toe Angle 5.5.1.8
Static Stability Ratios 11.5.2.4	Suspension 5.1.1
Static Toe 5.5.1.9	Suspension and Steering 5
Steady State 8.1.1	Suspension Components 5.2
Steady-State Response 9.2.4	Suspension Corner 5.1.1.3
Steer and Camber Angles 5.5.1	Suspension Motions 5.6
Steer Angle 5.5.1.1	Suspension Ride 5.6.3
Steer Arm 5.3.5.2	Suspension Ride Camber 5.7.1.7
Steer Camber 5.7.3.1	Suspension Ride Camber Gradient 5.7.1.8
	Suspension Ride Caster 5.7.1.9
	Suspension Ride Caster Gradient 5.7.1.10
	Suspension Ride Displacement 5.6.5

- Suspension Ride Rate 5.8.2
Suspension Ride Steer 5.7.1.13
Suspension Ride Steer Gradient 5.7.1.14
Suspension Ride Toe 5.7.1.11
Suspension Ride Toe Gradient 5.7.1.12
Suspension Roll 5.6.4
Suspension Roll Angle 5.6.6
Suspension Roll Angle Gradient 11.3.2.6
Suspension Roll Camber 5.7.2.1
Suspension Roll Camber Gradient 5.7.2.2
Suspension Roll Caster 5.7.2.5
Suspension Roll Caster Gradient 5.7.2.6
Suspension Roll Inclination 5.7.2.3
Suspension Roll Inclination Gradient 5.7.2.4
Suspension Roll Rate 5.8.4
Suspension Roll Steer 5.7.2.7
Suspension Roll Steer Gradient 5.7.2.8
Suspension Roll Stiffness 5.8.4
Suspension Trim Height 4.1.5
Suspension Trim Height Gradient 10.2.2.2
Tangent Point 4.2.2.1.9
Tangent Speed 11.3.5.1
Tangential Acceleration 4.2.1.2.5
Throttle Position 9.1.1.3.2
Tie Rod 5.3.5.1
Tilt-Table Ratio 11.5.2.4.3
Tire 7.2.1
Tire Aligning Moment 7.9.11
Tire Aligning Moment Coefficient 7.13.3
Tire Aligning Moment Load Sensitivity 7.13.4
Tire Aligning Stiffness 7.13.7
Tire Aligning Stiffness Coefficient 7.13.9
Tire Aligning Inclination Stiffness 7.13.8
Tire Aligning Torque 7.9.11
Tire Aspect Ratio 7.2.6
Tire Axis System 3.15
Tire Braking / Driving Stiffness 7.11.5
Tire Braking / Driving Stiffness Coefficient 7.11.8
Tire Braking Coefficient 7.11.2.2
Tire Braking Force 7.9.6.2
Tire Braking Force Coefficient 7.11.2.2
Tire Camber Coefficient 7.11.10
Tire Camber Stiffness 7.11.7
Tire Camber Stiffness Coefficient 7.11.10
Tire Coordinate System 3.16
Tire Cornering Coefficient 7.11.9
Tire Cornering Stiffness 7.11.6
Tire Cornering Stiffness Coefficient 7.11.9
Tire Deflection 7.12.1
Tire Designation 7.2.11
Tire Driving Coefficient 7.11.2.1
Tire Driving Force 7.9.6.1
Tire Driving Force Coefficient 7.11.2.1
Tire Face 7.2.7
Tire Force 7.9.1
Tire Forces and Moments 7.9
Tire Fore-Aft Force 7.9.6
Tire Friction Ellipse 7.14.1
Tire Friction Ellipse Boundary 7.14.2
Tire Inclination Stiffness 7.11.7
Tire Inclination Stiffness Coefficient 7.11.10
Tire Lateral Force 7.9.7
Tire Lateral Force Coefficient 7.11.3
Tire Lateral Force Load Sensitivity 7.11.4
Tire Lateral Force Response Phase Angle 7.11.12
Tire Lateral Load Transfer 11.1.1
Tire Lateral Load Transfer Distribution 11.1.3
Tire Lateral Velocity 7.5.4
Tire Load 7.7.3
Tire Load Index 7.2.8
Tire Load Limit 7.7.3.1
Tire Load Rating 7.7.3.1
Tire Longitudinal Force 7.9.6
Tire Longitudinal Force / Longitudinal Slip Gradient 7.11.5
Tire Longitudinal Force Coefficient 7.11.2
Tire Longitudinal Slip Ratio 7.6.4
Tire Longitudinal Slip Velocity 7.6.3
Tire Longitudinal Stiffness 7.11.5

Tire Longitudinal Stiffness Coefficient 7.11.8	Tire Vertical Velocity 7.5.5
Tire Longitudinal Velocity 7.5.3	Tire/Road Friction 7.14
Tire Moment 7.9.8	Tire/Wheel Assembly 7.3.1
Tire Normal Force 7.9.2	Tire/Wheel Disturbance Input 9.1.4.4
Tire Normal Stiffness 7.12.2	Tires and Wheels 7
Tire Normalized Aligning Moment 7.13.3	Toe Angle 5.5.1.7
Tire Normalized Braking Force 7.11.2.2	Torsional Shake 12.1.2.1
Tire Normalized Driving Force 7.11.2.1	Total Tire Lateral Load Transfer 11.1.2
Tire Normalized Lateral Force 7.11.3	Total Toe Angle 5.5.1.8
Tire Normalized Longitudinal Force 7.11.2	Track 4.1.3
Tire Normalized Overturning Moment 7.13.1	Track Bar 5.2.12
Tire Normalized Rolling Moment 7.13.2	Track Width 4.1.3
Tire Normalized Shear Force 7.11.1	Trailer Pitch Articulation Angle 4.2.2.1.12
Tire Orientation Angles 7.4	Trailer Roll Articulation Angle 4.2.2.1.13
Tire Outside Diameter 7.2.4	Trailer Wheelbase 4.1.2
Tire Overall Diameter 7.2.4	Trailer Yaw Articulation Angle 4.2.2.1.11
Tire Overall Width 7.2.3	Trailer Yaw Articulation Angle Gradient 11.3.2.9
Tire Overturning Moment 7.9.9	Trailing Link 5.2.9.3
Tire Overturning Moment Coefficient 7.13.1	Tramp 12.2.1.1.2
Tire Overturning Stiffness 7.13.5	Transient Response 9.2.5
Tire Overturning Inclination Stiffness 7.13.6	Transient State 8.1.2
Tire Radial Force 7.9.2	Translational Motion Variables 4.2.1
Tire Radial Stiffness 7.12.2	Trim 8.1.1
Tire Relaxation Length 7.11.11	Turn Center 4.2.3.4
Tire Rolling Characteristics 7.5	Understeer 11.3.3.3
Tire Rolling Moment 7.9.10	Understeer / Oversteer Gradient 11.3.3.1
Tire Rolling Moment Coefficient 7.13.2	Understeer and Oversteer 11.3.3
Tire Rolling Resistance Moment 7.9.10	Unsprung Mass 4.1.9
Tire Section Height 7.2.5	Unsprung-Mass Center of Gravity 5.4.1
Tire Section Width 7.2.2	Unsprung-Mass Moments of Inertia 5.4.2
Tire Shear Force 7.9.5	Unsprung-Mass Pitch Moment of Inertia 5.4.2.2
Tire Shear Force Coefficient 7.11.1	Unsprung-Mass Roll Moment of Inertia 5.4.2.1
Tire Shear Force Vector 7.9.4	Unsprung-Mass Vibration 12.2
Tire Side Force 7.9.7	Unsprung-Mass Yaw Moment of Inertia 5.4.2.3
Tire Speed Symbol 7.2.9	Unsprung Weight 4.1.8
Tire Spring Rate 7.12.2	Upright 5.2.8
Tire Trajectory Velocity 7.5.2	Variable Proportioning 6.3.3
Tire Vertical Load 7.9.3	Vehicle 4

Vehicle Acceleration 4.2.1.2.1	Wheel Coordinate System 3.18
Vehicle Angular Acceleration 4.2.2.3.1	Wheel Cylinder 6.2.5
Vehicle Angular Orientation 4.2.2.1.1	Wheel Flutter 12.2.3.1
Vehicle Angular Velocity 4.2.2.2.1	Wheel Hop 12.2.1.1
Vehicle Axis System 3.11	Wheel Kick 12.2.3.5
Vehicle Center of Gravity 4.1.22	Wheel Nomenclature 7.1
Vehicle Coordinate System 3.12	Wheel Plane 7.3.3
Vehicle Euler Angles 4.2.2.1.2	Wheel Plane Geometry 7.3
Vehicle Force 4.3.1.1	Wheel Plane Orientation 7.4.1
Vehicle Lateral Response 11	Wheel Rate 5.8.2
Vehicle Longitudinal Response 10	Wheel Spin and Tire Slip 7.6
Vehicle Moment 4.3.2.1	Wheel-Spin Axis 7.3.2
Vehicle Operating Mass 4.1.20	Wheel-Spin Velocity 7.6.1
Vehicle Operating Weight 4.1.19	Wheel Torque 7.8
Vehicle Path 4.2.3.2	Wheel Track 4.1.3
Vehicle Pitch Moment of Inertia 4.1.24.2	Wheel Vibration Modes 12.2.1
Vehicle Plane of Symmetry 3.8	Wheel Wobble 12.2.3.2
Vehicle Reference Point 3.13	Wheelbase 4.1.1
Vehicle Response 9.2.1	Wheelfight 12.2.3.4
Vehicle Roll Angle 4.2.2.1.6	Windup Compliance 5.9.2.4
Vehicle Roll Moment of Inertia 4.1.24.1	Wishbone 5.2.4
Vehicle Roll Stiffness 5.8.5	Yaw Acceleration 4.2.2.3.4
Vehicle Roll-Yaw Product of Inertia 4.1.24.4	Yaw Angle 4.2.2.1.3
Vehicle Sideslip Angle 4.2.2.1.8	Yaw Damping 11.6.1.5
Vehicle Speed 4.2.1.1.2	Yaw Moment 4.3.2.4
Vehicle Trajectory 4.2.3.1	Yaw Moment Reserve 11.6.3.4
Vehicle Trajectory Measures 4.2.3	Yaw Moment / Roll Angle Derivative 11.6.1.6
Vehicle Trim Height 4.1.4	Yaw Moment / Sideslip Derivative 11.6.1.4
Vehicle Velocity 4.2.1.1.1	Yaw Moment / Steering-Wheel Angle Derivative 11.6.2.2
Vehicle Yaw Moment of Inertia 4.1.24.3	Yaw Moment / Yaw Velocity Derivative 11.6.1.5
Velocities 4.2.1.1	Yaw Rate 4.2.2.2.4
Vertical Acceleration 4.2.1.2.4	Yaw Velocity 4.2.2.2.4
Vertical Force 4.3.1.4	Yaw Velocity Gain 11.3.1.3
Vertical Velocity 4.2.1.1.5	Yaw Velocity Overshoot 11.4.2.1
Warm Inflation Pressure 7.7.2	Yaw Velocity Peak Response Time 11.4.1.4
Warp 12.1.1.4	Yaw Velocity Response Time 11.4.1.3
Warp Couple 12.1.1.5	Yaw Velocity Rise Time 11.4.1.3
Watt Linkage 5.2.13	Zero Damping Speed 11.3.5.4
Wheel 7.1.1	
Wheel Axis System 3.17	
Wheel Center 7.3.4	

APPENDIX B - SYMBOLS

B.1 UPPER-CASE GREEK		
Γ	Trailer Yaw Articulation Angle	4.2.2.1.11
$\Delta\theta$	Trailer Pitch Articulation Angle	4.2.2.1.12
$\Delta\phi$	Trailer Roll Articulation Angle	4.2.2.1.13
$\Delta\psi$	Trailer Yaw Articulation Angle	4.2.2.1.11
B.2 LOWER-CASE GREEK		
α	Slip Angle	7.4.2
β	Vehicle Sideslip Angle (Attitude Angle)	4.2.2.1.8
γ	Inclination Angle [alternate symbol]	7.4.3
δ	Steer Angle (Road Wheel Steer Angle)	5.5.1.1
δ_A	Included Ackermann Steer Angle	5.5.1.6
δ_H	(Hand Wheel Angle)	9.1.1.1.1
δ_{REF}	Included Reference Steer Angle	5.5.1.5
δ_{SW}	Steering-Wheel Angle	9.1.1.1.1
ε	Inclination Angle	7.4.3
θ	Pitch Angle	4.2.2.1.2, 4.2.2.1.4
κ	Path Curvature (Curvature of Trajectory)	4.2.3.5
μ_p	Peak Coefficient of Friction	7.1.4.3
μ_s	Slide Coefficient of Friction	7.1.4.4
ν	Course Angle	4.2.3.7
$\sigma_F \sigma_R$	Front, Rear Axle Sideslip Angles	4.2.2.1.10
ϕ	Roll Angle	4.2.2.1.2, 4.2.2.1.5
ϕ_v	Vehicle Roll Angle	4.2.2.1.6
ψ	Yaw Angle (Heading Angle)	4.2.2.1.2, 4.2.2.1.3
ω	Vehicle Angular Velocities	4.2.2.2
ω_w	Wheel-Spin Velocity	7.6.1
ω_{w_0}	Reference Wheel-Spin Velocity	7.6.2
B.3 UPPER-CASE ARABIC		
A	Rim Width	7.1.2.1
C	Tire Force and Moment Stiffnesses and Coefficients [subscripted]	7.11.5 - 7.11.10, 7.13.5 - 7.13.9
C_N	Normalized Yaw Moment	11.6.3.1
C_y	Normalized Lateral Force	11.6.3.2
D	Rim Diameter (Specified Rim Diameter)	7.1.2.2
$D_F D_R$	Front, Rear Cornering Compliances	11.3.3.5
F	Vehicle Forces	4.3.1
F_H	(Hand Wheel Rim Force)	9.1.1.1.3
F_{SW}	Steering-Wheel Rim Force	9.1.1.1.3
F_T	Tire Forces	7.9, 7.10
H	Vehicle Center of Gravity Height	4.1.22

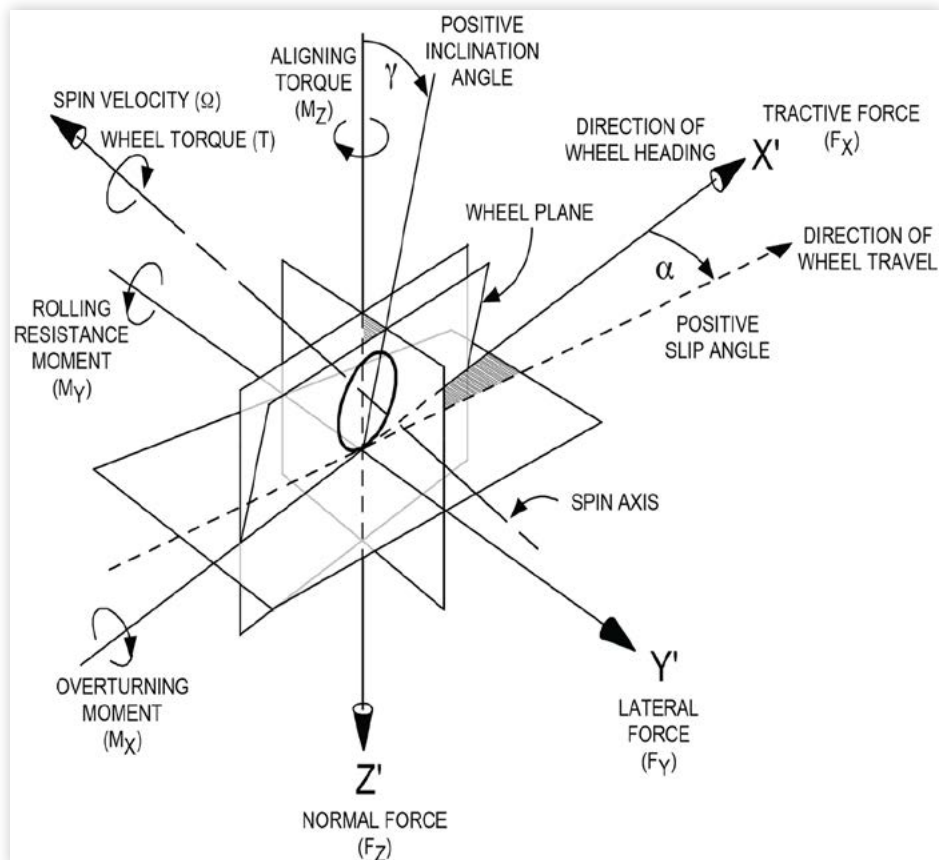
K	Stability Factor	11.3.4.3
L	Wheelbase	4.1.1
L	Stability Derivatives [subscripted]	11.6.1
M	Vehicle Moments	4.3.2
M_H	(Hand Wheel Torque)	9.1.1.1.2
M_{SW}	Steering-Wheel Torque	9.1.1.1.2
M_T	Tire Moments	7.9, 7.10
N	Stability and Control Derivatives [subscripted]	11.6.1, 11.6.2
R	Path Radius	4.2.3.3
R_L	Loaded Radius	7.3.7
S_x	Tire Longitudinal Slip Ratio	7.6.4
SLR	Static Loaded Radius	7.3.8
SSF	Static Stability Factor	11.5.2.2
T	Track	4.1.3
T_w	Wheel Torque	7.8
U	Understeer / Oversteer Gradient	11.3.3.1
W	Vehicle Operating Weight	4.1.19
X	Longitudinal Axis [subscripted or non-subscripted]	3.9, 3.11, 3.14, 3.15, 3.17
Y	Lateral Axis [subscripted or non-subscripted]	3.9, 3.11, 3.14, 3.15, 3.17
Y	Stability and Control Derivatives [subscripted]	11.6.1, 11.6.2
Z	Vertical Axis [subscripted or non-subscripted]	3.9, 3.11, 3.14, 3.15, 3.17

B.4 LOWER-CASE ARABIC		
a	Vehicle Accelerations	4.2.1.2
a, b	Longitudinal distance from the vehicle center of gravity to the front and rear axle center lines	4.1.22
h	Vehicle Center of Gravity Height	4.1.22
k_{YY}	Radius of Gyration in Pitch	4.1.26
k_{ZT}	Tire Normal Stiffness	7.12.2
k_{ZZ}	Radius of Gyration in Yaw	4.1.27
v	Vehicle Velocities	4.2.1.1
v_{CH}	Characteristic Speed	11.3.5.2
v_{CR}	Critical Speed	11.3.5.3
v_T	Tire Velocities	7.5.2 - 7.5.5
v_{ZD}	Zero Damping Speed	11.3.5.4
x	Longitudinal Coordinates [subscripted]	3.10, 3.12, 3.16, 3.18
y	Lateral Coordinates [subscripted]	3.10, 3.12, 3.16, 3.18
z	Vertical Coordinates [subscripted]	3.10, 3.12, 3.16, 3.18

APPENDIX C - SUPERSEDED TIRE AXIS SYSTEM

Previous editions of SAE J670 and the 1998 edition of SAE J2047 defined the Tire Axis System shown in [Figure C1](#). This edition of SAE J670 defines two tire axis systems - the Z-Up Tire Axis System and the Z-Down Tire Axis System, shown in [Figures 2A](#) and [2B](#), respectively. These tire axis systems replace the former SAE Tire Axis System. The orientation of the axes in the superseded Tire Axis System is identical to that of the Z-Down Tire Axis System shown in [Figure 2B](#). The sign conventions used for tire forces and moments in the Z-Down Tire Axis System are shown in [Figure 10B](#), and follow conventional mathematical practice for a right-handed axis system. The superseded Tire Axis System reversed the signs of wheel torque and wheel-spin velocity from accepted mathematical conventions. Positive wheel torque was previously defined as a driving torque, and positive wheel-spin velocity was previously defined to be consistent with vehicle motion in the positive X direction. In this Recommended Practice, the signs of wheel torque and wheel-spin velocity are determined using the right-hand rule for both Z-Up and Z-Down axis orientations.

FIGURE C1 Superseded Tire Axis System



The sign conventions used for wheel torque and wheel-spin velocity in previous editions of this Recommended Practice may need to be considered when analyzing legacy data. It is for that purpose that the previously defined sign conventions are shown in [Figure C1](#).

The terminology and symbols shown in [Figure C1](#) are those used in previous editions of SAE J670. [Table C1](#) provides a conversion of the terminology and symbols used in the superseded Tire Axis System to the terminology and symbols used in the current Z-Down Tire Axis System.

TABLE C1 Relationships between Superseded Tire Axis System and Z-Down Tire Axis System

Tire Axis System			
	Superseded	Z-Down	
Axes	X'	=	X _T
	Y'	=	Y _T
	Z'	=	Z _T
	Spin Axis	=	Wheel-Spin Axis
Forces	Tractive Force (F _x)	=	Longitudinal Force (F _{xt})
	Lateral Force (F _y)	=	Lateral Force (F _{yt})
	Normal Force (F _z)	=	Normal Force (F _{zt})
Moments	Overturning Moment (M _x)	=	Overturning Moment (M _{xt})
	Rolling Resistance Moment (M _y)	=	Rolling Moment (M _{yt})
	Aligning Torque (M _z)	=	Aligning Moment (M _{zt})
Angles	- Wheel Torque (T)	=	Wheel Torque (T _w)
	Slip Angle α	=	Slip Angle α
Velocities	Inclination Angle γ	=	Inclination Angle ε
	- Spin Velocity (Ω)	=	Wheel-Spin Velocity (ω_w)
	Direction of Wheel Travel	=	Tire Trajectory Velocity (V _T)

appendix B: SAE J6a Ride and Vibration Data Manual

Report of Riding Comfort Research Committee approved July 1946 and last revised by the Vehicle Dynamics Committee October 1965. It is no longer published by the SAE but is included in this book in its entirety.

Table of Contents

Section 1. Basic Relationships

- 1.1 Acceleration versus static deflections
- 1.2 Undamped natural frequency of sprung mass
- 1.3 Relations in simple harmonic motion
- 1.4 Resonant speed on uniformly spaced road disturbances

Section 2. Vibration Systems

- 2.1 List of symbols
 - 2.1.1 Vibrating system parameters
 - 2.1.2 Vibratory motion
- 2.2 Free vibration with coulomb damping
- 2.3 Free vibration with viscous damping
- 2.4 Forced vibration with viscous damping
 - 2.4.1 Force applied to suspended mass
 - 2.4.1.1 Peak exciting force constant
 - 2.4.1.2 Exciting force increasing as square of frequency
 - 2.4.1.3 Equivalent impedance
 - 2.4.2 Excitation applied to spring support
 - 2.4.2.1 Absolute amplitude ratio
 - 2.4.2.2 Relative amplitude ratio
- 2.5 Forced vibration with coulomb damping
- 2.6 Force transmission through suspension
 - 2.6.1 Direct excitation of mass with viscous damping
 - 2.6.1.1 Constant peak driving force
 - 2.6.1.2 Driving force on mass proportional to square of speed with viscous damping
 - 2.6.1.3 Equivalent impedance
 - 2.6.2 Comparison of viscous and coulomb damping
 - 2.6.3 Vibrating system with two degrees of freedom
- 2.7 References

Section 3. Energy Absorption and Impact

- 3.1 List of symbols
- 3.2 Mathematical relations
 - 3.2.1 Impact from free fall
 - 3.2.2 Impact without gravity acceleration

Section 4. Vibration Limits for Passenger Comfort

- 4.1 Response to vertical vibrations
- 4.2 Vertical vibration limits for passenger comfort
- 4.3 Subjective responses of the human body to vibratory motion

Section 5. Bibliography

Foreword

This is the third edition of Ride and Vibration Data to be issued by the SAE Vehicle Dynamics Committee, formerly the Riding Comfort Research Committee.

The first edition, prepared in 1945, was confined to basic relationships involved in vehicle suspension and impact energy absorption. However, the treatment of vibration did not go beyond the characteristics of undamped simple harmonic motion.

The second edition, issued in 1950, consisted essentially of the original material with the addition of a section on human vibration tolerance.

In this new edition, the editorial subcommittee has attempted to include a graphical presentation of damped vibrating system characteristics, aimed at applications to vehicle ride and vibration problems. A detailed description of the scope of this subject matter is given in the Introduction to Section 2.

SAE Vehicle Dynamics Committee: William Le Fevre, Chairman

Editorial Subcommittee:

R. N. Janeway, Chairman, Janeway Engineering Co.
 William Le Fevre, Le Fevre Co.
 W. C. Oswald, Bostrom Research Labs.
 John Versace, Ford Motor Co.

1. Basic Relationships

1.1 Acceleration versus Static Deflection

Figure 1 shows the acceleration of a mass to which a force is applied through a spring. It expresses the relation $A = x/\delta$, based on Newton's second law:

$$a = \frac{xk}{m}$$

$$A = \frac{a}{g} = \frac{xk}{mg} = \frac{x}{\delta}$$

where:

A = Acceleration, g units

a = Acceleration, in./ s^2

g = Acceleration of gravity, 386 in./ s^2

k = Spring rate, lb/in.

$m = w/g$ is mass, lb-sec 2 /in.

w = Weight of mass, lb

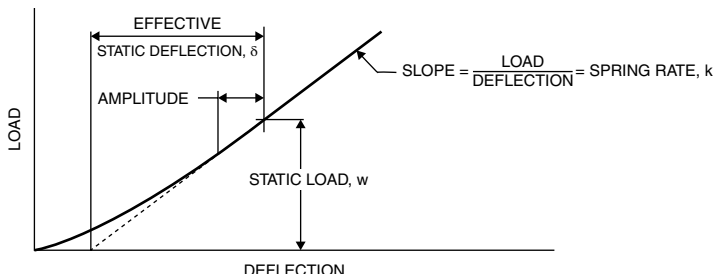
$\delta = w/k$ is the effective static deflection, in.

x = amplitude is the deflection of spring from static equilibrium, in.

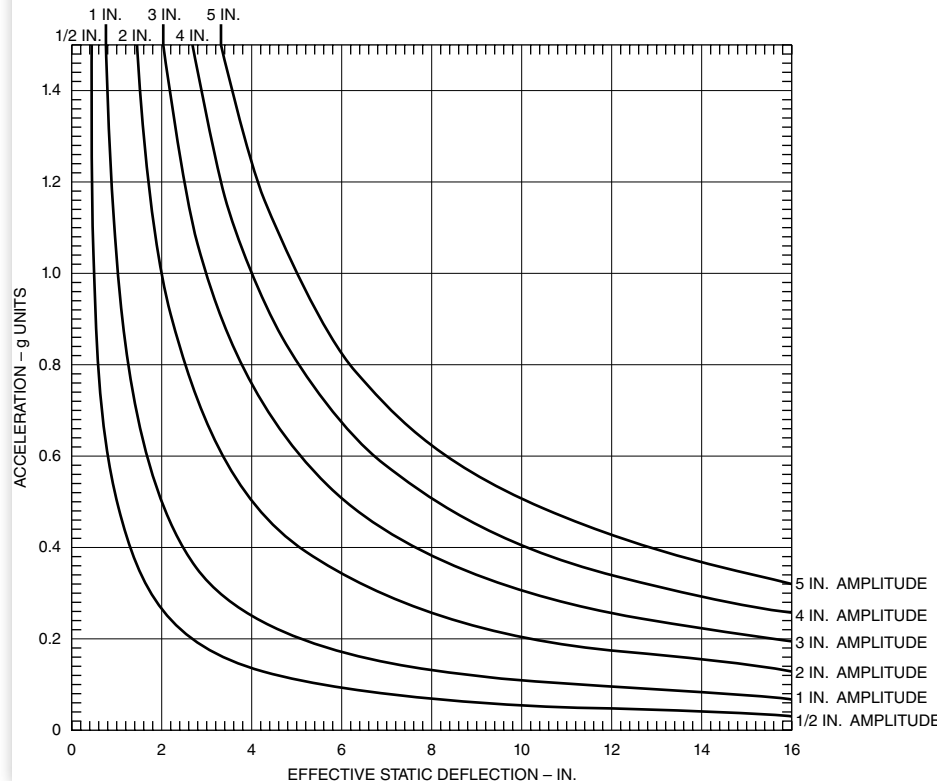
Referring to Figure 1A, note that the dynamic deflection (amplitude) of the spring is the relative displacement of the ends of the spring and can be caused by the displacement of the mass or of the support or of both. Also note that the effective static deflection

FIGURE 1 Acceleration versus static deflection at given amplitudes.

(A)



(B)



is not necessarily equal to the total loaded deflection. The relations expressed in this chart are not restricted to cyclic vibrations. They apply equally to the acceleration produced by a single sudden displacement. The figure refers to instantaneous values of acceleration and deflection, not to maxima only, for zero damping force.

The scales of [Figure 1B](#) can be changed in conformity with the relation $A = x/\delta$. Either x and δ can be multiplied by the same number, leaving A as given; or A and x can be multiplied by the same number, leaving δ as given.

EXAMPLE: A vehicle is sprung with 8 in. effective static deflection. The wheel is suddenly pushed 2 in. upward. What is the resulting acceleration?

ANSWER: At the intersection of the 8 in. vertical with the 2 in. amplitude curve read 0.25 g acceleration.

1.2 Undamped Natural Frequency of Sprung Mass*

The fundamental physical quantity which determines the natural vibration frequency of an undamped single degree of freedom system is the acceleration of the suspended mass produced by unit displacement from its static position. This is developed to give the basic frequency equation in [Figure 2A](#). Note that the spring rate must be measured in the direction of the motion and at the static loaded position. The simplified system diagram in [Figure 2A](#) assumes a constant spring rate. However, the effective static deflection is not necessarily equal to the total spring deflection at the static load, as illustrated in [Figure 1A](#).

[Figure 2C](#) shows the relation between static deflection and natural frequency in ordinary (Cartesian) coordinates; it gives a visual impression of the characteristic.

[Figure 2D](#) shows the same relationship by means of fixed logarithmic scales. It can be used to obtain quantitative values with satisfactory accuracy up to 50 cycles per second.

[Figure 2B](#) illustrates another important type of system with single degree of freedom, namely, angular motion about a fixed pivot. In this case the acceleration per unit displacement is

$$\ddot{\alpha} = \frac{\text{Restoring force moment per radian}}{\text{Mass moment of inertia}}$$

The deflection at the spring per radian = L_1 = Distance from pivot to spring center.
The restoring force at the spring per radian = kL_1 .

The restoring force moment per radian = kL_1^2 .

The moment of inertia of the mass, m , about the pivot = $m(i^2 + r^2)$,

where:

i = Radius of gyration about the c.g.

r = Distance of example from pivot

* See Refs. [1, 2, 3].

FIGURE 2 Undamped natural frequency versus static deflection.

(A)

$$\rho^2 = (2\pi f)^2 = \text{Acceleration per unit displacement}$$

$$f = \frac{1}{\pi} \sqrt{\text{Acceleration per unit displacement}}$$

$$\text{Force per unit displacement} = k$$

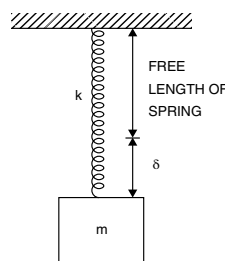
$$\text{Acceleration per unit displacement} = \frac{\text{Force}}{\text{Mass}} = \frac{k}{m}$$

$$\text{Acceleration} = \frac{k}{w} g = \frac{g}{\delta}$$

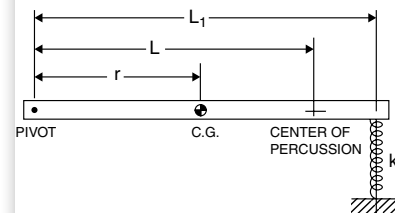
$$\text{Then } f = \frac{\sqrt{g}}{2\pi} \sqrt{\frac{1}{\delta}}$$

$$= 3.13 \sqrt{\frac{1}{\delta}}$$

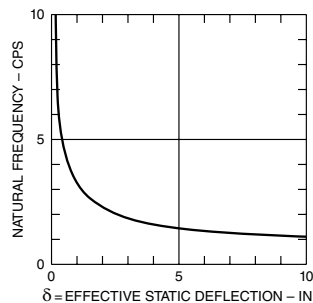
$$\text{or } f = \sqrt{\frac{10}{\delta}} \text{ cps approximately}$$



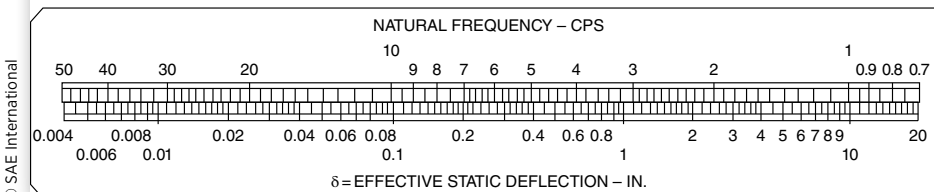
(B)



(C)



(D)



© SAE International

In this case it is useful to apply the concept of center of percussion which is located at the distance, L , from the pivot such that $L = r + i^2/r$.

Therefore, $r^2 + i^2 = rL$, and the moment of inertia $= mrL$. Then, the frequency,

$$f = \frac{1}{2\pi} \sqrt{\ddot{\alpha}} = \frac{1}{2\pi} \sqrt{\frac{kL_1^2}{mrL}} = \frac{\sqrt{g}}{2\pi} \sqrt{\frac{kL_1^2}{wrL}}$$

Since the load on the spring, $R = \frac{wr}{L_1}$

the static deflection, $\delta = \frac{wr}{L_1 k}$

$$\text{and } f = \frac{\sqrt{g}}{2\pi} \sqrt{\frac{L_1}{\delta L}}$$

Therefore, the frequency is again dependent on the static spring deflection but modified by the relation of the spring center to the center of percussion. It is important to note, however, that when $L_1 = L$, that is, spring is located at the center of percussion, the frequency is determined by the static deflection alone, as in the case of rectilinear motion. Figure 2C and 2D apply also to this special case of angular motion.

1.3 Relations in Simple Harmonic Motion

In simple harmonic motion, the distance, x , a vibrating mass is displaced from the static position at a given time, t , can be approximated closely by the equation

$$x = x_0 \sin(2\pi f t) = x_0 \sin \omega t$$

where:

- x = Instantaneous displacement from static position, in.
- x_0 = Maximum displacement from static position (amplitude), in.
- t = Time from zero displacement, sec
- f = Frequency of oscillation, cps
- $\omega = 2\pi f$, radians per second

From this equation, the following relationships for peak values can also be derived:

$$\text{Maximum velocity: } v_m = 2\pi f x_0 = \omega x_0 \quad \text{in./s}$$

$$\text{Maximum acceleration: } a_m = 4\pi^2 f^2 x_0 = \omega^2 x_0 \quad \text{in./s}^2$$

$$\text{Maximum jerk (rate of change of acceleration): } j_m = 8\pi^3 f^3 x_0 = \omega^3 x_0 \quad \text{in./s}^3$$

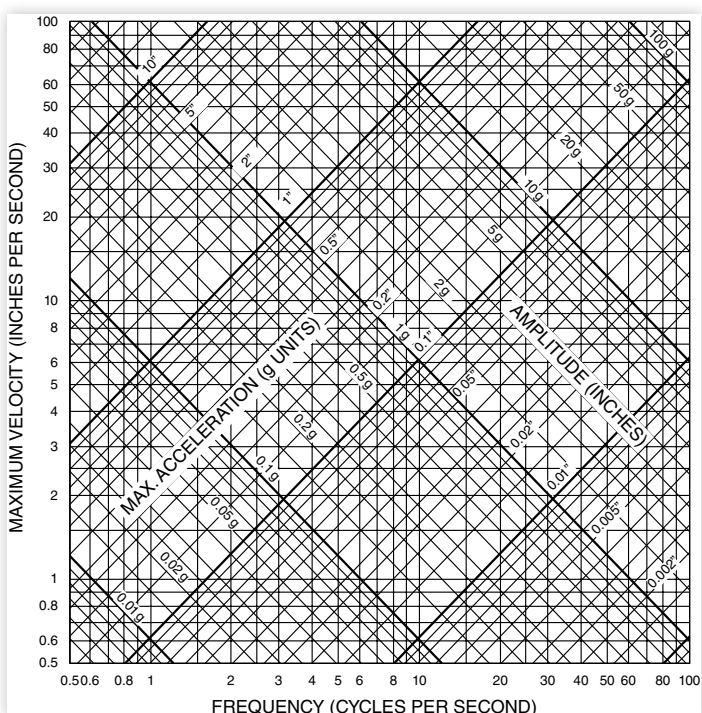
The interrelationships of frequency, velocity, amplitude, and acceleration are shown in [Figure 3](#).

Any deviation from true simple harmonic motion shows up more and more as higher derivatives of the motion are taken (or as we go from displacement to velocity, to acceleration, to jerk).

EXAMPLE: A mass has an amplitude of 1 in. at a frequency of 1 cycle/s. What are the maximum velocity and the maximum acceleration?

ANSWER: Follow the vertical line at frequency 1 to the intersection with the diagonal line for 1 in. amplitude. Reading horizontally to the left-hand scale gives approximately 6.2 in./s maximum velocity. Reading diagonally on the maximum acceleration scale gives approximately 0.1 g.

FIGURE 3 Relations in simple harmonic motion.



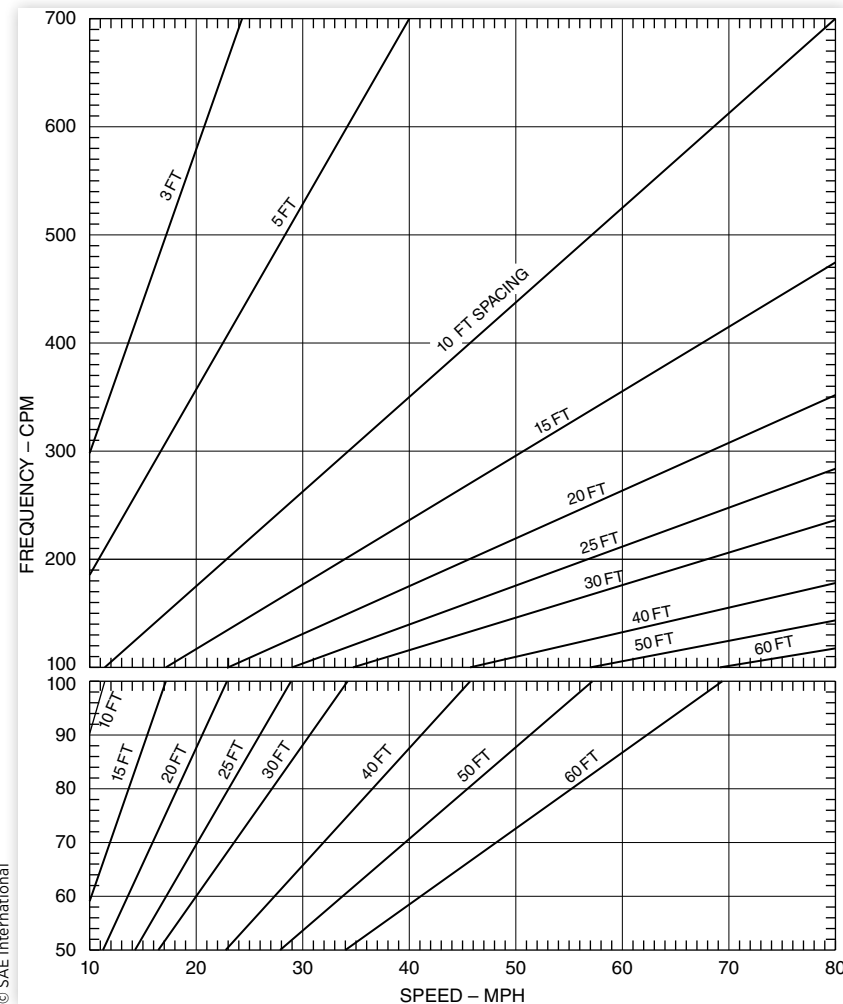
1.4 Resonant Speed on Uniformly Spaced Road Disturbances*

Periodic force impulses, such as those produced by uniformly spaced road joints or washboard surfaces, can excite resonant vibration in a vehicle system if any natural frequency of the system is equal to, or an even multiple of, the impulse frequency. In the latter case, however, the induced vibration is usually of minor intensity because of the greater time available for damping between impulses.

It should be noted that the occurrence of this type of resonance is not related to the time duration of the individual impulse, but is determined by the uniform time period between impulses. Thus, impulse frequency, cpm = mph × 88/spacing (ft).

For convenient reference, Figure 4 has been prepared to relate spacing distance between disturbances and vehicle speed to impulse frequency. The lines are plotted with frequency as ordinate, from 50 to 700 cpm, and speed as abscissa, from 10 to 80 mph.

FIGURE 4 Resonant speed on uniformly spaced road disturbances.



* See Ref. [5, p. 2-36].

Each line represents a periodic spacing, varying in steps from 3 to 60 ft. The ordinate scale is expanded below 100 cpm to enable more accurate reading of the chart in the passenger-car range of sprung mass frequency.

The following examples of the use of this chart have been selected to bring out some of the situations in which disturbing resonances are commonly experienced (all values are based on resonance with the fundamental of the road disturbance):

- a. A truck has a natural pitching frequency of 300 cpm of the entire mass on the tires alone, due to friction in the suspension. At what speed will resonance be excited by road joints uniformly spaced at 15 ft?
At intersection of the 15 ft line with the 300 cpm horizontal line, read 50 mph.
- b. A passenger car has a front-end unsprung mass natural frequency of 11.7 cps or 700 cpm. At what speed will unsprung mass resonance occur on a road with 10 ft joint spacing?
At intersection of the 10 ft line with the horizontal line through 700 cpm, read 79.8 mph.
- c. The natural frequency in vertical bounce of a driver on the seat cushion of a truck is 240 cpm. At what speed is he likely to experience resonant bouncing on the cushion on a road with 20 ft joint spacing?
At intersection of the 240 cpm horizontal with the 20 ft line, read 55 mph.

It will be noted that none of these cases of resonance could occur in the operating speed range with uniform joint spacing of 25 ft or more. Unevenly spaced joints would largely eliminate the possibility of resonance.

2. Vibration Systems

This section presents the basic quantitative relationships in generalized vibration systems with a single degree of freedom. Both free and forced steady-state vibrations are described, including damping effects. Undamped conditions are automatically covered by the same equations, corresponding to zero value of the damping constant.

With the exception of the coulomb damping condition, only linear systems with viscous damping are considered. Such systems must meet the following conditions (refer to SAE J670 JAN2008, Vehicle Dynamics Terminology which appears in Appendix A.):

- a. The mass or masses have only one mode of vibratory motion, along a prescribed path. This is seldom strictly true, but the relations shown are sufficiently accurate if the constraining supports or guides are much stiffer than the elastic restraint along the path of motion.
- b. The elastic or spring restoring forces produced by displacement of the mass must be proportional to the displacement. Even though the spring rate may not be constant over the entire range of load, sufficient accuracy can usually be obtained by taking the average rate over the actual range of displacement.
- c. Since viscous damping is assumed, the damping force, by definition, is proportional to the relative velocity between the points of attachment of the damper.

In each case of forced vibration, a sinusoidal driving force is assumed. All the forces acting upon the system, then, can be represented graphically by rotating vectors. This type of diagram is used throughout to derive the basic relationships. The important advantages of this procedure are:

- a. Differential equations are entirely eliminated.
- b. The reader can readily visualize the mechanics of the vibration.

2.1 List of Symbols

2.1.1 Vibrating System Parameters

m	= Mass, lb-s ² /in.
k	= Spring constant, lb/in.
F	= Coulomb friction, lb
c	= Viscous damping constant, lb-s ² /in.
c_c	= Critical damping constant, lb-sec ² /in. = $2\sqrt{km}$
b	= Damping ratio = c/c_c

2.1.2 VIBRATORY MOTION

t	= Time, s
f	= Forcing frequency, cycles/s
f_n	= Undamped natural frequency, cps
f_d	= Damped natural frequency, cps
ω	= Vector angular velocity at forcing frequency = $2\pi f$, radians/s
ω_n	= Vector angular velocity at undamped natural frequency = $2\pi f_n$, radians/s
ω_d	= Vector angular velocity at damped natural frequency = $2\pi f_d$, radians/s
a_0	= Amplitude of sinusoidal excitation of spring support, in.
X_0	= Initial mass amplitude in free vibration, in.
X'_0	= Mass amplitude after one-half cycle in free vibration, in.
X_1, X_2, \dots, X_n	= Mass amplitude after successive cycles in free vibration, in.
ΔX	= Mass amplitude decrement per cycle in coulomb damping, in.
x_0	= Mass amplitude in steady-state forced vibration, in.
x_{st}	= Static deflection of mass corresponding to peak force steadily applied, in.
x'_{st}	= Static deflection of mass corresponding to peak force at undamped natural frequency, in.
y_0	= Amplitude of relative motion between mass and vibrating spring support, in.
P_m	= Peak value of sinusoidal exciting force, lb
P_0	= Peak value of sinusoidal exciting force, at undamped natural frequency, lb
P	= Instantaneous variable sinusoidal force, lb
P_t	= Peak value of force transmitted to the spring support, lb
ϕ	= Phase angle

2.2 Free Vibration with Coulomb Damping*

Coulomb damping is produced when a constant friction force, F , opposes the vibratory motion. Referring to the force-displacement diagram (Figure 5B), the decrement in amplitude can readily be derived from the energy relationships:

$$[\text{The work done in accelerating the mass}]_1 = k(X_0)^2 / 2 - FX_0$$

$$[\text{The work done in decelerating the mass}]_5 = k(X'_0)^2 / 2 - FX'_0$$

Since the vibrating mass starts from rest and again comes to rest after each half cycle,

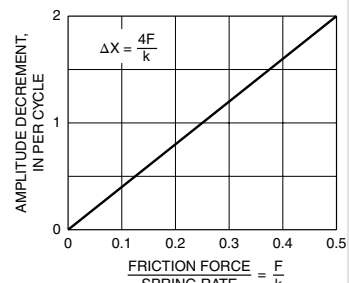
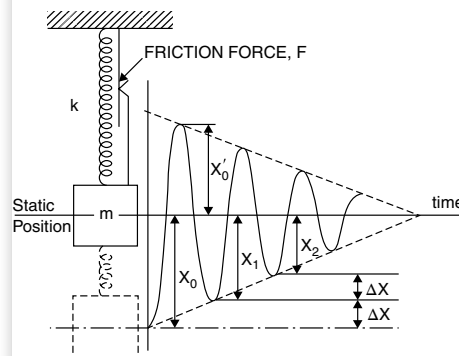
$$k(X_0)^2 / 2 - FX_0 = kX'^2 / 2 + FX'_0$$

$$(k/2)[X_0^2 - X'^2] = F(X_0 + X'_0)$$

$$X_0 - X'_0 = 2F/k \text{ per 1/2 cycle}$$

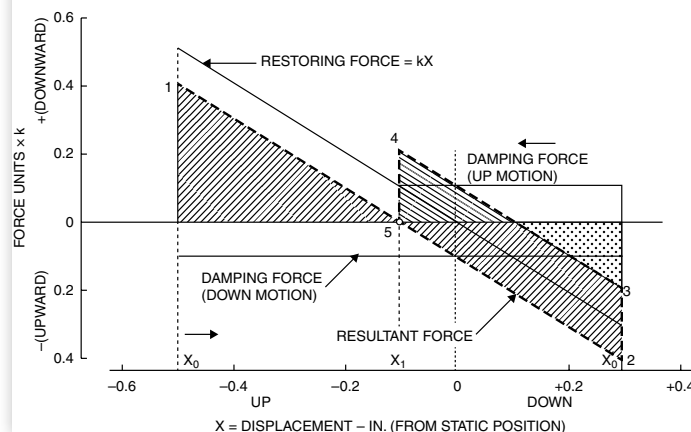
FIGURE 5 Free vibration with coulomb damping.

(A) Amplitude decrement



Conditions: initial deflection (upward) = 0.5 in.
Friction, lb = 0.10 × spring rate (k)

(B) Force – displacement diagram



* See Ref. [4].

Thus, in free vibration, coulomb damping produces a constant decrement of amplitude per cycle, $\Delta X = 4F/k$, which depends only on the ratio of friction force to spring rate. Amplitude decrement in inches as a function of the ratio of damping friction force to spring rate is shown in [Figure 5A](#).

Referring again to the force-displacement diagram ([Figure 5B](#)), the damping force is assumed to be 1/10 the spring force at unit deflection or 1/10 the spring rate, k . The friction force opposes the spring force to produce the resultant force line 1-5-2 which, of course, determines the motion of the vibrating mass. Since the vibrating mass starts from rest, and comes to rest again after each half cycle, the positive work of acceleration must be equal to the negative work of deceleration represented by the shaded areas above and below the baseline. The same condition must be met on the return motion so that at the end of one cycle, the displacement is 1/10 in. (point 4) with a reduction in amplitude of 4/10 in. equal to four times the ratio of friction to spring rate in accordance with the above equation. The mass has, in one cycle, come to rest at a displacement of 1/10 in. because the spring restoring force and the friction force are equal at this position, and velocity is zero.

The force-displacement diagram also shows that the mass will come to rest at zero elongation of the spring, only if the initial displacement is an even multiple of $4F/k$. The natural frequency of a free vibration determined by the equation in [Figure 3](#) is unchanged by friction damping.

2.3 Free Vibration with Viscous Damping*

Viscous damping is produced when the force opposing the motion is proportional to the velocity of the vibrating mass relative to the spring support. This type of damping in free vibration forms an amplitude decrement in which the amplitude between any two consecutive cycles is reduced by a constant ratio, according to the equation

$$\frac{X_1}{X_0} = \frac{X_2}{X_1} = \frac{X_{(n+1)}}{X_n} = e^{-2\pi b/\sqrt{1-b^2}}$$

where:

$b = c/c_c$ = Damping factor which is the ratio of damping constant to the critical damping value, $c_c = 2\sqrt{km}$

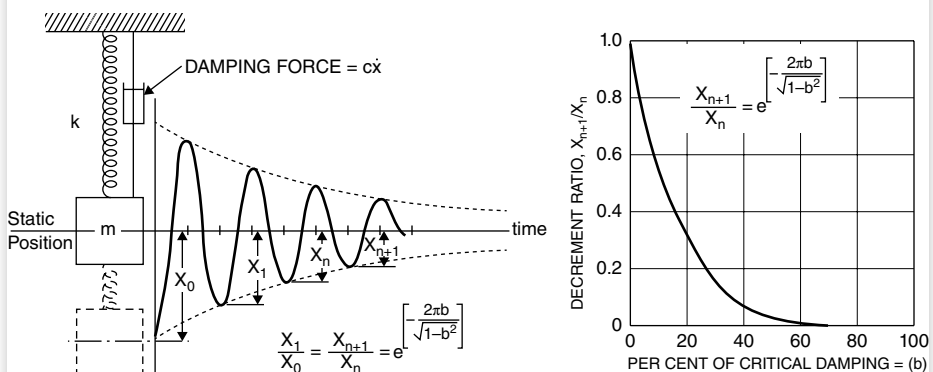
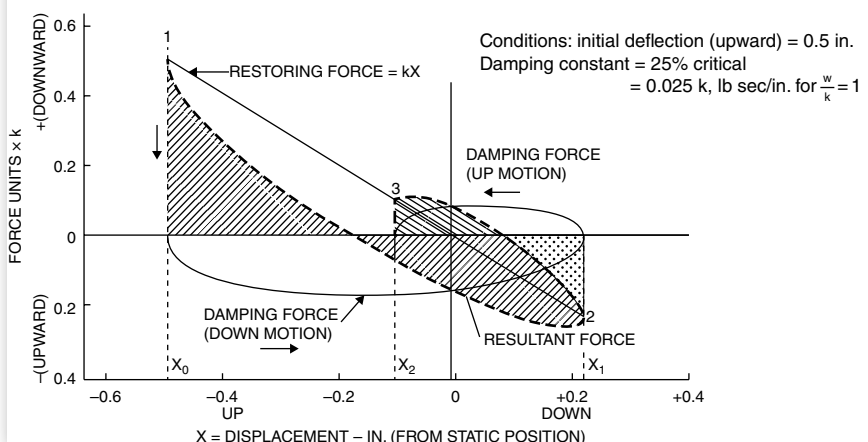
$\frac{X_{(n+1)}}{X_n}$ = Amplitude ratio between any two consecutive cycles

A typical displacement trace is illustrated in the graph in [Figure 6A](#). The amplitude decrement ratio as a function of percent of critical damping is shown plotted in the curve 6A.

[Figure 6B](#) shows a force-displacement diagram for free vibration with viscous damping at 25% of critical damping. The damping force, in this case, is variable in contrast to a constant force for friction damping. The resultant force curve meets the condition that the work of acceleration equals the work of deceleration represented by the shaded areas in the diagram. Damping force is a maximum at maximum velocity of the vibrating mass and is zero at points of maximum displacement where velocity is zero. Therefore, the maximum resultant deceleration force acting on the mass is out of phase with the maximum displacement.

After one complete cycle, the mass has momentarily come to rest at point 3, but oscillation will continue with a constant ratio in reduction of amplitude until displacement is small enough for extraneous friction to stop the motion.

* See Ref. [4].

FIGURE 6 Free vibration with viscous damping.**(A) Amplitude decrement****(B) Force – displacement diagram**

© SAE International

Viscous damping reduces the natural frequency (f_d) below that of undamped free vibration (f_n) according to the equation

$$f_d = \frac{1}{2\pi} \sqrt{\frac{k(1-b^2)}{m}} \quad \text{or} \quad \frac{f_d}{f_n} = \sqrt{1-b^2}$$

The effect on frequency is slight in the ordinary damping range. For example, if $b = 0.25$ (25% of critical damping), the frequency is reduced only by 3%. However, when $b = 1$ (critical damping), the frequency becomes zero, indicating the absence of vibratory motion. Instead, the mass, when displaced, will gradually creep back to its neutral position without a change in direction of the spring force.

2.4 Forced Vibration with Viscous Damping*

2.4.1 Force Applied to Suspended Mass

2.4.1.1 Peak Exciting Force Constant. This case is represented by the system diagram ([Figure 7A](#)) in which the suspended mass, m , is driven directly by a sinusoidal force, and is also acted upon by a viscous damper interposed between the mass and the spring support.

If the frequency of the driving force is f , and its maximum value is P_m , the generalized force can be written as $P = P_m \sin(\omega t + \phi)$, where $\omega = 2\pi f$ and ϕ = phase angle by which maximum force leads the maximum displacement. The variable driving force can be graphically generated by a rotating vector of magnitude P_m , having a constant angular velocity = $2\pi f$, as in [Figure 7B](#). Then, the vector component along the coordinate of vibratory motion at any instant equals the relative driving force. For steady-state vibration, the spring restoring force, inertia force, and damping force can also be represented by similar vectors having the proper relative magnitudes and phase relations. Note that the damping force, being proportional to, and in phase with, the mass velocity, is represented by a vector that lags the displacement by 90 degrees.

For simplicity in deriving the equations, the vector diagram is drawn for the instant when the mass displacement is at its maximum positive value ($\omega t = \pi/2$). Then for force equilibrium, the sum of vertical vector components and sum of horizontal vector components must each equal zero. Therefore,

Sum of vertical components

$$= kx_0 - m\omega^2 x_0 - P_m \cos\phi = 0 \quad (1)$$

Sum of horizontal components

$$= c\omega x_0 - P_m \sin\phi = 0 \quad (2)$$

In vertical force equation and [Figure 7B](#), note that inertia force is always in phase with displacement, while spring restoring force is opposed to displacement.

Combining [Equations \(1\)](#) and [\(2\)](#),

$$x_0 = \frac{P_m / k}{\sqrt{\left(1 - \frac{\omega^2}{\omega_n^2}\right)^2 + \left(2 \frac{c}{c_c} \frac{\omega}{\omega_n}\right)^2}} \quad (3)$$

Since P_m/k is the deflection X_{st} , corresponding to the maximum force if steadily applied, the magnification factor is

$$\frac{x_0}{X_{st}} = \frac{1}{\sqrt{\left(1 - \frac{\omega^2}{\omega_n^2}\right)^2 + \left(2 \frac{c}{c_c} \frac{\omega}{\omega_n}\right)^2}} \quad (4)$$

We may consider the undamped condition a special case in which $c = 0$.

*See Ref. [1, p. 48].

Then

$$\frac{x_0}{x_{st}} = \frac{1}{1 - (\omega / \omega_n)^2} \quad (5)$$

Equation (4) is the generalized magnification factor and is independent of the magnitude of the applied force. Values of this factor are plotted in Figure 7C against frequency ratio, for various constant damping intensities, expressed as the ratio, b, to the critical value.

2.4.1.2 Exciting Force Increasing as Square of Frequency. Note that the magnification factor curves also define the amplitude ratio for the specific case where the maximum force remains constant as the frequency varies. However, another important type of forced vibration encountered in practice is that in which the maximum exciting

FIGURE 7 Forced vibration with viscous damping (driving force applied to suspended mass).

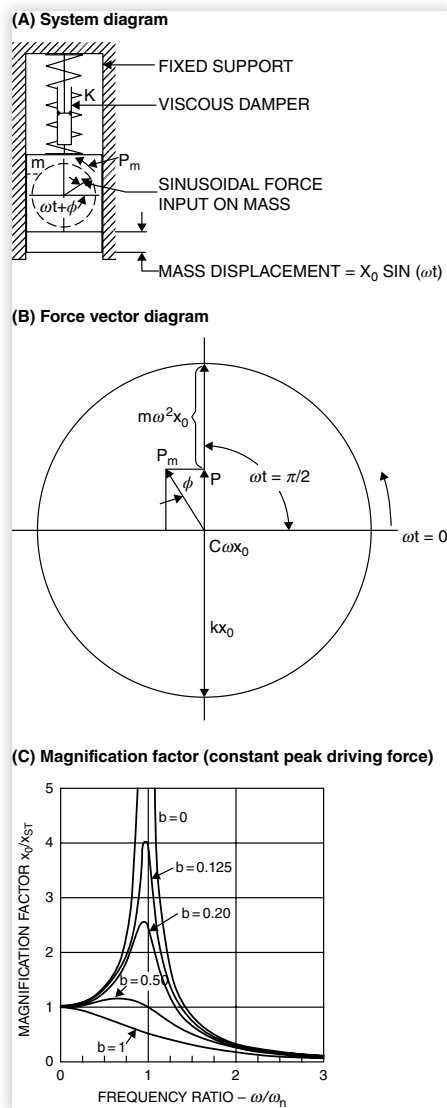
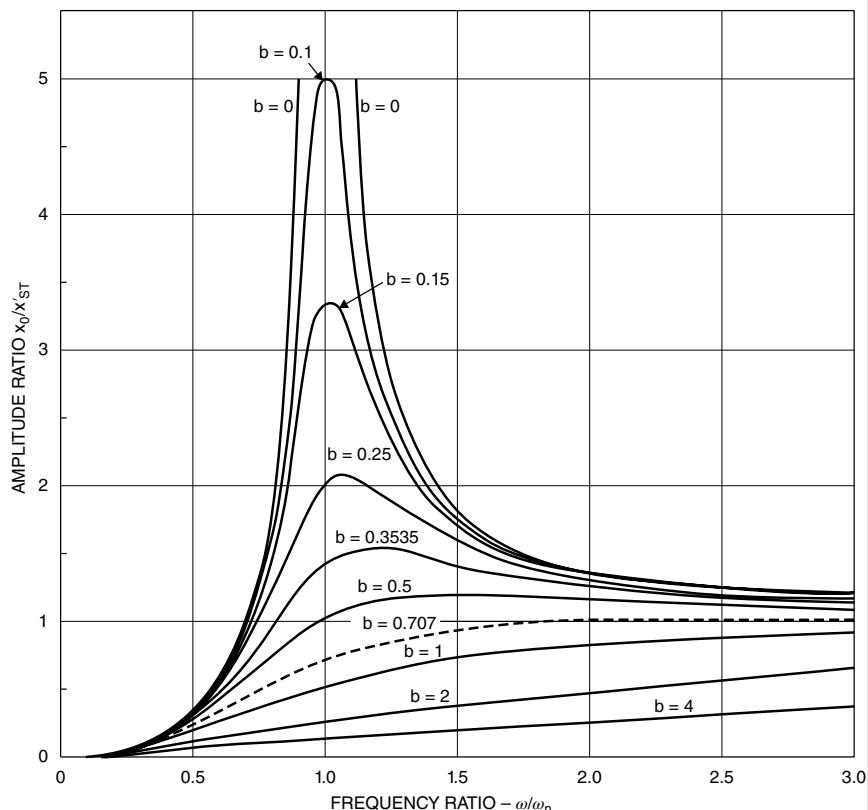


FIGURE 7 (Continued) Forced vibration with viscous damping (driving force applied to suspended mass).

(D) Amplitude ratio when peak driving force is proportional to $(\omega/\omega_n)^2$



(E) Phase angle, ϕ

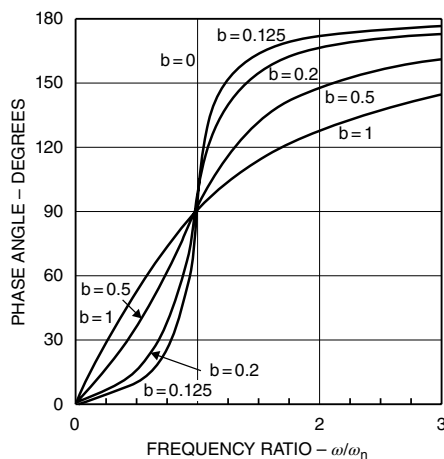


TABLE 1

Force condition	Amplitude ratio at $\omega/\omega_n = 1$	Amplitude ratio, max	ω/ω_h at max amplitude	Range of damping ratio
$P_m = \text{const.}$	1/2b	$\begin{cases} \frac{1}{2b\sqrt{1-b^2}} & \sqrt{1-2b^2} \\ 1 & 0 \end{cases}$	$b < .707$	$b < .707$
$P_m = P_0 \left(\frac{\omega}{\omega_n} \right)^2$	1/2b	$\begin{cases} \frac{1}{2b\sqrt{1-b^2}} & \frac{1}{\sqrt{1-2b^2}} \\ 1 & \infty \end{cases}$	$b < .707$	$b > .707$

Note that the phase angle is independent of the magnitude of the driving force, so that the curves of [Figure 7E](#) apply equally to both cases considered. At $\omega/\omega_n = 1$, ϕ becomes 90 degrees regardless of the degree of damping.

For values of ω/ω_n greater than 1, $\tan \phi$ becomes negative, corresponding to phase angles between 90 and 180 degrees.

force increases as the square of frequency. The most common situation of this kind occurs in machines having unbalanced rotating and/or reciprocating masses.

In this case, the maximum force may be written as $P_m = P_0(\omega/\omega_n)^2$, where P_0 = maximum force at resonance ($\omega/\omega_n = 1$). Substituting for P_m in [Equation \(3\)](#), we get for amplitude ratio

$$\frac{x_0}{x'_{st}} = \frac{(\omega/\omega_n)^2}{\sqrt{\left(1 - \frac{\omega^2}{\omega_n^2}\right)^2 + \left(2b\frac{\omega}{\omega_n}\right)^2}}$$

where:

$$x'_{st} = P_0 / k$$

[Figure 7D](#) shows how the amplitude ratio varies with frequency for different damping intensities, in this case. It will be seen that, regardless of damping, the amplitude ratio is zero at zero frequency and approaches unity at infinite frequency.

Since ω_n is the undamped natural frequency by definition, resonance occurs at $\omega/\omega_n = 1$ only for very low damping values. It will be observed in [Figure 7C](#) and [7D](#) that the resonant frequency (corresponding to peak amplitude) departs progressively further from the undamped resonant frequency as damping intensity increases. [Table 1](#) summarizes the equations which define the amplitude ratio at nominal resonance ($\omega/\omega_n = 1$), the maximum amplitude, and the frequency of maximum amplitude as functions of damping ratio, for the two cases considered previously.

Referring again to [Equations \(1\)](#) and [\(2\)](#), the phase angle, ϕ , is readily derived by evaluating $\sin \phi$ and $\cos \phi$ and dividing $(\sin \phi)$ by $(\cos \phi)$. (x_0) drops out and we get

$$\tan \phi = \frac{2b\omega/\omega_n}{1 - (\omega^2/\omega_n^2)}$$

2.4.1.3 Equivalent Impedance. The impedance concept, as applied to mechanical vibrating systems, expresses the ratio of applied force to the induced motion at the point of force application. Thus, displacement impedance is the force required per unit of peak displacement; velocity impedance is the force required per unit of peak velocity.

The term “mobility” is used to designate the reciprocal of impedance. Thus, displacement mobility is the peak displacement per unit of driving force.

These quantities are obviously variable with frequency ratio, but are independent of the magnitude of the driving force.

For the case of vibration excited by a force applied directly to a suspended mass, the impedance and mobility functions become

$$\text{Displacement Impedance, } Z_d = P_m/x_0$$

$$\text{Velocity Impedance, } Z_v = P_m/x_0\omega$$

Substituting the value of x_0 as a function of frequency ratio ([Equation 3](#)),

$$x_0 = \frac{P_m}{k \sqrt{\left[1 - \left(\frac{\omega}{\omega_n}\right)^2\right]^2 + \left(2b\frac{\omega}{\omega_n}\right)^2}}$$

$$Z_d = k \sqrt{\left[1 - \left(\frac{\omega}{\omega_n}\right)^2\right]^2 + \left(2b\frac{\omega}{\omega_n}\right)^2}$$

$$Z_v = \frac{k}{\omega} \sqrt{\left[1 - \left(\frac{\omega}{\omega_n}\right)^2\right]^2 + \left(2b\frac{\omega}{\omega_n}\right)^2}$$

Likewise, Displacement Mobility

$$M_d = \frac{x_0}{P_m} = \frac{1}{k \sqrt{\left[1 - \left(\frac{\omega}{\omega_n}\right)^2\right]^2 + \left(2b\frac{\omega}{\omega_n}\right)^2}}$$

Velocity Mobility

$$M_v = \frac{\omega x_0}{P_m} = \frac{\omega}{k \sqrt{\left[1 - \left(\frac{\omega}{\omega_n}\right)^2\right]^2 + \left(2b\frac{\omega}{\omega_n}\right)^2}}$$

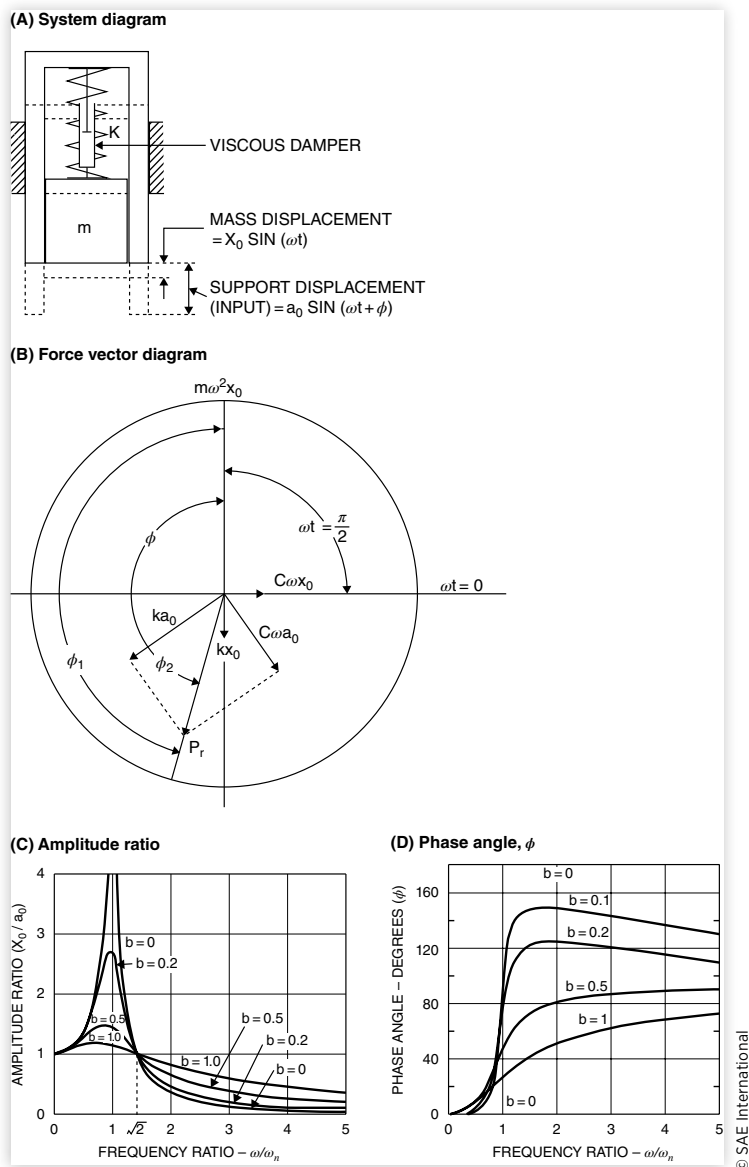
Note that the displacement mobility varies with frequency in exactly the same way as the peak displacement for a constant harmonic force intensity.

2.4.2 EXCITATION APPLIED TO SPRING SUPPORT

2.4.2.1 Absolute Amplitude Ratio. When the system shown in [Figure 8A](#) is excited by sinusoidal vibration of the spring support at a constant amplitude, a_o , instead of by a force applied directly to the suspended mass, the absolute amplitude of the mass is obtained by deriving the equivalent force acting on the mass. It is important to note, in this case, that the spring force component due to the support motion acts on the mass in the same direction as the support displacement, as opposed to the spring force due to mass displacement.

Referring to the vector diagram [Figure 8B](#) (for the condition $\omega/\omega_n = 2$, $b = 0.2$), it will be seen that the rotating force vector P_m , of [Figure 7B](#) has been replaced by two

FIGURE 8 Forced vibration of spring support at constant amplitude (absolute amplitude ratio).



© SAE International

rotating force vectors at 90 degrees to each other, ka_0 and $c\omega a_0$, corresponding respectively to the spring force and to the damping force components of the exciting amplitude. The resultant of these forces is

$$P_r = \sqrt{(ka_0)^2 + (c\omega a_0)^2} = a_0 k \sqrt{1 + \left(2b \frac{\omega}{\omega_n}\right)^2}$$

and the absolute amplitude of the mass, x_0 , is determined by the same magnification factor as in [Equation \(4\)](#), Paragraph 2.4.1.1.

$$x_0 = P_r / k \quad (\text{M.F.})$$

Substituting in this expression the equation for P_r , the magnification factor yields

$$\frac{x_0}{a_0} = \sqrt{\frac{1 + \left(2b\frac{\omega}{\omega_n}\right)^2}{\left(1 - \frac{\omega^2}{\omega_n^2}\right)^2 + \left(2b\frac{\omega}{\omega_n}\right)^2}}$$

Referring to Figure 8C, the values of this amplitude ratio are plotted for various damping intensities over a range of frequency ratios. It is significant to note that damping is beneficial in reducing amplitude only for frequency ratios lower than $\sqrt{2}$. At higher ratios the amplitude increases progressively with the damping intensity. However, with zero damping the amplitude ratio reduces to the same equation as that for constant force excitation applied directly to the mass (Equation 4). Thus, the curves for $b = 0$ are identical in Figures 7C and 8C.

The general expression for the phase angle between the mass and support motions is derived as follows (refer to Figure 8B):

ϕ_1 = Phase angle between P_r and x_0

ϕ_2 = Phase angle between P_r and a_0

φ = Phase angle between a_0 and x_0 = $\phi_1 - \phi_2$

$$\tan\phi_1 = \frac{2b\left(\frac{\omega}{\omega_n}\right)}{1 - \left(\frac{\omega}{\omega_n}\right)^2} \quad (\text{See Paragraph 2.4.1.2.})$$

$$\tan\phi_2 = \frac{ca_0\omega}{a_0k} = \frac{c\omega}{k} = 2b\left(\frac{\omega}{\omega_n}\right) \quad (\text{See Figure 8B.})$$

$$\tan\phi = \tan(\phi_1 - \phi_2) = \frac{\tan\phi_1 - \tan\phi_2}{1 + \tan\phi_1 \tan\phi_2}$$

Substituting,

$$\tan\phi = \frac{2b\left(\frac{\omega}{\omega_n}\right)^3}{1 - \left(\frac{\omega}{\omega_n}\right)^2 + \left(2b\frac{\omega}{\omega_n}\right)^2}$$

This equation is shown plotted in Figure 8D for various frequency ratios and for different damping intensities.

The frequency ratio at which maximum amplitude occurs is given by the expression

$$\left(\frac{\omega}{\omega_n}\right)_m = \frac{1}{2b} \sqrt{\sqrt{1 + 8b^2} - 1}$$

For finite values of b , $(\omega/\omega_n)_m$ is less than 1, but approaches unity as b approaches zero.

The maximum amplitude ratio for a given damping intensity, b , may be determined directly from the relation

$$\left(\frac{x_0}{a_0}\right)_m = \sqrt{\frac{\sqrt{1+8b^2}}{\left\{1 - \frac{1}{4b^2} [\sqrt{1+8b^2} - 1]\right\}^2 + \sqrt{1+8b^2} - 1}}$$

For small values of b (less than 0.15), this equation can be reduced to the approximate form

$$\left(\frac{x_0}{a_0}\right)_m = \sqrt{\frac{\sqrt{1+8b^2}}{\sqrt{1+8b^2} - 1}}$$

2.4.2.2 Relative Amplitude Ratio. Figure 9 illustrates the method of deriving the equations for the relative motion between vibrating mass and support in the same system as in Figure 8, where the excitation is applied to the support. Knowledge of the relative motion is needed in such important practical problems as designing vibration instruments and providing for clearance between components of a vibrating system.

Referring to the vector diagram in Figure 8B, it can be seen that the separate spring and damping force vectors associated with the respective motions of mass and support can be combined into resultants as shown in Figure 9B, in terms of the relative motion, y , between the mass and support. The resultant spring and damping forces are necessarily in 90 deg. phase relationship, while the inertia force on the mass remains in phase with the absolute mass displacement. In Figure 9C, the complete force vector diagram is seen to reduce to the simple form in which the only forces acting on the mass are the inertia force due to its absolute motion, the spring restoring force due to the relative displacement between mass and support, and the damping force due to the relative velocity between the mass and support. It is clear that for equilibrium the resultant between the spring and damping forces must be equal and opposite to the inertia force. The equations are readily derived as follows:

Denoting the phase angle between the relative motion and absolute motion as ϕ_3 and summing up the vertical and horizontal forces when the relative displacement is a maximum (y_0) (when $\omega t = \pi/2$):

Sum of the vertical forces

$$-m\omega^2 x_0 \cos\phi_3 + ky_0 = 0$$

therefore

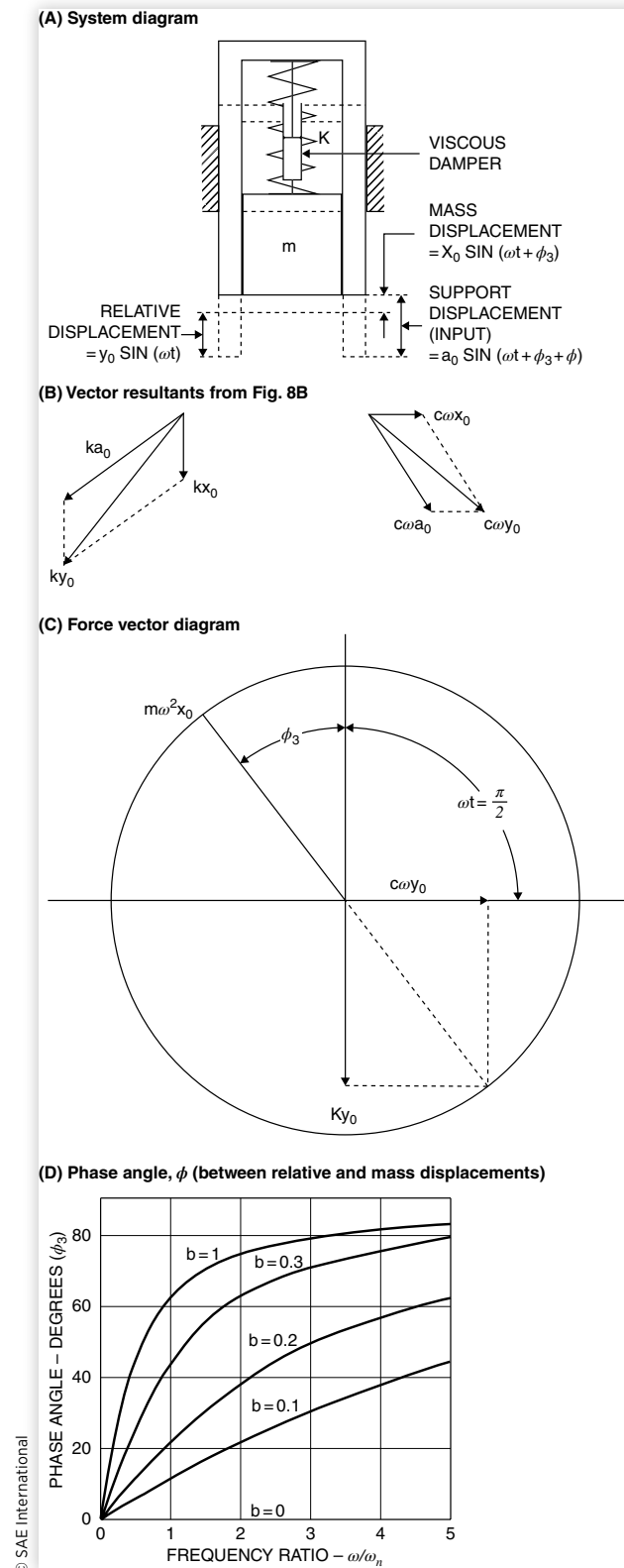
$$\cos\phi_3 = \frac{ky_0}{m\omega^2 x_0}$$

Sum of the horizontal forces

$$-m\omega^2 x_0 \sin\phi_3 + c\omega y_0 = 0$$

therefore

$$\sin\phi_3 = \left[\frac{c\omega y_0}{m\omega^2 x_0} \right]$$

FIGURE 9 | Forced vibration of spring support at constant amplitude (relative motion between mass and support).

Since $\sin^2 \phi_3 + \cos^2 \phi_3 = 1$:

$$\left[\frac{c\omega y_0}{m\omega^2 x_0} \right]^2 + \left[\frac{ky_0}{m\omega^2 x_0} \right]^2 = 1$$

$$y_0^2 = \frac{(x_0 m \omega^2)^2}{k^2 \left[1 + (c\omega/k)^2 \right]}$$

$$y_0 = \frac{x_0 \omega^2 / \omega_n^2}{\sqrt{1 + (c\omega/k)^2}}$$

From Paragraph 2.4.2.1, the absolute amplitude ratio is

$$\frac{x_0}{a_0} = \sqrt{\frac{1 + \left(2b \frac{\omega}{\omega_n} \right)^2}{\left(1 - \frac{\omega^2}{\omega_n^2} \right)^2 + \left(2b \frac{\omega}{\omega_n} \right)^2}}$$

so

$$\frac{y_0}{a_0} = \frac{\omega^2 / \omega_n^2}{\sqrt{\left(1 - \omega^2 / \omega_n^2 \right)^2 + \left(2b\omega / \omega_n \right)^2}}$$

Note that the expression for relative amplitude ratio is identical with that in Paragraph 2.4.1.2, when the mass is excited directly by a force varying as the square of the frequency ratio. Thus, the curves of [Figure 7D](#) apply to this case.

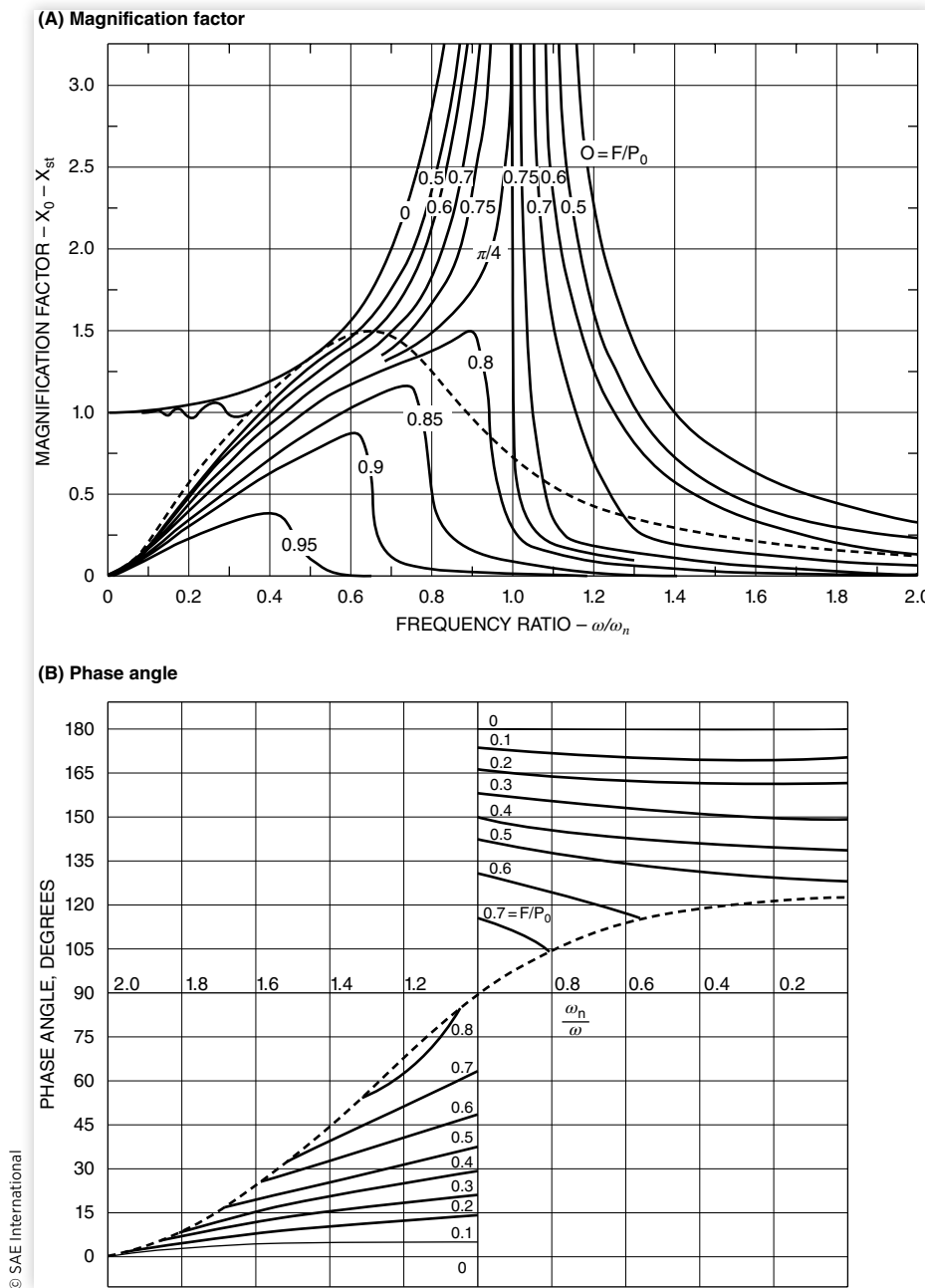
$$\tan \phi_3 = \sin \phi_3 / \cos \phi_3 = c\omega / k = 2b\omega / \omega_n$$

This phase angle relationship is shown in [Figure 9D](#) for various damping intensities and frequency ratios.

2.5 Forced Vibration with Coulomb Damping

As pointed out earlier in this section, a system with coulomb (constant friction) damping is nonlinear and the solution of the differential equations becomes complicated. Den Hartog (Ref. [1]) has arrived at an exact solution, which gives amplification factors and phase angles as shown in [Figure 10A and B](#), for specified ratios of friction to maximum driving force (F/P_0), over a range of frequency ratios (ω/ω_n).

Den Hartog points out that the dotted line in [Figure 10A](#) defines the limits below which the vibratory motion is not continuous, but involves a “stop” or dwell every half cycle. His analysis also emphasizes an important limitation of coulomb damping in that it will not restrict the amplitude of resonant vibration unless the friction force is greater than $\pi P_0/4$. This can be seen from the fact that the work done by a harmonic driving force at resonance is equal to $\pi P_0 x/4$, whereas the work done by the constant friction force, F, is equal to Fx . Consequently, if F is less than $\pi P_0/4$, the amplitude will increase on successive cycles to infinity. Coulomb damping is not applicable to a system which is subjected to steady-state vibration at resonance unless the maximum value of the driving force has a known limitation.

FIGURE 10 Forced vibration with coulomb damping.

An approximate solution for this case is also given in the cited reference, but its use is not recommended because of the very limited range of conditions for which it is valid.

An interesting approximate solution for the use of combined viscous and friction damping is given by Timoshenko (Ref. [3, p. 96]). This solution is applicable when the friction damping is small relative to the viscous component.

2.6 Force Transmission through Suspension

2.6.1 DIRECT EXCITATION OF MASS WITH VISCOUS DAMPING

2.6.1.1 Constant Peak Driving Force. From the standpoint of vibration isolation, when a directly excited mass is flexibly mounted, we are interested in the magnitude of the force transmission to the support. Thus, referring to the force vector diagram Figure 7B for the forced vibration system with constant maximum driving force and viscous damping, it will be seen that the spring force, kx_0 , and damping force, $c\omega x_0$, both react on the support. Since the two force components are 90 degrees out of phase, their vector resultant as shown in Figure 11A is

$$\begin{aligned} P_t &= \sqrt{(x_0 k)^2 + (c\omega x_0)^2} = x_0 k \sqrt{1 + (c\omega/k)^2} \\ &= x_0 k \sqrt{1 + (2b\omega/\omega_n)^2} \end{aligned}$$

Since (from Equation 3, Paragraph 2.4.1.1)

$$\begin{aligned} x_0 &= \frac{P_m / k}{\sqrt{\left(1 - \frac{\omega^2}{\omega_n^2}\right)^2 + \left(2b\frac{\omega}{\omega_n}\right)^2}} \\ P_t &= \frac{P_m \sqrt{1 + (2b\omega/\omega_n)^2}}{\sqrt{\left(1 - \frac{\omega^2}{\omega_n^2}\right)^2 + \left(2b\frac{\omega}{\omega_n}\right)^2}} \end{aligned}$$

This resultant is obviously the maximum force transmitted to the support when $\omega t = \tan^{-1} k/c\omega = \tan^{-1} 2b(\omega/\omega_n)$. This is the position shown in Figure 11.

Thus, the transmissibility, defined as the ratio of maximum transmitted force to driving force, is

$$\frac{P_t}{P_m} = \sqrt{\frac{1 + (2b\omega/\omega_n)^2}{\left(1 - \frac{\omega^2}{\omega_n^2}\right)^2 + \left(2b\frac{\omega}{\omega_n}\right)^2}}$$

This equation is shown plotted in Figure 11B and will be seen to be identical with that for absolute amplitude ratio, when a constant vibration amplitude is applied to the support (Figure 8C).

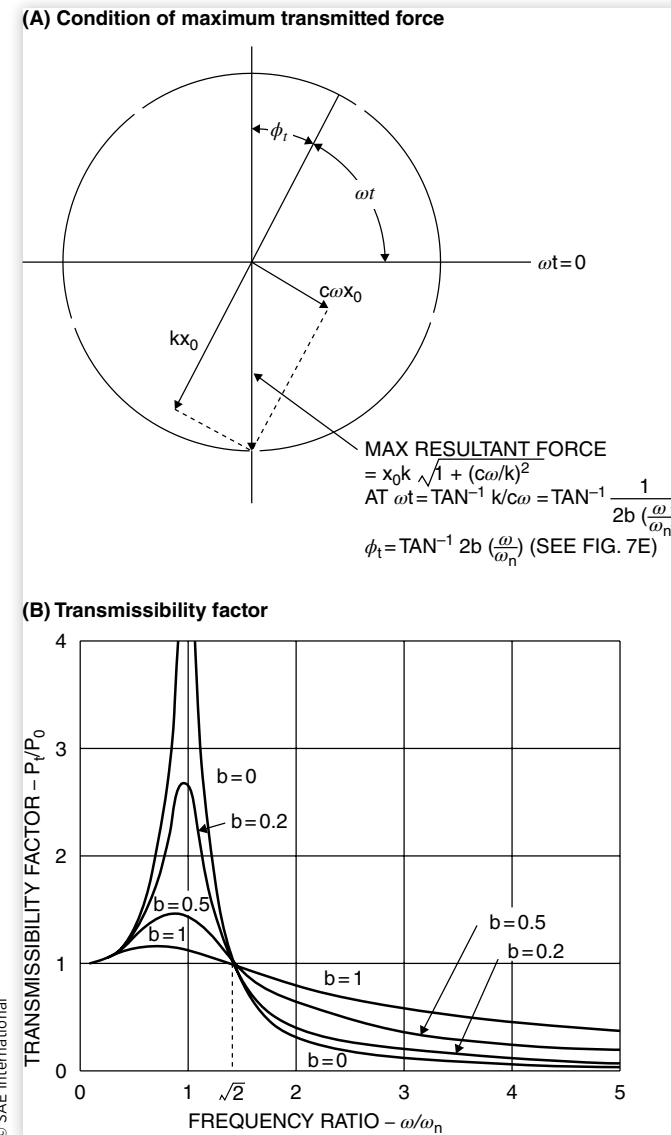
It will be noted that damping reduces the transmissibility for frequency ratios less than $\sqrt{2}$ but increases it for higher ratios. Thus, the undamped system has smaller transmissibility for frequency ratios larger than $\sqrt{2}$.

The force vector diagram, Figure 11A, shows that the transmitted force reaches its maximum value at $\omega t = \tan^{-1} 1/2b(\omega/\omega_n)$, and at 180 deg. intervals thereafter. Since the mass displacement is a maximum at $\omega t = \pi/2$ or $3\pi/2$, the phase angle, ϕ_t , by which the transmitted force leads the mass displacement is

$$\phi_t = \frac{\pi}{2} - \tan^{-1} \frac{1}{2b\left(\frac{\omega}{\omega_n}\right)} = \tan^{-1} 2b\left(\frac{\omega}{\omega_n}\right)$$

FIGURE 11 Force transmission through suspension.

CASE 1: Constant maximum driving force on mass, with viscous damping.



© SAE International

This is identical with the phase relationship previously derived between relative displacement and mass displacement under constant amplitude excitation of the support. Therefore, the curves of Figure 9D also define the value of ϕ_t as a function of frequency ratio and damping intensity.

2.6.1.2 Driving Force on Mass Proportional to Square of Speed with Viscous Damping*. Instead of a constant driving force, let the driving force on the mass increase with the square of the frequency ratio so that $P = P_0 (\omega/\omega_n)^2$, where P_0 is the maximum driving force at resonance ($\omega/\omega_n = 1$).

* See Ref. [2].

Although the transmissibility (ratio of transmitted force to applied force) remains the same as in Case 1 (Figure 11), the absolute value of transmitted force obviously varies in the same ratio as the applied force, or as $(\omega/\omega_n)^2$. The transmitted force thus becomes

$$P_t = P_0 \left(\frac{\omega}{\omega_n} \right)^2 \times \text{transmissibility}$$

$$\frac{P_t}{P_0} = \left(\frac{\omega}{\omega_n} \right)^2 \sqrt{\frac{1 + (2b\omega/\omega_n)^2}{\left(1 - \frac{\omega^2}{\omega_n^2} \right)^2 + \left(1b \frac{\omega}{\omega_n} \right)^2}}$$

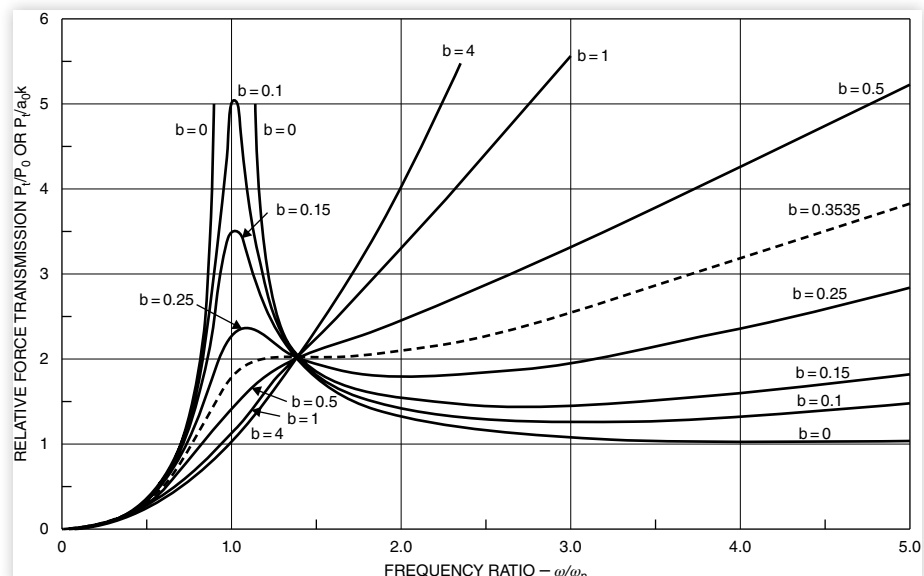
Figure 12 shows the ratio of force transmission, P_t/P_0 , plotted against frequency ratio, ω/ω_n , for various damping intensities. Comparison with Figure 7D shows that the amplitude gives no indication of the detrimental effect of even a small amount of viscous damping at frequency ratios greater than $\sqrt{2}$, when the applied force is a function of the square of frequency. It is evident that at high values of ω/ω_n , the force transmitted to the support is primarily through the damper.

In the case of vibration excited by oscillation of the spring support at constant amplitude, the transmitted force vector is likewise equal to the resultant of the relative spring and damping force vectors. In Figure 9C this resultant, P_t , is shown to be equal to the inertia force, $m\omega^2 x_0$. By substituting for x_0 , its value as derived in Paragraph 2.4.2.1, we get

$$P_t = m\omega^2 a_0 \sqrt{\frac{1 + (2b\omega/\omega_n)^2}{\left(1 - \frac{\omega^2}{\omega_n^2} \right)^2 + \left(2b \frac{\omega}{\omega_n} \right)^2}}$$

FIGURE 12 Transmission through suspension.

CASE 2: Driving force on mass proportional to square of speed (T.F. = P_t/P_0) or spring support excited at constant amplitude (T.F. = $P_t/a_0 k$)



The maximum force transmission, relative to $(a_0 k)$ as nominal input force, becomes

$$\frac{P_t}{a_0 k} = \frac{\omega^2}{\omega_n^2} \sqrt{\frac{1 + (2b\omega/\omega_n)^2}{\left(1 - \frac{\omega^2}{\omega_n^2}\right)^2 + \left(2b\frac{\omega}{\omega_n}\right)^2}}$$

It is evident that the force reaction formula so derived is identical with the formula given above for directly applied excitation to the suspended mass variable as the square of the frequency. Therefore, the curves of [Figure 12](#) apply equally when the spring support is excited at constant amplitude. The corresponding maximum acceleration of the sprung mass is

$$A_m = \frac{P_t}{m} = a_0 \omega^2 \sqrt{\frac{1 + (2b\omega/\omega_n)^2}{\left(1 - \frac{\omega^2}{\omega_n^2}\right)^2 + \left(2b\frac{\omega}{\omega_n}\right)^2}}$$

This relationship is fundamental to the ride problem, since it covers the condition of a vehicle traversing a series of periodic sine wave irregularities of constant amplitude at variable speed.

2.6.1.3 Equivalent Impedance. When excitation is applied to the spring support, the input force must be an equal reaction to the force transmitted to the mass. The impedance relationships, thus, become

$$Z_d = \frac{P_t}{a_0} = m\omega^2 \sqrt{\frac{1 + (2b\omega/\omega_n)^2}{\left(1 - \frac{\omega^2}{\omega_n^2}\right)^2 + \left(2b\frac{\omega}{\omega_n}\right)^2}} \quad (\text{Displacement})$$

$$Z_v = \frac{P_t}{a_0 \omega} = m\omega \sqrt{\frac{1 + (2b\omega/\omega_n)^2}{\left(1 - \frac{\omega^2}{\omega_n^2}\right)^2 + \left(2b\frac{\omega}{\omega_n}\right)^2}} \quad (\text{Velocity})$$

The corresponding mobility equations, as reciprocals, are

$$M_d = \frac{1}{m\omega^2} \sqrt{\frac{\left(1 - \frac{\omega^2}{\omega_n^2}\right)^2 + \left(2b\frac{\omega}{\omega_n}\right)^2}{1 + (2b\omega/\omega_n)^2}}$$

$$M_v = \frac{1}{m\omega} \sqrt{\frac{\left(1 - \frac{\omega^2}{\omega_n^2}\right)^2 + \left(2b\frac{\omega}{\omega_n}\right)^2}{1 + (2b\omega/\omega_n)^2}}$$

It is important to note that the above equations are entirely different from the corresponding expressions in Paragraph 2.4.1.3 for the case of driving force applied directly to the mass. This comparison brings out the wide variability of the impedance characteristic of a vibrating system, depending on where the driving force is applied.

2.6.2 COMPARISON OF VISCOUS AND COULOMB DAMPING*: To compare the effects of viscous and coulomb damping, assume the following alternative conditions (driving force on mass assumed proportional to square of frequency, $P_m = P_0(\omega/\omega_n)^2$ in both cases):

- The friction force of coulomb damping is equal to the driving force at resonance ($\omega/\omega_n = 1$), $F = P_0$.
- Viscous damping is 25% of critical damping.

These conditions are chosen to give about the same transmissibility in the resonant frequency range.

In Figure 13A, the undamped and viscous damping curves have been transposed from Figure 7D. The coulomb damping curve is obtained by interpolation from the curves of Chart 10A, as follows:

Up to $\omega/\omega_n = 1$, for $F/P_0 = 1$, amplitude = 0.

Taking $F = P_0$,

$$\text{For } \frac{\omega}{\omega_n} > 1, \quad P_m = P_0 \left(\frac{\omega}{\omega_n} \right)^2 \quad \text{and} \quad \frac{F}{P_m} = \frac{P_0}{P_0 \left(\frac{\omega}{\omega_n} \right)^2} = \left(\frac{\omega_n}{\omega} \right)^2$$

From Figure 10A, the value of x_0/x_{st} is obtained for a given value of ω/ω_n at intersection with curve corresponding to $F/P_0 = F/P_m = (\omega_n/\omega)^2$.

$$\text{Since } x'_{st} = P_0/k, \quad x_{st} = P_m/k = (\omega/\omega_n)^2 P_0/k = (\omega/\omega_n)^2 x'_{st}$$

$$\text{Then } x_0/x_{st} = (x_0/x_{st})(\omega/\omega_n)^2$$

At frequency ratios above 2.5, there is no difference in displacement amplitude for either viscous or coulomb damping or for no damping. This comparison gives no indication of the force transmission to the support through the suspension, especially for viscous damping.

As with viscous damping, the same curves apply to vibration excited by sinusoidal motion of the support at constant amplitude a_0 . In this case, however, the ordinate scale gives amplitude ratio in terms of (y_0/a_0) , where y_0 is the relative displacement amplitude between mass and support (see Paragraph 2.4.2.2).

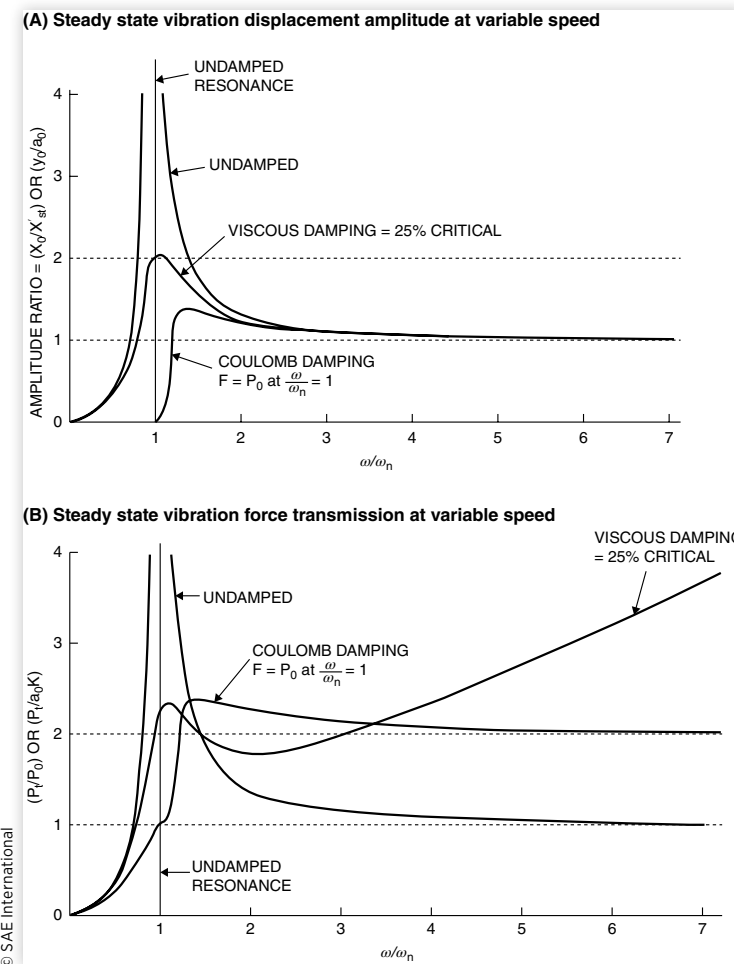
Figure 13B shows the comparative force transmission. For direct excitation of the mass, the ordinate scale defines the force transmitted to the support in terms of the ratio P_i/P_0 ; for excitation of the support, the ordinate scale gives the ratio $P_i/a_0 k$, as in Figure 12. It can be seen that the undamped suspension, although capable of infinite amplitude at resonance, gives the lowest force transmission at high frequency ratios.

With viscous damping at 25% of critical damping, the force transmission at high frequencies increases continuously above a frequency ratio of about 2.0.

With the specified coulomb damping, the maximum force transmission at resonance is nearly the same as for viscous damping but thereafter reduces continuously with increase in frequency ratio, approaching $2P_0$ as a limit. Thus at high frequency ratios, coulomb damping adds to the force transmission only by the amount of the damping friction force.

* Ref. [4]

FIGURE 13 Comparison of viscous and coulomb damping on displacement amplitude and force transmission.



In general, it can be said that the optimum damping characteristic for any given suspension is a compromise between a minimum penalty of force transmission and the required amplitude control.

2.6.3 VIBRATING SYSTEM WITH TWO DEGREES OF FREEDOM: The previous section is confined to consideration of systems having a single degree of freedom. A great many practical vibration problems, however, involve two degrees of freedom. In keeping with the definition in the introduction to Section 2, this means that the system either contains two masses, each capable of a single type of independent motion, or a single mass capable of two independent types of motion.

A primary example of the latter configuration, which is basic to ride problems, is a vehicle mass having two spaced spring supports. Considering only degrees of freedom in the longitudinal plane, the mass has two independent modes of motion, namely, vertical displacement of the center of gravity and angular displacement about the center of gravity.

In order to present in a useful form the effects of the principal parameters, the standard equations for frequencies and centers of oscillation (Ref. [3], p. 201) have been reduced to a few dimensionless terms.

Thus, if $r = \text{ratio of static spring deflection at the supports} = \delta_2/\delta_1$ where $\delta_2 \geq \delta_1$

$$d = i^2 / AB = \text{dynamic index}$$

where:

i = Radius of gyration about c.g.

A = Distance of the example from spring support at δ_1

B = Distance of the example from spring support at δ_2

$a = N(A+B)$

Then, if

f_1 is the bounce frequency (about center outside of spring supports), cycles per second

f_2 is the pitch frequency (about center between spring supports), cycles per second

m/B is the relative distance from the example to pitch center ((-) toward δ_2)

n/A is the relative distance from the example to bounce center ((+) toward δ_1)

NOTE: For values of $d > 1$ bounce and pitch frequencies and centers are reversed.

Then

$$f_1^2 = 4.9 / \delta_2 \left[C - \sqrt{D^2 + E} \right]$$

$$f_2^2 = 4.9 / \delta_2 \left[C + \sqrt{D^2 + E} \right]$$

where:

$$C = a \left(\frac{1}{d} - 1 \right) (r - 1) + \frac{1}{d} + r$$

$$D = a \left(\frac{1}{d} + 1 \right) (r - 1) + \frac{1}{d} - r$$

$$E = \frac{4}{d} a (1-a) (r-1)^2$$

Likewise,

$$\frac{m}{B} = \frac{2a(1-r)}{D + \sqrt{D^2 + E}} \quad \frac{n}{A} = \frac{2(1-r)(1-a)}{D - \sqrt{D^2 + E}}$$

Note that $(m/B \cdot n/A) = d = i^2/AB$, a useful relationship for checking purposes.

The curves of Figure 14 show in relative terms the characteristic changes in frequencies and centers of oscillation with variation in the ratio δ_2/δ_1 , for four values of dynamic index, namely, $d = 1.2, 1, 0.8$, and 0.6 . The chart values have been calculated for a center-of-gravity position equidistant from the spring centers ($a = 0.5$). Nevertheless, these curves are applicable to the usual passenger-car range of the example position ($a = 0.5$ to 0.6), with negligible error as to frequencies, and without exceeding $\pm 5\%$ error in centers of oscillation. However, for accurate determination in commercial vehicles, where the example usually falls outside this range, the values should be calculated from the general equations.

It will be seen in Figure 14 that only the pitch frequency is sensitive to the suspension deflection ratio and to the dynamic index. However, both frequencies increase as the dynamic index diminishes and are a minimum when the static spring deflections are equal. When $d = 1$, each of the two modes consists of an independent vibration at one spring about the other spring as a center of oscillation.

It is important to note that when $d = 1$, and the springs have the same static deflection ($\delta_2/\delta_1 = 1$), there are two other possible modes of vibration, since the two principal vibrations have the same frequency. One is a uniform bounce of the mass, when both springs act in the same phase, the other a pitch about the example when both springs act in opposite phase. The curves of pitch center show that this condition exists whenever $\delta_2/\delta_1 = 1$, regardless of the dynamic index. This situation is definitely undesirable because

FIGURE 14 Vibrating system with two degrees of freedom. Natural frequencies and centers of oscillation versus ratio of static deflections, δ_2/δ_1 , and dynamic index, d.

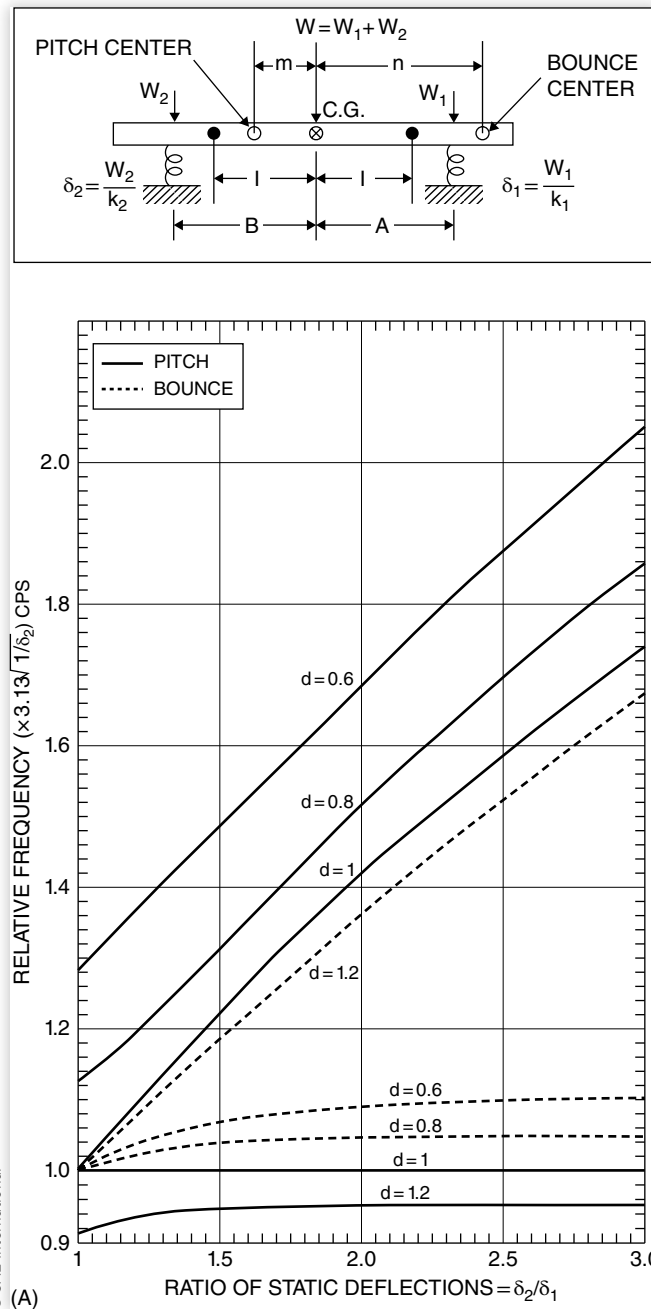
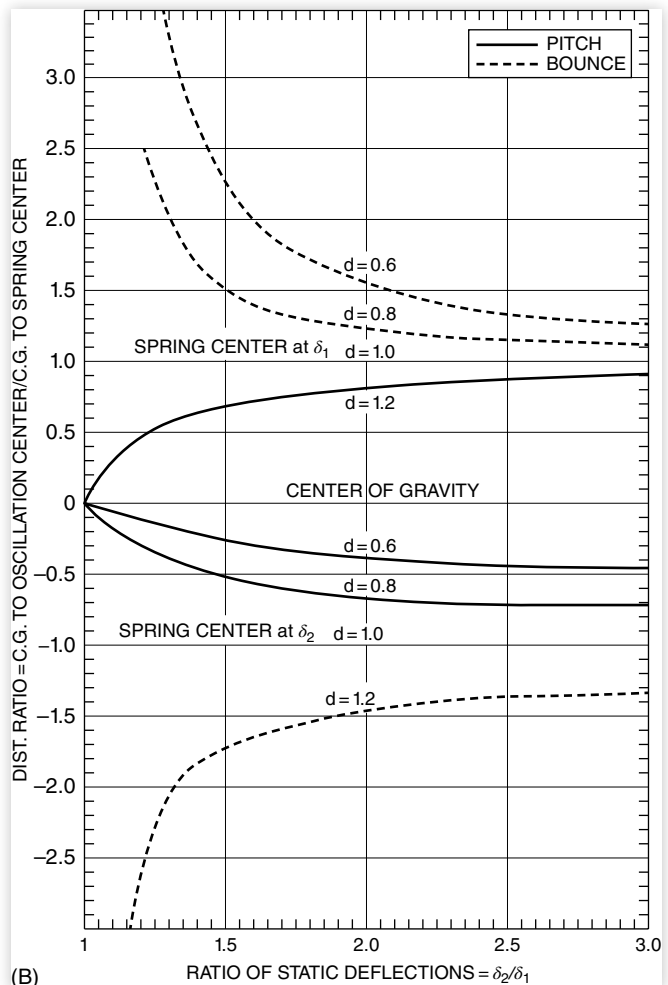


FIGURE 14 | (Continued) Vibrating system with two degrees of freedom. Natural frequencies and centers of oscillation versus ratio of static deflections, δ_2/δ_1 , and dynamic index, d.



© SAE International

it produces the maximum angular amplitude for a given vertical displacement at the springs. Consequently, this condition should be avoided in practice.

As long as there is a differential of static deflection between the two springs, a dynamic index of 1 gives the best vehicle ride because angular amplitudes are minimized and there is no interaction between springs.

2.7 References

1. J.P. Den Hartog, *Mechanical Vibrations*. McGraw-Hill, New York, N.Y., (4th ed.).
2. N.O. Myklestad, *Fundamentals of Vibration Analysis*, McGraw-Hill, New York, NY.
3. S. Timoshenko, *Vibration Problems in Engineering*, D. Van Nostrand Co., Princeton, NJ, (3rd ed.).
4. R. N. Janeway, "Problems in Shock and Vibration Control," *Industrial Mathematics*, 5 (1955).

3. Energy Absorption and Impact

Figures 15-17 are designed to facilitate the solution of problems involving the absorption of energy in bringing a moving mass to rest. Each chart provides an essential step in relating the resistance characteristic of the absorption gear to the displacement and resultant deceleration of the mass for any given initial velocity. These charts are particularly applicable to extreme operating conditions of vehicle suspensions and to normal operating conditions of airplane landing gears.

Absorption systems usually combine the elastic resistance of springs with friction or damping forces, so that the resultant variation in resistance with displacement becomes

FIGURE 15 Mean deceleration versus displacement for constant impact velocity.

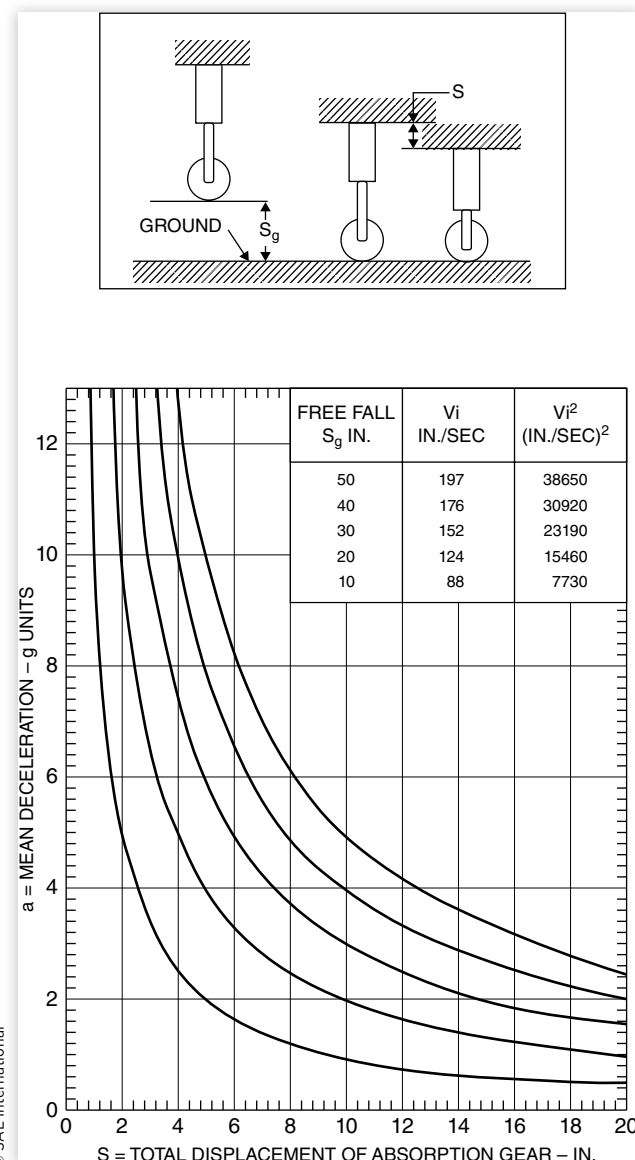
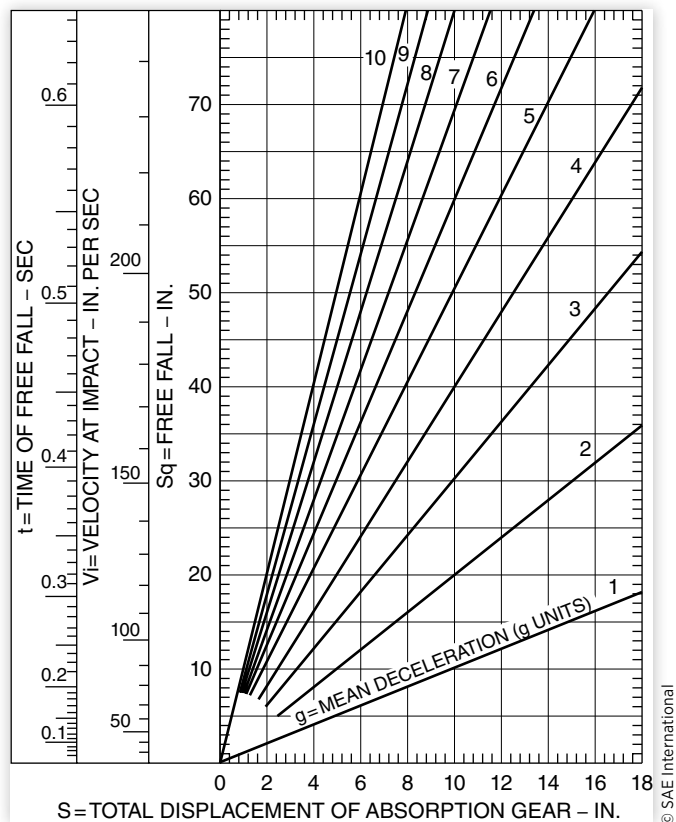
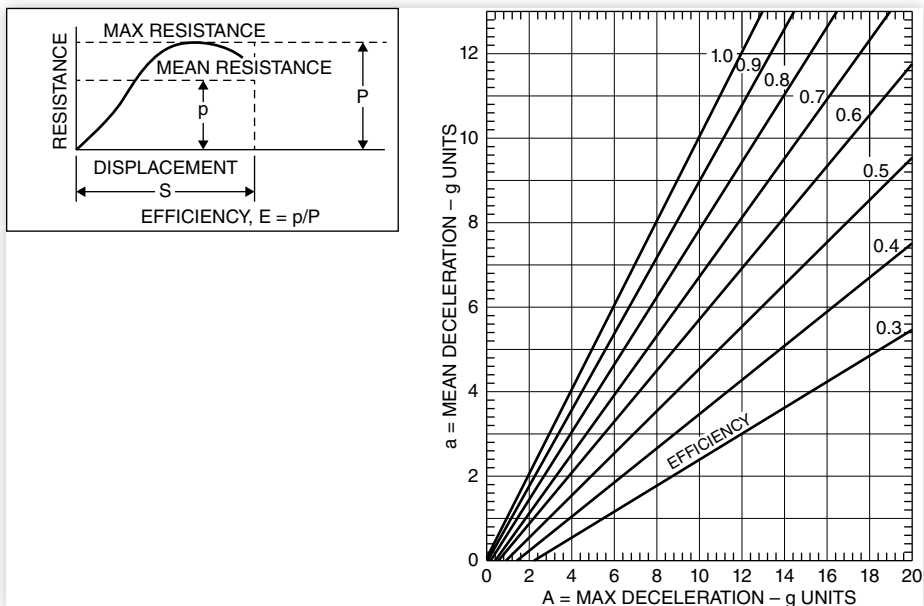


FIGURE 16 Freefall conditions.

© SAE International

FIGURE 17 Freefall conditions, mean versus maximum deceleration at given efficiencies.

© SAE International

complex. In order to make the charts readily applicable to any resistance characteristic, the resistance is reduced to a simple efficiency value. As shown diagrammatically in [Figure 17](#), the efficiency is taken as the ratio of mean to maximum resistance over the total displacement of the absorption gear.

The relations between velocity at impact, total displacement, and mean deceleration, shown in [Figures 15](#) and [16](#), apply equally whether gravity acceleration is present or not. But, in relating the resistance of the absorption gear to the resultant deceleration, the force of gravity, if present, must be reckoned with as an additional component. Cases with and without gravity must, therefore, be treated differently as shown on the following pages. Where gravity is not involved, the relations between mean and maximum deceleration and efficiency of the gear are simple and direct.

Note that, while [Figure 17](#) applies only to free fall conditions, it extends all the way to zero impact, that is, a mass falling freely from rest in contact with the absorption gear. Since both the initial and final velocities are zero, the mean deceleration is also zero. Therefore, the maximum deceleration for any efficiency value is defined by the intersection of the constant efficiency line with the abscissa. Thus, [Figure 17](#) can be applied to a sprung mass, initially at rest but displaced from its static position.

3.1 List of Symbols

S_g = Distance of free fall to point of contact, in.

V_i = Velocity at impact, in./s

t = Time of free fall, s

S = Total displacement of absorption gear in bringing mass velocity to zero, in.

a = Mean deceleration of moving mass, g units

A = Maximum deceleration of moving mass, g units

p = Mean resistance of absorption gear over total displacement, lb

P = Maximum resistance of absorption gear, lb

E = Efficiency of absorption gear, p/P

W = Total moving weight, lb

g = 386 in./s²

3.2 Mathematical Relations

3.2.1 IMPACT FROM FREE FALL

$$V_i^2 = 2gS_g \quad V_i = 27.8\sqrt{S_g}$$

$$t = \sqrt{2S_g / g} = 0.072\sqrt{S_g}$$

$$a = S_g / S \text{ or } a = V_i^2 / (2gS)$$

$$a = (p/W) - I \quad A = (P/W) - I$$

$$E = p/P = (a + 1)/(A + I)$$

$$a = E(A + 1) - 1 \quad A = [(a + 1)/E] - I$$

Example:

Given: Free fall, $S_g = 40$ in.

Maximum displacement of gear, $S = 10$ in.

Maximum deceleration = $7g$

To find: Required efficiency of gear and maximum resistance

From [Figures 15 or 16](#) for $S_g = 40$ in. and $S = 10$ in. (read) $a = 4g$.

Required efficiency: From [Figure 17](#) for $a = 4g$ and $A = 7g$ (read) $E = 62.5\%$.

Maximum resistance: $A = (P/W) - 1 = 7$

$$P = 8W$$

3.2.2 IMPACT WITHOUT GRAVITY ACCELERATION

$$a = V_i^2 / (2gS)$$

$$a = p / W \quad A = P / W$$

$$E = p / P = a / A$$

Example:

Given: Velocity at impact, $V_i = 176$ in./s

Maximum displacement of gear, $S = 10$ in.

Maximum deceleration = $7g$

To find: Required efficiency of gear and maximum resistance

From [Figure 15](#), for $V_i = 176$ and $S = 10$ in. (read) $a = 4g$

Required efficiency: $E = p/P = a/A = 4/7 = 57.2\%$

Maximum resistance: $P = AW = 7W$

4. Vibration Limits for Passenger Comfort

A study of the subject indicates that there is no absolute standard of human comfort or discomfort expressed in physical terms such as amplitudes or acceleration at a given frequency. However, there is enough agreement among the test data from various investigators so that a zone may be outlined, above which vibration is certainly intolerable and below which it is immaterial. A limit of acceptable vibration can only be drawn by combining a judgment factor with analysis of the laboratory test data.

Three independent analyses appear in this section, each based on data from many investigators, and each with the author's own comments. The Burton-Douglas chart ([Figure 19](#)) presents the conclusions of aircraft engineers, the Janeway recommendations ([Figure 20](#)) are directed at automobile and railroad practice, and the Goldman presentation ([Figure 21](#)) represents a broad biological viewpoint.

A comparison of these three presentations shows that above a frequency of cps, the disagreement is minor, so that all analyses can be considered identical. Below this frequency, the presentations differ, partly because the data used are not entirely the same, but also because each author takes a different point of view based upon his particular field of interest. Note that all three are superimposed in [Figure 18](#) to show how they are related to each other in the 1-10 cps frequency range. It is significant that Janeway's recommended limits agree very closely with Goldman's mean discomfort threshold, while both fall well inside the very disagreeable threshold of the Burton-Douglas chart.

For practical use, that chart should be selected which has been derived with the particular field of application in mind.

It will be noted that these criteria apply specifically to vertical vibration. For lateral vibrations, recently published experimental evidence from railway tests indicates that tolerable amplitudes for passenger comfort are 30% lower in the 1-2 cps frequency range.

The latest publications* on the subject strongly confirm the validity of constant peak jerk intensity as the comfort criterion for vertical vibration in the 1-6 cps frequency range. (See [Figure 20](#).)

4.1 Response to Vertical Vibrations

E.F. Burton, Douglas Aircraft Co.

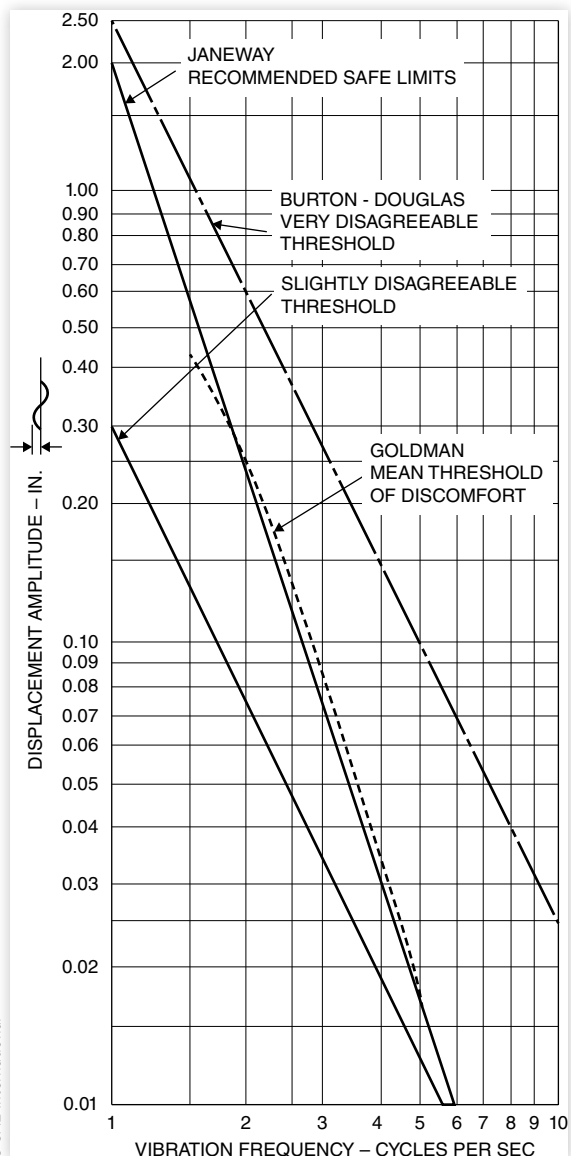
Passengers and crew in aircraft are subject to complex oscillatory disturbances, the effects of which must be evaluated in planning for comfort. The data on which such evaluations can be based are not extensive and are on sinusoidal oscillations, chiefly in a vertical plane, for a seated or standing person.

The accompanying chart ([Figure 19](#)) is a simplified graph based on a careful comparison and evaluation of ten original studies ranging from motion sickness and ordinary vibration table studies down to fingertip sensitivity experiments. The assumption that the comfort classification is continuous over a wide range of frequencies and amplitudes, even though the physiological responses may differ within these ranges, permits the engineer to employ a single set of standards in judging the vibration experience in aircraft.

The graph applies to simple harmonic motions, but if each major component of the complex steady-state vibration in an airplane is separately evaluated as if it were the only motion, a useful first approximation of the experience will be obtained. In the absence of other data, the graph may also serve as an approximate guide to the evaluation of fore and aft and lateral oscillations.

The family of three curves shown in the graph is taken from Lippert[†]. Janeway's description in terms of maximum acceleration and maximum velocity is applied to each curve.

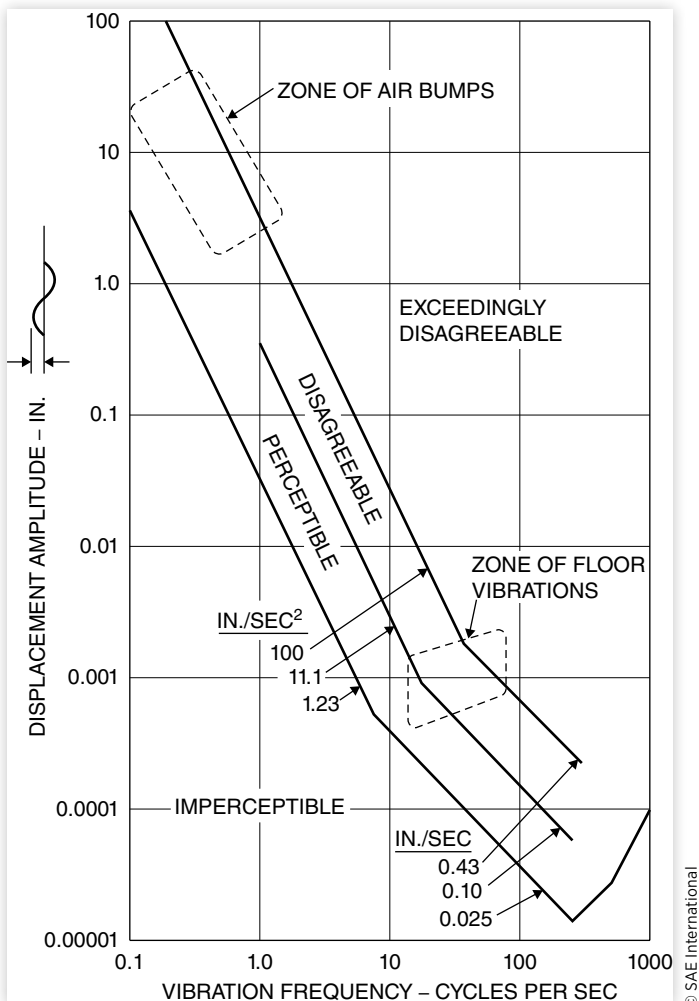
FIGURE 18 Discomfort thresholds—comparison at low frequencies.



© SAE International

* See Bibliography, Refs. [1, 4, 10, 11].

[†] See Bibliography, Refs. [14, 15].

FIGURE 19 Response to vertical vibrations.

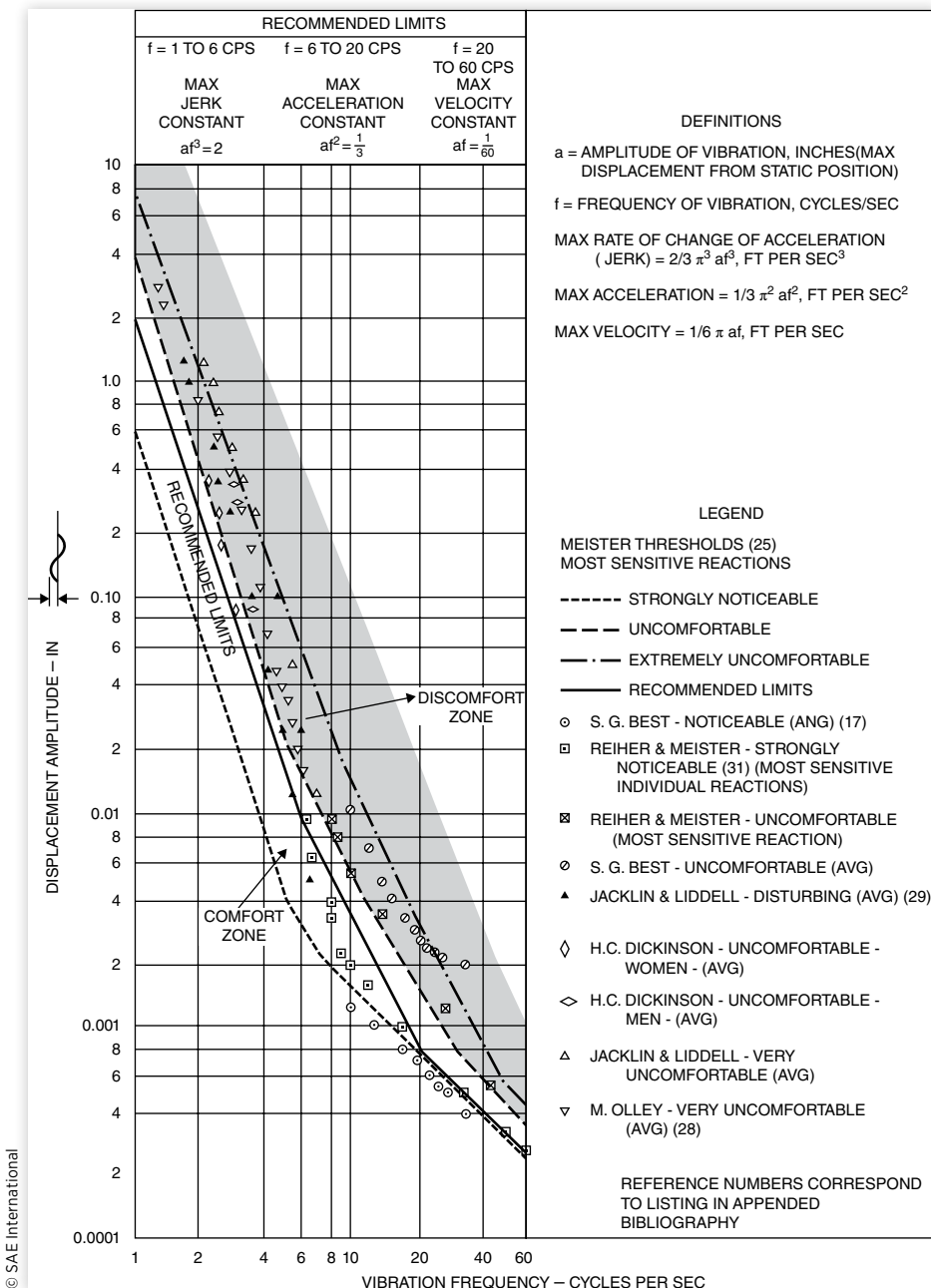
4.2 Vertical Vibration Limits for Passenger Comfort*

R.N. Janeway, Janeway Engineering Co.

In dealing with human reactions to vibration, limits for comfort cannot be fixed objectively but must be derived by interpreting the available experimental data. The problem is complicated by the variations in individual sensitivity and the diversity of test method and sensation level adopted by different investigators.

All the pertinent data available are correlated in Figure 20 in terms of vibration amplitude versus frequency. The three broken lines define the sensation thresholds, respectively, of "strongly noticeable," "uncomfortable," and "very uncomfortable" for the most sensitive

* Based on Bibliography, Ref. [13].

FIGURE 20 Human reaction to vertical vibration.

subjects at frequencies from 1 to 60 cycles per second, according to F.J. Meister.* Adjacent threshold lines encompass the results on at least 90% of all individuals tested and, therefore, also define the probable range of variation. The average results obtained by the other investigators confirm these boundaries remarkably well. The probable zones of "comfort" and "discomfort" are indicated on both sides of Meister's "uncomfortable" threshold.

* See Bibliography, Ref. [25].

TABLE 2

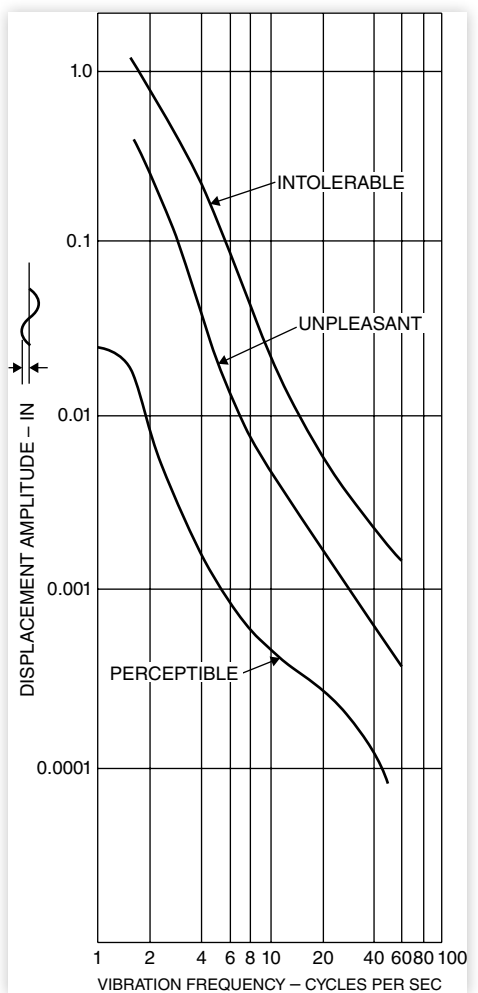
Frequency range, cps	Amplitude versus frequency, in
1-6	$af^3 = 2$ (constant peak jerk)
6-20	$af^2 = 1/3$ (constant peak acceleration)
20-60	$af = 1/60$ (constant peak velocity)

Example: At $f = 2$, the recommended amplitude limit is $a = 1/4$ in.

The following should be noted in studying this figure:

1. All values are based on vertical sinusoidal vibration of a single frequency. Where two or more components of different frequencies are present, there is no established basis on which to evaluate the resultant effect. It is probable, however, that the component, which taken alone represents the highest sensation level, will govern the sensation as a whole.
2. A relatively low noise level is assumed so that the vibration alone determines the sensation. No data are available to indicate how to evaluate the resultant sensation where vibration and noise are of comparable intensities in terms of human reaction.
3. All data used were obtained with subjects standing (Refs. [25, 31]) or sitting on a hard seat. In any case where a cushion is used, it must be evaluated independently. Only the resultant vibration transmitted to the passenger should be related to the chart values.

FIGURE 21 Subjective response of the human body to vibratory motion.



The heavy line shows recommended limits which include a judgment factor and should be well within the comfort range even for the most sensitive person. It is important to note that the experimental data are all based on short exposure time of five minutes or less. Vibration, as actually encountered in vehicles, tends to be more prolonged the higher the frequency. For this reason, the recommended limits allow a greater margin of safety as the frequency increases.

As indicated at the top of Figure 20, the recommended criterion consists of three simple relationships, each covering a portion of the frequency range, as shown in Table 2.

4.3 Subjective Responses of the Human Body to Vibratory Motion*

David E. Goldman, Naval Medical Research Inst.

Figure 21 shows mean amplitudes of simple harmonic vibration at frequencies up to 60 cycles per sec, at which subjects: (I) perceive vibration, (II) find it unpleasant, or (III) refuse to tolerate it.

Each point on the chart represents an average of 4-9 different values based on measurements reported by various investigators. The data are for short duration exposure (a few minutes) of the body standing or sitting on a vibrating support subjected to vertical oscillation.

* Based on Bibliography, Ref. [12].

5. Bibliography

1. Richard Fine, "Correlation of Vertical Acceleration and Human Comfort in a Passenger Car," SAE Technical Paper 630314 (733C), Sept. 1963.
2. C.B. Notess, "A Triangle-Flexible Airplanes, Gusts, Crew," *Cornell Aero. Lab. Memo No. 343*, May 1963.
3. Goldman, D.E., "The Effects of Shock and Vibration on Man," ASA Report, June 1963, *Shock and Vibration Handbook*, Chap. 44, McGraw-Hill, 1961.
4. H.C.A. von Eldik Thieme, "Passenger Riding Comfort Criteria and Methods of Analyzing Ride and Vibration Data," SAE Technical Paper 610173 (295A), January 1961.
5. Ziegenruecker, G.H. and Magid, E.G., "Short Time Human Tolerance to Sinusoidal Vibrations," WADC, TR 59-391, July 1959.
6. Radke, A.O., *Proceedings of the ASME*, New York, December 1957.
7. Simons, A.K., "Mechanical Response of Human Body to Wheeled Vehicle Vibration, I-6 cps," Paper presented at *40th Annual Conference of Human Engineers*, NYU, Sept. 1956.
8. Getline, G.L., *Shock and Vibration Bulletin*, 22. Supplement DOD, Washington, DC, 1955.
9. Steele, J.E., "Motion Sickness," *Shock and Vibration Bulletin*, 22. Supplement DOD, Washington, DC, 1955.
10. Haack, M., "Tractor Seat Suspension for Easy Riding," *SAE Transactions*. 63 (1955).
11. Haack, M., "Stressing of Human Being by Vibration of Tractor and Farm Machinery," *Grundlagen der Landtechnik*, 4, 1953 (Germany).
12. Goldman, D. E., "A Review of Subjective Responses to Vibratory Motion of Human Body," Report No. I, Naval Medical Research Institute, March 16, 1948.
13. Janeway, R.N., "Vehicle Vibration Limits to Fit the Passenger," Paper presented before SAE, March 5, 1948.
14. S. Lippert, "Comprehensive Graph for the Collection of Noise and Vibration Data," *J. Aviat. Med.*, August 1948.
15. Lippert, S., "Human Response to Vertical Vibration," Paper presented before SAE, October 1946.
16. Dart, E.E., "Effects of High Speed Vibrating Tools on Operators Engaged in the Aircraft Industry," *Occupational Medicine*, I, (1946), 515.
17. Best, S.G., "Propeller Balancing Problems," *SAE Journal*, November 1945.
18. Alexander, S.J., et al., "Effects of Various Accelerations upon Sickness Rates," *Journal of Psychology*, July 1945.
19. Postlethwaite, F., "Human Susceptibility to Vibration," *Engineering (British)*, 157, (1944), 61.
20. Geldard, F.A., "The Perception of Mechanical Vibration," Part III, *Journal of General Psychology*, 22, (1940), 281-289.
21. G. Von Bekesy, "The Sensitivity of Standing and Sitting Human Beings to Sinusoidal Shaking," *Akustische Zeitschrift*, 4, (1939), 360.
22. G. Von Bekesy, "Vibration Sensation," *Akustische Zeitschrift*, 4, (1939), 316.

23. R. Coermann, "Investigation of the Effect of Vibrations on the Human Organism," *Jahrbuch der Deutschen Luftfahrtforschung*, III, (1938), 142.
24. H.M. Jacklin, "Human Reactions to Vibration," *SAE Trans.*.. 39, (1936), 401.
25. Meister, F.J., "Sensitivity of Human Beings to Vibration," *Forschung* (V.D.I. Berlin), May-June 1935.
26. Constant, H., "Aircraft Vibration," British Air Ministry Report No. 1637, October 1934.
27. L.D. Goodfellow, "Experiments on the Senses of Touch and Vibration," *A.S.A. Journal*, July 1934.
28. Maurice Olley, "Independent Wheel Suspension - Its Whys and Wherefores," *SAE Journal*, March 1934.
29. Jacklin, H.M. and Liddell, G.J., "Riding Comfort Analysis," *Engineering Bulletin, Research Series-No. 44*, Purdue Univ., May 1933.
30. S.J. Zand, "Vibration of Instrument Boards and Airplane Structures," *SAE Journal*, November 1932.
31. Reiher, H. and Meister, F.J., "Sensitiveness of the Human Body to Vibrations," *Forschung* (V.D.I. Berlin), November 1931.
32. Moss, F.A., "Measurement of Riding Comfort (General)," *SAE Journal*, April 1932, May 1931, July 1930, April 1930, and September 1929.
33. G.B. Upton, "Report on Lecture by Prof. Lemaire (France) at Cornell Univ," *Sibley Journal of Engineering*, 34, (1925), 354.

appendix C: Ride index structure and development methodology

J2834™ OCT2019

SURFACE VEHICLE RECOMMENDED PRACTICE	Issued 2013-10 Reaffirmed 2019-04 Revised 2019-10 Superseding J2834 APR2019
-------------------------------------------------	--------------------------------------------------------------------------------------

Ride Index Structure and Development Methodology

Table of Contents

RATIONALE

FOREWORD

INTRODUCTION

1 SCOPE

1.1 Purpose

2 REFERENCES

2.1 Applicable Documents

2.1.1 SAE Publications

2.1.2 ISO Publications

2.1.3 IEC Publications

SAE Technical Standards Board Rules provide that: "This report is published by SAE to advance the state of technical and engineering sciences. The use of this report is entirely voluntary, and its applicability and suitability for any particular use, including any patent infringement arising therefrom, is the sole responsibility of the user."

SAE reviews each technical report at least every five years at which time it may be revised, reaffirmed, stabilized, or cancelled. SAE invites your written comments and suggestions.

Copyright © 2018 SAE International

All rights reserved. No part of this publication may be reproduced, stored in a retrieval system or transmitted, in any form or by any means, electronic, mechanical, photocopying, recording, or otherwise, without the prior written permission of SAE.

TO PLACE A DOCUMENT ORDER

Tel: 877-696-7323 (inside USA and Canada)

Tel: 877-606-7323 (inside USA and

Tel: +1 724-776-49

Fax: 724-776-0790

SAE values your input. To provide feedback
on this Technical Report, please visit
http://standards.sae.org/J2834_201910

SAE WEB ADDRESS:

<http://www.sae.org>

2.2 Related Publications

2.2.1 SAE Publications

2.2.2 ISO Publications

2.2.3 Other Publications

3. DEFINITIONS

4. SYMBOLS, SUBSCRIPTS AND ABBREVIATIONS

4.1 Symbols

4.2 Subscripts

5. SUBJECTIVE AND OBJECTIVE DATA REQUIREMENTS

5.1 Psychometric Ratings for Human Sensitivity Data

5.1.1 Discomfort Ratings

5.1.2 Human Subjects

5.1.3 Rating Scales and Usage

5.1.4 Subject Experimental Protocols

5.2 Objective Motion and Vibration Measurement

5.2.1 General

5.2.2 Motion and Vibration Measurement

5.2.3 Signal Conditioning

5.2.4 Duration of Measurement

5.2.5 Vehicle Speed Measurement

5.2.6 Reporting of Measurement Conditions

5.3 Processing of Vibration Data

5.3.1 Basic Processing Method Using Weighted Root-Mean-Square and Root-Mean-Quad Acceleration

5.3.2 Applicability of the Basic Processing Method

5.3.3 Frequency Weighting

5.4 Prediction of Discomfort Ratings

5.4.1 Rough Road Ride Specimens

5.4.2 Transient Ride Specimens

5.5 Statistical Method for Determining the Ride Discomfort Models

5.5.1 Jury Model

5.5.2 RPRED Statistic

5.5.3 Domain-of-Validity

6. NOTES

6.1 Revision Indicator

APPENDIX A MATHEMATICAL DEFINITION OF THE FREQUENCY WEIGHTINGS

APPENDIX B OTHER PUBLICATIONS

APPENDIX C SUPPORTING RATIONALE

Figure 1 Example discomfort rating scale developed using psychometric methods

Figure 2 Basicentric axes of the human body

Figure 3 Frequency weighting curves for human discomfort weightings

Figure 4 Frequency weighting curve for steering wheel/hands discomfort weighting

Table 1 Guide for the application of human discomfort frequency-weighting curves

Table 2 Human discomfort frequency weightings in one-third octaves

Rationale

This recommended practice indicates the current state of technology regarding the relationship between the human-to-vehicle interface vibration magnitude and human discomfort. The appendix is concerned with providing a uniform and convenient method of indicating the subjective severity of the motion and vibration but does not present limits. It is in no way related to quantifying health and safety aspects of motion and vibration for which an entirely different methodology would be needed. This methodology is intended to predict human sensitivity to motion and vibration for comparative purposes (i.e., condition A versus condition B) relative to a global (i.e., absolute) adjectival psychometric scale. See [Appendix C](#) for additional supporting rationale.

This revised edition incorporates changes due to the expanded scope of SAE J1441 to include vehicle ride, and a revised [Figure 1](#) to clarify the potential non-equal spacing of adjectives for a rating scale developed using psychometric adjectives.

Foreword

This new recommended practice was prepared by the SAE J6 Task Force as partial replacement for the SAE J6a “Ride and Vibration Data Manual.” This new recommended practice represents a substantial updating and expansion of state-of-the-art in ride development methods used compared to the J6a Ride Vibration Data Manual which it partially replaces.

The J6a Ride Vibration Data Manual was last revised by the SAE Vehicle Dynamics Committee in October 1965. It is no longer published by the SAE but is included in [Appendix B](#) of Gillespie (1992).

Introduction

This recommended practice is a method for developing an objective model of human sensitivity to vibration due to road induced disturbances in the automotive driving environment (a.k.a., “ride”). This method is based on statistical analysis of a database of juried vehicle occupant discomfort ratings and measured acceleration at the various human to vehicle contact surfaces during representative over-the-road driving events with stationary or transient characteristics within the finite time period of interest. The database for this analysis should cover an array of roads, vehicles, raters and driving conditions that well represent the application domain of interest.

The recommended discomfort model is hierachal in order to provide for allocation of performance objectives to various subsystems, ride diagnosis, and to reduce the statistical uncertainty of fitting a single stage model. The top level of the model expresses overall motion and discomfort as the weighted sum of several “interface” discomfort ratings. Each interface discomfort rating (e.g., seat back, steering wheel...) is the weighted sum of the discomfort ratings for the various axes of vibration at that interface (typically vertical, lateral and longitudinal). The axis discomfort ratings are based on frequency weighted acceleration signals. The frequency response filters are primarily taken from ISO 2631-1.

ISO 2631-1 is a very comprehensive and widely accepted standard for describing human sensitivity to vibration, but not specifically for the automotive driving environment. It is as relevant for vibrations in a building environment as it is in the automotive driving environment. It is based on human subjects seated on a rigid flat seat and subjected to a single axis of vibration at a time without the distractions and ancillary sensations of driving. This report describes a method for developing a human sensitivity model based on data taken in an actual ride environment.

1. Scope

This recommended practice defines methods for the measurement of periodic, random and transient whole-body vibration. It indicates the principal factors that combine to determine the degree to which a vibration exposure will cause discomfort. Informative appendices indicate the current state of knowledge and provide guidance on the possible effects of motion and vibration on discomfort. The frequency range considered is 0.5 Hz to 80 Hz. This recommended practice also defines the principles of preferred methods of mounting transducers for determining human exposure. This recommended practice is applicable to light passenger vehicles (e.g., passenger cars and light trucks). This recommended practice is applicable to motions transmitted to the human body as a whole through the buttocks, back and feet of a seated occupant, as well as through the hands of a driver.

This recommended practice offers a method for developing a ride performance index but does not specifically describe how to apply this index to assessment or comparison of specific vehicles.

NOTE: This recommended practice may also be applicable to other types of ground vehicles (e.g., medium and heavy duty road vehicles) with seated occupants having similar seating posture, occupant/vehicle interfaces, and vibration magnitudes, frequencies, and durations as light passenger vehicles.

1.1 Purpose

The primary purpose of this recommended practice is to define methods of quantifying human sensitivity to occupant motion and vibration in passenger cars and light trucks based on objective measurements of acceleration and sound in order to simplify and standardize the reporting, comparison and assessment of motion and vibration conditions. It contains methods for the evaluation of vibration containing occasional large peak values (i.e., having large crest factors). Human sensitivity is

quantified in terms of predicted subjective discomfort levels, based on suitable psychometric and statistical methodologies. Passenger cars and light trucks and vans expose occupants to periodic, random and transient mechanical vibration which can cause various levels of subjective discomfort. This recommended practice does not contain vibration exposure limits and does not address potential effects of motion and vibration on health and safety, or on motion sickness, which involve different phenomena. This recommended practice does not address the potential effects of intense vibration on human task performance since these involve different phenomena which depend critically on the biomechanical and ergonomic details related to the operator, the situation and the task. Appendix C provides rationale for the assessment of human discomfort due to motion and vibration. More information may be obtained from the scientific literature, a portion of which is listed in 2.2.1 and Appendix B. Motion and vibration is often complex, contains many frequencies, occurs in several directions and changes over time. The effects of motion and vibration on human discomfort may be manifold. Exposure to whole-body vibration causes a complex distribution of oscillatory motions and forces within the body. There can be large variations between subjects with respect to discomfort effects. Whole-body motion may cause sensations (e.g., discomfort or annoyance). The presence of oscillatory force (i.e., vibration) with little whole-body motion may cause similar effects.

2. References

2.1 Applicable Documents

The following standards contain provisions which, through reference in this text, constitute provisions of this recommended practice. At the time of publication, the editions indicated were valid. All standards are subject to revision, and users of this recommended practice are encouraged to investigate the possibility of applying the most recent editions of the standards indicated below. Members of IEC and ISO maintain registers of currently valid International Standards.

2.1.1 SAE PUBLICATIONS: Available from SAE International, 400 Commonwealth Drive, Warrendale, PA 15096-0001, Tel: 877-606-7323 (inside USA and Canada) or +1 724-776-4970 (outside USA), www.sae.org.

SAE J670 Vehicle Dynamics Terminology
SAE J1441 Subjective Rating Scale for Vehicle Ride and Handling

2.1.2 ISO PUBLICATIONS: Available from International Organization for Standardization, ISO Central Secretariat, 1, ch. de la Voie-Creuse, CP 56, CH-1211 Geneva 20, Switzerland, Tel: +41 22 749 01 11, www.iso.org.

ISO 2041:2005 Vibration and Shock - Vocabulary
ISO 5805:1997 Mechanical Vibration and Shock - Human Exposure - Vocabulary

2.1.3 IEC PUBLICATIONS: Available from IEC Central Office, 3, rue de Varembe, P.O. Box 131, CH-1211 Geneva 20, Switzerland, Tel: +41 22 919 02 11, www.iec.ch.

IEC 1260:1995 Electroacoustics - Octave-Band and Fractional-Octave-Band Filters

2.2 Related Publications

The following publications are provided for information purposes only and are not a required part of this SAE Technical Report.

2.2.1 SAE PUBLICATIONS: Available from SAE International, 400 Commonwealth Drive, Warrendale, PA 15096-0001, Tel: 877-606-7323 (inside USA and Canada) or +1 724-776-4970 (outside USA), www.sae.org.

SAE J1477 Measurement of Interior Sound Levels of Light Vehicles

Amman, S., Meier, R., Trost, K., and Gu, P., "Equal Annoyance Contours for Steering Wheel Hand-arm Vibration," SAE Technical Paper 2005-01-2473, 2005, <https://doi.org/10.4271/2005-01-2473>.

Griffin, M., "Evaluation of Vibration with Respect to Human Response," SAE Technical Paper 860047, 1986, <https://doi.org/10.4271/860047>.

Herrick, T., "A Ride Metric System Utilized to Benchmark and Develop a Superior Riding Sport Utility Vehicle," SAE Technical Paper 942273, 1994, <https://doi.org/10.4271/942273>.

Mousseau, C., Karamihas, S., Gillespie, T., Sayers, M. et al., "Computer Synthesis of Light Truck Ride Using a PC Based Simulation Program," SAE Technical Paper 1999-01-1796, 1999, <https://doi.org/10.4271/1999-01-1796>.

Van Auken, R.M., Zellner, J., and Kunkel, D., "Correlation of Zwicker's Loudness and Other Noise Metrics with Drivers' Over-the-Road Transient Noise Discomfort," SAE Technical Paper 980585, 1998, <https://doi.org/10.4271/980585>.

von Gierke, H., "The ISO Standard Guide for the Evaluation of Human Exposure to Whole-Body Vibration," SAE Technical Paper 751009, 1975, <https://doi.org/10.4271/751009>.

Gillespie, T.D., (1992) Fundamentals of Vehicle Dynamics, SAE International, Warrendale, PA.

2.2.2 ISO PUBLICATIONS: Available from International Organization for Standardization, ISO Central Secretariat, 1, ch. de la Voie-Creuse, CP 56, CH-1211 Geneva 20, Switzerland, Tel: +41 22 749 01 11, www.iso.org.

ISO 2631-1:1997 Mechanical Vibration and Shock - Evaluation of Human Exposure to Whole-Body Vibration - Part 1: General Requirements

ISO 5128:1980 Acoustics - Measurement of Noise Inside Motor Vehicles

ISO 5349-1:2001 Mechanical Vibration - Measurement and Evaluation of Human Exposure to Hand-Transmitted Vibration - Part 1: General Requirements

ISO 5349-2:2001 Mechanical Vibration - Measurement and Evaluation of Human Exposure to Hand-Transmitted Vibration - Part 2: Practical Guidance for Measurement at the Workplace

- ISO 8041:2005 Human Response to Vibration - Measuring Instrumentation
ISO 8608:1995 Mechanical Vibration - Road Surface Profiles - Reporting of Measured Data
ISO 10326-1:1992 Mechanical Vibration - Laboratory Method for Evaluating Vehicle Seat Vibration - Part 1: Basic Requirements

2.2.3 OTHER PUBLICATIONS: The references for these publications are listed in Appendix B.

3. Definitions

For the purposes of this recommended practice, the terms and definitions given in SAE J670, ISO 2041, and ISO 5805 apply. In addition, the following definitions apply.

3.1 Motion

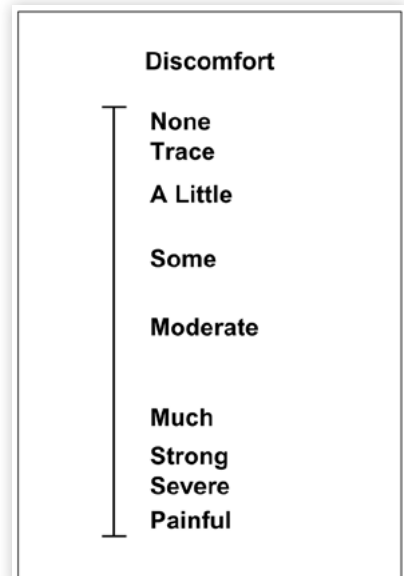
Whole-body dynamic movement of a human, periodic or aperiodic in nature, the frequency content of which is typically mainly at the lower end of the relevant frequency range (e.g., below 5 Hz).

3.2 Psychometric

Pertaining to the measurement of the subjective impression of a person exposed to a given condition, by requesting the person to place a mark on a vertical linear scale, which has a subjective title describing a psychological state (i.e., “discomfort”) and adjectives positioned along its length describing the intensity of the psychological state (e.g., “a little”), such adjectives being positioned from least at the top to most at the bottom, based on adjectival placement data previously collected using a suitable experimental protocol (see Figure 1).

NOTE: A global, continuous, interval, adjectively anchored psychometric rating scale is better suited for correlating large numbers of subjective ratings with objective measurements spanning a wide range of input levels than relative rating or threshold detection methods sometimes used in psychoacoustics research, which have different purposes.

FIGURE 1 Conceptual discomfort rating scale developed using psychometric methods (e.g., SAE 980585)



3.3 Rough Road Ride Event

An over-the-road ride event which at a given vehicle speed results in continuous and typically random-like motion and vibration disturbance of the occupant with stationary characteristics within the finite time period of interest (i.e., 8 seconds minimum and ideally the same measurement period for all rough road ride specimens), as further defined in 5.3.2.1.

3.4 Transient Ride Event

An over-the-road ride event which at a given vehicle speed results in one or more discrete motion and vibration disturbance(s) of the occupant, within

the finite time period of interest (i.e., 8 seconds minimum and ideally the same measurement period for all transient ride specimens), as further defined in 5.3.2.1.

3.5 Vibration

Periodic dynamic movement of that surface of a human which is in contact with a given vehicle interface, and typically involving frequency content at the middle or upper end of the relevant frequency range (e.g., above 5 Hz).

4. Symbols, Subscripts and Abbreviations

4.1 Symbols

- DR Numerical discomfort rating. The numerical value of the discomfort rating corresponds to a unique location on a psychometric discomfort rating scale developed by suitable psychometric methods (see [Figure 1](#)).
- a Vibration acceleration. Translational acceleration is expressed in meters per second squared (m/s^2) and rotational acceleration is expressed in radians per second squared (rad/s^2). Values are quoted as root-mean-square (RMS) or root-mean-quad (RMQ) unless stated otherwise.
- f Frequency expressed in Hz.
- $H(s)$ Transfer function, or gain, of a filter expressed as a function of the imaginary angular frequency (complex frequency).
- $j = \sqrt{-1}$ The imaginary unit number.
- $s = j2\pi f$ Imaginary angular frequency.
- W Frequency weighting.
- ω Frequency expressed in radians per second.

4.2 Subscripts

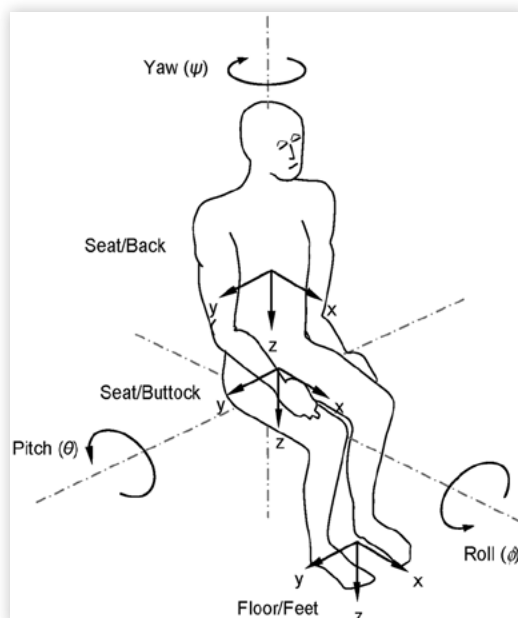
- $0, b, c, d, e, sl$ Refer to the various human discomfort frequency-weighting curves recommended for evaluation with respect to motion and vibration comfort and discomfort (see [Table 1](#)).
- w Refers to frequency-weighted acceleration values.
- x, y, z For translational or rectilinear motion, refer to the fore-aft, lateral and vertical directions of motion and vibration (see [Figure 2](#)).
- $\varphi, \theta, \text{ and } \psi$ Refer to roll, pitch and yaw rotational motion about x -, y -, and z -axes, respectively (see [Figure 2](#)).

TABLE 1 Guide for the application of human discomfort frequency-weighting curves

Frequency weighting	Occupant interface and direction
W_o	All
W_b	z-axis, seat/buttock interface x -, y -, z -axes, floor/feet interface
W_c	x -axis, seat/back interface
W_d	x -, y -axes, seat/buttock interface y -, z -axes seat/back interface
W_e	ϕ , θ , and ψ -axes, seat/buttock interface
W_{sl}	x -, y -, z -axes, steering wheel/hands interface

NOTE: The recommended W_b , W_c , W_d , and W_e frequency weightings for the seat/buttock, seat/back, and floor/feet interfaces are based on SAE 860047. The W_b weighting is within 3 dB of the ISO 2631-1 (1997) weighting W_k in the 0.4 to 100 Hz frequency range.

NOTE: A recommended weighting for the steering wheel/hands interface has not been established. W_{sl} is a low frequency realizable approximation to the W_s weighting from Giacomin et al. (2004). The Giacomin W_s weighting is based on rotational hand-arm vibration. W_h from ISO 5349-1 is for workplace hand vibration issues that are more severe than passenger vehicle driving comfort applications. Preliminary indications (SAE 2005-01-2473 and Giacomin et al. (2004)) are that the constant velocity sensitivity of W_{sl} is appropriate for passenger vehicle steering wheel comfort from 10 to 60 Hz. For steering wheel comfort, the frequency of peak sensitivity seems to be about 2 to 3 Hz for x and z , and perhaps 1 Hz for y (rather than the ISO 5349-1 W_h peak at 10 Hz). WorkSafeBC used ISO 5349-1 for steering wheel vibration (Eaton, 2003).

FIGURE 2 Basicentric axes of the human body

NOTE: The basicentric x-y-z axes define a right-handed orthogonal coordinate system at each human body/vehicle interface. The x-axis is nominally aligned with the fore-aft direction, the y-axis aligned with the lateral direction, and the z-axis nominally aligned with the vertical direction. The z-axes of the seat/buttock and floor/feet interfaces are in the direction normal to the respective interface contact planes and may not necessarily be parallel to the gravity vector. The x-axis of the seat/back interface is in the direction normal to the interface contact plane and may not necessarily be horizontal. The basicentric y-axes are parallel to and in the same direction as the vehicle y-axes.

NOTE: A right-handed z-down coordinate system is illustrated in [Figure 2](#). A z-up coordinate system may also be used. A right-handed axis system is recommended but not required. It is also recommended but not required that the directions of the axes be nominally aligned (i.e., within 15 degrees) with the vehicle axis system as defined in SAE J670.

5. Subjective and Objective Data Requirements

5.1 Psychometric Ratings for Human Sensitivity Data

Subjective data describing human sensitivity to motion and vibration shall be based on psychometric discomfort ratings (associated with correspondingly measured objective acceleration data) obtained from several human subjects, vehicles, and ride specimens, using suitable human subject experimental protocols for controlled in-vehicle over-the-road tests, or alternatively, simulator tests which replicate real, recorded in-vehicle over-the-road motions at all interfaces, in all axes, and across the frequency range of interest, to within 3 dB.

5.1.1 DISCOMFORT RATINGS: The separate psychometric discomfort ratings shall include, at a minimum:

- Overall Motion and Vibration Discomfort;
- Seat/Buttock Interface Discomfort;
- Seat/Back Interface Discomfort;
- Steering Wheel/Hands Interface Discomfort (for drivers only);
- Floor/Feet Interface Discomfort.

NOTE: Sound may influence the perception of motion and vibration discomfort (Howarth and Griffin, 1990). Therefore, a psychometric acoustic Noise Discomfort Rating is also recommended.

5.1.2 HUMAN SUBJECTS: The human subjects shall comprise a representative sample of the relevant vehicle occupant physical and market segment characteristics. The ride index models should be based on data for a minimum of 12 human subjects in order to reduce the effects of subject-to-subject variation on the jury average ratings.

NOTE: The predictive capability of the resulting ride index model is substantially degraded when there are fewer than 20 non-expert evaluators or 10 expert evaluators.

5.1.3 RATING SCALES AND USAGE The subjective rating data shall be collected using the global, continuous, interval, adjectively anchored psychometric rating scale shown in [Figure 1](#). The scale shall not have numbers on it which are visible to the human subjects. Each rating scale shall be presented in printed or in electronic form to each human subject.

A separate rating scale for each of the five discomfort categories listed in 5.1.1 shall be presented to each human subject for each motion and vibration condition, with the category (e.g., “Seat/buttock interface”) displayed above the “Discomfort” title of each scale.

Each human subject shall report a discomfort rating for each vehicle and ride specimen by marking or otherwise indicating the position on the scale which corresponds most closely to his or her subjective feeling of discomfort for that specimen.

The ratings marked or otherwise indicated on this scale shall be digitized on a 100-point basis, with zero at the bottom extremity and 100 at the top extremity, in order to obtain a numerical rating suitable for correlation with objective indices.

NOTE: SAE J1441 describes a ten point subjective rating scale for vehicle handing. The ratings on the ten point scale of SAE J1411 were developed for comparative evaluations for a given set of conditions and therefore may not be suitable for the subjective evaluation of ride discomfort in terms of a global (i.e., absolute) adjectively anchored psychometric rating scale that can be digitized and correlated with objective indices. For example the adjectives on the SAE J1441 rating scale such as “Good” or “Excellent” are not related to ride discomfort.

5.1.4 SUBJECT EXPERIMENTAL PROTOCOLS: Subject experimental protocols shall be used to minimize repeat-run and subject-to-subject rating variation. This shall include:

- Subject screening with regard to ability to discern different motion and vibration conditions on a gross level (e.g., can the subject detect a difference between an extremely smooth ride and a severely rough ride), ability to place adjectives on a blank rating scale in roughly the same order and spacing as a sample of subjects (e.g., comprehension typicality of the subject), and training (i.e., ability to follow relevant instructions).
- Reporting the ratings as soon as possible (e.g., ideally within a few seconds and always within 1 minute) after exposure to each ride specimen, so that memory effects are minimized.

Include at least one repeat run of each vehicle-ride specimen.

NOTE: The accuracy of the results depends on the frequency bandwidth and time duration of the ride specimen and the number of repeated runs. See note in 5.2.4.

5.1.4.1 Rating Interval and Description. Each human subject shall be exposed to each ride specimen for the same interval of time (or at the same location and distance interval on the road) and at the same target vehicle speed within ± 4 km/h (see 5.2.5). This may be done by using landmarks along the side or on the surface of the road. The subject shall be instructed to ignore all motion and vibration discomfort which occurs before or after the specified interval.

5.1.4.1.1 Rough Roads Ride Events. For rough road ride specimens, the subject shall be instructed to rate the average motion and vibration discomfort during the interval.

5.1.4.1.2 Transient Ride Events. For transient ride specimens, the subject shall be instructed to rate the worst motion and vibration discomfort during the interval.

5.2 Objective Motion and Vibration Measurement

5.2.1 GENERAL: The primary quantity of motion and vibration magnitude shall be acceleration (see 1.1).

NOTE: Sound may influence the perception of motion and vibration discomfort, therefore sound measures such as sound pressure or sound pressure level are also recommended (refer to SAE J1477).

5.2.2 MOTION AND VIBRATION MEASUREMENT

5.2.2.1 Direction. Motion and vibration shall be measured according to an orthogonal rectilinear coordinate system originating at a point from which vibration is considered to enter the human body. The principal relevant basicentric coordinate systems are shown in Figure 2.

If it is not feasible to obtain precise alignment of the motion and vibration transducers with the preferred basicentric axes, the sensitive axes of transducers may deviate from the preferred axes by up to 15 degrees about the y-axis (i.e., pitch) where necessary. For a person seated on an inclined seat, the relevant orientation should be determined by the axes of the body, and the z-axis will not necessarily be vertical with respect to gravity. The orientation of the basicentric axes to the gravitational field should be noted.

Transducers located at each measurement location shall be positioned orthogonally. Translational accelerometers orientated in different axes at a single measurement location shall be as close together as possible. If rotational accelerations are to be calculated from pairs of translational accelerometers, each translational accelerometer in the pair should be separated by as much distance as possible, and both accelerometers shall be attached to a mount which has a lowest resonant frequency in the axis of interest which is greater than the frequency range specified in this recommended practice (see 5.3.3.1.1).

5.2.2.2 Location. Transducers shall be located so as to indicate the motion and vibration at the interface between the human body and the respective vehicle surface. Motion and vibration which is transmitted to the body shall be measured at the interface between the body and that surface.

A minimum of three principal areas shall be used for measurement of motion and vibration of seated occupants: the supporting seat/buttocks surface, the seat/back surface and the floor/feet surface. For drivers, the steering wheel/hands surface shall also be measured. Measurements on the supporting seat/buttocks surface should be made beneath the ischial tuberosities. Measurements on the seat/back surface should be made in the area of principal support of the body. Measurements at the floor/feet should

be made on the surface on which the feet are most often supported. In all cases the location of measurement shall be fully reported.

NOTE: The principal areas of contact between the body and a surface may not always be self-evident.

Motion and vibration which is transmitted to the body from a non-rigid or resilient material (e.g., the seat cushion) shall be measured with the transducer interposed between the person and the principal contact areas of the surface. This should be achieved by securing the transducers within a suitably formed mount which has a lowest resonant frequency in the axis of interest which is greater than the frequency range specified in this recommended practice. The mount should not greatly alter the pressure distribution on the surface of the resilient material. The mount may be covered with a comfort retaining material such that the rated stationary interface discomfort of seated occupants is similar to that which occurs without the mount and its sensors being present. For measurements on non-rigid surfaces, a person shall use a normal position and posture.

NOTE: A commonly used design for accelerometer mount for seat vibration measurements is given in ISO 10326-1.

5.2.3 SIGNAL CONDITIONING: The motion and vibration evaluation procedures for rough road conditions defined in this recommended practice incorporate methods of averaging motion and vibration over time and over frequency bands.

The frequency response of the vibration transducer and associated signal conditioning prior to signal processing shall exhibit deviations no greater than 1 dB from a flat response across the range of frequencies specified in the relevant clauses of this recommended practice.

The dynamic range of the signal-conditioning equipment shall be adequate for the highest and lowest signals recorded. Signals to be recorded for later analysis may first be passed through a low-pass filter of at least sixth order having a cutoff (-3 dB) frequency of approximately 1.5 times the highest frequency of interest in order to maximize the signal-to-noise ratio and the phase characteristic shall be linear within the range of frequencies specified in the relevant clauses of this recommended practice. The signal-to-noise ratio of each channel of the data acquisition system, defined as the ratio of the data acquisition output range to the root-mean-squared signal level of each sensor when the sensor is at rest, electrically excited and connected to the data acquisition system, measured at the output of the data acquisition system, and scaled in the same units as the data acquisition system range, shall be at least 66 dB.

5.2.4 DURATION OF MEASUREMENT: The duration of measurement shall be sufficient to ensure reasonable statistical precision and to ensure that the vibration is typical of the exposures which are being assessed. The duration of measurement shall be reported. The measurement duration shall be a minimum of 8 seconds. The location of the specimen may be defined by using landmarks along the side or on the surface of the road. During the recording, the speed of the vehicle shall be displayed to the driver and shall remain constant to within ± 4 km/h.

NOTE: The choice of measurement duration depends on a number of factors, constraints and tradeoffs, including the type of ride events (e.g., rough road or transient), the availability of suitable over-the-road ride specimens, the ability to

subjectively evaluate the vehicle-ride events, the frequency weighted bandwidth of the driver interface accelerations, and the desired accuracy (refer to Bourne (1993)). It is recommended that the duration of measurement be the same for all ride specimens (i.e., 8 seconds minimum) in order to eliminate the measurement duration as a source of variation in the results when comparing the results to the ratings from a global (i.e., absolute) adjectively anchored psychometric rating scale and to the results from other ride specimens. For stationary random signals, the accuracy depends on the signal bandwidth and measurement duration. For example, to obtain a measurement error of less than 3 dB at a confidence level of 90% requires a minimum duration of 108 seconds for a one-third octave bandwidth signal centered at 1 Hz (i.e., 0.23 Hz total bandwidth). However, it may be not be practical or even feasible to measure over-the-road ride specimens with such long durations, particularly at higher travel speeds or for transient ride events, due either to physical space limitations or the likely presence of (dissimilar types of) transients. Instead it may be more practical and feasible to measure the same vehicle-ride specimen multiple times (e.g., six repeated runs) and assess the accuracy of the results based on the observed run-to-run variation. The number of repeated runs can then be increased until the desired accuracy of the mean value for the vehicle-ride specimen is achieved.

5.2.5 VEHICLE SPEED MEASUREMENT: Vehicle forward speed shall be measured and shall be recorded using the same data acquisition system used for the motion and vibration recording, for purposes of quality control screening of runs and documentation. The speed shall be measured with a sensor within an accuracy of $\pm 1\%$.

5.2.6 REPORTING OF MEASUREMENT CONDITIONS: Proper use of this recommended practice should result in clear documentation of results. This should involve a reference to the appropriate clauses and appendices of this recommended practice and to one or more of the frequency weightings.

Users of this recommended practice should report both the magnitude and duration of any motion and vibration exposure being assessed. If additional evaluation methods are applied both the basic value and the additional value shall be reported. If alternative methods are applied, the methods used shall be clearly reported. If the crest factor is determined, the time period of its measurement should be reported.

The specification of the severity of complex motion and vibration conditions by one, or a few, values should be provided. However, more detailed information on vibration conditions should also be made available. Reports should include information on the frequency content (i.e., vibration spectra), vibration axes, how conditions change over time, and any other factors which may influence the effect.

NOTE: Other factors may also affect human sensitivity to motion and vibration: population type (age, sex, size, fitness, etc.); experience, expectation, arousal, and motivation (e.g., difficulty of task to be performed); body posture; activities (e.g., driver or passenger); financial involvement. Therefore, a jury comprising a representative sample of subjects and recording and/or controlling for such variables by means of suitable protocols is recommended.

5.3 Processing of Vibration Data

5.3.1 BASIC PROCESSING METHOD USING WEIGHTED ROOT-MEAN-SQUARE AND ROOT-MEAN-QUAD ACCELERATION: The vibration processing according to this recommended practice shall always include measurements of the weighted root-mean-square (RMS) acceleration for rough road ride conditions, and root-mean-quad (RMQ) acceleration for transient ride conditions, as defined in this sub clause.

The weighted RMS acceleration is expressed in meters per second squared (m/s^2) for translational vibration and radians per second squared (rad/s^2) for rotational vibration. The weighted RMS acceleration shall be calculated in accordance with the following equation or its equivalents in the frequency domain.

$$\text{RMS}(a_w, T) = \left[\frac{1}{T} \int_0^T a_w^2(t) dt \right]^{\frac{1}{2}} \quad (\text{Eq. 1})$$

where:

$a_w(t)$ = Frequency-weighted translational or rotational acceleration as a function of time (time history), in meters per second squared (m/s^2) or radians per second squared (rad/s^2), respectively;

T = Duration of the measurement, in seconds.

NOTE: It is assumed that the frequency-weighted acceleration has zero mean value.

The weighted RMQ acceleration is expressed in meters per second squared (m/s^2) for translational vibration and radians per second squared (rad/s^2) for rotational vibration. The weighted RMQ acceleration shall be calculated in accordance with the following equation.

$$\text{RMQ}(a_w, T) = \left[\frac{1}{T} \int_0^T a_w^2(t) dt \right]^{\frac{1}{4}} \quad (\text{Eq. 2})$$

Frequency-weighting curves recommended and/or used for the various directions and their applications are listed in [Table 1](#) and discussed in the following sub clauses. Numerical values of the weighting curves are given in [Table 2](#) and exact definitions are given in [Appendix A](#).

5.3.2 APPLICABILITY OF THE BASIC PROCESSING METHOD

5.3.2.1 Categorizing Rough Versus Transient Specimens. The ratio of the RMQ/RMS shall be calculated to determine whether the ride specimen shall be processed using the RMS method for rough roads or the RMQ method for transient ride specimens. If the RMQ/RMS ratio is greater than 1.5, then the ride specimen should be considered to be a transient ride specimen. Otherwise, the ride specimen should be considered to be a rough road ride specimen.

NOTE: The RMQ/RMS ratio for ideal stationary Gaussian random signals is approximately 1.32. See rationale in C.3.3.

TABLE 2 Human discomfort frequency weightings in one-third octaves

Frequency band number ¹⁾ k	Frequency f Hz	W_o factor $\times 1000$	dB	W_b factor $\times 1000$	dB	W_c factor $\times 1000$	dB
-10	0.1	62.4	-24.10	24.4	-32.27	62.4	-24.10
-9	0.125	97.2	-20.25	37.9	-28.42	97.2	-20.25
-8	0.16	158	-16.03	61.7	-24.20	158	-16.03
-7	0.2	243	-12.30	94.6	-20.48	243	-12.30
-6	0.25	364	-8.78	142	-16.96	364	-8.78
-5	0.315	527	-5.56	205	-13.76	527	-5.56
-4	0.4	707	-3.01	275	-11.22	708	-3.01
-3	0.5	842	-1.49	326	-9.73	843	-1.48
-2	0.63	927	-0.65	358	-8.92	929	-0.64
-1	0.8	970	-0.26	372	-8.59	972	-0.24
0	1	987	-0.11	376	-8.49	991	-0.08
1	1.25	995	-0.05	377	-8.47	1000	0.00
2	1.6	998	-0.02	383	-8.34	1007	0.06
3	2	999	-0.01	408	-7.80	1012	0.10
4	2.5	1000	0.00	482	-6.34	1017	0.15
5	3.15	1000	0.00	646	-3.79	1022	0.19
6	4	1000	0.00	868	-1.23	1024	0.20
7	5	1000	0.00	1001	0.01	1013	0.11
8	6.3	1000	0.00	1030	0.26	974	-0.23
9	8	1000	0.00	1001	0.01	891	-1.00
10	10	1000	0.00	952	-0.43	776	-2.20
11	12.5	1000	0.00	885	-1.06	647	-3.79
12	16	1000	0.00	791	-2.03	512	-5.82
13	20	999	-0.01	691	-3.21	409	-7.77
14	25	998	-0.02	586	-4.65	325	-9.76
15	31.5	995	-0.04	481	-6.36	256	-11.84
16	40	987	-0.11	384	-8.31	199	-14.02
17	50	970	-0.26	305	-10.31	156	-16.13
18	63	929	-0.64	234	-12.63	118	-18.53
19	80	842	-1.49	167	-15.52	84.4	-21.47
20	100	707	-3.01	113	-18.96	56.7	-24.94

¹⁾ Index k is the frequency band number according to IEC 1260 for reference purposes only.

NOTE: For tolerances of the frequency weightings, see 5.3.3.1.2.

NOTE: The values have been calculated including frequency band limitation.

TABLE 2 Human discomfort frequency weightings in one-third octaves (continued)

Frequency band number ¹⁾ k	Frequency f Hz	W_d		W_e		W_s	
		factor × 1000	dB	factor × 1000	dB	factor × 1000	dB
-10	0.1	62.4	-24.09	62.5	-24.08	62.4	-24.10
-9	0.125	97.3	-20.24	97.5	-20.22	97.2	-20.25
-8	0.16	158	-16.01	159	-15.98	158	-16.03
-7	0.2	243	-12.28	245	-12.23	243	-12.30
-6	0.25	365	-8.75	368	-8.67	364	-8.78
-5	0.315	530	-5.52	536	-5.41	527	-5.56
-4	0.4	713	-2.94	723	-2.81	708	-3.00
-3	0.5	853	-1.38	862	-1.29	844	-1.48
-2	0.63	944	-0.50	939	-0.55	930	-0.63
-1	0.8	992	-0.07	941	-0.53	974	-0.23
0	1	1011	0.10	880	-1.11	993	-0.06
1	1.25	1008	0.07	772	-2.25	1003	0.03
2	1.6	968	-0.28	632	-3.99	1011	0.09
3	2	890	-1.01	512	-5.82	1017	0.15
4	2.5	776	-2.20	409	-7.77	1022	0.19
5	3.15	642	-3.85	323	-9.81	1024	0.20
6	4	512	-5.82	253	-11.93	1011	0.10
7	5	409	-7.76	202	-13.91	972	-0.24
8	6.3	323	-9.81	160	-15.94	891	-1.00
9	8	253	-11.93	125	-18.03	767	-2.30
10	10	212	-13.91	100	-19.98	638	-3.91
11	12.5	161	-15.87	80.1	-21.93	516	-5.75
12	16	125	-18.03	62.5	-24.08	403	-7.90
13	20	100	-19.99	50.0	-26.02	320	-9.89
14	25	80.0	-21.94	39.9	-27.97	255	-11.88
15	31.5	63.2	-23.98	31.6	-30.01	201	-13.95
16	40	49.4	-26.13	24.7	-32.15	156	-16.12
17	50	38.8	-28.22	19.4	-34.24	123	-18.22
18	63	29.5	-30.60	14.8	-36.62	93.2	-20.62
19	80	21.1	-33.53	10.5	-39.55	66.4	-23.55
20	100	14.1	-36.99	7.07	-43.01	44.6	-27.02

¹⁾ Index k is the frequency band number according to IEC 1260 for reference purposes only.

NOTE: For tolerances of the frequency weightings, see 5.3.3.1.2.

NOTE: The values have been calculated including frequency band limitation.

5.3.2.2. Determination of the Domain-of-Validity. The RMS or RMQ values for each ride specimen should be tested to determine whether it is within the domain-of-validity of the respective ride metric. For each interface, compute the following.

$$z = T(x - x_0) \quad (\text{Eq. 3})$$

where:

z is a p by 1 matrix of z-scores;

p = Number of interface axes ($p=6$ for the seat/buttock interface, $p=3$ otherwise);

x is a p by 1 matrix comprising the natural logarithm of the RMS or RMQ acceleration values;

x_0 = Mean value for x values in the original database used to develop the ride metric;

T is a p by p transformation matrix.

The values for x_0 and T should be determined according to 5.5.3.1.

If $z_{min} < z < z_{max}$ is satisfied, where:

z_{min} and z_{max} are p by 1 matrices that specify the range of z values in the original database used to develop the ride metric;

then the ride specimen given by x is within the domain-of-validity of the ride metric.

The values for z_{min} and z_{max} should be determined according to 5.5.3.2. The results of this test should be reported for each ride specimen along with the ride discomfort value calculated in 5.4.

5.3.3 FREQUENCY WEIGHTING

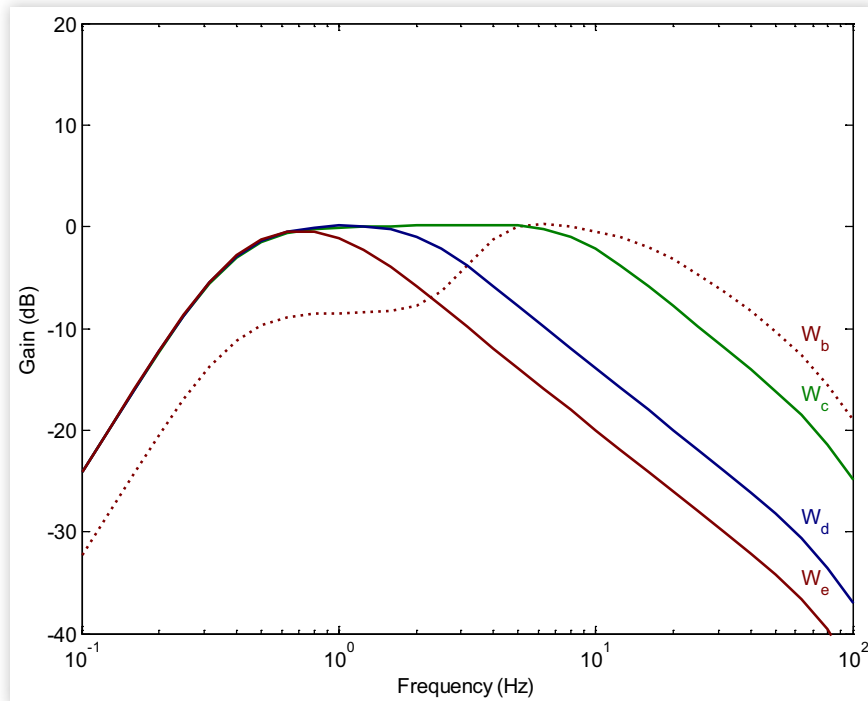
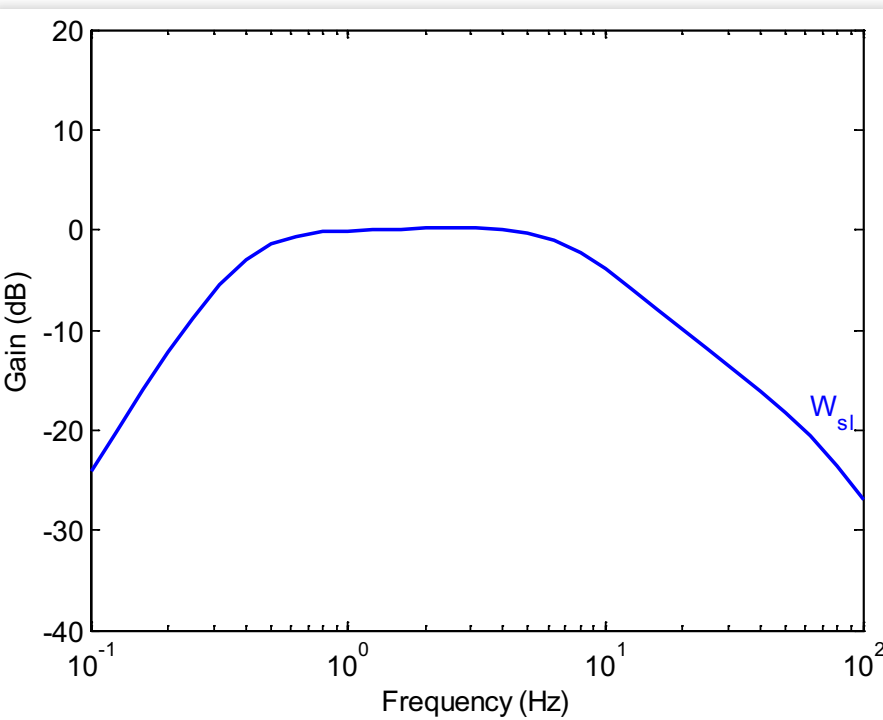
5.3.3.1. Frequency Weighting of Acceleration Time History. For integration of the frequency-weighted acceleration time history, the frequency weighting shall be determined from Tables 1 and 2, as applicable.

The frequency weightings listed in Table 1 for each of the applicable axes and locations of vibration shall be used.

The human discomfort frequency weightings listed in Table 2 for the respective axes shall be used. The corresponding frequency weighting curves are shown in Figures 3 and 4, respectively.

The frequency weightings may be implemented by either analog or digital methods. They are defined in a mathematical form familiar to filter designers, in Appendix A.

The frequency weightings given in Table 2 and illustrated in Figures 3 and 4 include the frequency band limitations. In Appendix A the equations for the frequency band limitation are expressed separately.

FIGURE 3 Frequency weighting curves for human discomfort weightings**FIGURE 4** Frequency weighting curve for steering wheel/hands discomfort weighting

5.3.3.1.1 Frequency Band Limitation. Lower and upper frequency band limitation shall be achieved by two-pole high-pass and low-pass filters, respectively, with Butterworth characteristics having an asymptotic slope of -12 dB per octave. The corner frequencies of the band-limiting filters shall be one-third octave outside the nominal frequency range of the relevant band.

Frequency weightings defined in [Appendix A](#) include the band-limiting filters (high pass at 0.4 Hz and low pass at 100 Hz) which shall be used with weightings W_b , W_c , W_d , W_e , and W_{sl} .

NOTE: The ISO 2631-1 (1997) weighting W_k is within 3 dB the W_b weighting in the 0.4 to 100 Hz frequency range.

5.3.3.1.2 Tolerances. Within the nominal frequency bands and one-third octave from the frequency limits, the tolerance of the combined frequency weighting and band limiting shall be ± 1 dB. Outside this range, the tolerance shall be ± 2 dB. One octave outside the nominal frequency bands, the attenuation may extend towards infinity.

NOTE: Also refer to ISO 8041 concerning tolerances.

5.3.3.2 Frequency Weighting of Acceleration Spectra. The acceleration signal of RMS weighted rough road accelerations may be analyzed and reported as either constant bandwidth or proportional bandwidth (e.g., as one-third octave band) spectra of unweighted acceleration. In the case of one-third octave bands the center frequencies shall be as stated in [Table 2](#). Any form of frequency analysis, analog or digital, direct one-third octave band or summation of narrow band data may be used. The data analysis method shall be consistent with the one-third octave band filter specification given in IEC 1260.

The frequency-weighted RMS acceleration shall be determined by weighting and appropriate addition of narrow band or one-third octave band data.

For the conversion of one-third octave band data, the weighting factors given in [Table 2](#) shall be used. The overall weighted acceleration shall be determined in accordance with the following equation or its digital equivalent in the time or frequency domain:

$$a_w = \left[\sum_k (W_k a_k)^2 \right]^{\frac{1}{2}} \quad (\text{Eq. 4})$$

where:

a_w = Frequency-weighted acceleration;

W_k = Weighting factor for the k th one-third octave band given in [Table 2](#);

a_i = RMS acceleration for the k th one-third octave band.

5.4 Prediction of Discomfort Ratings

5.4.1 ROUGH ROAD RIDE SPECIMENS: The predicted numerical discomfort rating of an occupant interface shall be calculated for a rough road ride specimen as follows:

$$DR_{int} = b_{r,int,0} + \sum_i b_{r,int,i} RMS(a_{w,i}) \quad (\text{Eq. 5})$$

where:

$a_{w,i}$ = Frequency weighted translational or rotational acceleration with respect to axis i , (e.g., $i=x, y, z$);

$b_{r,int,0}$ and $b_{r,int,i}$ are rough road ride interface discomfort model coefficients.

The overall motion and vibration discomfort rating for an occupant shall be calculated for a rough road ride specimen as follows:

$$DR_{omv} = b_{r,omv,0} + \sum_{int} b_{r,omv,int} DR_{int} \quad (\text{Eq. 6})$$

where:

$b_{r,omv,0}$ and $b_{r,omv,int}$ are rough road overall motion and vibration discomfort model coefficients.

The rough road ride discomfort model coefficients in Equations 5 and 6 shall be determined based on data collected from suitable human psychometric experiments as described in 5.1 and 5.2 and the statistical methods as described in 5.5. These coefficients may have different values depending on the occupant type (i.e., driver or passenger), occupant physical characteristics (e.g., age and sex), vehicle market segment and road specimen sample.

NOTE: Sound may influence the perception of motion and vibration discomfort, therefore terms for noise discomfort or sound indices may also be included in Equation 5 (refer to SAE 980585).

5.4.2 TRANSIENT RIDE SPECIMENS: The discomfort rating of an occupant interface shall be calculated for a transient ride specimen as follows:

$$DR_{int} = b_{t,int,0} + \sum_i b_{t,int,i} RMQ(a_{w,i}) \quad (\text{Eq. 7})$$

where:

$a_{w,i}$ = Frequency weighted translational or rotational acceleration with respect to axis i , (e.g., $i=x, y, z$);

$b_{t,int,0}$ and $b_{t,int,i}$ are transient ride interface discomfort model coefficients.

The overall motion and vibration discomfort rating for an occupant shall be calculated for a transient ride specimen as follows:

$$DR_{omv} = b_{t,omv,0} + \sum_{int} b_{t,omv,int} DR_{int} \quad (\text{Eq. 8})$$

The transient ride discomfort model coefficients in Equations 7 and 8 shall be determined based on data collected from suitable human psychometric experiments as described in 5.1 and statistical methods as described in 5.5. These factors may have different values depending on the occupant type (i.e., driver or passenger), occupant physical characteristics (e.g., age and sex), vehicle market segment, and road specimen sample.

NOTE: Sound may influence the perception of motion and vibration discomfort, therefore terms for noise discomfort or sound indices may also be included in Equation 7 (refer to SAE 980585).

5.5 Statistical Method for Determining the Ride Discomfort Models

Determine the rough road and transient ride discomfort model coefficients from experimental data using multi-variable linear regression methods (e.g., Draper and Smith, 1981).

Determine models representing a jury, comprised of several subjects, by combining the regression models for individual subjects. The terms in the models shall be selected to maximize the fit and predictive capability, on average, of the subject models, as quantified by the linear regression RPRED statistic described in 5.5.2.

5.5.1 JURY MODEL: Given the following set of linear regression models for individual (driver or passenger) subjects,

$$y_j = b_{j,0} + \sum_{i=1}^p b_{j,i} x_i, \text{ for } j = 1, m \quad (\text{Eq. 9})$$

where:

y_j = Discomfort rating reported by the j th subject,

x_i are the model inputs (either frequency weighted accelerations or interface discomfort ratings),

p = Number of model inputs,

$b_{j,0}$ and $b_{j,i}$ are the subject model coefficients, and

m = Number of subjects,

calculate the jury model coefficients as follows:

$$b_0 = \frac{1}{m} \sum_j^m b_{j,0} \quad (\text{Eq. 10})$$

$$b_i = \frac{1}{m} \sum_j^m b_{j,i} \quad (\text{Eq. 11})$$

5.5.2 RPRED STATISTIC: Calculate the RPRED statistic of a candidate linear regression model according to the equation:

$$RPRED_j = 1 - \frac{PRESS_j}{SS_{TOT,j}} \quad (\text{Eq. 12})$$

$$PRESS_j = \sum_{k=1}^{n_j} (y_{j,k} - \hat{y}_{j,k,-k})^2 \quad (\text{Eq. 13})$$

$$SS_{TOT,j} = \sum_{k=1}^{n_j} (y_{j,k} - \bar{y}_j)^2 \quad (\text{Eq. 14})$$

$$\bar{y}_j = \frac{1}{n_j} \sum_{k=1}^{n_j} y_{j,k} \quad (\text{Eq. 15})$$

where:

$y_{j,k}$ = Reported discomfort rating value of the k th data observation for the j th subject,

$\hat{y}_{j,k,-k}$ the discomfort rating value predicted by the candidate model estimated with the k th data observation removed, and

n_j = Number of observations for the j th subject.

The jury average RPRED statistic shall be calculated as follows:

$$RPRED_{jury} = \frac{1}{m} \sum_j RPRED_j \quad (\text{Eq. 16})$$

The ride discomfort ratings shall be predicted by jury models with large values for $RPRED_{jury}$.

5.5.3 DOMAIN-OF-VALIDITY: Determine the magnitude domain-of-validity of each interface discomfort model comprising the ride metric as follows:

5.5.3.1 Z-Score Transformation Parameters. Compute the following for each ride specimen in the database used to estimate the interface discomfort model:

$$\mathbf{x}_k = \begin{bmatrix} \ln(\text{RMS or RMQ acceleration of axis 1}) \\ \ln(\text{RMS or RMQ acceleration of axis 2}) \\ \vdots \\ \ln(\text{RMS or RMQ acceleration of axis } p) \end{bmatrix} \quad (\text{Eq. 17})$$

where:

\mathbf{x}_k is a p by 1 matrix,

k = Index of the ride specimen,

p = Number of interface axes ($p=6$ for the seat/buttock interface, $p=3$ otherwise).

Compute the mean value for \mathbf{x}_k in the database according to the equation:

$$\mathbf{x}_0 = \frac{1}{n} \sum_{k=1}^n \mathbf{x}_k \quad (\text{Eq. 18})$$

where:

n = Number of ride specimen used to estimate the ride metric model coefficients.

Compute a p by p matrix \mathbf{C} (representing the covariance of x_k) according to the equation:

$$\mathbf{C} = \frac{1}{n-1} \sum_{k=1}^n (\mathbf{x}_k - \mathbf{x}_0)(\mathbf{x}_k - \mathbf{x}_0)^T \quad (\text{Eq. 19})$$

Compute the eigenvalues and eigenvectors of \mathbf{C} such that:

$$\mathbf{CV} = \mathbf{VD} \quad (\text{Eq. 20})$$

where:

\mathbf{D} is a p by p diagonal matrix comprising the eigenvalues of \mathbf{C} , ordered such that:

$$D_{1,1} \geq D_{2,2} \geq \dots > 0$$

\mathbf{V} is a p by p matrix comprising the corresponding eigenvectors of \mathbf{C} .

NOTE: The eigenvalues and eigenvectors of \mathbf{C} can be computed using the EISPACK routine RS (Smith et al., 1976), LAPACK routine DSYEVR (Anderson et al., 1999) or other equivalent computer software.

Compute the p by p transformation matrix \mathbf{T} according to the equation:

$$\mathbf{T} = \mathbf{D}^{-1/2} \mathbf{V}^{-1} \quad (\text{Eq. 21})$$

5.5.3.2 Z-Score Domain-of-Validity. Compute the z-scores for each ride specimen in the original database according to the equation:

$$\mathbf{z}_k = \mathbf{T}(\mathbf{x}_k - \mathbf{x}_0) \quad (\text{Eq. 22})$$

The method in 5.3.3.3 may be used to compute \mathbf{z}_{min} and \mathbf{z}_{max} if the z-scores are normally distributed; otherwise, use the method in 5.3.3.4.

5.5.3.3 Normally Distributed Z-Score Limits. Compute the standard deviation of each element of the z-scores as follows:

$$s_i = \sqrt{\frac{1}{n-1} \sum_{k=1}^n z_{k,i}^2} \quad (\text{Eq. 23})$$

Determine $t_{0.005,n-1}$, the critical value for the 0.005 tail area probability of t-distribution with $n - 1$ degrees-of-freedom.

If $n > 120$ use the following approximation,

$$t_{0.005,n-1} = 2.576$$

NOTE: The value for $t_{0.005,n-1}$ can be found in Table B1 of Box (1978) or other equivalent table.

Then, compute z_{min} and z_{max} according to the equation:

$$\begin{aligned} z_{min,i} &= t_{0.005,n-1} s_i \\ z_{max,i} &= t_{0.995,n-1} s_i \end{aligned} \quad (\text{Eq. 24})$$

5.5.3.4 Not Normally Distributed Z-Score Limits. If the distribution of z-scores is not normally distributed, then the following method may be used to calculate z_{min} and z_{max} . For each element of \mathbf{z} sort the n values for $z_{k,i}$ from the smallest to the largest value. Then determine the 0.5th and 99.5th percentile values as follows:

$$\begin{aligned} z_{min,i} &= z_{k_{min,i}} \\ z_{max,i} &= z_{k_{max,i}} \end{aligned} \quad (\text{Eq. 25})$$

where:

$$\begin{aligned} k_{min,i} &= \text{nearest integer}\left(0.005(n+1)\right) \\ k_{max,i} &= \text{nearest integer}\left(0.995(n+1)\right) \end{aligned} \quad (\text{Eq. 26})$$

where nearest integer(x) indicates to round x to the nearest integer value.

6. Notes

6.1 Revision Indicator

A change bar (l) located in the left margin is for the convenience of the user in locating areas where technical revisions, not editorial changes, have been made to the previous issue of this document. An (R) symbol to the left of the document title indicates a complete revision of the document, including technical revisions. Change bars and (R) are not used in original publications, nor in documents that contain editorial changes only.

PREPARED BY THE SAE VEHICLE DYNAMICS STANDARDS COMMITTEE

APPENDIX A - MATHEMATICAL DEFINITION OF THE FREQUENCY WEIGHTINGS

A.1 Parameters of the Transfer Functions

The parameters of the transfer functions are given in [Table A1](#).

TABLE A1 - Parameters of the transfer functions of the human discomfort frequency weightings

Weighting	Band-limiting		Acceleration-velocity transition (a-v transition)			Upward step			
	f_1 Hz	f_2 Hz	f_3 Hz	f_4 Hz	Q_4	f_5 Hz	Q_5	f_6 Hz	Q_6
W_o	0.4	100	-	-	-	-	-	-	-
W_b	0.4	100	16.0	16.0	0.55	2.5	0.90	4	0.95
W_c	0.4	100	8.0	8.0	0.63	-	-	-	-
W_d	0.4	100	2.0	2.0	0.63	-	-	-	-
W_e	0.4	100	1.0	1.0	0.63	-	-	-	-
W_{sl}	0.4	100	6.3	6.3	0.63	-	-	-	-

NOTE: The W_{sl} weighting specified by the parameters in [Table A1](#) is a realizable analytic approximation for the asymptotic W_s weighting reported by Giacomin et al. (2004) within the 0.5 to 80 Hz frequency range.

A.2 Transfer Functions

The frequencies f_1, \dots, f_6 and the resonant quality factors Q_4, \dots, Q_6 are parameters of the transfer function which determine the overall frequency weighting (referred to acceleration as the input quantity). The transfer function is expressed as a product of several factors as follows.

Band-limiting (two-pole filter with Butterworth characteristic).

High pass:

$$|H_h(s)| = \left| \frac{s^2}{s^2 + \sqrt{2}\omega_1 s + \omega_1^2} \right| = \sqrt{\frac{f^4}{f^4 + f_1^4}} \quad (\text{Eq.A1})$$

where:

$s = j2\pi f$ is the imaginary angular frequency where $j = \sqrt{-1}$;

f = Frequency in Hz;

$\omega_1 = 2\pi f_1$;

f_1 = Corner frequency in Hz (intersection of asymptotes).

Low pass:

$$|H_l(s)| = \left| \frac{\omega_2^2}{s^2 + \sqrt{2}\omega_2 s + \omega_2^2} \right| = \sqrt{\frac{f_2^4}{f^4 + f_2^4}} \quad (\text{Eq. A2})$$

where:

$$\omega_2 = 2\pi f_2;$$

f_2 = corner frequency in Hz.

Acceleration-velocity transition (proportionality to acceleration at lower frequencies, proportionality to velocity at higher frequencies):

$$|H_t(s)| = \left| \frac{s + \omega_3}{s^2 + \frac{\omega_4}{Q_4} s + \omega_4^2} \cdot \left(\frac{\omega_4^2}{\omega_3} \right) \right| = \sqrt{\frac{f^2 + f_3^2}{f_3^2}} \cdot \sqrt{\frac{f_4^4 \cdot Q_4^2}{f^4 \cdot Q_4^2 + f^2 \cdot f_4^2 (1 - 2Q_4^2) + f_4^4 \cdot Q_4^2}} \quad (\text{Eq. A3})$$

where:

$$\omega_3 = 2\pi f_3;$$

$$\omega_4 = 2\pi f_4.$$

Upward step (steepness approximately 6 dB per octave, proportionality to jerk):

$$|H_s(s)| = \left| \frac{s^2 + \frac{\omega_5}{Q_5} s + \omega_5^2}{s^2 + \frac{\omega_6}{Q_6} s + \omega_6^2} \right| = \frac{Q_6}{Q_5} \cdot \sqrt{\frac{f^4 \cdot Q_5^2 + f^2 \cdot f_5^2 (1 - 2Q_5^2) + f_5^4 \cdot Q_4^2}{f^4 \cdot Q_6^2 + f^2 \cdot f_6^2 (1 - 2Q_6^2) + f_6^4 \cdot Q_6^2}} \quad (\text{Eq. A4})$$

where:

$$\omega_5 = 2\pi f_5;$$

$$\omega_6 = 2\pi f_6.$$

The product $H_h(s) \cdot H_l(s)$ represents the band-limiting transfer function; it is the same for all weightings.

The product $H_t(s) \cdot H_s(s)$ represents the actual weighting transfer function for a certain application.

$H_t(s) = 1$ for weighting W_o ;

$H_s(s) = 1$ for weighting W_o , W_c , W_d and W_e .

This is indicated by the absence of quality factors in the tables.

The total weighting function is:

$$H(s) = H_h(s) \cdot H_l(s) \cdot H_t(s) \cdot H_s(s) \quad (\text{Eq. A5})$$

In the most common interpretation of this equation (in the frequency domain) it describes the modulus (magnitude) and phase in the form of a complex number as a function of the imaginary angular frequency, $s = j2\pi f$.

NOTE: Sometimes the symbol p is used instead of s . If the equation is interpreted in the time domain then s represents $\frac{d}{dt}$ (the differential operator). This then leads directly to the digital realization of the weighting, where $\frac{d}{dt}$ is approximated by $\frac{\Delta}{\Delta t}$ provided the sampling interval Δt is small enough. Alternately s may be interpreted as the variable of the Laplace transform.

The weighting curves in [Figures 2](#) and [3](#) show the modulus (magnitude) of H (i.e., $|H|$) versus the frequency f in a double-logarithmic scale.

APPENDIX B - OTHER PUBLICATIONS

Anderson, E., et al. (1999), LAPACK Users' Guide, Third Edition, Society for Industrial and Applied Mathematics, Philadelphia, PA.

Bennett, C.A., and Franklin, N.L. (1954) Statistical Analysis in Chemistry and the Chemical Industry, John Wiley & Sons, New York.

Bongers, P.M., Boshuizen, H.C., Hulshof, C.T.J., Koerneester, A.P. (1988) Exposure to vibration and back disorders in crane operators. *Int. Arch. Occup. Environ. Health*, 60, pp. 129-137.

Bongers, P.M., Hulshof, C.T.J., Groenhout, H.J., Dijkstra, L., Boshuizen, H.C., Valken, E. (1990) Backpain and exposure to whole-body vibration in helicopter pilots. *Ergonomics*, 33, pp. 1007-1026.

Bongers P.M., Boshuizen H.C. (1990) Back disorders and whole-body vibration at work. Published: Thesis University of Amsterdam, Amsterdam.

Boshuizen, H.C., Hulshof, C.T.J., Bongers, P.M. (1990) Long-term sick leave and disability pensioning of tractor drivers exposed to whole-body vibration. *Int. Arch. Occup. Environ. Health*, 62, pp. 117-122.

Boshuizen, H.C., Bongers, P.M., Hulshof, C.T.J. (1990) Self-reported back pain in tractor drivings exposed to whole-body vibration. *Int. Arch. Occup. Environ. Health*, 62, pp. 109-115.

Boshuizen, H.C., Bongers, P.M., Hulshof, C.T.J. (1992) Self-reported back pain of fork-lift truck and freight-container tractor drivers, exposed to whole-body vibration. *Spine*, 17, pp. 59-67.

Bourne, S.M., Zellner, J.W., Matthews, C.C. (1993) On the methodology for development of discomfort models for passenger car rough road ride, C466/035/93, Institute of Mechanical Engineers.

Bovenzi, M., Zadjni, A. (1992) Self-reported back symptoms in urban bus drivers exposed to whole-body vibration. *Spine*, 17(9), pp. 1048-1059.

Bovenzi, M., Betta, A. (1994) Low-back disorders in agricultural tractor drivers exposed to whole-body vibration and postural stress. *Applied Ergonomics*, 25, pp. 231-240.

Box, G.E.P, Hunger, W.G., Hunter, J.S. (1978) Statistics for Experimenters, John Wiley & Sons, New York.

Broyde, F., Donati, P., Galmiche, J.P. (1989) Assessing the discomfort of whole-body vibration containing transients: r.m.s. or r.m.q. method? Proceedings of the meeting on Human Response to Vibration, AFRC, Silsoe, UK.

Christ, E., Brusl, H., Donati, P., Griffin, M., Hohmann, B., Lundström, R., Meyer, J., Straatsa, H. (1989) Vibration at work. Published by the International research section of ISSA¹.

Corbridge, C., Griffin, M.J. (1986) Vibration and comfort: vertical and lateral motion in the range 0,5 to 5,0 Hz. *Ergonomics*, 29(2), pp. 249-272.

¹ Institut national de recherche et de sécurité (INRS), 30, rue Olivier-Noyer, 75680 Paris, Cedex 14, France.

- Corbridge, C., Griffin, M.J. (1991) Effects of vertical vibration on passenger activities: writing and drinking. *Ergonomics*, 34(10), pp. 1313-1332.
- Donati, P., Grosjean, A., Mistrot, P., Roure, L. (1983) The subjective equivalence of sinusoidal and random whole-body vibration in the sitting position (an experimental study using the floating reference vibration method). *Ergonomics*, 26(3), pp. 251-273.
- Draper, N.R., Smith, H. (1981) *Applied Regression Analysis*, John Wiley & Sons, New York.
- Dupuis H., Christ, E. (1972) Untersuchung der Möglichkeit von Gesundheitsschädigungen im Bereich der Wirbelsäule bei Schlepperfahren. Max-Planck-Institut für Landarbeit und Landtechnik, Bad Kreuznach, Report Heft A 72/2.
- Dupuis, H., Zerlett, G. (1984) Beanspruchung des Menschen durch mechanische Schwingungen. BG Schriftenreihe des Hauptverbandes der gewerblichen Berufsgenossenschaften e.V.
- Dupuis, H., Zerlett, G. (1986) *The effects of whole-body vibration*. Springer-Verlag, Berlin/Heidelberg/New York/Tokyo.
- Eaton, S. (2003) Bus driver & human vibration, ARCS Reference No. 0135-20, Worker's Compensation Board of BC, Vancouver.
- Fairley, T.E., Griffin, M.J. (1988) Predicting the discomfort caused by simultaneous vertical and fore-and-aft whole-body vibration. *Journal of Sound and Vibration*, 124(1), pp. 141-156.
- Giacomin, J., Shayya, M.S., Dormegnie, E., Richard, L. (2004) Frequency weighting for the evaluation of steering wheel rotational vibration, *International Journal of Industrial Ergonomics*, 33, pp 527-541.
- von Gierke, H.E., Brammer, A.J. (1996) Effects of shock and vibration on humans. In: *Shock and vibration handbook*. (Harris C.M., ed.). McGraw Hill, New York.
- Grenander, U., Pollak, H. O., and Slepian, D. (1959). The distribution of quadratic forms in normal variates: A small sample theory with applications to spectral analysis. *Journal of the Society for Industrial and Applied Mathematics*, 7(4), 374-401.
- Griffin, M.J. (1976) Subjective equivalence of sinusoidal and random whole-body vibration. *The Journal of the Acoustical Society of America*, 60(5), pp. 1140-1145.
- Griffin, M.J. (1990) *Handbook of human vibration*. Academic Press, London/New York.
- Griffin, M.J. (1988) International Standard 2631 and British Standard 6841: A comparison of two guides to the measurement and evaluation of human exposure to whole-body vibration and repeated shock. *Proceedings of joint French-British Meeting, Groupe Français des Études des Effets des Vibrations sur l'Homme and UK Informal Group on Human Response to Vibration*, INRS, Vandoeuvre, France.
- Griffin, M.J., Whitham, E.M. (1980) Discomfort produced by impulsive whole-body vibration. *Journal of the Acoustical Society of America*, 68(5), pp. 1277-1284.
- Gruber, G.J. (1976) Relationships between whole-body vibration and morbidity patterns among interstate truck drivers. U.S. Department of Health, Education and Welfare

(DREW) of the National Institute for Occupational Safety and Health (NIOSH). Publication No. 77-167.

Gruber, G.J., Ziperman, H.H. (1974) Relationship between whole-body vibration and morbidity patterns among motor coach operators. U.S. Department of Health, Education and Welfare (DREW) of the National Institute for Occupational Safety and Health (NIOSH). Publication No. 75-104.

Guignard, J.C. (1985) Vibration. In: Patty's Industrial Hygiene and Toxicology, Biological Responses. (Lewis Cralley and Lester Cralley, eds.). John Wiley, Vol. 3B, 2nd edn., pp. 653-724.

Guignard, J.C., Landruivi, G.J., Reardon, E. (1976) Experimental evaluation of international standard ISO 2631-1974 for whole-body vibration exposures. University of Dayton Research Institute (UDRI). Technical Report 76-79.

Heide, R., Seidel, H. (1978) Folgen langzeitiger beruflicher Ganzkörpervibrationsexposition (Kurzfassung einer Literaturstudie). Consequences of long-term occupational exposure to whole-body vibration (an abridged literature survey). Zeitschrift für die gesamte Hygiene und ihre Grenzgebiete, 24(3), pp. 153-159.

Howarth, H.V.C., Griffin, M.J. (1987) The frequency dependence of subjective reaction to vertical and horizontal whole-body vibration at low magnitudes. The Journal of the Acoustical Society of America, 83(4), pp. 1406-1413.

Howarth, H.V.C., Griffin, M.J. (1990) Subjective Response to Combined Noise and Vibration: Summation and Interaction Effects. Journal of Sound and Vibration, 143(3), pp. 443-454.

Howarth, H.V.C., Griffin, M.J. (1991) Subjective reaction to vertical mechanical shocks of various waveforms. Journal of Sound and Vibration, 147(3), pp. 395-408.

Hulshof, C.T.J., Veldhuyzen Van Zanten, O.B.A. (1987) Whole-body vibration and low-back pain. A review of epidemiologic studies. Int. Arch. Occup. Environ. Health, 59, pp. 205-220.

Kelsey, J.L., Githens, P.B., O'Conner, T., Wei, J.U., Calogero, J.A., Holford, T.R., White, A.A., Walter, S.D., Ostfeld, A.M., Southwick, W.O. (1984) Acute prolapsed lumbar intervertebral disc. An epidemiologic study with special reference to driving automobiles and cigarette smoking. Spine, 9(6), pp. 608-613.

Kelsey, J.L., Hardy, R.J. (1975) Driving of motor vehicles as a risk factor for acute herniated lumbar intervertebral disc. American Journal of Epidemiology, 102(1), pp. 63-73.

Kjellberg, A., Wikstrom, B.-O. (1985) Subjective reactions to whole-body vibration of short duration. Journal of Sound and Vibration, 99(3), pp. 415-424.

Kjellberg, A., Wikstrom, B.-O., Dimberg, U. (1985) Whole-body vibration: exposure time and acute effects — experimental assessment of discomfort. Ergonomics, 28(3), pp. 545-554.

McDonnell, J.D. (1968) Pilot Rating Techniques for the Estimation of Handling Qualities. AFFDL-TR-68-76. Air Force Flight Dynamics Laboratory. Wright Patterson Air Force Base, Ohio.

- Miller, J.L., The Role of the Bandwidth-Duration Product WT in the Detectability of Diotic Signals, Ph.D. Thesis, Victoria University of Wellington, New Zealand, 1999.
- Mistrot, P., Donati, P., Galmiche, J.P., Florentin, D. (1990) Assessing the discomfort of the whole-body multi-axis vibration: laboratory and field experiments. *Ergonomics*, 33(12), pp. 1523-1536.
- Miwa, T. (1967) Evaluation methods for vibration effect. Part 1: Measurements of threshold and equal sensation contours of whole body for vertical and horizontal vibrations. *Industrial Health*, 5, pp. 183-205.
- Miwa, T., Yonekawa, Y. (1969) Evaluation methods for vibration effect. Part 9: Response to sinusoidal vibration at lying posture. *Industrial Health*, 7, pp. 116-126.
- Parsons, K.C., Griffin, M.J. (1978) The effect of the position of the axis of rotation on the discomfort caused by whole-body roll and pitch vibrations of seated persons. *Journal of Sound and Vibration*, 58(1), pp. 127-141.
- Parsons, K.C., Griffin, M.J. (1988) Whole-body vibration perception thresholds. *Journal of Sound and Vibration*, 121(2), pp. 237-258.
- Sandover, J. (1983) Dynamic loading as a possible source of low-back disorders. *Spine*, 8(6), pp. 652-658.
- Sandover, J. (1988) Behaviour of the spine under shock and vibration. A review. *Clinical Biomechanics*, 3, pp. 249-256.
- Seidel, H., Bastek, R., Bräuer, D., Buchholz, Ch., Meister, A., Metz, A.-M., Rothe, R. (1980) On human response to prolonged repeated whole-body vibration. *Ergonomics*, 23(3), pp. 191-211.
- Seidel, H., Heide, R. (1986) Long-term effects of whole-body vibration. A critical survey of the literature. *Int. Arch. of Occup. Environ. Health*, 58, pp. 1-26.
- Seidel, H., Bluthner R., Hinz, B. (1986) Effects of whole-body vibration on the lumbar spine: the stress-strain relationship. *Int. Arch. Occup. Environ. Health*, 57, pp. 207-223.
- Shoenberger, R.W. (1975) Subjective response to very low-frequency vibration. *Aviation, Space and Environmental Medicine*, 46(6), pp. 785-790.
- Shoenberger, R.W., Harris, C.S. (1971) Psychophysical assessment of whole-body vibration. *Human Factors*, 13(1), pp. 41-50.
- Smith, B.T., Boyle, J.M., Dongarra, J.J. (1976) Matrix eigensystem routines — EISPACK guide, Lecture Notes in Computer Science, Springer-Verlag, Berlin.
- Spear, R.C., Keller, C., Behrens, V., Hudes, M., Tarter, D. (1976) Morbidity patterns among heavy equipment operators exposed to whole-body vibration, U.S. Department of Health, Education and Welfare (DREW) of the National Institute for Occupational Safety and Health (NIOSH). Publication No. 77-120.
- Spång, K. (1997) Assessment of whole-body vibration containing single event shocks. *Noise Control Eng. J.*, 45(1), pp. 19-25.

APPENDIX C - SUPPORTING RATIONALE

C.1 Introduction

This appendix indicates the current state of technology regarding the relationship between the vibration magnitude and human discomfort. The appendix is concerned with providing a uniform and convenient method of indicating the subjective severity of the motion and vibration but does not present limits. It is in no way related to quantifying health and safety aspects of motion and vibration for which an entirely different methodology would be needed. This methodology is intended to predict human sensitivity to motion and vibration for comparative purposes (i.e., condition A versus condition B) relative to a global (i.e., absolute) adjectival psychometric scale.

C.2 Discomfort

C.2.1 ENVIRONMENTAL CONTEXT: A particular motion and vibration condition may be considered to cause severe discomfort in one situation but may be classified as little discomfort in another. Many factors combine to determine the degree to which discomfort may be noted or tolerated. Discomfort expectations and annoyance tolerance are quite different among various categories and market segments of vehicles, and in different regions (e.g., from the viewpoint of user demographics, highway design, maintenance, wear, and weathering, etc.), and this must be accounted for in the design of experiment and vehicle, road and human subject sample selection.

C.3 Objective Assessment of Motion and Vibration Discomfort

C.3.1 USE OF WEIGHTED RMS ACCELERATION: For rough road ride specimens, for example when the RMQ/RMS ratio is less than 1.5, it is possible to evaluate the effects of vibration on human discomfort by using the frequency-weighted RMS acceleration (weighted according to [Tables 1](#) and [2](#)). The RMS is related to the 2nd statistical moment of the acceleration and is a measure of on-the-average acceleration magnitude. Provided the acceleration data are stationary and normally distributed the RMS and RMQ values tend to be proportional; however the RMS value is less sensitive to the peak values and has less run-to-run variation than the RMQ value, resulting in better fit and predictive capability (as noted in Bourne (1993, Fig 7) and Griffin (1990, p 85)).

The RMS can also be calculated in the frequency domain, which may be advantageous for the diagnosis of rough road ride discomfort.

NOTE: It is recognized that the crest factor is an uncertain method of deciding whether or not the acceleration data have sufficiently stationary characteristics and that the RMS acceleration can be used to assess human response to vibration. In case of doubt the ride specimen should be treated as a rough road ride specimen (5.4.1) if the RMQ/RMS ratio is less than 1.5, and the ride specimen should be treated as a transient ride specimen (5.4.2) if the RMQ/RMS ratio is greater than 1.5. See C.3.3.

C.3.2 USE OF WEIGHTED RMQ ACCELERATION: For transient ride specimens, for example when the RMQ/RMS ratio is larger than 1.5, it is preferred to evaluate the effects of vibration on human discomfort using the frequency-weighted RMQ acceleration instead of RMS acceleration. The RMQ is related to the 4th statical moment of the acceleration, which is descriptive of the presence of contaminants (as noted in Bennett (1954)) or narrow band processes, and more heavily weights larger amplitude accelerations.

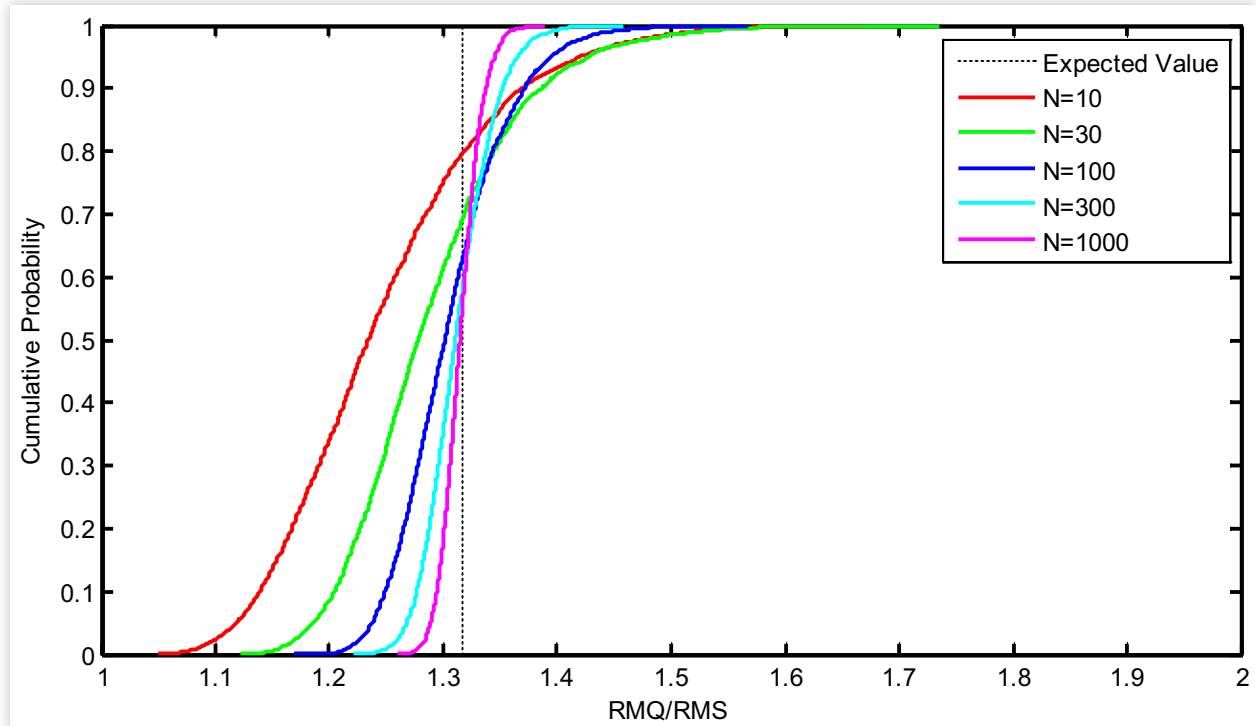
NOTE: Discomfort can be significantly influenced by peak values and underestimated by methods involving RMS averaging.

NOTE: Odd numbered moments would imply asymmetric human sensitivity to positive and negative accelerations for which there is no known supporting data. Higher statistical moments, such as the maximum or peak acceleration, would measure the most extreme acceleration, but may have increased run-to-run variation that is not correlated with human perception of discomfort.

Vibration values obtained in one environment may be compared with those obtained in another environment so as to compare the discomfort.

C.3.3 USE OF RMQ/RMS RATIO FOR CATEGORIZING ROUGH VERSUS TRANSIENT SPECIMENS: The RMQ/RMS ratio is equal to the fourth root of the kurtosis statistic of the washout weighted acceleration and is related to the weighed RMS and RMQ accelerations ([Equations 1](#) and [2](#)). Ideal stationary random band limited signals tend to have a Gaussian distribution due to the averaging over time involved in band limiting (i.e., filtering) according to the Central Limit Theorem. The expected value for the RMQ/RMS ratio for ideal stationary Gaussian random signals is approximately 1.32, however actual values will tend to vary from this value depending on the bandwidth of the data (B) times the signal duration time interval (T). [Figure C1](#) illustrates the cumulative probability distribution of the RMQ/RMS ratio for degrees-of-freedom N varying from 10 to 1000, based on simulation. The number of degrees-of-freedom N is approximately equal to $2 \cdot B \cdot T$ where B is the bandwidth in hz and T is the duration in second (Grenander et al 1959; Miller 1999). The distributions in [Figure C1](#) indicate that if the signal is a stationary Gaussian signal then the probability of the RMQ/RMS ratio being greater than 1.5 is small (i.e., less than 0.05). Therefore if the RMQ/RMS ratio is greater than 1.5 then it is statistically unlikely that the signal is a stationary Gaussian signal. Light passenger vehicle transient ride specimens with W_o frequency weighting tend to have a RMQ/RMS ratio greater than 1.5.

FIGURE C1 Cumulative probability Distribution of RMQ/RMS ratio for an ideal stationary Gaussian random signal with N degrees-of-freedom



C.3.4 USE OF FREQUENCY WEIGHTINGS: Simulator experiments reported in SAE 860047 and by others have demonstrated that the human sensitivity to discomfort depends on the frequency of the vibration.

index

- A-arm front suspension, 195
Acceleration control input, 365
Acceleration *vs.* static deflection, 396–398
Ackerman geometry, 158, 159
Ackermann error, 342
Active suspensions
dive control, 217
full-active suspensions, 216
height control, 216–217
passive suspensions, 215
performance, 217–218
ride control, 216
road holding, 217
roll control, 217
self-leveling suspensions, 215–216
semi-active suspensions, 216
squat control, 217
Air dams, 78
Air spring suspensions, 126–127
Aligning moment offset (M_{ZT0}), 357
Anti-lock brake systems, 57–58
Automatic control input, 365
Axis and coordinate systems, 316
earth-fixed axis system, 316
earth-fixed coordinate system, 317
ground plane, 316
inertial reference, 316
intermediate axis system, 317
ISO 8855 axis orientation, 314
reference frame, 316
road plane, 316
road surface, 316
SAE J670 axis orientation, 314
schematic diagram, 314, 315
tire axis system, 317, 318
tire coordinate system, 319
vehicle axis system, 317
vehicle coordinate system, 317
vehicle plane of symmetry, 316
vehicle reference point, 317
wheel axis system, 318, 319
wheel coordinate system, 319
Z-Down orientation, 314
Z-Up orientation, 314
Axis discomfort ratings, 440
Bandwidth, 367
Basicentric axes of human body, 445, 446
Brakes
anti-lock brake system, 345
components, 346
definition, 345
disc brake, 345
drum brake, 345
friction brake, 345
pressure, 346
proportioning, 346
regenerative brake, 345
torque, 346
Braking control input, 365
Braking performance
aerodynamic drag, 44
anti-lock brake systems, 57–58
basic equations, 41
brake factor, 45–47
comprehensive analysis, 42
constant deceleration, 42
deceleration with wind
resistance, 43
driveline drag, 44
drum brake and disc brake, 45
duo-servo brake, 46
efficiency, 58–59
energy/power, 43
Federal requirements, 51–52
front and rear braking force, 42
inertia dynamometer torque
measurements, 46
pedal force gain, 61–62
proportioning
brake force, 55
deceleration, 52
definition, 52, 55
FMVSS 105 braking standard, 55
inertia-proportioning valve, 56
instability, 55
load-sensing proportioning
valves, 56
maximum brake force, 52–54
peak coefficient of friction, 52
pressure proportioning valves, 56
proportioning design, 55
rear *vs.* front brake forces, 54–56
rear wheel lockup, 59–61
road grade, 44–45
rolling resistance, 44
“self-servo” action, 46
tire-road friction
adhesion component, 47
adhesive and hysteretic
friction, 48
adhesive friction contribution, 48
braking coefficient *vs.* slip, 49
braking deformations, 48
bulk hysteresis mechanism, 48
inflation pressure, 49
peak coefficient, 48
primary mechanisms, 47, 48
surface adhesion, 47
velocity, 49
vertical load, 49
torque performance, 46
Bumper spoilers, 78
Cars and trucks, acceleration
capabilities, 23
circa 1769, first motor vehicle, 1, 2
Conicity aligning moment
($M_{ZT(CON)}$), 357
Conicity lateral force ($F_{YT(CON)}$), 356
Conicity residual aligning moment
($M_{ZTR(CON)}$), 358
Constant radius method, 182–183
Constant speed method, 183–184
Control response, 366
Control system input, 365
Cornering stiffness, 288
Crosswind sensitivity
aerodynamic properties, 87
crosswind lateral acceleration
response, 87, 89
neutral steer point, 87, 89
tire cornering stiffness, 89
tire properties, 88
vehicle’s passive crosswind
response, 88
yaw rate response, 87, 88
“d’Alembert force,” 10
Deck lid spoilers, 78
de Dion system, 193–194

- Disc brake, 45
 Discomfort expectations and annoyance tolerance, 469
 Discomfort model, 440
 Disturbance input, 365
 Disturbance response, 366
 Driver control input, 365
 Driver settings, 365
 Drum brake, 45
 Duo-servo brake, 46
 Dynamic axle loads
 aerodynamic or acceleration effects, 12
 composite mass, 13
 downhill attitude, 11
 forces acting on vehicle under arbitrary conditions, 10
 loads on grades, 12
 low-speed acceleration, 11
 moments of inertia, 13–14
 Road Grade, 12
 static loads on level ground, 11
 uphill attitude, 11
- Earth-fixed coordinate system, 8–9
 Electronic stability control (ESC), 253, 266–267
 Equivalent time of initiation, 366
 Euler angles, 9
- Federal Motor Vehicle Safety Standards (FMVSS), 51, 264
 Fishhook maneuver, 269–271
 Forced vibration
 with coulomb damping, 416–417
 with viscous damping
 absolute amplitude ratio, 411–414
 amplitude ratio, 410
 equivalent impedance, 410–411
 magnification factor curves, 408
 peak exciting force constant, 407–409
 relative amplitude ratio, 414–416
 undamped natural frequency, 410
 Forces and moments, 328–329
 Four-link rear suspension, 193
 Four-wheel steering (4WS)
 active steering, 243
 high-speed cornering, 244–245
 low-speed turning, 243–244
 passive steering, 243
 4WS. *See* Four-wheel steering (4WS)
 Frederick William Lanchester (1868–1946), 3
 Front-wheel-drive (FWD) vehicles
 drive forces and moments, 240–241
 fore/aft load transfer, 242
 throttle on/off changes, 242–243
 tractive force on aligning moment, 242
 tractive force on tire cornering stiffness, 241, 242
 Fuel economy effects, 97, 98
 FWD vehicles. *See* Front-wheel-drive (FWD) vehicles
 Gasoline and diesel engines, performance characteristics, 21, 22
 Gasoline engines, 2
 Giacomin W_s weighting, 445
 Gottlieb Daimler (1834–1900), 2
 Hardware-in-the-loop testing
 Fishhook maneuver, 269–271
 Slowly Increasing Steer maneuver, 269
 TruckSim-based HIL Platform, 268, 269
 Hooke's Law, 33
 Hotchkiss drive, 192–193
 Human discomfort frequency-weighting curves, 445
 Human sensitivity, 440–441
 Independent suspension roll centers
 double A-arm suspension, 211
 inclined parallel links, 213–214
 “jacking” forces, 211
 MacPherson Strut, 214–215
 negative swing arm geometry, 212–213
 parallel horizontal links, 213
 positive swing arm geometry, 212
 swing axle, 215
 of symmetric independent suspension, 212
 Independent suspensions
 A-arm front suspension, 195
 advantage, 194
 MacPherson Strut suspension, 195–196
 multi-link rear suspension, 196, 197
 semi-trailing arm rear suspension, 197–198
 swing-axle rear suspension, 198–199
 trailing-arm rear suspension, 196, 197
 International Roughness Index (IRI), 105
 ISO 611, 314
 ISO 612, 314
 ISO 1176, 314
 ISO 2631-1, 440
 ISO 3833, 314
 ISO 3877, 314
 ISO 3911, 314
 ISO 4223, 314
 ISO 6725, 314
 ISO 6726, 314
 ISO 7237, 314
 ISO 8855:1991, 312, 313
 ISO 11838, 314
 ISO/SAE Z-up vehicle-fixed coordinate system, 8
 ISO vehicle coordinate system, 6, 7
 James Watt (1736–1819), 1
 Karl Benz (1844–1929), 2
 Lateral force offset (F_{YT0}), 355
 Lumped mass, 6–7
 MacPherson Strut suspension, 195–196
 Marginal indicia, 380
 Maurice Olley, 3
 Model T to Fusion Hybrid, 4
 Motion, 443
 Motion and vibration discomfort assessment, 469–471
 Motion variables, 8
 Multi-link rear suspension, 196, 197
 National Highway Traffic Safety Administration (NHTSA), 261, 266
 Newton's second law, 9–10
 Nicholas Joseph Cugnot (1725–1804), 1
 Noise, 103
 Normal Force, 9
 Overshoot, 367
 Peak response time, 367
 Peak to steady-state ratio, 367
 Percent overshoot, 367
 Plysteer aligning moment ($M_{ZT(PLY)}$), 357
 Plysteer lateral force ($F_{YT(PLY)}$), 356
 Plysteer residual aligning moment ($M_{ZTR(PLY)}$), 359
 Plysteer residual lateral force ($F_{YTR(PLY)}$), 356–357
 Power-limited acceleration

- automatic transmissions
effort-speed characteristics,
 automatic transmission, 28
- fuel consumption map, V-8
 engine, 30
- gear ratios selection, 29, 30
- inverse capacity factor, 28
- off-the-line acceleration
 performance, 28
- torque amplification
 characteristics, 28
- torque converter characteristics,
 27, 28
- engines, 21–23
- powertrain
 constant engine power line, 26
 effective mass, 26
 effort-speed characteristics,
 manual transmission, 26
 engine torque, 23
 mass factor, 26
 mechanical losses, 25
 primary elements, 23, 24
 rotational accelerations of engine,
 transmission, and driveline, 25
 tractive force, 25, 26
 transmission inertia, 24
 vehicle acceleration, 25
 viscous losses, 25
- Power spectral density (PSD) function,
 104–107
- Powertrain
 constant engine power line, 26
 effective mass, 26
 engine torque, 23
 mass factor, 26
 mechanical losses, 25
 primary elements, 23, 24
 rotational accelerations of engine,
 transmission, and driveline, 25
 tractive effort-speed
 characteristics, 26
 tractive force, 25, 26
 transmission inertia, 24
 vehicle acceleration, 25
 viscous losses, 25
- Proportioning, braking performance
 brake force, 55
 deceleration, 52
 definition, 52, 55
- FMVSS 105 braking standard, 55
- inertia-proportioning valve, 56
- instability, 55
- load-sensing proportioning
 valves, 56
- maximum brake force, 52–54
- peak coefficient of friction, 52
- pressure proportioning valves, 56
- proportioning design, 55
- rear *vs.* front brake forces, 54–56
- Psychometric methods, 443
- Quasi-static rollover
 of rigid vehicle, 250–253
 of suspended vehicle, 253–255
- Residual aligning moment (M_{ZTR}), 357
- Residual lateral force (F_{YTR}), 356
- Revision indicator, 461
- Ride
 driveline excitation
 arrangements, 113, 114
 cross-type (Cardan or Hooke)
 universal joints, 115
 driveshaft, 113
 mass imbalance, 114
 secondary couples, 114–115
 spectral map of vibrations,
 115, 116
 torque variations, 115
 dynamic system, 104
 engine and transmission, 116–119
 lower-frequency ride vibrations, 104
 response properties, 104
 ride quality, 147
 road roughness
 acceleration amplitude
 coefficient, 108
 “average” road properties, 106
 broad-band random signals, 104
 definition, 104
 elevation, velocity, and
 acceleration PSDs, 106, 107
 general amplitude level, 105
 high-speed profilometer, 105
 IRI, 105
 pitch and bounce modes, 108
 PSD function, 104–106
 “ride isolation” properties, 107
 road elevation profiles, 105
 roll excitation characteristics, 108
 sine wave representation, 107
 spectral contents, 106
 spectral density, 108
 vertical acceleration, 106
 sprung-mass vibration, 379
- tire/wheel assembly
 dimensional variations, 109
 lateral force variations, 113
 mass unbalance, 109
- radial force variations, 110, 112
- radial nonuniformities, 111–112
- radial spring model, 109, 110
- stiffness variations, 109
- tractive force variations, 112
- tolerance to seat vibrations
 frequency domain
 information, 151
 human tolerance limits, 148
- International Organization for
 Standardization, 147
- inverse filtering, 149
- ISO tolerance curves, 151
- mean-square vibration, 151
- measurements, 152
- NASA discomfort curves, 148, 149
- ride vibration variables, 148
- steering-wheel and cab-shake
 vibrations, 153
- tire/wheel nonuniformities on
 highway tractor, 152, 153
- unsprung-mass vibration, 379–380
- vehicle response properties (*see*
 Vehicle response properties)
- Rise time (response time), 367
- Road loads
 aerodynamic aids
 air dams, 78
 bumper spoilers, 78
 deck lid spoilers, 78
 optimization, 79, 80
 window and pillar treatments, 78–79
- aerodynamic forces, 67, 73–74
- air flow around vehicle
 adverse pressure gradient, 70
 Bernoulli’s equation, 68, 69
 boundary layer development,
 69, 70
 favorable pressure gradient, 70
 form drag, 70
 friction drag, 70
 Newton’s Second Law, 68
 pressure and velocity
 gradients, 69
 separation point, 70
 streamtubes, 68
 vortex action, 70, 71
- crosswind sensitivity
 aerodynamic properties, 87
- crosswind lateral acceleration
 response, 87, 89
- neutral steer point, 87, 89
- tire cornering stiffness, 89
- tire properties, 88
- vehicle’s passive crosswind
 response, 88
- yaw rate response, 87, 88

- drags
- aerodynamic drag, 79
 - aerodynamic shielding, 76
 - air density, 79–80
 - air flow pattern inside engine compartment, 76, 77
 - air flow recirculation in wheel well, 76, 77
 - cooling system, 76
 - drag coefficient, 81–83
 - flow management in cooling system, 76
 - forebody drag, 74
 - front end design, 74, 76
 - main sources, 74, 75
 - protuberances, 76
 - rear end inclination angle, 74, 75
 - semi-empirical models, 79
 - stagnation point, 74
 - windshield angle, 75, 76
- lift force, 84–85
- pitching moment, 85, 86
- pressure distribution
- adverse pressure gradient, 71
 - aerodynamic lift and drag forces, 72, 73
 - aerodynamic viewpoint, 72
 - along centerline of car, 70, 71
 - Kamm-back characteristic shape, 72
 - separation point effect on dirt deposition, 72, 73
 - vortex systems, 72
- rolling moment, 86–87
- rolling resistance
- property, 90
 - tire inflation pressure/load, 91–92
 - tire material and design, 92–94
 - tire slip, 94
 - tire temperature, 91
 - total rolling resistance, 90
 - velocity, 92, 93
- side force, 83–84
- total road loads, 96–98
- typical coefficients, 94–96
- yawing moment, 85, 86
- Road roughness
- acceleration amplitude coefficient, 108
 - “average” road properties, 106
 - broad-band random signals, 104
 - definition, 104
 - elevation, velocity, and acceleration PSDs, 106, 107
 - general amplitude level, 105
 - high-speed profilometer, 105
- IRI, 105
- pitch and bounce modes, 108
- PSD function, 104–106
- “ride isolation” properties, 107
- road elevation profiles, 105
- roll excitation characteristics, 108
- sine wave representation, 107
- spectral contents, 106
- spectral density, 108
- vertical acceleration, 106
- Roll center analysis
- definition, 207
 - independent suspension roll centers, 211–215
 - “instantaneous” axes, 207
 - roll axis, 207
 - solid axle roll centers, 207–211
- Roll moment distribution
- cornering stiffness, 172–174
 - force analysis, 169–171
 - on front and rear axles, 171–172
 - lateral force–vertical load characteristics of tires, 168, 169
 - lateral load transfer, 170
 - load sensitivity effect, 172
 - roll center, 170
 - roll stiffness, 170
 - steer angle, 173
- Rollover
- accident experience
 - of cars and utility vehicles, 263, 264
 - driver characteristics, 264
 - “first harmful event,” 263
 - FMVSS, 264
 - methodical analysis, 263
 - off-road mobility, 263
 - off-road rollover accidents, 262
 - road environment, 264
 - of small cars, 263
 - for tractor-semitrailer vehicles, 265
 - vehicle control and handling stability, 264
 - vehicle wheelbase, 265
 - cross-slope/superelevation, 250
 - definition, 249
 - dynamic stability testing
 - ESC, 266–267
 - NHTSA, 266
 - Sine with Dwell test series, 267–268
 - yaw stability and rollover stability, 266
 - hardware-in-the-loop testing
 - Fishhook maneuver, 269–271
- Slowly Increasing Steer maneuver, 269
- TruckSim-based HIL Platform, 268, 269
- quasi-static rollover
- of rigid vehicle, 250–253
 - of suspended vehicle, 253–255
- transient rollover
- simple roll models, 256–258
 - tripping, 260–262
 - yaw-roll models, 259–260
 - tripped rollover, 249
 - un-tripped rollover, 249
- Rough road ride event, 443
- SAE J670, 312, 313
- SAE J1451, 313
- SAE J1594, 313
- SAE J1982, 313
- SAE J2047, 313
- SAE J2564, 313
- SAE M-105, 313
- SAE R-159, 313
- SAE vehicle axis system, 6, 7
- Semi-trailing arm rear suspension, 197–198
- Settling time, 367
- Simple harmonic motion, 400
- Sine with Dwell test series, 267–268
- Slowly Increasing Steer maneuver, 269
- Solid axle roll centers
- four-link rear suspension, 208–209
 - four-link with parallel arms, 209–210
 - Hotchkiss suspension, 210, 211
 - three-link rear suspension, 209
 - virtual reaction point, 207
- Sprung-mass vibration, 379
- States and modes
- control modes, 363–364
 - equilibrium, 363
 - neutral stability, 363
 - non-oscillatory stability, 363
 - oscillatory stability, 363
- Steady-state cornering
- handling, 157
 - high-speed cornering
 - characteristic speed, 164
 - critical speed, 164–165
 - lateral acceleration gain, 165
 - sideslip angle, 165–167
 - static margin, 167–168
 - steady-state cornering equations, 160–163
 - tire cornering forces, 159–161

- understeer gradient, 163–164
 yaw velocity gain, 165, 166
 low-speed turning, 158–159
 “open-loop” behavior, 157, 158
 suspension effects—
 aligning torque, 178
 camber change, 174–176
 cornering compliance, 168
 cornering model with tractive forces, 178–181
 lateral force compliance steer, 177–178
 roll moment distribution, 168–174
 roll steer, 176–177
 understeer and oversteer, Olley’s definitions, 168
 understeer gradient, 157, 181
 constant radius method, 182–183
 constant speed method, 183–184
 definition, 181
 four test methods, 181
 Steady-state response, 366
 Steam-powered vehicle, 1
 Steering system
 Ackerman turning geometry, 223, 224
 axle windup compliance, 345
 braking stability, 238–239
 camber and steer compliances, 344
 components, 331–333
 control input, 364
 directional control, 221
 forces and moments
 aligning torque, 234
 lateral force, 233
 on right-hand road wheel, 230
 rolling resistance and overturning moments, 234
 SAE tire force and moment axis system, 229
 tractive force, 233
 vertical force, 230–232
 forward-steer configuration, 222
 four-wheel steering
 active steering, 243
 high-speed cornering, 244–245
 low-speed turning, 243–244
 passive steering, 243
 front-wheel-drive vehicles
 drive forces and moments, 240–241
 fore/aft load transfer, 242
 throttle on/off changes, 242–243
 tractive force on aligning moment, 242
 tractive force on tire cornering stiffness, 241, 242
 front-wheel geometry, 227–229
 function of, 221
 gearbox, 222
 geometry error
 CAD programs, 225
 definition, 224
 ideal steering geometry, 225
 roll steer behavior, 227
 steering geometry error, 226
 toe change, 225–226
 kinematics, 341–342
 lateral compliance at contact center, 345
 lateral compliance at wheel center, 345
 linkage booster power steering, 236
 linkages model, 234, 235
 longitudinal compliance, 345
 modeling equations, 236
 open-loop directional response, 234
 rack-and-pinion system, 222, 223
 rear-steer configuration, 222
 shimmy problems, 3
 steer and camber angles, 334–337
 steering-axis geometry, 337–338
 steering ratio, 237
 steering torque *vs.* steer angle., 224
 trapezoidal tie-rod arrangement, 223
 understeer gradient, 237–238
 wheel connects, 222
 windup compliance, 345
 Subjective and objective data
 requirements
 discomfort ratings prediction, 457–458
 human sensitivity data,
 psychometric ratings
 discomfort ratings, 446
 human subjects, 446–447
 rating scales and usage, 447
 subject experimental protocols, 447–448
 objective motion and vibration measurement
 crest factor, 450
 duration of measurement, 449–450
 principal relevant basicentric coordinate systems, 448
 of seated occupants, 448–449
 signal conditioning, 449
 translational accelerometers, 448
 vehicle speed measurement, 450
 ride discomfort models
 domain-of-validity, 459–461
 Jury model, 458
 RPRED statistic, 459
 vibration data processing
 domain-of-validity
 determination, 454
 frequency weighting, 454–456
 human discomfort frequency weightings, 451–453
 root-mean-quad (RMQ)
 acceleration, 451
 rough *vs.* transient specimens, 451
 weighted root-mean-square (RMS) acceleration, 451
 Superseded tire axis system, 392–393
 Suspension
 active suspensions
 dive control, 217
 full-active suspensions, 216
 height control, 216–217
 performance, 217–218
 ride control, 216
 road holding, 217
 roll control, 217
 self-leveling suspensions, 215–216
 semi-active suspensions, 216
 squat control, 217
 anti-characteristics, 342–343
 anti-dive suspension geometry, 204–205
 anti-squat and anti-pitch suspension geometry
 equivalent trailing arm analysis, 199–201
 four-wheel drive, 204
 front solid drive axle, 203
 independent front-drive axle, 203
 independent rear drive, 202–203
 Power Squat, 199
 rear solid drive axle, 201–202
 weight transfer effect, 199
 components, 330–331
 independent suspensions, 329
 A-arm front suspension, 195
 advantage, 194
 MacPherson Strut suspension, 195–196
 multi-link rear suspension, 196, 197
 semi-trailing arm rear suspension, 197–198

- swing-axle rear suspension, 198–199
 trailing-arm rear suspension, 196, 197
 masses and inertias, 334
 motions, 338
 passive suspensions, 215
 primary functions, 191
 properties of, 191
 ride and roll stiffness, 343–344
 ride kinematics, 339–340
 roll center analysis
 definition, 207
 independent suspension roll centers, 211–215
 “instantaneous” axes, 207
 roll axis, 207
 solid axle roll centers, 207–211
 roll kinematics, 340–341
 solid axles, 329
 de Dion system, 193–194
 four-link rear suspension, 193
 Hotchkiss drive, 192–193
 suspension corner, 329
 understeer/oversteer gradient, 339
- Suspension effects of cornering
 aligning torque, 178
 camber change, 174–176
 cornering compliance, 168
 cornering model with tractive forces, 178–181
 lateral force compliance steer, 177–178
 roll moment distribution, 168–174
 roll steer, 176–177
 understeer and oversteer, Olley’s definitions, 168
- Swing-axle rear suspension, 198–199
- Tire-road friction, braking performance
 adhesion component, 47
 adhesive and hysteretic friction, 48
 adhesive friction contribution, 48
 braking coefficient vs. slip, 49
 braking deformations, 48
 bulk hysteresis mechanism, 48
 inflation pressure, 49
 peak coefficient, 48
 primary mechanisms, 47, 48
 surface adhesion, 47
 velocity, 49
 vertical load, 49
- Tires
 aligning moment
 path curvature, 296
- slip angle, 294–295
 steer deflection angles, 296
 basic functions, 275
 camber thrust
 camber stiffness, 292
 Carpet plot, bias-ply tire, 292
 inclination angle, 291
 inflation pressure, 293–294
 load, 293
 passenger-car tires, 292, 293
 surface texture, 294
 tread design, 294
 vertically oriented tire, 292
 combined braking and cornering
 brake and lateral forces, 297
 directional or yaw response, 300
 friction circle, 297–299
 front-wheel lockup, 300
 longitudinal slip, 300
 radial vs. bias-ply tire, 299
 rear-wheel lockup, 300
 conicity and ply steer, 300–301
 construction, 276–277
 cornering properties
 bias-belted tires, 289
 bias-ply tire, 289
 inflation pressure, 290
 load, 290
 for passenger-car tires, 289
 radial tires, 289
 size and width, 290–291
 slip angle, 286–289
 tread design, 291
 understeer gradient, 291
 cornering stiffness, 360
 durability forces, 302–303
 forces and moments, 352–354
 inclination stiffness, 360
 lateral force coefficient, 359
 lateral force load sensitivity, 360
 lateral force response phase angle, 360
 Load Index, 278
 longitudinal force coefficient, 359
 longitudinal stiffness, 360
 mechanical structure, 276
 mechanics of force generation, 280–281
 moment properties, 361
 normal force properties, 360–361
 operating conditions, 275
 orientation angles, 349–350
 pneumatic tire, 348–349
 pull forces and moments, 355–359
 relaxation length, 360
 road friction, 361–362
- rolling characteristics, 350–351
 SAE tire axis system, 279–280
 shear force coefficient, 359
 size and load rating, 277
 slip, 351
 standard loads and inflation pressures, 352
 tractive properties
 anti-lock braking systems, 285
 brake force vs. slip, 282, 283
 deformation mechanism in contact patch, 281, 282
 inflation pressure, 283
 longitudinal stiffness, 282
 longitudinal traction properties, 285
 peak coefficient, 285
 sliding coefficient of friction, 285
 slip, 282
 speed, 285
 surface friction, 284
 vertical load, 283, 284
 vibrations, 303–305
- Traction-limited acceleration
 coefficient of friction, 32
 differential unit, 36–37
 of front-wheel-drive vehicle, 38–39
 independent rear suspension, 35
 maximum tractive force, 35
 for rear-drive passenger car, 37–38
 solid front drive axle with locking differential, 36
 solid front drive axle with non-locking differential, 36
 solid rear axle with locking differential, 35
 solid rear axle with non-locking differential, 35
 transverse weight shift, 32–35
- Traction-limited gradeability, 16, 17
- Trailing-arm rear suspension, 196, 197
- Transfer functions, 462–464
- Transient response, 366–367
- Transient ride event, 443–444
- Transient rollover
 simple roll models, 256–258
 tripping, 260–262
 yaw-roll models, 259–260
- Travel speeds of production automobiles, 3
- Tripped rollover, 249
- TruckSim-based HIL Platform, 268, 269
- Ttire dynamometer, 3

- Undamped natural frequency of sprung mass, 398–399
- Understeer gradient, 157, 163–164, 181
constant radius method, 182–183
constant speed method, 183–184
definition, 181
four test methods, 181
- Uniformly spaced road disturbances, resonant speed, 401–402
- Unsprung-mass vibration, 379–380
- Un-tripped rollover, 249
- Vehicle**
angular motion variables
 angles, 324–327
 angular accelerations, 327–328
 angular velocities, 327
dynamics, 4–6
Euler angles, 324
geometry and masses
 articulation point, 320
 base vehicle mass, 321
 base vehicle weight, 321
 curb mass, 321
 curb weight, 321
 dynamic index-pitch, 322
 dynamic index-yaw, 322
 effective unsprung mass, 320
 hitch point, 320
 load condition, 321
 mass moments of inertia, 321, 322
 passenger mass, 321
 payload, 321
 sprung mass, 321
 sprung-mass center of gravity, 321
 sprung-mass pitch moment of inertia, 322
 sprung-mass roll-yaw product of inertia, 322
 sprung-mass yaw moment of inertia, 322
 sprung weight, 320
 suspension trim height, 320
track T, 319
trailer wheelbase, 319
unsprung mass, 320
unsprung weight, 320
vehicle center of gravity (C.G.), 321
vehicle operating mass, 321
vehicle operating weight W, 321
vehicle trim height, 319
wheelbase L, 319
- translational motion variables
 accelerations, 323–324
 velocities, 322–323
vehicle trajectory measures, 328
- Vehicle-fixed coordinate system**, 7
- Vehicle lateral response**
 characterizing speeds, 374–375
 directional response limits, 376
 gain/sensitivity measures, 370–371
 gradient measures, 371–372
 lateral load transfer, 369
 linear range, 370
 minimum steering sensitivity, 376
 nonlinear range, 370
 on-center range, 370
 overshoot measures, 376
 rearward amplification, 376
 rise-time measures, 375
 rollover resistance, 376–377
 stability and control derivatives, 377–378
 stability measures, 374
 understeer and oversteer, 372–374
- Vehicle longitudinal response**
 braking performance, 369
 gain measures, 368
 gradient measures, 368
 longitudinal load transfer, 368
 pitch angle overshoot, 368
 transient brake system response, 368–369
- Vehicle response properties**, 366
 active control, 130–134
 bounce/pitch frequencies
 coupling coefficient, 141
 natural frequencies of front and rear suspensions, 142, 143
 Olley criteria, 143
 pitch motion, 141, 142
 pitch plane model, 140
 rear suspensions, vehicle bounce, 143–144
 vertical motion, 141
- damping
 “blow-off” valve, 130
 nominal effect, 127
 ratio curve, 127
 shock absorbers, 127
 in suspension jounce and rebound directions, 128
 tuning, 128
- twin tube and gas-pressurized monotube shock absorbers, 129–130
- unsprung mass, tuning, 128–129
- Rigid body bounce/pitch motions of heavy trucks**, 139
- Pitch resonance frequency**, 139
- Pitch response**, 139
- Roughness excitation**, 137
- Vertical vibration response**, 139
- Wheelbase filtering**, 137–139
- Suspension isolation**
 amplitude ratios, 121, 122
 bounce natural frequency, 120
 damped natural frequency, 120
 isolation of road acceleration, 123, 124
 quarter-car model, 119, 122
 response gain, 123
 “ride isolation” properties, 119
 ride rate, 119
 sprung and unsprung masses, 121
 sprung-mass acceleration spectrum, 123
 sprung-mass response, 123
 static deflection, 120
 stiffness and damping, 119
 suspension damping ratio, 120
 undamped natural frequency vs. static deflection, 120, 121
- Suspension nonlinearities**, 135–136
- Suspension stiffness**, 124–127
- Transmissibility**, 119
- Wheel hop resonances**, 134–135
- Vertical Force**, 9
- Vibration data processing**
 domain-of-validity determination, 454
 frequency weighting, 454–456
 human discomfort frequency weightings, 451–453
 root-mean-quad (RMQ) acceleration, 451
 rough vs. transient specimens, 451
 weighted root-mean-square (RMS) acceleration, 451
- Vibration systems**
 advantages, 403
 forced vibration
 with coulomb damping, 416–417
 with viscous damping, 407–416
 force transmission through suspension
 constant peak driving force, 418–419
 degree of freedom, 423–426
 driving force on mass proportional to square of speed, 419–421

- equivalent impedance, 421
- viscous and coulomb damping,
422–423
- free vibration
 - with coulomb damping,
404–405
 - with viscous damping, 405–406
- undamped conditions, 402
- vibrating system parameters, 403
- vibratory motion, 403
- Wheels
 - plane geometry, 349
 - rim, 347–348
- road wheel, 347
- spin, 351
- standard loads and inflation
pressures, 352
- Yaw-roll models, 259–260

Fundamentals of Vehicle Dynamics, Revised Edition

An SAE Core Title

Thomas D. Gillespie

A world-recognized expert in the science of vehicle dynamics, Dr. Thomas Gillespie has created an ideal reference book that has been used by engineers for 30 years, ranging from an introduction to the subject at the university level to a common sight on the desks of engineers throughout the world.

As with the original printing, **Fundamentals of Vehicle Dynamics**, Revised Edition, strives to find a middle ground by balancing the need to provide detailed conceptual explanations of the engineering principles involved in the dynamics of ground vehicles with equations and example problems that clearly and concisely demonstrate how to apply such principles.

A study of this book will ensure that the reader comes away with a solid foundation and is prepared to discuss the subject in detail.

Ideal as much for a first course in vehicle dynamics as it is a professional reference, **Fundamentals of Vehicle Dynamics**, Revised Edition, maintains the tradition of the original by being easy to read and while receiving updates throughout in the form of modernized graphics and improved readability.

Inasmuch as the first edition proved to be so popular, the Revised Edition intends to carry on that tradition for a new generation of engineers.

This book provides valuable insight into the dynamics of one of the most fascinating systems known to humankind

Saied Taheri
Professor, Virginia Tech
Director, Center for Tire Research
(CentiRe)

RELATED RESOURCES:

Race Car Vehicle Dynamics

Authors: William F. Milliken and Douglas L. Milliken
Product Code: 978-1-56091-526-3

Road Vehicle Dynamics

Authors: Rao V. Dukkipati, Jian Pang, Mohamad S. Qatu, Gang Sheng, Zuo Shuguang
Product Code: 978-0-7680-1643-7

SAE International Journal of Vehicle Dynamics, Stability, and NVH

ISSN: 2380-2162
eISSN: 2380-2170

ISBN: 978-1-4686-0176-3



9 781468 601763